THE STRUCTURAL PERFORMANCE OF TALL WOOD-FRAME WALLS UNDER AXIAL AND TRANSVERSAL LOADS

by

DANIEL LEONARD

B.A.Sc., The University of British Columbia, 2002

A THESIS SUBMITTED IN PARTIAL FULFILMENT OF
THE REQUIREMENTS FOR THE DEGREE OF

MASTERS OF APPLIED SCIENCE

in

THE FACULTY OF GRADUATE STUDIES

(Department of Civil Engineering)

We accept this thesis as conforming
to the required standard

....
Dr. H.G.L. Prion

....
Dr. T. Haukaas

....
Dr. M. Popovski

THE UNIVERSITY OF BRITISH COLUMBIA

October 2004

Library Authorization

In presenting this thesis in partial fulfillment of the requirements for an advanced degree at the University of British Columbia, I agree that the Library shall make it freely available for reference and study. I further agree that permission for extensive copying of this thesis for scholarly purposes may be granted by the head of my department or by his or her representatives. It is understood that copying or publication of this thesis for financial gain shall not be allowed without my written permission.

DANIEL EDWARD LEONARD
Name of Author *(please print)*

08/10/04
Date (dd/mm/yyyy)

Title of Thesis: THE STRUCTURAL PERFORMANCE OF TALL WOOD-FRAME WALLS UNDER AXIAL AND TRANSVERSAL LOADS

Degree: MASTERS OF APPLIED SCIENCE Year: 2004

Department of CIVIL ENGINEERING
The University of British Columbia
Vancouver, BC Canada

ABSTRACT

Tall wood-frame walls have emerged as a viable alternative to steel, concrete, and masonry in the construction of large industrial, commercial, and institutional buildings in North America. The construction of tall wood-frame walls incorporates the advantages of typical residential wood-frame platform construction, which include fast construction times and the use of relatively unskilled labour to deliver lightweight buildings proven to be durable over many years of usage. Some of the restrictions placed on the construction of residential wood-frame walls by applicable building codes are also currently placed on the construction of tall wood-frame walls. This study focused on the response of tall wood-frame walls under axial and transversal, or out-of-plane, loading with particular emphasis on addressing the appropriateness of certain current code restrictions on this type of construction. The axial loads represented the loads applied to the walls from the roof structure including the loads from snow, rain, and wind. The loads in the transversal direction represented either compression or suction to the face of the wall due to wind pressure.

Because of the inherent variability and non-linear behaviour of wood, many of the components of tall wood-frame walls were tested separately prior to testing the full-scale wall specimens. These component tests were used to determine the bending stiffness of each material component individually. In addition to the lateral and withdrawal stiffness of nailed connections, the bending stiffness of composite studs with sheathing, and the response of sheathing panels under racking loads with varied stud spacing was investigated. The tests of the sheathing panels showed that the current limit on stud spacing in the Canadian Wood Design Code is not

appropriate for this type of wall construction. Because these types of walls are designed using an equivalent static wind pressure rather than a true representation of the dynamic characteristics of wind, monotonic tests were primarily conducted on all of the components and the full-scale walls. The experimental results from the component tests were used to verify linear analytical models representing the load-deformation behaviour of composite T-beams, consisting of a stud connected to a tributary width of sheathing, under transversal loads. These models were then used to verify more sophisticated linear models representing the load-deformation behaviour of full-scale walls under axial and transversal loads. Non-linear finite element models of full-scale walls were also verified using the results from the component tests. Design equations were presented that accurately account for the composite action that exists between the sheathing and the studs. Finally, some design and construction recommendations are discussed regarding several aspects of tall wood-frame walls based on the results of the full-scale wall tests.

TABLE OF CONTENTS

LIST OF TABLES

LIST OF FIGURES

ACKNOWLEDGEMENTS

This project was conducted with the financial and in-kind support from Natural Resources Canada (Canadian Forest Service), the Natural Sciences and Engineering Research Council of Canada, the Department of Civil Engineering at the University of British Columbia, and Forintek Canada Corp. and its industry members. The support of all of these institutions is gratefully acknowledged.

I would like to thank my two supervisors, Dr. Marjan Popovski at Forintek and Dr. Helmut Prion at UBC, for their guidance, technical advice, and financial support. They both gave me a great deal of freedom in pursuing this research topic but were always available when I needed assistance. I would also like to thank Dr. Ricardo Foschi at UBC and Dr. Erol Karacabeyli at Forintek for their professional advice during the research project.

The extensive experimental portion of this thesis would not have been possible without the assistance of the engineers, technologists, and technicians at Forintek. I would like to thank Henley Fraser, Paul Symons, Tony Thomas, Len Stroh, Jules Gardy, Roy Abbott, and Bill Deacon for their involvement in this research. I am especially grateful to Henley Fraser and Paul Symons for their advice and guidance on the experimental test program and their knowledge of wood construction.

I would like to thank my parents, Frank and Elaine, who have supported me immeasurably and have inspired me to strive to produce the best work that I am capable of.

1. INTRODUCTION

1.1 PROBLEM OVERVIEW

In North America, wood-frame construction utilizing dimension lumber has been in use since the early 19th century. There are many examples of houses built with this system that are more than 100 years old and still continue to perform their original function. Although the system has evolved and changed over time, wood-frame construction still remains simple in concept and well within the scope of the average builder. Wood-frame construction with its comfort, economy, energy efficiency and use of renewable resources, is so practical and effective that more than ninety percent of North American homes are still constructed using this building method. A wall system utilizing regular residential wood-frame construction methods commonly found in North America is shown in Figure 1.1.

Efforts have been made to extend the use of this method to non-residential applications. Developments such as hotels, motels, low-rise commercial properties, community centres and other building applications are all benefiting from the advantages that wood-frame construction has to offer. In spite of this market expansion, the proportion of non-residential buildings constructed with wood remains relatively low compared to other construction materials such as steel, concrete or masonry. For applications such as hotels and motels, the wood-frame construction concept can be used with little modification from its residential version. That is not the case, however, for most industrial or commercial buildings. These buildings usually require larger open spaces and greater heights than other non-residential buildings.

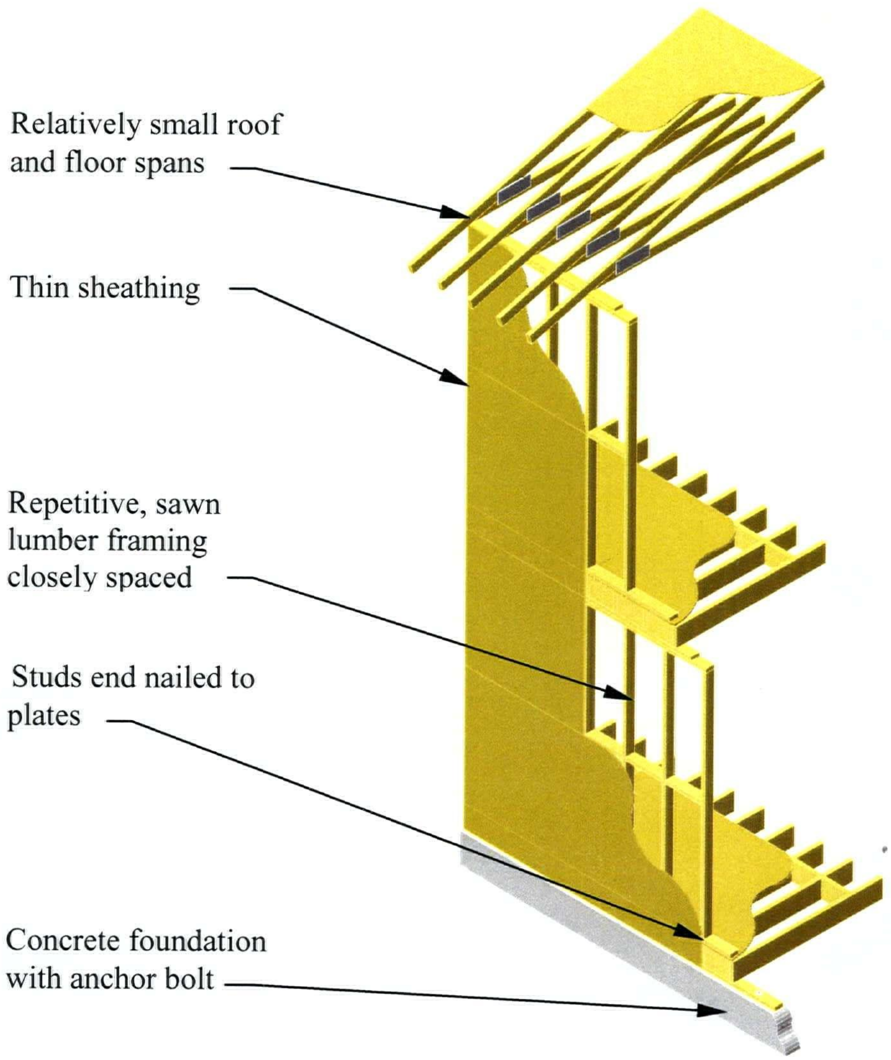

Figure 1.1. Regular residential wood-frame construction in North America.

To assist the specifiers of larger commercial and industrial structures, the Canadian Wood Council has issued two publications during the last four years. The "Design and Costing Workbook" gives detailed design and costing information on single storey buildings with a floor area of up to 14,400 square metres (CWC, 1999). The follow up publication "Tall Walls Workbook" (CWC, 2000) provides information on tall wall design for commercial and industrial structures. Tall walls are an extension of platform wood-frame construction into non-residential applications, where wall heights are usually from 4.8 m (16 ft) to 10.7 m (35 ft). The Tall Walls Workbook provides stud tables for lumber studs and studs made from selected engineered wood products up to 10.7 m (35 ft) in height. The engineered wood products considered include SelecTem™ (LVL), TimberStrand® (LSL) and Westlam® (Glulam). A typical tall wood-frame wall system is shown in Figure 1.2.

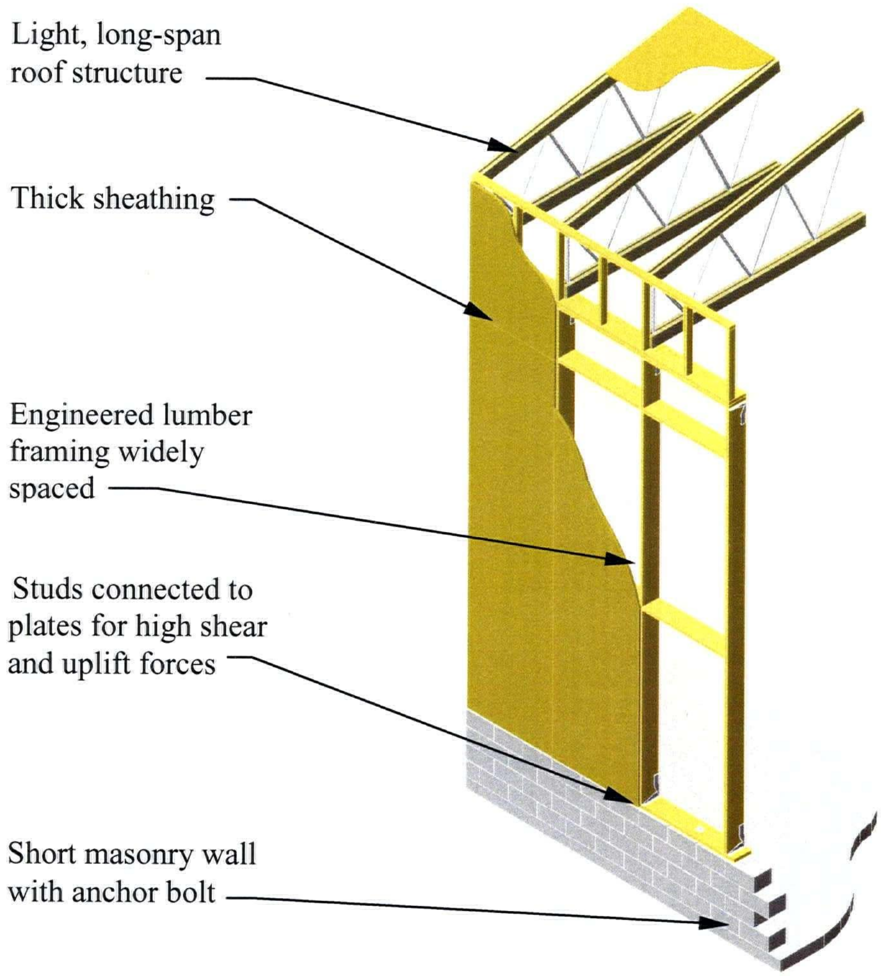

Figure 1.2. Tall wood-frame wall construction.

The publications mentioned above provide an excellent foundation for the use of tall walls in commercial structures. They are built on the long-term positive experience of using wood-frame construction in residential applications. Incremental research contributions, however, are needed if tall walls are to make further inroads into the non-residential construction market. Some of the current restrictions on wood-frame construction in the Canadian Wood Design Code seem overly conservative and may not be appropriate for tall wood-frame walls. By using thicker sheathing on the walls, for example, deflection criteria under design wind loads could easily be met by accounting for the composite action that exists between the sheathing and the stud. The inclusion of composite action is currently not permitted in the code. The most important parameter that affects the amount of composite action in a wall system is the stiffness of the connection between the sheathing and the studs, which typically consists of nails alone or nails combined with adhesive. There is currently very little test data available on the load-displacement response of these types of connections when thick sheathing or engineered wood products are used, and the degree of composite action that can be achieved.

Of the test programs that have investigated composite action between wall sheathing and studs in wood-frame walls over the past thirty years, none have included components and connections that significantly increased the bending stiffness of the walls. These tests were mostly concerned with determining the amount of composite action in existing structures that were built with regular wood-frame construction techniques. For larger walls, an increase in the stud spacing would certainly be an option worth investigating, as it would likely result in a more efficient building system. The maximum spacing currently allowed by the code seems overly restrictive as it is based on research conducted on regular wood-frame shearwalls with thin sheathing. Using thicker sheathing as required to span the longer distance between studs will also most likely increase the composite action in the wall system and allow for greater stud spacing.

The studs in regular wood-frame walls are typically only connected to the top and bottom wall plates with two or three nails. Due to the increased wall heights and roof spans found in buildings with tall walls, the stud connections are subjected to much higher loads necessitating the use of special connectors. These connectors, and the labour involved in their installation, can increase the total cost of construction significantly. More economical connection solutions are needed while maintaining the overall performance of the tall wood-frame walls under axial and transversal, or out-of-plane, loads. For larger buildings with large free-standing walls the axial loads from snow, rain, and wind on the roof, combined with the transversal wind loads on the wall surface, will require construction detailing that is beyond the realm of regular wood-frame construction. To achieve economically competitive solutions, more sophisticated design methods and analysis models are required.

Sophisticated mathematical models for the analysis of tall wood-frame walls under axial and transversal loads are an essential tool to extend the application of experimental results, predict the load-deflection response, and perform parametric studies on their performance. Once analytical models have been verified against test results, the models can then be used to determine factors for use in design, and to validate simpler and user-friendly analysis tools for use in design offices.

1.2 RESEARCH OBJECTIVES

For the reasons mentioned above, Forintek Canada Corp. initiated a research program on the structural performance of tall walls in Canada in 2003. The objective of this program is to assist the forest products industry in expanding its share of the market in the construction of box-type buildings in the commercial and industrial sectors using tall wood-frame walls. This thesis focuses on the structural performance of tall walls under axial and transversal loads. A subsequent study will focus on the performance of these walls under in-plane lateral loads due to wind and earthquakes. The main objectives of this thesis on tall wood-frame walls can be summarized as follows:

- Increase the body of knowledge on the performance of wood-frame walls under axial and transversal loads and their component properties with special attention to the use of engineered wood product studs and thick, oversized sheathing;

- Determine the factors that influence the response of tall wood-frame walls under axial and transversal loads;
- Investigate the appropriateness of the limit on stud spacing currently found in the Canadian Wood Design Code for wood-frame walls;
- Determine economical stud connections for tall wood-frame walls to resist axial and shear loads and study the influence of these connections on the overall performance of tall walls under axial and transversal loads;
- Verify linear equations to predict composite action for use in design and verify non-linear finite element models for use in future research;
- Propose a simple analysis model for tall walls that can be used in engineering practice

1.3 SCOPE

To meet the objectives outlined above, a research program was devised, which consists of five parts:

1. A literature review on wood-frame construction including previous research on composite construction and full-scale wall testing;
2. Monotonic testing on the individual material components, individual connections, and composite stud elements of a full-scale tall wood-frame wall;
3. Monotonic testing to determine the buckling characteristics of sheathing panels under racking loads to determine the validity of the restriction on stud spacing;
4. Monotonic testing of full-scale tall wood-frame walls under axial and transversal loads;
5. An analytical study to verify mathematical models to expand the test results to different design conditions and establish appropriate design factors.

There have been numerous formulations and computer models developed over the past fifty years to analyze the response of composite wood-frame diaphragms. A review of these studies was needed to determine accurate and straightforward methods for predicting the response of the tests conducted in this study, and that could also be easily incorporated into standard design practice.

Because of the inherent variability and non-linearity of wood, many of the components of tall wood-frame walls were tested separately prior to testing full-scale wall specimens. The properties obtained from these component tests are required input values in the analytical models. A chart showing the organization of the tests conducted in this study is shown in Figure 1.3. Because the non-linearity of the individual connections between the sheathing and the studs were greater than that of the larger composite components and full-scale walls, many more connections types were tested in order to build a database that could be incorporated into future analytical studies.

Tests were subsequently conducted on composite T-beams, comprising a stud and a tributary width of sheathing, in bending to study the sensitivity of composite action to specific properties such as connection stiffness, modulus of elasticity, sheathing thickness, and the presence of gaps in the sheathing. Shearwall tests were conducted to determine the out-of-plane buckling characteristics of sheathing panels subjected to lateral loads. The shearwall tests were conducted to validate the use of large stud spacing in the full-scale wall tests. Additional properties of tall wood-frame walls were also investigated throughout the course of the full-scale tests. These included: the interaction of axial and transversal load; the presence of non-structural sheathing; the effect of load reversal on bending stiffness; in-plane load distribution effects; the effect of end support conditions on mid-height deflections; and response of several stud connection types to axial and transversal loads. The stud materials used for both the composite T-beam and full-scale wall tests were spruce-pine-fir sawn lumber and laminated strand lumber. The nails used to connect the sheathing to the studs for all tests were spiral nails, as these are commonly used in the construction of wood-frame walls.

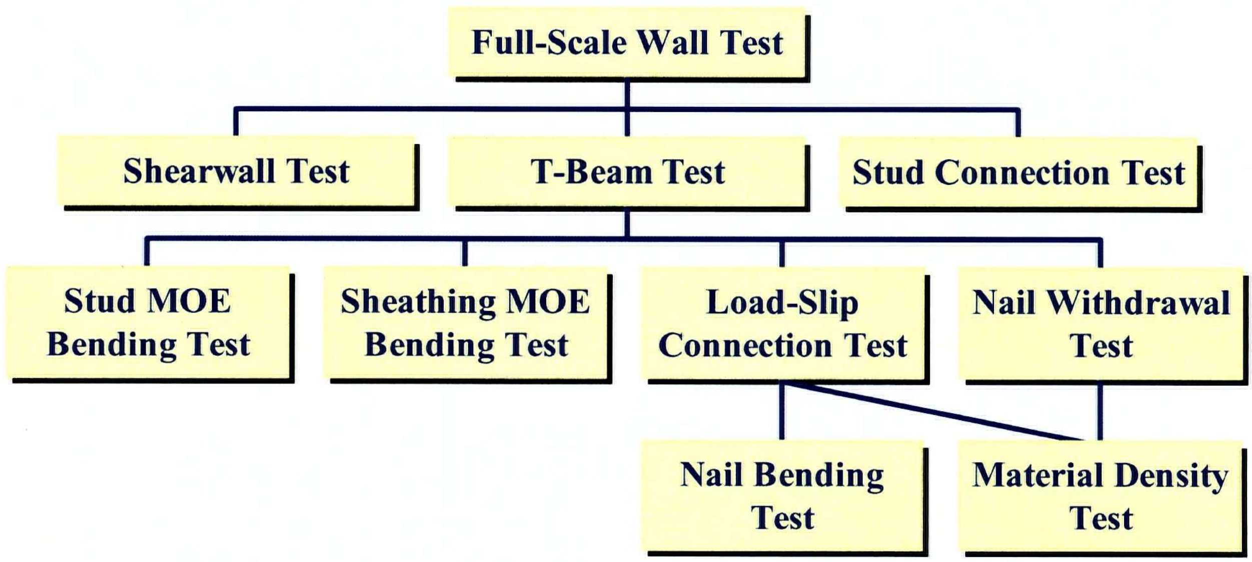

Figure 1.3. Tests conducted over the course of this study.

1.4 THESIS OUTLINE

The thesis presents the different steps followed in the study to achieve the research objectives. An overview of wood-frame construction in North America, past performance of wood-frame buildings, the advantages and disadvantages of wood, concrete, steel, and masonry materials when used in non-residential construction, and the corresponding literature review on issues concerning tall wood-frame walls are given in the second chapter. Chapters 3 and 4 describe the monotonic tests conducted on a number of different nailed connections under lateral and withdrawal loads, respectively. In Chapter 5 the monotonic and cyclic tests on composite T-beams under transversal loads are described, in addition to analytical predictions using linear approximations. A discussion of issues regarding composite action is also presented in this chapter. Chapter 6 describes the monotonic lateral load tests conducted on the shearwalls. The monotonic tests that were conducted on full-scale tall wood-frame walls under axial and transversal loads are presented in Chapter 7. Several issues affecting the performance of tall wood-frame walls are also addressed in this chapter. Results and discussion on the test results from all chapters include load-deformation characteristics and maximum loads. Analytical predictions of the full-scale tall wall tests are presented in Chapter 8. Finally, in Chapter 9 a summary of the results of the study is given. The chapter also provides recommendations for changes that could be made to current design practice and recommendations for further research. A list of references is given in Chapter 10 in the thesis.

2. LITERATURE REVIEW

2.1 WOOD-FRAME CONSTRUCTION IN NORTH AMERICA

The research investment into the engineering properties of Canadian wood species in the 1970's and 1980's yielded enormous returns for the Canadian lumber industry and paved the way for its current domination in the residential market in North America. In the construction market most of the Canadian wood products exported are used in residential construction, while only a small percentage is used in non-residential construction. The North American non-residential market is vast and comparable in size to the residential market. It is currently valued at about US$300 billion a year, and as such it should be a major target for the wood products industry. The total value of non-residential construction in the United States alone in 1999 was US$273.5 billion, which is nearly 80% of the value of new residential homes in the same year (USBC, 2000).

In the past, wood and engineered wood products have made only modest inroads into this steel and concrete dominated market. This is especially surprising given the fact that about 90 percent of all non-residential construction activity is four stories or less and could incorporate wood products in structural applications according to most building codes. Yet, the non-residential construction market used less than 11% of the amount of wood products used in residential construction in 1995, and this figure is in decline from a previous study conducted in 1985 (McKeever and Adair, 1998). It is difficult to estimate the exact value of this missed opportunity, but a rough estimate taking into account building code restrictions, is that an additional 9.9 million cubic metres (7.5 billion board feet) of lumber and 560 million square metres (6 billion square feet) of panels could have been used in the United States for non-residential construction in 1995 alone.

The need to examine new wood markets becomes even more urgent as steel and concrete slowly continue to erode wood's dominance in the residential sector. It is estimated that capturing an additional 2% of the non-residential market share would result in an increase of the industry income of US$5.4 billion per year (USBC, 2000). Furthermore, this value does not take into account the fact that the greater the use of wood in structural applications, the greater its use becomes for non-structural and finishing purposes as well. For all these reasons, a successful penetration of the forest products industry into the non-residential market is critical at this time.

The direct market impact of a tall wood-frame wall solution is difficult to estimate at this point. The most recent non-residential wood usage data available does not contain sufficient detail to accurately make such an estimate (McKeever and Adair, 1998). The details required for an accurate estimate would include specific usage and building code information for the aggregate data reported by McKeever and Adair. New non-residential buildings constructed in 1995 totalled approximately 260 million square metres (2.8 billion square feet) of area, contained 140 million square metres (1.5 billion square feet) of exterior walls, and had a total construction value of US$185 billion. Wood was used in only 10% of exterior walls. When wood is used at all in non-residential buildings, it is preferred for roofs (19% of non-residential roofs use wood), upper-story floors (14%), and interior walls (13%).

A 2001 study explored the reasons why wood is not used more often in non-residential construction (Gaston et. al., 2001). Code limitations, which restrict the use of wood to smaller buildings and may forbid it entirely for some building types, were cited as a primary reason. Wood is least restricted as a roof material, which may explain why its non-residential usage is greatest in roof applications. Another key hurdle for wood is total design and installed costs: wood was cited as not cost-competitive with other materials, particularly pre-engineered steel. Steel is quickly and inexpensively erected for simple warehouse-style structures, which is why it is a strongly preferred material in this market. In other tall wall cases, concrete has a major advantage over wood for its impact and vandal resistance in, for example, prisons, schools, and warehouses with moving forklifts and machinery.

Assuming that a tall wood-frame wall is cost-competitive with steel, masonry, and tilt-up concrete and can meet all the performance expectations of these materials for a given building application, then the market potential can be examined in a rough manner by considering only the size of the market for building types which might include tall walls. In other words, ignoring the segment of the market that would not choose wood due to cost or specific usage issues. The segments of the market with particularly stringent code restrictions on wood, for example, buildings that would be classified under code as "hazardous" categories will also be ignored. Some tall wall building applications, such as many factories, would fall into those occupancies. Ignoring current building code restrictions is a reasonable assumption for a long-term forecast, as it is expected that the objective-based codes to be adopted in near future will probably place no such limitations on material as a function of combustibility.

If a tall wall is defined as one with a height somewhere in the range of 3.6 m to 10.7 m (12’ to 35’), then the majority of non-residential buildings would qualify as the target market, as a 3.6 m or larger floor-to-floor height is typical for non-residential buildings. A more realistic estimate for market potential can be derived by considering which types of buildings have tall walls, perhaps 5 m (16.5’) and higher, where wood-frame structures are expected to be more competitive with other materials. Factories, warehouses and big box retail stores are the most obvious examples of these building types, which actually represent the majority of non-residential construction. In 1995, the categories of "stores" and "industrial buildings" together accounted for 58% of all non-residential floor area built. The potential incremental volume for wood in these categories is 2.0 million cubic metres (1.5 billion board feet) of lumber and 140 million square metres (1.5 billion square feet) of panels for stores, and 340,000 cubic metres (255 million board feet) of lumber and 130 million square metres (1.4 billion square feet) of panels for industrial buildings. Combined, this is 2.2 million cubic metres (1.7 billion board feet) of lumber and 270 million square metres (2.9 billion square feet) of panels, for a total value in 2002 dollars of CAD$1.94 billion. This represents the maximum potential incremental market for wood in the retail and industrial categories of buildings, and assumes that all other appropriate elements of the building are also made of wood along with the tall exterior walls. Under present code scenarios, some of these buildings would be precluded from wood due to a hazardous occupancy class and/or a floor area above the maximum for combustible construction. However, other building categories hold strong potential for application of a tall wood-frame wall solution: schools, offices, public buildings and health care facilities. It is difficult to estimate what fraction of these would convert to wood if a set of wood-based tall wall structural solutions were offered to designers.

2.2 PAST PERFORMANCE OF WOOD-FRAME BUILDINGS

Even though wood-frame structures represent a significant portion of the existing building stock in North America, relatively little is known about how these structures perform under high wind forces from the standpoint of engineering behaviour (Rosowsky et. al., 2000). The need for further research is warranted, as wind forces are the most common source of damage to light wood-frame construction (FEMA, 1997). Despite that fact, it has been documented that wood-frame construction has performed well under high wind forces and that a lot has been done to better understand these forces and how they affect buildings. Recent work has led to increased design wind speeds in building codes for many areas. And advances like hold-downs, bracing, and fastening systems have resulted in a building system that can resist even the most extreme forces of hurricanes (CWC, 2002).

Determining how actual wind forces are applied to a structure is very complicated and depends on several variables. Factors such as geographic location, variations in topography, building size and configuration, openings in the building, and building stiffness all effect wind behaviour and velocity. Wind near the earth's surface is a dynamic phenomenon, causing an erratic and unpredictable condition called gusting. This occurs when wind suddenly changes direction, totally reversing its motion. The distribution of wind velocity varies over the height of a building. Roughness elements on the earth's surface, which can range from grass to other buildings, slow down the wind velocity near the ground. It is clear, therefore, that low-rise buildings are more greatly affected by the presence of these elements than are larger structures.

The presence of large openings in a building can have a significant impact on the magnitude of wind forces on a structure. Buildings that have many large openings such as warehouses and industrial facilities are especially prone to high wind forces for this reason. Figure 2.1 shows the distribution of wind forces on a low-rise building that is enclosed. Because a different atmospheric pressure exists inside the building than exists outside, both internal and external pressures act simultaneously on the surfaces of the building. The internal pressures are smaller than the external but they are always added. In contrast, if the building has a large opening (Figure 2.2) then the internal pressures are approximately the same magnitudes as the external pressures creating significant wind forces on the surfaces of the building.

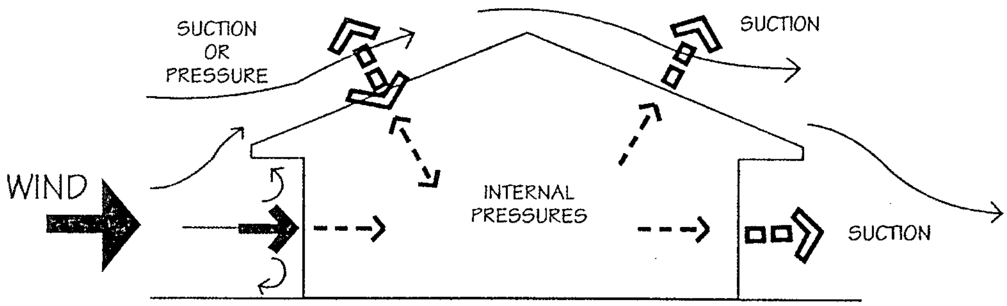

Figure 2.1. Distribution of wind pressure on an enclosed building (FEMA, 1997).

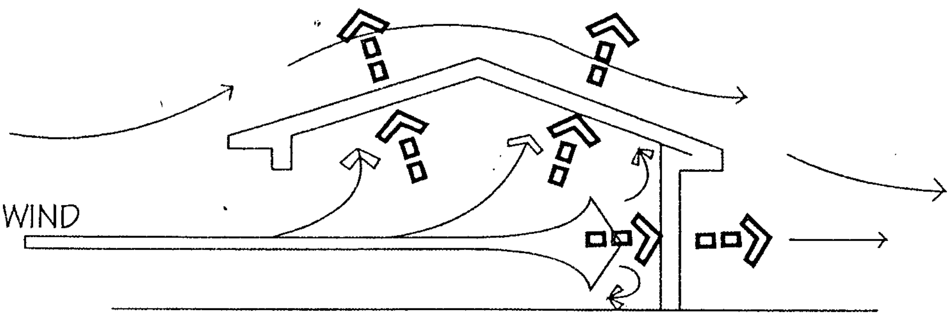

Figure 2.2. Distribution of wind pressure on a building with an opening (FEMA, 1997).

Because the distribution and magnitude of wind forces on a building is difficult to predict, building codes have simplified this phenomenon so that it can be easily incorporated into design. Forces are determined from wind velocities for specific geographic locations multiplied by internal pressure, external pressure, and gust coefficients based on the building type and particular building surface of interest. Despite its dynamic nature, wind forces are treated as a static load case in building codes. For wood design, this assumption is offset by a duration of load factor that increases the strength of wood for short-term loading. The load-duration effect is applied to both wood members and connections. Such a phenomenon, however, has never been documented in connections and it has recently been shown that an increase in strength may not exist at all in some types of wood connections (Rosowsky Reed, and Tyner, 1998).

2.3 WOOD AS A STRUCTURAL MATERIAL

If the tall wood-frame wall system is to make significant expansion in the non-residential market, it has to take market share away from its competitors in the market. The biggest competitors in the market currently are tilt-up concrete structures, masonry structures, and steel structures. Some of the most important characteristics, advantages, and disadvantages of tilt-up concrete, masonry, and steel construction are presented in this section, following a similar analysis of tall wood-frame walls.

2.3.1 Tall Wood-Frame Walls

2.3.1.1 Advantages of Tall Wood-frame Walls

The expansion of the use of tall wood-frame walls as a structural system in non-residential applications can benefit from the experience and the success of tilt-up concrete and prefabricated steel construction. The ultimate wood-based solution has to include a fast construction sequence, simplicity, and flexibility, while applying the advantages of the wood-based materials and their properties. These advantages are primarily realized by the following:

- Wall fabrication is faster than in concrete tilt-up and masonry construction. In the case of tilt-up concrete, the construction process includes the fabrication of perimeter forms, installation of reinforcement steel and lifting inserts, blocking the door and window openings, and placing the concrete. With a tall wood-frame wall system the framing crew can fabricate the entire wall assembly at one time;
- Wood-frame construction does not require curing time for the wall panels, which in the case of concrete tilt-up construction is typically ten days before the panels can be lifted;

- When using wood-frame walls there is no concern about delays due to cold and freezing weather conditions. When using concrete tilt-up in cold weather situations, the contractor must provide tenting, supplemental heat, and insulation blankets for curing of the concrete. If the temperature drops below -5^{0}C the concrete should not be placed at all;
- Smaller, more readily available and less expensive mobile cranes can be employed to lift the wood-frame panels. Wood-frame panels typically weigh around 10% of comparable size concrete wall panels;
- Labour costs for wood-frame construction are usually lower due to reduced number of skilled trades necessary to frame the walls. Masonry construction requires highly trained labour that is more expensive. Concrete tilt-up construction requires the use of several subcontractors, which increases the building cost. For example, in tilt-up construction a framing subcontractor is needed to construct perimeter forms, followed by a reinforcing steel subcontractor, concrete subcontractor for placing and finishing of the concrete, structural steel subcontractor, lifting accessories supplier, crane and rigging subcontractor, welding subcontractor, and sealant subcontractor;
- Concrete tilt-up is further limited in flexibility by limited casting space. If the ratio of building wall to floor area is high, it becomes difficult to lay out and cast all of the wall panels at once. Wood-frame tilt-up walls, however, can be placed on top of each other after assembly, thus conserving space and allowing greater freedom of movement for materials and equipment on the construction site;
- Because the mass of wood-based walls is much lower than that of concrete walls, the connections between the walls and the roof become relatively inexpensive. Such connections are massive and expensive in concrete tilt-up construction.

- Foundations for wood-frame walls are expected to be smaller than for tilt-up concrete because they do not need to support the high dead loads associated with concrete or masonry walls;
- The most important benefit of using lighter tall wood-frame walls will be in the regions with high seismic activity, where large seismic forces are generated in buildings that use concrete or masonry walls. This is a significant issue since the proposed peak accelerations of ground motions (and seismic loads) for most cities in Canada and the United States will increase according to proposed codes.
- Wood-based wall systems are expected to have a lower cost of interior wall finishing necessary for office applications compared to that of concrete tilt-up or masonry solutions.
- Light industrial and commercial buildings with tall wood-frame walls are perceived as more warm and aesthetic than other types of buildings;
- Wood buildings usually do not have the problems with isolation and air-conditioning associated with buildings in other competitive materials;
- Wood is a renewable material and wood-based solutions for structural systems are better choices from an environmental point of view;
- General contractors may prefer wood-frame solutions because they give them more control over the key components of the building. With other systems they may depend on sub-trades to keep up with the schedule. Wood is also a flexible and forgiving material on the construction site allowing easier adjustments and alterations than other materials;
- It is easier to achieve the required insulation values in wood-frame construction than in concrete tilt-up, masonry, or steel construction. Tilt-up concrete is not a good system for extreme climates. Steel studs, on the other hand, have no insulating properties and thus conduct cold through an insulated wall, reducing the overall insulation value. In such cases

insulation has to be installed on the outside face of the building, which adds costs not incurred with wood-frame walls.

2.3.1.2 Disadvantages of Tall Wood-frame Walls

Disadvantages of wood-frame construction used in tall wall solutions include the following:

- Lack of technical solutions for tall walls with various wood-based materials used for the studs and the sheathing;
- Lack of design capacities for such technical solutions for tall walls with various stud spacing and sheathing thickness, subjected to gravity, wind and seismic loading;
- Lack of technical solutions and design values for connections used in tall walls;
- External durability concerns related to water penetration;
- Internal durability concerns related to building damage caused by moving equipment or machinery;
- Concerns related to building break-in and vandalism;
- Higher insurance premiums.

Disadvantages related to the use of wood as a structural material include shrinkage, warping, swelling, decay, discoloration, mildew, and termite problems.

2.3.2 Concrete Tilt-Up Construction

2.3.2.1 Description and Development

Tilt-up concrete construction, which began in southern California in the late 1950's as an economical and fast way to construct concrete walls for warehouses, has become a multi-billion dollar industry today, accounting for over 10,000 buildings annually. It is now used for shopping centres, distribution facilities, warehouses, manufacturing plants, office buildings, prisons, schools churches, or in other words, in nearly every type of one to four-story building. According to a survey by the Tilt-Up Concrete Association (TCA), over 60 million square metres (600 million square feet) of tilt-up buildings were constructed in 2001 alone (TCA, 2003). That area equates to an estimated 12,000 buildings, ranging in size from 400 square metres (4,000 square feet) to over 100,000 square metres (one million square feet). Those figures conservatively place the area of tilt-up walls at 40 million square metres (400 million square feet), which at an average in-place cost of US$70.00 per square metre translates into an annual wall market of US$2.8 billion. Clearly, this is a huge market with room for new entries, not necessarily using concrete as the construction material.

The term "tilt-up" was coined in the late 1940's to describe a method for constructing concrete walls rapidly and economically without the formwork necessary for poured-in-place walls. It is a two-step process: First, slabs of concrete, which will comprise sections of wall, are cast horizontally on the building floor slab, or separate casting slab. Then, after attaining proper strength, they are lifted (tilted) with a crane and set on prepared foundations to form the exterior walls. These large slabs of concrete usually weigh 40 tonnes or more, and have an average thickness of 152 mm to 200 mm (6" to 8"). There is little formwork, since only perimeter forms are required to contain the concrete. When they have attained sufficient strength, usually in seven to ten days, a mobile truck crane is brought to the job site to lift them and set them on prepared foundations. The erected panels are temporarily braced, connected, and the joints between them caulked. The roof structure is then constructed and attached to the walls to complete the building shell. Construction time for a tilt-up building, from completion of the floor slab to completion of the building shell is often less than four weeks (Ruhnke and Schexnayder, 2002).

Over the years the investment in research of tilt-up concrete construction made by the concrete industry resulted in numerous refinements in design and construction methods. The refinements resulted in construction methods able to tilt panels higher than 12 metres (40 feet), faster erection time, with lifting, setting, and bracing of 20 to 30 panels per day, achieved through well-trained crews and innovative ground-release lift attachments, as well as a wide choice of finishes available for architectural attractiveness. Design and construction of tilt-up concrete structures is constantly being fine-tuned by researchers, and highly skilled workers, using state-of-the-art techniques. To assure that qualified field personal are available, a certification program is being developed jointly by the Tilt-Up Concrete Association and the American Concrete Institute.

In the sun-belt states today, an estimated 75% of all new one-story industrial buildings are of tilt-up construction, with California leading the way with nearly 90%. The geographical distribution of tilt-up construction across the United States is the following: California 36%, Texas and the Southwest 20%, Oregon and Washington States 20%, Florida 11%, Southeast and Southern States 9%, Great Lakes States and the Midwest 3%, and Northeast States 1% (Brooks, 1999). Annual growth in recent years has averaged nearly 20%, with an increasing number of contractors, developers and building owners becoming aware of its many advantages. Recently there has also been considerable tilt-up concrete construction in Mexico, Canada, Australia, and New Zealand. The largest under-one-roof tilt-up building, to date, is a 160,000 square metre (1.7 million square foot) distribution centre near Columbus, Ohio (Figure 2.3). The tallest tilt-up panel erected is a 28 m (91') high panel for a Houston, Texas church. The record for the heaviest single panel goes to a 16 m (51') wide by 13 m (42') high, 300 mm (12") thick wall panel for a distribution centre in Ontario, California, weighing 150 tonnes. Although tilt-up construction has been introduced in every state of the United States, it still remains unfamiliar construction method in many geographical areas (typically in the East and Northeast United States).

Figure 2.3. The largest tilt-up building to date, a 160,000 square metre distribution centre near Columbus, Ohio.

2.3.2.2 Advantages of Concrete Tilt-Up Construction

The non-residential construction market in North America is highly competitive, and tilt-up construction is chosen only when its advantages, given the site and circumstances of a project, clearly favour it. The North American forest products industry, using tall wall solutions, should be able to capitalize on the opportunities where tilt-up construction is not the preferred construction option of choice.

To use tilt-up effectively and economically some basic criteria should be met. The building should be at least 600 square metres (6,000 square feet) in floor size. Usually the larger the building, the more economical it is, allowing enough room to cast the panels and use the crane and rigging crew in an effective way. Tilt-up construction requires the existence of extensive wall surfaces, so that it can be divided into liftable panels. The panels should not weigh more than 40 to 60 tonnes each, and there should not be over 50% of surface area in openings in the panels. While one and two-story buildings are the most economical, many tilt-up structures have three or four stories. When basic conditions of building size are met, tilt-up construction offers the following advantages over other construction types (Brooks 1999):

- **Economy** - In areas where tilt-up design and construction expertise are available, particularly a trained crane and rigging crew, tilt-up can be more economical than competing construction methods for similar types of buildings;
- **Speed of Construction** - The growth of concrete tilt-up construction can be attributed in large part to the desire of building owners to shorten the construction process, in other words to condense the time it takes to go from breaking ground to tenant occupancy. From the time the floor slab is placed, the typical elapsed time from starting to form the panels until the building shell is completed is four to five weeks (TCA, 2003). This allows building owners to minimize their construction financing costs and maximize their revenue stream;
- **Durability** - Tilt-up buildings usually show less visible signs of aging, although architectural styling is an issue in older buildings.
- **Fire Resistance** - Concrete offers high fire protection. A 180 mm thick monolithic wall, for example, has a four-hour fire resistive rating (NBCC, 1995);
- **Low Maintenance Costs** - Sometimes the only thing that tilt-up structures need is a coat of paint every six to eight years;

- **Lower Insurance Rates** - The high fire resistance of tilt-up concrete walls results in low insurance premiums, although this might not be the decisive argument for the selection of the structural system;
- **Architectural Attractiveness** - The architect has relative freedom to arrange and assemble the panels, and a wide choice of surface finishes;
- **Expandability** - By planning for the possibility of expansion, panel connections can be designed so that the panels can be detached and relocated;
- **Security** - Unlike steel and wood-frame buildings, forced entry through walls can only be made through door and window openings;
- **Value Appreciation** - Low insurance costs, along with building durability and security, assure a desirable investment for the buyer;
- **Sound Insulation** - Concrete construction in general provides better sound insulation than wood-frame construction.

2.3.2.3 Disadvantages of Concrete Tilt-Up Construction

The disadvantages of the concrete tilt-up construction can be summarized as follows:

- **Poor Seismic Performance** - The seismic performance of concrete tilt-up buildings is one of the biggest concerns among the engineering community. Because the tilt-up walls are held vertically in place by a precarious connection to the roof, structures built in the tilt-up style are among the most dangerous to occupants in the event of an earthquake. The first warning about the seismic deficiencies of tilt-up buildings came during the 1964 Alaskan earthquake (Magnitude of 8.4), in which three of the five bays of an Elmendorf Air Force Base warehouse fell to the ground. According to a City of Los Angeles report, quoted in the

October 14th, 1999 issue of "Metro", the California Silicon Valley's weekly newspaper, the 1994 Northridge California Earthquake left more than 400 tilt-up buildings with a partial roof or exterior wall collapse in the San Fernando Valley, out of 1,200 existing in the area (Figure 2.4 and 2.5). Fortunately no one was killed by falling debris largely because the earthquake took place before normal working hours.

- **Expensive Connections** - Connections in tilt-up structures have to be designed to sustain large loads, sometimes in excess of 250 kN (50,000 lbs.), which make them expensive.
- **High Heating and Cooling Costs** - Costs associated with heating and cooling in tilt-up structures are usually higher than those in other types of structures;
- **Skilled Labour** - Tilt-up construction requires the use of skilled labour that increase construction costs;
- **High Weight** - The heavy weight of tilt-up structures requires that large cranes be used to lift the panels. This process is very expensive and cannot be economically feasible for smaller buildings.

(a)

(b)

Figure 2.4. Earthquake damage on older tilt-up structures during the 1994 Northridge earthquake.

Figure 2.5. Earthquake damage on a tilt-up construction site during the 1994 Northridge earthquake.

Some of the advantages and disadvantages presented above represent general trends. The building size, location, occupancy type, design and performance criteria requested by the owner can change some of the general advantages into disadvantages and vice versa. A detailed cost analysis of the design solutions for a particular building with various construction materials is needed to determine the exact construction costs of each solution.

2.3.3 Masonry Construction

Masonry is one of the oldest forms of construction known to man. Through civilization, builders have chosen masonry for its durability, providing structures that can withstand the normal wear and tear for centuries.

The methods for producing brick have continued to evolve through the time. Currently, the standard United States brick size is 64 mm by 95 mm by 203 mm (2.5" x 3.75" x 8"). The evolution of brick construction also led to the development of the concrete masonry block.

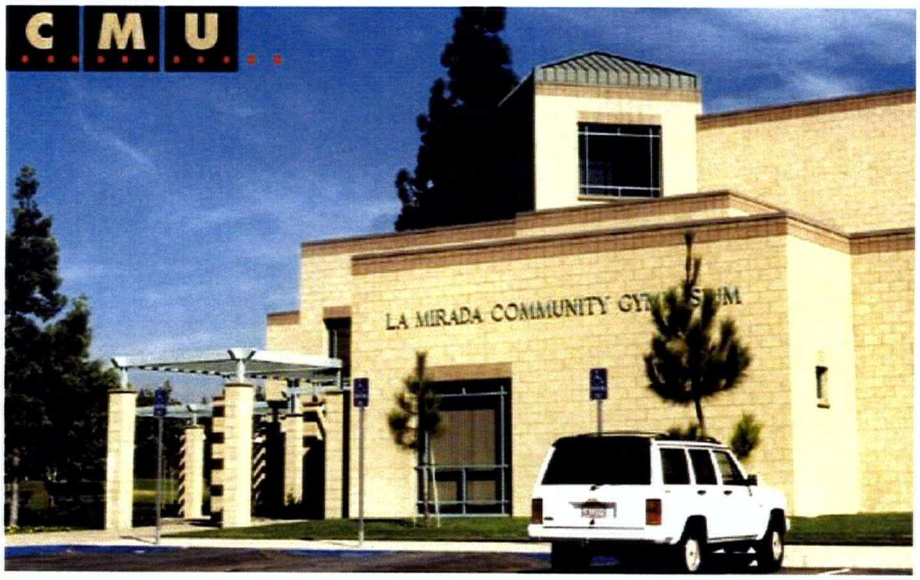

Figure 2.6. Example of a concrete masonry building: La Mirada Community Gymnasium that is 2,000 square metres.

Today's multi-coloured, multi-textured concrete products give designers the chance to create single and multi-family residences, office buildings, warehouses, municipal buildings, religious buildings, manufacturing facilities, correctional facilities, learning institutions, and hospitals. An example of modern masonry structure is shown in Figure 2.6. According to the National Concrete Masonry Association (NCMA, 2003), the market for masonry building in North America today is valued to be 15 times larger than that of concrete tilt-up, or approximately US$40 billion annually. While concrete tilt-up construction is the most prevalent type of construction in the western part of the United States, concrete masonry prevails in the Northeast United States.

2.3.3.1 Advantages of Masonry Construction

The advantages of masonry construction over other construction types are listed below. As for the concrete tilt-up examples, some of the advantages and disadvantages presented represent general trends. Advantages of using masonry construction include:

- **Economy** - Masonry construction will compete favourably with concrete tilt-up and wood-frame construction for smaller buildings (under about 600 square metres) or where inexpensive masonry materials and labour are available. Crane time is uneconomical for such small buildings in the case of tilt-up concrete;
- **Low Maintenance** - Ease of maintenance played a major role in the use of concrete masonry tall slender walls over tilt-up technologies. Usually coloured concrete masonry retains its original appearance with more consistency than the painted finish on tilt-up walls;
- **Durability** - Concrete masonry has a proven record of durability and resistance to "abuse" that is required for some types of buildings such as industrial or correctional facilities;
- **Fire Resistance** - Masonry construction has high fire resistant properties. A solid brick unit of 178 mm thickness has a four hour fire protection rating (NBCC 1995);
- **Low Maintenance** - Similarly to tilt-up structures, masonry structures have low maintenance costs;
- **Lower Insurance Rates** - The fire resistance and durability of masonry structures results in low insurance premiums;
- **Insulation and Energy Efficiency** - The energy efficiency of concrete masonry can be improved by isolating the hollow-core units. When using tilt-up technology, insulation is required on the inside of the wall where it is visible and unattractive, or requires that panels be pre-cast with insulation sandwiched between them;
- **Bed Casting** - No floor or large working space is needed prior to wall construction;
- **Sound Insulation** - Masonry construction provides better sound insulation than most construction types;

- **Life Cycle Cost Analysis** - Masonry structures can have higher initial costs in some cases but the life cycle costs are usually lower;
- **Finishing** - From an architectural point of view, a wide variety of finishing textures and patterns exist for concrete masonry applications.

2.3.3.2 Disadvantages of Masonry Construction

Disadvantages of masonry construction include the following:

- **Expensive Buildings** - The initial construction cost of masonry buildings is usually higher than that of tilt-up concrete or steel buildings;
- **Expensive and Highly Trained Labour** - One of the reasons why the initial costs are so high is because masonry construction is a labour intensive process. Depending on the location, labour can be very expensive in North America;
- **Low Earthquake Resistance.** - Unreinforced masonry construction has the lowest resistance to earthquake loads of any type of construction. A combination of high stiffness, large weight, and low ductility of the material used, make this construction very vulnerable even to moderate earthquakes. There have been numerous examples of wide spread damage to masonry structures during the past earthquakes (Figure 2.7). To improve the earthquake resistance of masonry structures, they need to be reinforced with vertical steel reinforcing bars during construction, which further increases the cost;
- **Water Absorption** - Masonry blocks are water absorbent and to avoid water penetration they must be isolated (weather-proofed) to provide a better painting (finishing) surface;
- **Modular Construction** - Concrete masonry construction is a modular construction using mainly 203 mm by 203 mm by 406 mm (8" x 8" x 16") nominal dimensions for the masonry block unit. It is thus difficult to have walls with odd dimensions, smooth curves, or smooth

thickness transitions. This is especially true for buildings with a clear height greater than 7.3 m (24') where tilt-up walls can vary more incrementally than the large jumps from 203 mm (8") to 305 mm (12") required for masonry block units;

- **Insulation** - Concrete masonry blocks have low insulation values and generally walls must be insulated, which is usually not an easy and inexpensive task;
- **Duration of Construction** - Masonry construction usually requires the longest period of construction of all competitive construction materials.

Figure 2.7. Damage to a masonry structure during the Northridge earthquake.

2.3.4 Steel Construction

Steel construction has one of the largest shares of the non-residential market in North America (AISI, 2003). The value of the steel non-residential market is conservatively estimated to be around US$90 billion a year. This includes all non-residential applications of steel, including high-rise office towers. The portion that corresponds to the low-rise steel structures, where wood-based solutions can compete for the structural system, is expected to be more than 50% of this market.

Figure 2.8. Typical example of a warehouse designed in prefabricated steel.

Figure 2.9. Typical example of the interior of a warehouse designed in prefabricated steel.

Steel structures in non-residential applications can be categorized in two types: conventional and pre-engineered steel structures. Conventional steel structures are built with hot rolled structural steel members, and an engineering consultant designs each structure separately. They require engineering design calculations and connection detailing for each separate building. Pre-engineered steel buildings, on other hand, use cold-formed steel structural elements. In this case the buildings are mainly constructed using standard pre-designed structural sections and connections, which are manufactured in a plant setting. Such elements are then shipped to the construction site for building assembly. Examples of steel construction for warehouses are shown in Figure 2.8 and 2.9.

2.3.4.1 Advantages of Steel Construction

Steel construction in non-residential applications offers the following advantages over other construction materials:

- **Strength** - Steel offers the highest strength-to-weight ratio (matched by that of clear wood) of any widely used structural material;
- **Light structure** - Steel structures, like wood structures, are much lighter than reinforced concrete or masonry structures, attracting lower horizontal forces due to earthquakes;
- **Foundations** - As lighter structures, steel buildings also require smaller foundations;
- **Material Efficiency** - Pre-engineered buildings can be an additional 30% lighter than conventional steel buildings, with even greater material efficiency. Primary structural members are usually tapered (varying depth) with larger depths in areas of high stress;
- **Inexpensive Design** - Construction design, shop details and erection drawings for prefabricated (off-the-shelf designs) are usually supplied free of charge from the manufacturer;
- **Construction Cost** - Material and erection costs are exactly known based on extensive experience with other similar buildings;

- **Delivery Time** - Delivery time for prefabricated structures is usually short, between six to eight weeks;
- **Design Accuracy and Quality Control** - Steel structures offer high accuracy of dimensions and uniform material quality due to close control of the pre-fabrication process in the plant. This significantly reduces the labour requirements at the construction site, which can be an important consideration in the face of growing shortages of skilled labour;
- **Combustibility** - Steel buildings are rated as non-combustible structures in buildings codes;
- **Expandability** - Manufacturers of pre-fabricated steel buildings usually keep all completed projects in electronic format for a long time, so that future expansions can be made easily and inexpensively;
- **Recycling** - Steel is a recyclable material;
- **Durability** - Steel is impervious to termites and other wood boring insects, thus eliminating the structural damage that can be caused by these insects in wood;

2.3.4.2 Disadvantages of Steel Construction

Disadvantages of steel structures can be summarized as follows:

- **Fire Resistance** - Although steel structures are rated as non-combustible, steel members may yield and subsequently loose strength and stability when subjected to high temperatures exhibited during a fire. Fire protection of all structural members is required, which increases the material and labour costs. In addition, the fire rating for steel structures is lower than that of concrete or masonry structures;
- **Material Costs** - Steel is an expensive material and much more expensive than masonry or concrete;

- **Environmental** - The major environmental concerns include the energy used in manufacturing, disruption of the affected area, and air and water quality degradation as a result of mining and manufacturing activities. Steel is one of the most energy-intensive industrial materials, generating pollution and waste during all stages of the manufacturing process, including coking coal, purifying iron, and galvanizing.
- **Insulation Properties** - Steel structures have lower insulation properties than other types of structures. In addition, steel is highly conductive, which increases the potential for thermal bridging;
- **Labour Costs** - In some areas it is difficult to find crews that are trained in constructing steel structures. This disadvantage usually raises the overall project cost;
- **Corrosion** - Steel components rust if they are left exposed in marine climates or in internal climates with high humidity and acidity.

2.4 TALL WOOD-FRAME WALL CASE STUDIES

Only a handful of buildings have been designed and constructed to date with tall wood-frame walls as the load-resisting system. Brief case studies on two buildings that are of significant importance for the topic are presented below.

2.4.1 Tembec Mill in Cranbrook, B.C.

As a manufacturer of wood products, Tembec Industries Inc. aimed to use wood for the major expansion of its Crestbrook plant in Cranbrook, British Columbia. The design solution, however, still had to make good business sense. The plant expansion was to house 2,024 square metres (22,000 square feet) of value-added manufacturing area for the production of finger-joined lumber (WoodWorks, 2003).

Figure 2.10. Construction of the Tembec Cresbrook Mill in Cranbrook, BC.

The production area of the new facility needed to have a large roof span of nearly 42.5 m (140') across, with no interior columns (Figure 2.10). For this type of structure, off-the-shelf steel and tilt-up concrete buildings have often proven to be most cost effective. Preliminary cost comparisons for this project, however, favoured a tall wood-frame wall solution. Moreover, with the natural insulating properties of wood, the insulating value of a wood-frame building is higher than that of steel. It was also recognized that using wood would benefit the local economy, whereas a steel alternative would likely be factory-built outside the province of British Columbia.

The building has a conventional concrete foundation and ground floor slab. Wall and roof components were assembled on the ground, and then lifted into place. Tall walls were framed with continuous Laminated Veneer Lumber (LVL) studs 7.6 m (25') in length, with horizontal LVL top and bottom plates. The studs were spaced at 610 mm (24") on centre. They were fastened to the top and bottom plates with specially manufactured steel brackets, using two lag screws and a thru-bolt in the stud (Figure 2.11). Information from building contractors suggests that those connections were actually the most time-consuming aspect of the construction process. They also suggested that having standardized connection details for such buildings would increase their competitiveness. The walls also had horizontal LVL blocking every 1,220 mm (48") to provide the strength necessary to carry the imposed lateral loads. On the exterior of the walls, 38 mm by 140 mm (2" x 6") rough-sawn, horizontal tongue and groove cladding was applied. The walls were built in 9 m (30') sections and tilted up by crane.

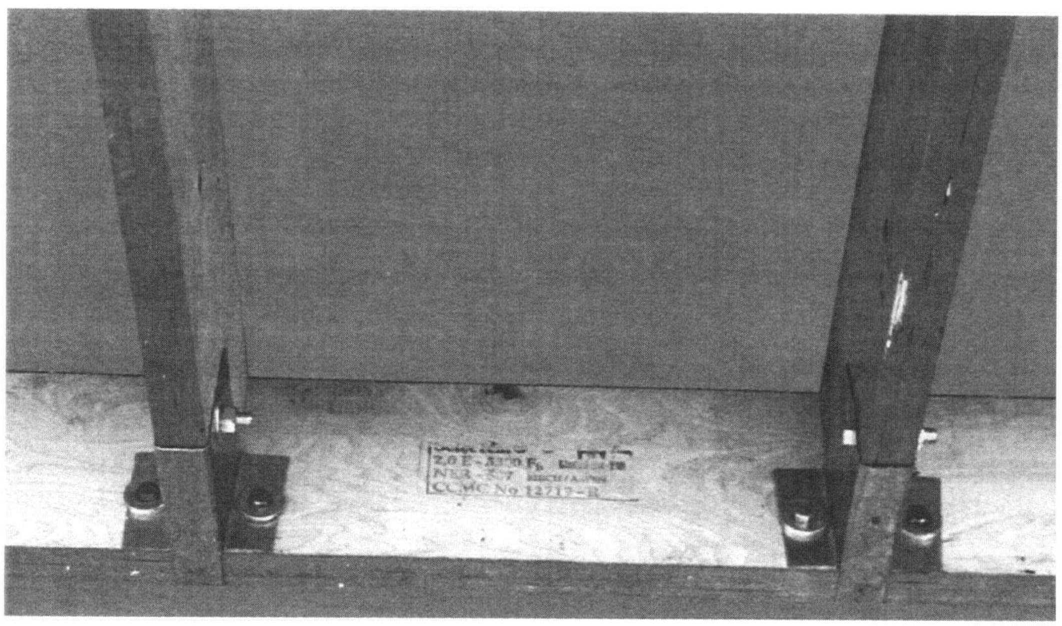

Figure 2.11. Connections between the studs and the bottom plate (CWC, 2000).

The roof consisted of pitched open web trusses spaced 610 mm (24") on centre. The trusses, which taper from 3,048 mm to 1,270 mm (120" to 50"), were manufactured in two pieces to facilitate transportation and then assembled on site. Four bays of trusses were connected together with bracing and oriented strandboard (OSB) sheathing to provide the rigidity necessary to avoid damage when lifting them by crane into place.

2.4.2 Trus Joist Research Center in Boise, Idaho

Another example of the successful use of tall wood-frame walls is the Trus Joist Technology Center in Boise, Idaho, completed in July 2000. This 16,350 square metre (176,000 square foot) facility was designed with the goal of providing an environment that would foster information and idea sharing between multiple groups focused on the research, development, engineering, marketing, sales, and manufacturing support of Trus Joist engineered wood products. The walls, roofs and floors were constructed primarily with engineered wood products. Total quantities of wood products included 300 cubic metres of Parallam® PSL, 800 cubic metres of TimberStrand® LSL, 10 cubic metres of Microllam® LVL, 1,250 m of TJI® Floor Joists, and 15,600 m of open web trusses (Taylor, 2000).

The manufacturing, research, and development functions of the building required a 30.5 m (100') clear roof span and a 12.2 m (40') building height constructed with exposed engineered wood products. The primary objective was to construct a functional and stimulating workspace while showcasing efficient, innovative structural framing systems with typical materials and connections for viewing by potential Trus Joist customers.

Tall walls were used as the primary structural system for resisting the vertical and horizontal loads in the building. Tall walls consisted of LSL studs, plates, and full billet sheathing (large uncut sheets of laminated strandboard). The lateral and vertical loads on the wall dictated the stud spacing as well as the stud and plate size. The stud system was framed using conventional carpentry methods and tilted in place by a crane in 21.9 m (72') long sections to reduce labour time (Figure 2.12). The full billet LSL panellized walls reduced the mass of the building when compared with masonry and concrete systems. Therefore, the tilt-up wood-based system significantly reduced the lateral shear requirements for the connections. The strength and integrity of the LSL allowed for the nails to be fastened at 38 mm on centre resulting in an allowable lateral load capacity of up to 12,690 N/m (9,360 lb./ft.) (Taylor, 2000).

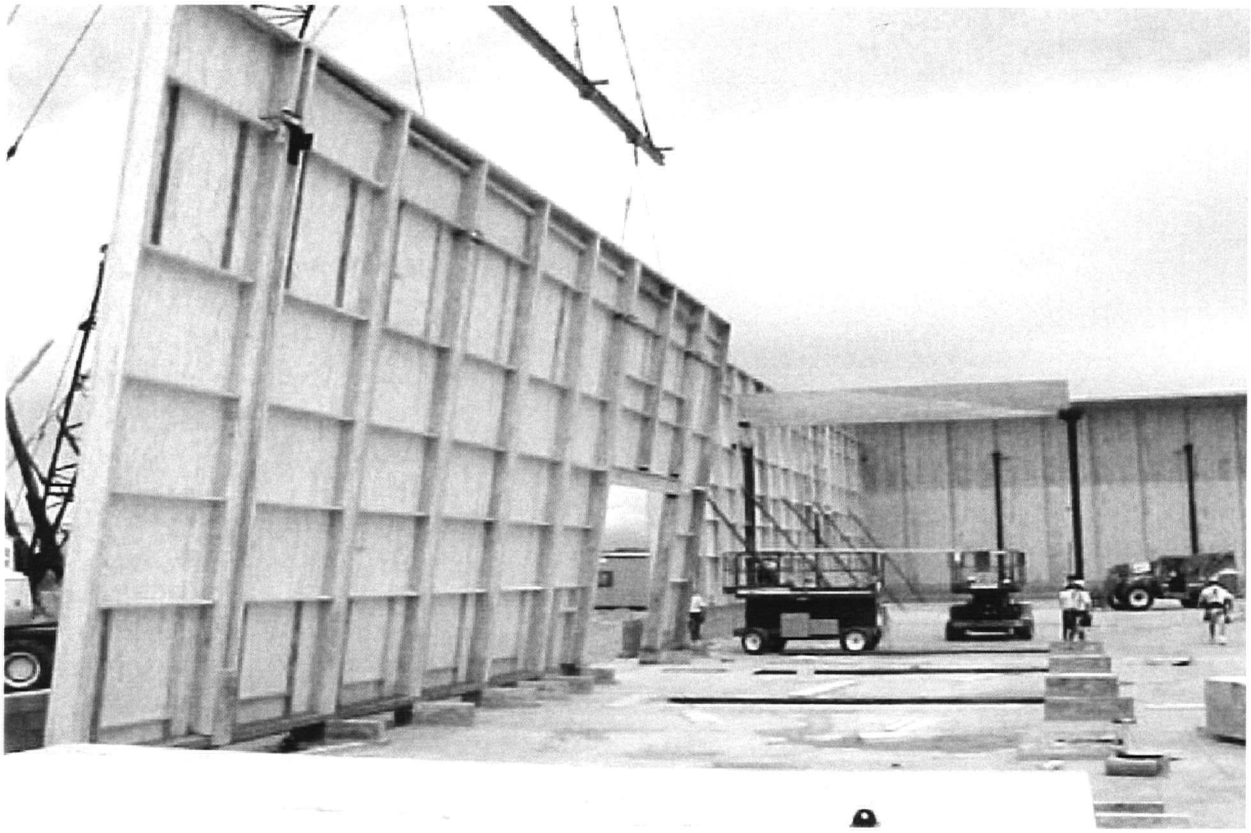

Figure 2.12. Lifting of a completed section of the wall in place at the Trus Joist Technology Center in Boisie, Idaho (Taylor, 2000).

Two configurations were used for the long span roof systems of the building. The first system was made of Parallam® PSL heavy timber trusses assembled on the ground and raised into place as three truss sections spanning 30.5 m (100'). The second system was constructed of Microllam® LVL flanged open web trusses delivered in continuous 30.5 m spans. The roof trusses were assembled on the ground in multiple truss sections before being put in place by a crane and fastened to the beam supports and tilt up wall systems.

2.5 PARTIAL COMPOSITE ACTION AND EFFECTIVE FLANGE WIDTH

Partial composite action is used to describe the interaction of two or more components of a structural member when interlayer slip can occur between the components. A beam without composite action and a fully composite beam are shown in Figure 2.13. While this phenomenon has been analyzed and codified for use with several structural materials, this section will focus

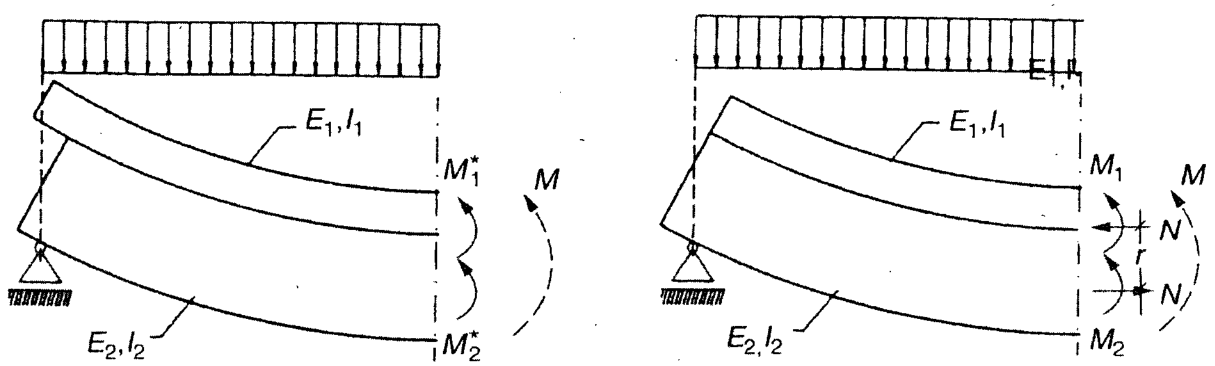

Figure 2.13. Comparison between (a) a beam without composite action and (b) a fully composite beam (Ceccotti, 2003).

on applications for wood construction. T-shape and I-shape sections are the most common when dealing with partially composite members in wood construction. Since the distribution of stress in the flanges of these members is not uniform, several methods have been developed to determine an equivalent flange width of uniform stress for use in the analysis of composite members (Figure 2.14). Methods for determining effective flange width in wood construction will also be discussed.

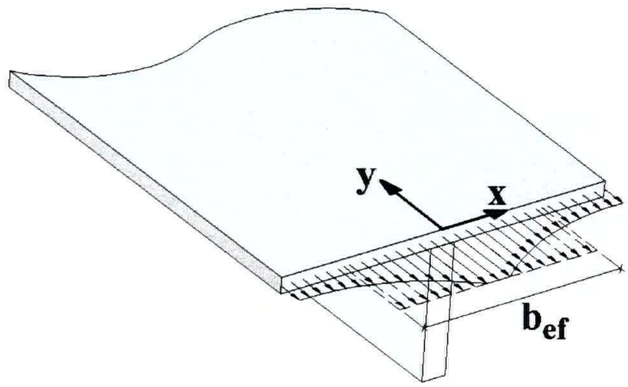

Figure 2.14. Stress distribution in the flange of a composite member (Raadschelders and Blass, 1995).

2.5.1 Partial Composite Action (Newmark, Seiss, and Viest)

The concept of partial composite action has been studied extensively over the past half century. Granholm (1949), reporting in Swedish, and Pleskov (1952), reporting in Russian, investigated composite timber members with Pleshkov also considering interlayer slip. Newmark, Seiss, and Viest (1951) investigated the incomplete interaction of composite steel and concrete T-beams (Figure 2.15). Their theoretical analysis incorporated the load-slip characteristics of steel channel shear connectors. Comparisons between test results and theoretical analyses were difficult because minimal slip occurred in the concrete and steel connections. Even though theoretical results were only compared with testing on these composite steel and concrete members with minimal measurable slippage, it was concluded that the theorem for composite beams with incomplete interaction was generally accurate and was not limited to that type of member as long as the basic assumptions were satisfied to a reasonable degree. Those assumptions were:

- The shear connection between elements was assumed to be continuous along the length of the member;

- The amount of slip permitted by the shear connection was directly proportional to the load transmitted;
- The distribution of strain throughout the depth of each element was linear; and
- The elements were assumed to deflect equal amounts at each cross section along the length of the member at all times.

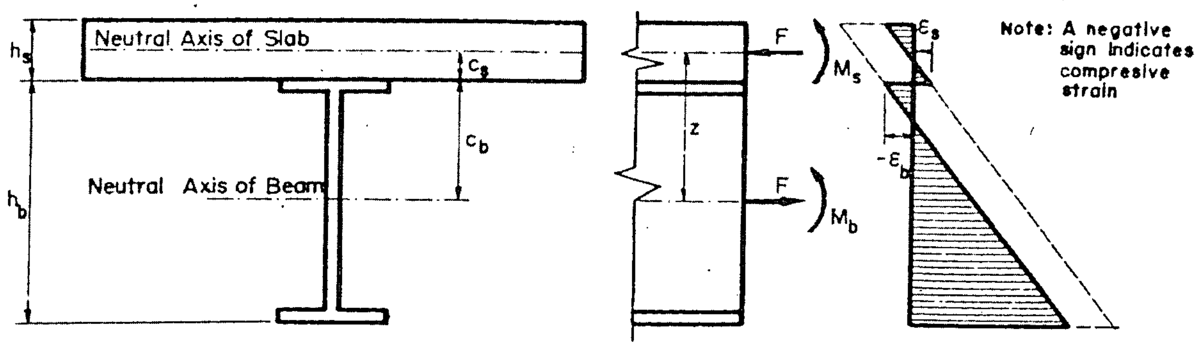

Figure 2.15. Composite T-beam with imperfect interaction (Newmark et. al., 1951).

The deflection of a simply supported T-beam under a single point load was given by:

$$\Delta = \frac{P\,L^3}{\overline{EI}}\left(1-\frac{u}{L}\right)\frac{y}{L}\left\{\frac{1}{6}\left[2\frac{u}{L}-\left(\frac{u}{L}\right)^2-\left(\frac{y}{L}\right)^2\right]+\frac{\overline{EA}\,r^2}{\sum EI}\frac{C}{\pi^2}\frac{F_L}{F_L'}\right\}, \tag{2.1}$$

where the force acting at the centroids of the two elements was:

$$F_L = \frac{\overline{EA}\,r}{\overline{EI}}P\,L\left\{\left(1-\frac{u}{L}\right)\frac{y}{L}-\frac{\sqrt{C}}{\pi}\frac{\sinh\left[\frac{\pi}{\sqrt{C}}\left(1-\frac{u}{L}\right)\right]}{\sinh\left(\frac{\pi}{\sqrt{C}}\right)}\sinh\left(\frac{\pi}{\sqrt{C}}\frac{y}{L}\right)\right\}; \tag{2.2}$$

$$F_L' = F_L \text{ at } C = 0,$$

$$C = \frac{1}{k}\frac{\pi^2\,\overline{EA}\sum EI}{L^2\,\overline{EI}}, \tag{2.3}$$

$$\overline{EI} = \sum EI + \overline{EA}\, r^2 \text{, and} \tag{2.4}$$

$$\frac{1}{\overline{\overline{EA}}} = \frac{1}{E_1 A_1} + \frac{1}{E_2 A_2}. \tag{2.5}$$

The parameter k is called the slip modulus. It was given by the equation:

$$k = \frac{K_n}{S} \tag{2.6}$$

Subscript 1 denotes the flange element and subscript 2 denotes the web element of the T-beam. In the previous formulation the symbols are defined as follows:

P = concentrated point load

u = the distance of the concentrated point load from the left support

L = length of the composite member

y = distance of the cross section from the left support

r = distance between the centroidal axis of the web and the flange

E_i = modulus of elasticity of the i^{th} component

I_i = moment of inertia of the i^{th} component

A_i = area of the i^{th} component that is equal to width, b_i, multiplied by height, h_i

K_n = stiffness of an individual connector

S = spacing of the connectors.

2.5.2 Partial Composite Action (Goodman and Popov)

Goodman and Popov later applied the theory developed by Newmark, Siess, and Viest to nailed, layered timber beams (Goodman and Popov, 1968; Goodman, 1969). The deflection of a simply supported beam member consisting of three identical layers connected by nails under a single point load was given by:

$$\Delta = \Delta_{\infty} + \frac{8}{9}\frac{1}{k}\frac{1}{h}F_L \text{, where} \tag{2.7}$$

$$F_L = \frac{C_2}{C_1}\frac{P}{\sqrt{C_1}}\frac{\sinh\left[\sqrt{C_1}(L-u)\right]\sinh\left[\sqrt{C_1}\ y\right]}{\sinh\left[\sqrt{C_1}\ L\right]} + \frac{C_2}{C_1}P\left(1-\frac{u}{L}\right)y, \tag{2.8}$$

$$C_1 = \frac{9\,k}{b\,h\,E}\text{, and} \tag{2.9}$$

$$C_2 = \frac{h\,k}{3\,EI}. \tag{2.10}$$

The parameters b and h, the width and height of each layer of the composite beam, are shown in Figures 2.16 and 2.17. Δ_{∞} is the deflection of a perfectly rigid composite beam. The other symbols have been defined previously.

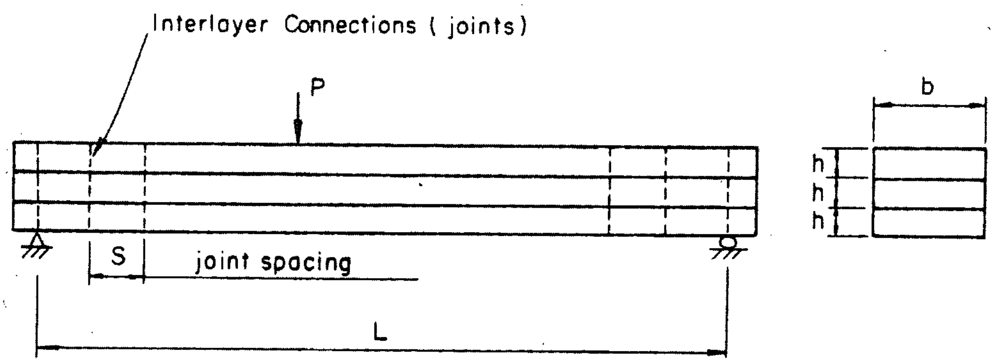

Figure 2.16. Layered beam system layout (Goodman, 1969).

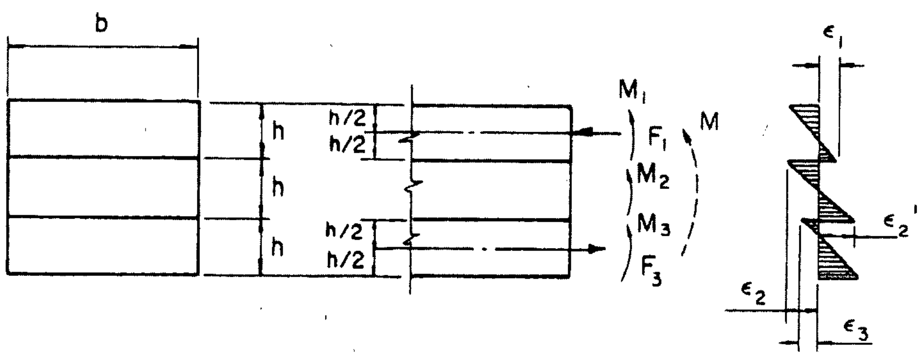

Figure 2.17. Three-layered beam internal forces and strains (Goodman, 1969).

Excellent agreement was found with the experimental tests that were performed to verify the developed theory. Theoretical equations to determine the deflection of a nailed beam with glued ends were also developed. It was found that the restraining effect of using a small amount of glue at the ends of nailed beams on deflection was significant. It was concluded that this scheme would provide an economical method of improving stiffness.

2.5.3 Partial Composite Action and Effective Width (Amana and Booth)

Amana and Booth developed a mathematical formulation to predict the response of glued plywood stressed-skin components (Amana & Booth, 1967). Equations were derived for three configurations, shown in Figure 2.18. The theoretical solutions compared well with experimental testing that was conducted on several specimens. This method included an allowance for an effective flange width that was embedded within the calculation for deflection. As well, the method could easily be applied to several loading configurations because it contained a Fourier series coefficient as an input parameter. The deflection of a partially composite T-beam was given by:

$$\Delta = \sum_{n=1}^{\infty} \frac{F_n \sin(\omega y)}{\omega^2 (EI)_o} \left[1 - \frac{r^2}{G(b') + C_s r^2 n^2} \right], \text{ where} \tag{2.11}$$

$$G(b') = \frac{(EI)_o}{h_1 E_1} \frac{s(b')}{f(b')} + \frac{(EI)_o}{E_2 A_2} + r^2, \tag{2.12}$$

$$C_s = (EI)_o \frac{1}{k} \frac{1}{r^2} \frac{\pi^2}{L^2}, \text{ was denoted as the non-dimensional positive joint constant,} \tag{2.13}$$

$$\begin{aligned} s(x) &= \left(p^2 + \nu_{xy}\omega^2\right)\cosh(p\,x) - \left(q^2 + \nu_{xy}\omega^2\right)\cosh(q\,x) \\ &+ \theta_n \left[\left(p^2 + \nu_{xy}\omega^2\right)\sinh(p\,x) - \left(pq + \frac{p}{q}\nu_{xy}\omega^2 \right)\sinh(q\,x) \right], \end{aligned} \tag{2.14}$$

$$f(x) = 2(p \cdot \sinh(p\,x) - q \cdot \sinh(q\,x)) + \theta_n (p \cdot \cosh(p\,x) - q \cdot \cosh(q\,x)), \tag{2.15}$$

$$\theta_n = -\left|\frac{\left(\lambda_2^2 + \nu_{xy}\right)\sinh(p\,b') - \frac{\lambda_2}{\lambda_1}\left(\lambda_1^2 + \nu_{xy}\right)\sinh(q\,b')}{\left(\lambda_2^2 + \nu_{xy}\right)\cosh(p\,b') - \left(\lambda_1^2 + \nu_{xy}\right)\cosh(q\,b')}\right|, \tag{2.16}$$

In the previous formulation, the symbols are defined as follows:

$$p = \lambda_1 \omega$$

$$q = \lambda_2 \omega$$

$$\lambda_1 = \sqrt{\alpha + \sqrt{\alpha^2 - \beta}}$$

$$\lambda_2 = \sqrt{\alpha - \sqrt{\alpha^2 - \beta}}$$

$$\beta = \frac{E_y}{E_x}$$

$$\alpha = \frac{E_y}{2G_{xy}} - \nu_{xy}$$

$(EI)_o =$ the stiffness of all beam parts as if unglued

$b' =$ one half the stud spacing

For a simply supported beam with a uniformly distributed load:

$$\omega = \frac{n\pi}{L}$$

$$F_n = \frac{4w}{L\omega^3}$$

$n = 1,3,5,\ldots$ It was determined that very few terms were required to achieve accurate results within one percent.

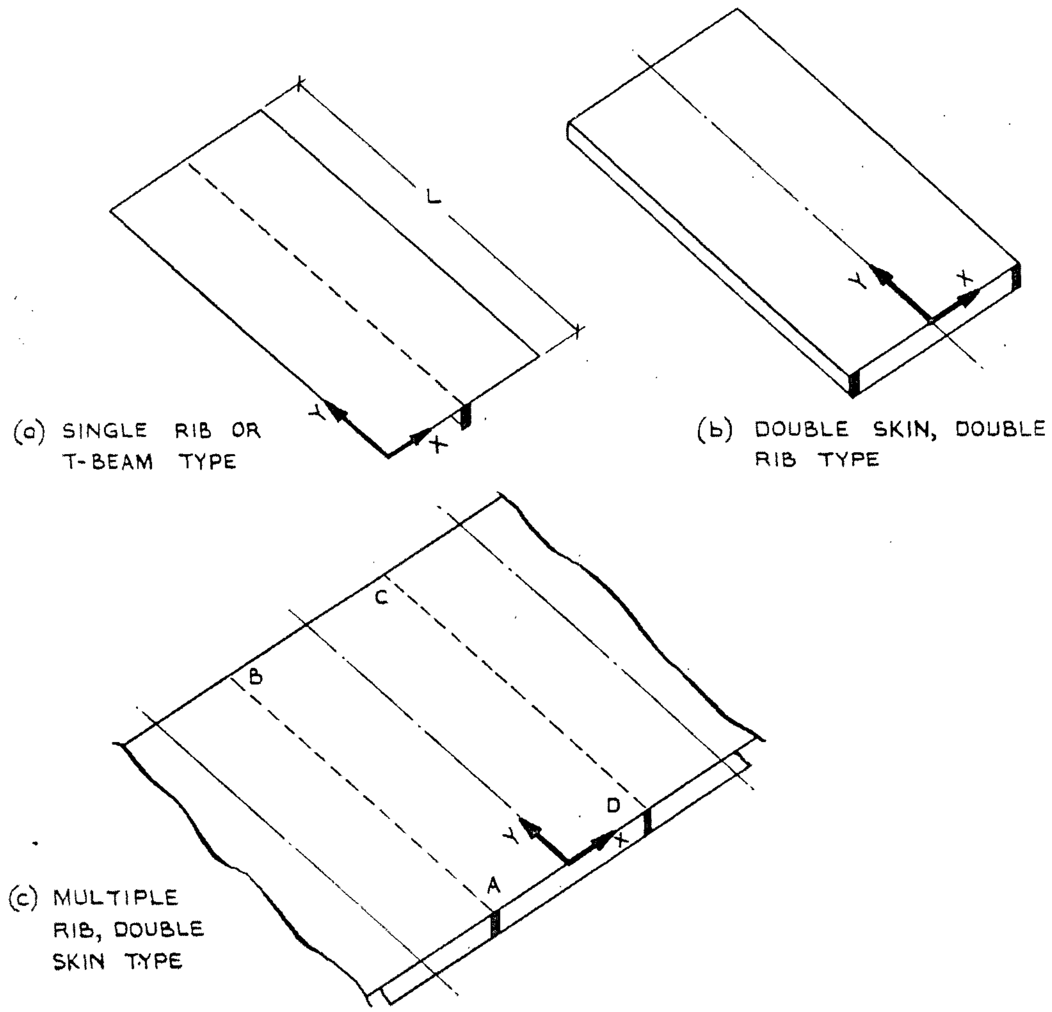

Figure 2.18. Different diaphragm configurations considered by Amana and Booth (1967).

Amana and Booth computed a stiffening factor, i, that was obtained by comparing the deflection of a composite beam with that of a bare stud as follows:

$$i = \frac{\Delta_o}{\Delta}\text{, where} \tag{2.17}$$

$$\Delta_o = \sum_{n=1}^{\infty} \frac{F_n \sin(\omega\, y)}{\omega^2 E_2 I_2}. \tag{2.18}$$

The stiffening factor could also be used to calculate an effective bending stiffness, which could be used in simplified beam equations. This was given by:

$$(EI)_{eff} = i \cdot E_2 I_2 . \tag{2.19}$$

While the determination of effective flange width is included in the calculation of deflection, it could also be calculated separately:

$$b_{eff} = \frac{\sum_{n=1}^{\infty} A_n f(b')\sin(\omega\, y)}{\frac{E_2}{E_1}\sum_{n=1}^{\infty} A_n s(b')\sin(\omega\, y)}, \text{ where} \tag{2.20}$$

$$A_n = \frac{r\, F_n}{f(b')\left[G(b') + C_s r^2 n^2\right]} . \tag{2.21}$$

It can be seen that both deflection and effective flange width are a function of the type of loading. The influence of the type of loading on these values will be discussed in detail later in this chapter.

2.5.4 Partial Composite Action and Effective Width (Polensek and Kazic)

Polensek and Kazic modified the solution by Amana and Booth in order to model a more complex system, shown in Figure 2.19, using reliability analysis (Polensek & Kazic, 1991). It was recognized that the solution by Amana and Booth only works when $\alpha > \beta^{1/2}$, which is not valid for systems with gypsum wallboard. In addition, the two flanges and flange connection types of a composite I-section typically have different properties when used in wall construction but the solution by Amana and Booth assumed that the composite I-section was symmetric. Therefore, the following solution was developed for a composite I-section, based upon the original work by Amana and Booth but with a new function that satisfies $\alpha > \beta^{1/2}$:

$$(EI)_{eff} = E_2 \cdot I_{eff}, \text{ where the effective moment of inertia,} \tag{2.22}$$

$$I_{eff} = I_2 + \frac{1}{K}\left[I_e + A_2\left(r_1^2 \overline{K}_1 E_2 K_{n1}^{-1} + r_3^2 \overline{K}_3 E_2 K_{n3}^{-1}\right)\right], \tag{2.23}$$

$$K = 1 + K_1E_2K_{n1}^{-1} + K_3E_2K_{n3}^{-1} + K_{13}E_2^2(K_{n1}K_{n3})^{-1}, \tag{2.24}$$

$$K_1 = \left(\frac{\pi}{L}\right)^2 S_1A_1(A_2 + A_3)\left(A\frac{E_1}{E_2}\right)^{-1}, \overline{K}_1 = K_1 \text{ with } A_2 = 0 \tag{2.25}$$

$$K_3 = \left(\frac{\pi}{L}\right)^2 S_3A_3(A_2 + A_1)\left(A\frac{E_3}{E_2}\right)^{-1}, \overline{K}_3 = K_3 \text{ with } A_2 = 0 \tag{2.26}$$

$$K_{13} = \left(\frac{\pi}{L}\right)^4 S_1S_3A_1A_2A_3\left(A\frac{E_1E_3}{E_2^2}\right)^{-1}, \tag{2.27}$$

$$I_e = A_1a_1^2 + A_2a_2^2 + A_3a_3^2, \tag{2.28}$$

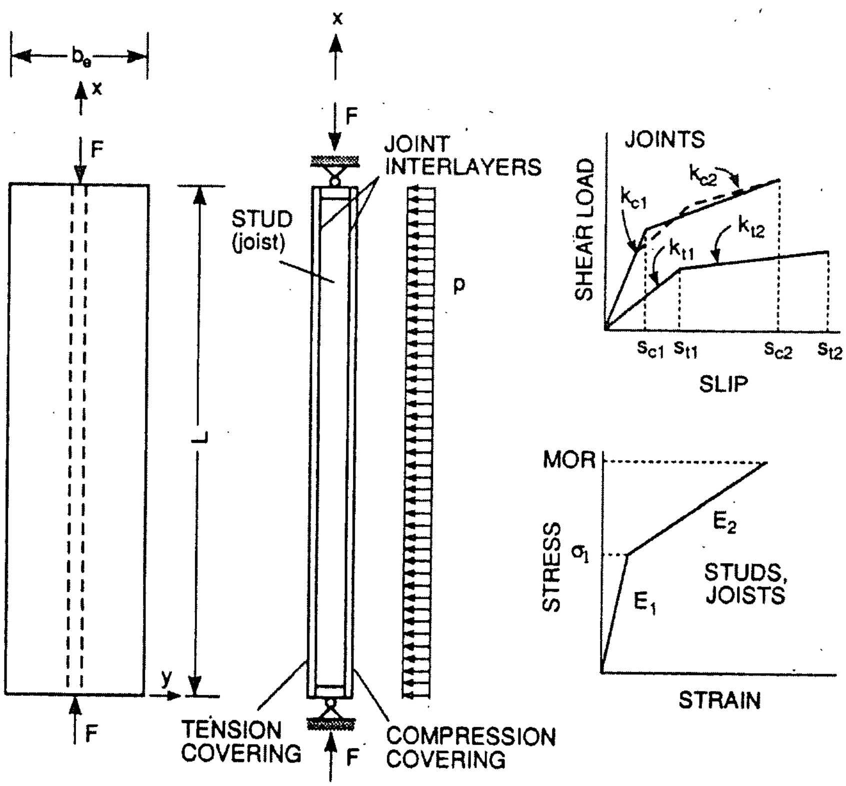

Figure 2.19. Bending and compression system with non-linear components (Polensek & Kazic, 1991).

In the previous formulation, the symbols are defined as follows (Figure 2.20):

$$a_2 = \frac{(r_3A_3 - r_1A_1)}{A}$$

$$a_1 = r_1 + a_2$$

$$a_3 = r_3 - a_2$$

$$A_1 = b_1 h_1 \frac{E_1}{E_2}$$

$$A_2 = b_2 h_2$$

$$A_3 = b_3 h_3 \frac{E_3}{E_2}$$

$$A = A_1 + A_2 + A_3$$

The other symbols have been defined previously. As can be seen, this solution for the effective member properties of a partially composite section is independent of the type of loading configuration. No testing was conducted in this study to verify the new solution.

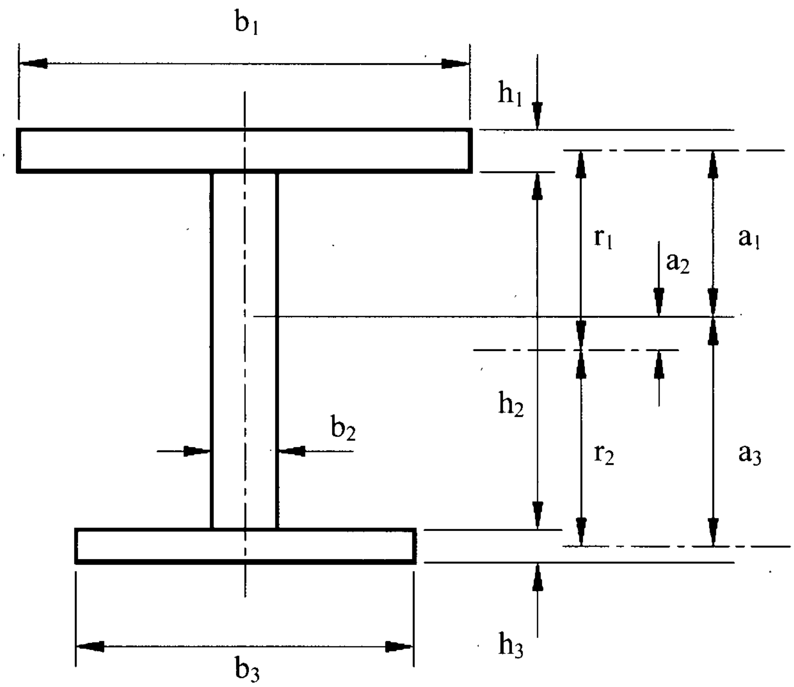

Figure 2.20. Cross-section of an I-shaped composite beam.

A new solution for effective flange width was also introduced and was found by applying appropriate boundary conditions to the function mentioned previously. It can be seen in the above solution that effective flange width is now an input parameter and not explicitly contained in the calculations for the composite properties of the member. The solution for effective flange width was simplified by taking n equal to one and expanding the trigonometric and hyperbolic functions into exponential series. As well, it was shown that ignoring terms containing Poisson's ratio affected the solution by less than five percent. The effective flange width was thus given by:

$$b_e = 2b\left[90\beta + 30\alpha\beta\overline{\omega} + \overline{\omega}^4\left(3\alpha^2\beta + \beta^2\right)\right]\left\{3\left[30\beta + 30\alpha\beta\overline{\omega}^2 + \overline{\omega}^4\left(\beta^2 + 5\alpha^2\beta\right)\right]\right\}^{-1}, \tag{2.29}$$

where

$$\overline{\omega} = \frac{\pi b}{L}.$$

The reliability analysis that was conducted accounted for the non-linear properties of the composite sections. This was achieved by changing the stiffness of the joints and the studs with increasing displacements (Figure 2.19). The member model consisted of a composite beam-column wall section under axial and transversal, or out-of-plane, loading. The deflection at the mid-height of the wall was given by:

$$\Delta = \frac{5\, M_{max} L^2}{48\,(EI)_{eff}}, \text{ where} \tag{2.30}$$

$$M_{max} = \frac{w\, L^2}{8}\left[1 + \frac{P\, L^2 w}{4\,(EI)_{eff}}\eta(u)\right], \tag{2.31}$$

$$\eta(u) = \frac{2\sec(u) - 2 - u^2}{u^4}, \tag{2.32}$$

$$u = \frac{1}{2\,L}\sqrt{\frac{P}{(EI)_{eff}}}. \tag{2.33}$$

2.5.5 Partial Composite Action (Kuenzi and Wilkinson)

Kuenzi and Wilkinson studied the response of composite beams of various construction configurations with fasteners of finite rigidity (Kuenzi & Wilkinson, 1971). Their solutions were based upon work done at the Forest Products Laboratory in the 1950's (Norris et al, 1952). Testing was conducted on twenty-four beams including double T-beams, double I-beams, rectangular beams, and box beams. Nail load-slip values were taken from previous testing by Wilkinson but shear load-slip data for construction mastic adhesives was determined from testing for this study. The mid-span deflection of a simply supported beam under a uniformly distributed load, w, was given by:

$$\Delta = K_{\Delta} \frac{5wL^4}{384\,(EI)_{\infty}} = K_{\Delta}\Delta_{\infty}\text{, where} \tag{2.34}$$

$$K_{\Delta} = 1 + \frac{12}{5}\left[\frac{(EI)_{\infty}}{(EI)_{o}} - 1\right]\left(\frac{2}{L\,\alpha}\right)^2\left[1 - 2\left(\frac{2}{\alpha\,L}\right)^2\left(1 - \frac{1}{\cosh\left(\frac{L\,\alpha}{2}\right)}\right)\right], \tag{2.35}$$

$$\alpha^2 = \frac{r^2 k}{(EI)_{\infty} - (EI)_{o}}\left[\frac{(EI)_{\infty}}{(EI)_{o}}\right]\text{, and} \tag{2.36}$$

$(EI)_{\infty}$ is the stiffness of the composite beam as if the components were glued together with rigid adhesive.

Better agreement was found between the theoretical and experimental data for the load-deflection results than for the load-slip results. The differences found from the comparisons of the load-slip results was thought to arise because of the assumption of constant shear stress throughout the thickness of all inner members.

2.5.6 Partial Composite Action (McCutcheon)

McCutcheon sought to simplify the solution provided by Kuenzi and Wilkinson by approximating the hyperbolic trigonometric functions used in their calculations (McCutcheon, 1977). His solution for the mid-span deflection of a simply supported beam under any type of loading was given by:

$$\Delta = \Delta_\infty \left\{ 1 + f_\Delta \left[\frac{(EI)_\infty}{(EI)_o} - 1 \right] \right\}, \text{ where} \tag{2.37}$$

$$f_\Delta = \frac{10}{(L\,\alpha)^2 + 10}. \tag{2.38}$$

f_Δ is an approximation of the factor containing hyperbolic trigonometric functions of $L\alpha$ that vary depending upon the type of loading. By using this factor it was then possible to compute the properties of a partially composite member independently from the type of loading configuration. Table 2.1 compares the approximation with the exact solutions for the three different loading configurations at the mid-span of a beam. The discrepancy between these values is small. The effective bending stiffness of a partially composite beam was then given by:

Table 2.1. Comparison of approximate and exact values of f_Δ (McCutcheon, 1977).

$L\alpha$	Approximate f_Δ	Exact f_Δ		
		Quarter-point loading	Distributed loading	Mid-span loading
0.0	1.000	1.000	1.000	1.000
1.0	0.909	0.907	0.908	0.909
2.0	0.714	0.708	0.711	0.715
5.0	0.286	0.276	0.281	0.291
10.0	0.091	0.084	0.088	0.096
50.0	0.004	0.003	0.004	0.005
100.0	0.001	0.001	0.001	0.001
∞	0.000	0.000	0.000	0.000

$$(\mathrm{EI})_{\mathrm{eff}} = \frac{(\mathrm{EI})_{\infty}}{1 + f_{\Delta}\left(\frac{(\mathrm{EI})_{\infty}}{(\mathrm{EI})_{\mathrm{o}}} - 1\right)}. \tag{2.39}$$

2.5.6.1 Influence of Gaps

McCutcheon identified the influence of gaps in the flange as being significant and it was subsequently included in the theorem. The amount of composite action was defined by f_{Δ}. Since α is a property of the cross section, it was determined that reducing the length value in the f_{Δ} factor should account for the reduction in stiffness due to the presence of gaps. Thus the presence of gaps was accounted for by rewriting equation (2.38) as:

$$f_{\Delta} = \frac{10}{(\mathrm{L}'\alpha)^2 + 10} \tag{2.40}$$

where L' is the distance between discontinuities (open gaps) in the sheathing in the direction of the span. It was assumed that the gaps were evenly spaced along the span.

Data from seven floors that were tested for this 1977 study along with data from T-beam tests conducted at Colorado State University and the NAHB Research Foundation provided sufficient information to validate this theoretical method. The specimens were subjected to both concentrated and uniform load tests. The computations performed by this method were found to match well with results obtained experimentally, validating the solution for a partially composite member with gaps in the flange.

2.5.6.2 Beam-Spring Analog

While McCutcheon identified the need to determine the distribution of the load in the transverse (in-plane) direction to the composite members in 1977, he did not publish his solution to this problem until 1984 (McCutcheon, 1984). Using what he called a beam-spring analog, a floor was modeled as a beam supported by elastic springs to account for two-way action due to the cross-member distribution properties of the sheathing. The progression of this model is shown in Figure 2.21. As stated, each composite member was represented by an elastic spring that was a constant ratio of member load to joist deflection. For each member, j, the spring constant was given by:

$$k_j = \frac{wL}{\Delta_j} \tag{2.41}$$

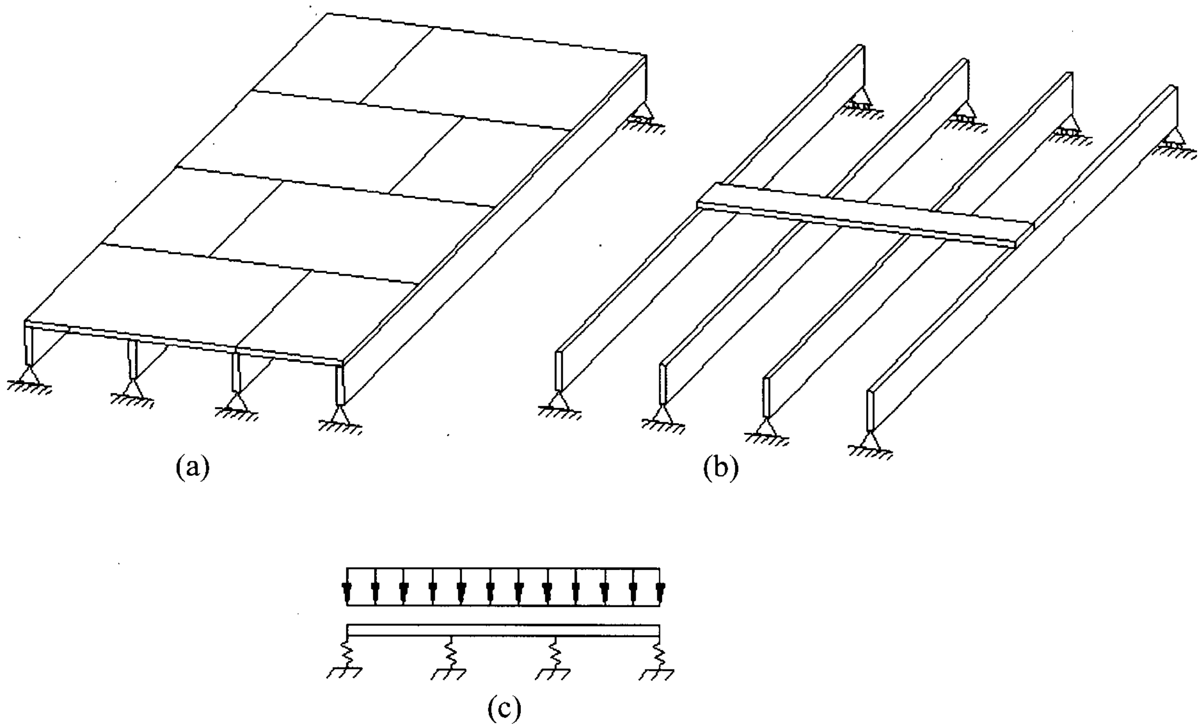

Figure 2.21. Progression of the beam-spring analog method (a) composite wood-frame floor, (b) transverse stiffness represented as an equivalent beam perpendicular to the joists, and (c) composite joists represented as springs supporting the equivalent transverse beam (McCutcheon, 1984).

The analog beam represents the aforementioned distributional properties of the sheathing along the length of the composite member. The bending stiffness of this beam is equal to the stiffness of the sheathing in the transverse direction and was given by:

$$(\mathrm{EI})_b = \frac{1}{12} E_s L t^3 \left(1 - \frac{s}{l'}\right), \text{ where} \tag{2.42}$$

E_s is the bending modulus of elasticity of the sheathing in the cross-joist direction, s is the composite member spacing, and l' is the length of sheathing in the cross-joist direction. As can be seen, this equation also accounts for gaps in the sheathing but in the transverse direction. In a typical floor or wall system the gaps in the sheathing in the transverse direction are staggered. This equation approximates the reduced stiffness of the analog beam by averaging the effects of these discontinuities.

The analog system can be solved using matrix analysis as the individual spring stiffness values and the beam stiffness are known. This method of analysis was compared with the finite element program FEAFLO (Thompson et al, 1977), described in Section 2.10.2, and with the data from the seven floors that were tested in the 1977 study by McCutcheon. The results were virtually identical to those obtained from the finite element program and very close to the data obtained from testing.

2.5.6.3 Generalized Model for Partial Composite Action

All of the work done by McCutcheon described previously had been for composite members with sheathing on one face only. He later reinterpreted his solution for the effective properties of a partially composite member to include sheathing on both faces (McCutcheon, 1986). The new solution was valid for a member with two different sheathing and connection types. The effective bending stiffness was given by:

$$(\mathrm{EI})_{eff} = (\mathrm{EI})_o + \overline{\mathrm{EA}}_1\, r_1^2 + \overline{\mathrm{EA}}_3\, r_3^2 - \overline{\mathrm{A}}\, \overline{y}^2, \text{ where} \tag{2.43}$$

$$\overline{EA}_i = \frac{E_i A_i}{1 + 10\dfrac{E_i A_i}{k_i L_i^2}} \qquad i = 1,3. \tag{2.44}$$

k_i is the interlayer slip for sheathing layer i, and L_i is the distance between discontinuities (open gaps) in sheathing layer i in the direction of the span. Additionally, the total area of the transformed section and the location of the neutral axis were respectively given by (Figure 2.22):

$$\overline{A} = E_2 A_2 + \overline{EA}_1 + \overline{EA}_3 \tag{2.45}$$

$$\overline{y} = \frac{r_1 \overline{EA}_1 - r_3 \overline{EA}_3}{\overline{A}} \tag{2.46}$$

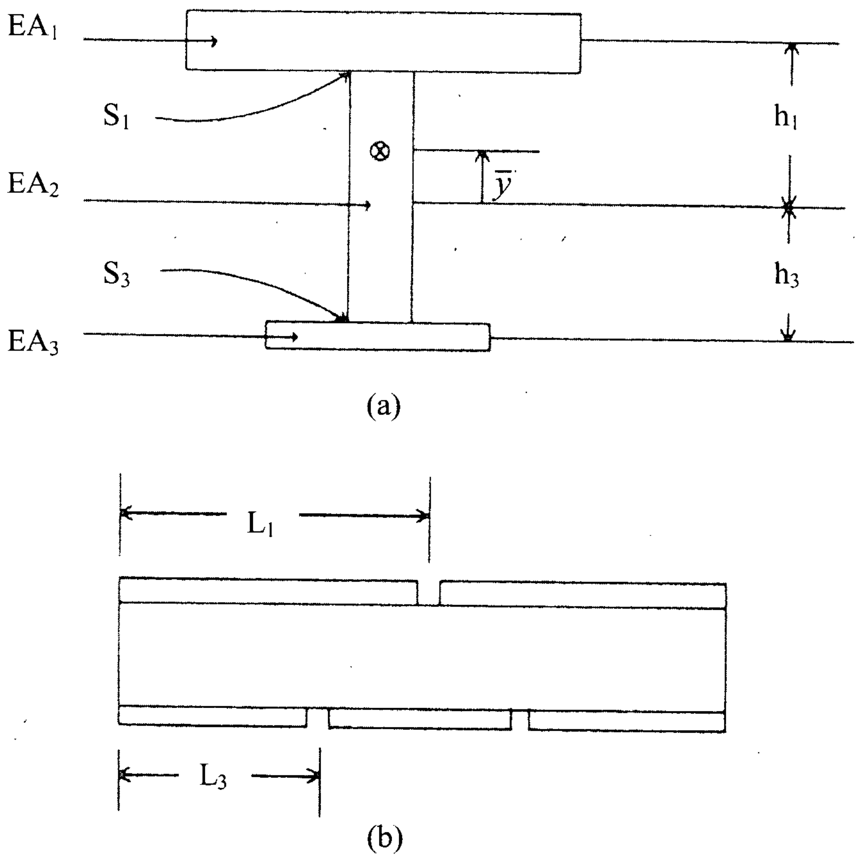

Figure 2.22. (a) cross-section and (b) side view of the revised model by McCutcheon (1986).

Numerous tests were conducted to validate this formulation, including twelve T-beams and twenty-four I-beams, under third-point loading. Once again, the comparison of load-deflection results with test data proved to be much closer than that of load-slip results. In this case, however, the difference in accuracy was attributed to the use of a linear nail load-slip relationship. Actual nail load-slip test data was shown to be highly non-linear.

2.5.7 Partial Composite Action (Itani and Brito)

A theoretical study for computing stresses and deflections in floors with gaps was developed by Itani and Brito (1978) concurrently with the study done by McCutcheon (1977). The theoretical results were verified against the experimental results on T-beams connected with elastomeric adhesive presented by Bessette (1977). Unlike the theoretical formulation developed by McCutcheon, the formulation by Itani and Brito is not as easily applied to different gap configurations as it is derived from a basic differential equation for each separate configuration. An example of a T-beam with gaps placed at the fourth points is shown in Figure 2.23 and the analysis methodology is shown graphically in Figure 2.24. The beam is modeled into four segments and the mid-span deflection is the sum of deflections at the ends of the equivalent beams. The equation for mid-span deflection of a composite T-beam under a uniformly distributed load, w, was given by (Itani, 1983):

$$\Delta = \frac{1}{(E_1 I_1 + E_2 I_2)} \left\{ \begin{array}{l} \dfrac{-13\,L^4}{3072}\left(\dfrac{w}{2} - Q_1 r\right) + \dfrac{r\,L}{4\sqrt{C_1}}\left[P_3 \tanh\left(\sqrt{C_1}\,L/8\right) - R_3\right].. \\ -\dfrac{67\,L^4}{3072}\left(\dfrac{w}{2} - Q_1 r\right) + \dfrac{r\,L}{4\sqrt{C_1}}\left[3\,P_4 \tanh\left(\sqrt{C_1}\,L/8\right) - 2\,R_4\right].. \\ -\dfrac{R_4 r\,L}{4\sqrt{C_1}}\cosh\left(\sqrt{C_1}\,L/4\right) \end{array} \right\} \tag{2.47}$$

where:

$$P_3 = \frac{w\,C_2}{C_1}\left(\frac{1}{C_1} - \frac{3\,L^2}{32}\right) \tag{2.48}$$

$$P_4 = \frac{w\,C_2}{C_1}\left(\frac{1}{C_1} - \frac{L^2}{8}\right) \tag{2.49}$$

$$R_3 = \frac{3\,w\,L^2}{32}\frac{C_2}{C_1}\operatorname{csc h}\left(\sqrt{C_1}\,L/4\right) \tag{2.50}$$

$$R_4 = \frac{w\,L^2}{32}\frac{C_2}{C_1}\operatorname{csc h}\left(\sqrt{C_1}\,L/4\right) \tag{2.51}$$

$$Q_1 = \frac{w\,C_2}{2C_1} \tag{2.52}$$

$$C_1 = k\left[\frac{\overline{EI}}{\overline{EA}(E_1 I_1 + E_2 I_2)}\right] \tag{2.53}$$

$$C_2 = \frac{k\,r}{(E_1 I_1 + E_2 I_2)} \tag{2.54}$$

The other terms in the proceeding equations have been defined previously.

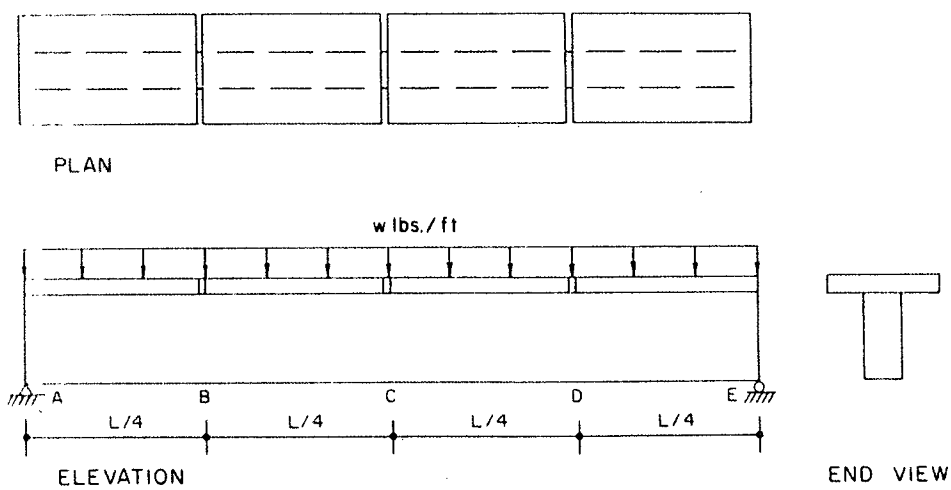

Figure 2.23. Beam with gaps at the fourth points (Itani, 1983).

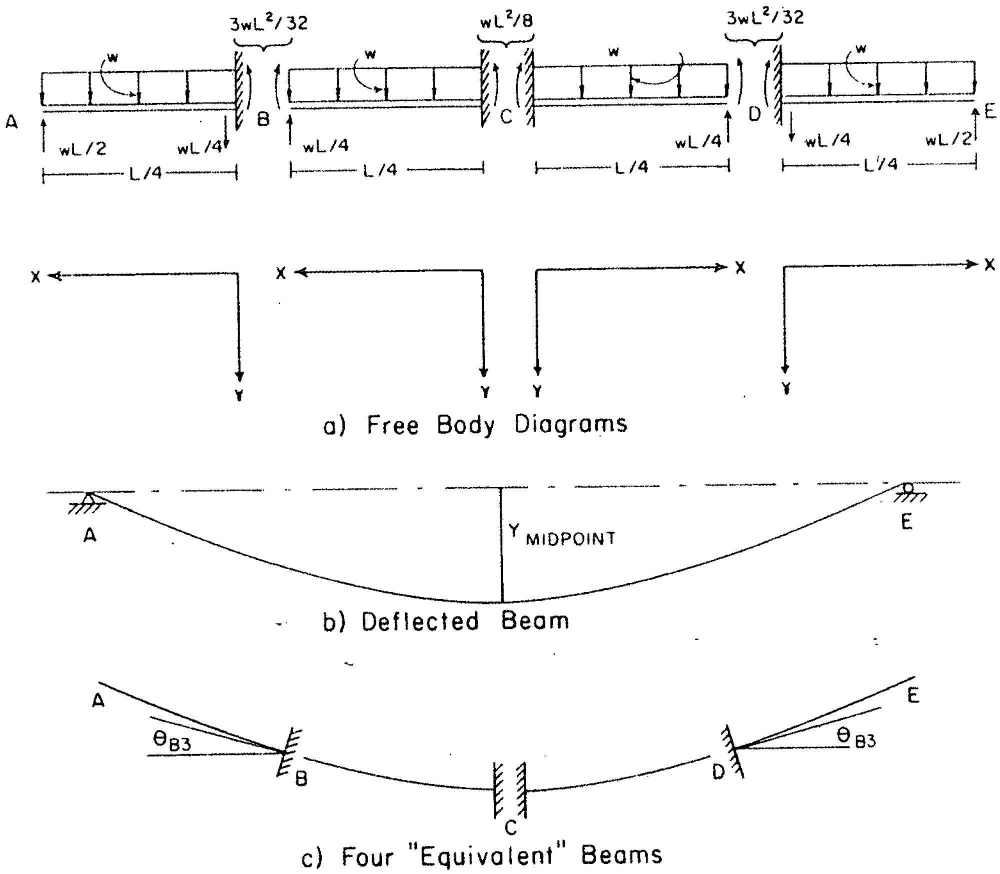

Figure 2.24. Analysis of the beam with gaps at the fourth points (Itani, 1983).

A parametric study was conducted using the same theory as the above example. The beams investigated varied with respect to span, sheathing thickness, and joist size. The sheathing width, uniformly distributed load, modulus of elasticity for the sheathing, modulus of elasticity for the joist, and connection stiffness were all held constant. The findings showed that sheathing discontinuities have a considerable effect on the deflection of a beam. The relationship between a discontinuous and a continuous floor system was not affected by joist depth or flange thickness but it was slightly affected by the thickness of the sheathing. It was concluded that the presence of open gaps redistributed stresses in the sheathing and joists causing a shift in the neutral axis of the composite beam.

2.5.8 Partial Composite Action (Girhammar and Gopu)

2.5.8.1 First-Order Solution

Girhammar and Gopu developed a solution for the response of a partially composite T-beam under axial and transversal loading that included the second order effects of axial load (Girhammar & Gopu, 1991; Girhammar & Gopu, 1993). Their first-order solution for the mid-span displacement of a simply supported T-beam under a uniformly distributed load, w, was given by:

$$\Delta = \frac{5\,w\,L^4}{384\,(EI)_\infty} + \frac{w}{\alpha^4 (EI)_\infty}\left(\frac{(EI)_\infty}{(EI)_o} - 1\right)\left[\frac{1}{\cosh\left(\frac{\alpha L}{2}\right)} + \frac{1}{8}\alpha^2 L^2 - 1\right], \text{ where} \tag{2.55}$$

$$\alpha^2 = k\left(\frac{(EA)_o}{(EA)_p} + \frac{r^2}{(EI)_o}\right), \tag{2.56}$$

$$(EA)_p = E_1 A_1 \cdot E_2 A_2\,, \tag{2.57}$$

$$(EA)_o = E_1 A_1 + E_2 A_2\,, \text{ and} \tag{2.58}$$

$$(EI)_o = E_1 I_1 + E_2 I_2\,. \tag{2.59}$$

2.5.8.2 Second-Order Solution

Both the first-order and second-order analyses include the assumption that axial load is shared by the web and flange members in proportion to their axial stiffness. This ensures that the axial load produces uniform strain over the cross section and does not contribute to the bending of the member. The second-order solution for the mid-span displacement of a simply supported T-beam under a uniformly distributed load was given by:

$$\Delta = \frac{w}{P}\frac{\theta_2^2}{\theta_1^2}\frac{\frac{\theta_1^2 (EI)_\infty}{\alpha^2 (EI)_o} - 1}{\left(\theta_1^2 + \theta_2^2\right)\cosh\left(\frac{\theta_1 L}{2}\right)} + \frac{w}{P}\frac{\theta_1^2}{\theta_2^2}\frac{\frac{\theta_2^2 (EI)_\infty}{\alpha^2 (EI)_o} - 1}{\left(\theta_1^2 + \theta_2^2\right)\cos\left(\frac{\theta_2 L}{2}\right)} - \frac{w}{P}\left(\frac{L^2}{8} + \frac{(EI)_\infty}{P}\right), \tag{2.60}$$

where

$$\theta_1 = \left(\frac{1}{2}\left\{\left(\alpha^2 - \frac{P}{(EI)_o}\right) + \left[\left(\alpha^2 - \frac{P}{(EI)_o}\right)^2 + 4\,\alpha^2 \frac{P}{(EI)_\infty}\right]^{1/2}\right\}\right)^{1/2}, \text{ and} \tag{2.61}$$

$$\theta_2 = \left(-\frac{1}{2}\left\{\left(\alpha^2 - \frac{P}{(EI)_o}\right) - \left[\left(\alpha^2 - \frac{P}{(EI)_o}\right)^2 + 4\,\alpha^2 \frac{P}{(EI)_\infty}\right]^{1/2}\right\}\right)^{1/2}. \tag{2.62}$$

The second-order analysis was used to solve many other section properties such as the shear force and bending moments in each member element as well. Results from the first-order and second-order formulations were compared for an example T-beam. The magnifications for several different beam properties were presented (Table 2.2). Subscripts 1 and 2 denote applied forces and bending moments in the flange and the web members, respectively. Table 2.2 shows that the magnification of displacements, forces, and bending moments is not constant but that it is approximately the same for the two most important parameters in design: maximum

Table 2.2. Comparison of approximate and exact second-order results (Girhammar and Gopu, 1991).

Displacement/ action	First-order analysis	Second-order analysis	Magnification
Δ_{max}	7.560 mm	9.276 mm	1.227
$M_{1,max}$	0.1659 kNm	0.2054 kNm	1.238
$M_{2,max}$	0.4977 kNm	0.6162 kNm	1.238
$N_{1,max}$	-50.863 kN	-53.897 kN	1.060
$N_{2,max}$	0.863 kN	3.897 kN	4.516
$V_{s,max}$	11.444 kN/m	13.878 kN/m	1.213

displacement and bending moment. The magnification of internal axial forces is different from magnifications obtained for other internal actions since only that portion of an internal axial force induced by bending is magnified by the second order effect.

2.5.8.3 Critical Buckling Load

The method outlined above can also be used to determine the critical buckling load and, subsequently, an effective bending stiffness. By setting w = 0 in the governing differential equation, the critical buckling load is given by:

$$P_{cr} = \frac{\theta_{2,cr}^2 (EI)_\infty}{1+\dfrac{\dfrac{(EI)_\infty}{(EI)_o}-1}{1+\dfrac{\alpha^2}{\theta_{2,cr}^2}}} = \frac{P_{cr,\infty}}{1+\dfrac{\dfrac{(EI)_\infty}{(EI)_o}-1}{1+\dfrac{\alpha^2}{\theta_{2,cr}^2}}} = P_{cr,\infty}\frac{(EI)_{eff}}{(EI)_\infty}, \text{ where} \tag{2.63}$$

$\theta_{2,cr}$ is a value associated with the buckling load. Approximate critical loads can be obtained by using the characteristic value of $\theta_{2,cr}$ given for columns with full composite action as:

$$\theta_{2,cr} \cong \frac{\pi}{\mu L}, \text{ where} \tag{2.64}$$

$\mu = 2$ Euler case 1, cantilever

$\mu = 1$ Euler case 2, simply supported

$\mu = 0.7$ Euler case 3, fixed-pinned

$\mu = 0.5$ Euler case 4, fixed-fixed

An approximate equation for the effective bending stiffness of a partially composite member was then given as:

$$(EI)_{eff} = \frac{(EI)_\infty}{1+\dfrac{\dfrac{(EI)_\infty}{(EI)_o}-1}{1+\dfrac{\alpha^2}{\theta_{2,cr}^2}}} = \frac{(EI)_\infty}{1+\dfrac{\dfrac{(EI)_\infty}{(EI)_o}-1}{1+\dfrac{(\alpha L)^2}{\pi^2}}}. \tag{2.65}$$

2.5.9 Partial Composite Action (Kreutzinger)

The design of partially composite members is codified in an appendix of Eurocode 5, the wood design code prevalent in Europe, and is explained in further detail by Kreutzinger (ENV 1995-1-1, 1993; Kreutzinger, 1995). This method is very simple to apply and understand. It is applicable to both T-beams and I-beams. The determination of section properties is independent of the loading configuration. Because a sinusoidal load configuration does not produce any hyperbolic functions in the solution of section properties, it was chosen as the base case. It has been shown previously in this chapter that the type of loading configuration has little effect on the bending stiffness of a composite beam at the mid-span. The mid-span effective bending stiffness of a partially composite member was given by:

$$(EI)_{eff} = \sum_{i=1}^{3}\left(E_i I_i + \gamma_i E_i A_i a_i^2\right) \tag{2.66}$$

where γ, the connection efficiency factor, was given by:

$$\gamma_i = \frac{1}{1+\dfrac{\pi^2 E_i A_i}{k_i L^2}}, \text{ for } i=1 \text{ and } i=3\text{, and } \gamma_2 = 1. \tag{2.67}$$

The connection efficiency factor is equal to one for a perfectly rigid connection and zero for no connection at all. The location of the neutral axis is found by using the following (Figure 2.25):

$$a_2 = \frac{\gamma_1 E_1 A_1 \dfrac{(h_1+h_2)}{2} - \gamma_3 E_3 A_3 \dfrac{(h_2+h_3)}{2}}{\sum_{i=1}^{3}\gamma_i E_i A_i}. \tag{2.68}$$

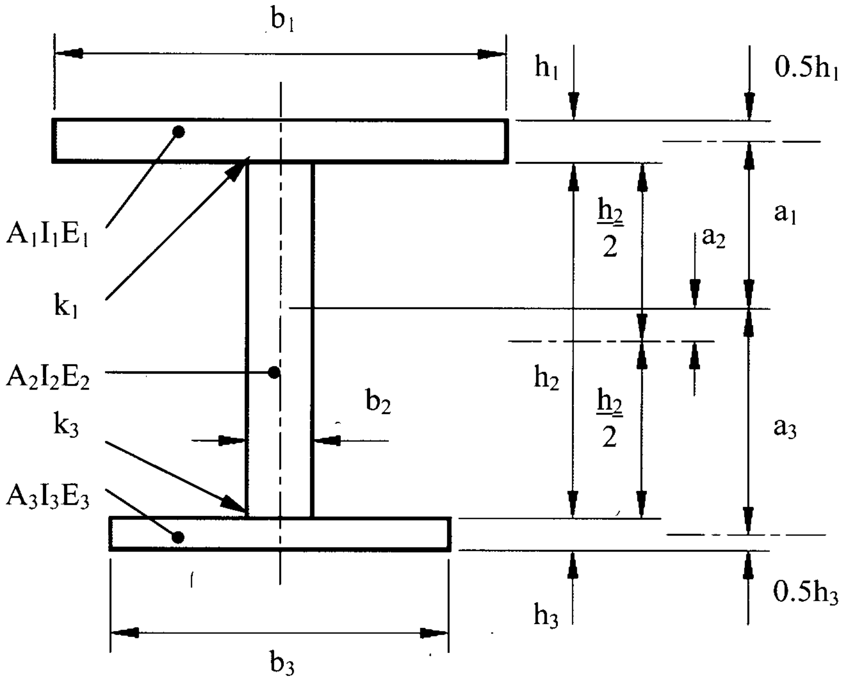

Figure 2.25. Cross-section of an I-shaped composite beam.

2.5.10 Partial Composite Action (Ceccotti)

Ceccotti also provided alternate solutions to the exact deflections of partially composite members under several loading configurations and showed the validity of assuming a sinusoidal load distribution as the basis for determining all member section properties independently from the loading configuration (Ceccotti, 2003). The general solution for the deflection of a simply supported partially composite T-beam member was given by:

$$\Delta = \Delta_\infty \frac{1}{\eta}, \tag{2.61}$$

where the factor accounting for partial composite action due to a uniformly distributed load, a central point load, and a sinusoidal load distribution at mid span was given by, respectively:

$$1/\eta_q = \left[1 + \frac{48\left(1-\beta^2\right)}{5\,\delta^2 L^2}\left(\frac{8\,\beta^2}{\delta^2 L^2}\left(\frac{1}{\cosh\left(\frac{L\,\delta}{2\,\beta}\right)} - 1\right) + 1\right)\right] \tag{2.69}$$

$$1/\eta_Q = \left[1 + \frac{12\left(1-\beta^2\right)}{L^2\delta^2}\left(1 - \frac{\tanh\left(\frac{L\,\delta}{2\,\beta}\right)}{\frac{L\,\delta}{2\,\beta}}\right)\right] \tag{2.70}$$

$$1/\eta_{\sin} = \frac{1+\left(\frac{\pi}{L\,\delta}\right)^2}{1+\beta^2\left(\frac{\pi}{L\,\delta}\right)^2}, \text{ where} \tag{2.71}$$

$$\delta^2 = \frac{k}{(EA)_r}, \text{ and}$$

$$\beta^2 = \frac{(EI)_0}{(EI)_\infty},$$

$$(EA)_r = \frac{E_1 A_1 \cdot E_2 A_2}{E_1 A_1 + E_2 A_2}. \tag{2.72}$$

The ratio between mid-span deflection for a timber-concrete T-beam with deformable connections and the deflection of the same beam with perfectly rigid connections was determined for each of the loading configurations described above (Table 2.3). As can be seen, and as was shown previously, the error in assuming a sinusoidal load distribution when determining the properties of a composite member at the mid-span is limited. This factor was also used to determine an effective bending stiffness for a composite member:

$$(EI)_{eff} = \eta_{\sin}(EI)_\infty. \tag{2.73}$$

Table 2.3. Ratio of mid-span deflection for different loading configurations (Ceccotti, 2003).

Loading Configuration	Short span T-beam	Long span T-beam
Concentrated load a mid-span	1.9313	1.3492
Uniform load	1.9039	1.3258
Sinusoidal load	1.9021	1.3190

In addition to providing exact solutions for determining deflections of partially composite members, Ceccotti also provided a variation on the approximate solutions for equivalent bending stiffness outlined previously. This approximate solution for equivalent bending stiffness was given by:

$$(EI)_{eff} = (EI)_o + \gamma\left[(EI)_\infty - (EI)_o\right], \text{ where} \tag{2.74}$$

$$\gamma = \frac{1}{1+\left(\dfrac{\pi}{L\,\delta}\right)^2} = \frac{1}{1+\dfrac{\pi^2 (EA)_r}{k\,L^2}}. \tag{2.75}$$

2.5.11 Effective Flange Width (Mohler)

Two solutions for the effective width of flange components have already been presented (Amana & Booth, 1967; Polensek & Kazic, 1991). Those solutions were derived in conjunction with the solution of either effective member properties or deflection. The solution by Mohler, as described by Raadscelders and Blass (1995), is a mathematical derivation of effective flange width for a simply supported beam that is uniformly loaded. This solution takes into account the shear deformation in the flange and was given by:

$$b_{ef} = 2\,L\frac{\lambda_1 \tanh(\varphi_1) - \lambda_2 \tanh(\varphi_2)}{\pi\left(\lambda_1^2 - \lambda_2^2\right)}. \tag{2.76}$$

In the previous formulation, the symbols are defined as follows:

$$\varphi_1 = \frac{\lambda_1 \pi \, b_f}{2\,L}$$

$$\varphi_2 = \frac{\lambda_2 \pi \, b_f}{2\,L}$$

$$\lambda_1 = \sqrt{\alpha + \sqrt{\alpha^2 - \beta}}$$

$$\lambda_2 = \sqrt{\alpha - \sqrt{\alpha^2 - \beta}}$$

$$\beta = \frac{E_y}{E_x}$$

$$\alpha = \frac{E_y}{2\,G_{xy}} - \nu_{xy}$$

b_f = the distance between web members minus the width of a web member (Figure 2.26).

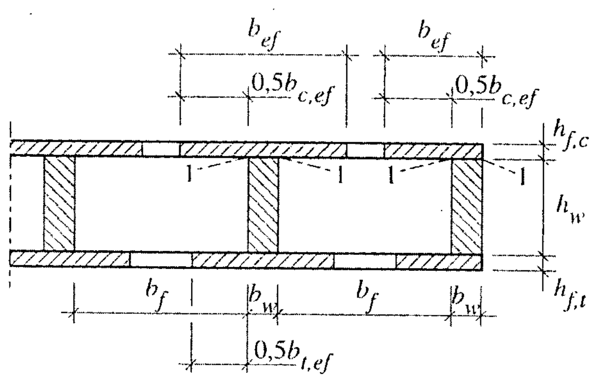

Figure 2.26. Cross-section of a thin-flanged diaphragm (Raadscelders & Blass, 1995).

2.5.12 Effective Flange Width (Eurocode 5)

Eurocode 5 gives the following approximation for the effective flange width of composite members in a wood-frame diaphragm (ENV 1995-1-1, 1993):

$b_{ef} = b_{c,ef} + b_w$ (or $b_{t,ef} + b_w$), where (2.77)

b_w = the width of the web member.

Values for effective flange width are given in Table 2.4 that account for plate buckling on the compression face and shear lag on the tension face of a composite member. Figure 2.27 shows the relationship between the simplified procedure presented in Eurocode 5 and the theoretical solution by Mohler.

Table 2.4. Effective flange width factors from Eurocode 5 (Raadscelders & Blass, 1995).

Flange Material	Shear lag	Plate buckling
Plywood, with grain direction in the outer plies		
Parallel to the webs	0.1 L	25 h_s
Perpendicular to the webs	0.1 L	20 h_s
Orientated strand board	0.15 L	25 h_s
Particleboard or fibreboard with random fibre orientation	0.2 L	30 h_s

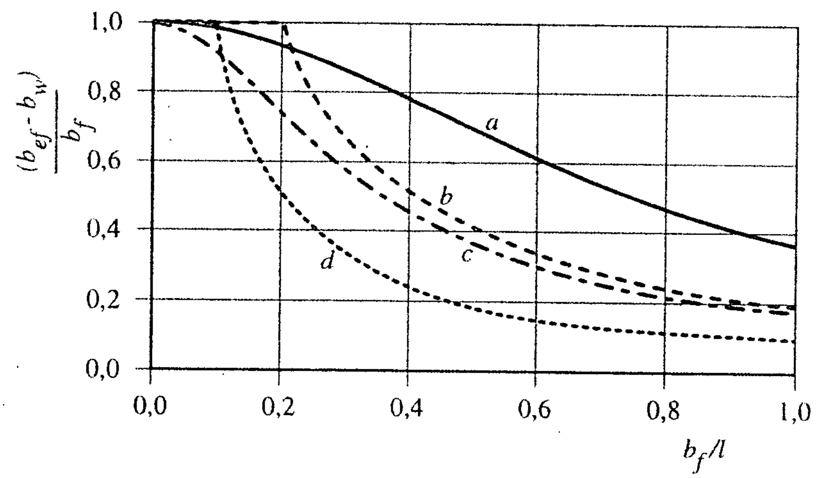

Figure 2.27. Effective flange width according to Mohler and EC5. (a) particleboard Mohler, (b) particleboard EC5, (c) plywood Mohler, (d) plywood EC5 (Raadscelders & Blass, 1995).

2.5.13 Effective Flange Width (Kikuchi)

A formula for effective flange width was developed by Kikuchi (2000) and contains factors based on the results of a sensitivity analysis conducted on glued stressed-skin panels with a single skin and double ribs. The basic panel that was analyzed is shown in Figure 2.28. The sensitivity analysis was conducted using the mathematical model developed by Amana and Booth described previously (Amana & Booth, 1967). The complete formula for effective flange width containing all of the modification factors was given by:

$$b_{eff} = K_1 K_2 K_3 K_4 K_5 b\left[1 - e^{-\alpha(L/b-\beta)}\right], \text{ where} \tag{2.78}$$

$\alpha = 0.3838$

$\beta = 0.4687$.

The exponent function in the brackets is related to rib spacing, and more specifically, to the rib spacing ratio of L/b. The α and β parameters are strictly for curve fitting.

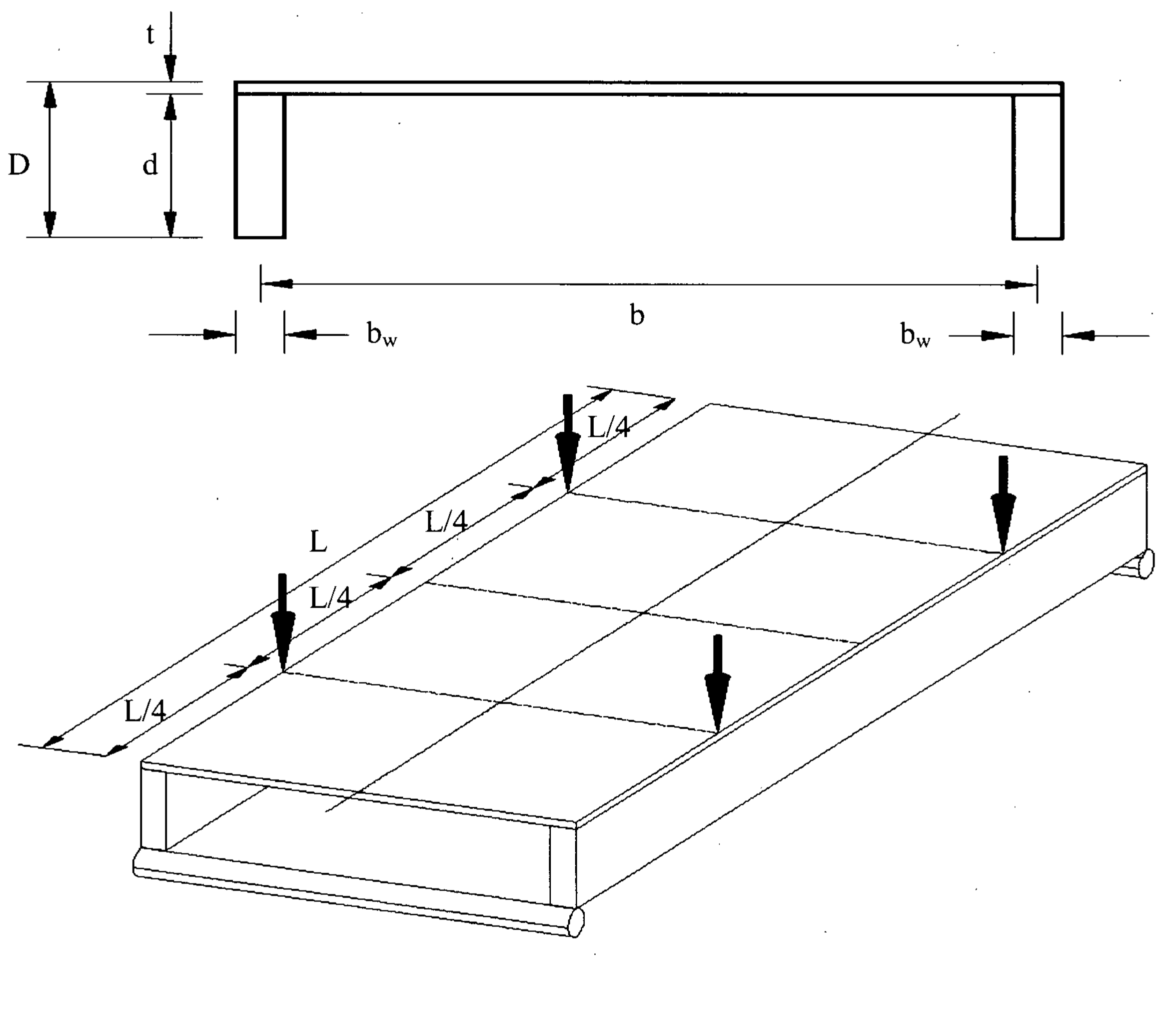

Figure 2.28. The basic panel that is the basis for the formulation by Kikuchi (Kikuchi, 2000).

The K_1 factor defines the effect of varying the rib depth on the effective flange width. This factor, based on a basic rib depth of 140 mm and a curve fitting parameter related to the rib spacing ratio, was given by:

$$K_1 = \left(\frac{140}{d}\right)^{1/\gamma} \quad \text{(d in mm)} \qquad \gamma = 2(L/b) + 12.5 \quad \text{for } L/b < 4 \tag{2.79}$$

$$\gamma = 11(L/b) - 23.5 \quad \text{for } L/b \geq 4$$

In contrast to the rib depth, it was determined that varying the rib width, b_w, or the modulus of elasticity of the rib did not have a significant effect on the effective flange width. Those two parameters were, therefore, neglected in the final formulation.

Three parameters related to the properties of the flange itself were found to be significant with respect to the determination of effective flange width except for panel configurations where the rib spacing ratio is large. A factor accounting for the variation in flange thickness, based upon a basic flange thickness of 12 mm, was given by:

$$K_2 = \frac{0.766}{9}\left(10 - \frac{L}{b}\right)\left(\frac{t}{12} - 1\right) + 1 \quad \text{(t in mm)} \qquad \text{for } L/b < 10 \tag{2.80}$$

$$K_2 = 1 \qquad \text{for } L/b \geq 10$$

The relationship between effective flange width and the modulus of elasticity of the flange, based upon a basic axial elastic modulus of the flange of 4,413 MPa, was given by:

$$K_3 = \frac{1}{9}\left(10 - \frac{L}{b}\right)\left(\sqrt{\frac{4413}{E_y}} - 1\right) + 1 \quad \text{(E in MPa)} \qquad \text{for } L/b < 10 \tag{2.81}$$

$$K_3 = 1 \qquad \text{for } L/b \geq 10$$

Variation in the value of shear modulus of elasticity was also found to have a significant effect on the determination of effective flange width. The following approximated this effect, where the basic shear elastic modulus of the flange was 392 MPa:

$$K_4 = \frac{1.2}{10}\left(10 - \frac{L}{b}\right)\left(\sqrt{\frac{G_{xy}}{392}} - 1\right) + 1 \quad \text{(G in MPa)} \qquad \text{for } L/b < 10 \tag{2.82}$$

$$K_4 = 1 \qquad \text{for } L/b \geq 10$$

Finally, the type of loading was found to have a significant effect on the effective flange width along the entire length of a simply supported panel. The variation of effective width along the span was expressed as a linear relation to the rib spacing ratio as follows:

$$K_5 = a(L/b) + b \tag{2.83}$$

where the parameters a and b are related to the location along the span and the type of loading applied to the panel. Those parameters are given in Table 2.5.

Table 2.5. Values for coefficients a and b found in equation (2.83) (Kikuchi, 2000).

	Fourth point loads (F.P.L.)			Central point load (C.P.L.)			Uniformly distributed load (U.D.L.)		
	y=0.5L	0.35L	0.1L	y=0.5L	0.35L	0.1L	y=0.5L	0.35L	0.1L
a	1	0.01067	0.01811	0.02226	0.00998	-0.01000	0.00972	0.01119	0.02035
b	1	0.8530	0.7247	0.6040	0.8754	1.1031	0.8554	0.8350	0.6533

2.6 SHEATHING BUCKLING

The current limit on the spacing of studs in shearwalls, as specified in the Canadian Wood Design Code, CSA O86-01 (CSA, 2001), was based on two papers that identified localized buckling of the sheathing as a mode of failure of typical shearwalls built in North America. Tissell looked at over one hundred tests that were compiled by the American Plywood Association since 1965 (Table 2.6) (Tissell, 1993). All shearwall specimens were fabricated with the longest panel length dimension parallel to the studs. From those tests, the potential for thin panels to buckle was identified and a reduced capacity was recommended for walls with 610 mm (24") stud spacing versus 406 mm (16") stud spacing with thin sheathing. The reduced capacity, however, was not necessary for sheathing panels that were at least 9.5 mm (15/32") thick. Therefore, the limit on stud spacing specified in the Canadian Wood Design Code is directly applicable to the one sheathing thickness less than 9.5 mm given in the design tables but has shown to be conservative for thicker sheathing thicknesses.

Table 2.6. Effect of stud spacing on shearwalls from (Tissell, 1993).

Stud Spacing (mm)	Fastener		Panel Thickness[a] (mm)	No. of Tests	Ultimate Loads (kN/m)			Target Design Shear (kN/m)	Load Factor
	Size	Spacing (mm)			Min.	Max.	Avg.		
Structural I Sheathing									
406	8d	76	9.5	1			26.91	8.03	3.4
610	8d	76	9.5	7	16.58	22.08	19.88	6.71	3.0
406	10d	76	11.9	1			32.43	9.70	3.3
610	10d	76	11.9	29	21.83	33.27	28.52	9.70	2.9
Rated Sheathing									
406	8d	76	9.5	14	19.38	24.44	21.38	7.15	3.0
610	8d	76	9.5	17	16.87	24.52	20.31	5.98	3.4
406	10d	76	11.9	1			27.74	8.76	3.2
610	10d	76	11.9	30	19.61	28.66	23.98	8.76	2.7
406	10d	76	15.1	2	24.50	28.11	26.30	9.70	2.7
610	10d	76	15.1	16	20.37	31.60	27.22	9.70	2.8

Notes:
(a) Minimum panel thickness for design shear, some walls sheathed with thicker panels
(b) The load factor is determined by dividing the ultimate load by the target design shear.

The second paper referenced in the Canadian Wood Design Code also identified the potential for localized buckling to occur in the sheets of a shearwall if the sheets are very thin (Kallsner, 1995). The work done in this paper was purely theoretical and was not related to test data. The critical shear stress in a sheathing panel was given as:

$$\tau_{cr} = k\frac{\pi^2 E}{12\left(1-\nu^2\right)}\left(\frac{t}{b}\right)^2. \tag{2.84}$$

For a sheet that is simply supported along all four edges, an approximate expression for the coefficient k was given by:

$$k = 5.35 + 4\left(\frac{b}{a}\right)^2. \tag{2.85}$$

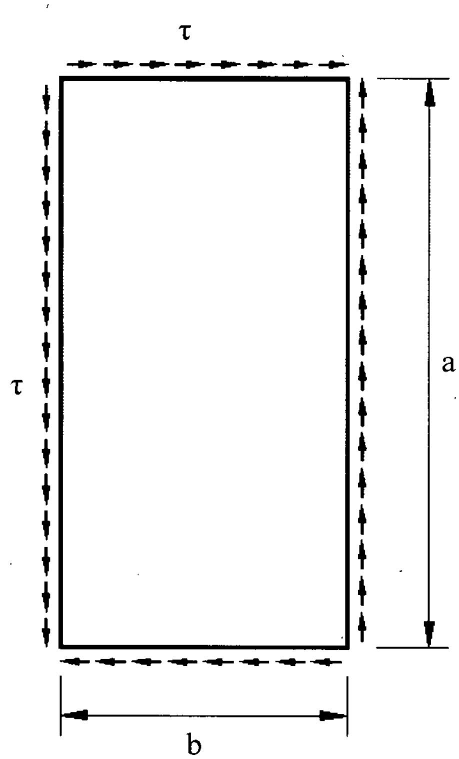

Figure 2.29. Sheathing panel loaded with a constant shear stress along the edges (Kallsner, 1995).

For a sheet that is clamped along all four edges, the coefficient k was given as:

$$k = 8.98 + 5.6\left(\frac{b}{a}\right)^2. \tag{2.86}$$

In equations (2.84) through (2.86), the symbols and terms are defined as follows:

E = modulus of elasticity of the sheathing panel

= Poisson's ratio

t = thickness of the sheathing panel

b = width of the sheathing panel (Figure 2.29)

a = length of the sheathing panel (Figure 2.29).

2.7 NAILED CONNECTION LOAD-SLIP MODELS

It was shown in section 2.5 that the effective member properties of a member with partial composite action are a function of the connection stiffness between the separate components. A parameter study conducted by Polensek showed that the ultimate load, maximum stresses, and maximum deflections of a composite member are greatly affected by the stiffness of the connection (Polensek, 1978). If the partially composite member is connected with nails then the load-displacement relationship of the connection is important with respect to the overall response of the member. To accurately predict the response of partially composite members connected with nails the load-displacement response of the nailed connections must, therefore, be quantified and characterized by one or more functions.

Two procedures will be used throughout the course of this study. The CEN procedure will be used to quantify specific properties of the load-displacement response of nailed connections in order to compare connections with varied parameters more easily (CEN, 1995). The CEN procedure defines initial stiffness by the line that connects to points on the load-slip curve at 0.1 F_{max} and 0.4 F_{max}, respectively (Figure 2.30). The yield load is the load on the curve that corresponds to the yield displacement, which is defined as the displacement at the interception of the initial stiffness line and a tangent line with stiffness equal to 1/6 of the initial value. The ultimate displacement corresponds to the displacement at which the load drops to 80% of the maximum load.

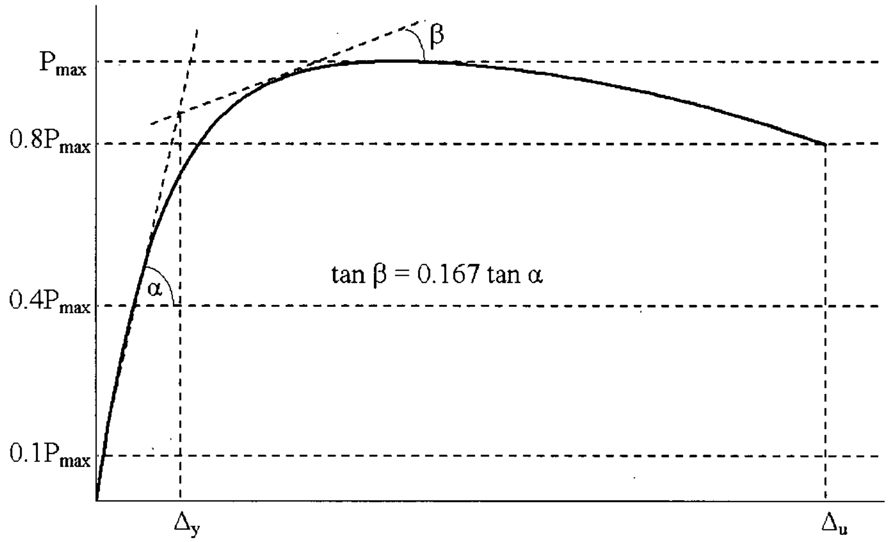

Figure 2.30. Definition of the parameters of the CEN procedure (CEN, 1995).

While the CEN procedure allows for ease of comparisons between load-displacement results, a function is required for computational ease of modeling composite members. A non-linear finite element program developed by Foschi for wood-frame diaphragm structures will be used to predict the response of full-scale test specimens later in this study. That program employs a five-parameter function to model the load-slip behaviour of timber joints, which was also developed by Foschi (1974). That function, shown in Figure 2.31, was given by the following equations:

$$P = (P_o + K_1 u)\left(1 - e^{-\frac{K_o u}{P_o}}\right) \qquad \text{if } u < u_{max} \qquad (2.87)$$

$$P = P_o + K_1 u_{max} + K_E (u - u_{max}) \qquad \text{if } u > u_{max} \qquad (2.88)$$

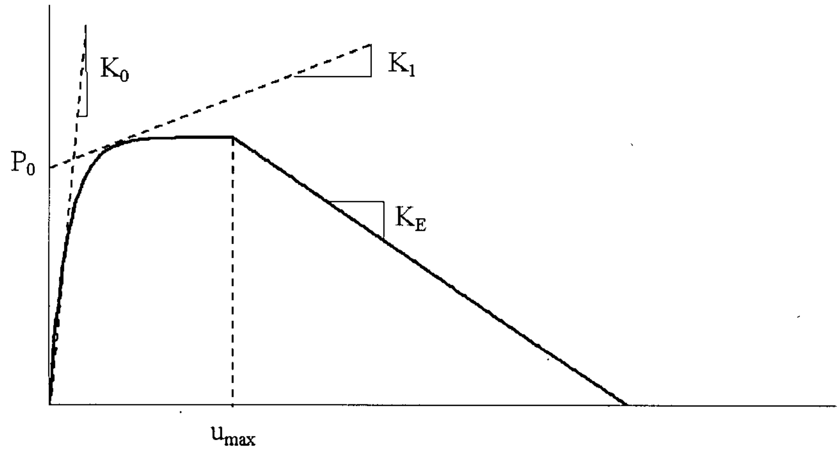

Figure 2.31. Definition of the parameters of the function by Foschi (Foschi, 1974).

It should be noted that a recent study has modified the function by Foschi to more accurately account for the softening behaviour of the joints (Girhammer et. al., 2004). The new function, shown in Figure 2.32, was given by:

$$P = (P_o + K_1 u)\left(1 - e^{-\frac{K_o u}{P_o}}\right) e^{-\frac{u^{\alpha}}{\beta}} \tag{2.89}$$

The solution to this five-parameter function was determined by forcing the function through the points (u_m, P_m) and (u_c, P_c). P_c corresponds to a defined point of total collapse. The non-linear curve fit was then reduced to finding the best value of three of the parameters defined by Foschi: K_0, K_1, and P_0. The parameters α and β were found by iteration using a solving process.

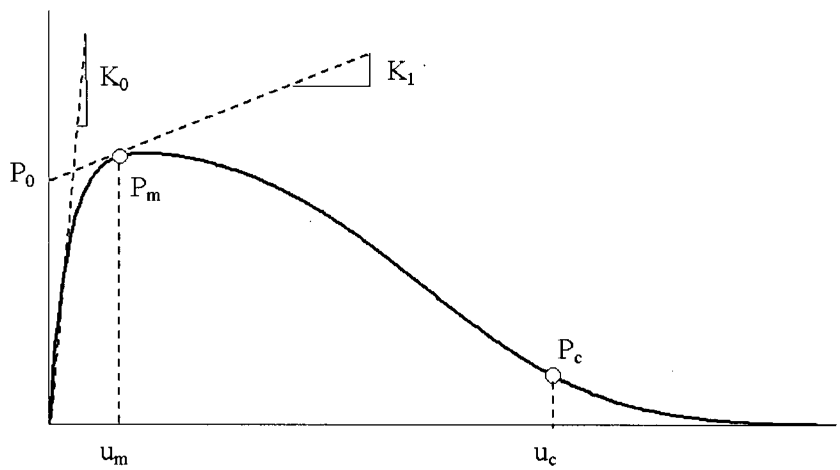

Figure 2.32. Load-slip curve modelled by a 5-parameter equation (Girhammer et. al., 2004).

2.8 LATERAL-TORSIONAL BUCKLING

Structural members loaded by transversal loads in the plane of greatest stiffness may deform laterally and twist (Figure 2.33). This type of stability problem is known as lateral-torsional buckling and results in the loss of increased resistance in the transversal loading direction. Providing adequate support to the compression face of a loaded member can prevent lateral-torsional buckling from occurring. Wood-frame tall walls are especially susceptible to lateral-torsional buckling for several reasons. Firstly, the engineered wood products that are used as studs in tall wall construction have a large slenderness ratio (the ratio of stud depth d to width b). As will be shown later, the resistance of rectangular members to lateral buckling is a function of stud depth and width. Second, unlike floor diaphragms, the transversal loads on walls due to wind pressure and suction can be approximately equal in magnitude. Therefore, both faces of

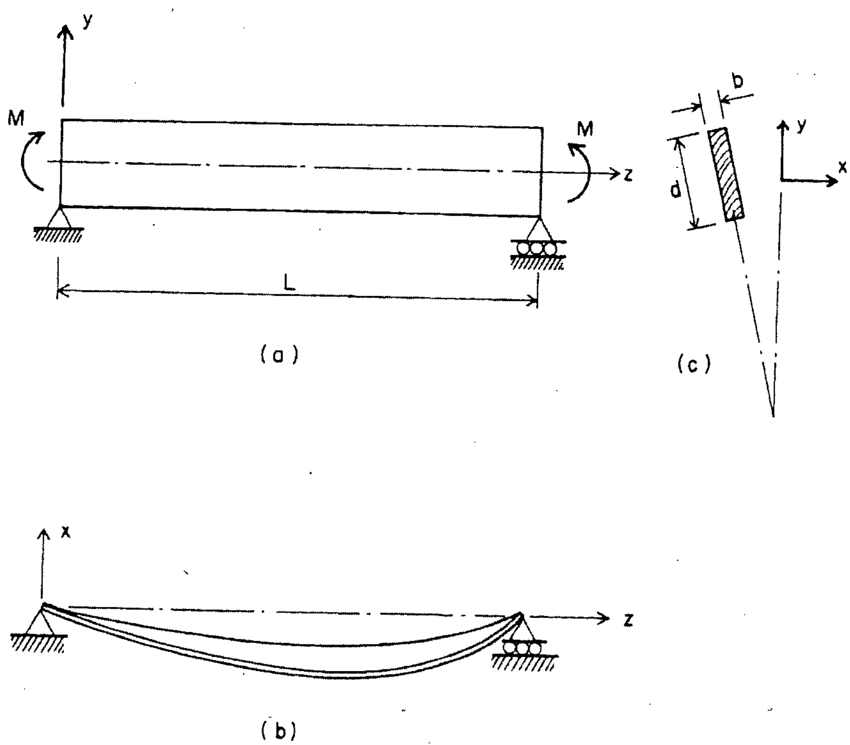

Figure 2.33. Lateral-torsional buckling of a simply supported beam (Hooley and Madsen, 1964).

the wall will be loaded to approximately the same compression stress. Finally, unlike regular wood-frame wall construction, buildings constructed with tall wood-frame walls often utilize oversized sheathing panels. This removes the need to provide blocking at small increments along the height of the wall to provide support to panel edges.

Lateral stability is addressed in the Canadian Wood Design Code in two ways (CSA, 2001). For regular wood-frame construction, criteria are defined for a lateral stability factor, K_L, based upon the slenderness ratio of a member. If the member meets the criteria set out and the slenderness ratio, then the lateral stability factor may be taken as unity. These requirements are based on the experience of what has worked over many years. Otherwise, the lateral stability factor may be calculated in accordance with the requirements for glued-laminated timber. These requirements for lateral stability are based upon a formulation, verified with testing, that was derived by Hooley and Madsen (1964). They identified that the resistance of a rectangular beam to lateral buckling is not related to the slenderness ratio but is governed by the ratio L_ed/b^2. L_e is the effective length of the member and can be a function of the entire length of the member, if it does not have any intermediate support, or the distance between intermediate supports.

A tall wood-frame wall often consists of slender studs with a large spacing between blocking, sheathed on the exterior face with structural panel sheathing and sheathed on the interior face with gypsum wallboard. For the case of wind pressure in the transversal direction, the exterior face of the stud member will be in compression. The commentary to the Canadian Wood Design Code defines diaphragm-forming panel sheathing as a suitable rigid diaphragm and so no reduction to the bending moment resistance is required in this direction and the lateral stability factor can be taken as unity. Zahn has shown that blocking contributes very little to preventing lateral torsional buckling, however, when used in conjunction with a stiff diaphragm (Zahn, 1984).

Conversely, gypsum wallboard does not meet the criteria for forming a rigid diaphragm on the interior face of the wall and often the wall does not meet the slenderness criteria for regular wood-frame walls. Therefore, the lateral stability factor must be determined based on the method presented for glued-laminated timber. In this case, the effective length is equal to the blocking spacing multiplied by 1.92. In many cases, the lateral stability factor can be less than 0.50, which means that the bending moment resistance in one direction is less than half of the bending moment resistance of the other direction even though the applied load is approximately equal.

The interpretation of the code requirements is varied in practice. A wood-frame wall design guide published by a producer of engineered wood products provides lateral stability factors for given blocking spacing and sheathing limits. Firstly, gypsum wallboard is described as an acceptable material to provide lateral support. Second, instead of increasing the distance between blocking supports by 92% to determine an effective length, this distance is reduced by 15% by assuming a buckling length coefficient of 0.85. For an example wall characterized by 38 mm by 235 mm studs with blocking spaced at 2,440 mm on centre, the result of this interpretation is that the code requires approximately a 70% reduction in bending moment resistance while the design guide prescribes only a 30% reduction. This clearly identifies the need for clarification on what is an acceptable design procedure to account for lateral-torsional buckling and possibly the need for further testing.

2.9 ROTATIONAL RESTRAINT AND STUD CONNECTIONS

The structural models that are typically used in design incorporate assumptions that are simplifications of actual structures. In almost all cases, the assumptions are conservative and result in a structural model that predicts the maximum displacements and member stresses to be larger than what occurs in actual structures. A simplification commonly employed when designing wood-frame structures is to model the supports at each end of a floor or wall diaphragm as being pinned. Therefore, the support does not provide any restraint against rotation. Polensek and Schimel identified the need to quantify the effect that intercomponent connections in light-frame wood buildings, such as those between walls, floors, and foundations, have on the displacement of wall diaphragms (Polensek and Schimel, 1986).

The research carried out by Polensek and Schimel included the creation of a non-linear finite element model to predict the actual response of the wall components that were tested. In addition to testing representative sections of wood-frame walls with connections commonly found in structures in North America, they tested wall sections with simple construction modifications that increased the amount of end restraint. A total of nine panels were tested three times with different modifications. The predicted deflections using the finite element model closely agreed with the corresponding experimental results. The typical connection system between wall, floor, and foundation that was investigated is shown in Figure 2.34.

For design purposes, a simple method to incorporate the reduction in mid-span deflection of a wall with support restraint was provided. Partial support restraint was accounted for by adding springs that restrained support rotation at the ends of a beam-column. The coefficient of restraint

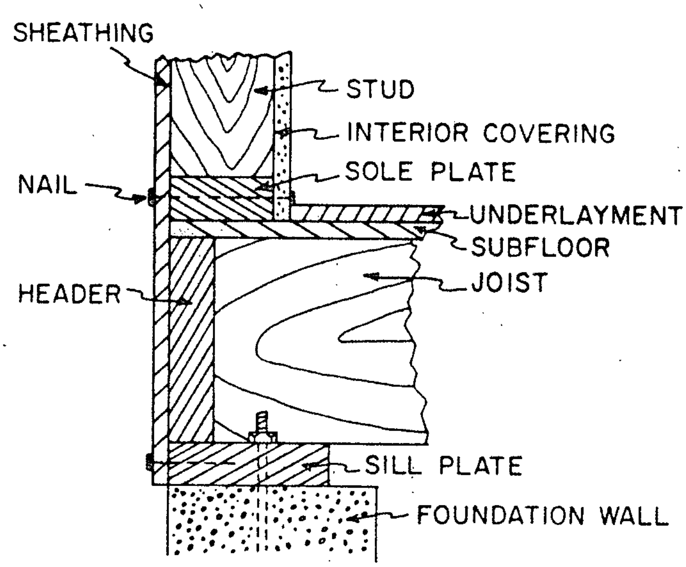

Figure 2.34 Typical intercomponent connection system between a wall, floor, and foundation (Polensek and Schimel, 1986).

was defined as the spring stiffness, α, of the beam-column model. The spring stiffness was determined from the ratio of the mid-span deflections of the restrained and unrestrained beam, y and y_o respectively. For uniform load, α was given as:

$$\alpha = \frac{10EIR}{[L(4-5R)]} \tag{2.90}$$

where $R = 1\text{-}y/y_o$.

Several important findings resulted from the testing and parametric study that was conducted using the finite element model. Firstly, the mid-span deflection reduction for walls constructed in the conventional way with 38 mm by 89 mm (2" x 4") studs was less than 2%. Hammering two additional nails at each stud between the sheathing and the sill plate and six additional nails at each stud between the sheathing and the header proved to be the most successful modification to the original connection and reduced the mid-span deflection by 13%. Finally, it was determined that the coefficient of support restraint gets smaller with increasing lateral load because of the non-linear behaviour of the wood components themselves and the connections of those components.

The axial load on a wall can either be in compression or in tension. Wind can cause suction on the leading edges of roofs. While most of the research to date on wood structures under wind uplift has focused on fastening the roof sheathing to the roof joists, a study was conducted at Clemsen University in South Carolina that addressed the uplift capacity of regular wood-frame stud walls (Rosowski, 2000). Some of the objectives of the research were to determine the failure modes of walls with various sheathing orientations and hurricane strap installations and to determine the ultimate load carrying capacities of the walls tested for comparison with theoretical predictions.

Four critical points on the load path of these walls were determined: the sheathing to the top plate connection; the connection from the sheathing to the wall stud; the nailing pattern at the inter-story detail; and the sheathing to bottom plate connection. The results indicated that horizontally oriented sheathing might be able to carry the uplift loads in a wall system, assuming that an adequate number of nails are present in the sheathing. In addition, top plate roll due to the eccentricity of the straps was identified as a failure mode with significant design implications. The capacity of the walls with this type of failure mode was up to 50% lower than walls with other types of connection details. Two solutions suggested to remedy this type of failure were to place the straps on the outside of the wall or to use a strap that directly connects the rafters to the studs on the inside of the wall.

2.10 WOOD DIAPHRAGM MODELS

Numerous simplified methods for determining the effective properties of composite members were presented in section 2.5. These members represented one stud or one joist of a larger wall or floor diaphragm. A method was also presented where the composite members were joined together to form a diaphragm using a beam-spring analog. Wood-frame structures are a complicated amalgam of non-linear members, however, joined together by hundreds of non-linear connections. To more accurately predict the response of an entire wood system a more advanced method of analysis is thus required. With the onset of personal computers in the late 1970's, researchers began to develop computer programs that used finite elements to model wood diaphragms. Over the years, researchers have attempted to predict the response of wood diaphragms with sophisticated models, some of which will now be presented.

2.10.1 FINWALL (Polensek)

FINWALL, one of the first computer programs to model wood diaphragms, was developed by Polensek at the University of Oregon (Polensek, 1976b). The program subjects walls to constant axial and increasing transversal loads. It is capable of both linear and non-linear analysis. The finite element method of analysis is combined with a linear step-by-step procedure to calculate wall performance. The stud and sheathing connection properties are assumed to be constant over the full height of a given stud and symmetrical about the mid-height of the wall. The finite element mesh is, thus, rather coarse (Figure 2.35).

A method for calculating partial composite action similar to that derived by Amana and Booth, described in section 2.5.3 (Amana and Booth, 1967), was used to calculate the stiffness of I-

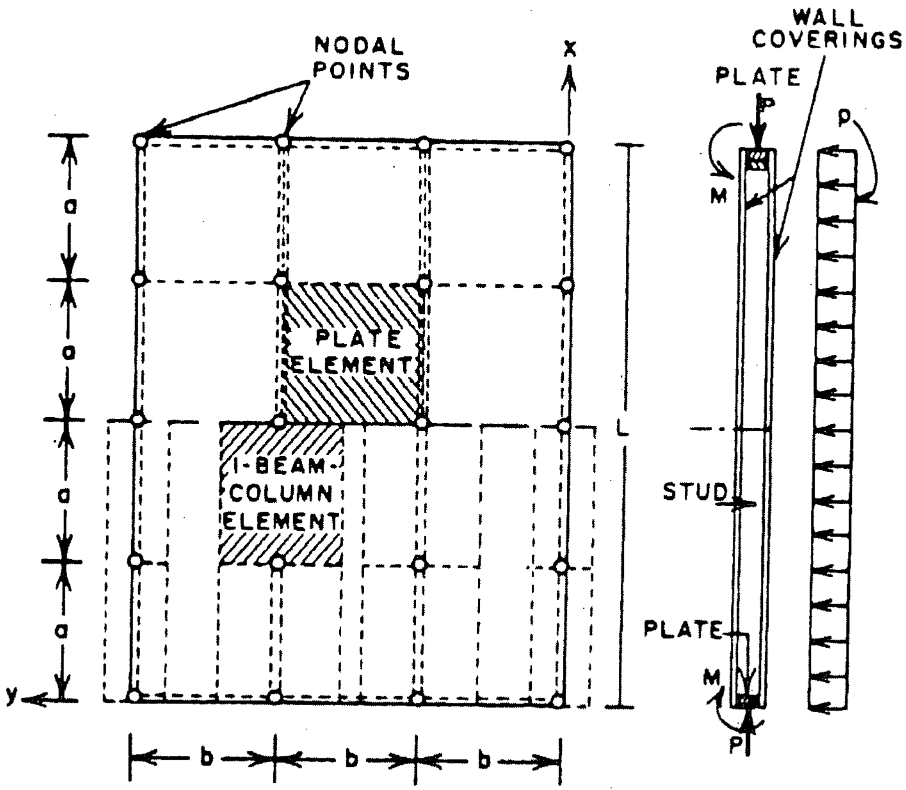

Figure 2.35. Finite element mesh for the FINWALL program (Polensek, 1976b).

beam column elements, comprised of a stud and two layers of sheathing (Figure 2.36). After the column stiffness of the I-beam was calculated, the contributions of the two layers of sheathing were analytically lumped into a single plate for evaluation of their load-distribution ability. It was assumed that the load-distribution properties of the plate could be modeled by simply adding the stiffness of the two layers of sheathing. Discontinuities in the sheathing layers were accounted for by reducing the sheathing stiffness at the discontinuity.

After the stiffness values were compiled in a stiffness matrix, the stresses and deflections in the wall were calculated. Secondary moments induced by axial loads were calculated by an iterative procedure. Failure of an individual stud was computed when the mid-height deflection of the stud exceeded the value input as its failure deflection. The failed stud was then assigned a near-zero stiffness in the stiffness matrix for the next iteration of the program. The program defined wall failure as the failure of two adjacent studs. The model assumed that wall failure was governed by the bending strength of the studs and that stud failures were complete. Based on tests that were conducted to verify the model, described later in this chapter, model accuracy was in the range of less than 10% error at first stud failure and up to approximately 20% at wall failure.

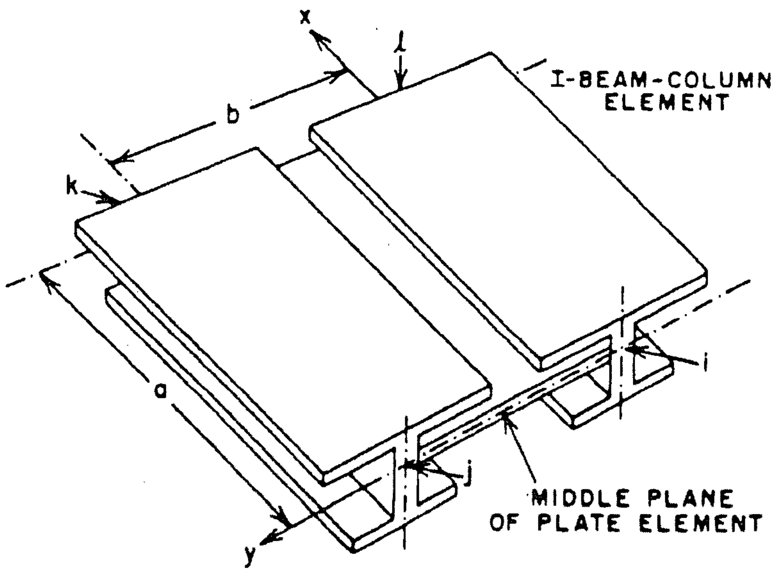

Figure 2.36. Assembly of I-beam column and plate elements (Polensek, 1976b).

2.10.2 FEAFLO and NONFLO (Thompson, Vanderbilt, and Goodman)

The differential equations developed by Goodman and Popov (1968), presented in section 2.5.2, were the basis for the Finite Element Analysis of FLOors (FEAFLO) program developed by Thompson, Goodman, and Vanderbilt at Colorado State University (Thompson et. al., 1975). The sheathing is modeled as a series of parallel strips perpendicular to the joists (Figure 2.37). The differential equations for the partially composite T-beams are coupled by strain compatibility at the common boundary of the sheathing strips. FEAFLO was able to account for interlayer slip between the joists and the sheathing, intralayer gaps between sheathing sheets, and composite and two-way action. The contribution from torsional stiffness was ignored since the ratio of sheathing modulus of rigidity to the modulus of elasticity is small in this case and because the torsional stiffness of a T-beam is small compared to its bending stiffness. The flange width was equal to the joist spacing.

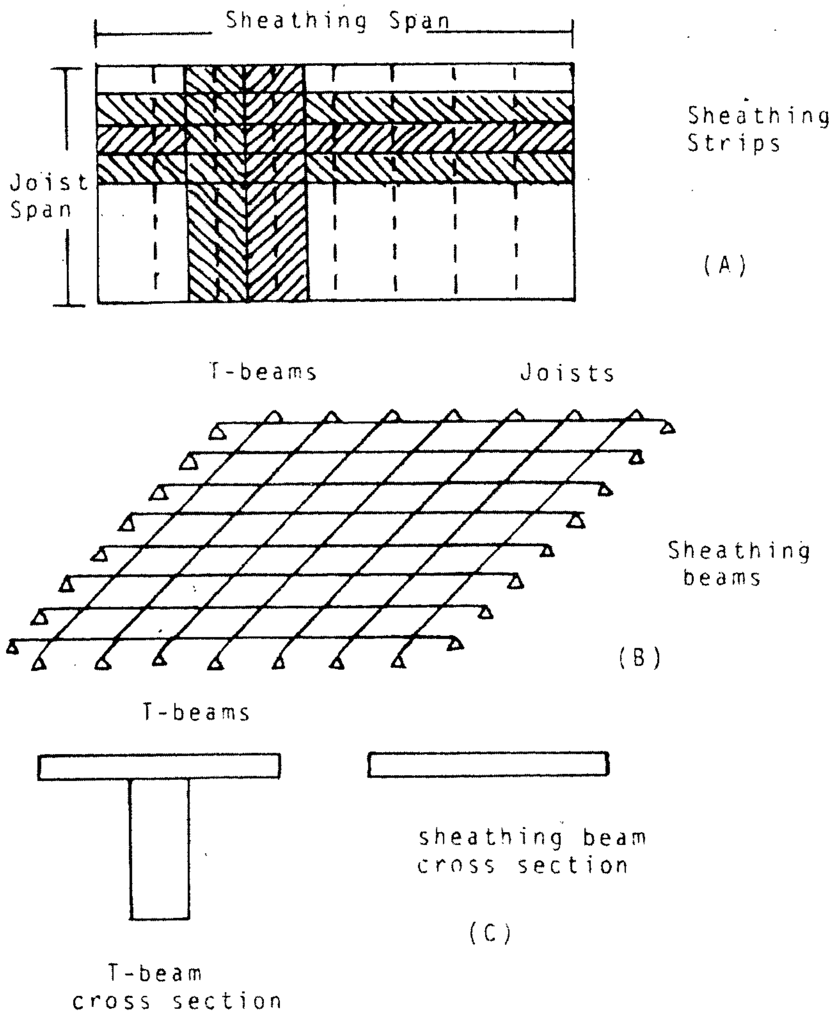

Figure 2.37. Idealization of a wood-joist floor system in FEAFLO (Pellicane and Robinson, 1997).

Since its development, several modifications to the basic program have been made. The ability to account for multiple load cases and evaluate interlayer shears, vertical shears, axial forces, and moment in the system was incorporated. Wheat, Vanderbilt, and Goodman made the most significant increase in accuracy by adding the effects of sheathing connection non-linearity to the finite element analysis (Wheat et. al., 1983). The new program called, NON-linear FLOor analysis (NONFLO), only considered the non-linearity due to connector deformations since this was deemed to be the major source of floor non-linearity for loads close to the failure load.

FEAFLO and its various incarnations have been used in numerous studies to predict the response of tested specimens. Deflection comparisons of floors showed that the predictions made by the non-linear program were more accurate than the earlier developed linear analysis program for behaviour at impending floor failure under short-term loading. In addition, far more realistic magnitudes of connector forces above the service load level were provided by the non-linear analysis (Wheat et. al., 1983).

2.10.3 FAP and PANEL (Foschi)

Foschi has developed several computer programs to model wood-frame diaphragm structures. They include: Floor Analysis Program (FAP) (Foschi, 1989); Wall Analysis Program (WAP) (Foschi, 1992); Diaphragm Analysis Program (DAP) (Foschi, 1993); and PANEL (Foschi, 1999). The programs were all based on his original program that was characterized by a combined Fourier series and finite element analysis of a wood floor (Foschi, 1982).

The structural idealization of the floor shown in Figure 2.38 was based on a finite strip formulation made up of an assemblage of T-beams. The deformations of the floor were represented by a Fourier series in the direction parallel to the joists and by a one-dimensional finite element discretization in the direction perpendicular to the joists. The model in this program included lateral and torsional deformation of the joists as degrees of freedom. This permited the consideration of the effect that joist bridging has on maximum floor deflection and maximum bending stresses. The FEAFLO model restricted those degrees of freedom and, therefore, resulted in a model that was stiffer than the actual structure, which was shown by experimental data (Thompson et. al., 1975). The original model by Foschi provided reliable estimates for deflections and the influence of different gaps configurations when compared with tests conducted on full-scale floors.

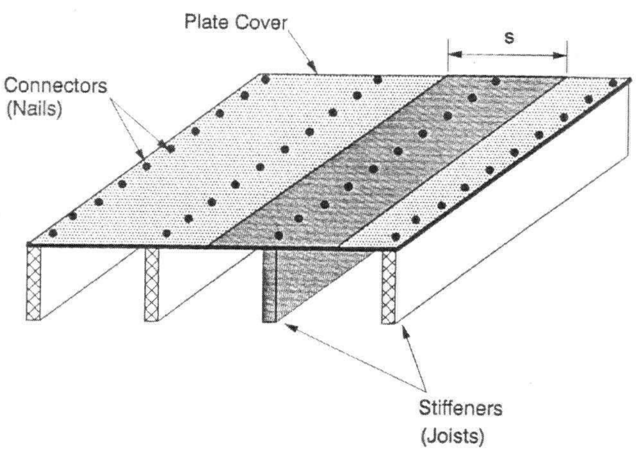

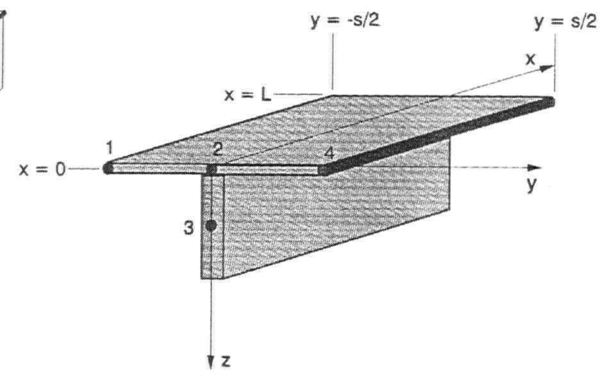

Figure 2.38. (a) wood floor assembly and (b) T-beam element strip (Foschi, 1989).

PANEL was used in this study to predict the response of full-scale wall specimens. It was designed to model stressed skin panels consisting of a frame connected to top and bottom covers. The connections were assumed to be non-rigid with non-linear load-slip properties. The loads, which could be applied in the transversal direction or in the plane of the wall, could be incremented simultaneously or individually until the ultimate capacity was reached. Ultimate capacity was defined by the following: excessive connection deformation; buckling of either of the sheathing layers; buckling of the frame; tearing of the edge of the covers implying local connection failure; or bending failure of the frame members. The models employed in this study are described in detail in Appendix C.

2.10.4 BSAF (Lui and Bulleit)

The programs described previously do not consider the post failure behaviour of the system components of a wood-frame diaphragm. Even programs that include the non-linear behaviour of the connections are not adequate in this regard since they do not include the non-linear behaviour of the partial composite members. The overload behaviour of wood systems is directly related to this non-linear behaviour of the partial composite members. The system-failure criteria of a system can only be predicted through the use of a program that incorporates the non-linear behaviour of all of the components of the system.

Lui and Bulleit incorporated the beam-spring analog method developed by McCutcheon, presented in section 2.5.6.2, into a computer program called Beam-Spring Analog for Floors (BSAF) (Lui and Bulleit, 1995). The program included: two-way action of the sheathing; partial composite action between the sheathing, connectors, and lumber members; the random mechanical properties of the lumber members; and the random post-yield properties of the partial composite members. A trilinear spring model (Figure 2.39) and a member-replacement technique were introduced to account for the non-linear behaviour of the partial composite members.

The program did not represent the wood-frame system using the finite element method and was thus an approximation with several assumptions to simplify the procedure. The tri-linear model and member replacement technique in BSAF to predict the non-linear behaviour of a sheathed lumber system compared well with test data on floors. Using this program, the primary factors affecting system overload behaviour were determined along with appropriate system-failure criteria.

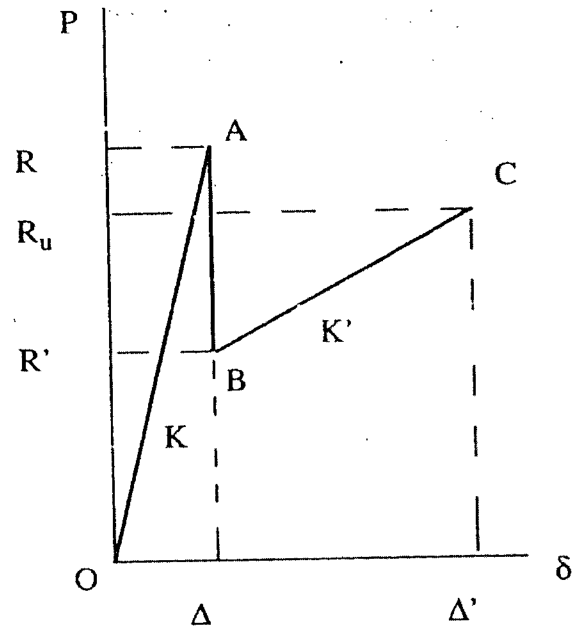

Figure 2.39. Spring load-deformation curve (Lui and Bulleit, 1995).

2.10.5 Equivalent Finite Element Model (Kasal and Leichti)

With the advent of modern structural modeling software, it is possible for consulting engineers to routinely use packaged finite element programs to design structures. Unlike the programs that have been described previously that assess the response of an isolated wall or floor in a building, it is now possible to predict the global response of a structure under load by modeling the entire structure. An actual wood-frame structure is very complex, however, and the number of degrees of freedom is enormous. To address this problem, Kasal and Leichti developed a simplified, or equivalent, finite element model of a wood-frame wall that could be used as a component in a three-dimensional model of an entire wood-frame structure (Kasal and Leichti, 1992).

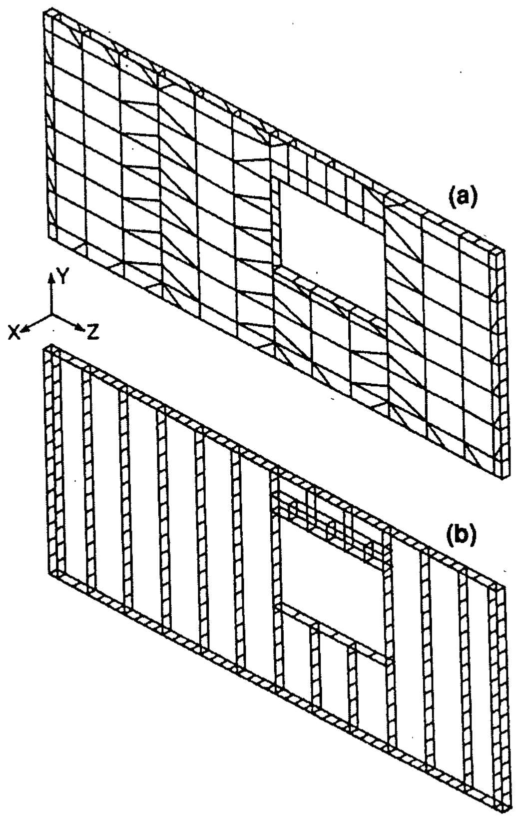

Figure 2.40. Finite element mesh of a (a) sheathed wall and (b) wall frame (Kasal and Leichti, 1992).

Using an off-the-shelf finite element program, a detailed model of an actual wood-frame wall was created (Figure 2.40). The studs and sheathing were modeled as linear two-dimensional shell elements. Three one-dimensional springs were used to represent the non-linear characteristics of each joint: one for withdrawal and one each for shear in each coordinate. In addition, gap elements were used where the sheathing was not continuous. Tests on walls without openings by Polensek were used to verify the detailed model (Polensek, 1975). Next, an equivalent model was developed in order to minimize the degrees of freedom while retaining the response of the detailed model under axial, transversal, and lateral loading. The degrees of freedom associated with the equivalent model were global degrees of freedom corresponding to geometrical locations in a real structure (Figure 2.41). The equivalent model had only 55 elements compared to over 2500 in the detailed model.

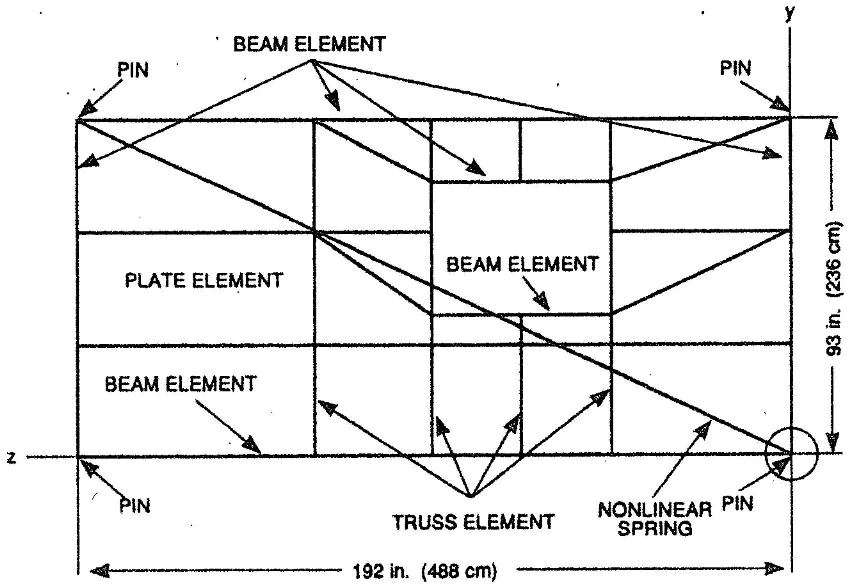

Figure 2.41. Finite element mesh of equivalent wall model (Kasal and Leichti, 1992).

2.11 PREVIOUS FULL-SCALE WALL TESTING

It is clear from section 2.5 that there has been extensive research conducted on the effects of composite member properties as they relate to wood-frame diaphragms. Most of this research has been compared with tests on single composite members, which represent the individual load resisting elements in a diaphragm, or with tests on full-scale floor diaphragms. Very few studies have conducted tests on full-scale wall specimens loaded under axial loads, representing the loads transmitted through a wall from the floors and roof of a structure, and transversal loads, representing loads due to wind pressure and suction on the face of a wall. Three test programs that have looked at this combination of loads on regular wood-frame walls will now be presented.

2.11.1 Polensek

The finite element program FINWALL, described in section 2.10.1, was verified against full-scale wall tests conducted by the author of the program at the Forest Research Laboratory at Oregon State University (Polensek, 1976b). The walls were loaded both axially and in the transversal direction (Figure 2.42). The transversal load was applied by using an inflated plastic bag to simulate a uniformly distributed load on the wall. The axial load was applied eccentrically to the top of the wall by a cantilevered weight on a steel roller.

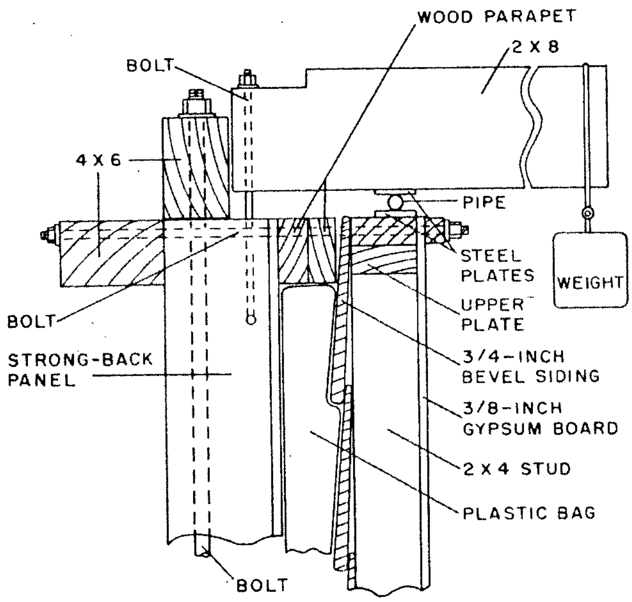

Figure 2.42. Wall test arrangement for tests by Polensek (Polensek and Atherton, 1976).

Although only four walls in total were constructed and tested in this study, tests on each component of the walls were also conducted in order to increase the accuracy of the analytical models. The modulus of elasticity of each stud was determined by non-destructive testing. Samples of all sheathing materials were tested to determine axial and bending moduli of elasticity. Double shear connection specimens were tested to determine the stiffness of one-nail joints. And finally, fifteen I-beams representing the composite load-resisting members in the walls were tested. Because of the detailed knowledge of the properties of each component of the walls tested, the analytical models accurately predicted their response.

2.11.2 Gromala

Ten full-scale walls with varied wall sheathing and stud spacing were tested by Gromala (1983) as part of the light-frame construction research program initiated at the Forest Products Laboratory in Madison, Wisconsin (Hans et. al., 1977). The goal of the study was to accurately predict the response of these walls. FINWALL was once again used for this purpose. The test set-up was very similar to one described in the previous section (Figure 2.43 and Figure 2.44). Once again, the axial load was applied eccentrically. In addition, the properties

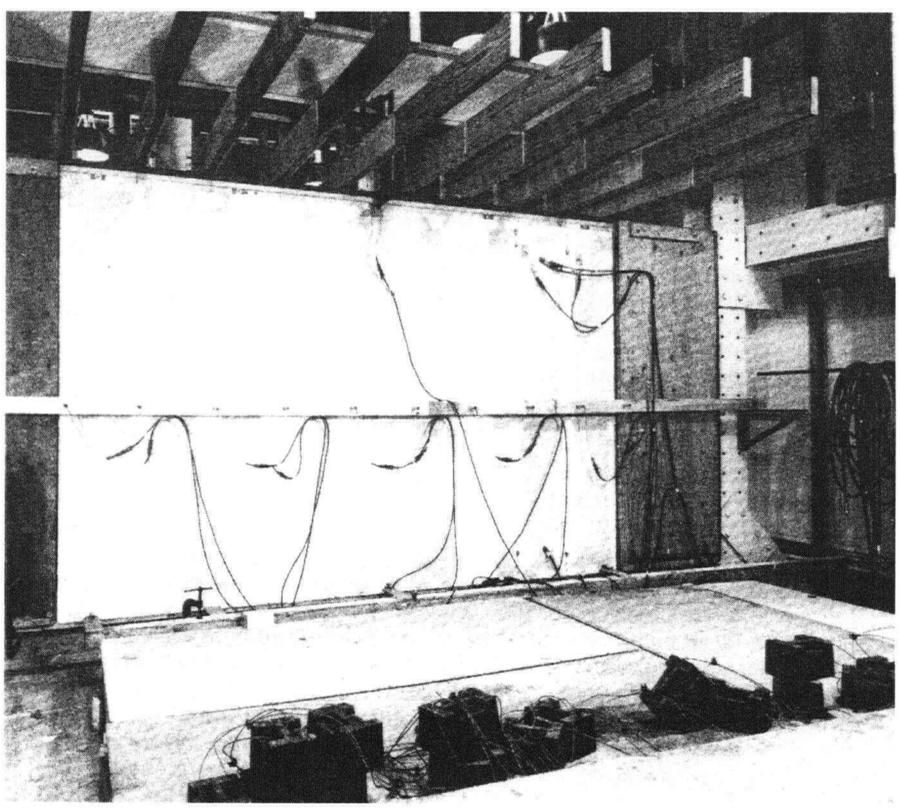

Figure 2.43. Photo of the overall test set-up (Gromala, 1983).

of all of the studs, sheathing materials, and connection configurations were determined as input values for the computer program. For some of the walls, internal deflection transducers were placed inside the wall to measure the slippage between the sheathing and the studs.

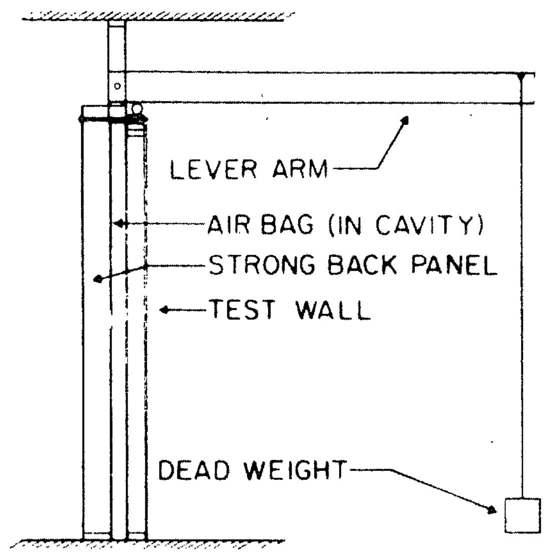

Figure 2.44. Schematic of the test set-up (Gromala, 1983).

The predictions of deflection by FINWALL were on average 6% higher than test values. Predictions for wall strength were not as accurate and proved to be very sensitive to the material properties used as input. Of significance to this study was the recommendation with respect to the effect of the test set-up. It was determined that the negative stud deflections induced by the applied eccentric axial load were sometimes not overcome until the application of a large transversal load. It was concluded that large axial loads might not be present in an actual structure when design-level transversal loads are present and so the 'reinforcing' effect of the eccentric load was deemed to be unrealistic. Therefore, the author recommended that future wall testing should not include an eccentric load that reinforces the wall.

2.11.3 Stefanescu et. al.

The finite element program PANEL, discussed in section 2.10.3, was verified with tests conducted on four walls at Clemsen University in South Carolina (Stefanescu et al., 2000). The walls had varied stud depth and nail spacing and were sheathed on both sides. The transversal loads were applied by inflating air bags. Hydraulic jacks just below the bottom beam applied the axial loads (Figure 2.45 and Figure 2.46). The properties of the studs, sheathing, and nailed connections were all determined prior to testing the full-scale walls. The walls were rotated 180 degrees about the middle stud between each of the four loading cycles to simulate both wind pressure and suction.

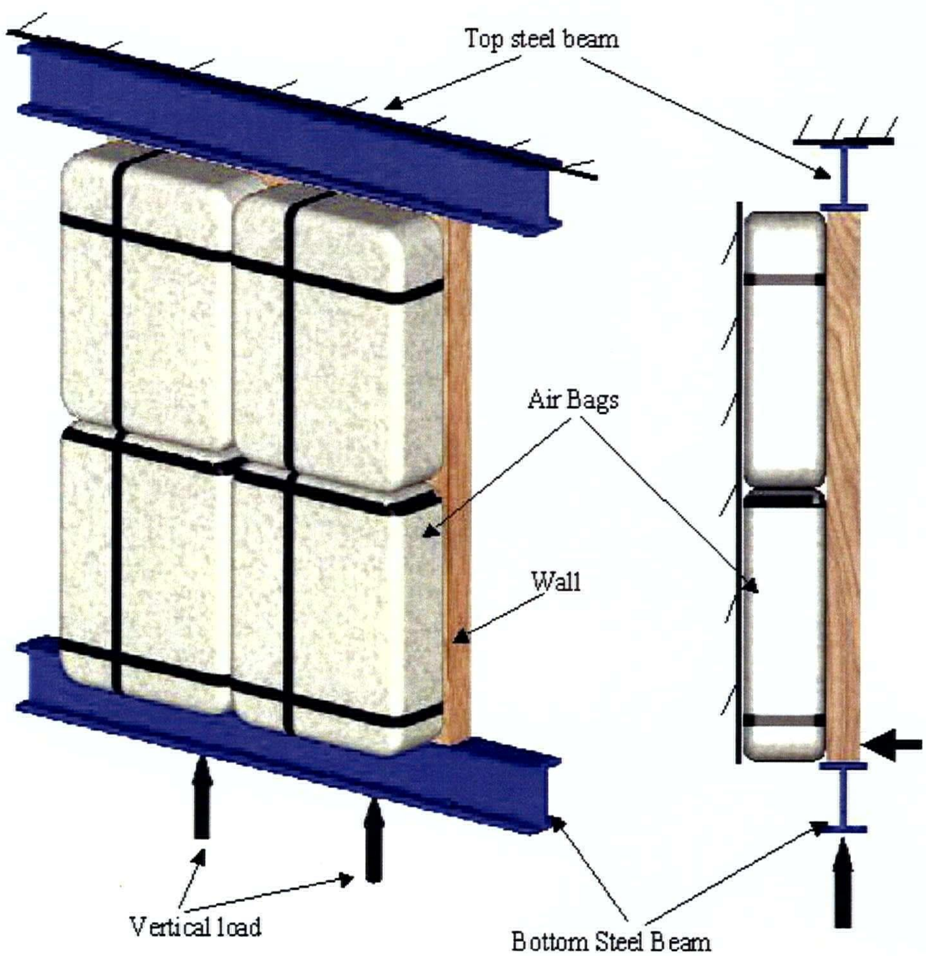

Figure 2.45. Schematic of the wall test set-up (Stefanescu et. al., 2000).

The end conditions affected the results of the analytical predictions for this study as well. The top steel beam was fixed on the columns of the testing frame while the bottom steel beam was free to rotate and move vertically. This caused partial fixity at the top of the wall. PANEL does not have the capability to apply partial fixity to the end reactions of a wall model by applying rotational springs and so two models were used to predict the response of each wall test: one assuming the top of the wall was fully fixed and one assuming it was free to rotate. It was concluded that the boundary conditions had less of an effect on the walls with deeper studs.

Figure 2.46. Photo of the wall test set-up described by Stefanescu et. al. (2000).

Because the experimental results fell in between the predictions using the two end reaction assumptions, it was concluded that the model was in good agreement with the test results. In addition, the comparisons between the predicted and experimental deflections may have been affected by the use of the average modulus of elasticity of all the studs tested for each stud in the models. This indirectly increased the transverse (in-plane) stiffness of the wall models by assuming that the stiffness of the studs along the length of the wall was uniform.

3. CONNECTION LOAD-SLIP TESTS

One of the most important parameters to quantify when attempting to calculate the amount of partial composite action between the studs and the sheathing of a wood frame wall is the connection stiffness. If this connection is glued then it can be assumed that the interface is fully rigid and the stiffness is infinite. If the sheathing is connected to the studs with mechanical fasteners, however, then the connection has a finite stiffness that can vary depending on the load level applied to it and the number of previous load cycles it has undergone. The most common mechanical fastener used to connect sheathing to studs in North America is the nail. Numerous studies have looked at the load-deformation, or load-slip, properties of sheathing-to-stud connections with a variety of nail types and sizes as well as sheathing and stud types. The tall walls in this study, and walls that have recently been designed in practice, have been constructed using combinations of nails, studs, and sheathing that have not previously been studied, which necessitate the testing of these particular combinations. Only monotonic testing was done because this study is concerned with the response of tall wood-frame walls under quasi-static axial and transversal loads as imposed by dead, live, and wind loads. Wind loads are here considered quasi-static, as it is commonly done in practice, although it could be argued that they should be treated as dynamic loads. The term monotonic indicates that the loads are applied in one direction only and at rates slow enough so that the material strain rate effects do not influence the results.

The findings from monotonic tests to determine the load-deformation response of connections associated with tall wood-frame walls are presented in this chapter. The load-deformation tests represent the first part of the experimental program presented in this thesis. The rest of the experimental program, which includes withdrawal connection tests, composite T-beam tests, shearwall tests to examine sheathing buckling, and full-scale tall wall tests are presented in the subsequent chapters.

3.1 OBJECTIVES AND SCOPE

The stiffness and load-deformation response of wood-frame walls under wind loading is influenced by the amount of composite action between the sheathing and the studs. Since in wood construction the sheathing is most commonly connected to the studs by nails, the first part of the experimental program was focused on determining the stiffness of these connections along with their associated failure modes. Once this information is known, analytical models for predicting the connection response can be developed and calibrated and further models can be used to predict the response of composite members and full-scale walls. Displacement controlled monotonic tests were conducted on several connections with different stud material, sheathing material, and nail sizes. The monotonic load-deformation connection tests were conducted in the Wood Engineering Laboratory of Forintek Canada Corp. in Vancouver.

3.2 METHODS AND MATERIALS

3.2.1 Connection Specimens

A large number of connection specimens, over 270, were tested in order to build a database of connection properties that is representative of the most common combinations of nails, sheathing, and stud types that are, or could be, used in wood tall wall construction. Only a few of these connection results have been used to predict the response of the component and full-scale tests described in subsequent chapters. The database, however, can now be drawn upon to provide stiffness values for tall wall response predictions not tested in this study, and in doing so determine the most efficient use of materials. Because of the large number of nails employed in connecting the sheathing to the studs in wall construction, the average nail properties are typically of interest to the designer, rather than the values at the tail ends of the distribution curve. Therefore, only five replicates of each specimen type were initially tested to determine a reasonable average response. For each test group, the variation of results within the group was quantified and additional replicates were tested if it was deemed that the variation was too high. This will be discussed further in this chapter.

Tall walls require a significant number of nails to be used to connect the sheathing to the studs during construction. For this reason, nails guns are almost always used for the task of connecting the two components. The most common type of nail currently being used in nail guns is the spiral nail. It is for this reason that spiral nails were used to connect the sheathing to the stud material in this test program. A typical connection test specimen is shown in Figure 3.1. As can be seen, the nailed connection is loaded in single shear. Three spiral nail lengths were used, namely 65 mm (2 ½"), 76 mm (3"), and 102 mm (4") as shown in Figure 3.2. The connection test matrix is shown in Table 3.1. The three nail lengths corresponded to the sheathing thickness they were connecting to, so that an appropriate embedment length, approximately 50 mm (2"), into the stud was left for each test.

Four stud materials were chosen for the load-slip connection testing: spruce-pine-fir No. 2 or better (SPF), laminated veneer lumber (LVL), laminated strand lumber (LSL), and SPF glued laminated lumber (glulam). The stud members were 38 by 76 mm (1-½" x 3") in cross section. The sheathing material corresponding to each stud consisted of five thicknesses of Canadian softwood plywood (CSP) and five thicknesses of oriented strandboard (OSB). The sheathing material was tested both parallel and perpendicular to the strong axis since sheathing in common construction practice can be installed with the strong axis being either vertical or horizontal. The

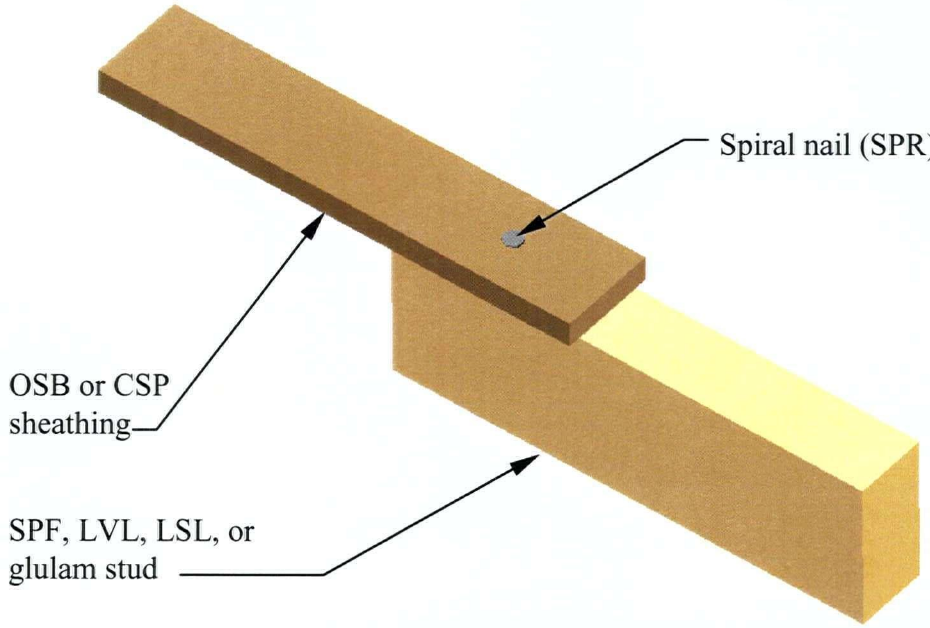

Figure 3.1. Typical detail of a nailed stud-to-sheathing connection.

results from previous load-slip tests on connections with nails have shown that the differences between connections tested with the stud strong direction parallel to the direction of loading and perpendicular to the direction of loading are within the margin of error (Jenkins et. al, 1979). Furthermore, because this study is primarily concerned with the response of tall wood-frame walls under axial and transversal, or out-of-plane, loading and not racking, the slippage between

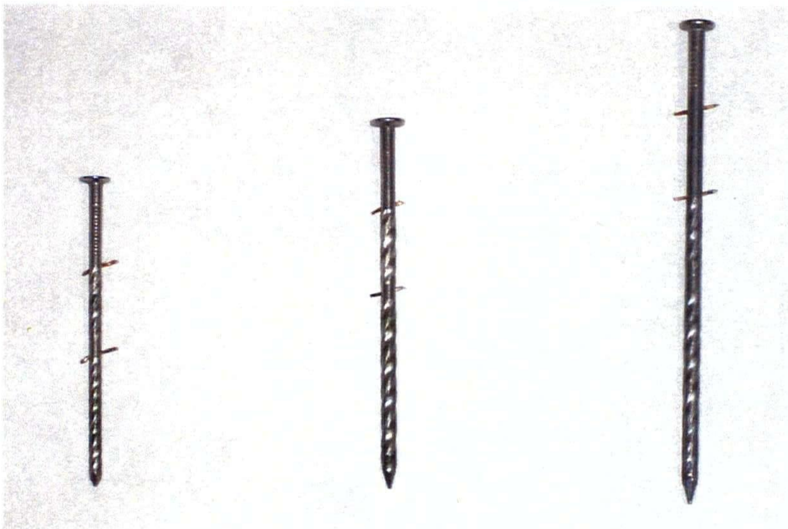

Figure 3.2. Spiral nail lengths used in connection testing.

Table 3.1. Connection load-slip test matrix

Specimen Group Number	Nail Length (mm)	Sheathing Material	Sheathing Orientation	Stud Member Material	Specimen Group Number	Nail Length (mm)	Sheathing Material	Sheathing Orientation	Stud Member Material
001	65	9.5 CSP	PAR	SPF	026	65	18.5 CSP	PAR	LSL
002	65	15.5 CSP	PAR	SPF	027	76	28.5 CSP	PAR	LSL
003	65	18.5 CSP	PAR	SPF	051	102	28.5 CSP	PAR	LSL
049	102	28.5 CSP	PAR	SPF	028	65	9.5 OSB	PAR	LSL
004	65	9.5 OSB	PAR	SPF	053	65	15.5 OSB	PAR	LSL
005	65	15.5 OSB	PAR	SPF	029	65	18.5 OSB	PAR	LSL
006	65	18.5 OSB	PAR	SPF	030	76	28.5 OSB	PAR	LSL
050	102	28.5 OSB	PAR	SPF	052	102	28.5 OSB	PAR	LSL
007	65	9.5 CSP	PERP	SPF	031	65	9.5 CSP	PERP	LSL
008	65	15.5 CSP	PERP	SPF	032	65	18.5 CSP	PERP	LSL
009	65	18.5 CSP	PERP	SPF	033	76	28.5 CSP	PERP	LSL
010	65	9.5 OSB	PERP	SPF	034	65	9.5 OSB	PERP	LSL
011	65	15.5 OSB	PERP	SPF	035	65	18.5 OSB	PERP	LSL
012	65	18.5 OSB	PERP	SPF	036	76	28.5 OSB	PERP	LSL
013	65	12.5 CSP	PAR	LVL	037	65	9.5 CSP	PAR	Glulam
014	65	18.5 CSP	PAR	LVL	038	65	18.5 CSP	PAR	Glulam
015	76	28.5 CSP	PAR	LVL	039	76	28.5 CSP	PAR	Glulam
016	65	12.5 OSB	PAR	LVL	040	65	9.5 OSB	PAR	Glulam
017	65	18.5 OSB	PAR	LVL	041	65	18.5 OSB	PAR	Glulam
018	76	28.5 OSB	PAR	LVL	042	76	28.5 OSB	PAR	Glulam
019	65	12.5 CSP	PERP	LVL	043	65	9.5 CSP	PERP	Glulam
020	65	18.5 CSP	PERP	LVL	044	65	18.5 CSP	PERP	Glulam
021	76	28.5 CSP	PERP	LVL	045	76	28.5 CSP	PERP	Glulam
022	65	12.5 OSB	PERP	LVL	046	65	9.5 OSB	PERP	Glulam
023	65	18.5 OSB	PERP	LVL	047	65	18.5 OSB	PERP	Glulam
024	76	28.5 OSB	PERP	LVL	048	76	28.5 OSB	PERP	Glulam
025	65	9.5 CSP	PAR	LSL					

the sheathing and the stud occurs along the stud length and not around the entire panel. It is for these reasons that tests were not conducted with the stud material strong direction perpendicular to the direction of loading.

The nailed connections were fabricated by hand using a hammer, since the nails could be more accurately placed when using a hammer rather than a nail gun. The LSL studs required that the nails be hammered into pre-drilled holes equal to 70% of the nail diameter in order to avoid bending of the nail. The Canadian Wood Design Code, CSA O86 (CSA, 2001), recommends that a pre-drilled hole be up to 75% of the nail diameter to avoid failure in the connection when placing the nail. All material used for testing was dry and had been stored in a laboratory environment at an average temperature of 20° ± 3°C and relative humidity of 60% ± 10% for at least one week. The LSL prisms were cut from larger specimens left over from previous testing that had been stored in the laboratory for at least six months. In accordance with the testing standard used, ASTM D 1761 (ASTM, 1995), the specimens were tested within one hour after assembly and not conditioned in the laboratory environment for an extended period of time to allow for the relaxation of the wood fibres around the nails.

3.2.2 Testing Apparatus and Instrumentation

A photo of the set-up is shown in Figure 3.3 and a schematic of the test set-up for the load-slip connection tests is shown in Figure 3.4. Each component of the connected specimen, the stud and the sheathing, were approximately 250 mm (10") in length, while the overall specimen length was approximately 400 mm (16"). Each end of the specimen was connected to the testing apparatus by friction using steel clamping plates and bolts. The bolts were tightened by hand so that the bolt was turned one full revolution after the plates were snug. The collars at the base were not placed directly adjacent to the clamping plate connector so that the specimen could rotate in two principal directions. The top of the specimen was only free to rotate in one principal direction.

Three data measurements were collected during the tests: applied load; movement of the actuator head (stroke); and the relative displacement of the stud with respect to the sheathing. The loading was unidirectional and downwards, or in compression, at a rate of 12.7 mm (1") per minute. Two load cells were used over the course of the testing program with 89 kN (20,000 lb.) and 22 kN (5,000 lb.) capacities. They were attached to a 222 kN (50,000 lb.) universal testing machine that delivered the load. Connection slip was measured using a displacement transducer (DCDT) that had a total displacement measuring range of 76 mm (3"). The transducer was connected to the stud by way of a mounting bracket that was in turn connected to the clamping plate. An angle bracket screwed to the sheathing provided a resting place for the extending end of the transducer. Data was acquired using Forintek's data acquisition software on a personal computer and was analysed using a commercial spreadsheet software package.

Figure 3.3. Photo of the test set-up for determining the load-slip properties of stud-to-sheathing connections.

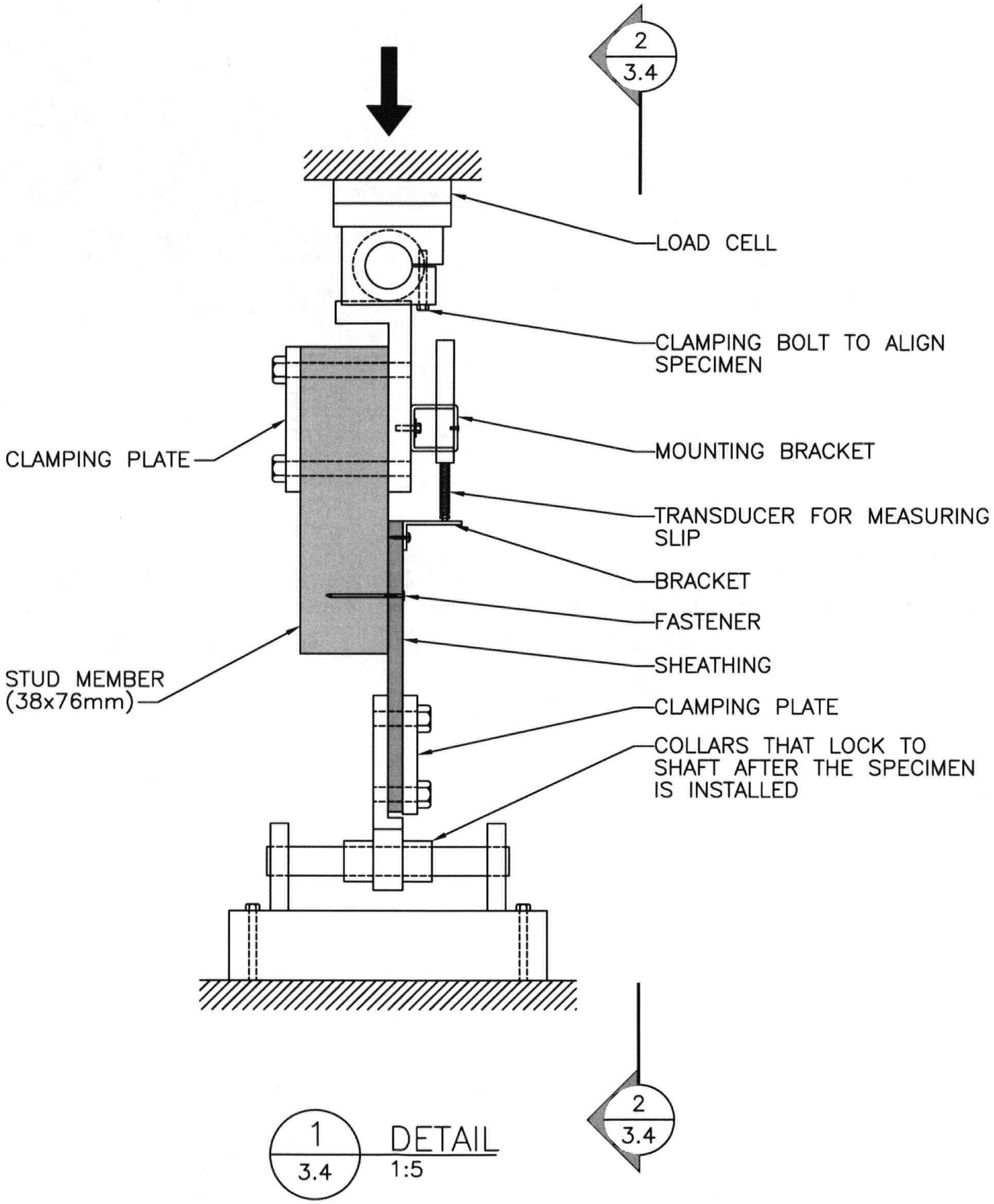

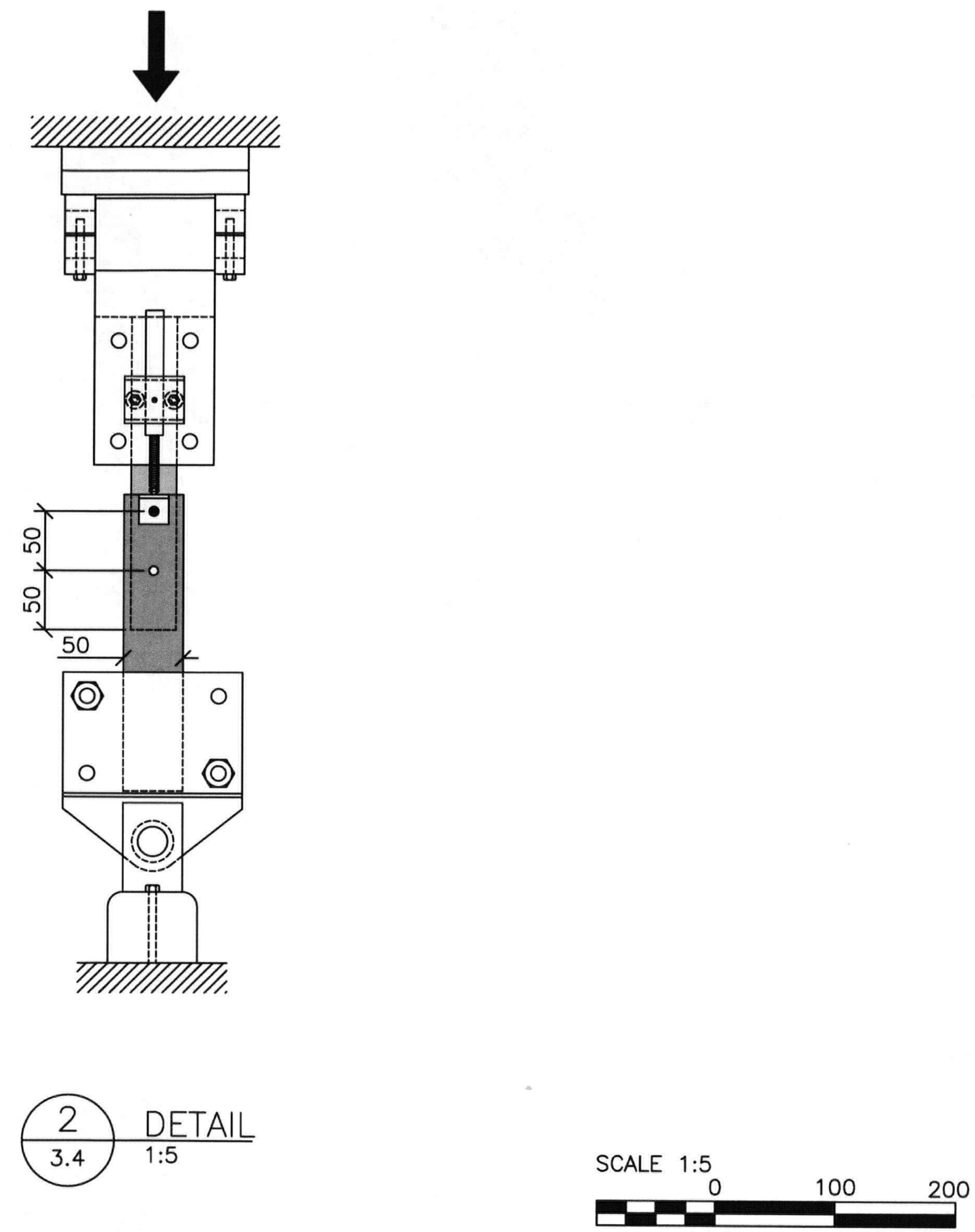

Forintek Canada Corp.	TALL WALL STRUCTURAL PERFORMANCE	DRAWN DEL	DATE OCT–04
		SCALE AS SHOWN	APPROVED
	SCHEMATIC OF LOAD–SLIP TEST SET–UP	DRAWING NUMBER FIG 3.4	REVISION PROJECT REF. 3910

3.2.3 Material Properties

Random samples of each of the tested materials were taken after testing was completed to determine their relative densities. From previously conducted tests on similar material specimens it was known that the material had a moisture content of approximately 5%. The average relative densities of the specimen materials are shown in Figure 3.5.

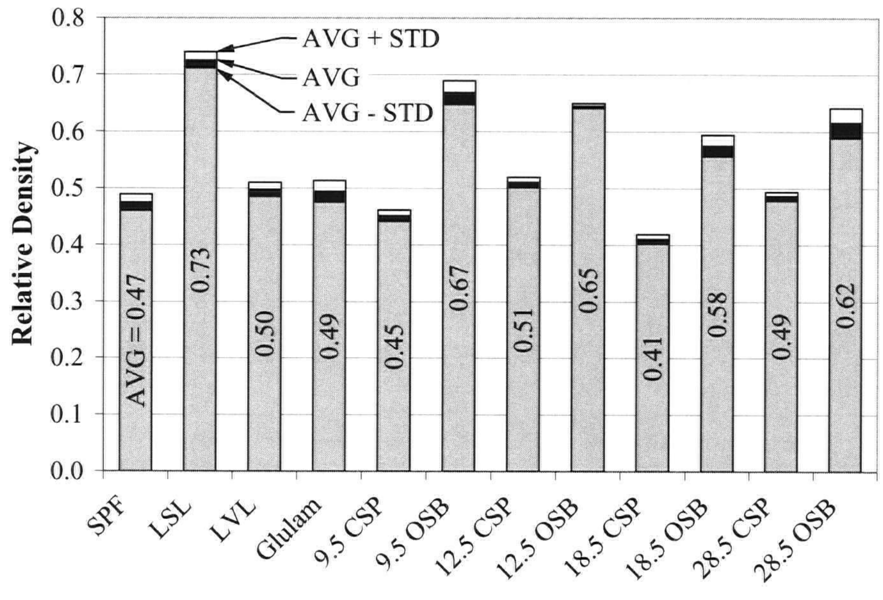

Figure 3.5. Relative wood densities of specimen materials.

Three of the stud materials that were used (Figure 3.6) are proprietary products that will be described in greater detail. Tembec Inc. of Ville-Marie, Quebec, manufactured the laminated veneer lumber that was used (Figure 3.6 (a)). The trade name of the product is SlecTem® LVL and this particular product was manufactured by laminating 3.2 mm thick veneers of aspen with the grain of the veneers orientated along the length of the member. The layers of veneer are bonded with an exterior-type adhesive (phenol-formaldehyde) and hot pressed under a specified time, pressure, and temperature cycle. Scarf joints are used to join shorter pieces along the length of the member and these joints are staggered between adjacent layers.

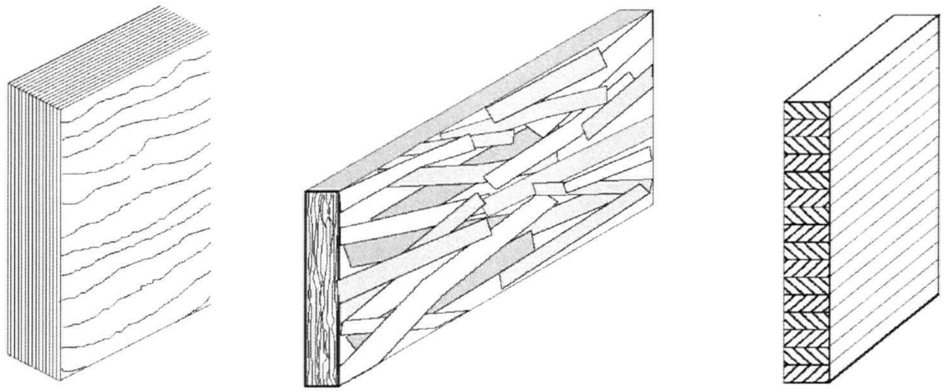

(a) (b) (c)

Figure 3.6. Proprietary products used in testing: (a) LVL, (b) LSL, (c) Glulam.

Trus Joist, a Weyerhaeuser business out of Boise, Idaho manufactured the laminated strand lumber used in testing, which has the trade name TimberStrand® LSL (Figure 3.6 (b)). This product is manufactured by blending wood species or species combinations oriented in a predominantly parallel direction with an isocyanate-based adhesive into formed mats of various thicknesses. A steam injection press is then used to press the mats to the required thickness.

Western Archrib, based in Edmonton, Alberta, manufactured the glued laminated lumber used in testing (Figure 3.6 (c)). The trade name for this product is Westlam® Structural Lumber (WSL) and it is constructed of western spruce and lodgepole pine boards. The grain of each 19 mm thick board is running mainly parallel to the length of the member. The boards are bonded together with an exterior-type phenol-resorcinol adhesive. End joints within each layer may be either a finger joint or a scarf joint.

The bending characteristics of the spiral nails used were also sought in order to predict ultimate load carrying capacities of the specimens tested and the corresponding failure modes. The nails were tested in the test apparatus that is shown in Figure 3.7 along with the test set-up. The apparatus is based on a fastener bending prototype developed in the Timber Engineering Laboratory of the University of Karlsruhe (Ehlbeck et. al., 1990). The fastener is placed into a fixing device and bent directly by hand and the applied loads as well as the bending angle are recorded.

A description of the nails and the average results from testing are shown in Table 3.2. Ten replicates of each of the three spiral nail lengths were tested. The load-deformation relationships in bending of each of the replicates are shown in Figure 3.8 along with the failure modes of the 102 mm long nails tested. Most of the nails had to be bent back to their starting position and thus do not show a significant bend. There are several definitions of yield moment depending upon which standard is being referenced. As will be described later in this chapter, the method presented in Eurocode 5 was used to characterize the load-slip response of the connections tested (ENV 1995-1-1, 1993). For this method, yield moment of a nail is defined as the smaller value of the maximum bending moment and the moment at a deformation of 45 degrees. This is how the yield moment values in Table 3.2 were determined. The Eurocode 5 methodology is less conservative than the method employed in the United States, which uses a 5% diameter offset from the initial stiffness to determine yield strength, but it contains a large adjustment factor to account for the variability.

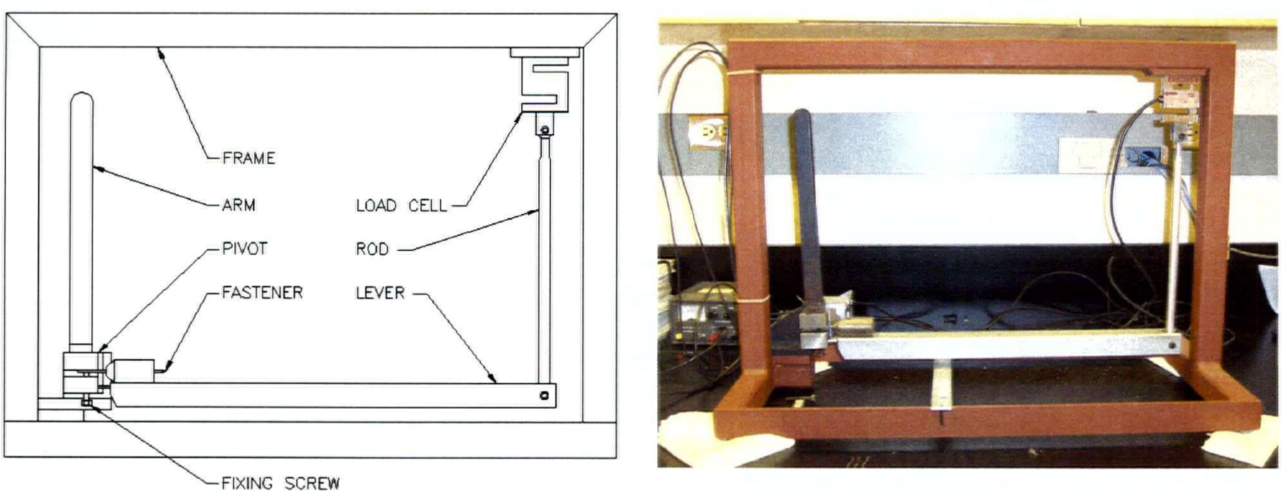

(a) (b)

Figure 3.7. Fastener bending (a) test apparatus and (b) test set-up.

Table 3.2. Average nail bending properties obtained from testing.

Specimen Group Number	Number of Specimens	Nail Length (mm)	Nail Diameter (mm)	Yield Moment of Nail (Nmm)	Coefficient of Variation (%)	Calculated Yield Stress (MPa)	Design Yield Moment (Eurocode 5)	Overstrength (Test/Design)
601	10	65	2.46	2437	6.18	982	1869	1.30
602	10	76	2.99	4257	5.32	955	3105	1.37
603	10	102	3.27	5666	1.79	972	3918	1.45

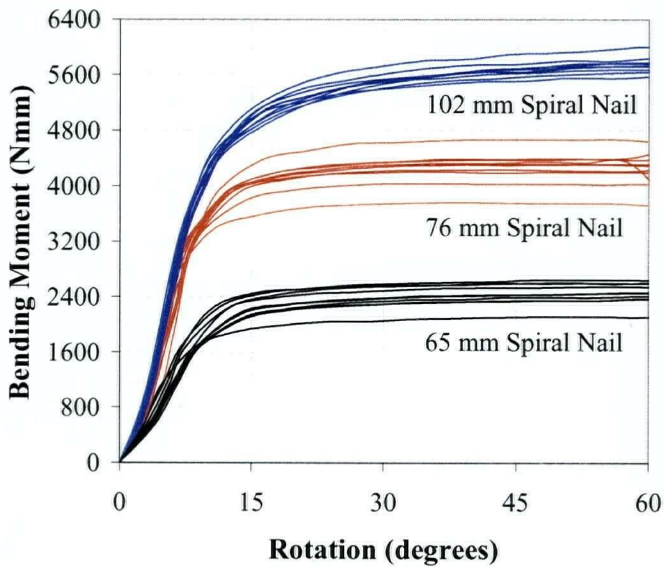

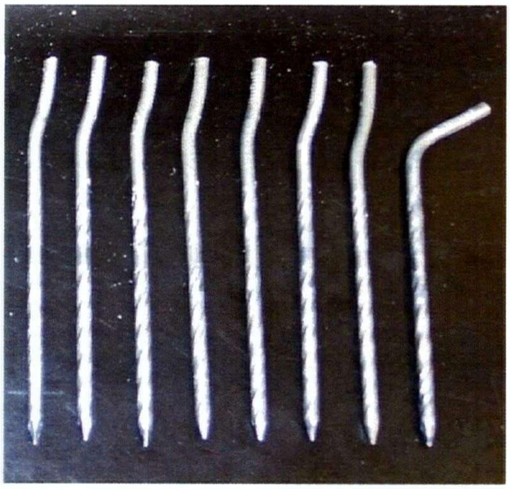

(a) (b)

Figure 3.8. (a) Load-deformation curves and (b) failure modes of spiral nails in bending.

The yield stress in Table 3.2 was calculated using the plastic section modulus and is given by the following equation:

$$\sigma_y = \frac{6 \cdot M_y}{d^3}, \tag{3.1}$$

where d is the diameter of the nail. The characteristic yield moment in Table 3.2, as defined in Eurocode 5, is as follows:

$$M_y = 180d^{2.6}. \tag{3.2}$$

3.3 RESULTS AND DISCUSSION

As mentioned previously, the purpose of conducting numerous load-slip connection tests was to build a database of values in order to interpret component and full-scale tests that were conducted later in this study. Therefore this section will not closely examine each and every connection group tested. Plots of all load-slip tests conducted are provided in Appendix A. This section will, however, provide results and illustrate general trends that were observed.

3.3.1 Connection Properties

A typical load-deformation curve obtained from monotonic compression tests on the nail connections is presented in Figure 3.9. Included in the figure are the average value of the replicates tested, the average value plus and minus the standard deviation of the replicates, and the coefficient of variation of the replicates of one test group. If the coefficient of variation obtained was higher than a reasonable value for this type of testing (in this case assumed at approximately 30 %) then additional replicates were tested so that the coefficient of variation

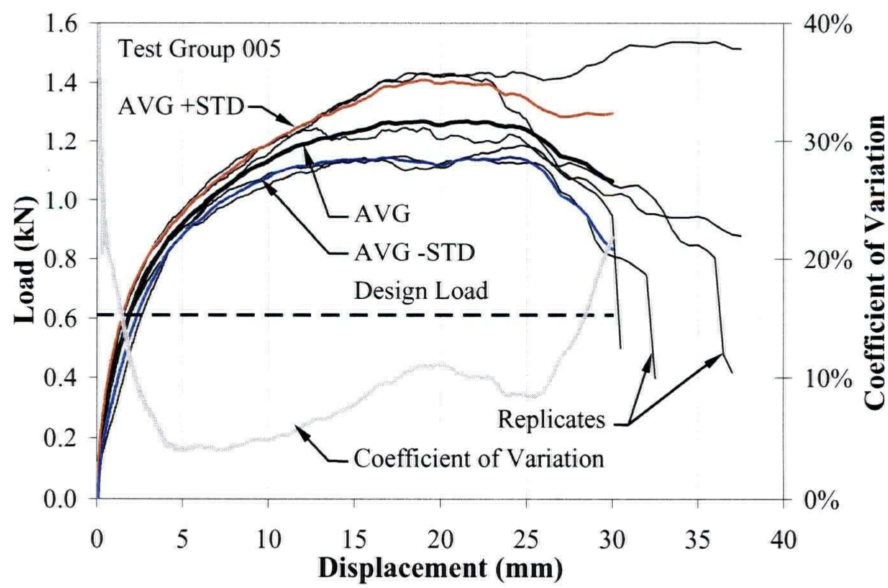

Figure 3.9. Typical connection load-slip results.

could be reduced. This was only necessary for one test group (023). In general, the coefficient of variation was below 20%. It was also found to increase with decreasing nail embedment length. This will be discussed further in the next chapter on nail withdrawal testing.

Average properties such as initial stiffness, ultimate load, yield load, ultimate displacement, and overstrength determined from each test group are presented in Table 3.3. The most important

Table 3.3. Average connection properties obtained from tests.

Specimen Group Number	Number of Specimens	Stud Member Material	Sheathing Thickness (mm)	Yield Load F_y (kN)	Yield Displacement Δ_y (mm)	Maximum Load F_{max} (kN)	Displacement at F_{max} (mm)	Ultimate Displacement Δ_u (mm)	Initial Stiffness (N/mm)	Ductility (Δ_u / Δ_y)	Overstrength (F_{max} / F_{design})
001	5	SPF	9.5	0.781	4.04	1.111	18.40	24.20	224	5.99	2.71
002	5	SPF	15.5	0.714	3.48	1.270	27.00	30.50	225	8.76	2.75
003	5	SPF	18.5	0.619	1.64	1.238	19.40	28.00	389	17.07	2.45
049	5	SPF	28.5	1.307	2.64	2.477	22.20	33.00	526	12.50	2.62
004	5	SPF	9.5	0.745	2.10	1.403	15.00	24.40	361	11.62	2.96
005	5	SPF	15.5	0.672	2.30	1.270	19.00	30.50	300	13.26	2.30
006	6	SPF	18.5	0.601	1.72	1.169	20.60	31.00	369	18.02	2.02
050	5	SPF	28.5	1.166	1.30	2.530	19.40	31.50	954	24.23	2.56
007	5	SPF	9.5	0.643	3.14	1.165	14.60	18.40	232	5.86	2.85
008	5	SPF	15.5	0.545	2.70	1.063	18.60	33.00	229	12.22	2.30
009	5	SPF	18.5	0.578	2.72	1.108	21.80	35.00	235	12.87	2.19
010	5	SPF	9.5	0.686	2.62	1.165	12.10	23.60	287	9.01	2.45
011	6	SPF	15.5	0.623	1.48	1.248	16.40	26.00	475	17.57	2.26
012	5	SPF	18.5	0.526	1.06	1.044	15.80	26.00	567	24.53	1.80
013	5	LVL	12.5	0.732	4.42	1.232	19.60	25.00	195	5.66	2.60
014	5	LVL	18.5	0.841	5.40	1.557	30.50	35.50	171	6.57	3.05
015	5	LVL	28.5	1.023	2.48	2.123	16.60	37.50	448	15.12	2.64
016	6	LVL	12.5	0.673	2.40	1.259	18.80	36.50	303	15.21	2.38
017	5	LVL	18.5	0.672	3.18	1.395	25.50	37.00	229	11.64	2.37
018	5	LVL	28.5	0.836	1.30	1.890	24.00	37.50	616	28.85	2.24
019	5	LVL	12.5	0.808	4.74	1.441	20.80	35.00	194	7.38	3.04
020	5	LVL	18.5	0.837	5.50	1.550	27.00	37.50	174	6.82	3.04
021	5	LVL	28.5	1.167	3.00	2.492	24.80	38.00	439	12.67	3.10
022	6	LVL	12.5	0.718	2.44	1.383	27.50	38.00	293	15.57	2.61
023	6	LVL	18.5	0.651	2.06	1.415	22.80	34.50	332	16.75	2.41
024	5	LVL	28.5	0.937	1.54	2.155	29.50	41.50	564	26.95	2.56
025	5	LSL	9.5	0.651	3.00	1.177	15.20	17.40	233	5.80	2.62

Table 3.3 Continued. Average connection properties obtained from tests.

Specimen Group Number	Number of Specimens	Stud Member Material	Sheathing Thickness (mm)	Yield Load F_y (kN)	Yield Displacement Δ_y (mm)	Maximum Load F_{max} (kN)	Displacement at F_{max} (mm)	Ultimate Displacement Δ_u (mm)	Initial Stiffness (N/mm)	Ductility (Δ_u / Δ_y)	Overstrength (F_{max} / F_{design})
026	5	LSL	18.5	0.759	2.94	1.427	17.60	22.00	264	7.48	2.61
027	5	LSL	28.5	1.557	3.06	3.324	21.80	30.00	556	9.80	3.75
051	5	LSL	28.5	1.670	3.14	3.597	24.40	34.50	557	10.99	3.41
028	5	LSL	9.5	0.863	2.08	1.768	15.00	17.80	437	8.56	3.35
053	6	LSL	15.5	0.890	2.22	1.773	13.80	22.80	419	10.27	2.93
029	5	LSL	18.5	0.766	1.30	1.739	14.70	21.60	579	16.62	2.66
030	5	LSL	28.5	1.379	1.64	3.064	17.40	25.50	869	15.55	3.26
052	5	LSL	28.5	1.294	1.26	2.782	14.10	21.40	1076	16.98	2.49
031	5	LSL	9.5	0.698	1.88	1.399	10.40	13.20	436	7.02	3.11
032	5	LSL	18.5	0.977	4.74	1.685	15.80	23.80	254	5.02	3.09
033	5	LSL	28.5	1.508	2.84	3.314	21.40	29.50	578	10.39	3.74
034	5	LSL	9.5	0.855	2.22	1.558	11.40	15.60	411	7.03	2.95
035	5	LSL	18.5	0.855	1.62	1.945	18.00	22.40	522	13.83	2.97
036	5	LSL	28.5	1.404	1.44	3.114	16.00	24.40	1036	16.94	3.31
037	5	GLU	9.5	0.626	1.76	1.127	22.60	25.50	358	14.49	2.73
038	5	GLU	18.5	0.704	2.78	1.445	22.00	27.50	268	9.89	2.83
039	5	GLU	28.5	0.956	1.66	2.098	20.60	39.00	591	23.49	2.62
040	5	GLU	9.5	0.615	1.82	1.221	16.20	28.50	367	15.66	2.55
041	5	GLU	18.5	0.604	1.14	1.329	19.20	34.50	491	30.26	2.26
042	5	GLU	28.5	0.860	1.70	1.836	19.40	39.00	531	22.94	2.18
043	5	GLU	9.5	0.713	2.02	1.392	14.30	21.00	377	10.40	3.37
044	5	GLU	18.5	0.624	1.80	1.365	19.20	34.50	359	19.17	2.68
045	5	GLU	28.5	0.901	1.48	1.985	18.20	38.00	625	25.68	2.47
046	5	GLU	9.5	0.773	3.56	1.403	18.20	23.60	228	6.63	2.92
047	5	GLU	18.5	0.588	0.86	1.357	23.00	34.50	690	40.12	2.31
048	5	GLU	28.5	0.903	1.58	1.926	17.80	34.00	618	21.52	2.29

parameter obtained from the test data is the initial stiffness because the displacements between the sheathing and the studs along the height of the studs in tall walls are relatively small. The procedure described in the European CEN protocol (CEN, 1995) was used to calculate the properties given in Table 3.3. The load-slip relationship developed by Foschi (Foschi, 1974) has been used to more accurately model the connection behaviour using finite element analysis in subsequent chapters, but it does not allow for easy comparison between test results. Thus the CEN protocol has been used for such a comparison of the test results. Figure 2.30 in Section 2.7 presented a typical load-deformation curve with the parameters defined by the CEN procedure.

The CEN procedure defines initial stiffness as the slope of the line that connects points on the load-slip curve at 0.1 F_{max} and 0.4 F_{max} respectively. The yield load is the load on the curve that corresponds to the yield displacement, which is defined as the displacement at the interception of the initial stiffness line and a tangent line with stiffness equal to 1/6 of the initial one. The ultimate displacement corresponds to the displacement at which the load drops to 80% of the maximum load. The overstrength factor is a ratio of the maximum load to the design load. The procedure set out in Eurocode 5, based upon a theory developed by Johansen for joints made with dowel-type fasteners in single shear, was used to calculate the design load. The member density values and nail bending strengths described previously were used in these calculations. The Canadian Wood Design Code was not used because it does not contain a procedure for determining the resistance of nailed connections using proprietary products. As can be seen in Table 3.3, the overstrength factor is quite variable, ranging from 1.80 to 3.75. This large variation in results may be due to the fact that Eurocode 5 only gives one set of equations for the characteristic embedment strength of the stud material based upon testing conducted on sawn lumber. Engineered lumber behaves differently than sawn lumber in many applications and may require alternative approximations for this material property. Additionally, Johansen's yield model does not include pullout or pull-through failures, which were the most common modes of failure observed and will be discussed in detail later in this chapter.

Several different comparisons are made between load-slip tests in Figure 3.10. While not every load-slip curve is shown, the ones that are shown provide insight into general trends that have been observed. The numbers in brackets refer to the specimen group number. The terms SPR

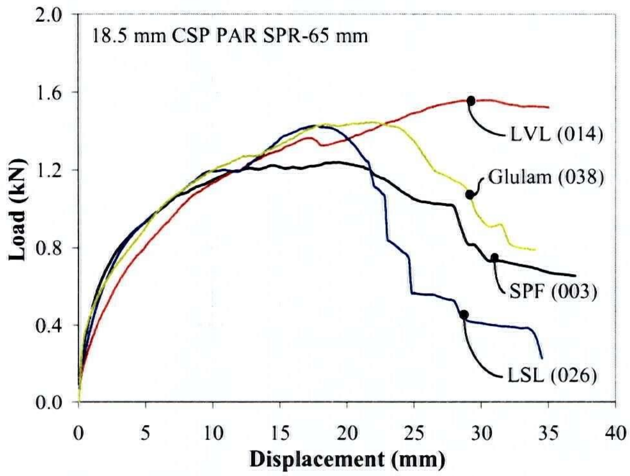

(a) 18.5 mm CSP sheathing

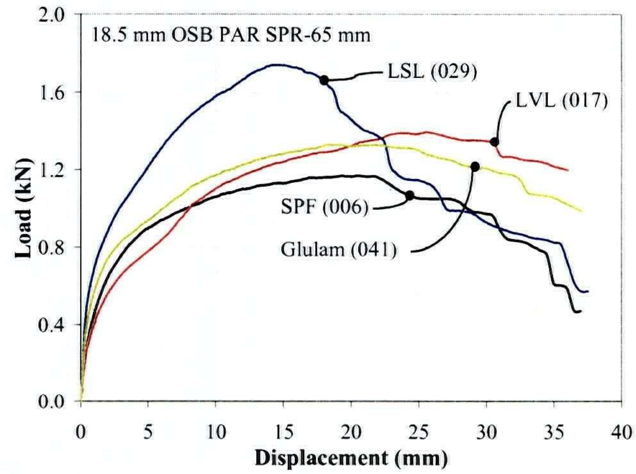

(b) 18.5 mm OSB sheathing

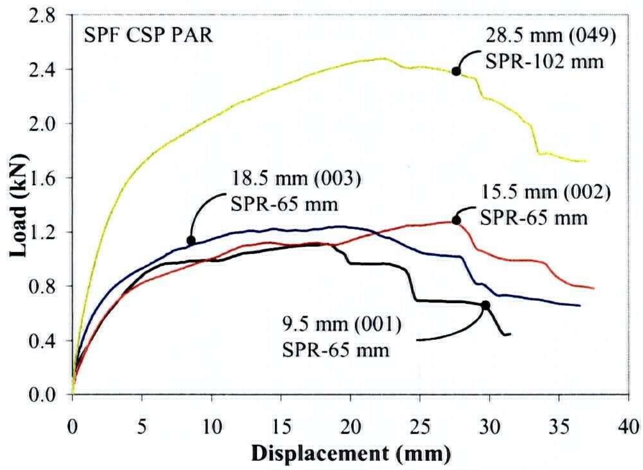

(c) CSP sheathing with SPF studs

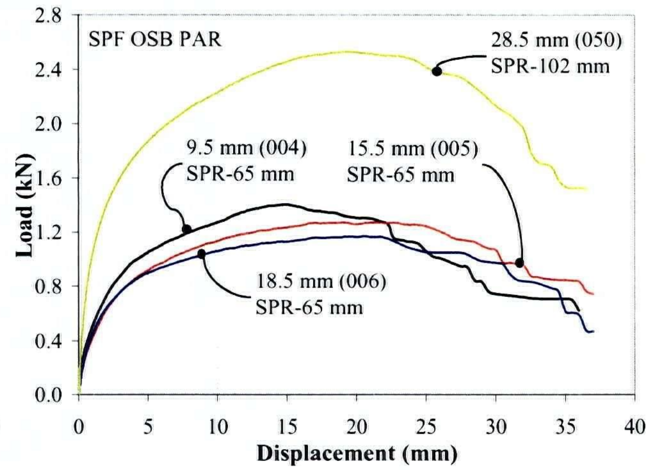

(d) OSB sheathing with SPF studs

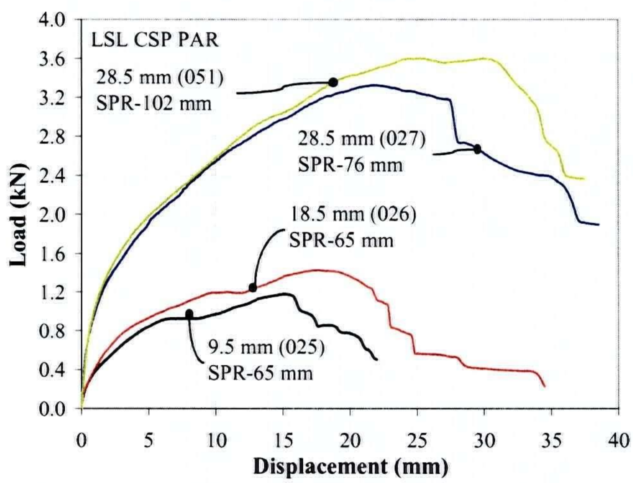

(e) CSP sheathing with LSL studs

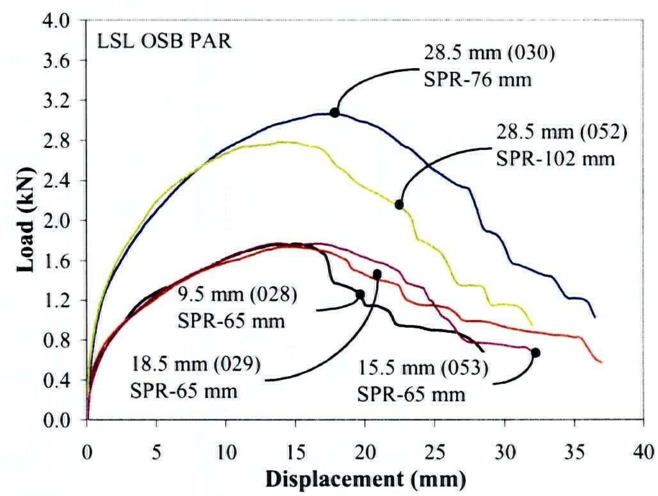

(f) OSB sheathing with LSL studs

Figure 3.10. Load-slip curves from testing.

and PAR refer to spiral nail length and parallel sheathing orientation, respectively. The sheathing thickness is shown either at the top of the graphs or before the specimen group number. In Figure 3.10 (a) the difference between the four stud materials tested for this particular sheathing thickness is very minimal. This can by explained be examining the relative density values of the stud materials and that of the 18.5 mm CSP sheathing given in Figure 3.5. The relative density of the sheathing is, in this case, less than the stud materials so the strength of the connection is governed by the embedment strength of the sheathing alone. This is contrasted with Figure 3.10 (b) where the relative density of the 18.5 mm OSB sheathing is larger than all of the stud materials except the LSL. The strength is once again related to the component with the weakest relative density, in this case the studs, which results in the load-slip response of each of these test groups being more varied than Figure 3.10 (a) because the relative density of the studs are varied.

It is clear from Figures 3.10 (c) and (d) that the strength of these particular connections is directly related to the withdrawal strength of the nail in the stud member. The relative densities of the CSP sheathing and the OSB sheathings are quite different but the average stiffnesses and maximum loads achieved in the connections are approximately the same. The mode of failure that occurred in these connections is characterized by the nail pulling out from the stud. The load-slip response is entirely due to the nail length irrespective of the sheathing type and thickness. This pattern did not emerge in the load-displacement responses of the connections shown in Figures 3.10 (a) and (b) because the sheathing did not consistently have a higher relative density compared with the stud material.

It is more difficult to pinpoint the failure mode of the curves in Figures 3.10 (e) and (f) because, as will be shown in the next chapter, the withdrawal strength of LSL is very high. It is clear that the relative density of the OSB sheathing is sufficiently large enough that the responses of the connections in Figure 3.10 (f) with 65 mm spiral nails are due to the nail and the stud member only because the average stiffnesses and maximum loads achieved by the connections with three different OSB thicknesses are approximately the same. This is in contrast to the connections with 65 mm spiral nails in Figure 3.10 (e) where the response is governed by the sheathing, as the relative density of the CSP is quite low compared to the LSL stud material. The average stiffness and strength of the connection with 18.5 mm CSP sheathing is higher than the connection with 9.5 mm CSP sheathing due to the mode of failure being concentrated in the weak sheathing component.

Two distinct modes of failure are evident from the curves of the load-slip response of 102 mm spiral nails with the LSL stud material with CSP and OSB sheathing. While the withdrawal strength of both of these connections should be approximately equivalent and quite large, the connection with the CSP sheathing produced a larger maximum load. This is due to the fact that OSB sheathing, because of the structure of the material, is more likely to have the nail pull through the sheathing as the mode of failure. In addition, the connection with OSB sheathing, an LSL stud, and a 102 mm long spiral nail was weaker than the same connection with a 76 mm long spiral nail (Figure 3.10 (f)). The longer nail had a higher withdrawal resistance than the shorter one and the sheathing pulled through at a lower lateral load. This pull-through failure will also be described in more detail later in this chapter.

3.3.2 Effect of Sheathing Orientation

As mentioned in this chapter, it has been shown in previous testing that there is very little difference in the load-deformation characteristics of nailed sheathing-to-stud connections having the stud length parallel or perpendicular to the direction of loading. The test results presented in Figures 3.11 (a) to (d) show the difference between the responses of nailed connections with different sheathing orientation, as sheathing can be placed in both the vertical and horizontal direction when constructing walls.

As can be seen from the figure, there is very little difference in the connection properties of sheathing orientated in the strong direction versus the weak, or perpendicular, direction of loading. Any difference that is observable is certainly within the coefficient of variation for

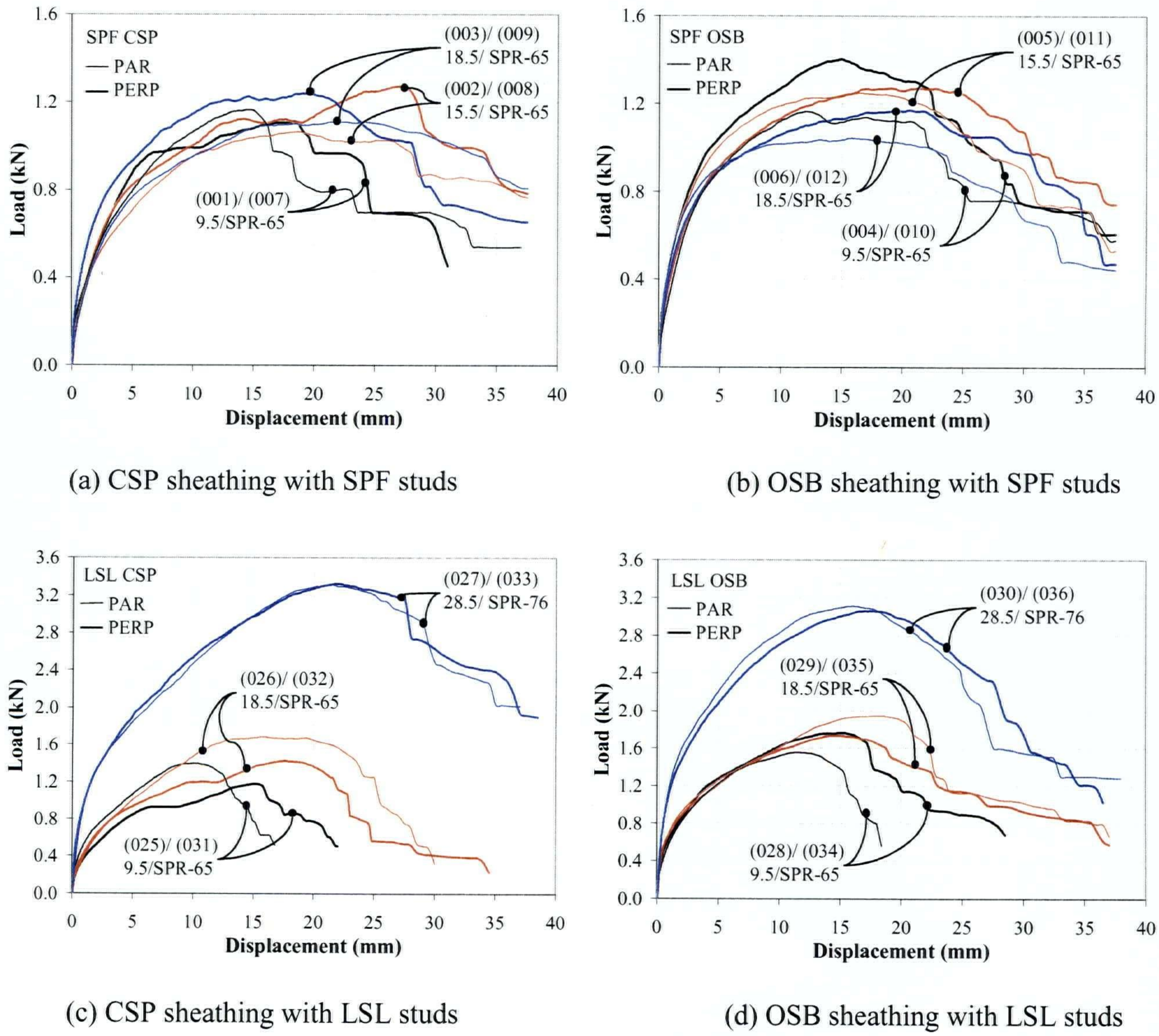

Figure 3.11. Load-slip curves with sheathing parallel and perpendicular.

these tests. This may be due to the modes of failure that were described previously. If the connection failed due to withdrawal of the nail from the stud, or pull-through of the nail through the sheathing, then a change in the sheathing orientation would not produce different results.

3.3.3 Failure Modes

Two distinct failure modes dominated the connection tests in this study: pullout and pull-through. These two failure modes are shown in Figures 3.12 and 3.13 respectively. Pullout involves the sheathing and the nail pulling out from the stud. This mode of failure is thus directly related to the withdrawal characteristics of the nail, which is the focus of the next chapter. Pull-through occurs when the head of the nail pulls through the sheathing, leaving behind the stud and the nail.

As mentioned previously, the analytical method employed to predict the strength of the connections does not include these two failure modes. Johansen's yield model predicts two other modes of failure for all of the connections that were modeled. They were: the formation of one plastic hinge in the nail in the stud, and the formation of two plastic hinges in the nail in both the

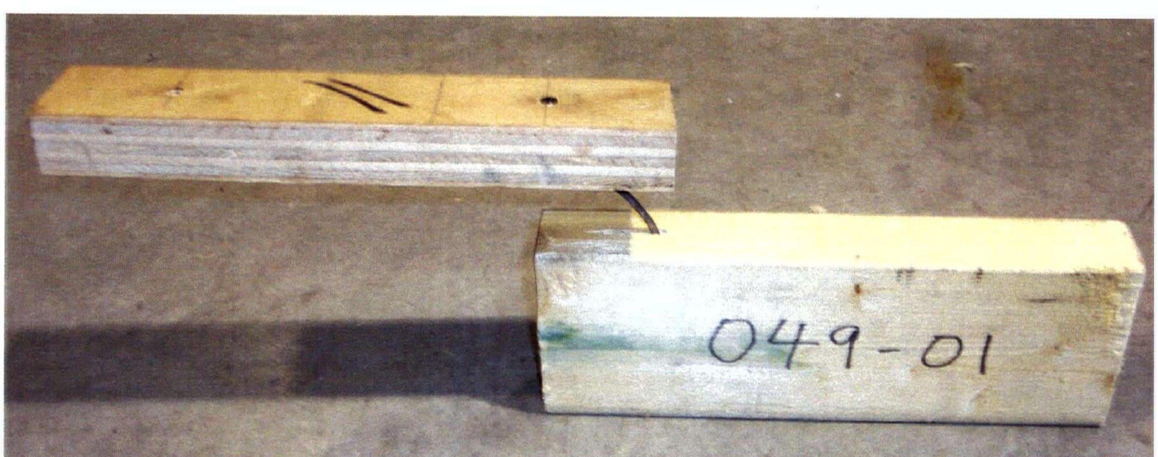

Figure 3.12. Pullout failure mode.

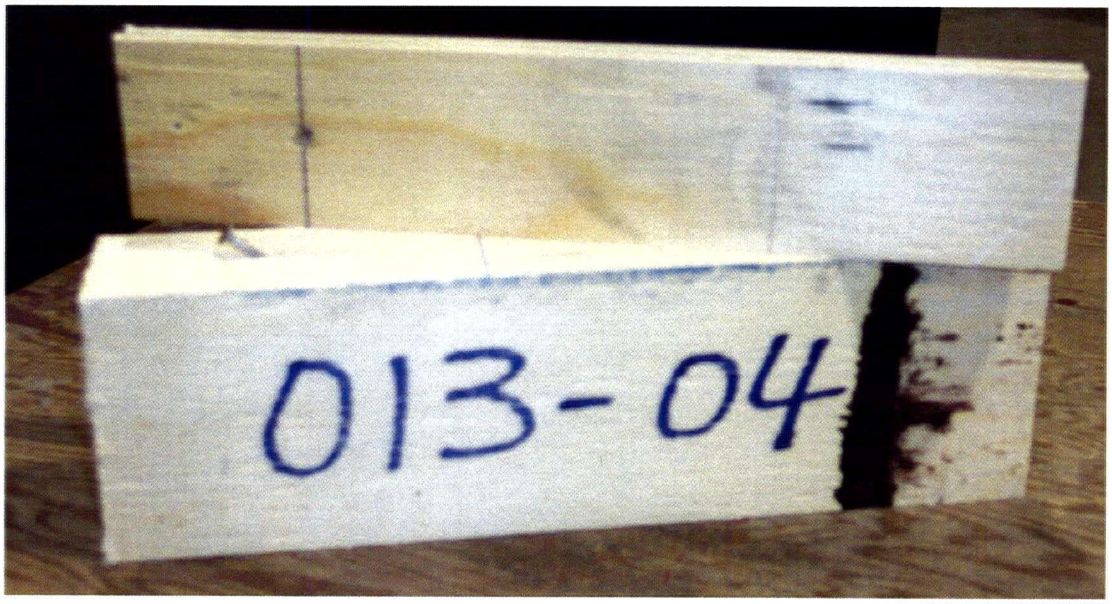

Figure 3.13. Pull-through the sheathing failure mode.

stud and the sheathing material. Most of the connections tested likely achieved one of the predicted failure modes prior to a pullout or pull-through failure. In real structures the sheathing is somewhat restrained from lifting off from the stud by the large number of nails that attach it to the stud member. This means that pullout and pull-through failures due to wind loading would be far less likely in actual structures than were found in this test program. A connection test with restrained sheathing would not likely result in increased stiffness and maximum strength but would have a much more pronounced load plateau than was found in the unrestrained tests that were conducted.

3.4 SUMMARY

The results of load-slip nail connection tests clearly demonstrate that having a connection with a high-strength component does not necessarily mean that the connection will become stronger. The mode of failure will usually find the weakest component of the system and so further increase of the strength of a stronger component in the connection does little to increase the overall strength of the connection. That said, however, the strength of a connection was shown to increase significantly when the failure mode was located in a denser stud or sheathing component or when changing a component moved the mode of failure to the other, stronger component in the connection. This increase is demonstrated most dramatically when comparing specimens 012 and 035 where the only difference between these two connections is the stud material. Specimen 035 with an LSL stud was found to have an average maximum load that was 86% greater than specimen 012 with an SPF stud.

Overall, connections with LSL studs proved to be stronger on average than connections with the other stud materials as the LSL studs are much denser. Connections with the other three stud materials gave similar results, as the densities of these studs are similar even though the manufacturing process used to make them is not. The initial stiffness of the connections, which will prove to be an important parameter with respect to partial composite action in subsequent chapters, varied significantly between connection specimens. Connections consisting of LSL studs with OSB sheathing gave the highest values for initial stiffness.

4. NAIL WITHDRAWAL TESTS

Like the connection load-slip tests, the results from nail withdrawal tests are needed in order to develop a more comprehensive model of the behaviour of tall wood-frame walls. Nail withdrawal resistances are required when analyzing a wall under suction loading but, as mentioned in the previous chapter, they also relate closely with the resistances of laterally loaded connections, as withdrawal of the nail is a mode of failure.

This chapter will present the findings from monotonic tests to determine the withdrawal response of the connection specimens presented in the previous chapter. The withdrawal test itself is rather simple in nature and the number of test specimens is greatly reduced from the previous chapter as there are only two parameters to consider: the stud and the nail.

4.1 OBJECTIVES AND SCOPE

Wind loading may act in both directions perpendicular to the face of the walls of a building. If the load is acting away from the building then suction will occur on the face of the wall. Under this scenario the load must be transferred from the sheathing to the studs through the nails in tension, or withdrawal from the studs. This part of the experimental program takes a look at the response of nails and studs typically found in tall wood-frame wall construction under withdrawal loading. This information is also valuable when analyzing the response of laterally loaded nailed connections, as one possible failure mode of this type of connection is withdrawal of the nail and sheathing from the stud. Displacement controlled monotonic tests were conducted on a small number of specimens with different stud material and nail sizes. The monotonic withdrawal tests were conducted in the Wood Engineering Laboratory of Forintek Canada Corp. in Vancouver.

4.2 METHODS AND MATERIALS

4.2.1 Withdrawal Specimens

The same combinations of studs and nails that were presented for the connections in the previous chapter were tested under withdrawal loading. This is representative of the possible combinations of nails and stud types that are, or could be, used in tall wood-frame wall construction. The average nail properties are once again of greater importance than the tail end of the distribution curves because of the large number of nails employed in connecting the sheathing to the studs in wall construction. The number of replicates for each specimen group was increased to seven from the five tested for the laterally loaded connections because withdrawal has a much wider scatter of results. The variation of results within each group was quantified and additional replicates were tested if it was deemed that the variation was too high based on the results of previous tests of this type.

The same three nail types and four stud materials described in the previous chapter were tested under withdrawal loading. A typical specimen is shown in Figure 4.1 and the withdrawal test

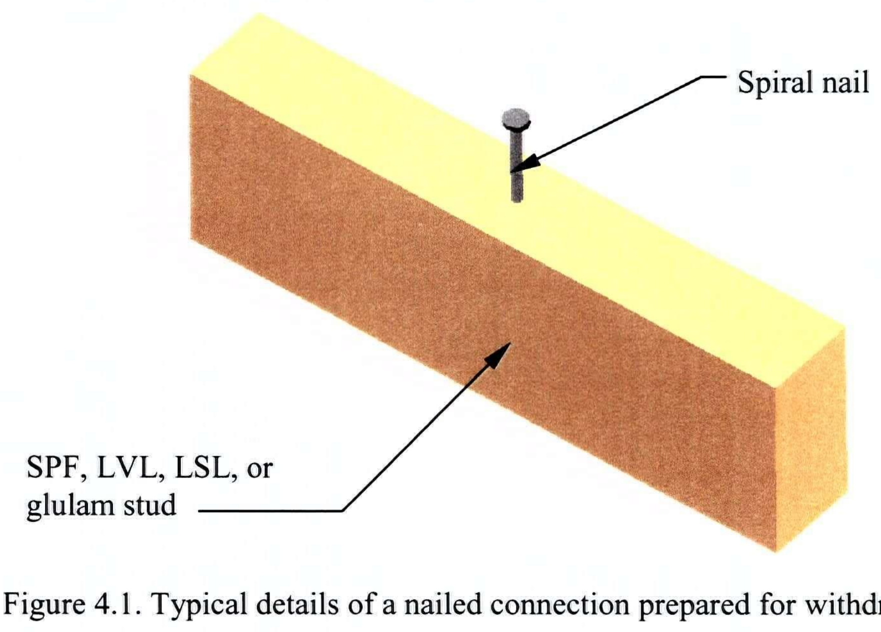

Figure 4.1. Typical details of a nailed connection prepared for withdrawal testing.

matrix is shown in Table 4.1. The embedment lengths shown in the table correspond to the depth the nails were driven into the studs. These lengths were chosen after obtaining the depth of embedment for each nail in the load-slip connection tests and calculating an average for the combinations of nails and studs shown in the matrix.

Table 4.1. Nail withdrawal connection test matrix

Specimen Group Number	Nail Length (mm)	Sheathing Material	Embedment Length (mm)
101	65	SPF	49.5
108	102	SPF	76.5
102	65	LVL	49.5
103	76	LVL	62.2
104	65	LSL	49.5
105	76	LSL	50.5
109	102	LSL	62.2
106	65	Glulam	49.5
107	76	Glulam	50.5

The connections were fabricated by hand using a hammer. Once again the LSL studs required that the nails be hammered into pre-drilled holes equal to 70% of the nail diameter in order to avoid bending of the nail. In all cases, studs that were used in the load-slip connection tests were re-used for the withdrawal tests. In accordance with the standard used, ASTM D 1761 (ASTM, 1995), the specimens were tested within one hour after assembly and not conditioned in the laboratory environment.

4.2.2 Testing Apparatus and Instrumentation

A photo of the test set-up is shown in Figure 4.2 and a schematic of the test set-up for the nail withdrawal tests is shown in Figure 4.3. Each end of the stud was connected to the testing apparatus using steel clamping angles and bolts. The bolts were tightened by hand so that the angles were snug. The stud was not free to rotate or displace in any direction and the nail was lined up to be withdrawn in a purely vertical direction.

Figure 4.2. Photo of the test set-up for determining the withdrawal characteristics of nails.

Three data measurements were collected during the tests: applied load; movement of the actuator head (stroke); and the relative displacement between the head of the nail and the stud. The loading was unidirectional and upwards, or in tension, at a rate of 12.7 mm (1") per minute. A 4.5 kN (1000 lb.) load cell was attached to the 89 kN (20,000 lb.) universal testing machine that delivered the load. The nail withdrawal was measured using a displacement transducer (DCDT) that had a displacement measuring range of 76 mm (3"). The transducer was connected to the bracket holding the nail head, which was rigidly connected to the load cell, and rested on the top of the stud. Data was acquired using Forintek's data acquisition software on a personal computer and was analyzed using a commercial spreadsheet software package.

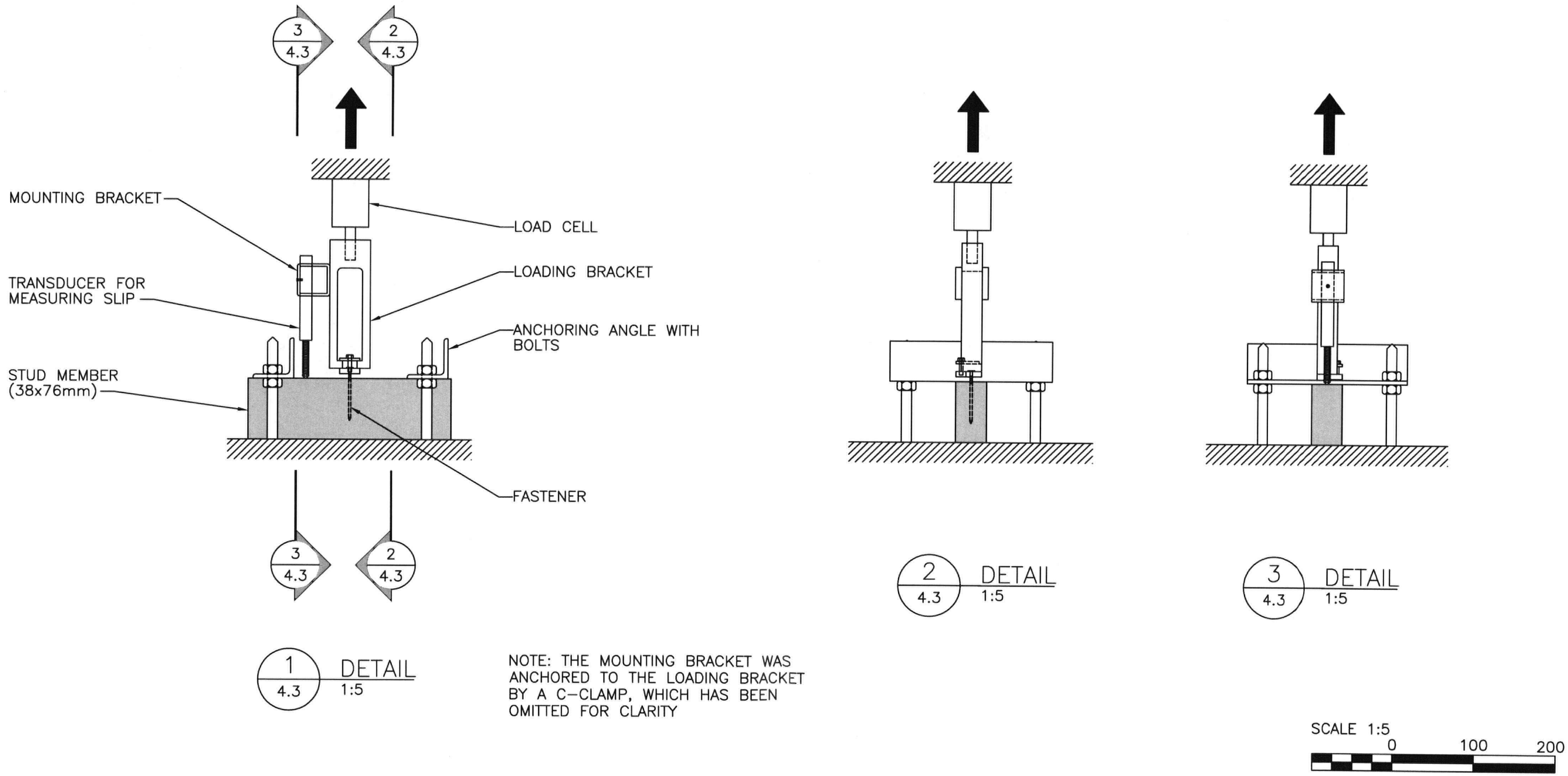

Forintek Canada Corp.	TALL WALL STRUCTURAL PERFORMANCE	DRAWN DEL	DATE OCT–04
		SCALE AS SHOWN	APPROVED
	SCHEMATIC OF WITHDRAWAL TEST SET–UP	DRAWING NUMBER FIG 4.3	REVISION
			PROJECT REF. 3910

4.2.3 Material Properties

The same stud specimens and the same nail types from the load-slip connection tests were used for the nail withdrawal tests. Therefore the results from the material tests from the load-slip connection tests are valid for the withdrawal testing as well. This data can be found in Figure 3.5. The properties of the spiral nails used in the withdrawal tests can be found in Table 3.2 and Figure 3.8 (a).

4.3 RESULTS AND DISCUSSION

4.3.1 Connection Properties

A typical load-displacement curve obtained from a monotonic withdrawal test is presented in Figure 4.4. Included in the figure are the average curve of the replicates tested, the average plus and minus one standard deviation curves of the replicates, and the coefficient of variation curve. If the coefficient of variation was higher than a reasonable value for this type of testing, in this case approximately 40%, then additional replicates were tested to determine if the coefficient of

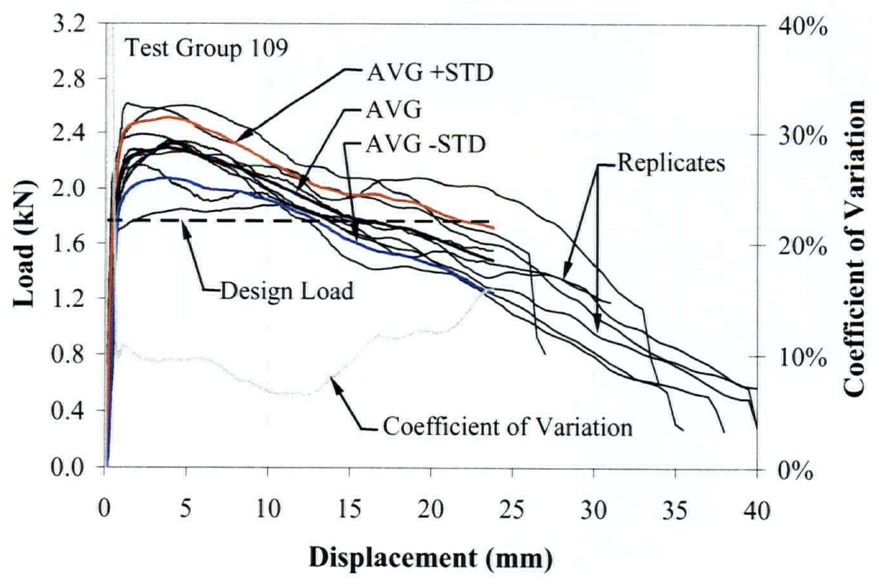

Figure 4.4. Typical withdrawal connection results.

variation could be reduced. Only one test group was re-tested to reduce the coefficient of variation (101). In general, the coefficient of variation was around 25% and was found to increase with decreasing nail penetration length. Because a larger penetration length results in the surface area of the nail coming in contact with a greater proportion of the cross section of the stud the results of the withdrawal test are more likely to reflect that of the average properties of the stud material and thus give similar results between replicates. Reducing the penetration length increases the chances of a defect in the stud negatively impacting the test results and thus increasing the variability between tests.

Properties such as initial stiffness, ultimate load, yield load, ultimate displacement, and overstrength were determined from each test group and are presented in Table 4.2. Once again, the procedure described in the European CEN protocol (CEN, 1995) was used to calculate the properties given in Table 4.2. This procedure has been shown graphically in Section 2.7 and described in Section 3.3.1. The overstrength factor is a ratio of the maximum load to the factored design load, which is based upon the procedure set out in Eurocode 5 (ENV 1995-1-1,

Table 4.2. Average connection properties obtained from tests.

Specimen Group Number	Number of Specimens	Yield Load F_y (kN)	Yield Displacement Δ_y (mm)	Maximum Load F_{max} (kN)	Displacement at F_{max} (mm)	Ultimate Displacement Δ_u (mm)	Initial Stiffness (N/mm)	Ductility (Δ_u / Δ_y)	Overstrength (F_{max} / F_{design})
101	7	0.437	0.36	0.694	3.22	11.60	1642	32.22	1.80
108	7	1.273	0.60	1.864	5.10	14.20	2802	23.67	2.01
102	7	0.527	0.42	0.762	3.18	13.20	1806	31.43	1.80
103	7	1.307	0.62	1.806	3.34	11.00	2681	17.74	3.04
104	9	0.879	0.52	1.417	4.30	8.10	2184	15.58	1.58
105	10	1.722	0.96	2.170	4.54	10.70	2054	11.15	2.11
109	9	1.705	0.62	2.296	3.78	14.00	3885	22.58	1.30
106	7	0.409	0.50	0.694	5.40	12.80	1280	25.60	1.66
107	7	0.979	0.60	1.417	4.10	7.50	1806	12.50	2.97

1993). The factored resistance of an axially loaded nail was given in Eurocode 5 as:

$$R_d = \min\begin{cases} f_{1,d}dl & \text{for all nails} \\ f_{2,d}d^2 & \text{for threaded nails} \end{cases} \tag{4.1}$$

$$f_{i,d} = \frac{k_{mod,i}\ f_{i,k}}{\gamma_M},\ i = 1, 2 \tag{4.2}$$

$$f_{1,k} = \left(18x10^{-6}\right)\rho_k^2 \tag{4.3}$$

$$f_{2,k} = \left(300x10^{-6}\right)\rho_k^2 \tag{4.4}$$

In the previous formulation, the symbols are defined as follows:

$f_{i,k}$ and $f_{i,d}$ = specified and factored characteristic strength

d = nail diameter

l = point side penetration length

ρ_k = mass density

$k_{mod,i}$ = load-duration factor (0.9 for short-term loading)

γ_M = material properties factor (1.3 for wood-based materials)

The overstrength factor is quite variable ranging from 1.30 to 3.04. This large variation in results may again be due to the fact that Eurocode 5 only gives one set of equations for the characteristic penetration strength of the stud material based upon testing conducted on sawn lumber. The overstrength factors for the two groups tested with sawn lumber, groups 101 and 108, have similar values of 1.80 and 2.01 respectively.

All the average load-displacement curves from the nine groups tested are presented in Figure 4.5. The numbers in brackets refer to the specimen group number. The terms SPR and PEN refer to spiral nail length and nail penetration length, respectively. The curves in Figure 4.5 (a) show the results of tests with the same nail type and penetration length but with different stud materials.

The three stud materials with similar relative densities have similar responses while the LSL stud, which has a much higher relative density, has a much higher withdrawal strength. This is shown again in Figure 4.5 (b) and (c) for the 76 mm and 102 mm spiral nails, although the penetration lengths are not the same for all of the groups. Finally, Figure 4.5 (d) shows that increasing penetration length for spiral nails with LSL studs increases the maximum load attained in withdrawal to a greater extent than increasing nail diameter. Because the LSL is very stiff, even a small increase in penetration length will have an effect on the withdrawal strength.

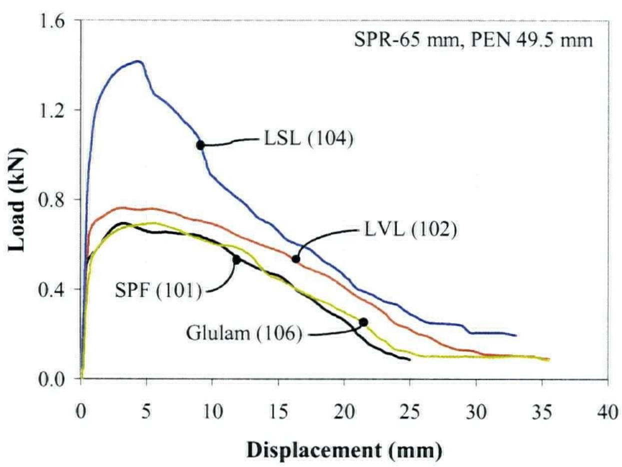

(a) 65 mm spiral nail.

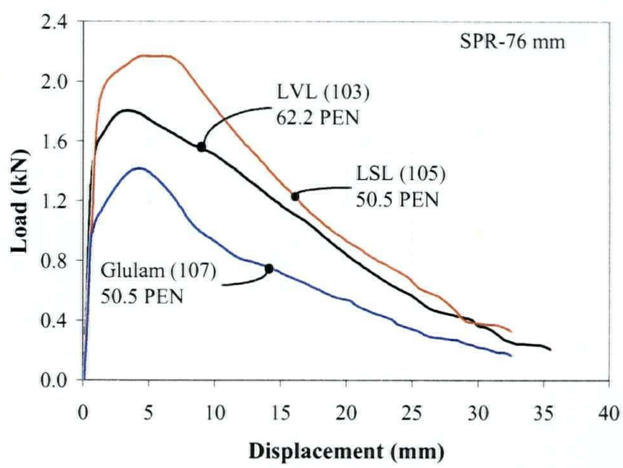

(b) 76 mm spiral nail.

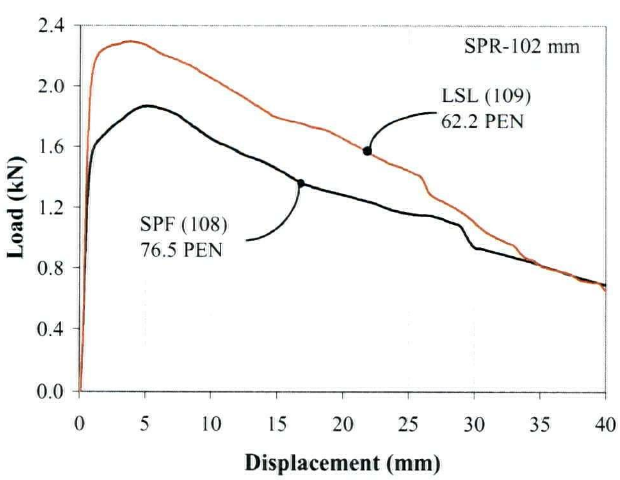

(c) 102 mm spiral nail.

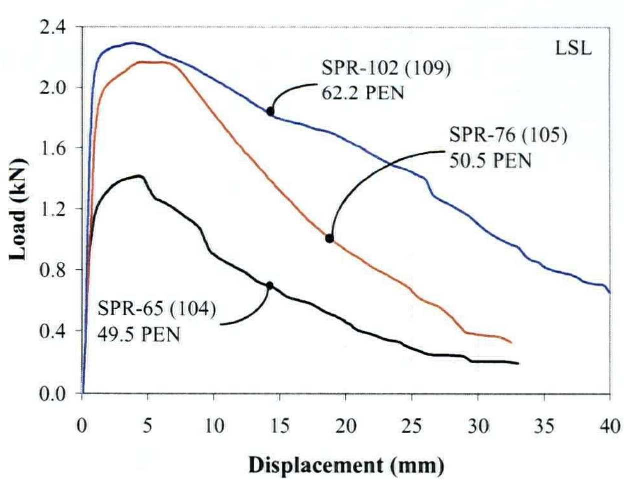

(d) LSL studs.

Figure 4.5. Load-deflection curves from withdrawal testing.

4.3.2 Failure Modes

There is only one desired failure mode for this type of testing: withdrawal of the nail from the stud. This type of failure is shown in Figure 4.6. Some of the test specimens failed, however, when the head of the nail fractured off or yielded in the cradle that was supporting them. A new cradle for the heads of the nails was fabricated after the first few occurrences of this failure mode. None of the tests that failed with the brittle fracture of the head of the nail were included in the results and all the replicates that were included had reached their maximum load prior to failure.

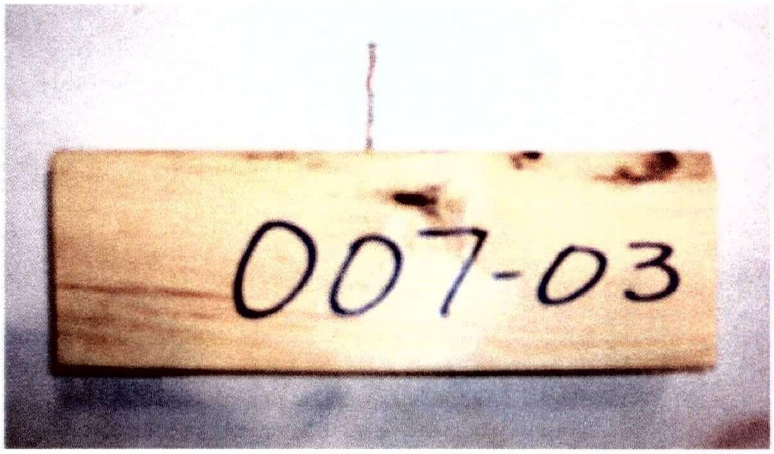

Figure 4.6. Typical nail withdrawal failure mode.

4.4 SUMMARY

The results from nail withdrawal testing show that the response is related to the density of the stud material, the length of penetration, and the diameter of the nail with the significance of each of those parameters being in the descending order that they were listed. The withdrawal resistance of these specimens is directly related to the load-slip response of the connections tested in the previous chapter since withdrawal of the sheathing and the nail was a common failure mode.

5. COMPOSITE T-BEAM TESTS

Several theoretical methods for determining the properties of a composite member were presented in chapter 2. This chapter includes the test results of monotonic and cyclic tests to determine the stiffness of composite T-beams, which consist of a stud and its tributary width of sheathing, and compare them with theoretical solutions. Such composite T-beam members are closely associated with tall wood-frame wall construction.

5.1 OBJECTIVES AND SCOPE

A main objective of this research is to determine the structural performance of tall wood-frame walls, so that they can be constructed in a way that makes them economically competitive with other materials currently being used by the construction industry. One way to make tall wood-frame walls more economically feasible is to consider some changes in the standard design approach for regular wood-frame walls. The current design approach allows the designer to only account for the studs in the wall as the sole load-resisting elements, and does not treat the entire wall system as an equivalent composite member consisting of all the elements that make up the wall. Composite action is implicitly taken into account only in the serviceability requirements by increasing the deflection limits for the studs by the same ratio for all types of wood frame construction (CSA, 2001). This test program attempts to not only accurately measure the amount of composite action for several different sheathing and stud configurations, but also to determine the best configurations for maximizing this effect.

A necessary piece of information needed to accurately predict the response of full-scale walls under axial and transversal, or out-of-plane, loading, which will be presented in detail in subsequent chapters, is the response of composite T-beam specimens in bending. Many of the composite member configurations tested in this program were later used in the full-scale wall tests. Displacement controlled monotonic tests and load controlled cyclic tests were conducted on several composite T-beams with different stud materials, sheathing thicknesses, and connection types. The T-beam tests were conducted in the Wood Engineering Laboratory of Forintek Canada Corp. in Vancouver.

5.2 METHODS AND MATERIALS

5.2.1 T-Beam Specimens

The configurations of the composite T-beams were chosen so that the results of the load-slip connections presented in Chapter 3 could be used to predict their response. The specimen groups tested were chosen to represent a wide spectrum of beam strength and stiffness properties. The test matrix for the T-beam specimens is shown in Table 5.1. Twelve specimen groups were tested but, as will be described later, specimens from some of the groups were modified, which resulted in a total of thirty specimen types. In nine of the specimen groups, spiral nails were used to connect the sheathing to the stud members and glue was used in the rest of the groups. Because each specimen contains many connectors, or a continuous glued connection, that share the shear load between wood components, the response of the T-beam is closely related to the average response of the connectors. The effect of variability of the stud and sheathing properties was slightly reduced by testing each component separately prior to constructing the composite beam. Therefore, only three replicates of each specimen type were tested. The variation of results will be presented later in this chapter and the validity of the number of replicates chosen will be discussed.

Two of the four stud materials used for the load-slip connection test specimens were used for stud members of the composite T-beam specimens. They were 38 mm by 235 mm (1-½" x 9-½") spruce-pine-fir No.2 or better (SPF) and 44 mm by 242 mm (1-¾" x 9-17/32") Laminated

Table 5.1. T-Beam test matrix.

Specimen Group Number	Configuration	Nail Length (mm)	Nail Spacing (mm)	Glue	OSB Thickness (mm)	Gap Spacing (mm)	Sheathing Orientation	Stud Member Material
301	C	65	152	No	9.5	1220	PERP	SPF
302	A	65	152	No	9.5	4880	PAR	SPF
	B	65	152	No	9.5	2440	PAR	SPF
	C	65	152	No	9.5	1220	PAR	SPF
	D	65	152	No	9.5	610	PAR	SPF
303	A	65	152	No	15.5	4880	PAR	SPF
304	A	65	152	No	15.5	4880	PAR	LSL
305	A	65	152	No	15.5	4880	PAR	LSL
	B	65	152	No	15.5	2440	PAR	LSL
	C	65	152	No	15.5	1220	PAR	LSL
	D	65	152	No	15.5	610	PAR	LSL
306	A	65	102	No	15.5	4880	PAR	LSL
307	A	65	76	No	15.5	4880	PAR	LSL
308	A	65	152	No	9.5	4880	PAR	LSL
309	A	102	152	No	28.5	4880	PAR	LSL
	B	102	152	No	28.5	2440	PAR	LSL
	C	102	152	No	28.5	1220	PAR	LSL
	D	102	152	No	28.5	610	PAR	LSL
310	A	65	76	Yes	15.5	4880	PAR	LSL
	B	65	76	Yes	15.5	2440	PAR	LSL
	C	65	76	Yes	15.5	1220	PAR	LSL
	D	65	76	Yes	15.5	610	PAR	LSL
311	A	65	76	Yes	15.5	4880	PAR	SPF
	B	65	76	Yes	15.5	2440	PAR	SPF
	C	65	76	Yes	15.5	1220	PAR	SPF
	D	65	76	Yes	15.5	610	PAR	SPF
312	A	102	76	Yes	28.5	4880	PAR	LSL
	B	102	76	Yes	28.5	2440	PAR	LSL
	C	102	76	Yes	28:5	1220	PAR	LSL
	D	102	76	Yes	28.5	610	PAR	LSL

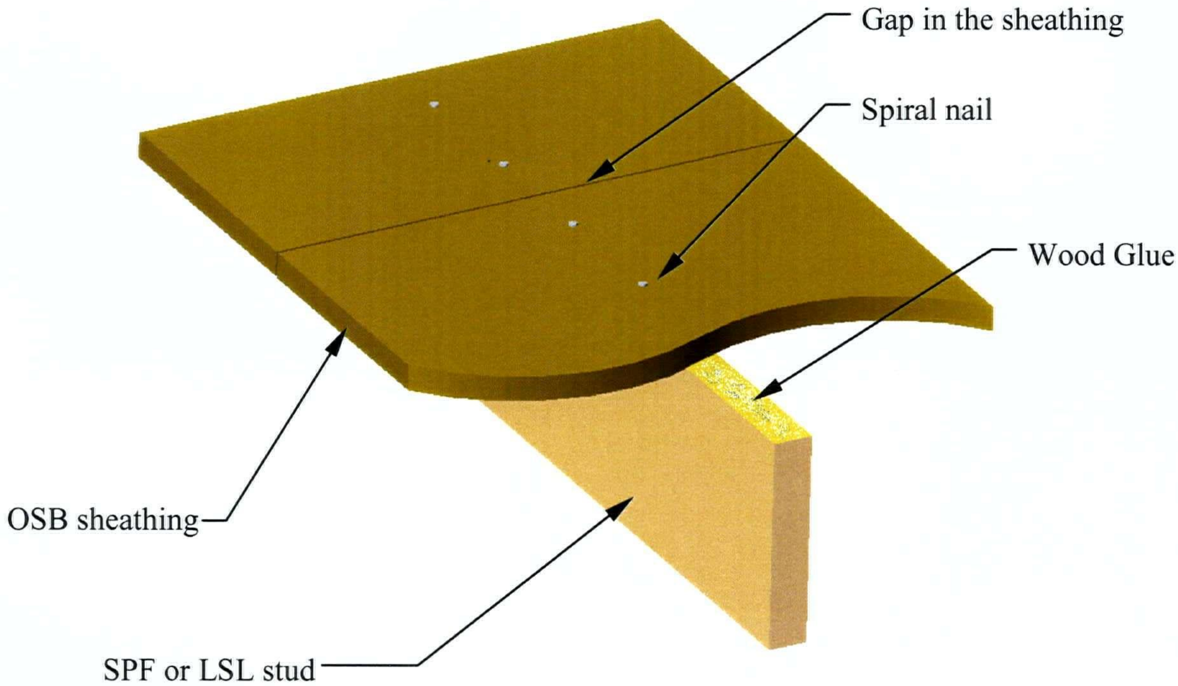

Figure 5.1. Typical details of a T-beam composite specimen.

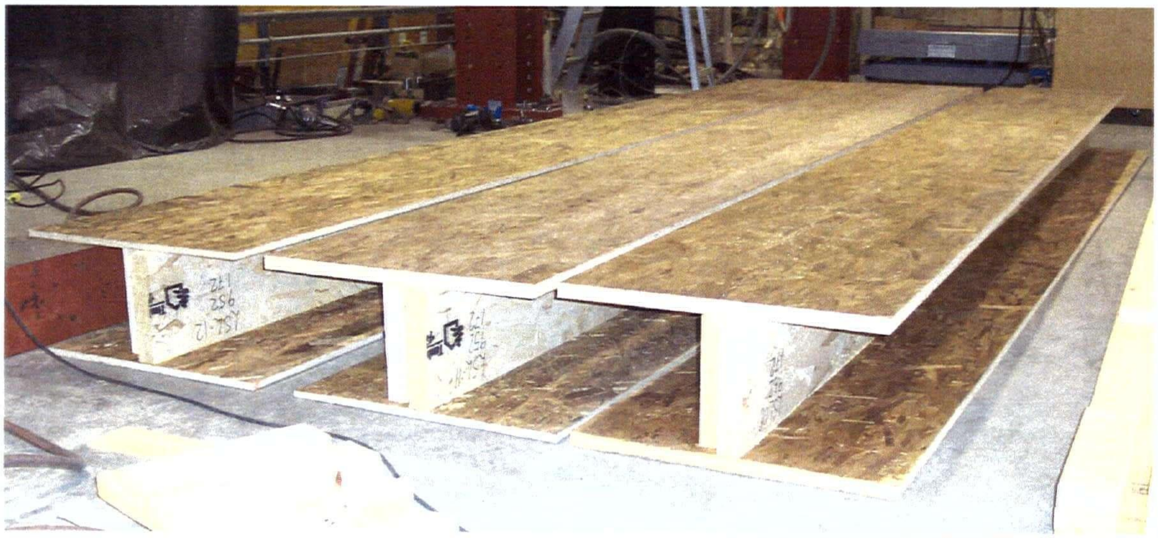

Figure 5.2. T-beam specimens prepared for testing (stacked two high).

Strand Lumber (LSL) produced by Trus Joist. These two were chosen because they represent the high and low ends of strength, stiffness, and variability of the original four materials. A portion of a typical T-beam specimen is presented in Figure 5.1. Prepared T-beam specimens are shown in Figure 5.2.

An important parameter that affects that amount of composite action between the sheathing and the stud is the distance between the gaps in the sheathing. Oriented strandboard (OSB) was used exclusively for the T-beam specimens since it is possible to purchase oversized sheets of OSB due to the nature of the manufacturing process of this material. Plywood, by contrast, is not readily available in large sheets. By using oversized sheets of OSB, some of the 4,880 mm (16') long T-beam specimens were tested without gaps in the sheathing. The effect of the distance between the gaps in the sheathing on member stiffness was investigated by cutting gaps into the sheathing of the already built T-beam specimens with a radial arm saw. This will be described in detail later in this chapter.

Spiral nails were once again used as a mechanical fastener. Only two spiral nail lengths were utilized as they corresponded to the sheathing thicknesses used in the connection specimens. The 65 mm (2 ½") spiral nails were driven using a pneumatic coil nail gun. The nail gun was not large enough to hold the 102 mm (4") spiral nails so they were driven by hand using a hammer. The density of the LSL was such that a pilot hole with a diameter of 70% of that of the nail had to be pre-drilled to allow the nail to be driven by hand without being bent. In practice, pilot holes would not be required when using a nail gun.

While nine test groups utilized nailed connections, the sheathing of three of the test groups was connected to the stud using both glue and nails. The intention of these T-beams was to have fully composite members with a rigid connection between the sheathing and the stud. Therefore, the nails do not provide any resistance and were only used to ensure that an adequate glued bond was developed between the sheathing and the stud. Because a rigid connection was desired and long-term serviceability issues were not taken into account, regular white wood glue was used as the bonding agent. This proved to be an excellent bonding agent because, as will be discussed later, there was no measurable slippage between the sheathing and the studs for the glued specimens. The edge of the stud was lightly sanded and both the stud and sheathing were cleaned of dust with an air gun prior to applying the glue. A thick layer of glue was applied to the entire edge of the stud using a small, flat piece of wood. The sheathing was then placed on the stud and nailed into place to ensure an adequate bond.

All material used for testing was dry and had been stored in a laboratory environment at an average temperature of 20° ± 3°C and a relative humidity of 60% ± 10% for at least one week. The specimens with nailed connections were tested within 24 hours of assembly. The specimens with glued connections were tested at least 72 hours after assembly to allow the glue to cure.

5.2.2 Testing Apparatus and Instrumentation

A picture of the T-beam bending test set-up with a specimen being tested is shown in Figure 5.3, while a schematic of the test set-up is shown in Figure 5.4. The specimens were loaded in third-point loading, which resulted in a distribution of bending moment along the beam is similar to

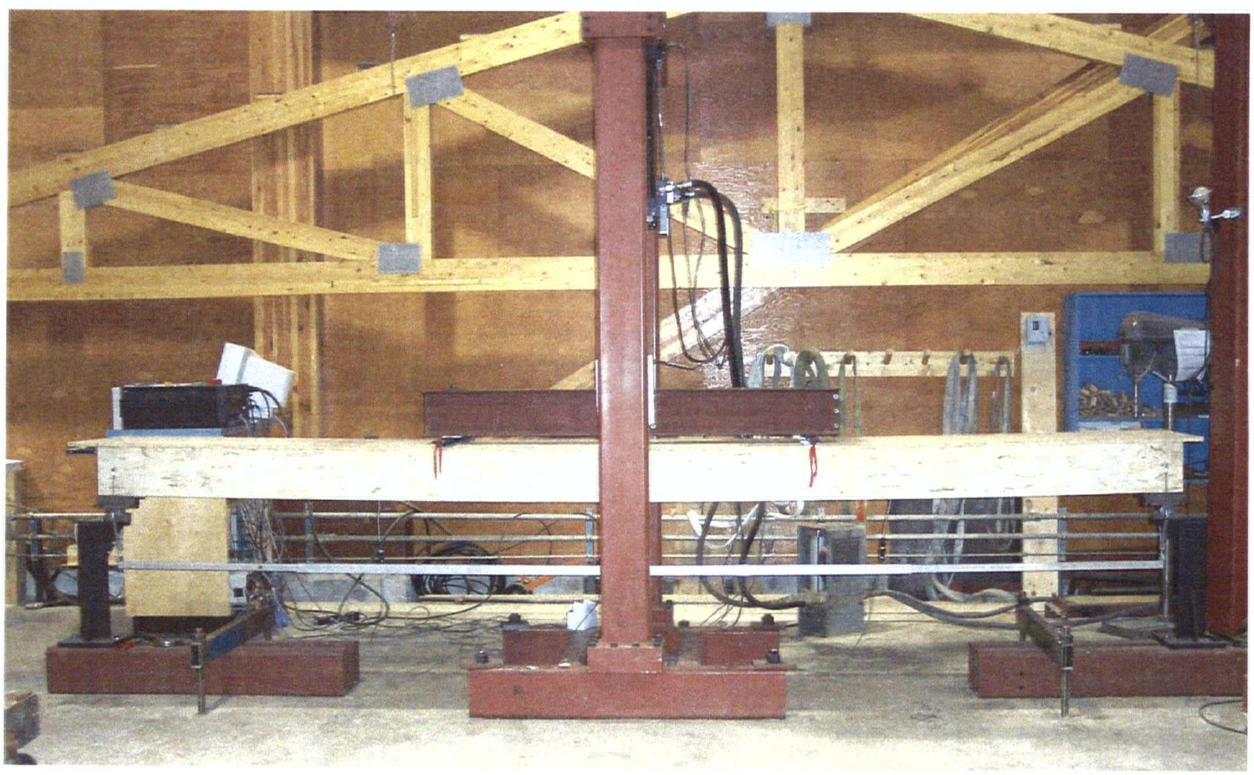

Figure 5.3. Photo of the T-beam test set-up.

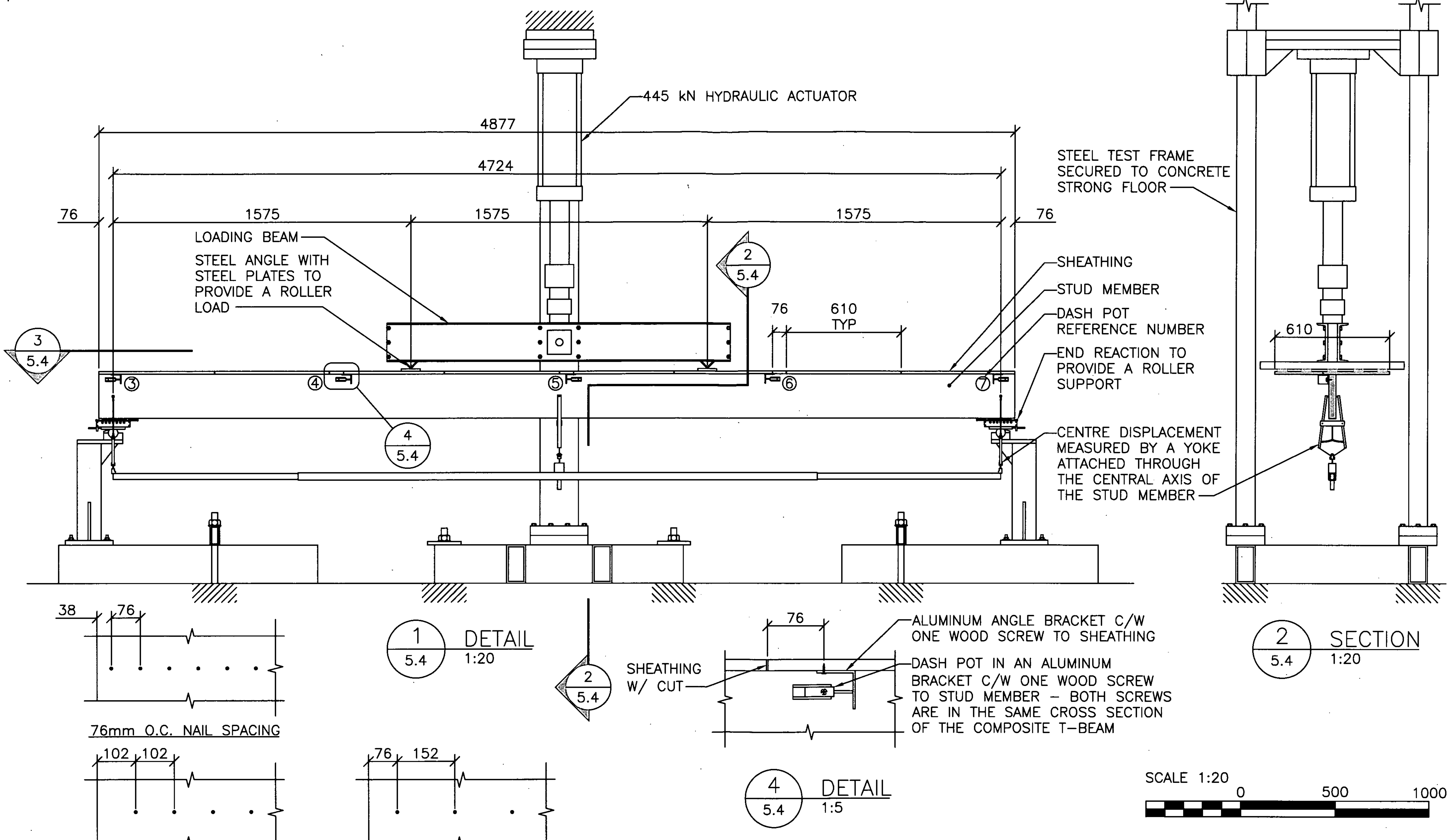

Forintek Canada Corp.	TALL WALL STRUCTURAL PERFORMANCE SCHEMATIC OF BEAM TEST SET-UP	DRAWN DEL	DATE OCT-04
		SCALE AS SHOWN	APPROVED
		DRAWING NUMBER FIG 5.4	REVISION
			PROJECT REF. 3910

FEB 04, 2004 ~FCC~C:/MY DOCUMENTS/BEAM BENDING TEST.DWG DLEON that of a beam under a uniformly distributed load, as experienced under wind loading. Each specimen was 4,880 mm (16') long and the distance between the supports of the test apparatus was 4,724 mm (15'-6"), so the distance between the loaded points was 1,575 mm (5'-2"). The end reactions approximated idealized roller supports by allowing movement in the longitudinal direction of the specimen and rotation. Steel angles were used to apply a knife-edge load at the third points to the entire 610 mm (24") width of the sheathing. This width was chosen because it represents the tributary width of sheathing for a wall with studs spaced 610 mm (24") on centre, and also because of geometry limitations of the testing frame. Small steel plates were placed under the angles along the width of the sheathing to allow the angles to slide over the sheathing and thus simulate a roller. The layout of the placement of the nails, from the end of the T-beam, is shown in Detail 3 of Figure 5.4.

Eight sets of data measurements were collected during the tests: applied load; movement of the actuator head (stroke); the relative transverse (vertical) displacement between the ends of the beam and the centre, along the middle of the beam; and the relative displacement between the sheathing and the stud measured at five locations along the length of the beam (Figure 5.4). The loading for both the monotonic and cyclic testing was unidirectional and downward, resulting in compression in the flange of the beam. A 445 kN (100,000 lb.) universal testing machine delivered the load. Two different load cells were used over the course of the testing program, with 89 kN (20,000 lb.) and 22 kN (5,000 lb.) capacities, respectively. The displacement of the beam at the centre of the span was measured using a yoke apparatus, which was connected to the beam at the mid-height of the stud member. The transducer (DCDT) used to measure the displacement of the beam had a total measurement range of 51 mm (2").

Five linear potentiometers (pots) measured the slippage between the sheathing and the stud and each had a total measurement range of 25 mm (1"). The locations where slippage was measured are shown in Figure 5.4. Brackets were connected to the sheathing and linear pots were connected to the stud member with wood screws at the same cross section. All data was acquired using Forintek's data acquisition software on a personal computer and was analysed using a commercial spreadsheet software package.

5.2.3 Testing Procedures

The purpose of the T-beam test program was to determine the stiffness of each specimen and not its ultimate strength. Three different loading programs (protocols) were used to determine stiffness for the different test groups, although the load range used to measure stiffness was the same for all of them to allow for a direct comparison of results. The first loading program (Figure 5.5 (a)) was used for specimens where the sheathing length was not reduced in future tests, specifically test groups 301, 303, 306, 307, and 308. All of these specimens had continuous sheathing except group 301, which had three gaps in the sheathing. In order to get a consistent stiffness value, each specimen was loaded at a displacement controlled rate of 25 mm (1") per minute to a load of 2.2 kN (500 lb.) three times. The member stiffness was calculated as the slope of the load deformation curve between two points on the curve, one at 0.9 kN (200 lb.) and the other at 2.2 kN (500 lb.). Next, the specimen was loaded at the same rate to 11.1 kN (2500 lb.) or to failure, whichever came first. The intention of this loading program was to obtain the load versus deflection curve for each specimen in both the linear and non-linear range. The highest load level that was applied, 11.1 kN (2500 lb.), corresponded to a uniformly distributed load of 5 kPa (104 psf).

As mentioned previously, the effect of gaps in the sheathing on member stiffness was one of the objectives of this research program. The second loading program, shown in Figure 5.5 (b), was developed to capture this effect. It was applied to test groups 302, 305, and 309 through 312.

Each specimen started out with continuous sheathing (configuration A) and was loaded three times to 2.2 kN (500 lb.) at 25 mm (1") per minute. Next, the specimens had a 3.2 mm (1/8") gap cut only into the sheathing, to be tested in accordance with the subsequent configuration type (Figure 5.6). This process was repeated for each configuration of a particular specimen

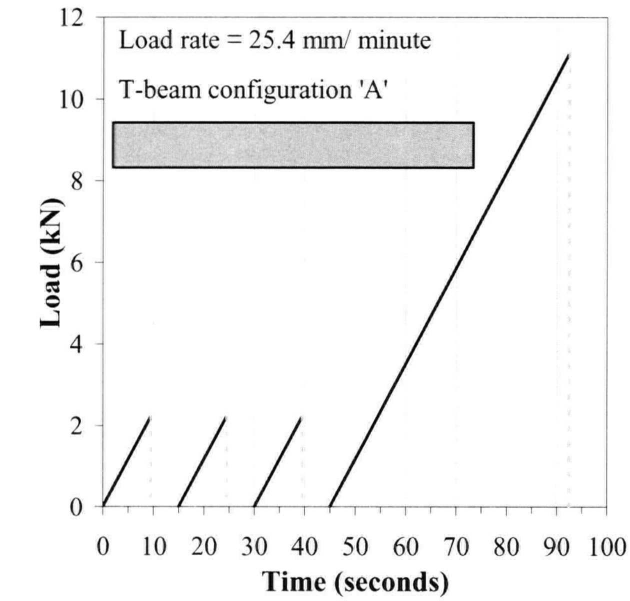

(a)

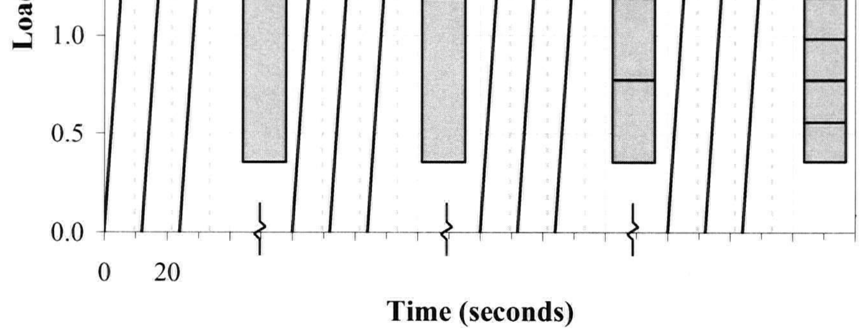

(b)

Figure 5.5. Monotonic loading programs (a) for stiffness in the linear and non-linear range and (b) for stiffness in the linear range with differing sheathing lengths.

Figure 5.6. Reducing the gap spacing by cutting the sheathing of an already tested T-beam specimen.

group. It was desirable to avoid non-linear effects over the course of the entire loading program, so the load was not increased past 2.2 kN for each T-beam configuration.

Finally, the specimens in group 304 were loaded cyclically using the protocol shown in Figure 5.7. The load in this case was applied at a rate of 14 kN (3147 lb.) per minute, which was approximately equal to the previously described rates of 25 mm per minute, taking into account the stiffness of the beams tested. Previous testing has shown that the stiffness of a nailed connection will degrade over time with repeated loading cycles (Jenkins et. al., 1979). This loading program consisted of applying cyclic load on the T-beams with several increasing load levels. After three cycles of each load level, an additional cycle was conducted that was equal in magnitude to the cycles used in the monotonic loading programs to determine the stiffness in the initial linear-elastic range. This additional cycle was used to determine the stiffness of the composite T-beams after each increasing load cycle. Thus, the effect of load level on the bending stiffness of a composite T-beam could be determined.

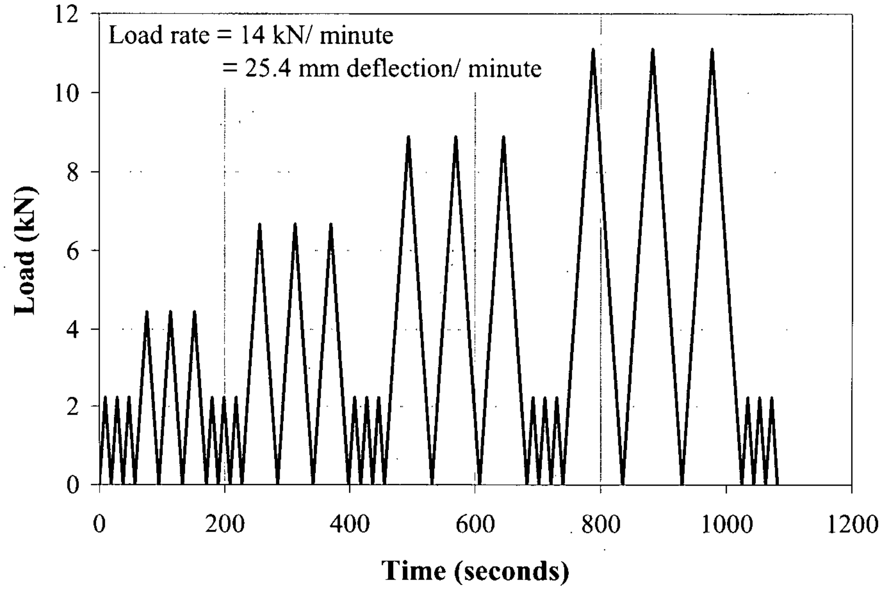

Figure 5.7. Cyclic loading protocol used for testing of composite T-beams.

5.2.4 Material Properties

A description of the two stud materials used for the T-beam tests can be found in Chapter 3 along with their relative densities. Each stud was also loaded at its third-points in the test frame described previously in this chapter to obtain its modulus of elasticity in bending prior to the T-beam tests. This is shown in Figure 5.8. A maximum load of 3.1 kN (700 lb.) was applied at a displacement controlled rate of 25 mm (1") per minute. The calculated values for stiffness were taken as the slope of the load-displacement curve between the 0.9 kN (200 lb.) and 2.2 kN (500 lb.) load points. The dimensions of the studs were measured with callipers. The normal cumulative distribution functions for the modulus of elasticity of each stud material are shown in Figure 5.9. As would be expected, the distribution for SPF was much wider than that of LSL with median values of 10,293 MPa and 11,680 MPa, respectively. The coefficients of variation for the SPF and LSL distributions were approximately 26% and 3%, respectively. The mean values of modulus of elasticity for the SPF and LSL, which were 9,500 MPa and 11,670 MPa,

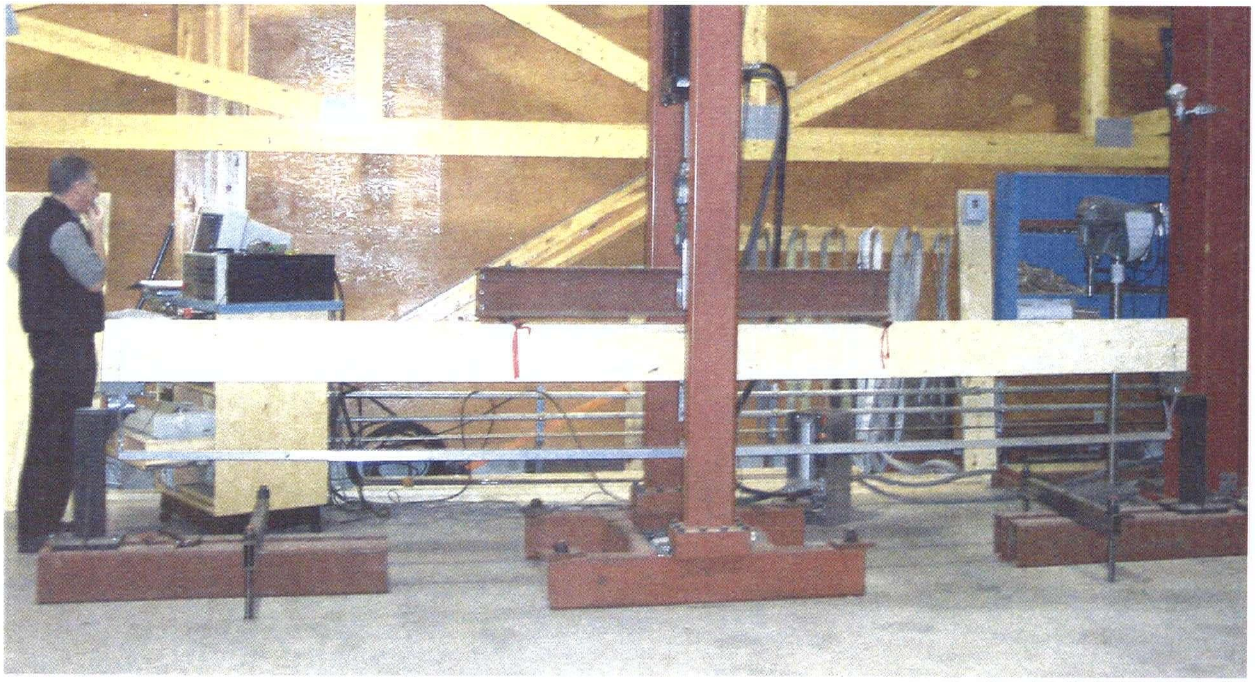

Figure 5.8. Loaded stud under third-point bending to obtain modulus of elasticity.

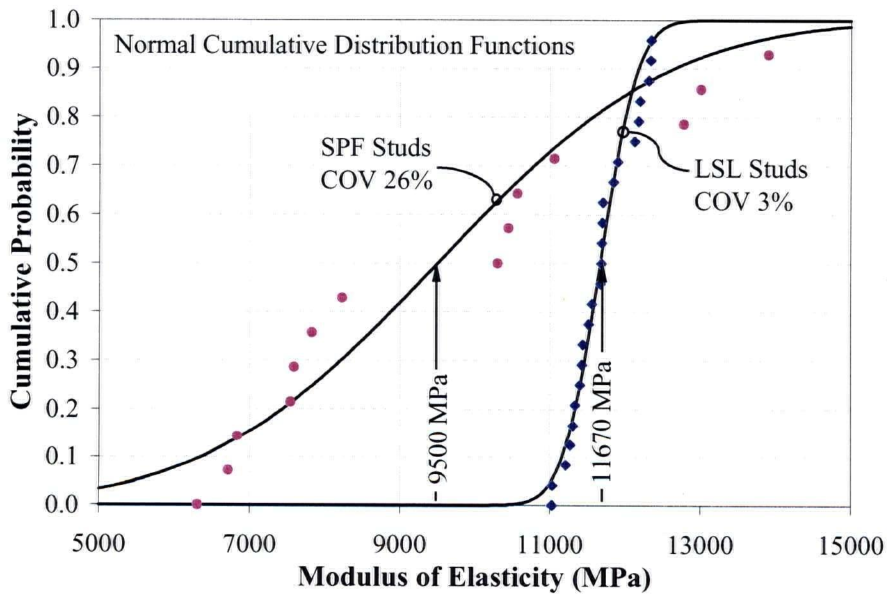

Figure 5.9. Cumulative distribution of modulus of elasticity for SPF and LSL studs.

respectively, relate quite closely with published values for use in design in the Canadian Wood Design Code and literature provided by the manufacturer.

The properties of the spiral nails used to fabricate the T-beam specimens can also be found in Chapter 3. As mentioned previously, standard white wood glue was used to provide a rigid connection between the stud and the sheathing for some of the specimens. The particular glue that was utilized was Elmer's Contractor's Grade Professional Strength Wood Glue for Interior Use.

The modulus of elasticity in bending of the sheathing was also determined in order to more accurately predict the response of the T-beams using an analytical model. This was achieved by loading sheathing specimens at the third points as shown in the photo in Figure 5.10 and in schematic form in Figure 5.11. The 295 mm by 1,067 mm (11 5/8" x 42") specimens were loaded at their third points with a displacement controlled rate of 51 mm (2") per minute over a total span length of 914 mm (36"). Displacement was measured by a transducer with a range of 25 mm (1") located at the middle of the span. An 89 kN (20,000 lb.) hydraulic actuator applied the load through a 4.5 kN (1,000 lb.) load cell.

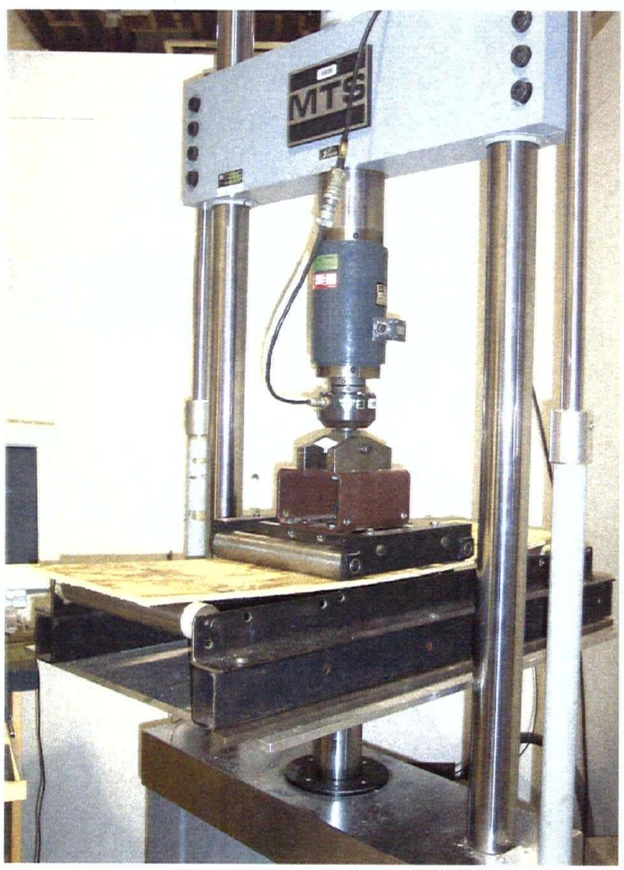

Figure 5.10. Photo of the test set-up for determining the stiffness and strength characteristics of OSB sheathing used in the testing program.

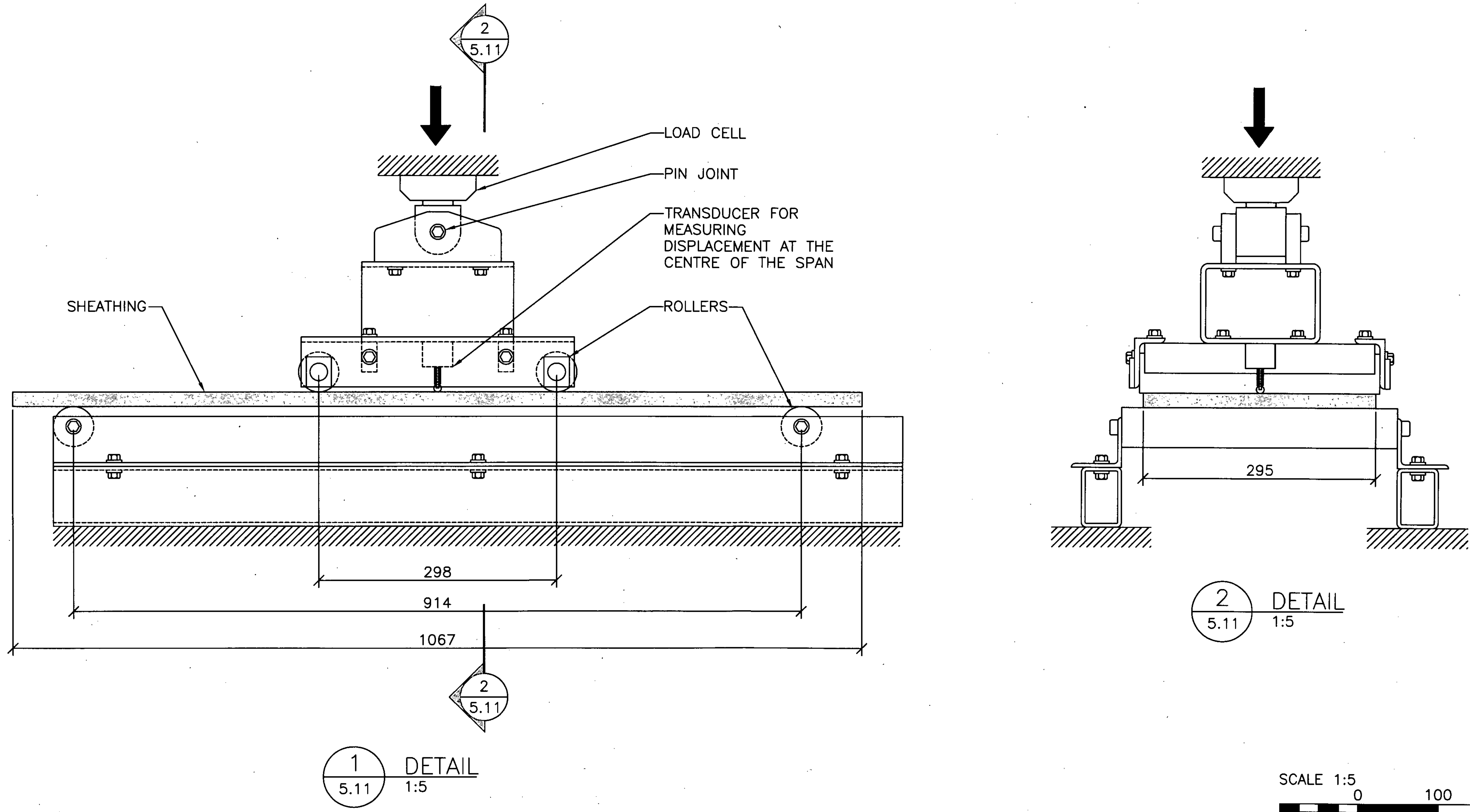

Forintek Canada Corp.	TALL WALL STRUCTURAL PERFORMANCE	DRAWN DEL	DATE OCT–04
		SCALE AS SHOWN	APPROVED
	SCHEMATIC OF SHEATHING BENDING TEST SET–UP	DRAWING NUMBER FIG 5.11	REVISION
			PROJECT REF. 3910

MAY 10, 2004 ~FCC~C:/MY DOCUMENTS/FIGURES/OSB MOE TEST.DWG DLEON

Five different types of sheathing were tested in both parallel and perpendicular directions to the axis of greater strength. The results from the testing are given in Table 5.2. Eight replicates of each type of sheathing in both directions were tested. Only the sheathing produced by the Ainsworth Lumber Company was used in the T-beam testing. The sheathing produced by Slocan Forest Products Ltd. (now owned by the Canfor Corporation) and Tolko Industries Ltd. was used in the shearwall tests that will be described in the next chapter. They are presented here for completeness.

Table 5.2. Sheathing modulus of elasticity in bending results.

Description	Measured Thickness (mm)	Parallel				Perpendicular			
		Lower Load (N)	Upper Load (N)	Mean MOE (MPa)	COV (%)	Lower Load (N)	Upper Load (N)	Mean MOE (MPa)	COV (%)
3/8" Slocan OSB Construction Sheathing	9.81	98	191	7779	6.80	62	89	3459	2.90
3/8" Ainsworth Construction Sheathing	9.68	98	191	7522	7.11	36	62	2866	3.47
19/32" Ainsworth Structural 1 Rated Construction Sheathing	15.11	267	534	7290	14.47	133	267	3501	8.72
23/32" Tolko OSB Rated Sturd I-Floor Construction Sheathing	18.49	387	774	7637	3.76	196	387	2652	4.78
1 1/8" Ainsworth Rimboard	28.05	890	1806	8353	6.66	445	903	3382	8.16

The upper and lower load levels used to calculate the modulus of elasticity for the sheathing specimens are based on predicted stress levels in the outer fibres of the sheathing of 7,584 MPa (1,100,000 psi). The modulus of elasticity was found to vary more in the perpendicular direction than in the direction parallel to the stronger axis. The published values in the Canadian Wood Design Code for bending stiffness per unit width for all thicknesses of sheathing are based on a single value of modulus of elasticity of 8,250 to 6,800 MPa (rating grade A to B) and 2,400 MPa (all rating grades) for the parallel and perpendicular directions, respectively. This relates well to the values determined from the testing.

The average relative density of eight replicates for each sheathing type is shown in Figure 5.12. These values relate closely with the corresponding densities shown in Figure 3.5 for the sheathing used in the load-slip connection tests, which was from different manufacturers. This validates the use of the load-slip connection data for use in predicting the response of the composite T-beam specimens.

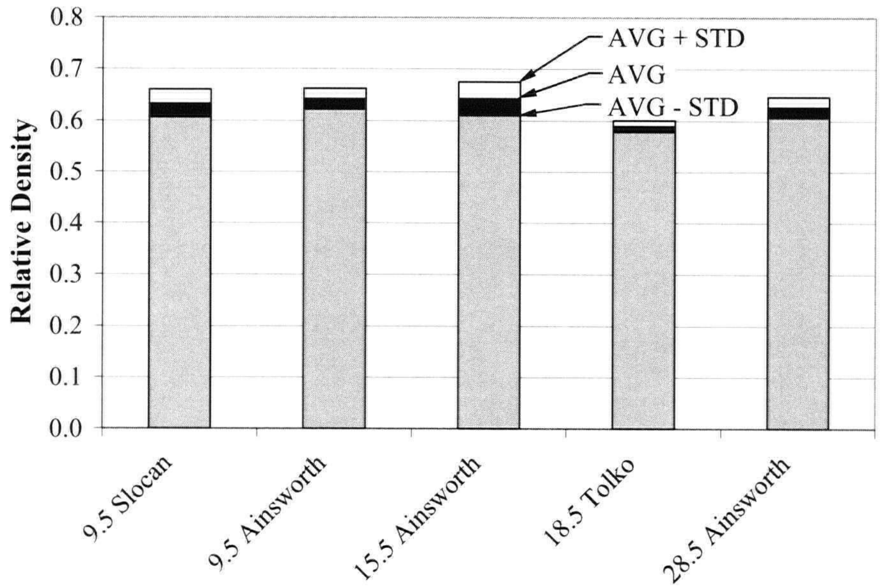

Figure 5.12. Relative densities of OSB sheathing specimens.

5.3 RESULTS AND DISCUSSION

Results from the numerous composite T-beam tests have allowed comparisons to be made between test groups with respect to individual beam components. The test data has also allowed verification of the partial composite action formulations for effective member properties and effective flange width, as presented in Chapter 2. While the monotonic tests are useful to compare beams with varying parameters, actual structures are loaded numerous times over the lifetime of the structure. Cyclic tests were conducted on specimens of one of the test groups to understand how the cycles of loading affect the stiffness properties of a beam with partial composite action.

5.3.1 Monotonic Tests

The average values of stiffness resulting from monotonic bending tests for the studs and the composite T-beams for each composite T-beam test group are presented in Table 5.3. Test results from the specimens of test group 304, which were loaded cyclically, will be presented later in this chapter. In a similar fashion to the procedure previously outlined for determining the stiffness of the stud members, the calculated values for stiffness for the composite T-beams were taken as the slope of the load-displacement curve between the 0.9 kN (200 lb.) and 2.2 kN (500 lb.) load points. The values presented are the average values of the three replicates of each test group. As can be seen, the coefficients of variation for the studs are relatively low for the SPF studs and very low for the LSL studs. In addition, the coefficients of variation of the composite T-beams are roughly equal, to or lower than, the coefficients of variation of the stud alone. Thus, the addition of the sheathing to the stud member does not increase the stiffness variability of the composite T-beam member, and in most cases reduces it significantly, compared to the bare stud. This validates the choice of only testing three replicates of each test group.

The last two columns of Table 5.3 present the average increase in the stiffness of the composite T-beam members over the stiffness of the bare studs themselves and the coefficient of variation of this average increase in stiffness. Once again, the coefficients of variation are very low, with the highest value being just over 4.5%. However, the best way to compare the increase in member stiffness is in a graphical form. Figure 5.13 presents several linear load versus displacement plots of the average stiffness values calculated for the composite T-beams tested

Table 5.3. Average T-beam stiffness values obtained from monotonic bending tests.

Specimen Group Number	Configuration	Nail Length (mm)	Nail Spacing (mm)	Glue	OSB Thickness (mm)	Head Side Member Orientation	Stud Member Material	Average Stiffness of Stud (N/mm)	Stud Stiffness COV (%)	Average Stiffness of Composite T-Beam (N/mm)	Composite T-Beam Stiffness COV (%)	Average Percent Increase in Stiffness (%)	Increase in Stiffness COV (%)
301	C	65	152	No	9.5	PERP	SPF	161	4.74	166	2.32	3.17	2.70
302	A	65	152	No	9.5	PAR	SPF	194	12.36	259	9.54	34.05	3.04
	B	65	152	No	9.5	PAR	SPF	194	12.36	211	10.84	9.06	1.43
	C	65	152	No	9.5	PAR	SPF	194	12.36	200	12.46	2.99	0.26
	D	65	152	No	9.5	PAR	SPF	194	12.36	196	12.97	1.09	0.93
303	A	65	152	No	15.5	PAR	SPF	231	3.61	326	1.04	41.29	4.51
305	A	65	152	No	15.5	PAR	LSL	329	2.24	528	2.52	60.55	2.90
	B	65	152	No	15.5	PAR	LSL	329	2.24	370	2.32	12.45	2.08
	C	65	152	No	15.5	PAR	LSL	329	2.24	341	2.17	3.50	1.07
	D	65	152	No	15.5	PAR	LSL	329	2.24	330	2.03	0.27	0.77
306	A	65	102	No	15.5	PAR	LSL	331	2.98	570	1.42	72.43	2.97
307	A	65	76	No	15.5	PAR	LSL	326	1.56	596	1.62	82.73	0.76
308	A	65	152	No	9.5	PAR	LSL	309	2.74	419	3.42	35.34	1.43
309	A	102	152	No	28.5	PAR	LSL	329	3.41	704	1.70	114.14	4.45
	B	102	152	No	28.5	PAR	LSL	329	3.41	425	2.38	29.37	2.26
	C	102	152	No	28.5	PAR	LSL	329	3.41	365	2.66	11.09	1.50
	D	102	152	No	28.5	PAR	LSL	329	3.41	343	2.76	4.43	0.82
310	A	65	76	Yes	15.5	PAR	LSL	317	1.43	602	1.47	90.10	0.71
	B	65	76	Yes	15.5	PAR	LSL	317	1.43	502	1.38	58.52	0.19
	C	65	76	Yes	15.5	PAR	LSL	317	1.43	449	1.01	41.86	0.57
	D	65	76	Yes	15.5	PAR	LSL	317	1.43	385	1.00	21.79	0.45
311	A	65	76	Yes	15.5	PAR	SPF	282	1.04	511	4.25	81.12	4.13
	B	65	76	Yes	15.5	PAR	SPF	282	1.04	431	2.96	52.80	3.02
	C	65	76	Yes	15.5	PAR	SPF	282	1.04	384	2.07	36.34	2.26
	D	65	76	Yes	15.5	PAR	SPF	282	1.04	331	1.74	17.41	2.14
312	A	102	76	Yes	28.5	PAR	LSL	314	1.62	786	0.21	150.17	1.80
	B	102	76	Yes	28.5	PAR	LSL	314	1.62	610	0.80	94.04	2.28
	C	102	76	Yes	28.5	PAR	LSL	314	1.62	520	0.48	65.52	1.52
	D	102	76	Yes	28.5	PAR	LSL	314	1.62	419	0.96	33.29	0.70

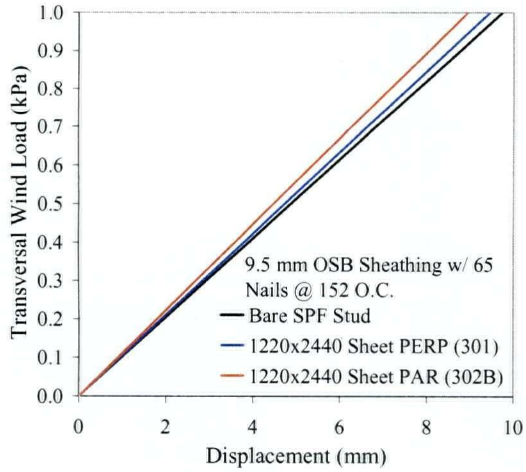

(a) Sheathing orientation.

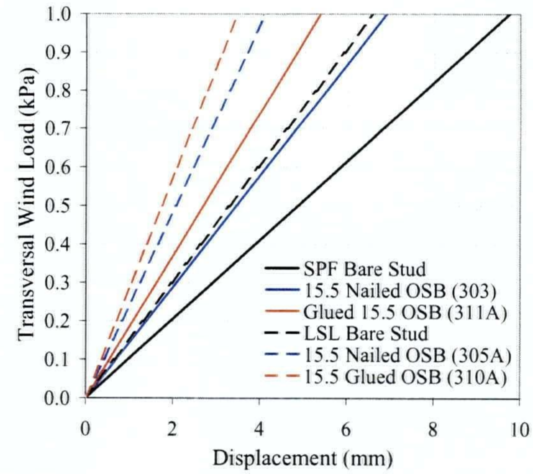

(b) Stud modulus of elasticity.

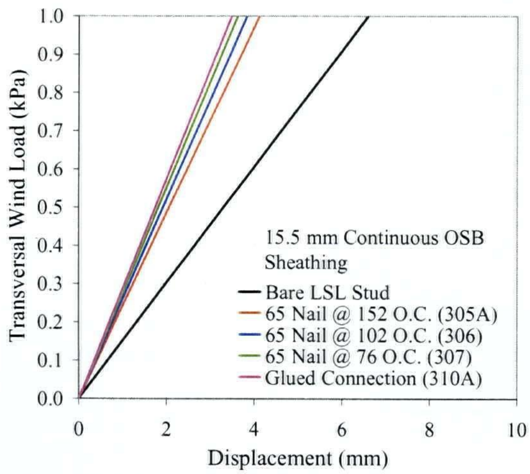

(c) Connection stiffness.

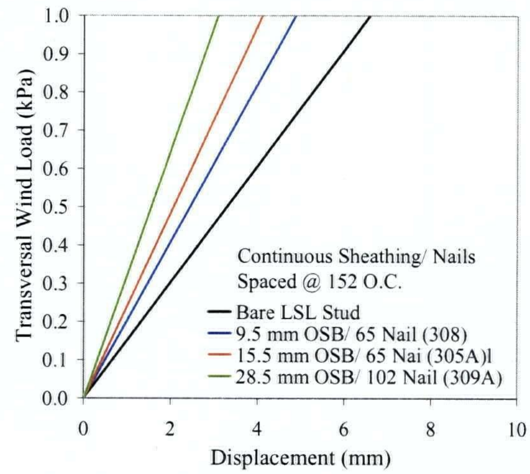

(d) Sheathing thickness.

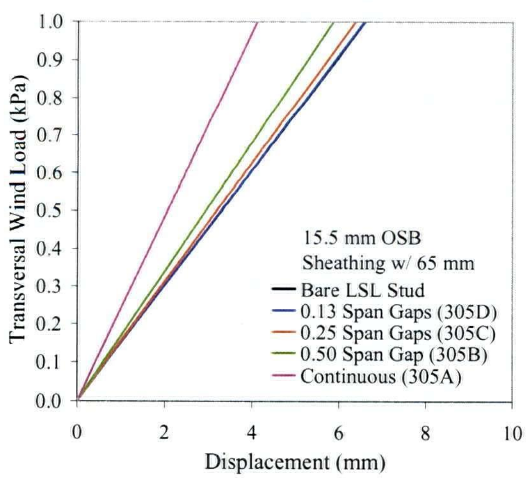

(e) Nailed connection with gaps.

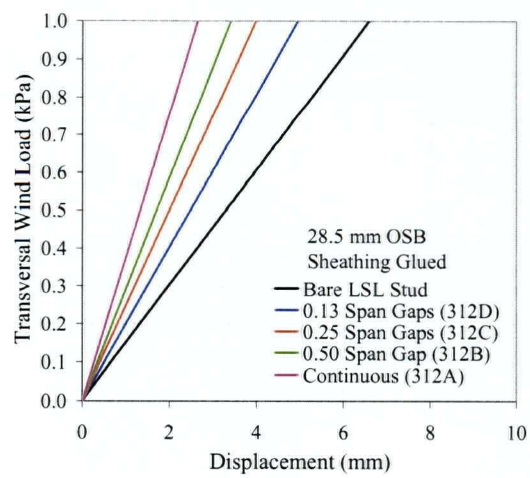

(f) Glued connection with gaps.

Figure 5.13. Load-displacement relationships obtained from testing.

under an increasing uniformly distributed transversal wind load. The curves for the bare SPF and LSL studs are based on the average modulus of elasticity values of all studs tested, which were shown in Figure 5.9 and are 9,500 MPa and 11,670 MPa, respectively. The average dimensions of the SPF and LSL studs were 38 by 234 mm and 44 by 242 mm, respectively.

The curves in Figure 5.13 are presented with a uniformly distributed wind load because that is the type of loading that these building components would be designed under if they were incorporated into a wall structure. The average load-displacement stiffness of each composite T-beam specimen type (Table 5.3) obtained from the third-point loading tests was transformed into an effective bending stiffness using simple beam theory. Effective bending stiffness is a cross-sectional property that is independent of the type of loading. These effective bending stiffness values were then used to calculate the load-displacement response of the composite T-beams under a uniformly distributed load using simple theory once again.

Figure 5.13 (a) shows the increase in composite member stiffness of T-beams with sheathing comprised of 1,220 by 2,440 mm sheets of 9.5 mm thick OSB oriented parallel along the length of the stud and the same sheathing oriented perpendicular to the length of the stud. The increase in stiffness of a composite member over the bare stud due to changing the orientation of the sheathing is not significant in this case (just under 6%). It has been shown, however, that it is possible to achieve a 30% increase in bending stiffness by changing the sheathing orientation for a 2,440 mm long (8') composite T-beam constructed with a similar cross section except using a 38 mm by 89 mm (2" x 4") SPF stud (McCutcheon, 1986). Thus, it is possible to significantly increase the stiffness of regular wood-frame walls with thin sheathing such as commonly used in the construction industry in North America by orienting the sheathing to be parallel along the length of the stud.

The effect of the modulus of elasticity of the stud, or stud member type, on the stiffness of composite T-beam members is presented in Figure 5.13 (b). These load-displacement relationships are for members with continuous sheathing. As can be seen, the increases in composite member stiffness over the bare stud stiffness are approximately the same for the members constructed with SPF and LSL studs. The responses of the composite members with LSL studs are merely shifted due to the increase in the stiffness of the LSL stud over the SPF stud. It should be noted that, since the existing provisions for light framing in the Canadian Wood Design Code do not allow for the explicit inclusion of composite action in design, the only way for the designer to increase the stiffness of a wall is by either changing the stud dimensions, the stud spacing, or the stud material. In this instance, changing the stud material from SPF to LSL resulted in an increase in member stiffness of approximately 48%. By including the effects of composite action for a member with an SPF stud and continuous nailed sheathing, the increase in stiffness is approximately 41%. By contrast, the increase in stiffness of that same composite member with an LSL stud over the bare SPF stud is 137%.

Figures 5.13 (c) and (d) show the effects of changing connection stiffness and sheathing thickness, respectively. While the increase in stiffness of a composite member with sheathing connected with 65 mm long spiral nails spaced 152 mm on centre may appear to be as large as a member with a glued connection (fully composite member), it should be noted that the results presented above correspond to initial member stiffnesses. As will be shown later in this chapter, the stiffness of nailed connections, and thus the stiffness of the partially composite members, decreases with repeated load cycles. As was mentioned in Chapter 2, partial composite action is used to describe the interaction of two or more components of a structural member when interlayer slip can occur between those components. Nailed connections are characterized by load-slip curves that were described in detail in Chapter 3 and thus composite members connected with nails are identified as being partially composite.

The increase in the stiffness of a composite member due to the increase in sheathing thickness can be significant. One of the objectives of this research program was to determine if it is safe and economically feasible to increase the spacing of studs in a wall beyond the 610 mm limit set out in the Canadian Wood Design Code. But, as can be seen in Figure 5.13 (d), any loss in wall stiffness due to the reduction of the number of studs in the wall (increased stud spacing) would be offset by including the effects of the partial composite action with thick sheathing. If the limit on stud spacing is increased significantly, or even eliminated, however, the sheathing may deflect excessively or fail in bending. Therefore, a design aid that specifies the minimum sheathing thickness required for a given stud spacing and a factored transversal wind load would be needed. Table 5.4 shows what this design aid could look like. The results are based on plate theory assuming pinned supports around the perimeter of each sheathing panel.

Deflection often governs the design of tall wood-frame walls. If it is assumed that deflection governs the design in this case then comparisons can be drawn from the test results, which show how an increase in stiffness can lead to an increase in stud spacing. Because the current code does not allow a designer to account for partial composite action, the average stiffness of a single 4,880 mm long bare SPF stud spaced at 610 mm on centre (206 N/mm) can be compared against the results of the partially composite T-beam tests. From the results, this wall configuration would have the same, or less, stiffness as a wall with LSL studs spaced at 1,220 mm on centre and either: 15.5 mm thick OSB without gaps in the sheathing and connected with nails; 28.5 mm thick OSB with gaps spaced at 2,440 mm on centre and connected with nails; or 15.5 mm thick

Table 5.4. Minimum sheathing thickness for a given stud spacing and factored wind load.

Sheathing Selection Tables

Horizontal Sheathing

Minimum Sheathing Thickness (mm)

Sheathing type	Stud spacing mm	Factored Wind Load (kPa) 1.0	1.4	1.8	2.2	2.6
OSB-A	305	9.5	9.5	9.5	9.5	9.5
	406	9.5	9.5	9.5	9.5	9.5
	610	9.5	9.5	9.5	9.5	11.0
	813	9.5	11.0	12.5	12.5	15.5
	1220	15.5	15.5	18.5	18.5	18.5
	2440	28.5				

Vertical Sheathing

Minimum Sheathing Thickness (mm)

Sheathing type	Stud spacing mm	Factored Wind Load (kPa) 1.0	1.4	1.8	2.2	2.6
OSB-A	305	9.5	9.5	9.5	9.5	9.5
	406	9.5	9.5	9.5	9.5	11.0
	610	11.0	15.5	15.5	15.5	15.5
	1220	28.5	28.5			

Notes:
1. Deflection criterion is length divided by 240 with the load unfactored.
2. Horizontal blocking for vertical sheathing panels is located at the panel edges only.
3. The wind load is equally distributed over the entire panel.
4. All studs are orientated vertically.

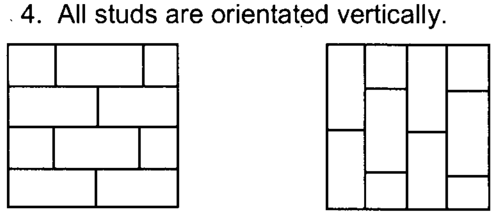

Horizontal sheathing

Vertical Sheathing

OSB with gaps spaced at 1,220 mm on centre and connected with glue. Alternatively, the average stiffness of a bare LSL stud (324 N/mm) spaced at 610 mm on centre would have the same, or less, stiffness as a wall with the same stud spaced at 1,220 mm on centre and either: 28.5 mm thick OSB without gaps in the sheathing and connected with nails; or 28.5 mm thick OSB without gaps in the sheathing and connected with glue.

The influence of the distance between the gaps in the sheathing of a composite member is presented in Figures 5.13 (e) and (f) for both nailed and glued connections, respectively. It is clear that adding gaps to the sheathing of a composite member dramatically decreases the stiffness of the composite member. Conversely, reducing the number of gaps in the sheathing can increase the stiffness of a composite stud member. It is common practice in wood-frame wall construction in North America to attach the sheathing to the studs horizontally, resulting in the maximum number of gaps in the sheathing along the height of a stud. Therefore, changing the orientation of the sheathing or using oversized sheathing panels to reduce the number of gaps over the height of the wall can significantly increase the stiffness of a composite wall system.

For the glued members without gaps in the sheathing, the average increase in member stiffness is approximately 150%. The average increase is still 33% for the glued members with gaps placed every 610 mm, which shows the significant effect that the connection stiffness can have on composite member properties. The increase in stiffness of a T-beam without gaps in the sheathing connected with nails is approximately 61% but that increase reduces to almost zero when gaps are placed every 610 mm in the sheathing. Thus the relationship between the gap spacing and the increase in member stiffness appears to be different for members with nailed connections and glued connections. The reason for this difference becomes clear when looking at the equations used to predict the response of partially composite members and the variables that affect that response. This will be addressed in detail next.

5.3.2 Analytical Prediction of Composite T-Beam Tests

The component tests that have been discussed in this, and previous, chapters were conducted to more accurately predict the response of the larger scale tests using analytical approximations. The composite T-beam test program was one of those large-scale test programs. Some of the properties of the sheathing components were not measured directly so reasonable engineering judgement was applied to measured values in order to provide an estimate of the unknown properties.

As will be shown later in this chapter, the effective stiffness in bending of a composite member is dependent upon the axial properties and the bending properties of the individual components. In addition, the calculation of effective flange width requires the shear rigidity of the sheathing members. Because only the bending stiffness of the sheathing in both principle directions was tested, the axial stiffness was calculated using the ratios between bending stiffness and axial stiffness values listed in Table 7.3C of Canadian Wood Design Code (CSA, 2001). Shear rigidity was calculated as a function of the modulus of elasticity with a Poisson's ratio of

Table 5.5. Sheathing properties based on sheathing bending test results.

Description	Nominal Thickness (mm)	Measured Thickness (mm)	Parallel			Perpendicular			Shear Rigidity (N/mm)
			MOE (MPa)	Bending Stiffness (N/mm^2/mm)	Axial Stiffness (N/mm)	MOE (MPa)	Bending Stiffness (N/mm^2/mm)	Axial Stiffness (N/mm)	
3/8" Ainsworth Construction Sheathing	9.5	9.68	7522	567800	42600	2866	216400	23300	11600
19/32" Ainsworth Structural 1 Rated Construction Sheathing	15.5	15.11	7290	2094500	64500	3501	1005900	44400	22000
1 1/8" Ainsworth Rimboard	28.5	28.05	8353	15363800	137200	3382	6221300	79600	39500

0.2. These values are listed in Table 5.5. Unlike the OSB sheathing, the axial modulus of elasticity of the studs was assumed to have the same value as the modulus of elasticity of the studs in bending.

5.3.2.1 Partial Composite Action

Extensive research has been conducted over the last fifty years on partial composite action with respect to wood structures. That research has produced several analytical formulations for predicting the response of members with partial composite action, some of which are presented in Chapter 2. Many of these studies have employed the same four assumptions to approximate this phenomenon: (i) the shear connection between elements is assumed to be continuous along the length of the member; (ii) the amount of slip permitted by the shear connection is directly proportional to the load transmitted; (iii) the distribution of strain throughout the depth of each element is linear; and (iv) the cross-sectional elements are assumed to deflect equal amounts at all points along their length at all times. Because the majority of these studies have included the same assumptions, they have been shown to give approximately the same results in the calculation of effective bending stiffness of a composite beam member.

Figure 5.14 shows the increase in stiffness of a typical T-beam member with partial composite action included over the stiffness of a bare stud, along the length of the beam, predicted by several analytical formulations. The example is 4,880 mm long with continuous sheathing connected to the stud with nails. The fraction of the span, referred to in the figure, is the ratio of the distance along the beam from the support to the total supported length of the beam. While some of the formulations attempt to predict effective member properties over the entire length of the beam, they all give similar results for effective member properties at the mid-span of the

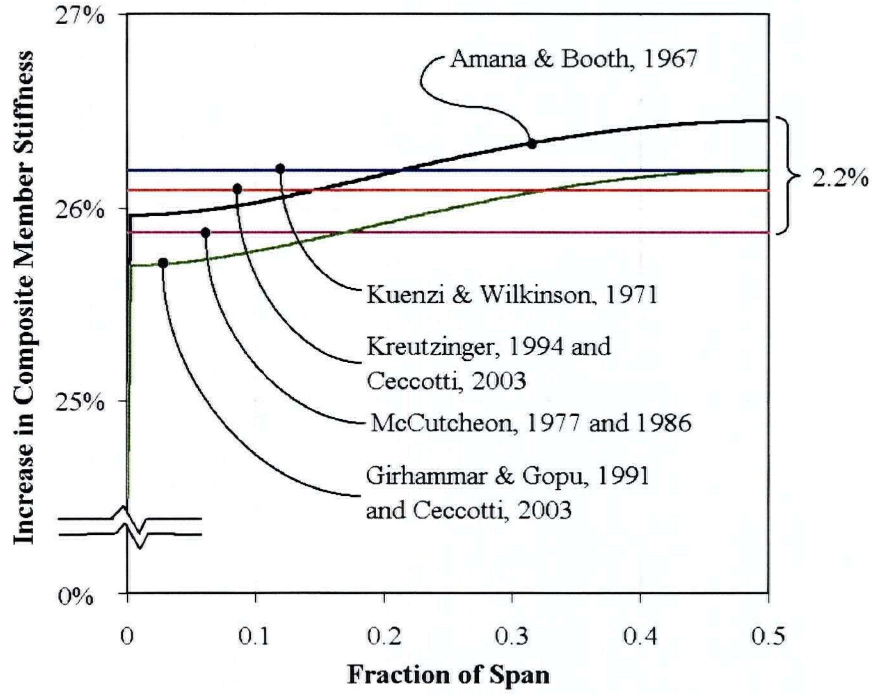

Figure 5.14. Variation of the increase in stiffness for several different formulations.

beam, in this case within 2.2%. Since all of the analytical formulations presented give approximately the same result for a typical beam member tested in this study, the formulation presented by Kreutzinger (1994) was chosen to predict the response of the composite beams tested in this study. This formulation is also included in the European standard for wood design – Eurocode 5 (ENV 1995-1-1, 1993). The effective bending stiffness of a partially composite member is thus given by:

$$(\mathrm{EI})_{\mathrm{eff}} = \sum_{i=1}^{2} \left(\mathrm{E}_i \mathrm{I}_i + \gamma_i \mathrm{E}_i \mathrm{A}_i \mathrm{a}_i^2 \right), \tag{5.1}$$

where γ_i is given by:

$$\gamma_i = \frac{1}{1 + \dfrac{\pi^2 \mathrm{E}_i \mathrm{A}_i}{\mathrm{k}_i \mathrm{L}^2}}, \text{ for } \mathrm{i} = 1,\ \gamma_2 = 1. \tag{5.2}$$

The location of the neutral axis is found by using the following (Figure 5.15):

$$a_2 = \frac{\gamma_1 E_1 A_1 \dfrac{(h_1 + h_2)}{2}}{\sum_{i=1}^{2} \gamma_i E_i A_i}. \tag{5.3}$$

In Equations (5.1) through (5.3), the symbols and terms are defined as follows:

i = identifier for each of the individual components of the composite member

E_i = modulus of elasticity of the i^{th} component

I_i = moment of inertia of the i^{th} component

A_i = area of the i^{th} component that is equal to width, b_i, multiplied by height, h_i

a_i = distance from the effective neutral axis to the centroids of the i^{th} component

γ_i = connection coefficient or connection efficiency factor of the i^{th} component, equal to 1 for a perfectly rigid connection and 0 for no connection at all

L = length of the composite member

k_i = per-unit-length slip modulus of the i^{th} component, equal to the slip modulus of an individual mechanical fastener divided by the fastener spacing.

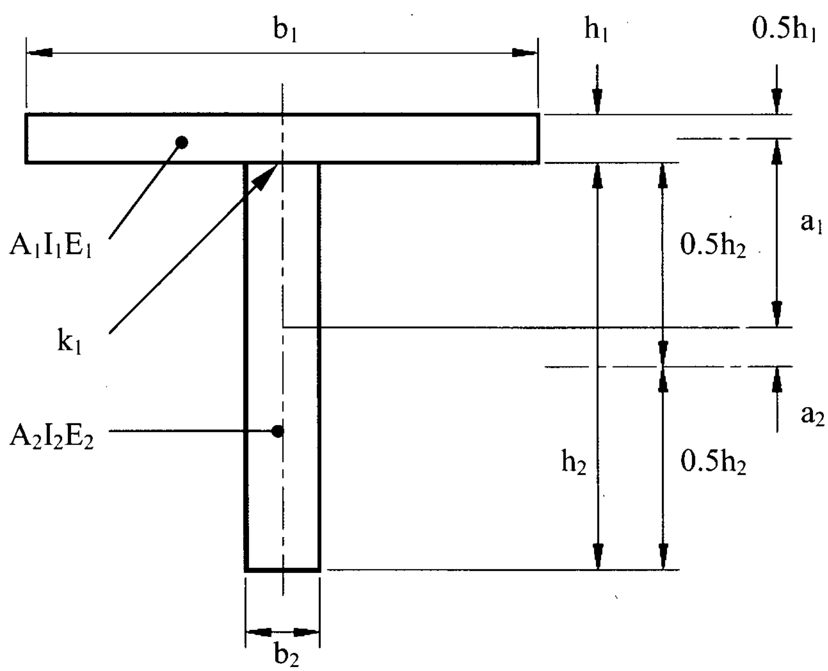

Figure 5.15. Cross-section of a T-shaped composite beam.

Unlike some of the other formulations, this one is independent of the type of load that is applied to the composite member and is therefore solely based upon the properties of the individual components of the member.

As was described in detail in Chapter 2, two research studies, one by McCutcheon (1977) and another by Itani and Brito (1978), concurrently identified the significance and quantified the effects of gaps in the flanges of composite members. Itani and Brito quantified this affect using a differential formulation leading to distinct equations for each beam configuration with gaps. McCutcheon, much more simply, included this effect into his formulation for effective bending stiffness by using the distance between the gaps as the length value in a factor that accounts for the amount of composite action. This principle can be applied to Equation 5.2 by exchanging the length value L in the connection efficiency factor, with the distance between the gaps in the sheathing L'. It was assumed that the gaps were evenly spaced along the span.

The Canadian Wood Design Code currently contains a formulation for calculating the effective properties of fully composite beams and stressed skin panels. This formulation is very similar to the one outlined above except that it does not contain a connection efficiency coefficient because the connections between components must be rigid. This standard does, however, also account for the partial composite action present in light framing floor, roof, and wall assemblies but not in a straightforward manner. The deflection limit set out for each type of assembly is higher than the target deflection limit to achieve the serviceability limit state because it is assumed that the affect of partial composite action from one or two sheathed faces will reduce the deflection calculated for the individual framing members and thus achieve the required serviceability target. The effect of partial composite action, both parallel and perpendicular to the framing members, is also included in system factors that increase the resistance values of the framing members. The problem with including the effect of partial composite action in common factors is that they apply to all assembly configurations equally. Thus a wall with very high partial composite action will receive the same increase in deflection limit for the bare stud as a wall with very little partial composite action. By providing the designer with a straightforward method to account for partial composite action a structure can use the wood materials more efficiently and at the same time meet all limit states.

5.3.2.2 Effective Flange Width

Since the distribution of stress in the flanges of composite members is not uniform, several methods have been developed to determine an effective flange width based on uniform stress distribution. Figure 5.16 shows the true and the effective distributions of stress in a typical T-beam. In contrast to the results from the calculation of the bending stiffness of partially composite members, the results for effective flange width can vary significantly among methods. An example of such variation is shown in Figure 5.17 with formulations outlined in Chapter 2.

This disparity between the methods of calculating an effective flange width has not been viewed as significant in previous research on regular wood-frame walls. Because the studs in regular walls are spaced relatively closely, the effective flange width is usually assumed to be the same as the stud spacing (Polensek, 1976; Gromala, 1983). In addition, because the sheathing on

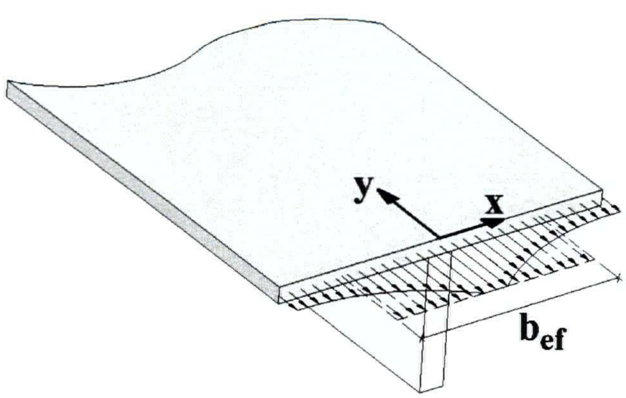

Figure 5.16. Stress distribution in the flange of a composite member.

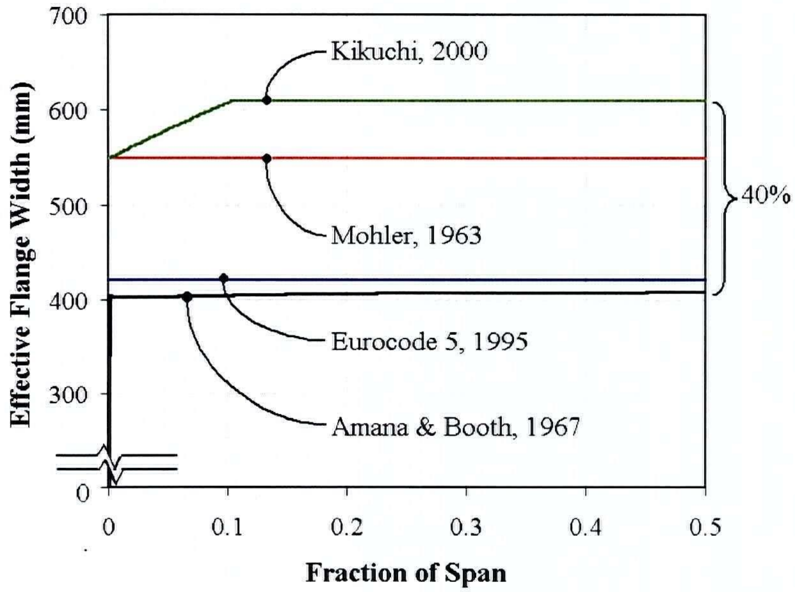

Figure 5.17. Variation of effective flange width for several different formulations.

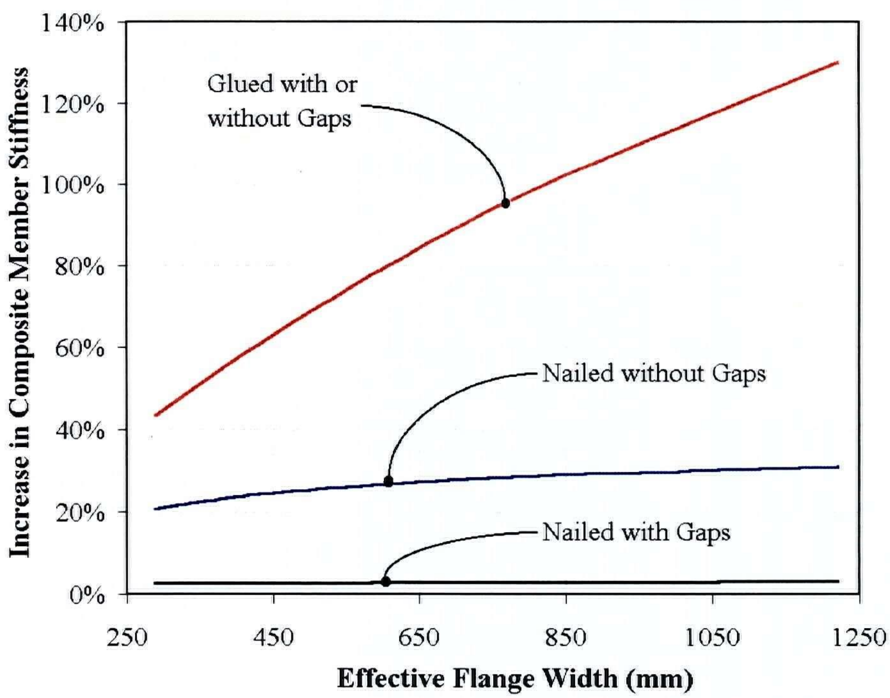

Figure 5.18. Increase in composite member bending stiffness with effective flange width.

regular walls is connected with nails at a large spacing, especially in the middle of sheathing panels, and the wall usually contains gaps between sheathing panels, the value chosen for the effective flange width does not have a significant impact on the determination of composite member properties. This can be observed in Figure 5.18, where the same T-beam used in Figures 5.14 and 5.16, is now shown with gaps placed at the quarter points of the total span. The value of effective flange width, however, does have a significant effect on tall wood-frame walls, as these walls are far more likely to have large stud spacing, thus requiring thicker sheathing connected to the studs with stiffer connections to increase the composite action between the two components. The same wall is also shown in Figure 5.18 with a glued, or fully rigid, connection. As the connection stiffness increases, so does the effect of the value chosen for effective flange width. It should be noted that the current methods for determining the effective flange width of a composite wood-frame member do not allow the designer to account for the effects of gaps in the sheathing.

Six T-beam test groups that included gaps in the sheathing showed two distinct curve shapes relating the increase in bending stiffness to the gap spacing in the sheathing (Figure 5.19). The curves of the nailed T-beams are influenced by two parameters: the connection efficiency factor and the effective width of the flange, but are dominated by the connection efficiency factor. In contrast, the curves of the glued T-beams are influenced only by the effective flange width parameter since the connection efficiency factor is unity.

Since the method for calculating effective flange width developed by Mohler (Raadschelders an Blass, 1995) is purely theoretical and is independent from the determination of composite member properties, it was chosen to approximate the test results. The equation to determine effective flange width is given by:

$$b_{ef} = 2L\frac{\lambda_1 \tanh(\varphi_1) - \lambda_2 \tanh(\varphi_2)}{\pi(\lambda_1^2 - \lambda_2^2)}, \text{ where} \tag{5.4}$$

$$\varphi_1 = \frac{\lambda_1 \pi b_f}{2L} \tag{5.5}$$

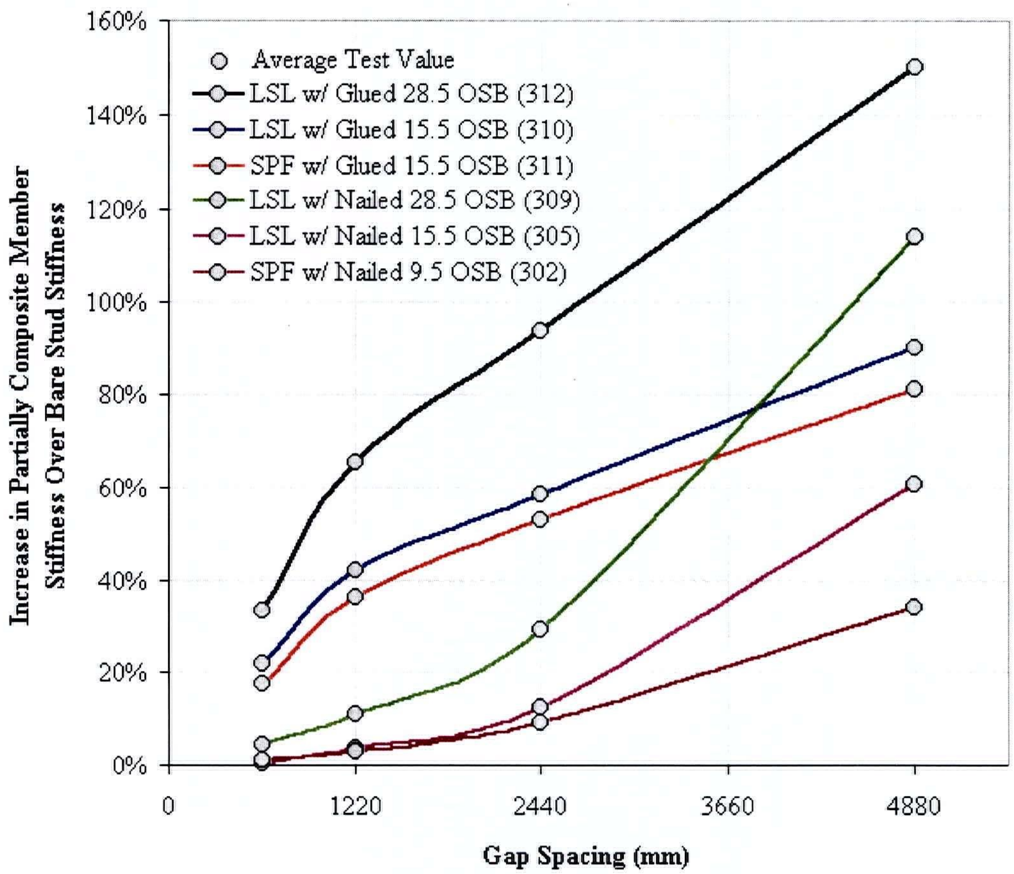

Figure 5.19. Increase in composite member bending stiffness with gap spacing.

$$\varphi_2 = \frac{\lambda_2 \pi b_f}{2L} \tag{5.6}$$

$$\lambda_1 = \sqrt{\alpha + \sqrt{\alpha^2 - \beta}} \tag{5.7}$$

$$\lambda_2 = \sqrt{\alpha - \sqrt{\alpha^2 - \beta}} \tag{5.8}$$

$$\beta = \frac{E_y}{E_x} \tag{5.9}$$

$$\alpha = \frac{E_y}{2G_{xy}} - \nu_{xy}\,. \tag{5.10}$$

where b_f is the clear flange width between the studs, L is the length of the beam, E_y is the modulus of elasticity parallel to the longitudinal axis of the beam, E_x is the modulus of elasticity perpendicular to the longitudinal axis of the beam, G_{xy} is the shear modulus of elasticity, and ν_{xy} is Poisson's ratio. Figure 5.20 shows that this formulation of effective flange width gives a good approximation to test results for the case of no gaps in the sheathing, where the length value is the entire span. It does not, however, approximate the tested T-beams with gaps very well using the distance between the gaps as the length value. The difference can be explained by looking at the distribution of axial stress in the flange as shown in Figures 5.21 and 5.22. Figure 5.21 shows the distribution of axial stress in the flange of a T-beam with progressively smaller distances between gaps in the flange obtained using the SAP2000 finite element analysis program (Wilson and Habibulah, 2000). In contrast, Figure 5.22 shows the same distribution of stress approximated by the Mohler formulation (Raadschelders and Blass, 1995) using the distance between the gaps as the length factor. By using the distance between the gaps as the length value, an effective width value from a shorter span is assumed and it is simply repeated along the length when there are gaps in the sheathing of the composite member. As shown in Figure 5.22, that is not in accordance with the finite element formulation.

The T-beam model represented in Figures 5.21 and 5.22 consisted of 25.4 mm by 25.4 mm (1" by 1") shell elements in SAP2000. The thickness and orthotropic properties of the shell elements in the sheathing and the stud corresponded to materials used for the specimens in group number 312. The sheathing elements were connected rigidly to the stud elements where they overlapped, which represented a glued connection. The total supported length of the beam was 4,880 mm (16') long. Pin supports were placed on the bottom two corners of the shell element at one end of the beam and rollers were placed on the bottom to corners at the other end. Gaps were placed in the sheathing by adding a new column of shell elements in the stud of the T-beam 3.2 mm (1/8") wide, which corresponded to the recommended gap between sheets by sheathing manufacturers and the gap width that was placed in the tested specimens.

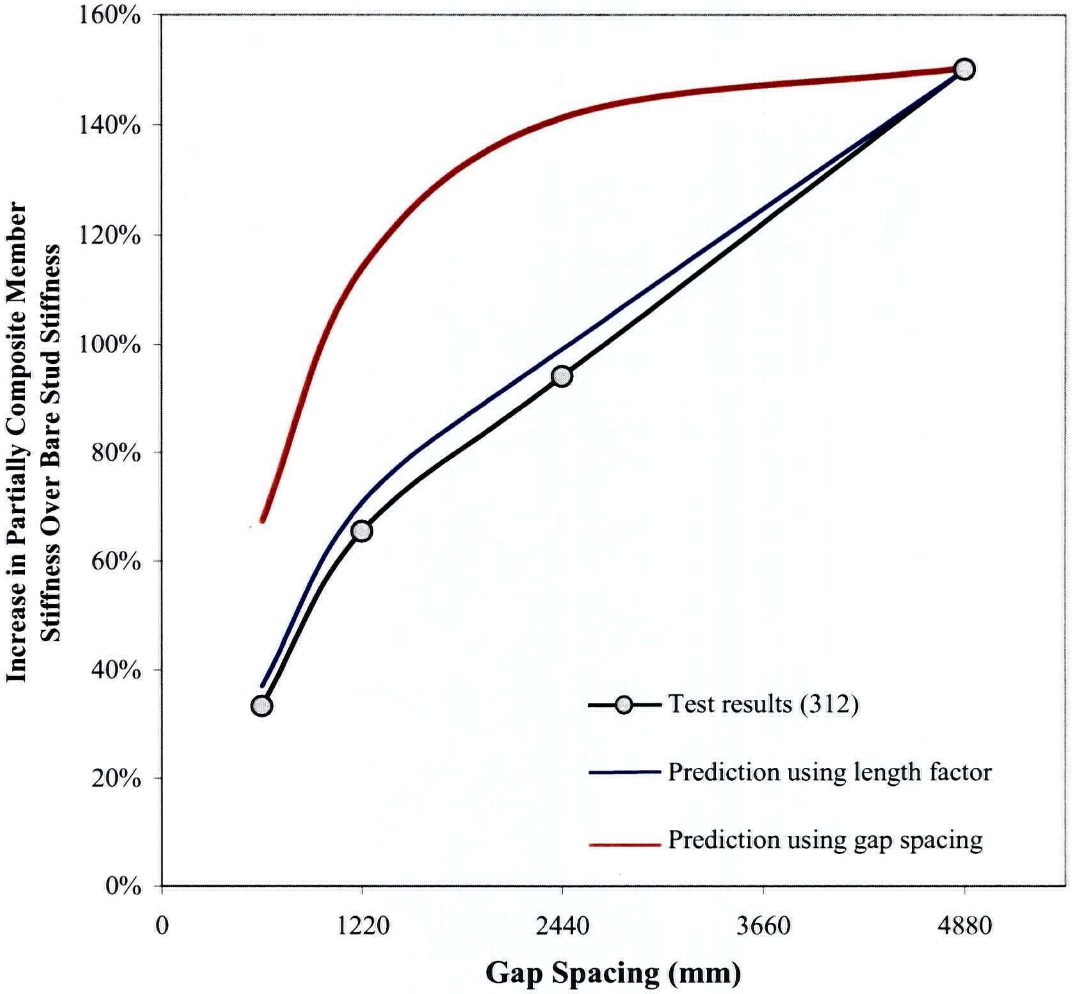

Figure 5.20. Comparison of the increase in stiffness of partially composite members over the bare stud stiffness with test results for a glued specimen with gaps.

As the only parameter that is not a cross-sectional property of the sheathing in the determination of the effective flange width in the formulation by Mohler (Raadschelders and Blass, 1995), the length value was varied to match the test results. For each of the three glued T-beam test groups, with three replicates each, a new length factor that closely approximated the test results was determined. It was found that this length factor was very similar for each of the three test groups. The average of the new length function is shown in Figure 5.23 as a ratio of the gap length to the total beam span. A new prediction based on test results using the new length factor

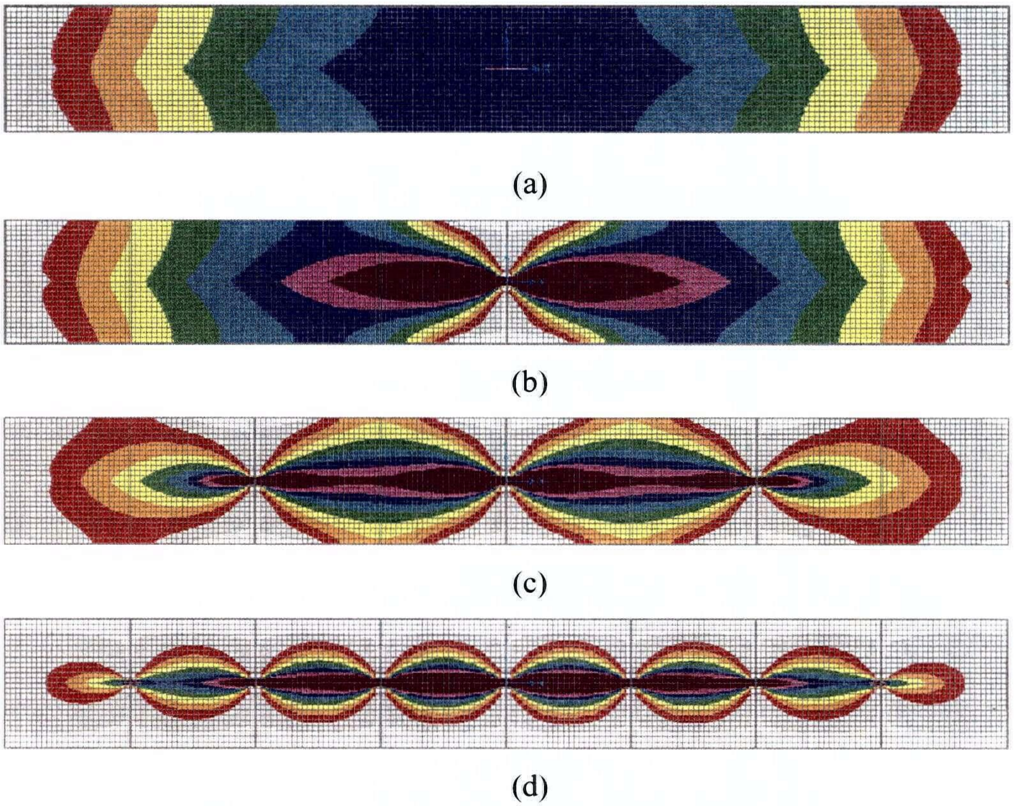

Figure 21. Distributions of axial stress in the flange from finite element models.

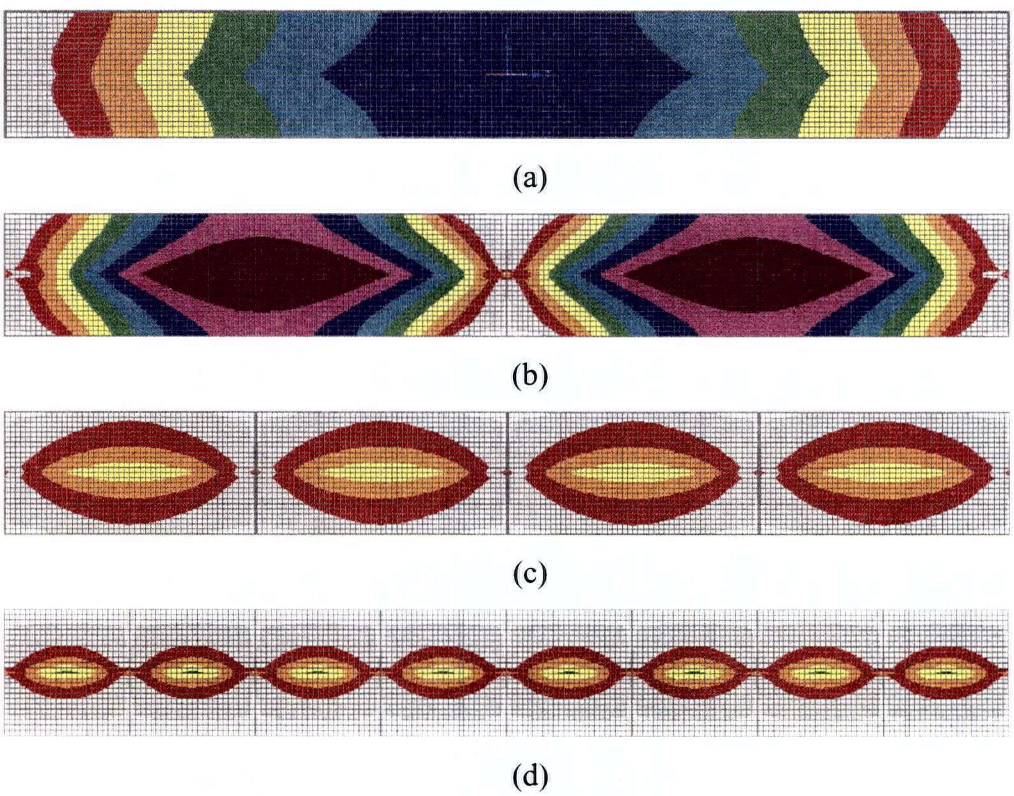

Figure 22. Approximated distributions of axial stress in the flange using gap length.

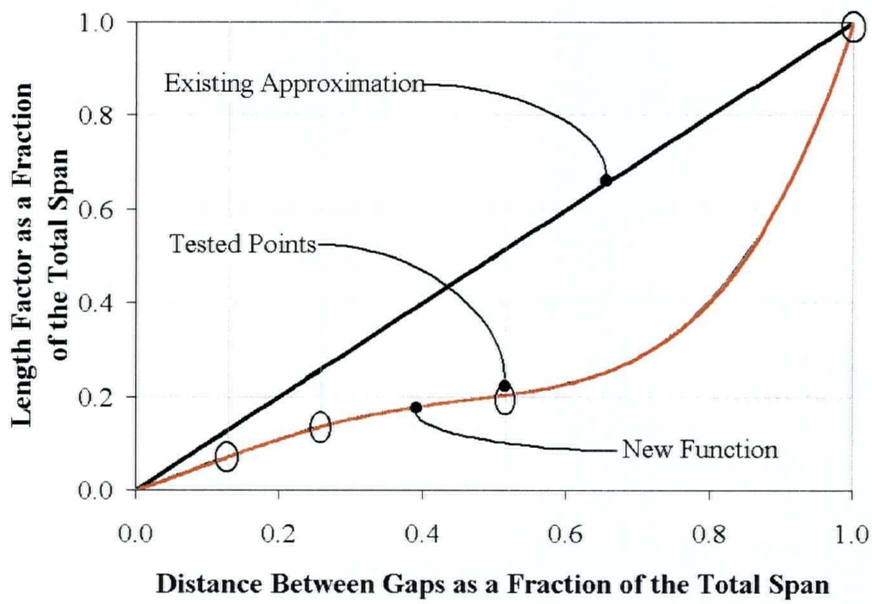

Figure 5.23. Length factor for use in effective flange width calculations.

is also given in Figure 5.20. As shown, it matches the test results much better than the approximation that uses the distance between the gaps as the length value in the effective flange width calculations.

The equation of the length function is as follows:

$$L_g = L\left\{3.6\left(\frac{L'}{L}\right)^4 - 4.1\left(\frac{L'}{L}\right)^3 + 0.94\left(\frac{L'}{L}\right)^2 + 0.49\left(\frac{L'}{L}\right)\right\} \tag{5.11}$$

L' is equal to the distance between the gaps in the sheathing and L is the total length of the beam. The length function has been fit to test results but a parameter study has not been undertaken to determine if it is a function of the member properties of the composite T-beams. In addition, since this equation has only been fit to a limited number of tested T-beams it is recommended that this factor be compared to test results or finite element analyses with a greater variation of cross-sectional member properties before it is used in the design of wood-frame floors or walls. The length factor, once validated with further study, could be applied in design as a tabulated factor for length based on the ratio of the distance between gaps in the sheathing to the total span length such as in Table 5.6.

Table 5.6. Length factor as a function of the ratio of gap spacing to total span length.

Gap Spacing Ratio L'/L	Length Factor L_g/L
0.125	0.07
0.250	0.13
0.500	0.20
0.75	0.33
1.00	1.00

5.3.2.3 Connection Stiffness

The per-unit-length connection slip modulus values used in the analytical formulations to predict the composite T-beam test results were obtained from the load-slip connection tests described in Chapter 3. Slippage measurements between the stud and the sheathing, described previously in this chapter, were taken for each T-beam test. The average maximum slippage measured in the T-beams with nailed connections was approximately 0.4 mm (0.016"). From the data measured during the load-slip connection tests, stiffness values were obtained for this range of slippage in the connection. No slippage was measured in any of the glued tests; therefore a rigid connection, or a connection efficiency factor equal to 1.0, was assumed for the analytical approximations.

When the load-slip connection stiffness values were used in the analytical predictions there was a relatively large disparity between the test results and the predicted response. This can be explained by looking at the load-slip connection test set-up shown in Chapter 3 and the actual T-beams connected with nails that were tested. The sheathing in the load-slip connection tests was not restrained from lifting off of the stud and in many cases the nail and sheathing withdrew from the stud prior to failure. In the T-beam tests not only was the sheathing prevented from lifting off from the stud by the other nails connecting the sheathing to the stud, but the applied load at the third points of the T-beam also prevented the sheathing from lifting off. Therefore, in addition to the resistance provided by the nail, there is a frictional component to the load-slip connection not accounted for in the load-slip connection tests.

The effect of friction can clearly be seen in Figures 5.24 (a) and (b). Four of the T-beam test groups were loaded beyond their initial linear range. The load-displacement response of one of those tests groups, 306, is shown in the figure. A high initial stiffness is overcome at approximately 2.2 kN (500 lb.) for the displacement at the mid-span of the beam (Figure 5.24 (a)) and for the slippage between the sheathing and the stud at the end of the beam (Figure 5.24 (b)) followed by another, lower linear stiffness range. This change in stiffness is due to overcoming the friction between the sheathing and the stud. Figure 5.25 shows comparisons between predicted stiffness values and stiffness values obtained from test results in both linear ranges. The comparisons in the initial linear range are not close and can differ by as much as 27%. The per-unit-length slip modulus is thus far too low. But when the predicted stiffness is compared with the test results in the range of lower stiffness the difference is much smaller, being less than 9% for each of the test groups.

Because the majority of the composite T-beams that were tested were only loaded in the initial linear stiffness range, i.e. prior to overcoming the effects of friction, it would be useful to determine a method to account for the frictional resistance in the nailed connections. But frictional effects are difficult to quantify in this case because they depend on a number of factors: weight of the sheathing which is a function of sheathing thickness; applied force imparted through the sheathing by each nail; nail spacing, as nails spaced closer together will produce a

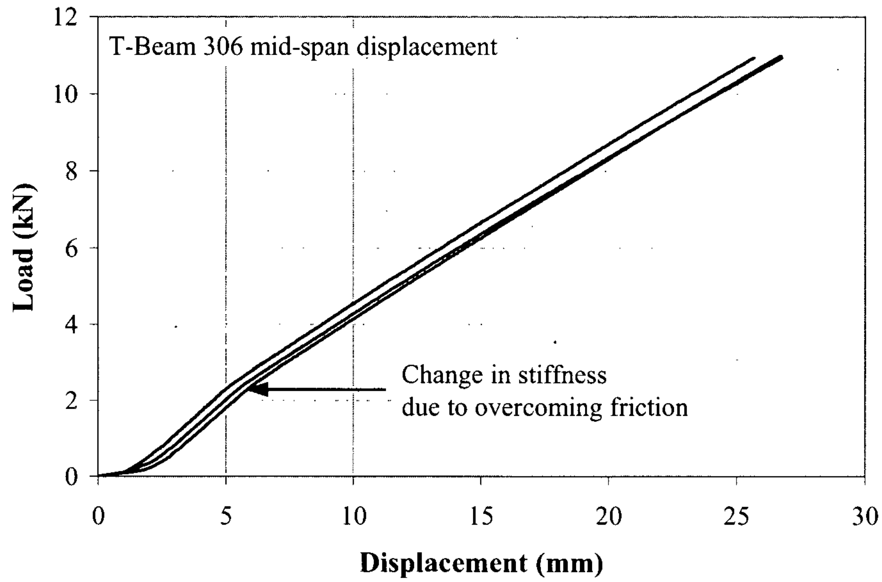

(a) Mid-span displacement

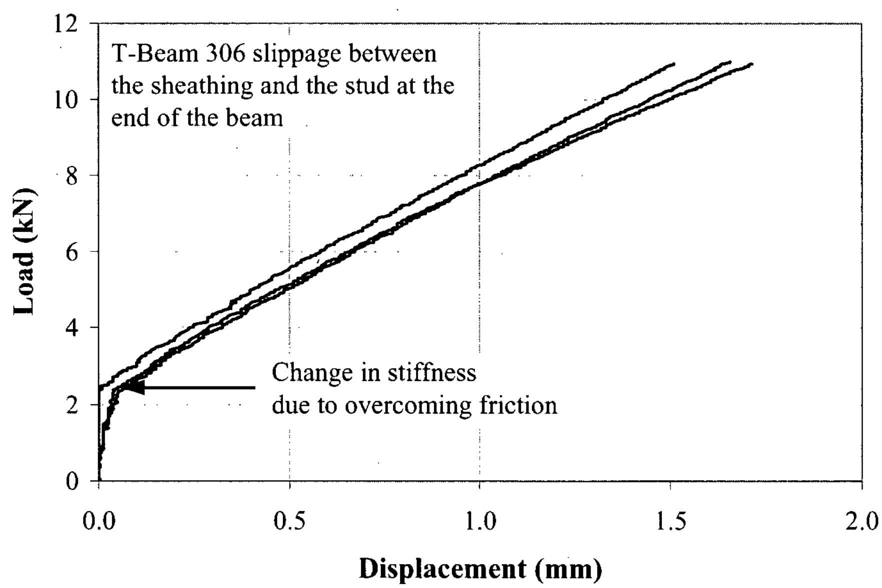

(b) Slippage between the sheathing and the stud

Figure 5.24. Load-displacement response of a T-beam loaded beyond the linear range.

higher frictional force per nail than the same nails at a larger spacing; and the frictional force produced by the load distribution beams at the third points of the composite T-beams. In addition, most T-beams with gaps were loaded several times after each gap was cut in the sheathing, so the frictional effects are expected to be reduced after each loading cycle.

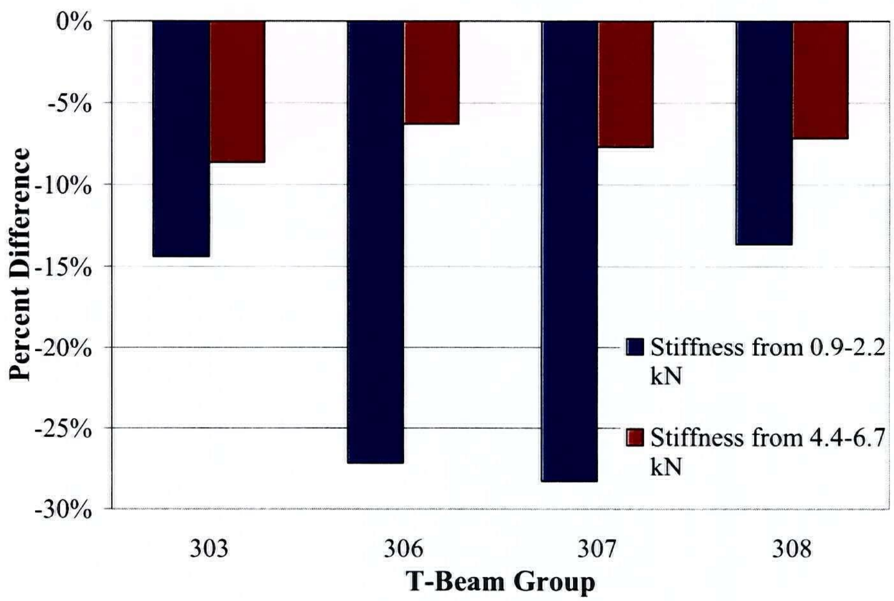

Figure 5.25. Percentage difference between test and analytically predicted results at different load levels.

Analytical predictions are presented in Table 5.7 for each of the specimen groups except group 304, which was loaded cyclically and will be discussed in detail in the next section. The reduced individual connector stiffness values for the specimen group numbers denoted with an 'H,' for the higher loading range, were obtained from the load-slip connection test results for larger deformations. The predicted effective bending stiffness for each group was determined using equations 5.1 to 5.3 with an effective flange width using equations 5.4 to 5.10. From the predicted effective bending stiffness values, predicted T-beam stiffness values were calculated based on the beam test set-up configuration. As mentioned previously, the T-beams with continuous flanges were considerably stiffer than the stud members alone and also much stiffer than the T-beams with gaps in the sheathing. In general, the analytical predictions gave very good estimates of composite beam stiffness. Figure 5.26 shows graphically how the test results compare with the predicted values. Only the comparisons between the predicted values and the test results for the higher loading range for the four specimen groups described previously have

Table 5.7. Average T-beam stiffness values compared with analytical predictions.

Specimen Group Number	Configuration	Individual Connector Stiffness (N/mm)	Predicted Effective Bending Stiffness, EI_{eff} (Nmm^2)	Effective Flange Width (mm)	Average Stiffness of Composite T-Beam (N/mm)	Average Percent Increase in Stiffness	Predicted Stiffness of T-Beam (N/mm)	Predicted Percent Increase in Stiffness	Percent Difference
301	C	392	3.041×10^{11}	320	166	3.17	163	0.72	-2.25
302	A	606	4.564×10^{11}	552	259	34.05	244	25.82	-5.82
302	B	606	3.705×10^{11}	345	211	9.06	198	2.15	-6.17
302	C	606	3.661×10^{11}	228	200	2.99	196	0.94	-2.00
302	D	606	3.636×10^{11}	102	196	1.09	194	0.25	-0.90
303	A	461	5.224×10^{11}	556	326	41.29	279	20.76	-14.39
303H	A	257	4.885×10^{11}	556	286	23.73	261	12.92	-8.63
305	A	611	7.360×10^{11}	551	528	60.55	393	19.46	-25.57
305	B	611	6.256×10^{11}	373	370	12.45	334	1.54	-9.69
305	C	611	6.204×10^{11}	255	341	3.50	332	0.69	-2.71
305	D	611	6.173×10^{11}	114	330	0.27	330	0.19	-0.07
306	A	611	7.773×10^{11}	551	570	72.43	415	25.56	-27.13
306H	A	389	7.345×10^{11}	551	419	26.66	392	18.64	-6.27
307	A	611	7.999×10^{11}	551	596	82.73	427	31.07	-28.27
307H	A	456	7.686×10^{11}	551	445	36.43	411	25.92	-7.68
308	A	566	6.763×10^{11}	546	419	35.34	361	16.88	-13.66
308H	A	296	6.389×10^{11}	546	368	18.96	341	10.41	-7.17
309	A	1153	8.644×10^{11}	547	704	114.14	462	40.40	-34.34
309	B	1153	6.391×10^{11}	351	425	29.37	342	3.80	-19.71
309	C	1153	6.270×10^{11}	235	365	11.09	335	1.83	-8.30
309	D	1153	6.193×10^{11}	105	343	4.43	331	0.59	-3.65
310	A	-	1.047×10^{12}	551	602	90.10	560	76.84	-6.97
310	B	-	9.253×10^{11}	373	502	58.52	494	56.21	-1.46
310	C	-	8.322×10^{11}	255	449	41.86	445	40.49	-0.96
310	D	-	7.067×10^{11}	114	385	21.79	378	19.31	-2.03
311	A	-	9.534×10^{11}	556	511	81.12	509	80.72	-0.22
311	B	-	8.384×10^{11}	375	431	52.80	448	58.93	4.02
311	C	-	7.512×10^{11}	255	384	36.34	401	42.41	4.46
311	D	-	6.344×10^{11}	113	331	17.41	339	20.26	2.44
312	A	-	1.440×10^{12}	547	786	150.17	770	144.82	-2.11
312	B	-	1.221×10^{12}	351	610	94.04	653	107.59	7.02
312	C	-	1.055×10^{12}	235	520	65.52	564	79.32	8.36
312	D	-	8.248×10^{11}	105	419	33.29	441	40.18	5.18

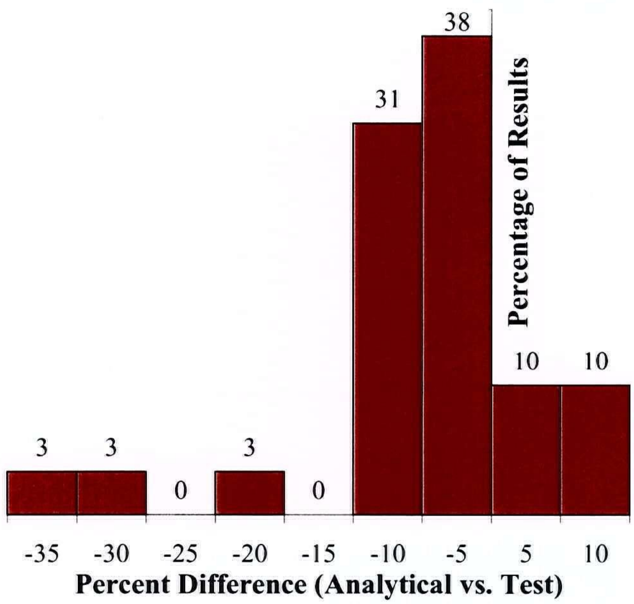

Figure 5.26. Histogram of analytical predictions versus test results for bending stiffness.

been included. Of the 29 stiffness computations included in Figure 5.26, 48% were within 5% of the test values and another 41% were within 10%. Only three predictions (9%) were off by more than 10%.

Several member properties can be determined in addition to effective bending stiffness. One of those properties, slippage between the sheathing and the stud, was measured in each T-beam test conducted at five locations along the length of the beam. This was shown in Figure 5.4. Using the second assumption listed in section 5.3.2.1 to derive predictions for effective member properties, that the amount of slip permitted by the shear connection is directly proportional to the load transmitted, the amount of slip at any point along the beam is given as:

$$\delta_i = \frac{\gamma_i E_i A_i a_i V}{(EI)_{eff} k_i} \tag{5.12}$$

where V is the shear force in the composite beam, which is a function of the total load applied. The other terms have been defined previously. Predicted slippage stiffness used for comparison with test results is determined by dividing the total load applied to the composite beam by the amount slippage at a particular point along the beam. Thus, for a composite beam loaded at the third points, the shear force at the ends of the beam are equal to half of the total load applied and the slippage stiffness is equal to:

$$\kappa_{y=0,L} = \frac{2k_i (EI)_{eff}}{\gamma_i E_i A_i a_i}. \tag{5.13}$$

Comparisons between predicted slippage stiffness at the ends and the quarter points for four composite T-beams are presented in Table 5.8. Each test result value represents six values: both sides of the three replicates tested for each group. The coefficient of variation for these results can be very high in comparison with those found for bending stiffness. These four T-beams had continuous sheathing and were loaded past the initial linear stiffness range. Unlike the prediction of effective bending stiffness, predicted slippage values for composite beams with gaps in the sheathing do not correspond well with test results. However, the predicted slippage stiffness at the ends of the four T-beam groups selected compares well with the test results. As mentioned, the amount of slip at a point along the beam is a function of shear force. Using Euler

Table 5.8. Average T-beam slippage values compared with analytical predictions.

Specimen Group Number	Configuration	Predicted Slippage Stiffness at the End (3rd Point Loading) (N/mm)	Average Slippage Stiffness at the Ends (N/mm)	COV of Slippage Stiffness at the Ends (N/mm)	Percent Difference at the Ends	Predicted Slippage Stiffness at the Quarter Point (UDL) (N/mm)	Average Slippage Stiffness at the Quarter Points (N/mm)	COV of Slippage Stiffness at the Quarter Points (N/mm)	Percent Difference at the Quarter Points (3rd Point Loading)	Percent Difference at the Quarter Points (UDL)
303H	A	3760	3954	8.39	-4.93	5640	5432	12.35	-30.79	3.82
306H	A	6305	6492	31.71	-2.88	9458	8426	16.48	-25.17	12.24
307H	A	7548	6688	10.11	12.86	11322	10655	23.32	-29.16	6.26
308H	A	5224	4729	13.69	10.47	7836	7026	19.59	-25.65	11.53

beam theory, the shear force at the quarter points of a beam loaded at its third points is the same as the shear force at the ends of the beam. Thus, according to equation 5.12, the amount of slip at the ends of the beam should be the same as the amount of slip at the quarter points of the beam. The differences between predicted values and test results at the quarter points using these assumptions were found to be very large, with an average of approximately 27%. The reason for this discrepancy is due to the fact that an assumption of Euler beam theory is not met: that plane sections of a beam remain plane. The cross sections of the partially composite members do not remain constant with increasing load as the sheathing slips past the stud members.

An additional comparison was made to the test results for slippage stiffness at the quarter points assuming that the beams are loaded uniformly along their length, which results in a linearly varying distribution of shear stress over the length of the beams. The distributed load was determined by making the maximum bending moments from the third point loading and uniformly distributed loading (UDL) configurations equal. As can be seen in Table 5.6, these predicted values are much closer to the slippage stiffness from test results due to the linear variation in shear force. It therefore appears that the real distribution of shear force is in between these two extremes.

5.3.3 Cyclic Tests

The previous section has shown the importance of the connections between the sheathing and the studs on the overall response of a composite member. In Chapter 3 it was stated that only the average load-slip connection response was required for predicting the response of composite T-beams and full-scale walls because they contain so many connectors. Reducing the load-slip response to a lower percentile value would therefore be too conservative. However, there may be other factors that would contribute to lowering the response of these connections over time.

Walls undergo many cycles of loading prior to a design event. For the case of wind loading, there may be dozens of storms with severe wind speeds in a particular location every year, although the top wind speeds are typically lower than the wind speed used in design. These repeated cycles of loading might have a detrimental effect on the stiffness of a composite wall system. To achieve a greater understanding of this effect on partial composite action, one group of composite T-beam specimens, 304, was loaded under the cyclic protocol described in Section 5.2.2 and shown in Figure 5.7.

Figure 5.27 shows the load-displacement response of one of these specimens. The cyclic load levels shown correspond to maximum bending moments produced by increments of a 1 kPa uniformly distributed load. Thus the maximum bending moment achieved in the composite T-beam at the highest load level corresponds to the maximum bending moment that would be achieved had the beam been loaded under a 5 kPa uniformly distributed load. Three cycles equal to the maximum load of the initial loading cycle followed each incremental increase in load level. Figure 5.28 shows the approximate linear stiffness of the average of these groups of three

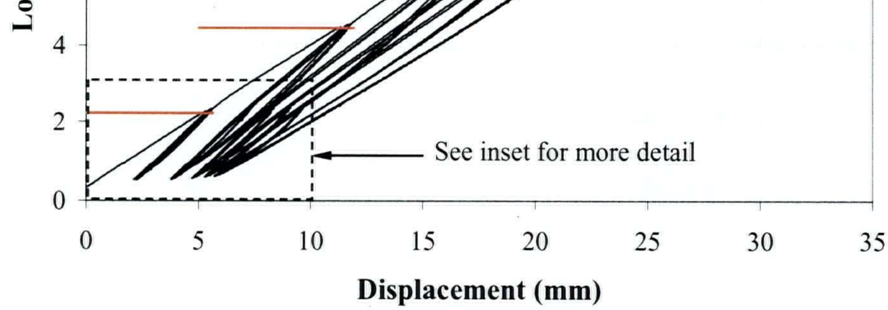

Figure 5.27. Load versus displacement for a typical cyclic test specimen.

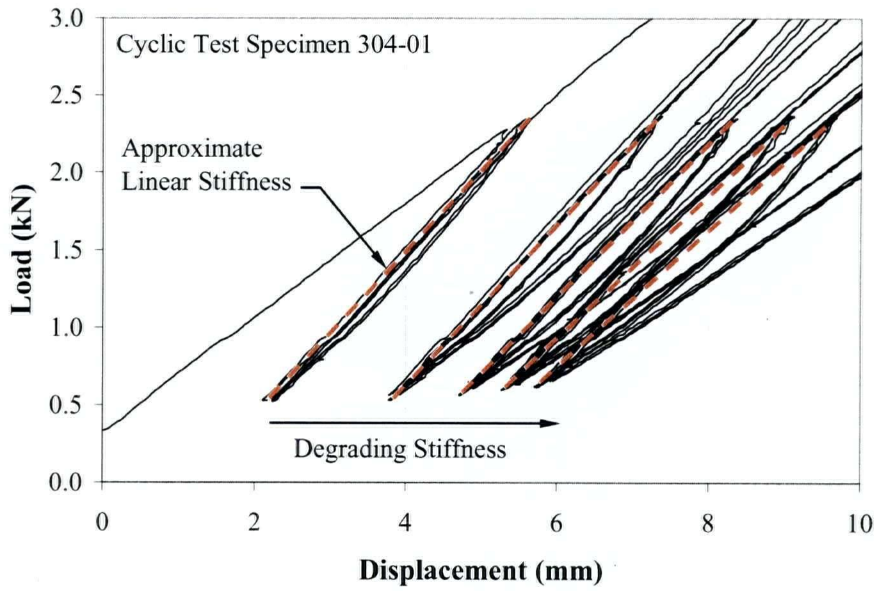

Figure 5.28 (Inset of Figure 5.27). Degrading stiffness with increasing load levels.

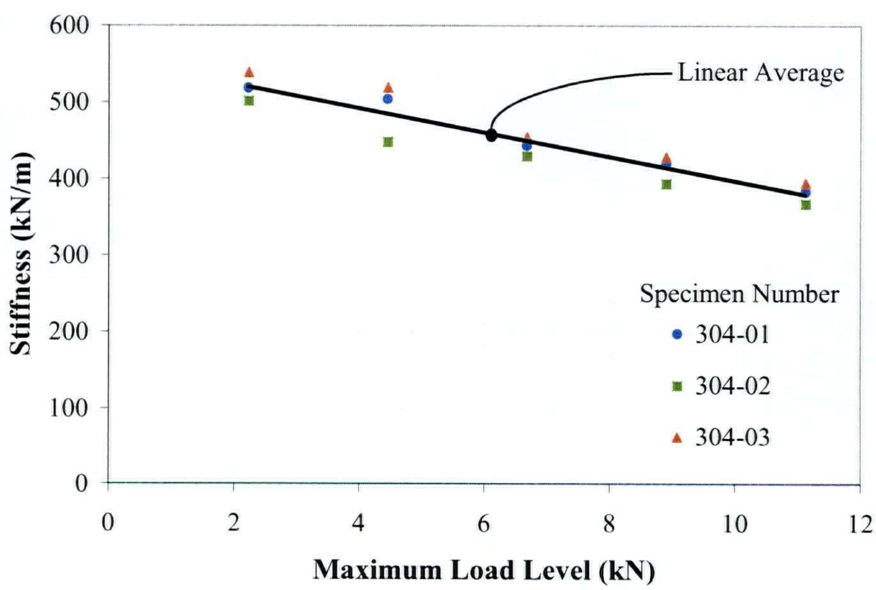

Figure 5.29. Degrading stiffness values under cyclic loading with increasing load levels.

lower load cycles for the same specimen in Figure 5.27. It is clearly evident that the stiffness of the composite T-beam is degrading after repeated increasing loading cycles. The relationship between bending stiffness and the maximum load level applied is shown in Figure 5.29. When a line is plotted through the average values of each of the three replicates tested it can be seen that this relationship is approximately linear. The total decrease in stiffness is approximately 26%.

The degradation in bending stiffness of the composite T-beam is related to the decrease in stiffness of the nailed connections due to the increasing slippage displacement of the joints. Figure 5.30 shows the load-displacement response of the connection between the sheathing and the stud at one end of the composite T-beam specimen. This curve is very similar to the curve in Figure 5.27, which shows the response of the entire composite T-beam. Therefore, although the average response of connections may be appropriate for use in the prediction of effective member properties with partial composite action, the connection stiffness should be reduced to account for the numerous cycles of varying load that a structure will be exposed to over its lifetime. To fully understand this phenomenon, and to develop connection stiffness reduction factors for inclusion into design codes, several different connection specimens or composite members should be loaded with a protocol based on recorded wind speeds at numerous locations over the lifetime of a structure.

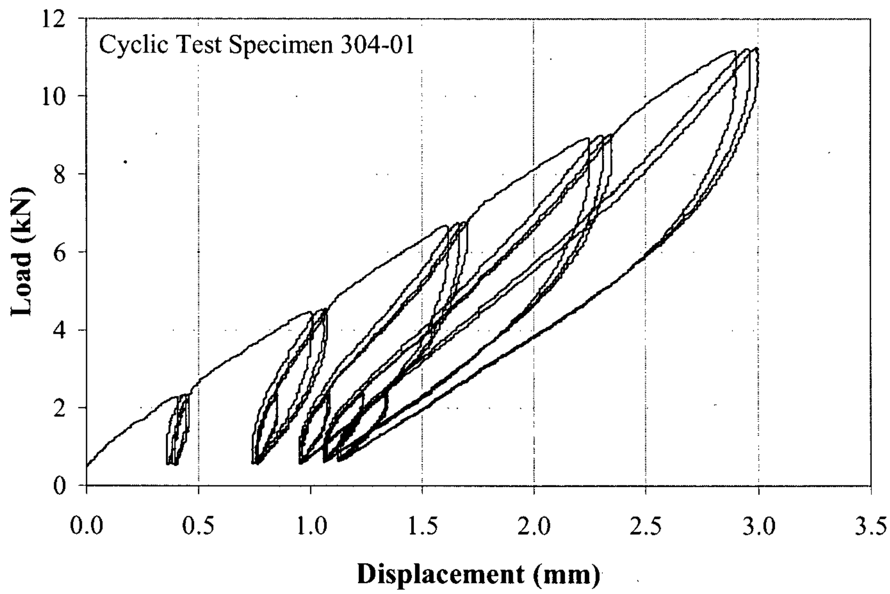

Figure 5.30. Slippage between sheathing and stud during cyclic loading.

In addition to loading cycles from external wind pressures, wood-frame walls may also be exposed to changing moisture levels over time that can produce internal forces between the components of the composite structure. This could cause slippage between the sheathing and the studs and also lead to degradation in the overall bending stiffness of the system over time. Several studies have looked at the response of timber and concrete composite structures under varying moisture levels (Kuhlmann and Schanzlin, 2004; Fragiacomo and Ceccotti, 2004). These studies are not directly applicable because the loading remained constant throughout the tests and, as mentioned, exterior walls undergo many loading fluctuations. However, this research has shown that moisture variations can also have a detrimental affect on the bending stiffness of a composite member over time.

5.3.4 Failure Modes

When tested to ultimate capacity, failure occurred in the SPF studs of two of the T-beam specimens in test group 301. The two failures are shown in Figure 5.31 and 5.32. The measured bending stiffnesses of these two studs were at the low end of the cumulative distribution presented in Figure 5.9 with calculated moduli of elasticity of 6,834 MPa and 7,585 MPa. The failure was in tension and originated in defects in the bottom tension face of the studs and propagated on a diagonal through the height of the stud in a brittle manner. The failures occurred at loads of 8.7 kN and 6.5 kN, respectively. The other specimens did not display any visible signs of failure. The intention of this testing program was to obtain stiffness values in the linear-elastic range of the T-beams and so the beams were for the most part undamaged after testing. Small slip did occur in the interface between the sheathing and the stud, with a maximum value of approximately 0.4 mm for the beams loaded in the initial elastic range and 3 mm for those loaded in the higher loaded range.

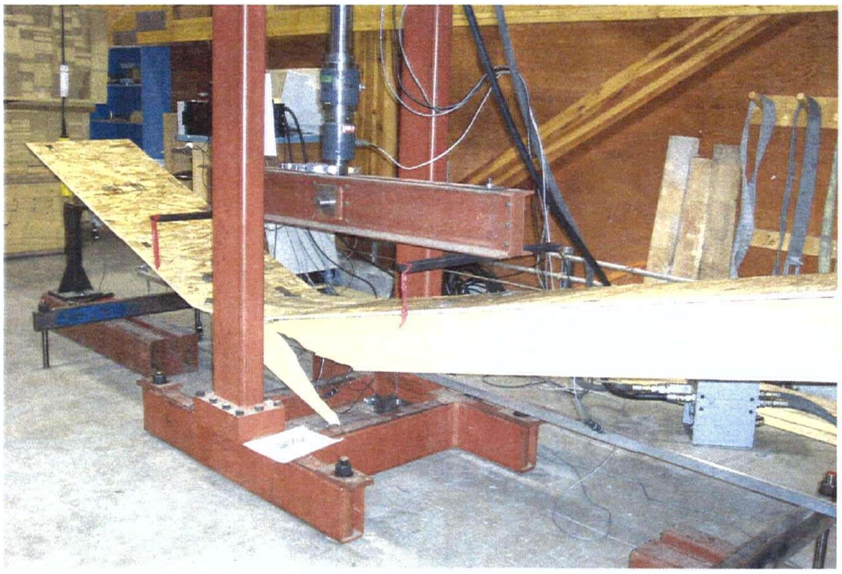

Figure 5.31. T-beam failure due to stud failure.

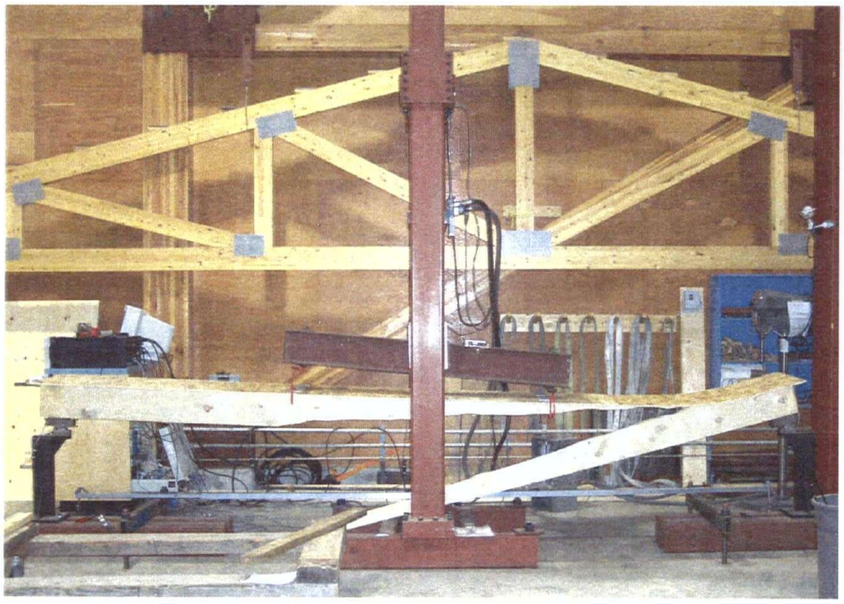

Figure 5.32. T-beam failure due to stud failure.

Although it has been shown that partial composite action can increase the bending stiffness of composite members, the bending capacity specified by design codes of a member designed with partial composite action may not increase to the same extent, if at all. This is because the distribution of stress in the stud member changes if the contributions from the flanges are taken into account compared with the bare stud alone. For the case of the T-beams described in this chapter, by connecting a flange to the stud the bending stresses in the stud are reduced but a uniform tension stress is added due to the force couple created by shifting the neutral axis towards the flange. Increasing the stiffness of the connection between these two components will further decrease the bending stresses in the stud but will increase the tension stress because the location of the neutral axis will move closer to the flange. The distribution of stress in an example composite T-beam is shown in Figure 5.33.

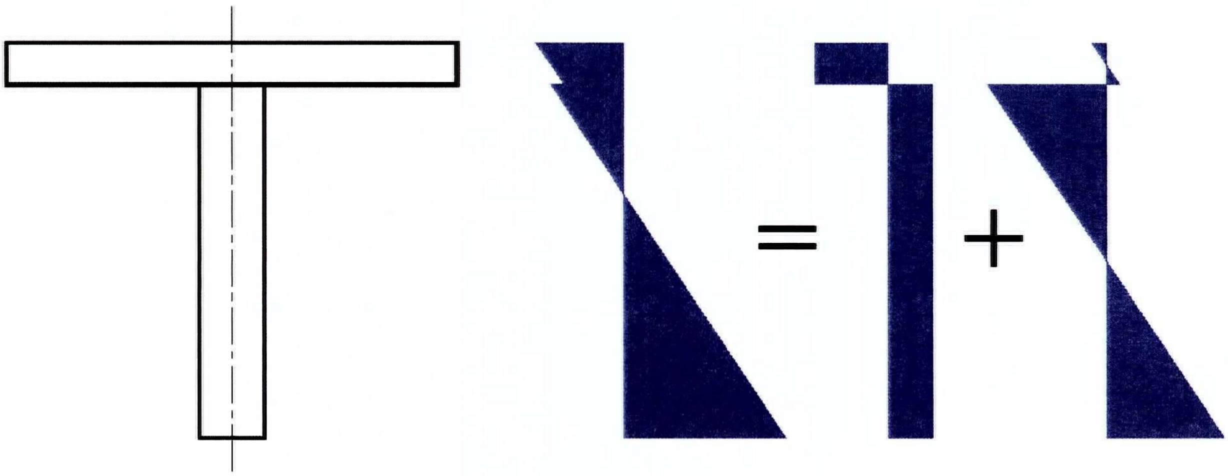

Figure 5.33. Distribution of stress for a composite T-beam.

The inclusion of axial stresses can dramatically change the distribution of stress in the components of composite bending members. Therefore, in order to evaluate the acceptability of stress in composite members it is necessary to treat each component as a member under combined axial and bending load using an interaction equation. A common interaction equation used in the design of wood structures is as follows:

$$\frac{f_a}{F_a} + \frac{f_b}{F_b} \leq 1.0 \tag{5.14}$$

where the lower case f values represent applied axial and bending stresses and the upper case F values represent allowable stresses. When this ratio is compared to the ratio of only applied bending stress to allowable bending stress for the case when the contribution of the sheathing is ignored, the values are very similar. This is because tension is a weaker property of wood than bending. From a reliability point of view, the phenomenon can also be explained by the fact that the stressed volume in tension is being increased through composite action, consequently increasing the probability of failure. The larger volumes of wood in tension thus negate the benefit of lower maximum tension stress. In summary, partial composite action therefore does not significantly affect the specified strength of composite members.

5.4 SUMMARY

The test results presented in this chapter have provided a basis for comparing variations in the cross-sections, configurations, and loading protocols of the 12 composite T-beam specimen groups that represent components of tall wood-frame walls. The variations included: stud material; sheathing material; sheathing thickness; connection type; length between the gaps in the sheathing; and monotonic and cyclic loading. The distance between the gaps in the sheathing and connection stiffness had the greatest influence on the stiffness of the specimens tested. With the incorporation of partial composite action into design standards and the elimination of the limit on stud spacing for regular wood-frame walls, more economically feasible wall configurations could be selected.

Because the majority of methods used to calculate partial composite action are based on the same assumptions and give approximately the same result, a simple approach was chosen predict the results of the tested T-beams. This formulation included a method for predicting effective flange width based on structural mechanics. The predictions compared well with test results for specimens without gaps that had been loaded past an initially high linear stiffness range, due to friction between the sheathing and the stud. A new length factor in the formulation of effective flange width, based on test results with glued connections, was determined to account for the affects of gaps in the sheathing. Using this new factor, the predicted stiffness values matched more closely with test results.

Walls found in structures will undergo many loading cycles over the lifetime of a building. These cycles will reduce the connection stiffness of mechanical fasteners and thus reduce the stiffness of the walls. A method to account for this reduction must be developed before partial composite action can be incorporated into codified design. In addition, attaching a flange to a stud will impart a tension stress over the depth of the stud in addition to reducing the bending stress applied. Therefore, each component of a composite beam must be designed as a member under combined axial and bending load using an interaction equation. Because tension is a weak property of wood, the effects of partial composite action may not increase the overall strength of a composite member.

6. SHEARWALL TESTS

The current guidelines for regular wood-frame shearwalls limit the stud spacing to 600 mm (nominal 2 ft) on centre. This limit in the Canadian Wood Design Code is to prevent sheathing panels from buckling under racking loads. This chapter presents the test results of monotonic pushover tests on shearwalls to assess whether this limitation on the stud spacing can be relaxed for tall wood-frame walls. The aim was to determine to what extent buckling of the sheathing panels of a shearwall occurs and, if so, what effect the buckling of the sheathing panels has on the overall response of the wall to racking loads.

6.1 OBJECTIVES AND SCOPE

Tall wood-frame walls are similar in many respects to regular wood-frame walls but they have certain characteristics that set them apart so that restrictions and limits in design codes that apply to regular walls do not necessarily apply directly to tall walls. Chapter 5 has demonstrated how the inclusion of partial composite action directly into the design of member resistance, currently restricted in the Canadian Wood Design Code, can lead to significant increases in composite member stiffness over the bare stud stiffness. With an increase in the overall stiffness of a composite wall, due to the inclusion of partial composite action, the stud spacing could be increased, resulting in a more economical structural system.

A major advantage of wood-frame construction is that the sheathing panels in a wall system serve a dual structural purpose. Unlike a wall constructed with structural steel, where braces are required to resist lateral forces and a system of sheathing and purlins is required to resist transversal, or out-of-plane, wind loads, the sheathing panels in wood-frame walls contribute to resisting both of these loads. Therefore, although this study is primarily concerned with the performance of tall wood-frame walls under transversal loads, it must be remembered that these walls also act as shearwalls that resist lateral loads due to wind and earthquakes. Clause 9.5.3.2 in the Canadian Wood Design Code, CSA O86-01 (CSA, 2001), states that the framing members in a shearwall shall be spaced no greater than 600 mm apart. The reasoning behind this limitation is provided in the commentary to the code. It states that "under specific test conditions, panels have been observed to buckle locally under lateral loads." This conclusion is based on theoretical work done by Kallsner (1995) and a report on shearwall testing compiled for the American Plywood Association by Tissell (1990). The testing showed that there is a reduction in the load carrying capacity of shearwalls with 9.5 mm sheathing and 600 mm stud spacing, compared to shearwalls with thicker sheathing.

The results presented in Chapter 5 clearly show that the use of thicker sheathing can have a significant effect on the increase in stiffness of a partially composite member over the stiffness of a bare stud alone. The use of thicker sheathing creates the possibility of increasing the stud spacing. One of the objectives of the full-scale wall tests, to be described in Chapter 7, was to test walls that had stud spacing in excess of the current code prescriptions. To validate the use of the large stud spacing in the full-scale wall testing, displacement controlled monotonic pushover tests were conducted on shearwalls with both thin and thick sheathing (9.5 mm and 18.5 mm), 610 mm and 1,220 mm stud spacing, and with varied connection stiffness. The purpose of this testing program was, therefore, not to analyze every aspect of the buckling of the sheathing under racking loads or to accurately predict when buckling would occur. Only general trends on the occurrence of buckling and its effect on the lateral load carrying capacity of a shearwall were sought. The shearwall tests were conducted in the Wood Engineering Laboratory of Forintek Canada Corp. in Vancouver.

6.2 METHODS AND MATERIALS

6.2.1 Shearwall Specimens

The failure mode of interest in this test program, localized buckling of the sheathing panels of a shearwall, was deemed independent of the height of the wall because it largely depends on the properties and the support conditions of the individual sheathing panels of a wall. Therefore, it was not considered necessary to construct and test tall shearwall specimens. The tested walls were nominally 2,440 mm (8') tall and 2,440 mm wide. A typical wall specimen is shown in Figure 6.1 and two pictures of specimens prepared for testing are shown in Figure 6.2. To increase the likelihood of localized buckling in the sheathing panels, modifications to standard shearwall construction practice were made. The framing members were all 38 by 140 mm

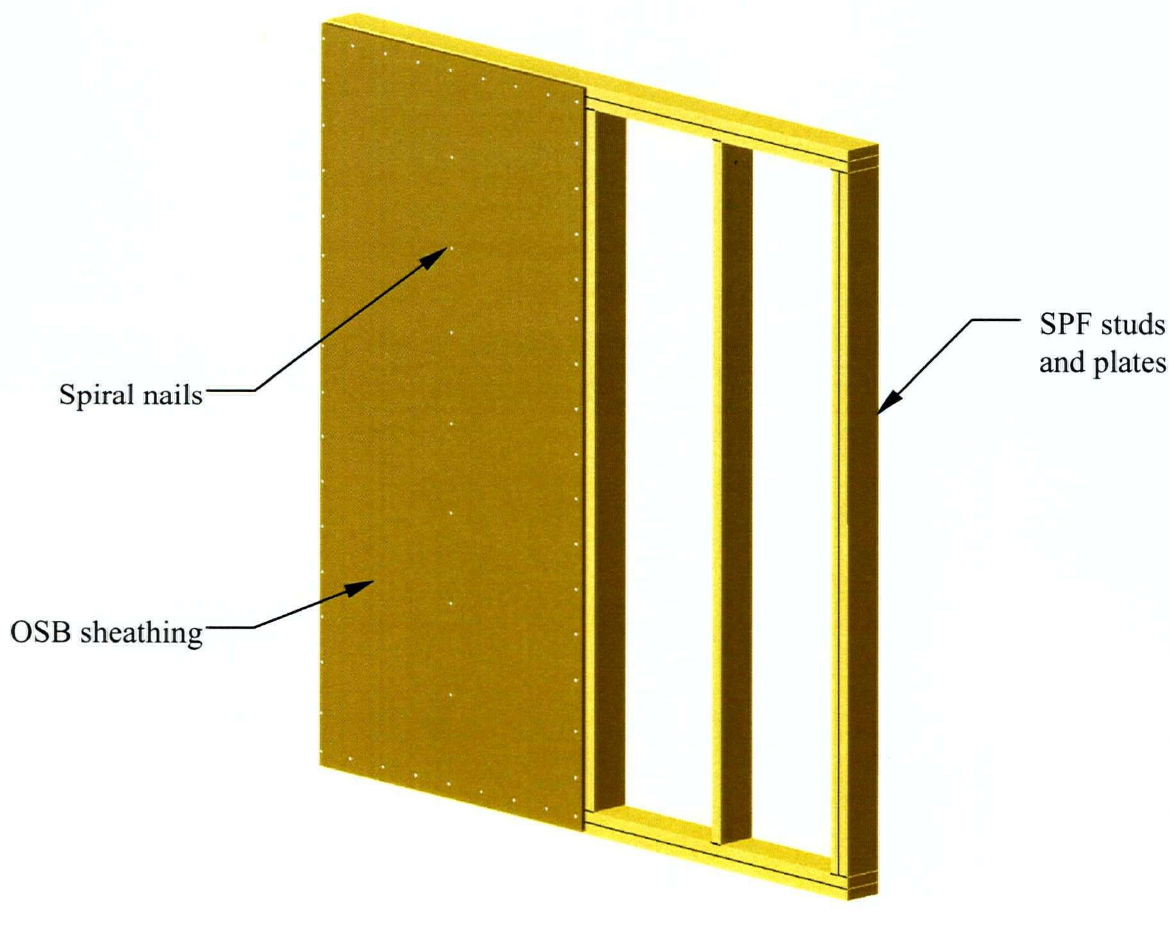

Figure 6.1. Typical details of a shearwall specimen.

(a) (b)

Figure 6.2. Shearwall specimen prepared for testing.

(2"x6") spruce-pine-fir (SPF) No. 2 or better. This framing member size was chosen to prevent axial failures in the studs of the walls. Additionally, the central stud and the bottom plate were doubled up, similar to the end studs and the top plate of the wall. This was done to minimize the possibility of tear-out failures occurring around the perimeter of the sheathing panels by maximizing the edge distance of the connectors.

Three frames for the walls were constructed, but as will be described later, each wall was modified after the first test and retested. The six wall configurations are listed in Table 6.1. The sheathing material chosen for the testing was oriented strandboard (OSB) because it was used exclusively in the composite T-beam tests and the full-scale wall tests. The studs and plates were cut from 4,880 mm (16') long members. It was possible to cut two studs or two plates from each 4,880 mm long member. To decrease the variability between wall 201 and wall 202 in terms of the framing material, the studs and plates were 'matched' for these two walls. Each

Table 6.1. Shearwall test matrix.

Specimen Group Number	Configuration	Fastener Type	Edge Fastener Spacing (mm)	Interior Fastener Spacing (mm)	Sheathing Material (Thickness in mm)	Sheathing Orientation w.r.t stud orientation	Stud Material	Stud Spacing (mm)
201	A	65 mm Spiral Nails	152	305	9.5 OSB	PAR	SPF	610
	B	#8x65 mm Wood Screws w/ 13 mm dia. washers	76	-	9.5 OSB	PAR	SPF	610
202	A	65 mm Spiral Nails	152	-	9.5 OSB	PAR	SPF	1220
	B	#8x65 mm Wood Screws w/ 13 mm dia. washers	76	-	9.5 OSB	PAR	SPF	1220
204	A	65 mm Spiral Nails	152	-	18.5 OSB	PAR	SPF	1220
	B	#8x65 mm Wood Screws w/ 13 mm dia. washers	76	-	18.5 OSB	PAR	SPF	1220

stud and plate in one wall was cut from the same member as the corresponding stud and plate in the other wall.

Walls 201 and 202 had the same sheathing but had different stud spacing. Wall 201 had fasteners in the interior of the sheathing panels because it had five studs due to the smaller stud spacing. Walls 202 and 204 had the same stud spacing but different sheathing thicknesses. It was determined that the test results from wall 203, which was characterized by 18.5 mm OSB sheathing with studs spaced at 610 mm on centre, were not required after viewing the results of test 201.

The sheathing panels were oriented vertically, or with the stronger axis parallel to the studs, for every wall. This was done so that the sheathing panels were only supported at the edges for the walls with 1,220 mm stud spacing. The sheathing was connected to the frame with either 65 mm (2 ½") spiral nails or with both spiral nails and #8 by 65 mm (#8x2 ½") wood screws and 4.8

mm thick by 19 mm (3/16" by 3/4") outside diameter steel washers. The spiral nails were driven using a pneumatic coil nail gun and the screws were attached using a power drill. The studs were end nailed to one plate member at the top and bottom of each wall using 76 mm (3") common nails. The double studs and plates were also connected together using 76 mm common nails. Two nails spaced at 102 mm (8") on centre were used for the studs and three nails at each stud location were used for the plates. Additional 89 mm (3 ½") common nails spaced at 102 mm on centre, which were clinched, were used to connect the double studs in wall 204 to prevent a shear failure mode found during a previous wall test from reoccurring.

All material used for testing was dry and had been stored in a laboratory environment at an average temperature of 20° ± 3°C and a relative humidity of 60% ± 10% for at least one week. The framing members were left over from a previous research program and had been stored in the laboratory for several months. Each wall specimen was tested within 24 hours of assembly.

6.2.2 Testing Apparatus and Instrumentation

A photo of the test set-up to determine the response of sheathing panels to racking loads is shown in Figure 6.3 and a schematic of the test set-up is shown in Figure 6.4. The upper steel transfer beam was attached to the top plate of each wall prior to the wall being placed onto the lower steel foundation member by an overhead crane. The steel foundation member was attached to the concrete strong floor of the lab with bolts to provide a rigid support. A 16 mm (5/8") diameter threaded tension rod was placed at each end of each wall to resist any overturning forces so that the walls themselves resisted only shear loads. The tension rods and the 12 mm (1/2") anchor bolts, placed at 406 mm (16") on centre along the top and bottom of the walls, were tightened by hand. Two steel guide frames with rollers to prevent out-of-plane displacements of the walls laterally supported the upper steel transfer beam.

Seven data measurements were collected during the tests: applied load; movement of the actuator head (stroke); the in-plane horizontal displacement of the top plate of the wall; and the in-plane relative displacements (shear) between the diagonally opposite corners of each sheathing panel (Figure 6.4). The loading for the monotonic testing was unidirectional and to the left in the photo and the schematic. A 222 kN (50,000 lb.) universal testing machine delivered the load that was measured using a 111 kN (25,000 lb.) load cell. The displacement controlled loading rate for each shearwall test was kept constant at 7.6 mm (0.3") per minute. The in-plane horizontal displacement of the bottom frame member of the top plate was measured using a coil spring-loaded transducer (DCDT) with a total measurement range of 3,050 mm (120").

The four corner-to-corner relative displacements were measured with displacement transducers with a measurement range of 76 mm (3"). The transducers were connected to mounting

Figure 6.3. Photo of the test set-up for determining the response of sheathing panels to racking loads.

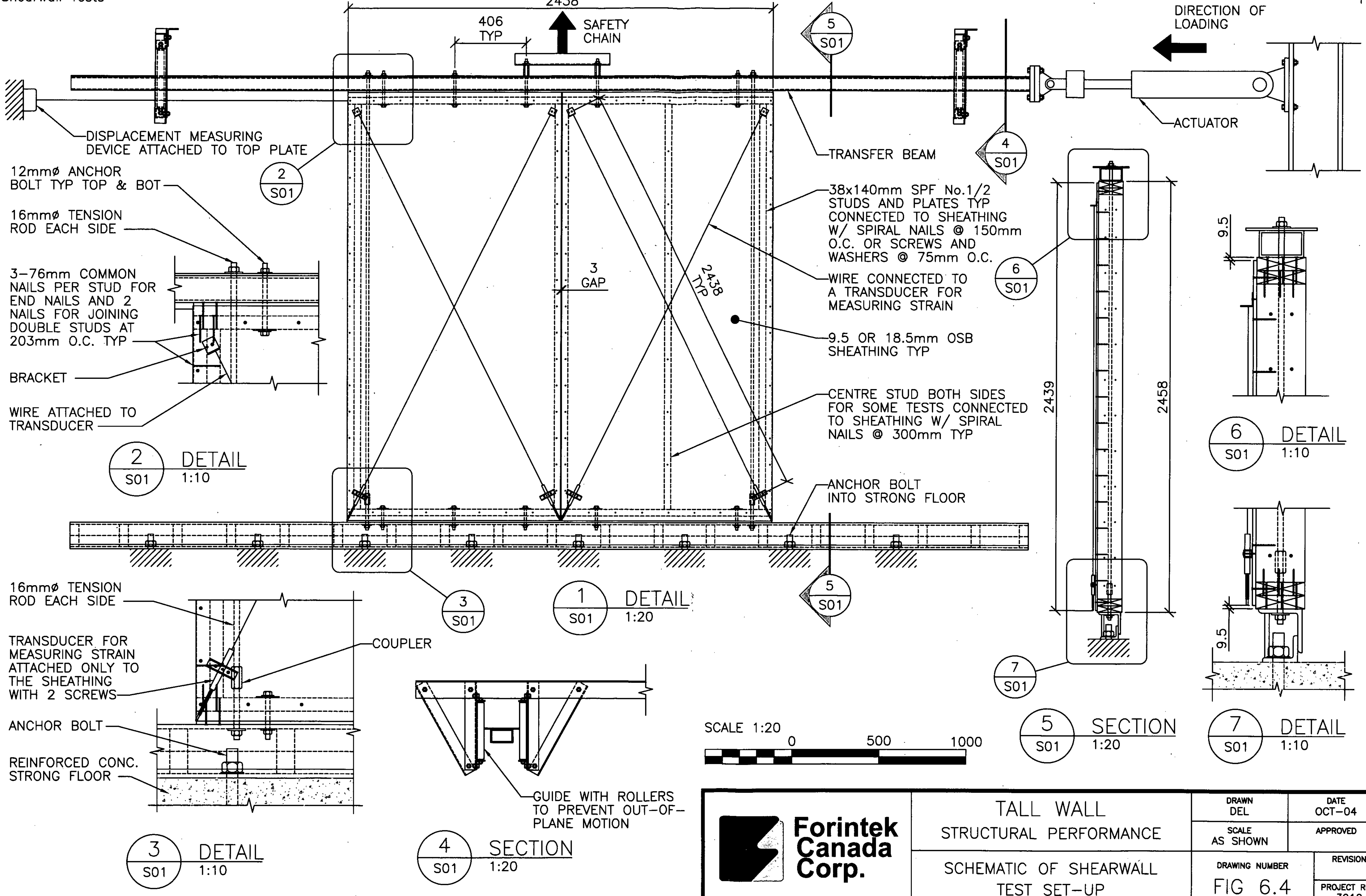

Forintek Canada Corp.	TALL WALL STRUCTURAL PERFORMANCE	DRAWN DEL	DATE OCT-04
		SCALE AS SHOWN	APPROVED
	SCHEMATIC OF SHEARWALL TEST SET-UP	DRAWING NUMBER FIG 6.4	REVISION
			PROJECT REF. 3910

OCT 21, 2003 ~FCC~C:/MY DOCUMENTS/SHEARWALL TEST.DWG DLEON brackets that were each in turn connected to the sheathing using two wood screws. The screws were long enough to pass through the full thickness of the sheathing panels without penetrating the framing members. A thin wire was attached to the spring end of each transducer. The wires were passed through each transducer and attached to angles that were connected to the two sheathing panels at the opposite corners to the transducers with wood screws. The length between the screws connecting the angles and the screws connecting the mounting brackets was kept constant for each diagonal measurement and each wall at 2,440 mm (8').

6.2.3 Testing Procedures

The testing procedure was largely governed by the fact that the buckling capacity of a sheathing panel is highly dependent on the support conditions around the edges of the panel. Since connection failures were likely to occur before buckling of the panels, additional racking tests were planned on (preferably the same) shearwalls, reinforced along the edges to prevent localized sheathing panel connection failures. To observe the buckling behaviour of sheathing panels that are connected in the common way found in construction practice and with a very rigid connection, each shearwall was strengthened with screws after its initial test and then retested.

Each wall was initially tested with the sheathing panels connected to the wood frame with spiral nails spaced at 152 mm (6") on centre around the perimeter of each panel. For wall 201, which had a stud in the middle of each panel, the nail spacing along this interior stud was 305 mm (12") on centre. After its initial test each wall was pulled back to its starting position. No damage was observed in any of the framing members after the initial tests. Any exposed nails connecting the sheathing to the frame were removed or the heads of the nails were cut off. The same sheathing panels were then connected to the frame around the perimeter of each panel with wood screws and washers spaced at 76 mm (3") on centre and a second test was conducted for each wall.

6.2.4 Material Properties

As was mentioned previously, the SPF frame members that were used to construct each shearwall were left over from a previous study conducted at Forintek Canada Corp. In that study, all 118 members were tested under third point loading to determine the modulus of elasticity of each member. The moisture content was also measured for each member and an average value of 17% was found. The normal cumulative distribution function for the modulus of elasticity of the SPF members is shown in Figure 6.5. The median value of modulus of elasticity was 9,715 MPa, the average was 9,681 MPa, and the coefficient of variation was 15%. The best members left over from the previous study were used as frame members in the shearwalls. It was therefore assumed that they could conservatively be characterized by the average modulus of elasticity.

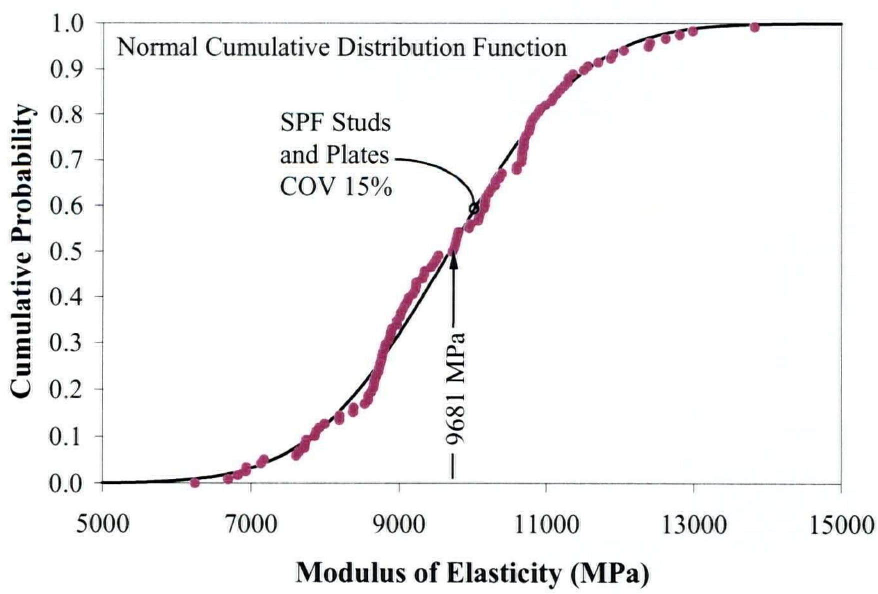

Figure 6.5. Cumulative distribution of modulus of elasticity for SPF studs and plates.

The same type of spiral nail that was used in the connection and T-beam tests, as described previously in Chapter 3, was used to construct the specimens for the shearwall tests. A photo of the nail is given in Figure 3.2 and the properties of the spiral nail itself are given in Table 3.2. The properties of the connection between the sheathing and the frame under lateral load and nail withdrawal are given in Table 3.3 and Table 4.2 respectively. The moduli of elasticity of the sheathing panels in both parallel and perpendicular directions to the axis of greater strength were determined under third point loading as described in section 5.2.4. These values are given in Table 5.2 and the density of the panels is shown in Figure 5.12.

6.3 RESULTS AND DISCUSSION

The purpose of the shearwall tests was to investigate the behaviour of the sheathing in walls with studs at a greater spacing than the limit specified in the Canadian Wood Design Code. Because a limited number of configurations were tested, only general observations and conclusions on the buckling behaviour of sheathing panels in walls under racking loads can be made. Based on the results of the composite T-beam tests and on previous tests on shearwalls conducted at Forintek Canada Corp., however, the variation of the shearwall results obtained were found to be very low, which can be attributed to the averaging effect from load distribution among a large number of connectors. The results from this limited sample size are thus deemed to be representative of the general population of similar shearwalls.

6.3.1 Pushover Results

The load-displacement response of each of the six shearwall configurations tested is shown in Figure 6.6 and the average properties of these curves are presented in Table 6.2. The European CEN protocol (CEN, 1995) was used to calculate those properties. The procedure is briefly outlined in section 3.3.1 and shown graphically in Figure 2.30 in Section 2.7.

The response of the three walls that were only connected with nails was approximately the same. The average maximum load achieved by the three walls was 20.63 kN and the coefficient of variation was 4.0%. The average initial stiffness of the three walls was 2,043 N/mm with a coefficient of variation of 7.2%. Thus, the response of the shearwalls under racking loads was, in this case, independent of sheathing thickness and stud spacing and directly related to the resistance of the nailed connection between the sheathing and the framing members and the nail spacing. No buckling of the sheathing was observed for the three tests with nailed connections.

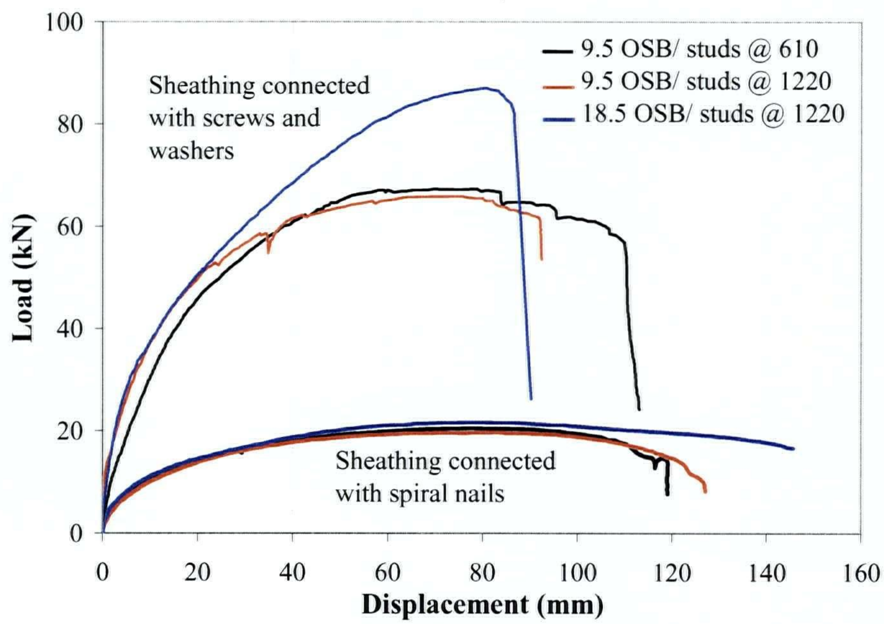

Figure 6.6. Load-displacement response of the shearwalls tested.

Figure 6.6 shows that the response of the two walls with 9.5 mm thick sheathing connected with screws and washers was approximately the same, while the wall with 18.5 mm thick sheathing sustained a significantly higher load. This shows that, as the stiffness of the connection between the sheathing and the frame was increased, the response became more sensitive to the material properties and thickness of the sheathing panels. An interesting observation is that, although the sheathing panels in wall 202 (9.5 mm OSB sheathing with studs spaced at 1,220 mm on centre and connected with screws and washers) visibly buckled prior to achieving maximum load, the load-displacement curve remained approximately the same as the walls where panel buckling did not occur. The maximum load achieved by wall 202 was only 2.2% lower than wall 201, which corresponded to the variation of results from the tests with nailed connections.

Table 6.2. Shearwall response parameters obtained from tests.

Specimen Group Number	Configuration	Yield Load F_y (kN)	Yield Displacement Δ_y (mm)	Maximum Load F_{max} (kN)	Displacement at F_{max} (mm)	Ultimate Displacement (at 0.8 Pmax) Δ_u (mm)	Initial Stiffness (N/mm)	Ductility ratio (Δ_u/ Δ_y)
201	A	14.4	12.12	20.5	78.3	111.69	953	9.21
	B	43.9	18.01	67.4	69.9	110.39	2631	6.13
202	A	10.6	11.17	19.7	83.5	116.75	1038	10.45
	B	38.2	10.74	65.9	72.7	92.35	3483	8.60
204	A	11.1	9.71	21.7	80.6	142.88	1137	14.71
	B	42.4	13.21	87.0	80.5	87.16	3584	6.60

The diagonal transducers shown in Figure 6.4 captured the localized buckling of the sheathing panels in wall 202. The load-displacement response captured by transducer number 5 is shown in Figure 6.7. The displacement corresponds to diagonal contraction since the panel is undergoing compression at that angle. From this graph it can be seen that buckling of the left-hand sheathing panel of wall 202 initially occurred at a load of approximately 35 kN. This was just over half of the maximum load achieved by the wall. No buckling was observed or measured in any of the other tests and this can also be seen in Figure 6.7 as the responses of the other walls remained linear elastic.

Photos of wall 202 after the sheathing panels buckled are shown in Figures 6.8 and 6.9. The two sheathing panels buckled out of plane in opposite directions, which is shown in Figures 6.9 (a) and (b). The results from the six tests of shearwalls under lateral load that were conducted show

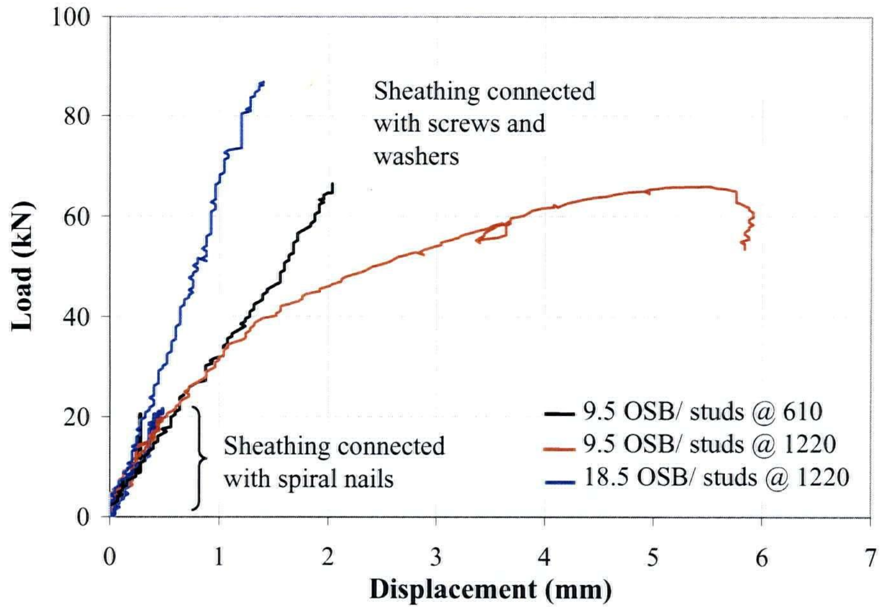

Figure 6.7. Diagonal deformation response of shearwalls tested.

Figure 6.8. Buckling of the sheathing of wall specimen 202A.

(a) (b)

Figure 6.9. (a) and (b) Buckling of the sheathing of wall specimen 202A.

that buckling of the sheathing panels is highly unlikely in walls where the sheathing is connected to the frame with nails because the nails will either pull-out from the frame or tear out at the edges of the sheathing at a much lower load than is required to cause buckling. Therefore, for a wall where the sheathing is connected to the frame with nails, localized buckling of the sheathing is not an important consideration for the wall performance because it is related to the response of the connections around the perimeter of each sheathing panel, which is independent from the stud spacing for the wall. Additionally, it has been shown that if the connections are stiff enough to cause the failure of the wall to be due to localized buckling of the sheathing panels, the wall will continue to resist increasing racking load and will achieve approximately the same maximum load as a similar wall where the sheathing panels have not buckled.

The current limit on the spacing of studs in shearwalls as specified in the Canadian Wood Design Code is based on two papers that identify buckling of the sheathing as a mode of failure of typical shearwalls built in North America. Tissell (1990) looked at over one hundred tests that have been compiled by the American Plywood Association since 1965. From those tests, the potential for thin panels to buckle was identified and a reduced capacity was recommended for walls with a 610 mm (24") stud spacing versus a 406 mm (16") stud spacing for thin sheathing. The reduced capacity, however, was not necessary for walls with sheathing panels of 9.5 mm (3/8") minimum thickness. Therefore, the limit on stud spacing specified in the Canadian Wood Design Code is directly applicable to the one sheathing thickness less than 9.5 mm given in the design tables but was shown to be conservative for walls with thicker sheathing panels.

The second paper, referenced in the Canadian Wood Design Code, identified that there is a risk that local buckling of the sheathing of a shearwall may occur if the sheets are very thin (Kallsner, 1995). The work done in this paper is purely theoretical and is not related to any test data. The critical shear stress in a sheathing panel was given as:

$$\sigma_{cr} = k \frac{\pi^2 E}{12\left(1-\nu^2\right)}\left(\frac{t}{b}\right)^2, \tag{6.1}$$

where, for a sheet simply supported along all four edges, an approximate expression for the coefficient k was given by:

$$k = 5.35 + 4\left(\frac{b}{a}\right)^2. \tag{6.2}$$

For a sheet clamped along all four edges the coefficient k was given as:

$$k = 8.98 + 5.6\left(\frac{b}{a}\right)^2. \tag{6.3}$$

In equations (6.1) through (6.3), the symbols and terms are defined as follows:

E = modulus of elasticity of the sheathing panel

ν = Poisson's ratio

t = thickness of the sheathing panel

b = width of the sheathing panel

a = length of the sheathing panel

Using equation (6.1), multiplied by the thickness of the sheathing panels and the total length of sheathing panels parallel to the applied load, the load at which localized buckling of the sheathing occurs can be calculated. Using the properties of the sheathing used for the tests and the geometry of wall 202, the predicted racking load that will produce localized buckling of the sheathing panels is 29.1 kN, assuming simply supported edges, and 47.6 kN assuming the edges are clamped. This relates closely with the load at which buckling was first measured, 35 kN, since the boundary conditions in practice are somewhere between the two support cases given in equations (6.2) and (6.3). However, the response of wall 202 with the sheathing connected with screws and washers shows that localized buckling of the sheathing panels does not result in global failure of the shearwall since the wall continued to resist increasing racking load.

6.3.2 Failure Modes

Several modes of failure were observed in addition to localized buckling of the sheathing panels. As was stated previously, the failure of all three walls tested where the sheathing was connected to the frame with nails was due to the failure of those connections. The majority of these failures were characterized by nail pullout from the frame members. The two walls where the sheathing was connected to the frame with screws and washers and the sheathing did not buckle, failed in a brittle manner. Photos of the failure modes of these two walls are shown in Figure 6.10 and Figure 6.11.

(a)

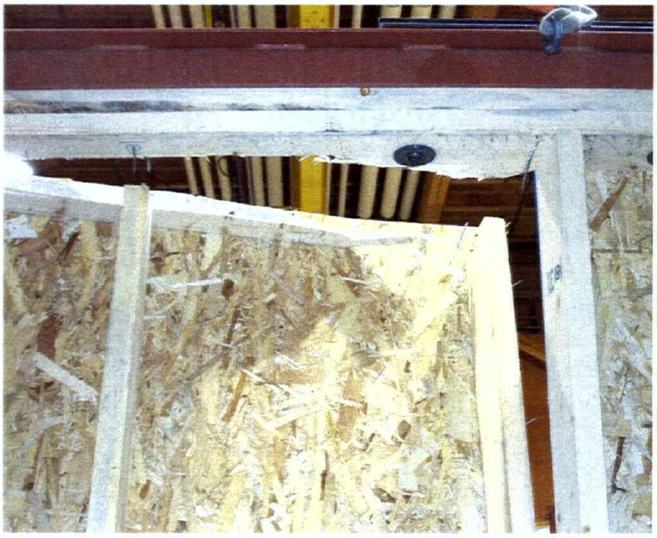

(b)

Figure 6.10. (a) and (b) Failure of the double central stud and top plate in wall 201B.

In wall 201 the connection between the two frame members of the centre stud failed and the top of one of the sheathing panels deflected out of the plane of the wall. The failure also caused the bottom member of the top plate to fail (Figure 6.10 (b)). The failure in wall 204 was due to the splitting of the top member of the bottom plate of the wall. This is shown in Figure 6.11 (a) and (b). In both instances, the frames were not strong enough to resist the racking loads required to induce localized buckling failure in the sheathing panels. The ultimate failure modes of the shearwalls tested were not of importance to this study, however, as the walls were primarily constructed to observe the response of the sheathing panels. That was the reason for using double plates and double studs, which are not found in regular walls.

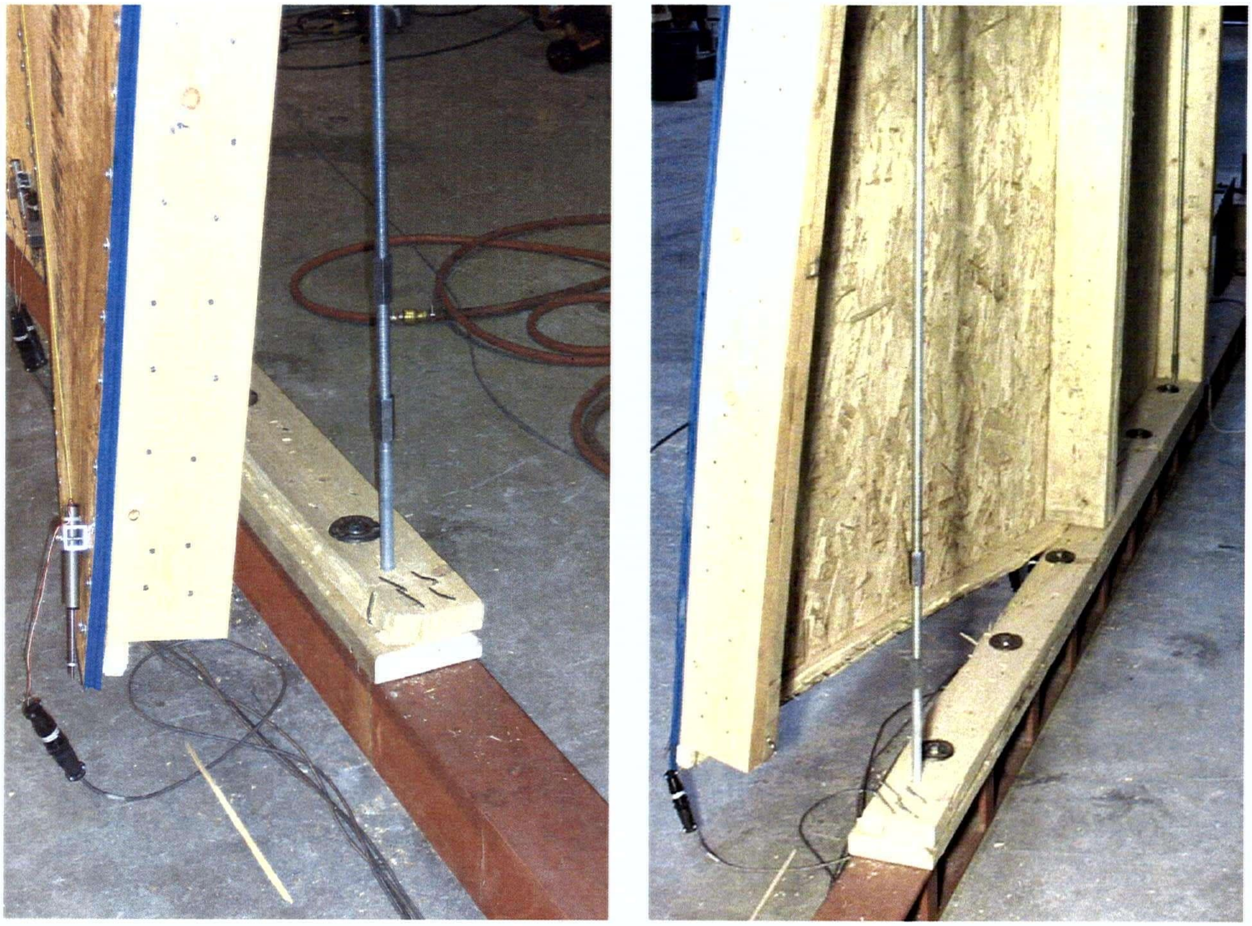

(a) (b)

Figure 6.11. (a) and (b) Failure of the bottom plate in wall 204A.

6.4 SUMMARY

Three shearwalls with two configurations each were tested under racking loads to determine if localized buckling of the sheathing panels would occur when stud spacing is larger than 600 mm on centre and if so, what effect it would have on the total response of the shearwalls. From the results of the limited tests that were conducted, several conclusions can be drawn. Firstly, walls with different sheathing thicknesses and stud spacings but with the same sheathing-to-frame nailed connections and nail layout have the same load-displacement response. Thus, the response of shearwalls where the sheathing is connected to the frame with nails is directly related to the response of that connection and is independent of the stud spacing. Secondly, the response of shearwalls under lateral or in-plane loads becomes increasingly related to the properties of the sheathing as the stiffness of the connections between the sheathing and the frame increases. Thirdly, the response of the wall in which the sheathing panels did buckle was approximately equal to that of a wall in which the sheathing did not buckle. Therefore, localized buckling of the sheathing panels of a shearwall under racking loads does not constitute global failure of the shearwall. Finally, brittle failure of the frame was observed in two walls where the sheathing was connected to the frame with screws and washers. In these cases, the frame was not strong enough to resist the racking load required to induce localized buckling of the sheathing panels, as was expected. The results of this test program validated the use of large stud spacing in the full-scale test program.

7. FULL-SCALE WALL TESTS

The testing described in previous chapters was on the components of a full-scale tall wood-frame wall. To better understand the response of those individual components in an actual structure, tests on full-scale tall walls under axial and transversal, or out-of-plane, loads were conducted with realistic support conditions. This chapter includes the results of those monotonic tests to determine several response parameters of full-scale tall walls. The results of the full-scale wall tests were used to compare the responses of different wall configurations and materials. The results will be compared with detailed analytical predictions that are presented in the next chapter.

7.1. OBJECTIVES AND SCOPE

The individual responses of the components of a full-scale wood structure are not always adequate to be able to accurately predict the response of those components in combination with each other. Discrepancies occur because wood exhibits a non-linear behaviour and because the assumptions used to analytically predict the response of actual wood-frame structures are not always a good representation of the actual structure. These assumptions can include equations for the interaction between axial and transversal loads and idealizations for the support conditions and applied loads. One objective of this research is to analyze how the results from individual component tests compare with full-scale wall tests using simple assumptions often incorporated into design. Therefore, it can be determined if the findings from the component tests, such as increased stiffness due to composite action and increased stud spacing, can be applied directly into actual structures.

It was shown in Chapter 5 how the stiffness of a wall stud can be significantly increased by accounting for the composite action that exists between the stud and the wall sheathing. The sheathing, along with the blocking between studs, can further increase the stiffness of a full-scale wall by optimizing the distribution of the applied transversal load with respect to the stiffness of the individual studs. In addition to structural panels, walls can be sheathed with non-structural, or architectural finishes, such as gypsum wallboard. Specific types of gypsum wallboard have recently been included into the Canadian Wood Design Code (CSA, 2001) to resist racking loads on wood-frame walls. Therefore, the effects of structural and non-structural sheathing in both principal directions of full-scale tall walls were examined.

One negative affecting the economic feasibility of wood-frame tall walls that has been identified in previous structures is the cost of stud to plate connections. Because of the scale of tall wood-frame walls, the connection of the studs in a wall to the top and bottom plates can be placed under high shear and axial loading, thus requiring more substantial connections than the commonly used toe-nailing. Another objective of this research was to test full-scale tall walls with different types of stud connections to determine economically feasible connection details that satisfy the load capacity and safety requirements of applicable building codes.

To meet the objectives outlined above, axial and transversal load controlled monotonic tests were conducted on several full-scale tall walls with different: stud material and spacing; sheathing thickness, orientation, and connection type; and stud connection type. One wall was tested with both exterior structural sheathing and interior gypsum wallboard sheathing. The walls were loaded in the transversal direction under increasing third-point bending load and single point loads and by both constant and increasing loads axially. The full-scale wall tests were conducted in the Wood Engineering Laboratory of Forintek Canada Corp. in Vancouver.

7.2. METHODS AND MATERIALS

7.2.1 Full-Scale Wall Specimens

One purpose of the component tests described in the previous chapters was to incorporate the results into an analytical model for predicting the response of full-scale wall specimens. Therefore, the full-scale wall specimens that were tested incorporated many of the materials and configurations that were used during the component tests. The test matrix for the full-scale wall specimens is shown in Table 7.1. A total of thirteen walls were tested but, as will be described later, some of the walls were tested in more than one orientation in the test frame. Specimen number 510, denoted as specimen type W3, was not tested due to the limitations of the test frame, which will be described later. The results of the composite T-beam tests presented in Chapter 5 showed that the variation between the three replicates of each specimen type that were tested was low, with the highest coefficient of variation for increased member stiffness being just over 4.5%. This low value for the coefficient of variation was due to the fact that the properties of each stud were known prior to testing the composite members. Since the material properties of the components of the full-scale walls were also known prior to testing it was decided to only test one specimen of each wall configuration.

The four specimen types that were tested are shown in Figure 7.1 (a) and (b) and Figure 7.2 (a) and (b). A wall specimen that was prepared for testing is shown in Figure 7.3 (a) and (b) before and after sheathing had been applied. Every specimen was constructed with 44 mm by 242 mm (1 23/32" x 9 17/32") laminated strand lumber (LSL) top and bottom plates. The total length of every wall was 4,890 mm (192 ½") and the width between the centrelines of the outside studs of every wall was 2,440 mm (96"). The walls had blocking spaced at 1,220 mm (48") on centre between each stud. The blocking material was the same as the studs used for the wall. The blocking was either end-nailed through the studs or toe nailed to the studs with three 89 mm (3 ½") common nails at each end using a pneumatic nail gun. The oriented strandboard (OSB) sheathing panels, representing the exterior sheathing of a wall, were connected to the studs, plates, and blocking with either 65 mm long spiral nails or, for wall number 508, with spiral nails and glue. Like the composite T-beams tested with glue, the intention with wall number 508 was to have full composite action with a rigid connection between the sheathing and the studs. The nails were not expected to provide any significant resistance until after the glued bond would break. The nails were primarily used to ensure that an adequate glued bond was

Table 7.1. Full-scale wall test matrix.

Specimen Number	Specimen Type	Nail Spacing[a] (mm)	Glue	OSB Thickness	Stud Spacing (mm)	Sheathing Orientation	Stud Material	Connector Type	Test Protocol
501	W1	152[b]	No	9.5	610	PERP	SPF	A	T1
502	W2	152	No	9.5	610	PAR	SPF	A	T1
503	W1	152	No	15.5	610	PERP	SPF	A	T1
514	W1	152	No	15.5	610	PERP	SPF	A[c]	T1
504	W2	152	No	15.5	610	PAR	LSL	B[c]	T2
505	W4	152	No	15.5	1220	PAR	LSL	B	T1
506	W1	152	No	11.1	1220	PERP	LSL	D	T1
507	W1	152	No	15.5	610	PERP	LSL	B	T3
508	W4	76	Yes	15.5	1220	PAR	LSL	B	T1
509	W2	152	No	9.5	610	PAR	LSL	B	T2
511	W5	152	No	15.5[d]	610	PAR	LSL	B	T4
512	W1	152	No	15.5	610	PERP	LSL	C	T2
513	W4	152	No	15.5	1220	PAR	LSL	C	T1

Notes:

(a) 65 mm long spiral nails were used to attach the sheathing on all walls tested.
(b) 305 mm nail spacing was used on the interior of the sheathing panels.
(c) Tension straps were used on every other stud, i.e. on three of the five studs in the wall.
(d) 15.9 mm gypsum wallboard attached with 41 mm coarse thread drywall screws spaced at 203 mm on centre for both the exterior and interior panel connections was applied to the interior side of the wall in addition to the sheathing on the exterior face.

developed between the sheathing and the stud. Because a rigid connection was desired and long-term serviceability issues were not taken into account, regular white wood glue was used as the bonding agent. A thick layer of glue was applied to the entire edge of the stud using a small, flat piece of wood. The sheathing was then placed on the wall frame and nailed into place to ensure an adequate bond.

Specimen type W1 had either 38 mm by 235 mm (1 ½" x 9 ¼") spruce-pine-fir No. 2 or better (SPF) studs, or 44 mm by 242 mm LSL studs spaced at 610 mm (24") on centre (Figure 7.1 (a)). The 1,220 mm by 2,440 mm OSB sheathing panels were positioned so that their axis of higher

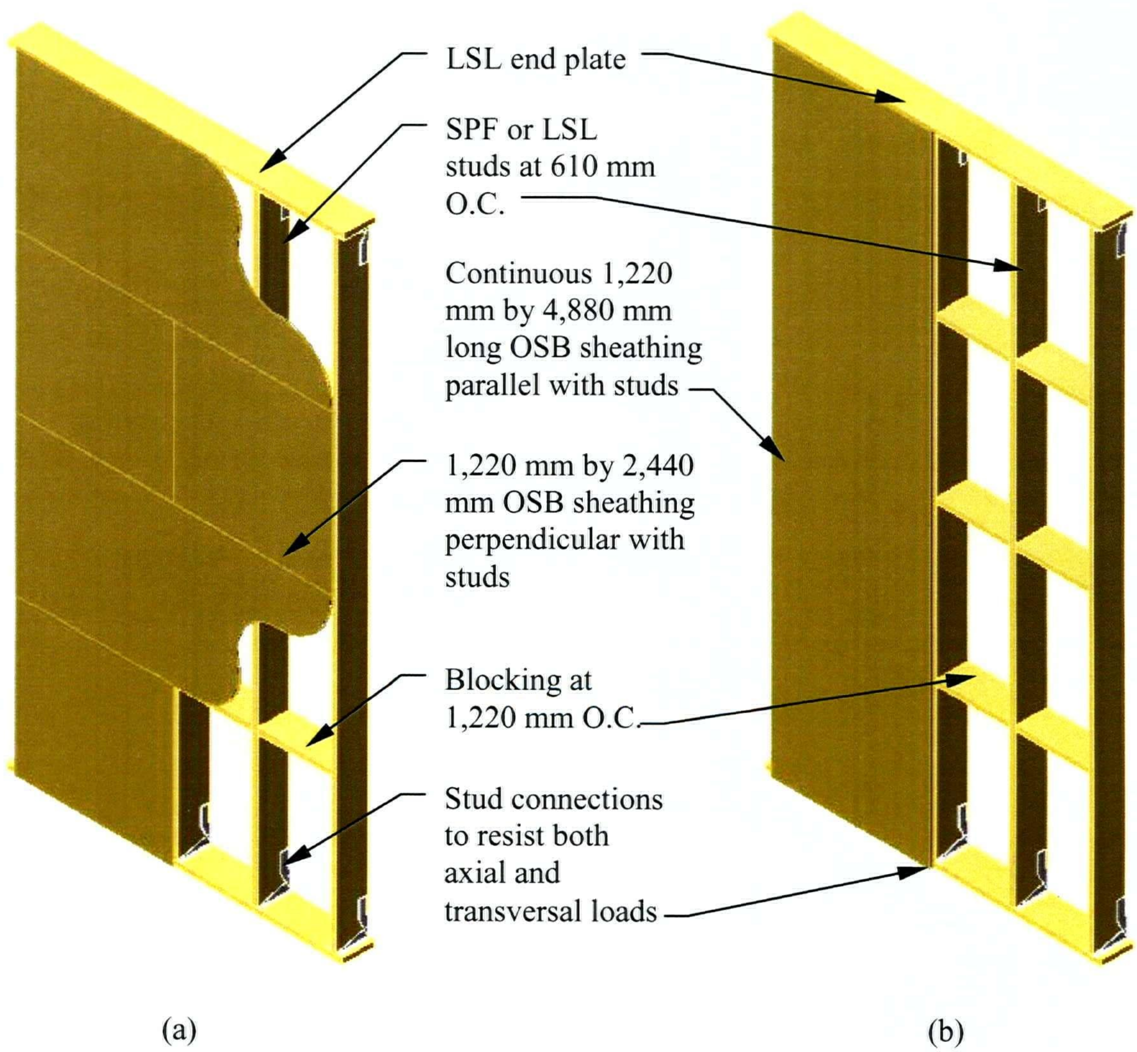

Figure 7.1. Details of a full-scale wall specimen types (a) W1 and (b) W2.

strength was perpendicular to the length of the studs and staggered across the width of each wall. This left gaps between sheathing panels along the length of the studs and across the width of the wall at two of the panel strips. The sheathing panels for wall number 501 were attached to the frame with spiral nails at 305 mm (12") on centre in the interior of each panel and at 152 mm (6") on centre around the perimeter of each panel. The sheathing panels for all other walls were attached to the frames with an interior and perimeter nail spacing of 152 mm on centre.

Specimen type W2 was similar to specimen type W1 except that it had two 1,220 mm by 4,880 mm (48" x 192") sheathing panels (Figure 7.1 (b)). In this case the axis of higher strength of the panels was parallel with the length of the studs. Specimen type W4 was similar to specimen type

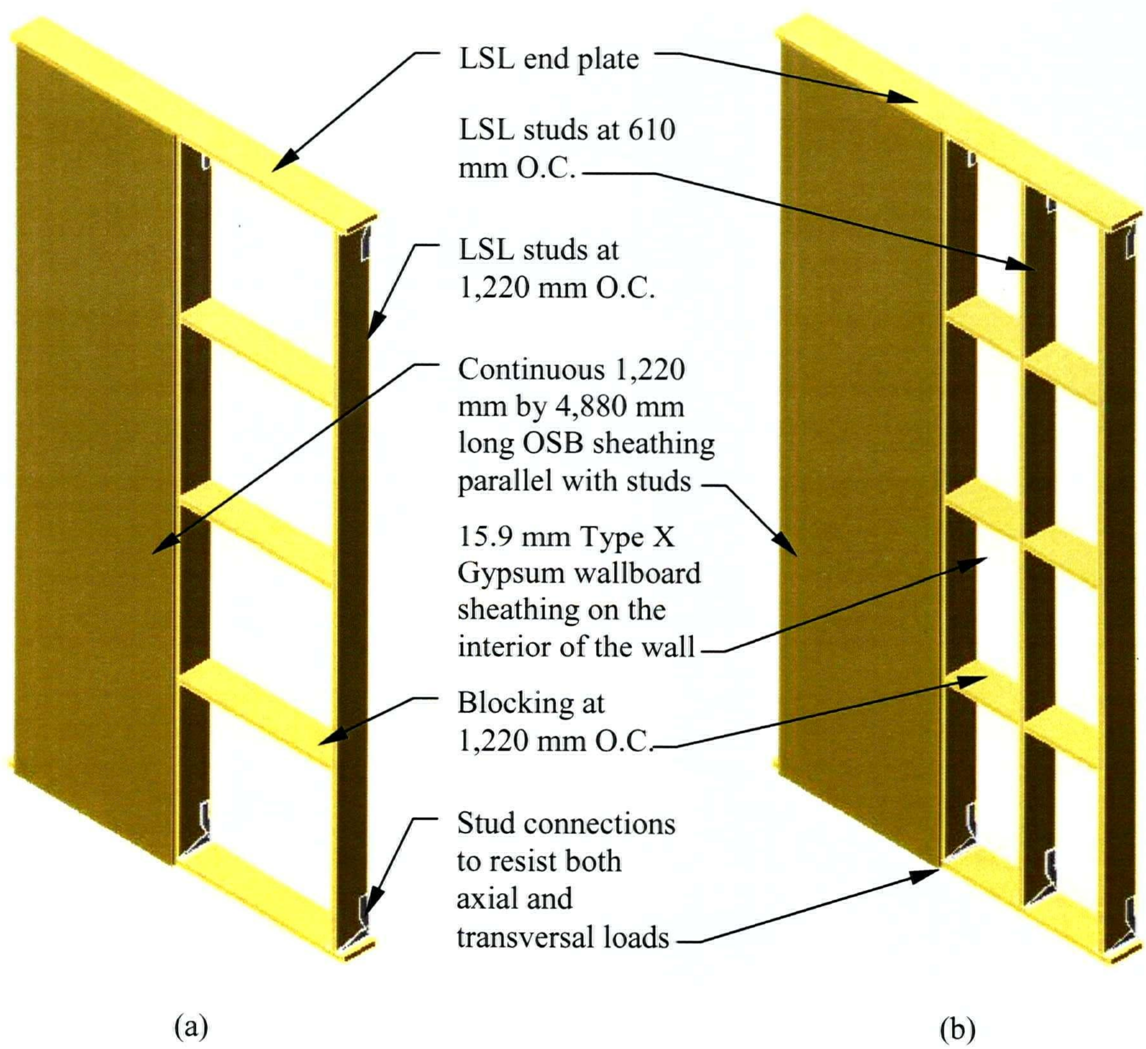

Figure 7.2. Details of full-scale wall specimen types (a) W4 and (b) W5.

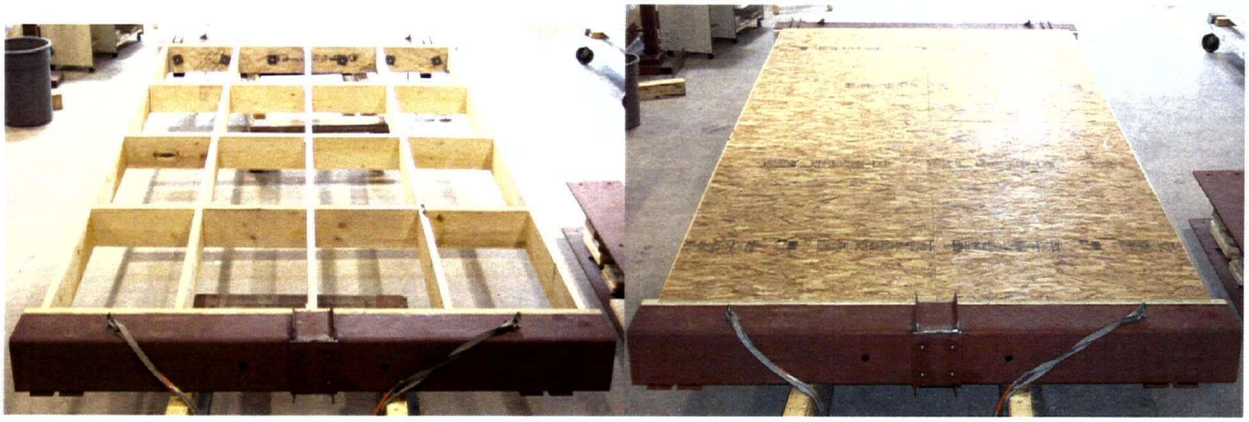

(a) (b)

Figure 7.3. Full-scale wall specimen (a) without sheathing and (b) with sheathing being prepared for testing.

W2 except that the studs were spaced at 1,220 mm on centre instead of 610 mm (Figure 7.2 (a)). Specimen type W5 was the same as W2 but it was also sheathed on the interior side of the wall with 15.9 mm (5/8") thick gypsum wallboard (Figure 7.2 (b)). The sheets were 1,220 mm by 2,440 mm and oriented with their long side perpendicular with the length of the studs. The sheets were not staggered so there were no gaps between sheets across the width of the wall. Coarse thread drywall screws, 41 mm (1 5/8") in length, were used to attach the wallboard to the

Figure 7.4. Tape and spackle being applied to gypsum wallboard on a full-scale wall specimen.

frame at a spacing of 203 mm (8") on centre both in the interior and around the perimeter of the sheets. Drywall tape and two layers of spackle were applied to the seams between sheets (Figure 7.4).

Four different connection types were used to connect the studs and the end plates along with two different types of connection configurations. The four different connections are shown in Figure 7.5 (a) through (d). This variation was driven by one of the objectives of this research, which was to develop more economically feasible connections for use in tall wood-frame wall construction. Connection types A, B, and D all consisted of readily available, or off-the-shelf, connector products manufactured by Simpson Strong-Tie Co. Inc (Simpson Strong-Tie Inc., 2004). Connection type A consisted of an LUS28 face mounted hanger to resist the transversal loads due to wind pressure or suction on a wall and an H6 hurricane tension tie to resist the tension force along a stud due to uplift on the roof of a structure from wind suction (Figure 7.5 (a)). Each hanger was attached to the end plates with six 3.75 mm diameter by 38 mm long (10d x 1 ½") common nails and to the studs with four 3.75 mm diameter by 76 mm long (10d x 3") common nails at 45 degrees to the plane of the end plates, as per the manufacturers specifications. The tension ties were attached to both the back of the end plates and to the side of the studs with eight 3.75 mm diameter by 38 mm long (10d x 1 ½") common nails. All nails were driven by hand using a hammer.

Connection type B was similar to type A, except that a different Simpson Strong-Tie hanger, HU9, was used for the LSL studs (Figure 7.5 (b)). The hangers were attached to the end plates with eighteen 3.75 mm diameter by 38 mm long (10d x 1 ½") common nails and to the studs with six common nails of the same type. Connection type D used the same hanger as type B but did not have a tension tie (Figure 7.5 (d)). Instead, the tension force in each stud was resisted by

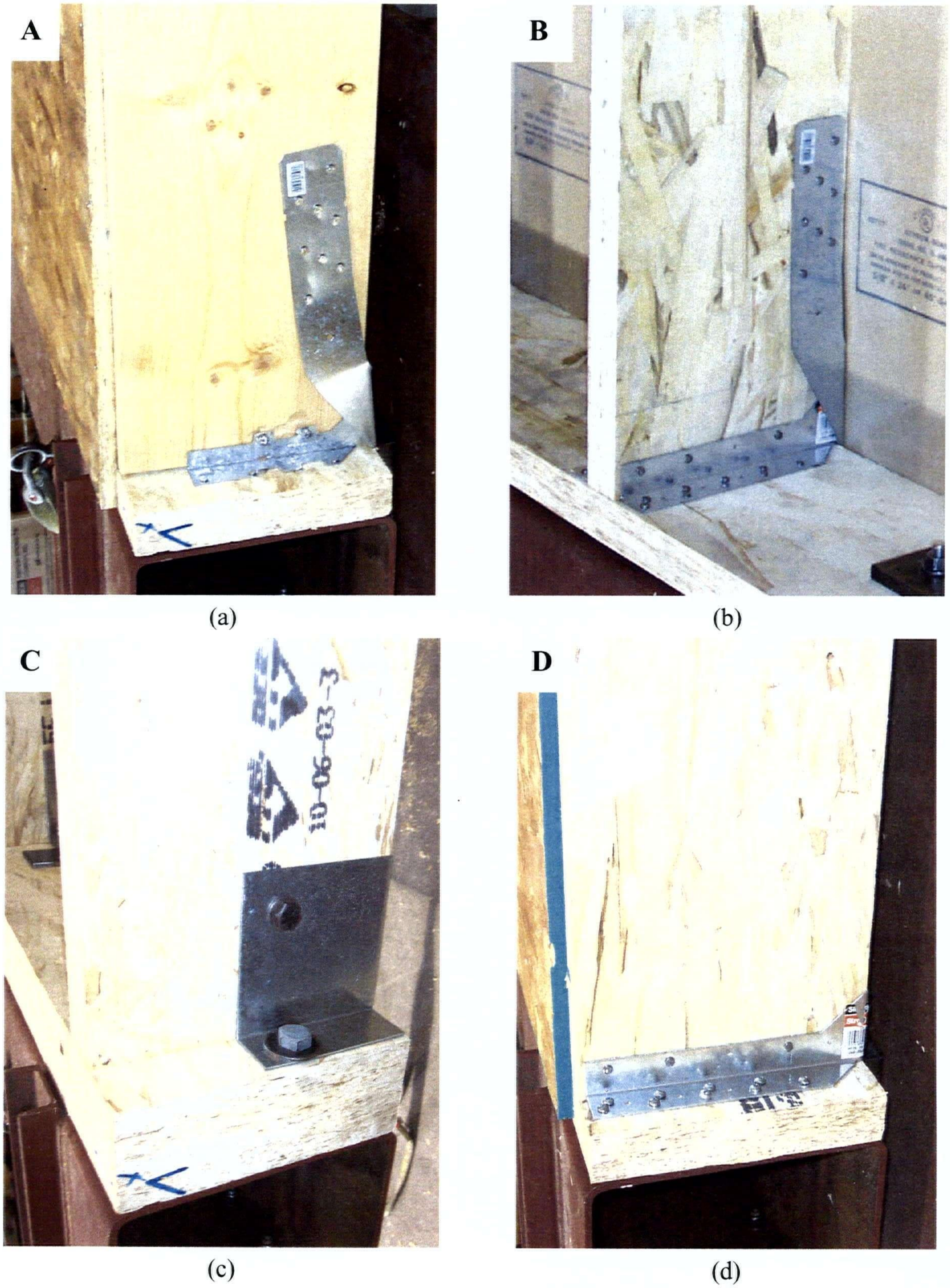

Figure 7.5. Full-scale wall stud connection types: (a) SPF joist hanger with tension strap; (b) LSL joist hanger with tension strap; (c) specially fabricated stud connector; and (d) LSL joist hanger connected to the end plate with screws.

connecting the hangers to the end plates with eighteen 3.75 mm diameter by 38 mm long (#10 x 1 ½") round head wood screws instead of the common nails. Common nails were used to attach the hangers to the studs. The screws were attached using a power drill.

Connection type C was specifically designed and fabricated for this testing program and was modeled after a connector that was used in a tall wood-frame structure that was built in Cranbrook, British Columbia (Figure 7.5 (c)). It was also shown as an example in the guide for the design of tall wood-frame walls published by the Canadian Wood Council (CWC, 2000). A description of the building is presented in section 2.4.1. The brackets were fabricated with 2.7 mm thick (12 gauge) steel. A schematic of the bracket is shown in Figure 7.6. The brackets were attached to the studs with a 12.7 mm (1/2") diameter bolt and to the end plates with two 15.9 mm diameter by 76 mm long (5/8" x 3") lag screws. A 12.7 mm pilot hole was drilled into the end plates the full length of the lag screw, following the specifications in the Canadian Wood Design Code. The bolt and the lag screws were tightened by hand. For the walls with connector type C, the end plates were doubled at each end to allow enough depth for the lag screws. The studs were shortened so that the overall length of the walls remained 4,890 mm (192 ½").

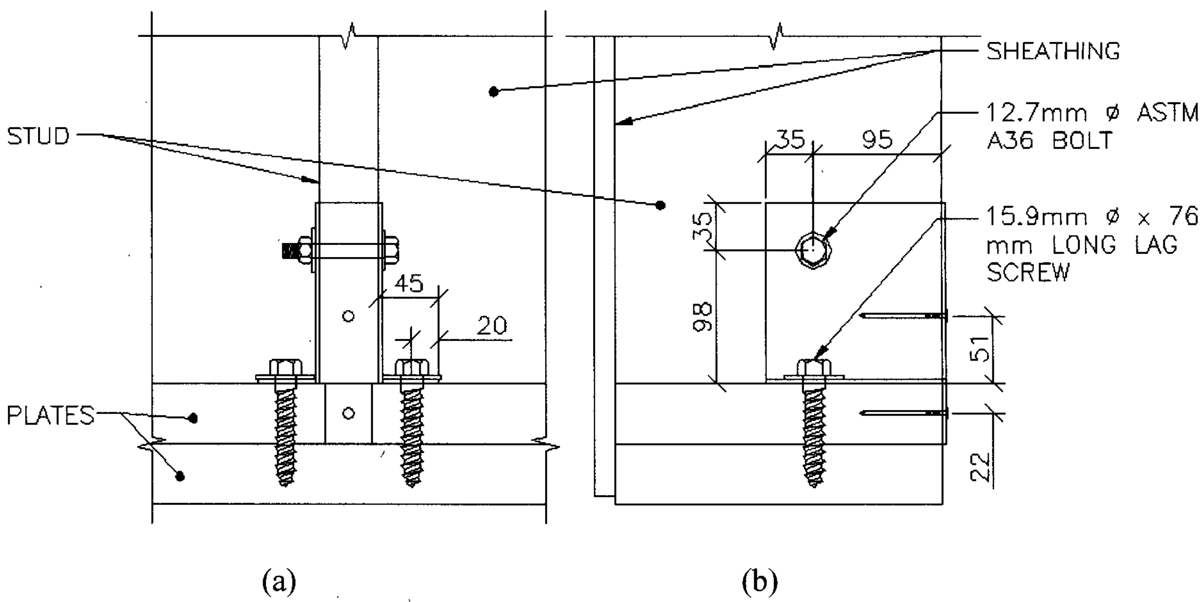

Figure 7.6. Schematic of connection type C (a) face view, and (b) side view.

All material used for testing was dry and had been stored in a laboratory environment at an average temperature of 20° ± 3°C and a relative humidity of 60% ± 10% for at least one week. The specimens with nailed connections were tested within 24 hours of assembly. The specimens with glued connections and with gypsum wallboard sheathing were tested at least 72 hours after assembly to allow for the glue to cure and the spackle to dry.

7.2.2 Testing Apparatus and Instrumentation

A photo of the full-scale wall test set-up with a specimen being tested is shown in Figure 7.7. The specimens were loaded in the transversal direction (perpendicular to the plane of the wall) in third-point loading to simulate a wind load, and axially to simulate the dead, live, and wind uplift loads from the roof of a structure. The schematic of the test set-up is shown in Figure 7.8. Although wind loading is an approximately uniformly distributed load over the height of a wall, this loading arrangement was deemed satisfactory since the distribution of bending moment along a beam loaded at its third points is similar to that of a beam under a uniformly distributed load. A more realistic loading method using airbags was considered, but proved to be impossible in the facilities available. Hollow rectangular steel beams were used to apply the transversal loads at the third points of the wall. To simulate rollers, the steel tubes were connected to the test frame with rocker washers that allowed the tubes to rotate in three different directions. It was also deemed that the small amount of friction between the tubes and the OSB sheathing would not prevent the tubes from sliding along the sheathing when required. Detailed schematics of the test frame are presented in Figures 7.10 and 7.11.

Realistic end conditions were simulated to more realistically predict the response of an actual wall in a structure. Both ends of the wall specimens were attached to large steel tubes with six 12.7 mm (1/2") diameter bolts spaced at 406 mm (16") on centre. The axial load was applied to the centre of the top distribution beam to simulate a uniformly distributed axial load across the top of the wall, assuming that the tube was rigid in comparison to the deflections of the wall specimens. In an actual building, by comparison, the structure supporting the roof typically rests on the top plate of the walls and is connected with brackets and bolts or light-gauge connectors and nails. In either case, these connections are designed to be pinned connections and thus do not restrain the top of the wall from rotating to a large extent. The axially loaded end of the wall specimens, or the end supporting the roof, was therefore left free to rotate by supporting the

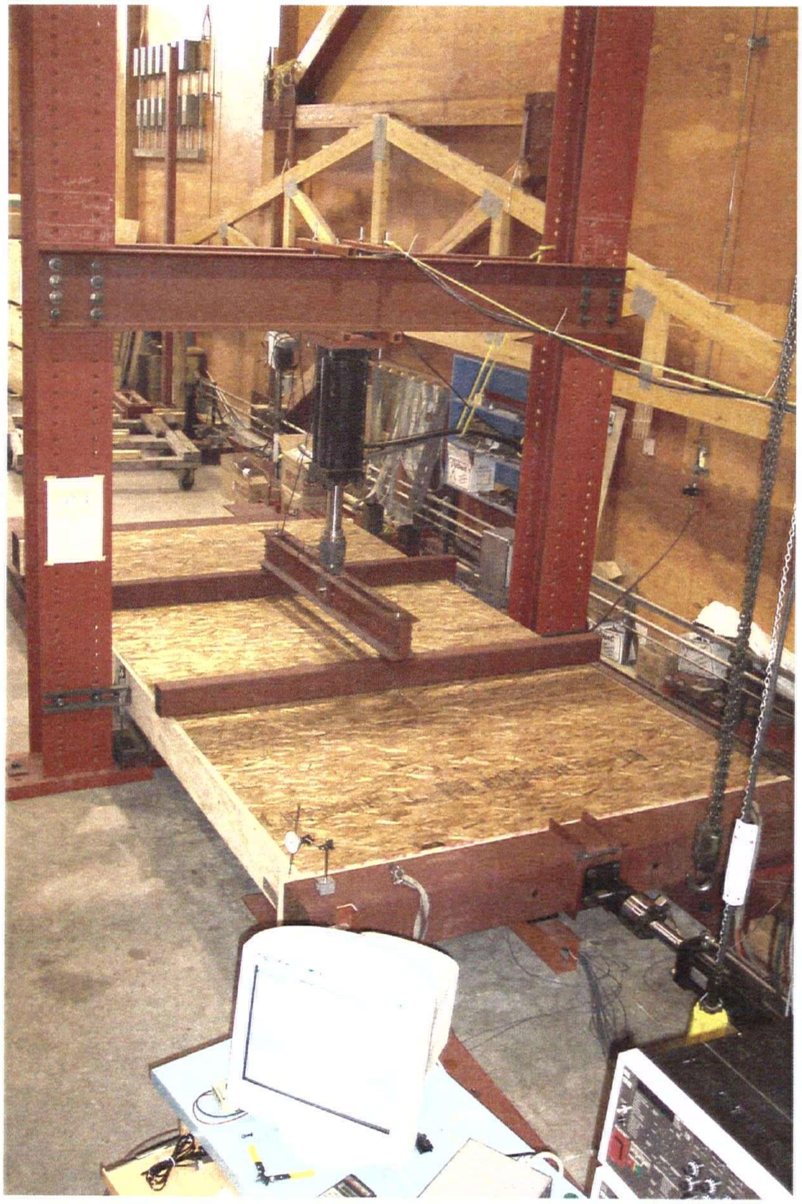

Figure 7.7. Photo of the test set-up for determining the response of full-scale walls under axial and transversal loads.

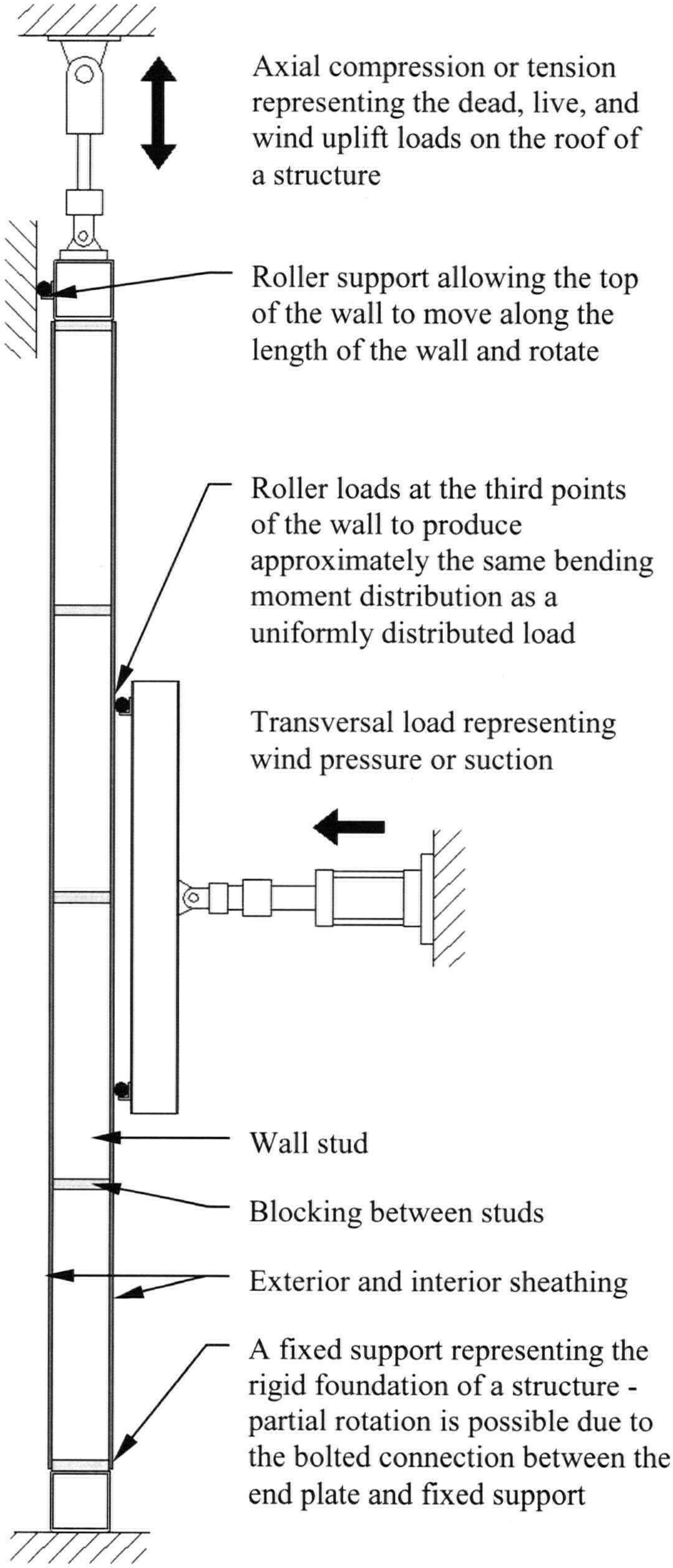

Figure 7.8. Idealization of the test set-up for determining the response of full-scale walls under axial and transversal loads.

distribution beam with rollers that sat on steel pedestals (Section 3 in Figure 7.11). The roller allowed the axially loaded end to move in the direction of the length of the studs. This compares well with a real wall which shortens due to transversal deflections.

To simulate the bottom wall support it was decided that, since the bottom of an actual tall wall typically rests on a rigid concrete foundation or a concrete masonry block up-stand wall with the bottom plate bolted to the foundation or up-stand wall with threaded anchors embedded into concrete, it should be modelled as fixed. To simulate this support configuration the bottom steel tube was connected at each end to steel brackets that were in turn connected to steel pedestals (Figure 7.11, Section 4). The brackets prevented the tube from rotating along its length and from displacing along the height of the wall specimens. Because tall walls are typically long in plan and continuously sheathed, they are stiff in the plane of the wall. Therefore, racking stops were placed at the mid-height of each wall to prevent the wall specimens from displacing in the plane of the wall perpendicular to the height of the wall under axial and transversal loads (Figure 7.9 (b)).

Data was collected continuously by a computer controlled data acquisition system. Up to twenty-four instrument measurements per data set were collected during each full-scale wall test. The measurements included: applied load in the axial (horizontal) and transversal (vertical) directions; movement of the actuator heads (stroke) in the axial and transversal directions; axial displacement of the loaded end; transversal displacement of the wall; and relative displacement along the wall height between the wall sheathing and the centre stud. The position of the displacement measurements is shown in Plan 1 of Figure 7.10. The loading in both axial and transversal directions was monotonic. For tests where both axial and transversal loads were applied to a wall specimen, the axial load was increased and held constant and then the

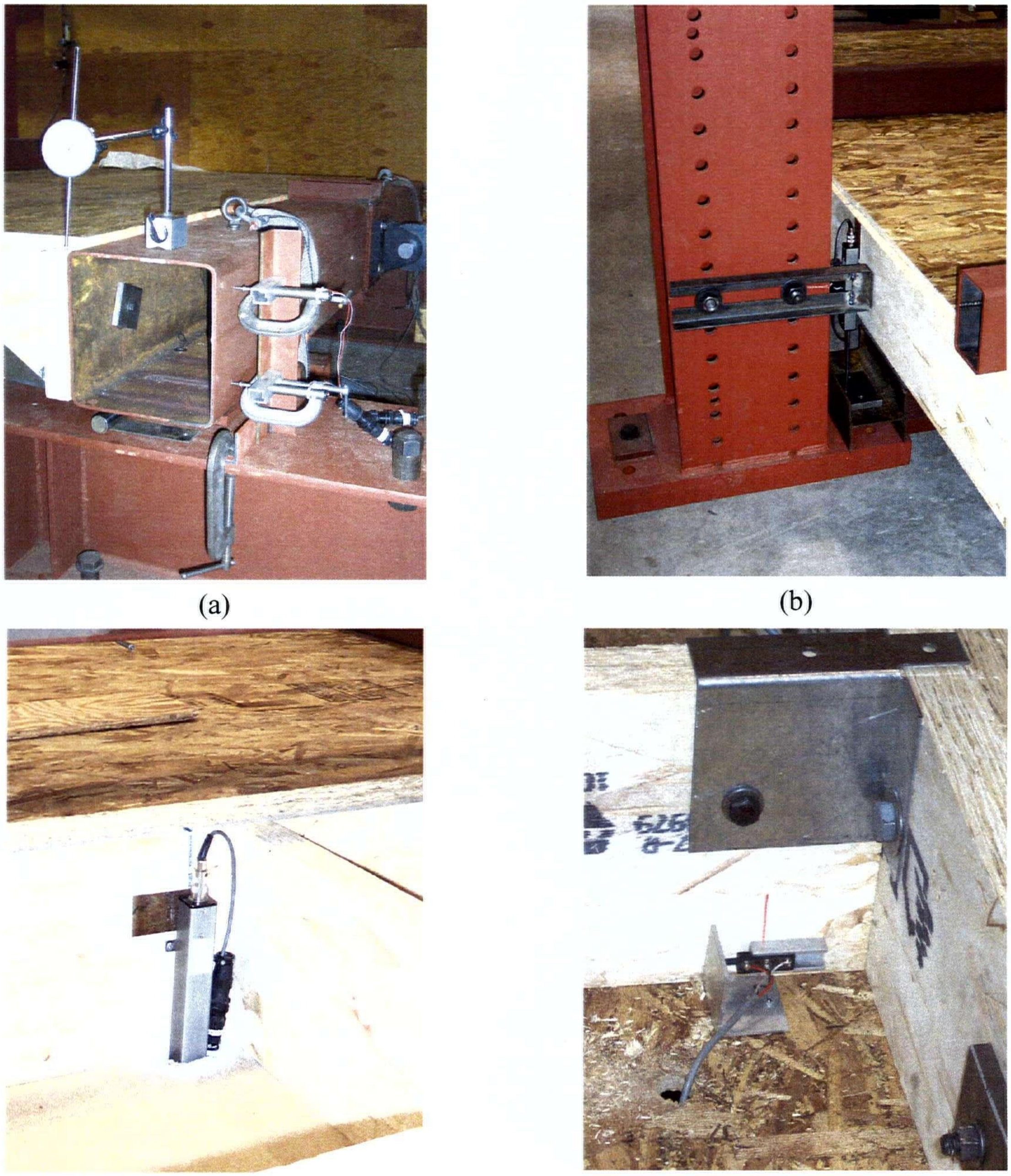

(a) (b)

(c) (d)

Figure 7.9. Full-scale wall test set-up details: (a) displacement and rotation transducers at roller-supported end; (b) racking stop and transversal displacement transducer at mid-span; (c) transversal displacement transducer at mid-span of the centre stud; and (d) slippage pot at the end of the centre stud.

transversal load was applied. The transversal load was applied downwards, causing flexural compression in the loaded face of the wall, and the axial load was applied in both directions, causing either tension or compression along the height of the wall. A 445 kN (100,000 lb.) servo controlled actuator delivered the transversal load through an 89 kN (20,000 lb.) load cell. The axial load was delivered by a 222 kN (50,000 lb.) servo controlled actuator and measured by a 111 kN (25,000 lb.) load cell.

Two displacement transducers with a measurement range of 76 mm (3") were placed at both ends of the distribution beam at the axially loaded end (Figure 7.9 (a) and Section 3 of Figure 7.11). They were set to be in line with the centreline of the outside studs along the length of the wall and 76 mm above and below the middle of the studs. By maintaining a known offset from the centreline of the outside studs it was possible to measure the axial displacement of the wall, the rotation of the top of the wall in the plane of the wall, and the rotation of the top of the wall about the width of the wall. The displacement of the centre of the distribution beam at the foundation end of the wall along the height of the wall was also measured. This was to ensure that the assumption of a rigid support was valid.

The transversal displacement of the walls was measured at five locations: at the ends and at the mid-height of the centre stud, and at the mid-height of the two outside studs. The displacement transducers that were used had a range of 152 mm (6") and were attached to the middle of each stud with two wood screws. It will be described later how some of the walls were tested on both sides, to simulate load reversal, and it has already been described how one of the walls had sheathing on both sides. In these cases, the sheathing on the tension face of the walls was cut using a jigsaw to allow the transversal displacement transducers to pass through (Figure 7.9 (c)). The displacement transducers at each end of the centre stud were located 102 mm (4") from the inside face of the outer end plates for walls with and without double end plates to ensure that the distance between these two measurements remained constant for all wall specimens tested.

Five linear potentiometers (pots) measured the slippage between the exterior sheathing and the centre stud and each had a measurement range of 25 mm (1"). The locations where slippage was

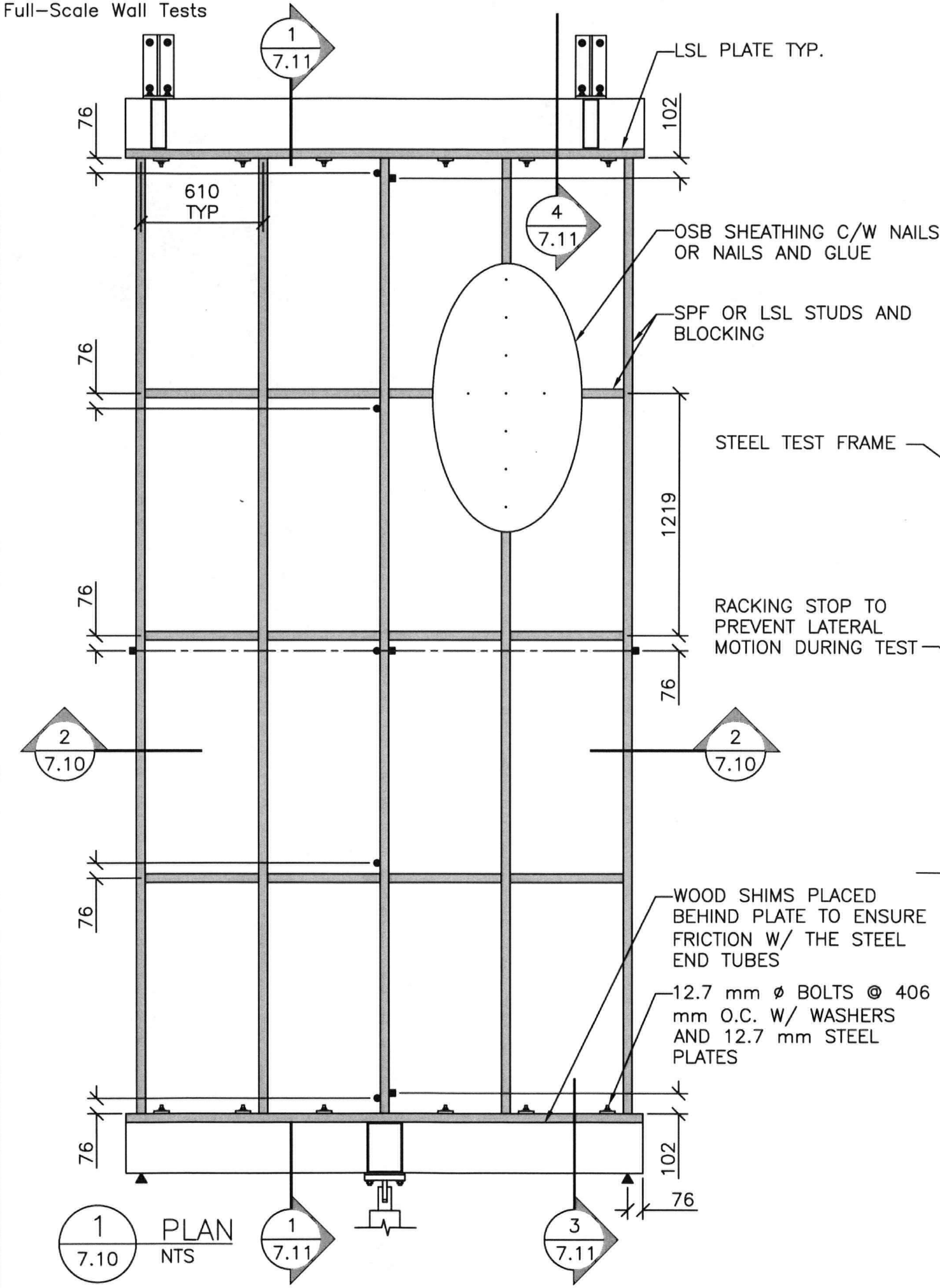

1 7.10 PLAN
NTS

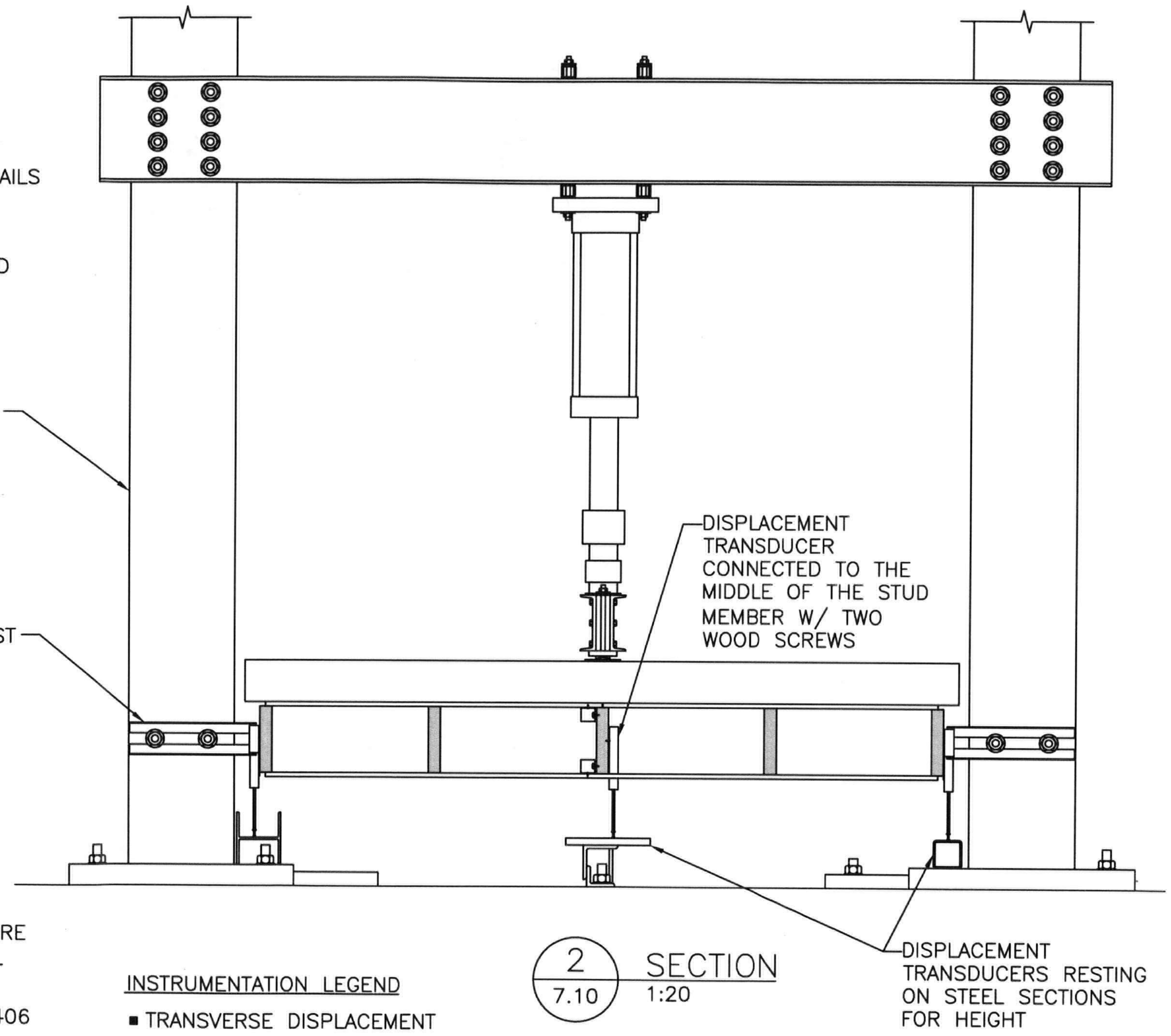

2 7.10 SECTION
1:20

INSTRUMENTATION LEGEND

- ■ TRANSVERSE DISPLACEMENT
- • SLIPPAGE POT
- ▲ AXIAL DISPLACEMENT AND ROTATION

SCALE 1:20
0 500 1000

Forintek Canada Corp.	TALL WALL STRUCTURAL PERFORMANCE	DRAWN DEL	DATE OCT-04
		SCALE AS SHOWN	APPROVED
	SCHEMATIC OF FULL-SCALE WALL TEST SET-UP	DRAWING NUMBER FIG 7.10	REVISION
			PROJECT REF. 3910

AUG 12, 2004 ~FCC~C:/MY DOCUMENTS/FULL-SCALE WALL TEST.DWG DLEON

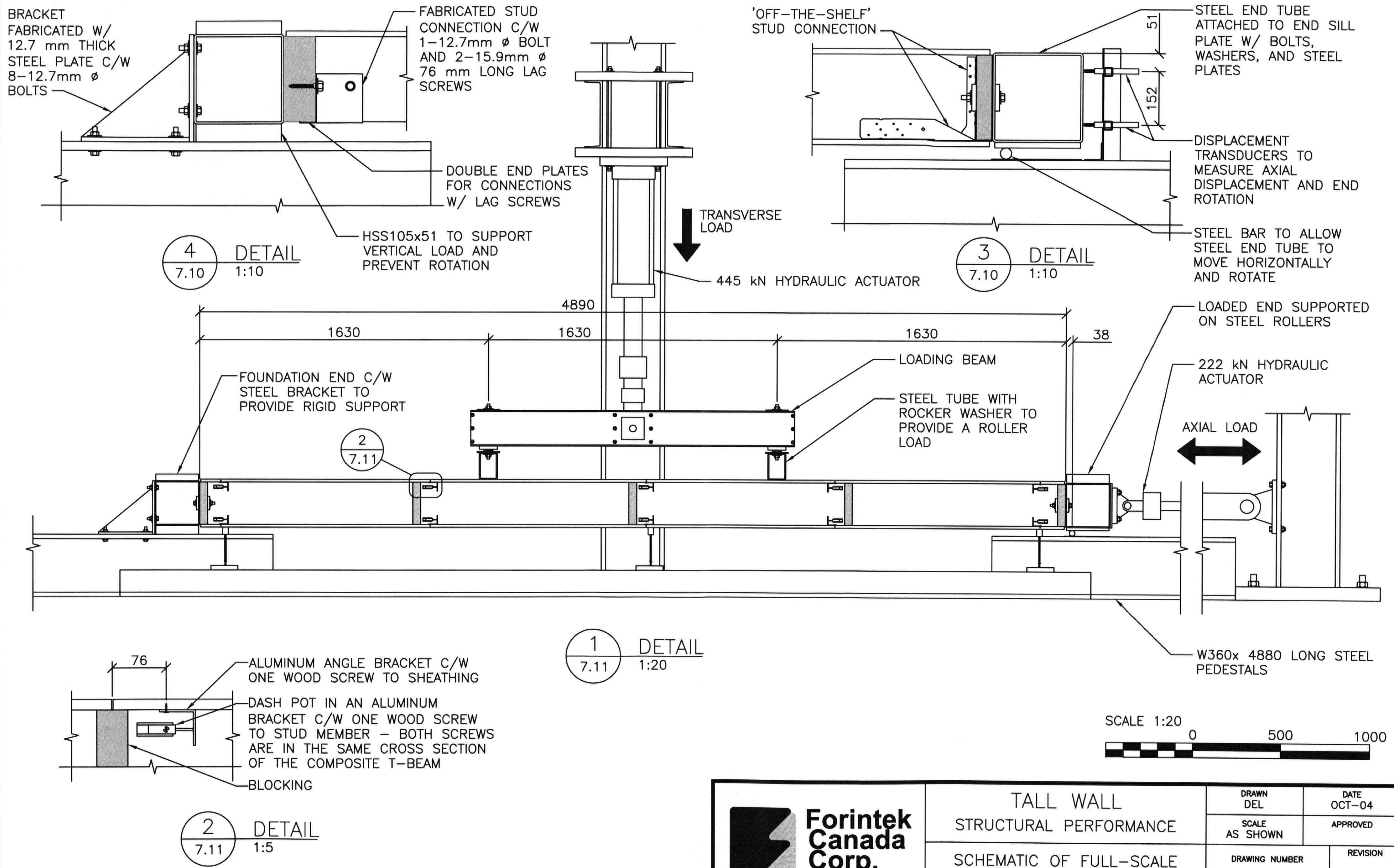

Forintek Canada Corp.	TALL WALL STRUCTURAL PERFORMANCE	DRAWN DEL	DATE OCT–04
		SCALE AS SHOWN	APPROVED
	SCHEMATIC OF FULL-SCALE WALL TEST SET-UP	DRAWING NUMBER FIG 7.11	REVISION PROJECT REF. 3910

AUG 12, 2004 ~FCC~C:/MY DOCUMENTS/FULL-SCALE WALL TEST.DWG DLEON measured are shown in Plan 1 in Figure 7.10. For the wall that had gypsum wallboard sheathing on the interior (bottom) face, five additional linear pots measured the slippage between that sheathing and the centre stud at the same cross-sectional locations as the pots on the exterior (top) face. Holes were drilled in the sheathing on the tension face of the walls that were tested on both sides or had sheathing on both faces to allow the data cables to be connected to the data-recording computer (Figure 7.9 (d)). The slippage pots at each end of the centre stud were located 76 mm (3") from the inner end plates for walls with and without double end plates.

7.2.3 Testing Procedures

Because of the many objectives outlined for the full-scale wall test program, many different loading protocols were employed over the course of testing. First, like the T-beam tests described in Chapter 5, the stiffness of the walls in the transversal direction was measured on a one-time basis. With the inclusion of axial load, however, it was necessary to measure the stiffness as it varies with changing axial load. To achieve this, constant axial load levels were applied to the wall specimens, while several monotonic tests with linearly increasing transversal load were conducted in the transversal direction. The four different test protocols referred to in Table 7.1 are presented in Figure 7.12. For each of the four test programs the transversal load was increased at a load-controlled rate of 66.7 kN (15,000 lb.) per minute. This approximately corresponded to the displacement-controlled rate of 25 mm (1") per minute previously used for the T-beam monotonic tests.

The different transversal load levels correspond to the different strengths of the walls. A transversal load of 24.5 kN (5,500 lb.) was applied to walls with SPF studs and to walls with LSL studs spaced at 1,220 mm (48") on centre (test protocol T1). A transversal load of 48.9 kN (11,000 lb.) was applied to walls with LSL studs spaced at 610 mm (24") on centre (test protocol

T2 and T3). The two transversal load levels produce maximum bending moments in the walls that correspond to uniformly distributed loads of 2.7 kPa (57 psf) and 5.4 kPa (114 psf) respectively. The final ramped transversal load shown for test protocols T1, T2, and T3 were not always conducted. When other failure modes were sought, the transversal load was increased to the same level as the previous cycles. Table 7.2 shows how each wall specimen was loaded. The axial load increment is equal to 24.5 kN (5,500 lb.). This corresponds to a uniform load at

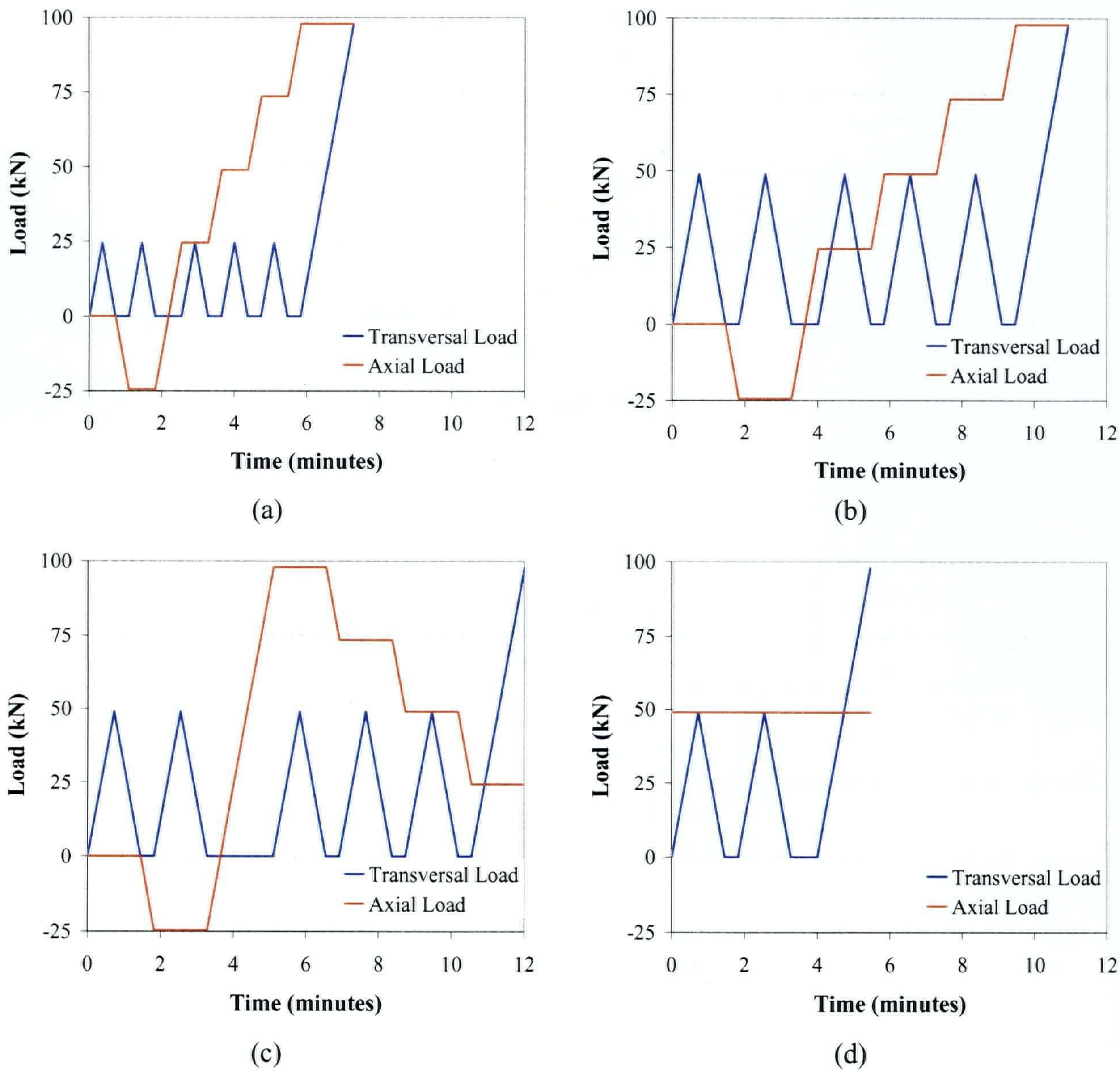

Figure 7.12. Transversal and axial loads as a function of time for test protocols: (a) T1; (b) T2; (c) T3; and (d) T4.

the top of the wall of 10 kN/m (688 lb./ft.). The increment was increased to a compression load of 97.8 kN (22,000 lb.) and decreased to a tension load of 24.5 kN. The different axial load level sequences seen in test programs T2 and T3 were used to determine if the sequence of load level had any affect on the interaction between axial load and transversal displacement.

One objective of the test program was to determine the effect of non-structural gypsum wallboard sheathing on the transversal stiffness of a tall wood-frame wall, specifically if the stiffness degraded with several transversal cycles with the same axial load. Test protocol T4 served this purpose and was used on wall number 511 where a constant axial load was applied while the three transversal load tests were conducted (Figure 7.12 (d)). Another objective was to determine if the direction of transversal loading had an effect on the stiffness of a wall. Several of the walls were inverted in the test frame and retested after the initial test program. A wall that

Table 7.2. Test schedule for each full-scale wall specimen.

Specimen Number	Test Protocol	Transversal Load Past Linear Range on Exterior	Specimen Inverted (Load Reversal)	Transversal Load Past Linear Range on Interior (Inverted Specimen)	Point Loaded	Axial Tension Load to Failure
501	T1	●				
502	T1	●				
503	T1	●				
514	T1					●
504	T2					●
505	T1	●				
506	T1				●	●
507	T3	●				●
508	T1	●	●		●	●
509	T2		●	●	●	
511	T4	●				
512	T2		●			●
513	T1					●

was inverted with an overhead crane and placed in the test frame is shown in Figures 7.13 (a) and (b), respectively. For these walls, the same test protocol was applied for each orientation. Because a uniform transversal displacement was applied at the third points of the wall by the comparatively rigid steel loading beams, the bending stiffness in the transverse (in-plane) direction could not be measured during most tests because each stud was displaced the same amount along each loading beam over the width of each wall. For three of the walls, however, a point load was applied at the mid-height of the centre stud in order to quantify this property. Finally, the response of the four stud connection types described previously was examined. Some of these walls were loaded under axial tension only until the walls failed. The axial loading rate was approximately 25 kN (5,600 lb.) per minute.

(a) (b)

Figure 7.13. Wall specimen being prepared for second test on internal side: (a) inverting a wall using an overhead crane; and (b) an inverted wall in test frame.

7.2.4 Material Properties

A description and the relative densities of the SPF and LSL stud materials used for the full-scale wall tests can be found in Chapter 3. The stiffness properties and relative density of the OSB sheathing used for the wall specimens can also be found in Chapter 3 along with the properties of the spiral nails. Standard white wood glue was used to provide a rigid connection between the frame and the sheathing for one specimen. The particular glue that was utilized was Elmer's Contractor's Grade Professional Strength Wood Glue for Interior Use.

Some of the studs from the T-beam test program had not been loaded beyond the linear-elastic range and were subsequently re-used as studs in the full-scale wall test program. The elastic properties of all the additional studs that were used in the wall were determined by loading at their third-points in the test frame shown in Figure 7.14. Some of the studs from the T-beam tests were also re-tested in this test frame to ensure that the results matched those determined using the test frame described in Chapter 3. The total span was 4,100 mm (161 ½"). A maximum load of 2.7 kN (600 lb.) was applied at a displacement-controlled rate of 25 mm (1") per minute. The calculated value for stiffness was taken as the slope on the load-displacement curve between the 1.3 kN (300 lb.) and 2.7 kN (600 lb.) load points. The dimensions of the studs were measured with callipers. The normal cumulative distribution functions for the modulus of elasticity of all studs tested from both the T-beam and full-scale wall test programs are shown in Figure 7.15. The stiffness values obtained for the studs tested previously were found to be consistently 6% lower in the subsequent tests as shown in Figure 7.14. All of the stiffness values obtained from the second test frame were therefore increased by this amount. The median values of the SPF and LSL distributions were 9,582 MPa and 11,570 MPa, respectively, and the coefficients of variation were approximately 22% and 3%, respectively. The mean values of modulus of elasticity for the SPF and LSL, which were 9,525 MPa and 11,661 MPa, respectively, relate quite closely with that found for the T-beam tests and with published values for use in design in the Canadian Wood Design Code and literature provided by the manufacturer.

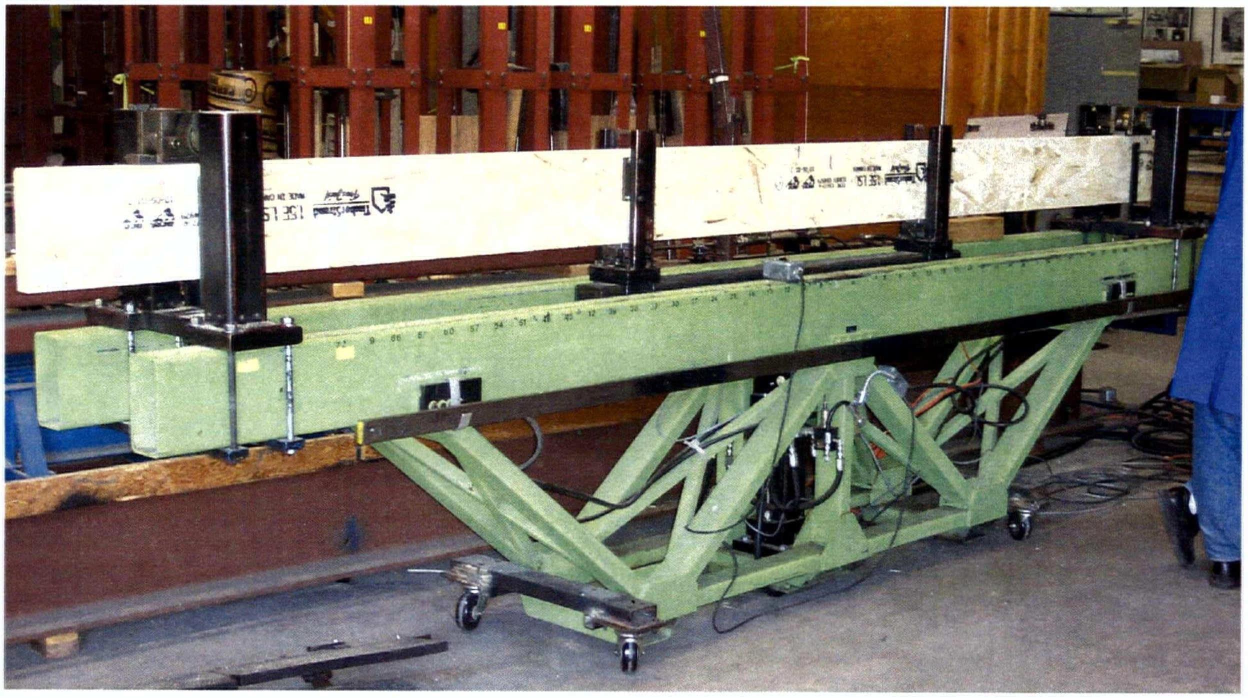

Figure 7.14. Full-scale wall studs tested under third point loading to determine modulus of elasticity.

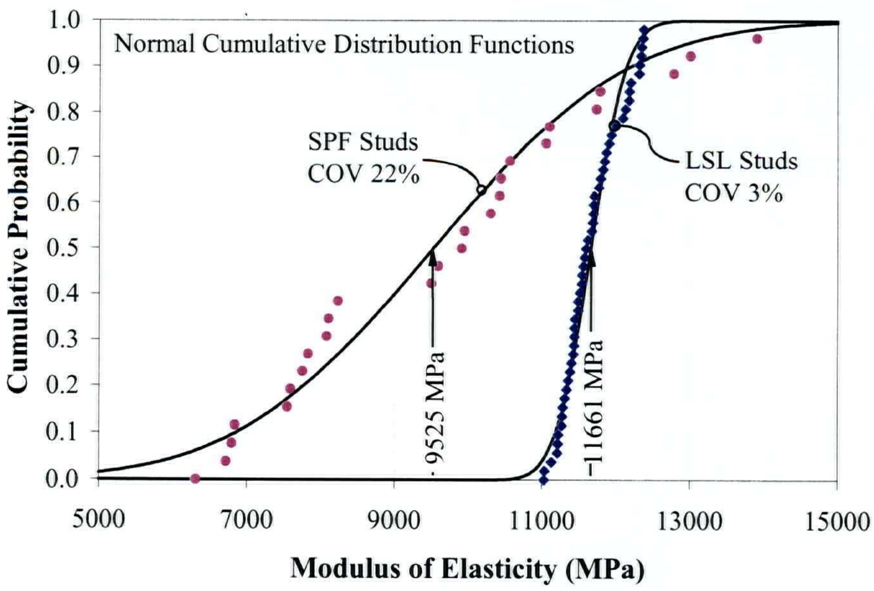

Figure 7.15. Cumulative distribution of modulus of elasticity for full-scale wall studs, plates and blocking.

The gypsum wallboard sheathing used as interior sheathing in wall specimen 511 was 15.9 mm (5/8") thick Fireguard Type X, manufactured in Canada by Georgia Pacific, Inc. It was specified as fire-rated sheathing and meets the specifications in ASTM C36. The most recent edition of the Canadian Wood Design Code includes limited design provisions for shearwalls constructed with gypsum wallboard conforming to Type X specifications for fire rating. Therefore, Type X gypsum wallboard was used instead of other more common types of wallboard since it is the only one currently referred to in the Canadian Wood Design Code. The properties of the gypsum wallboard sheets or the load-slip response of the screwed connections were not determined.

7.3 RESULTS AND DISCUSSION

The full-scale wall tests that were conducted have extended the knowledge of composite action and allowed for new insight into the behaviour of an entire wall structure. Although similar comparisons presented in Chapter 5 have been made with respect to wall construction, the full-scale tests allowed for new comparisons to be made with regards to load interaction, the direction of loading, transverse effects, end connections, and the effect of the end support conditions on the bending stiffness of walls. Tests with monotonic transversal loading and constant axial load were conducted to obtain bending stiffnesses in both the in-plane and out-of-plane directions and strength values. Additional tests with monotonic axial load only were conducted to obtain axial strength values.

7.3.1 Load-Displacement Results

The stiffness values from monotonic transversal third point loading with constant axial loads for each wall specimen are presented in Table 7.3. Axial compression is denoted with a negative sign. The transversal displacements were measured at the mid-height of the centre stud of the walls. As mentioned previously, some of the walls were inverted and tested again. Those tests, with transversal loads applied to the interior face of the walls, are denoted in the table with a B. The stiffness of the walls is presented for two loaded ranges. The first, which is referred to as the initial stiffness, corresponds to the load levels used to determine the initial stiffness of the T-beam specimens described in Chapter 5. For those tests, stiffness was measured as the slope on the load-displacement curve between the 0.9 kN (200 lb.) and 2.2 kN (500 lb.) load points. For the full-scale wall tests, two loading ranges were used. According to the first one, initial stiffness was chosen to be either three or five times that of the T-beam tests depending on whether there were three or five studs in the wall specimen. Therefore, the initial stiffness loading range for walls that had three studs spaced at 1,220 mm (48") on centre was between 2.7 kN (600 lb.) and 6.7 kN (1,500 lb.) and for walls with five studs spaced at 610 mm (24") on centre it was between 4.5 (kN) (1,000 lb.) and 11.1 kN (2,500 lb.). The largest load values in the initial stiffness range for the two wall types produce maximum bending moments in the walls equivalent to the bending moments produced by uniformly distributed loads of 0.6 kPa (13 psf) and 1.0 kPa (21 psf) respectively, assuming that the walls are simply supported. The second loading range used to determine stiffness was constant for all of the walls and was taken between 11.1 kN (2,500 lb.) and 24.5 kN (5,500 lb.). The largest load value in this stiffness range corresponds to a uniformly distributed load of 2.2 kPa (45 psf).

The predicted wall bending stiffness with bare studs only, Column (5) in the table, was determined by summing up the individual stiffness values for each stud in a wall using simple beam theory and the modulus of elasticity (MOE) for each stud as calculated previously, assuming that the studs were simply supported. This method was chosen since this is the procedure currently used in the design of wood-frame walls, except that the modulus of elasticity for all the studs would of course be the same, as is specified in the building code. The average

Table 7.3. Full-scale wall bending stiffness values from tests with monotonic transversal loads and constant axial loads.

(1) Specimen Number/ Stud Numbers within Specimen	(2) MOE of Studs within Wall Specimen (MPa)	(3) Specimen Test Number	(4) Axial Load Applied to Wall Specimens (kN)	(5) Predicted Wall Bending Stiffness with Bare Studs Only (N/mm)	(6) Maximum Transversal Load used to obtain Initial Stiffness (kN)	(7) Initial Wall Bending Stiffness from Tests (N/mm)	(8) Stiffness Increase (7) to (5) (%)	(9) Wall Bending Stiffness from Tests (11.1 - 24.5 kN) (N/mm)	(10) Stiffness Increase (9) to (5) (%)
501		01	0.0	1051	11.1	1270	20.8	1073	2.1
SPF 01	12771	02	24.5	1080	11.1	1289	19.4	1098	1.7
SPF 12	7823	03	-24.6	1023	11.1	1220	19.2	1037	1.4
SPF 06	7540	04	-49.0	995	11.1	1236	24.3	1047	5.2
SPF 14	13896	05	-73.4	966	11.1	1252	29.5	1034	7.0
SPF 08	12998	06	-97.9	938	11.1	1222	30.3	1006	7.2
502		01	0.0	841	11.1	1071	27.3	964	14.6
SPF 02	8224	02	24.5	869	11.1	1076	23.8	1089	25.3
SPF 09	6711	03	-24.5	813	11.1	1033	27.0	1043	28.3
SPF 20	7746	04	-48.9	784	11.1	1011	28.9	1008	28.5
SPF 04	10293	05	-73.4	756	11.1	1033	36.7	996	31.8
SPF 05	11046	06	-97.9	728	11.1	1033	42.0	983	35.1
503		01	-0.1	920	11.1	1188	29.2	1068	16.1
SPF 25	8072	02	24.4	948	11.1	1178	24.2	1108	16.9
SPF 26	9904	03	-24.5	891	11.1	1095	22.8	1049	17.6
SPF 24	9582	04	-49.0	863	11.1	1100	27.4	1055	22.2
SPF 23	9490	05	-73.4	835	11.1	1092	30.8	1043	24.9
SPF 18	11093	06	-98.0	806	11.1	1098	36.2	1028	27.5
504		01	0.0	1448	11.1	2167	49.7	1755	17.7
LSL 44	11760	02	24.5	1476	11.1	2182	47.8	1831	20.5
LSL 46	12084	03	-24.5	1419	11.1	2092	47.4	1741	19.1
LSL 45	12169	04	-49.0	1391	11.1	2079	49.5	1700	18.6
LSL 37	11930	05	-73.5	1362	11.1	2035	49.3	1660	18.2
LSL 41	11204	06	-98.0	1334	11.1	1897	42.2	1622	17.9
505		01	-0.1	828	6.7	1491	80.2	1006	21.6
LSL 51	11434	02	24.5	856	6.7	1472	71.9	1105	29.0
LSL 48	11122	03	-24.5	799	6.7	1350	68.9	1057	32.2
LSL 47	11263	04	-48.9	771	6.7	1334	73.0	1018	32.0
		05	-73.4	743	6.7	1227	65.2	984	32.5
		06	-97.9	714	6.7	1243	74.0	955	33.8
506		01	-0.1	882	6.7	794	-10.0	874	-0.9
LSL 17	12189	02	24.5	911	6.7	937	2.9	850	-6.7
LSL 16	12304	03	-24.5	854	6.7	901	5.5	879	3.0
LSL 18	11552	04	-49.0	825	6.7	998	20.9	887	7.5
		05	-73.4	797	6.7	1000	25.4	878	10.2
		06	-97.9	769	6.7	979	27.4	868	12.9

Table 7.3 Continued. Full-scale wall bending stiffness values from tests with monotonic transversal loads and constant axial loads.

(1) Specimen Number/ Stud Numbers within Specimen	(2) MOE of Studs within Wall Specimen (MPa)	(3) Specimen Test Number	(4) Axial Load Applied to Wall Specimens (kN)	(5) Predicted Wall Bending Stiffness with Bare Studs Only (N/mm)	(6) Maximum Transversal Load used to obtain Initial Stiffness (kN)	(7) Initial Wall Bending Stiffness from Tests (N/mm)	(8) Stiffness Increase (7) to (5) (%)	(9) Wall Bending Stiffness from Tests (11.1 - 24.5 kN) (N/mm)	(10) Stiffness Increase (9) to (5) (%)
507		01	0.0	1472	11.1	1713	16.4	1548	5.1
LSL 14	12329	02	22.3	1498	11.1	1713	14.4	1524	1.8
LSL 13	11896	03	-97.7	1359	11.1	1771	30.3	1531	12.6
LSL 04	12170	04	-73.4	1387	11.1	1751	26.3	1525	9.9
LSL 06	11419	05	-49.0	1415	11.1	1749	23.6	1509	6.6
LSL 05	12336	06	-24.5	1444	11.1	1702	17.9	1485	2.9
508		01	0.0	841	6.7	1760	109.3	1571	86.9
LSL 29	11214	02	24.5	869	6.7	1665	91.5	1576	81.3
LSL 32	11613	03	-24.5	812	6.7	1751	115.6	1584	95.0
LSL 28	11533	04	-49.1	784	6.7	1771	125.9	1580	101.5
		05	-73.5	756	6.7	1605	112.4	1580	109.1
		06	-98.2	727	6.7	1567	115.5	1544	112.4
508B		01	0.0	841	6.7	1936	130.2	1532	82.2
LSL 28	11533	02	24.4	869	6.7	1873	115.5	1575	81.3
LSL 32	11613	03	-24.5	813	6.7	1815	123.3	1556	91.5
LSL 29	11214	04	-49.0	784	6.7	1783	127.4	1529	95.0
		05	-73.4	756	6.7	1741	130.4	1490	97.2
		06	-97.8	728	6.7	1713	135.5	1467	101.6
509		01	0.1	1418	11.1	2018	42.3	1656	16.8
LSL 36	11484	02	24.5	1446	11.1	2016	39.4	1710	18.2
LSL 35	11374	03	-24.5	1389	11.1	1997	43.7	1653	19.0
LSL 33	12363	04	-48.9	1361	11.1	1980	45.5	1637	20.3
LSL 25	11429	05	-73.5	1332	11.1	1959	47.0	1628	22.2
LSL 27	11277	06	-98.0	1304	11.1	1875	43.7	1609	23.4
509B		01	-0.1	1418	11.1	2045	44.2	1565	10.4
LSL 27	11277	02	24.5	1446	11.1	1975	36.6	1658	14.6
LSL 25	11429	03	-24.6	1389	11.1	1897	36.6	1591	14.5
LSL 33	12363	04	-49.0	1361	11.1	1942	42.7	1589	16.8
LSL 35	11374	05	-73.4	1333	11.1	2029	52.2	1600	20.1
LSL 36	11484	06	-97.9	1304	11.1	2048	57.0	1610	23.4
511		01	-48.9	1352	11.1	3107	129.9	1819	34.6
LSL 10	11686	02	-48.9	1351	11.1	2421	79.1	1763	30.4
LSL 21	12119	03	-48.9	1351	11.1	2342	73.3	1715	26.9
LSL 22	11024								
LSL 23	11030								
LSL 24	11680								

Table 7.3 Continued. Full-scale wall bending stiffness values from tests with monotonic transversal loads and constant axial loads.

(1) Specimen Number/ Stud Numbers within Specimen	(2) MOE of Studs within Wall Specimen (MPa)	(3) Specimen Test Number	(4) Axial Load Applied to Wall Specimens (kN)	(5) Predicted Wall Bending Stiffness with Bare Studs Only (N/mm)	(6) Maximum Transversal Load used to obtain Initial Stiffness (kN)	(7) Initial Wall Bending Stiffness from Tests (N/mm)	(8) Stiffness Increase (7) to (5) (%)	(9) Wall Bending Stiffness from Tests (11.1 - 24.5 kN) (N/mm)	(10) Stiffness Increase (9) to (5) (%)
512		01	0.0	1443	11.1	1906	32.1	1488	3.2
LSL 42	11484	02	24.6	1471	11.1	1862	26.6	1584	7.7
LSL 43	12355	03	-24.5	1414	11.1	1834	29.7	1517	7.3
LSL 52	11348	04	-49.0	1386	11.1	1828	31.9	1506	8.7
LSL 50	11783	05	-73.4	1358	11.1	1815	33.7	1492	9.9
LSL 49	11979	06	-97.9	1329	11.1	1842	38.6	1474	10.9
512B		01	0.0	1443	11.1	1742	20.7	1432	-0.8
LSL 42	11484	02	24.5	1471	11.1	1655	12.5	1471	0.0
LSL 43	12355	03	-24.5	1414	11.1	1606	13.5	1437	1.6
LSL 52	11348	04	-49.0	1386	11.1	1613	16.4	1470	6.1
LSL 50	11783	05	-73.5	1358	11.1	1609	18.5	1465	7.9
LSL 49	11979	06	-97.9	1329	11.1	1645	23.8	1466	10.3
513		01	0.0	852	6.7	1218	43.0	962	12.9
LSL 42	11484	02	24.5	880	6.7	1207	37.1	1101	25.0
LSL 52	11348	03	-24.5	824	6.7	1179	43.1	1042	26.5
LSL 49	11979	04	-49.0	795	6.7	1172	47.3	1039	30.6
		05	-73.4	767	6.7	1159	51.1	1033	34.8
		06	-97.9	738	6.7	1174	59.0	1020	38.2
514		01	0.0	993	11.1	1290	30.0	1137	14.5
SPF 16	11775	02	24.5	1021	11.1	1257	23.1	1145	12.1
SPF 17	10416	03	-24.5	965	11.1	1231	27.6	1138	18.0
SPF 22	11729	04	-49.1	936	11.1	1218	30.2	1127	20.5
SPF 19	8100	05	-73.6	908	11.1	1208	33.1	1108	22.1
SPF 15	9941	06	-98.0	879	11.1	1179	34.1	1078	22.5

dimensions for the SPF and LSL studs used in the calculations were 38 mm by 234 mm and 44 mm by 242 mm, respectively. The predicted change in stiffness of the bare stud members with varying axial loads will be discussed later. The increase in stiffness values for both loading ranges were determined by dividing the stiffness values determined from testing by the predicted stiffness of the bare studs.

It was shown in Chapter 5 that the coefficient of variation for the increase in composite member bending stiffness over the bending stiffness of the bare stud alone for the three replicates of each T-beam specimen type tested was very low, with the highest value being just over 4.5%. Although only one replicate of each full-scale wall specimen was tested, some of the wall specimens were constructed in the same way except for their stud connection types. By comparing the values of increase in stiffness for the three pairs of walls at the higher loading range with a chosen axial load level, it can be seen that the composite stiffness properties of these walls were indeed similar. The higher loading range for determining stiffness was chosen to avoid secondary effects resulting from the different stud connections on the initial stiffness. The axial load level chosen was 48.9 kN (11,000 lb.) in compression; this load level is used repeatedly throughout the rest of this chapter for comparisons purposes. The increase in stiffness over the stiffness of the bare studs in the wall for the three pairs of similar wall specimens tested are as follows: 22.2% for wall number 503 and 20.5% for wall number 514; 32.0% for wall number 505 and 30.6% for wall number 513; and 6.6% for wall number 507 and 8.7% for wall number 512. The largest difference between the walls with similar constructions was 2.1%.

The linear load-vs-displacement plots presented in Figure 5.13 of Chapter 5 have been repeated in Figure 7.16 for the full-scale walls tested. The comparisons are based on the initial bending stiffness values obtained from testing applied to a simply supported wall under a uniformly distributed load using simple beam theory. Although bending stiffness is a cross-sectional property that is independent of the type of loading, it was deemed appropriate to use a uniformly distributed load, as is commonly used for the design of walls in actual structures under transversal loads. The values of bending stiffness obtained from testing are from tests with an applied axial load of 48.9 kN (11,000 lb.). The curves for the bare SPF and LSL studs are based

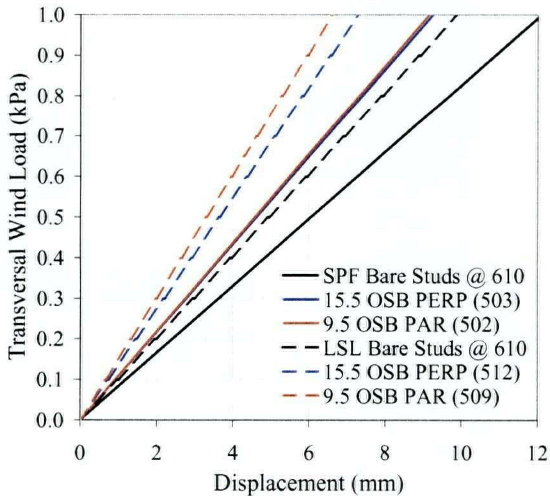

(a) Stud modulus of elasticity.

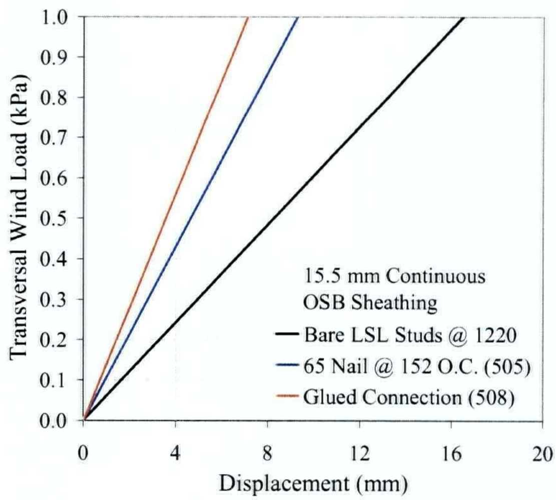

(b) Connection stiffness.

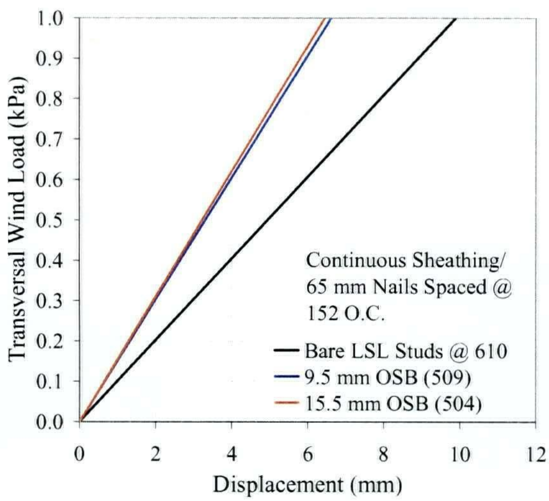

(c) Sheathing thickness.

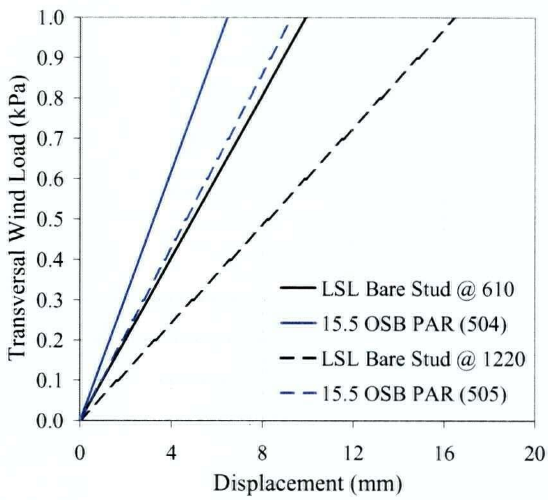

(d) Stud spacing.

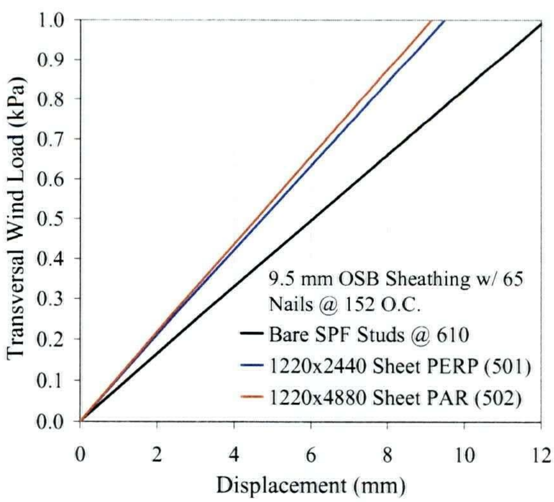

(e) SPF with gaps in the sheathing.

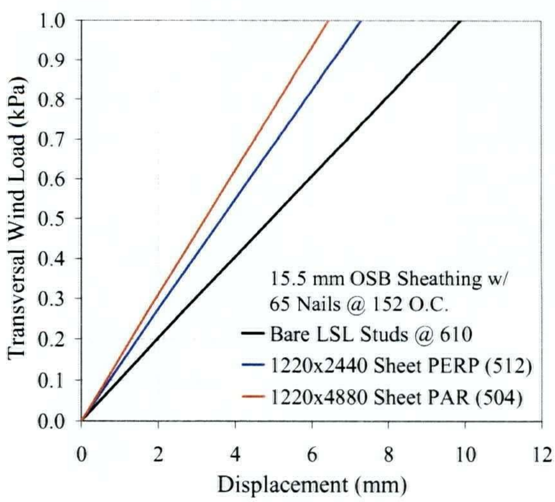

(f) LSL with gaps in the sheathing.

Figure 7.16. Load-displacement relationships obtained from full-scale wall testing.

on the average modulus of elasticity values of all studs tested, which were shown in Figure 7.15 and were 9,525 MPa and 11,661 MPa, respectively.

The effect of the modulus of elasticity of the stud, or the stud member type, on the stiffness of wall specimens is presented in Figure 7.16 (a). The load-displacement relationships compare walls with 15.5 mm thick OSB sheathing oriented perpendicular to the length of the studs and walls with continuous 9.5 mm thick OSB sheathing oriented parallel to the length of the studs. Similar to the comparison of the effect of stud modulus of elasticity on the stiffness of composite T-beams shown in Figure 5.13 (b), the increase in stiffness of the walls with 15.5 mm thick OSB sheathing over the bare studs is approximately the same for the specimens constructed with SPF and LSL studs, namely 27.4% and 31.9%, respectively. The increase in stiffness of the wall with continuous 9.5 mm thick OSB sheathing and LSL studs is greater than the increase for the wall with the same sheathing and SPF studs, namely 45.5% and 28.9, respectively. In both cases, however, the bending stiffness values of the walls with LSL studs are increased by approximately the same amount due to the increase in stiffness of the LSL studs compared to the SPF studs.

The effect of sheathing-to-stud connection stiffness on the bending stiffness of walls with LSL studs spaced at 1,220 mm O.C. and continuous 15.5 mm thick OSB sheathing is shown in Figure 7.16 (b). A similar comparison for T-beams with an LSL stud and 610 mm wide, continuous 15.5 mm thick OSB sheathing was presented in Figure 5.13 (c). In that case the difference between the connection with 65 mm spiral nails spaced at 152 mm on centre and a glued connection was 29.6%. For the wall specimens, the difference between walls with those same connections was 52.9%. It was shown in Chapter 5 that the stiffness of nailed connections, and thus the stiffness of the partially composite T-beams or walls with those connections, decreases with increasing load due to the loss of frictional resistance and with repeated load cycles due to degradation of the connection. The T-beams in Figure 5.13 (c) were not loaded past the initial stiffness range. The wall specimens in Figure 7.16 (b) were loaded past the initial stiffness range and the difference between the increases in stiffness for the two sheathing connection types was increased from 52.9% to 69.5% at the higher load level. Although this clearly shows how the degradation in nail stiffness with increasing load can effect the overall bending stiffness of a wall, it should be noted that the discrepancy between the T-beam tests and the full-scale wall tests may have been due in part to the effect that the glued sheathing had on end rotational restraint at the foundation end of the wall, which will be discussed in detail later in this chapter.

It was stated in Chapter 5 that the increase in the stiffness of a composite member due to the increase in sheathing thickness could be significant. This was shown graphically in Figure 5.13 (d). In that example, the difference in the increase in member stiffness between T-beams with LSL studs and 9.5 mm versus 15.5 mm thick continuous OSB sheathing was 25.2%. The results of full-scale walls with similar construction are shown in Figure 7.16 (c) and indicate that the difference between these walls is only 4%. No clear conclusion can be drawn from this discrepancy because both of these increase in stiffness values for the wall specimens lay in between the values determined from the T-beam tests. The increase in stiffness for the wall specimen with 9.5 mm sheathing was approximately 10% higher than the average increase for the corresponding T-beam specimens and the increase in stiffness was approximately 10% lower for the wall specimen with 15.5 mm sheathing. An overall trend is not possible because the thickest sheathing used in the T-beam tests was not used in the full-scale wall tests.

The load-displacement response of wall specimens with differing stud spacing but with the same stud material, sheathing, and connection type are presented in Figure 7.16 (d). Both specimens had continuous 15.5 mm thick OSB sheathing connected to LSL studs with 65 mm spiral nails spaced at 152 mm on centre. The increase in stiffness of the wall specimen with studs spaced at

610 mm on centre over the stiffness of the bare studs was less than that for the wall specimen with studs spaced at 1,220 mm on centre, namely 49.5% versus 73.0%, respectively. This trend also continued at the higher loading range used to determine the bending stiffness. The difference may be due to the influence of larger effective flange widths for the wall with the larger stud spacing. The predictions made in Section 5.3.1, based on the bending stiffness results of the composite T-beam tests, showed however that it would require 28.5 mm thick continuous OSB sheathing with LSL studs spaced at 1,220 mm on centre to surpass the stiffness of a wall with bare LSL studs spaced at 610 mm on centre. The stud spacing comparison was made because the current Canadian Wood Design Code does not allow for the inclusion of partial composite action into the calculations of member stiffness. The full-scale wall tests showed that, in the initial stiffness range, a wall with continuous 15.5 mm thick OSB sheathing connected to LSL studs spaced at 1,220 mm on centre was stiffer than simply supported LSL studs spaced at 610 mm on centre.

Figure 7.16 (e) and (f) show the composite stiffness of wall specimens sheathed with 1,220 mm by 2,440 mm sheets of OSB oriented perpendicular to the length of the studs and with 1,220 mm by 4,880 mm sheets of OSB oriented parallel to the length of the studs. Figure 7.16 (e) shows the response of walls with SPF studs sheathed with 9.5 mm thick OSB and Figure 7.16 (f) shows the response of walls with LSL studs sheathed with 15.5 mm thick OSB. For the T-beams, the difference in the increase in bending stiffness for beams with different sheathing orientations and similar construction to the wall specimens with SPF studs was found to be approximately 6% (Figure 5.13 (a)). For the wall specimens, the difference was 4.6%, which again is not a significant increase even though there were no gaps in the sheathing for the wall with the sheathing oriented parallel to the length of the studs. In a reference to previous testing, it was stated in Chapter 5 that changing the sheathing orientation for a composite member with thin sheathing and small, short studs can increase stiffness of that member by approximately 30%.

The stiffness increase due to changing the sheathing orientations for the walls with LSL studs and 15.5 mm thick OSB sheathing was found to be 17.6%. This can be compared directly with the findings presented in Figure 5.13 (e) for T-beams with LSL studs and 15.5 mm thick OSB sheathing with different distances between gaps in the sheathing. The difference between the stiffness increase for T-beams with continuous sheathing and T-beams with gaps in the sheathing spaced at one-quarter of the span length was just over 57%. Although the stiffness increase of the wall with continuous sheathing compares well with the increase found in the T-beam tests, 49.5% versus 60.6%, the reduction in stiffness due to the presence of gaps in the sheathing is not as significant for the full-scale walls in this case. This may have been due to the fact that the same T-beam specimens were loaded repeatedly with additional gaps cut in the sheathing after each test. The reduction in the stiffness of nailed connections, due to repeated load cycles in the T-beam specimens, would have been less in the wall specimens as these were not loaded as many times.

7.3.2 Load Interaction

Many design codes contain an interaction equation for determining the resistance of beam-columns, which are structural elements subjected to both axial forces and bending moments, due to loads in the out-of-plane direction or applied bending moments, in one or more axes. Due to secondary effects, the applied bending moments in the beam-column are increased as the axial load is applied. The displacement of the beam-column out-of-plane due to the bending moments causes the axial load to become eccentric with respect to the centreline of the beam-column. This eccentricity amplifies the bending moments in the beam-column. The amount of amplification is a function of the ratio of the axial load to the Euler load, P_E, which is the axial load that is predicted to cause the beam-column to buckle out-of-plane without any applied bending moments. In the Canadian Wood Design Code a linear interaction equation must be satisfied for beam-columns with applied axial loads and bending moments. The equation is given by:

$$\frac{P_f}{P_r}+\frac{M_f}{M_r}\leq 1\text{, where} \tag{7.1}$$

$$M_f = M'_f\left[\frac{1}{1-\dfrac{P_f}{P_E}}\right], \tag{7.2}$$

$$P_E = \frac{\pi^2 EI}{(k_e L)^2}. \tag{7.3}$$

In the above equations, the symbols are defined as follows:

P_f = applied axial load

P_r = axial load resistance

M'_f = applied bending moment

M_f = applied bending moment amplified by the applied axial load

M_r = bending moment resistance

EI = bending stiffness of the beam-column, which equals the modulus of elasticity, E, multiplied by the moment of inertia, I

L = length of the beam-column

k_e = effective length factor, which is a function of the end restraints of the beam-column

The applied axial load also amplifies the out-of-plane displacement of the beam-column. The Canadian Wood Design Manual suggests the same amplification factor for displacements that is used for bending moments. The out-of-plane displacement that is amplified by the applied axial load is given as follows:

$$\Delta = \Delta' \left[\frac{1}{1 - \frac{P_f}{P_E}} \right]. \tag{7.4}$$

Δ' is the transversal displacement resulting from the applied bending moments or loads in the transversal direction. Each tested wall specimen was loaded under six different levels of constant axial load with a repeated monotonic transversal load. The stiffness values from the load-displacement responses for each of the axial load levels are presented in Table 7.3.

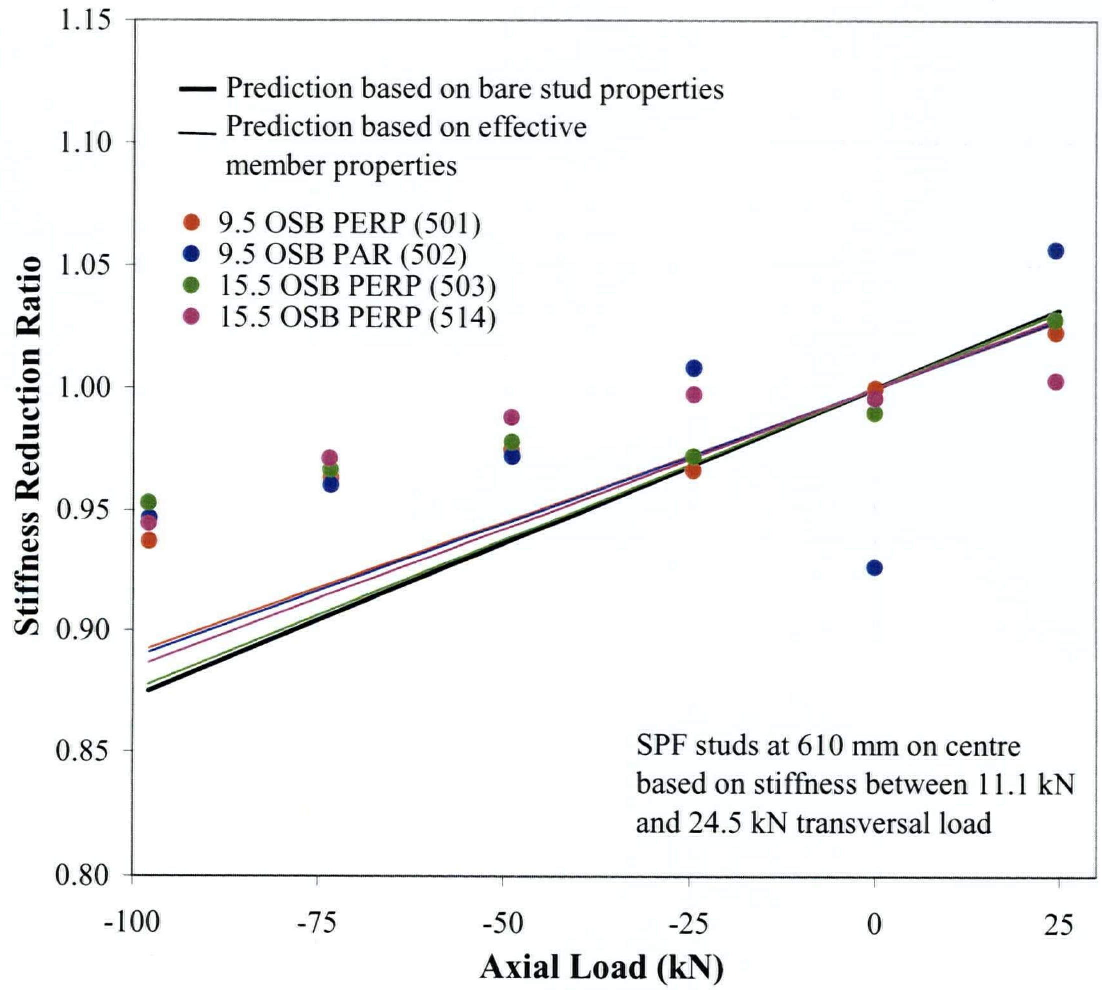

Figure 7.17. Reduction in bending stiffness due to axial load for wall specimens with SPF studs spaced at 610 mm on centre.

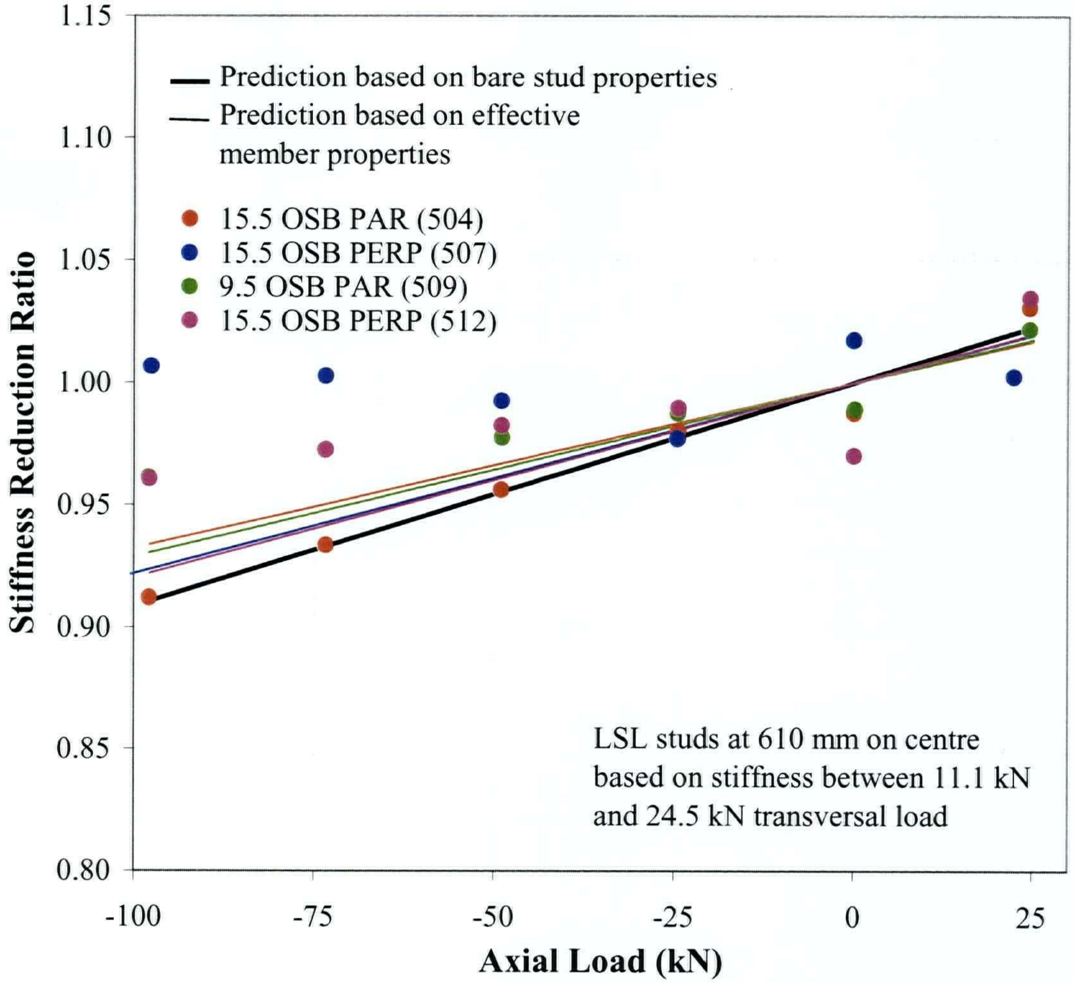

Figure 7.18. Reduction in bending stiffness due to axial load for wall specimens with LSL studs spaced at 610 mm on centre.

Stiffness is here defined as the change in applied transversal load divided by the change in transversal displacement at different load levels. The inverse of the amplification factor presented in equation (7.4) thus represents a stiffness reduction factor, which is compared with the stiffness values obtained from testing for the six different axial load levels. This comparison is shown graphically in Figures 7.17 through 7.19 for three different frame types: SPF studs spaced at 610 mm on centre, LSL studs spaced at 610 mm on centre, and LSL studs spaced at 1,220 mm on centre.

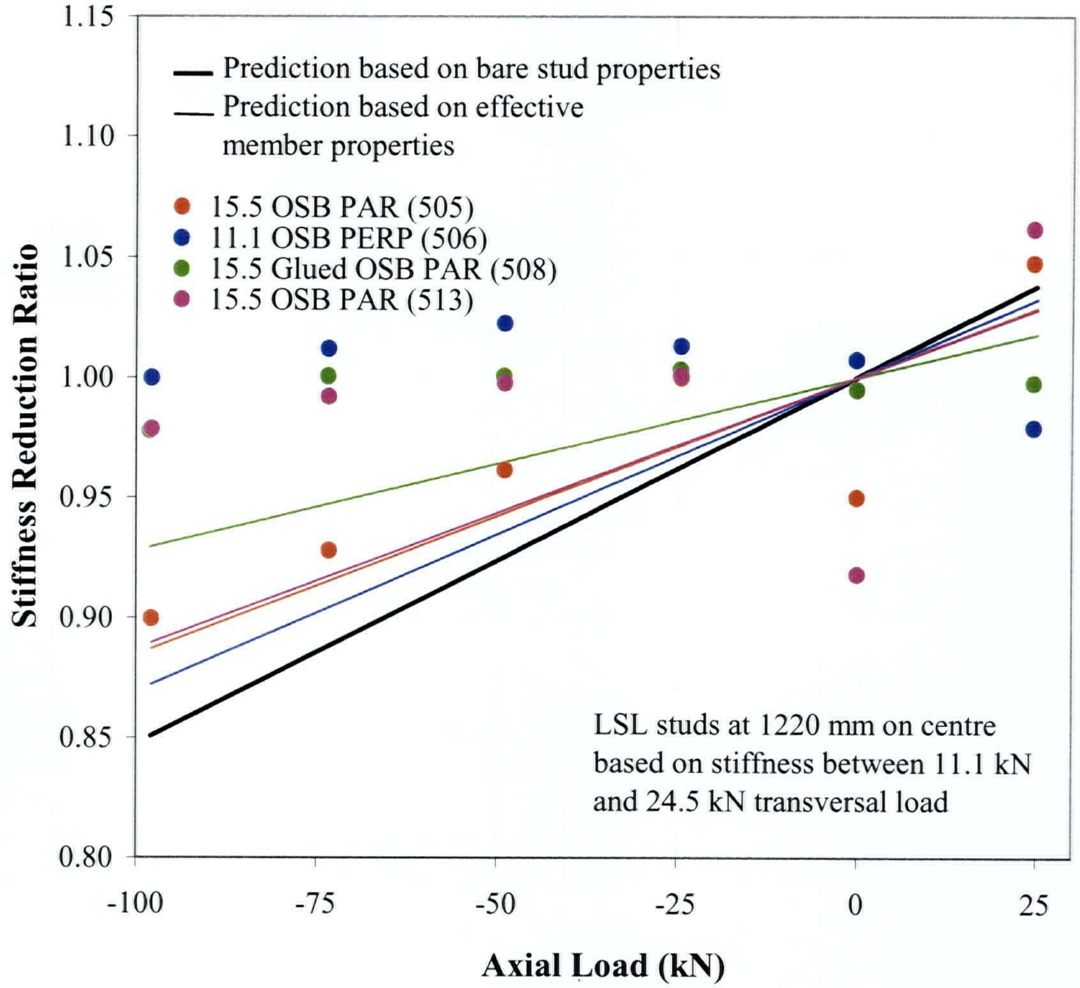

Figure 7.19. Reduction in bending stiffness due to axial load for wall specimens with LSL studs spaced at 1,220 mm on centre.

The points plotted on the graphs are from the tests that were conducted and each point represents one test. A linear regression line of stiffness versus axial load level, which is not shown, was plotted through the six stiffness values for each wall specimen. The stiffness reduction ratio for the tests was determined by dividing the stiffness values obtained from testing at each axial load level by the stiffness on the linear regression line at an axial load of zero. The basic stiffness values were taken from the higher load range (11.1 – 24.5 kN) so that the load range was constant for all of the wall specimens. The linear lines in the graphs are the predicted stiffness reduction ratios based on the bending stiffness of the bare stud alone, which is what is currently specified in the code, and the predicted bending stiffness of the composite wall based on the procedure outlined in Section 5.3.2.1. The values of modulus of elasticity used for the bare stud predictions were taken as the average value E as specified in the Canadian Wood Design Code for SPF stud grade lumber and literature published by the manufacturer of the LSL studs, namely 9,500 MPa and 10,345 MPa, respectively (CSA, 2001, Trus Joist, 2000). The bending stiffness of the composite members was based on the actual material properties of the components and connections of the walls, which were determined from testing. As the Euler load in the stiffness reduction ratio is a function of bending stiffness, increasing the predicted stiffness of a wall by accounting for composite action reduces the slope of the line. A member with infinite bending stiffness, for example, would therefore have a stiffness reduction ratio equal to 1.00 for all levels of axial load.

For each of the three frame configurations, the predicted values for the stiffness reduction ratio appear to be conservative for most wall specimens, especially at the higher axial compression load levels. This is the case even when using composite wall properties to determine the stiffness reduction ratio. It should be noted, however, that the predicted stiffness reduction ratio values are based on a structural model with simple supports. As was described previously, one end of the wall specimens tested was left free to rotate and the other was attached to a rigid support, which would have increased the stiffness of the wall. The amount of end rotational restraint provided by this support condition will be discussed in detail later in this chapter. Other factors that may have affected the results include the loss of bending stiffness in the wall specimens due to repeated loading cycles and due to the looseness of the stud connections after the walls were placed under axial tension. Figure 7.18 shows that there was a difference between the results for wall 504 and for wall 507, both of which were constructed in the same way but were loaded under different test protocols. Therefore, the sequence of axial load levels also may have affected the load interaction results.

7.3.3 Direction of Loading and Contributions from Gypsum Wallboard

In some cases, structural sheathing is applied to the interior face of wood-frame walls and non-structural cladding is applied to the exterior face. The non-structural cladding is able to distribute the transversal wind load to the studs but it does not contribute to the bending stiffness of the composite wall or to the resistance of the wall to racking loads. Theoretically, the composite properties of such a wall should remain the same regardless of whether the transversal loads are applied to the exterior of the wall or to the interior of the wall. Or, in other words, the composite properties of the wall should remain the same if the sheathing is placed in tension or compression.

7.3.3.1 Direction of Loading

Three of the walls tested were loaded in the transversal direction on both faces of the wall. All three of the walls had sheathing on only one side and, in each case, the sheathed side was loaded first. Figures 7.20 (a) through (c) show the load-displacement responses of each of these walls under transversal loading in the two directions for the case of 48.9 kN axial compression. The tests where the walls were loaded on the un-sheathed side appear to be less stiff than when the walls were loaded on the sheathed side. Looking at Table 7.3, however, it can be seen that the difference between the stiffness values obtained in both loaded ranges for walls 508 and 509 was less than 4% with an axial load of 48.9 kN in compression. For wall 512, the difference was approximately 13% in the initial loading range but it was less than 3% in the higher loading range. The larger displacements for the case when the walls were loaded on the un-sheathed sides were also affected by the different orientation of the stud connections. In other words, the connectors used to resist shear load were not loaded in their strongest direction for the walls that

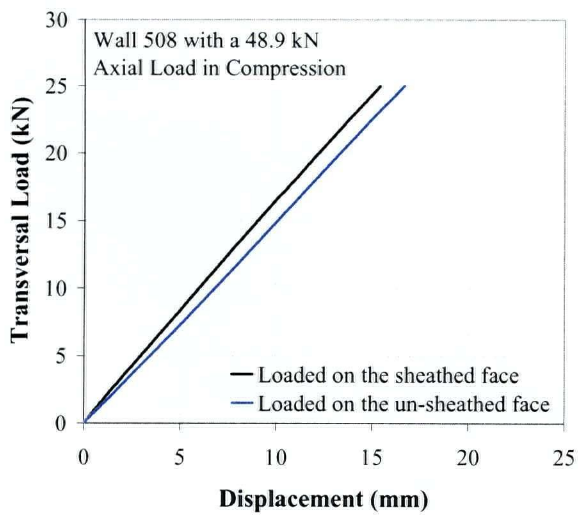

(a) Wall 508

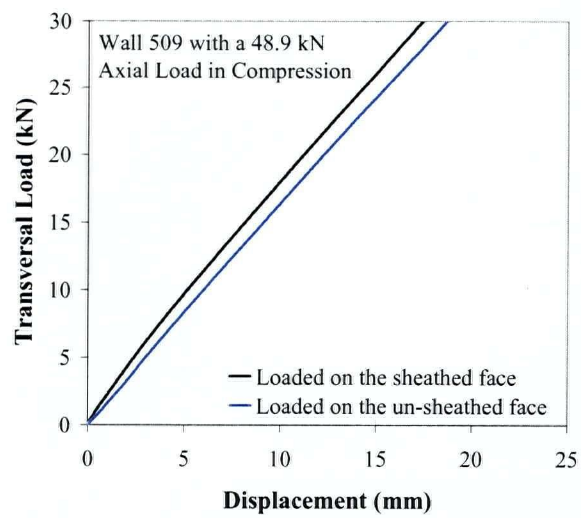

(b) Wall 509

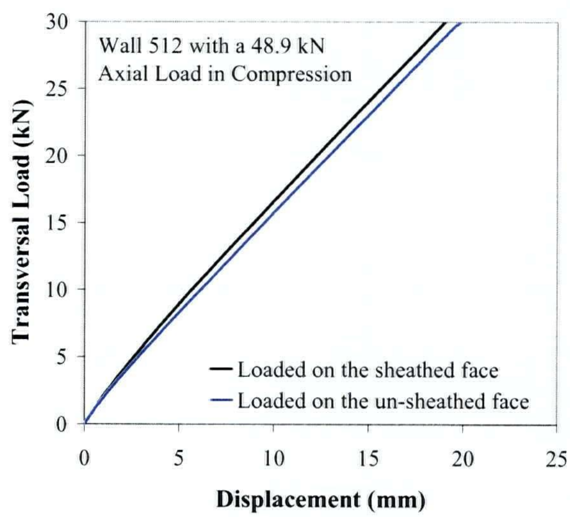

(c) Wall 512

Figure 7.20. Load-displacement response of wall specimens loaded in the transversal direction on the sheathed and un-sheathed faces.

were loaded on their un-sheathed side. Furthermore, the sheathing also contributes to the connection of the stud to the end plates when it is on the loaded side.

When a wall is loaded in the transversal direction so that the compression edge of the studs undergoing bending is not supported sufficiently, the studs may fail in lateral-torsional buckling. In such a case the stud loaded in the transversal direction deforms laterally and twists. Structural sheathing and blocking at a small spacing is typically sufficient to support the compression edges of studs. Unlike floor diaphragms, where the primary loading is in one direction only, the transversal loads on walls due to wind pressure and suction can be almost equal in magnitude. Therefore, an un-sheathed face of a wall that does not properly support the compression edge of the studs with blocking is especially susceptible to lateral-torsional buckling. This type of failure is shown in Figure 7.21. Furthermore, the engineered wood products that are commonly used as studs in tall wall construction are typically designed to higher efficiencies, leading to large section slenderness ratios (the ratio of stud depth d to width b), which increase the susceptibility to lateral-torsional buckling and the need for additional bracing. Unlike regular wood-frame wall construction, buildings constructed with tall wood-frame walls might use oversized sheathing panels. This removes the need to provide blocking at small increments along the height of the wall and reduces the support at the compression edge of the studs.

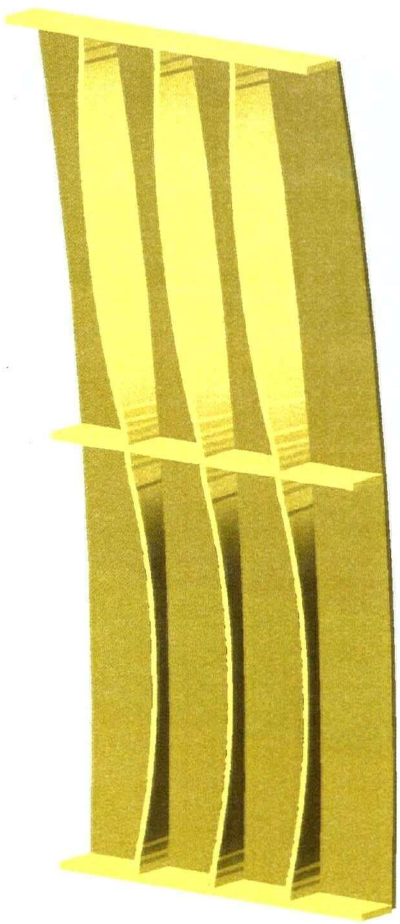

Figure 7.21. Lateral-torsional buckling of the studs in a tall wood-frame wall.

A description of how lateral-torsional buckling is addressed in the current edition of the Canadian Wood Design Code and in literature published by a manufacturer of engineered wood products was presented in Section 2.8. Lateral-torsional buckling was not observed in this testing program in any studs for the walls that were loaded on their un-sheathed face. This was because adequate blocking was provided for all of the walls tested during the course of this study. As was mentioned in Section 2.8, however, there is a need for further research into appropriate factors to account for lateral-torsional buckling to remove the discrepancies currently found in design practice.

7.3.3.2 Gypsum Wallboard Sheathing

One type of non-structural sheathing that is commonly applied to the interior face of both regular and tall wood-frame walls is gypsum wallboard. Previous full-scale tests conducted on regular wood-frame walls have quantified the contributions of gypsum wallboard to the overall bending stiffness of composite walls (Polensek and Atherton, 1976). For walls sheathed on the exterior face with bevel siding and on the interior with gypsum wallboard, a decrease in transversal displacement was attributed to increased load sharing due to the presence of gypsum wallboard compared to walls sheathed only with bevel siding.

One wall specimen, 511, was tested with gypsum wallboard to quantify the effect of this type of sheathing on the bending stiffness of a tall wood-frame wall. The wall was sheathed with 15.5 mm thick continuous OSB sheathing on the loaded, or exterior, face and 15.9 mm thick gypsum wallboard on the opposite, or interior, face. The gypsum wallboard was oriented with its length perpendicular to the length of the LSL studs, which were spaced at 610 mm on centre. The joints were taped and spackled. Previous tests on full-scale walls have shown that these joints significantly contribute to the structural continuity in the gypsum wallboard up to a lateral load equal to 80% of the ultimate load in a regular wood-frame wall (Polensek and Atherton, 1976).

Figure 7.22 shows the load-displacement response of the wall with gypsum wallboard (511) and a wall with the same configuration without gypsum wallboard (504). All of the curves were for tests with an axial compressive load of 48.9 kN. As can be seen, there was no noticeable effect on the stiffness due to the presence of the wallboard. As a matter of fact, the stiffness of the wall without wallboard was slightly higher than the wall with wallboard. The values of bending stiffness provided in Table 7.3 show that the stiffness of the wall with gypsum wallboard is much higher than the wall without wallboard in both load ranges used to determine stiffness. There was a 50% reduction in the increase in stiffness over the bare studs, however, between the first and second loading cycles for the wall with gypsum wallboard. This occurred because the load-slip response of the connections between gypsum wallboard and wood studs is typically characterized by a very high initial stiffness followed by a rapid decrease in strength (Gromala, 1983). Deformation of the connection results from irreversible crushing of the gypsum. When

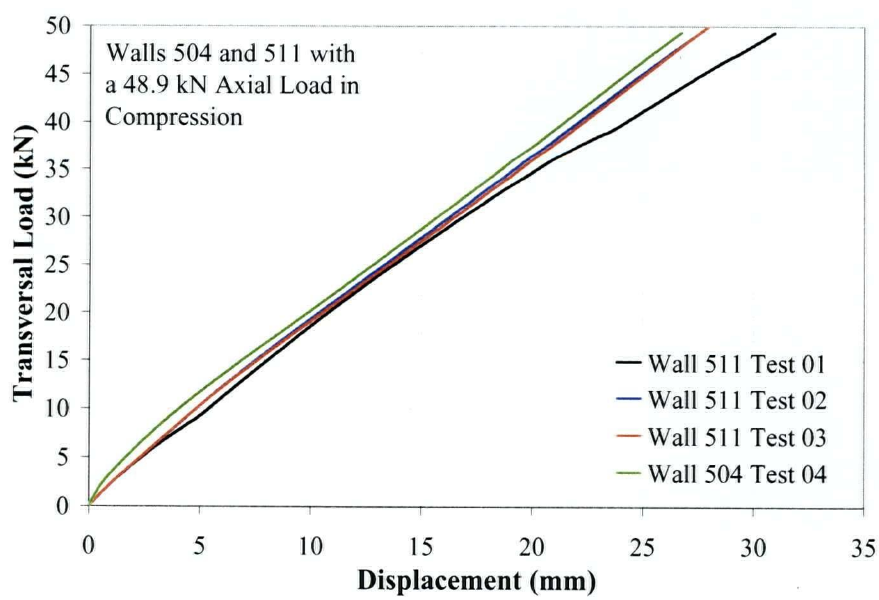

Figure 7.22. Load-displacement response of walls loaded in the axial and transversal directions with and without gypsum wallboard on the interior face.

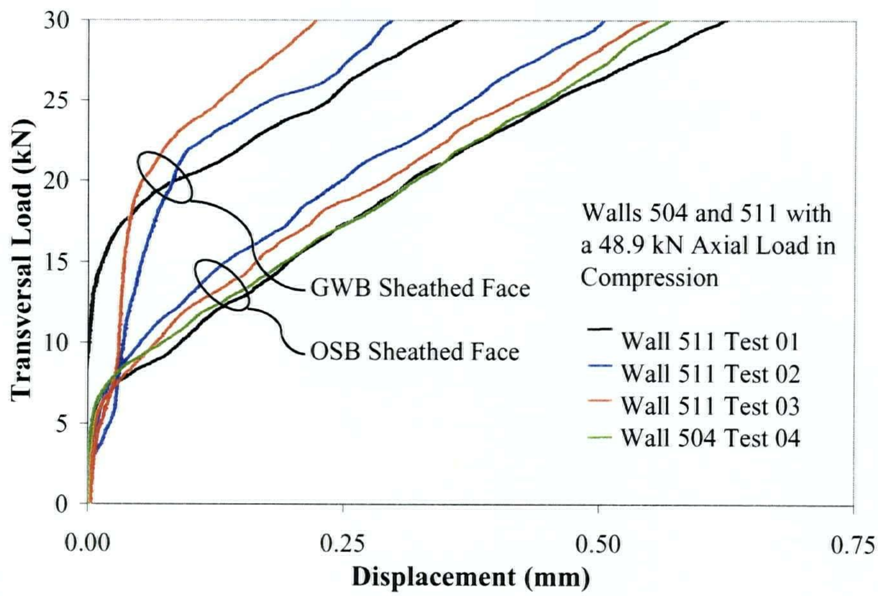

Figure 7.23. Load-slip response of the pots located nearest to the roller-supported end of the walls with and without gypsum wallboard on the interior face.

the large numbers of fasteners in the wall were loaded to different levels along the length of the wall, this abrupt decrease in fastener stiffness was smeared out over the length of the wall and thus resulted in gradual stiffness degradation. This is shown in Figure 7.23, where the displacement of the slippage pots at the roller supported end for both sheathed faces and for the OSB sheathing in wall 504 are plotted against the transversal load. Despite the reduction in stiffness during the first cycle, the difference in the increase in stiffness over the bare studs between the two walls after the first cycle was approximately 24% in the initial load range and 8% in the higher load range. Therefore, the wall with gypsum wallboard did see an increase in bending stiffness over the wall without wallboard and the larger displacements were due to variations in the behaviour of the end connections.

7.3.3.3 Transversal Displacement Criteria

The Canadian Wood Design Code treats the studs in a wood-frame wall as wind columns for the purpose of satisfying serviceability limit states. The maximum deflection suggested for walls under an applied wind load is equal to the height of the wall divided by 180 (L/180), where the calculation for deflection is typically based only on the properties of the studs themselves. This maximum value is in place to avoid discomfort to occupants and to limit damage to non-structural members and materials such as gypsum wallboard. Implicit in this deflection criterion, however, is the presumption that a wall designed to this limit would in fact deflect less because the studs are connected to sheathing or cladding, which increases the stiffness of the composite wall system. This can be inferred from a statement in the Appendix of the Canadian Wood Design Code, which says, "the deflection criteria that evolved from this approach have provided satisfactory system performance based on calculated single member deflections" (CSA, 2001). The implication of this statement is that if the composite member properties of a wall are used to determine the maximum deflection of a wall directly, then more stringent deflection criteria than those suggested in the code would have to be adopted.

The wall sheathed on the interior face with gypsum wallboard was loaded in the transversal direction up to a displacement of just over 80 mm (Figure 7.24), which corresponds to L/60. The transversal load required to reach this level of displacement was approximately 114 kN, which corresponded to the maximum bending moment that would have been produced by applying a uniformly distributed load of approximately 10 kPa. The load was not increased past 114 kN because the capacity of the testing frame had been reached. The stiffness of the wall at this very high load level (between 75 kN and 100 kN) was approximately 12% lower than the predicted stiffness of the bare studs because those predictions were based on the linear-elastic responses of the studs. It is interesting to note that the change in stiffness occurred at a displacement of 28 mm, which approximately corresponds to L/180.

No damage was observed in the gypsum wallboard sheathing, or any other part of the wall, throughout the entire loading range. Based on this test, it can thus be concluded that a deflection

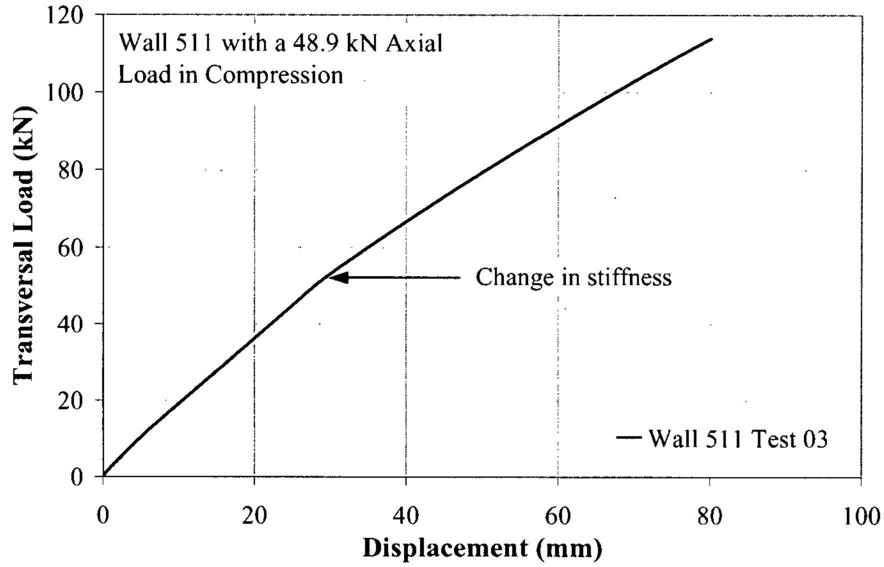

Figure 7.24. Load-displacement response of the wall with gypsum wallboard loaded beyond the linear-elastic range.

limit of L/180 seems to be an acceptable criterion to prevent damage to non-structural materials attached to the wall even when the calculated stiffness is based on the composite properties of the wall. It is felt that a larger deflection limit might even be acceptable for tall wood-frame walls in general, especially when used in industrial applications. The National Building Code of Canada allows such a relaxation of rules by stating that "(defection limits) do not apply to industrial buildings or sheds if it is known by experience that greater movement will have no significant adverse effect on the strength and function of the building" (NBCC, 1995). To determine more generally applicable deflection limits for tall wood-frame walls, it is suggested here that further testing should be done on full-scale walls, using different types of non-structural cladding and different fastening methods.

7.3.4 Transverse Load Distribution Effects

It has been known for many years that the presence of sheathing and blocking can increase the stiffness and strength of wood-frame diaphragms. The transverse load distributional effects of sheathing and blocking allow parallel members to provide mutual support in a structurally redundant system and thereby increase the capacity of the system beyond the predicted strength and stiffness of a single member alone. Since the Canadian Wood Design Code specifies that wood-frame diaphragms should be designed using a single member equation, a system modification factor, K_H, which accounts for load sharing in the determination of strength, was introduced to compensate for this simplification, while maintaining acceptable levels of reliability.

The following three justifications for the inclusion of a system factor in design are provided in the commentary to the Canadian Wood Design Code:

1. In a system with load sharing, the stresses in a load-resisting member may be less than what would be predicted based on the tributary area for the applied load as the loads are typically distributed to the members based on their relative stiffness.
2. The composite action of the sheathing and fasteners enhances the performance of each member in the system.
3. The probability that a weak member is placed in the location of higher stress is reduced in a repetitive system (CSA, 2001).

The system (load sharing) factors are not included for deflection calculations as the load sharing effects are accounted for by using the average modulus of elasticity of the frame members instead of the 5th percentile value, which is used in strength calculations.

The system factors given in the code were based on research conducted on wood-frame floors at the University of British Columbia (Foschi, 1989). For the case of a wood-frame system in bending, there are two values for the system factor provided for sawn lumber, based on two different framing configurations, and one value given for engineered wood products. The system factor for systems consisting of sawn lumber is 1.10 when at least three parallel members spaced at not more than 610 mm on centre with some form of mutual support share the load. The factor is 1.40 for similar systems consisting of joists and sheathing, that also meet specific requirements for the type of sheathing and nail spacing. The system factor for engineered wood products is 1.04 if the requirements of the first system described above are met. The reason why the system factor for engineered wood products is lower than it is for sawn lumber is because the variation of strength and stiffness properties in a large sample of engineered wood product members is much less than it is for sawn lumber. The population at large thus has less overstrength that can be utilized when averaging takes place.

Because the contributions from composite action are already accounted for in the second system factor for sawn lumber, it is not clear if this factor should also be used when composite member properties are determined explicitly. If composite action is explicitly included in the determination of the strength of a wood-frame wall with sawn lumber then, according to the requirements for the two cases, a system factor of 1.10 should be used instead of 1.40. To provide further insight, it might be of interest to note that, as shown in Chapter 5, the increase in strength of a composite T-beam member over the bare stud, according to the code, is not as great as the increase in stiffness. This is because the inclusion of the flange creates a force couple that induces additional tension in the web member. Since the tension strength of sawn lumber is adversely affected by an increase in the stressed volume, the interaction of tension and bending stresses in the web member effectively reduces the design tension stress. This means that the calculated bending capacity of the composite member is likely not significantly higher compared to that of the bare stud alone. Therefore, it is unlikely that the 27% (1.40 divided by 1.10) reduction in calculated capacity due to the use of the lower system factor can be regained by including the effects of composite action for sawn lumber.

As it stands now, it is difficult to de-couple the contributions from composite action and transverse load sharing affects in the system factors because they were determined from structural models that contained both of these properties. No reference is given in the Canadian Wood Design Code as to the origin of the lower value for the system factor for sawn lumber. It is felt that the 27% reduction in strength due to the inclusion of composite properties, and therefore foregoing the benefits of a case 2 system factor, may be too conservative. To shed light on this matter, further research on load sharing in composite wood systems would be required.

For walls constructed with engineered wood products, the effects of composite action are not included in the system factor, as it only requires that transverse load distribution elements are present. The findings in Chapter 6 revealed that the 610 mm on centre limit on stud spacing that is currently in the code for wood-frame diaphragms is too conservative for walls with sheathing thicknesses 9.5 mm and greater. The system factor would therefore not apply for most tall walls where the studs are spaced greater than 610 mm on centre. The author feels that some benefits may be gained from load sharing even when studs are widely spaced. To quantify this benefit, however, further research is required on the strength of walls with studs spaced greater than 610 mm, which have explicit transverse load distribution elements. For the walls with engineered studs spaced at 1,220 mm on centre tested in this study, the average increase in stiffness over the predicted stiffness of the bare studs alone was approximately 30%.

By foregoing the benefits of the system factor, as it stands now, design calculations for strength can offset this conservatism through increases in strength and stiffness that are gained by explicitly accounting for composite action, and also from material efficiencies resulting from increased stud spacing.

To aid in the deliberations about transverse load distribution, the transverse stiffness of three wall specimens was measured by applying a transversal point load to the middle of the central stud of the walls without any axial load (Figure 7.25). The displacement at the middle of the central stud and the two outside studs was measured. In the remainder of the tests, the transverse stiffness of the walls could not be determined because the steel spreader beams at the third point loading lines imposed equal displacements on all the studs in each wall. Wall 510, which was not specified to have blocking, was not tested because the transverse stiffness of the wall could not be measured when loaded at the third points. The wall with the same configuration as Wall 510 except with blocking would most likely have had the same transversal load-displacement response at all points on the wall. A method for predicting the transverse stiffness of the sheathing of a wood-frame diaphragm was presented in Section 2.5.6.2. An equation for the bending stiffness of a width of sheathing, equal to the distance between the gaps in the sheathing parallel to the length of the studs, multiplied by a factor that included a ratio of the spacing of the stud members to the distance between gaps in the sheathing perpendicular to the length of the studs was presented (Equation 2.42). The equation did not account for the contributions of the blocking to the transverse stiffness of the diaphragm, mainly because blocking elements are not

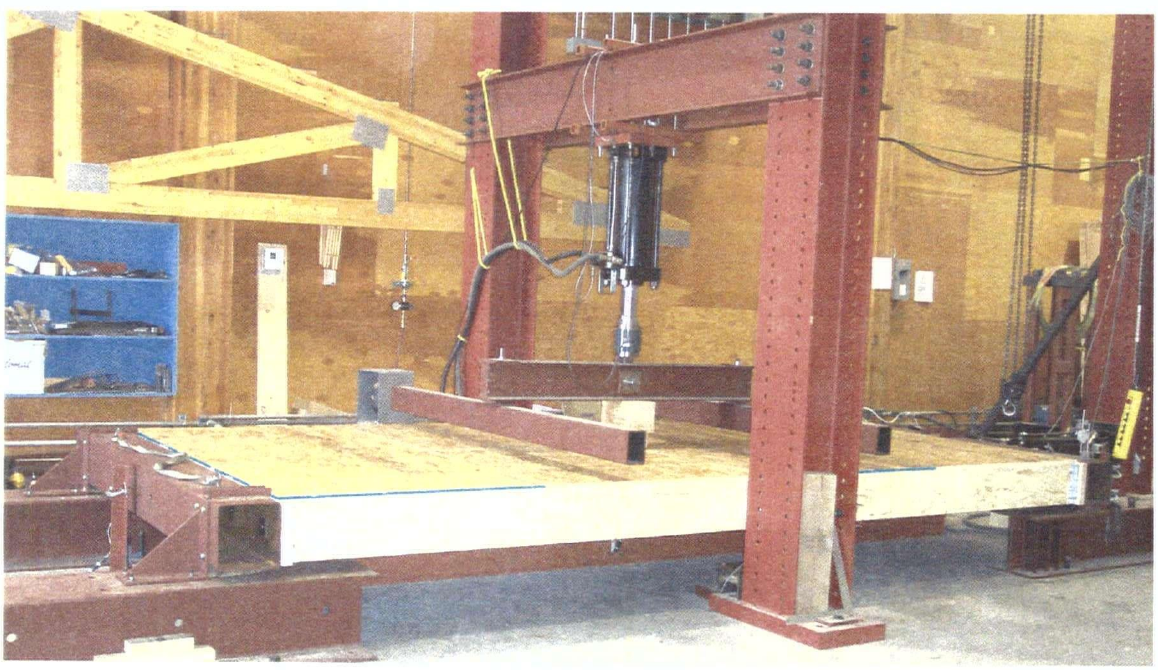

Figure 7.25. Transversal point load applied to the middle of the central stud of a wall specimen.

continuous and the stiffness of these transverse elements thus depends largely on the connections to the studs, which can vary from toenailing to elaborate metal clips. All three of the walls tested with a point load had blocking spaced at 1,220 mm on centre, attached to the studs with toenailing.

The equation for predicting the transverse stiffness of the sheathing in a wood-frame diaphragm was part of an extensive procedure for predicting the overall stiffness of the system by employing a beam-spring analog wall model. This was also presented in Section 2.5.6.2. The wall was modeled as a beam, with its bending stiffness properties representing the wall bending stiffness in the transverse direction, supported by springs, each of which represented the bending stiffness properties of each individual stud along the length of the wall. This method will be discussed in greater detail in Chapter 8. The actual transverse stiffness of each of the three walls tested was determined using this method. These values were then compared with the predictions for transverse stiffness based on the properties of the sheathing alone given by Equation 2.42 (Table 7.4). The bending stiffness of each composite stud in each of the walls was determined using the procedures for calculating partial composite action outlined in Section 5.3.2. These values were then compared with the actual bending stiffness of the walls that were determined from the third-point loading tests. The actual transverse bending stiffness was determined by matching the beam-spring analog model results with the slope on the load-displacement curve for the single-point load test results between 8.9 kN and 13.3 kN.

It appears from Table 7.4 that the blocking had a significant effect on the transverse bending stiffness of the walls tested. This is illustrated by the difference in the analytically predicted transverse stiffness of the sheathing alone versus the total transverse bending stiffness that was obtained from tests, which represented the contributions from the blocking and the sheathing. It

Table 7.4. Transverse bending stiffness of sheathing alone and sheathing and blocking.

Specimen Number	Analytically Predicted Transverse Bending Stiffness of Sheathing, EI_b (Nmm^2)	Total Transverse Bending Stiffness Matched to Test Results, EI_b (Nmm^2)	Bending Stiffness of Middle (M) and Outside (O) Studs from Testing (8.9 - 13.3 kN) (N/mm)	Bending Stiffness of Middle (M) and Outside (O) Studs Using Matched Transverse Stiffness (N/mm)
506	2.47×10^8	2.35×10^{10}	2591 (O)	2601 (O)
			319 (M)	333 (M)
			2535 (O)	2463 (O)
508	0.00×10^0	7.00×10^{10}	3563 (O)	3432 (O)
			732 (M)	731 (M)
			3330 (O)	3496 (O)
509	5.28×10^8	2.00×10^9	-60437 (O)	-10705 (O)
			542 (M)	476 (M)
			-10222 (O)	-10510 (O)

is very difficult to predict the transverse stiffness of blocking without using a finite element program, however, because of the complicated connections that occur at the studs. The blocking for these walls was toe nailed and end nailed to the studs but significant transfer of bending moment across the studs occurred because of the presence of the sheathing. It is interesting to note that the analytically predicted transverse bending stiffness of the sheathing for wall 508 was zero because the width of the sheathing was equal to the spacing of the studs. This resulted in a gap being placed between sheathing panels down the entire length of the middle stud. The transverse stiffness obtained from testing for this wall, however, was the highest of the three walls. As mentioned previously, the code does not allow the system factor to be included in the calculation of stud strength for configurations where the studs are spaced greater than 610 mm on centre. The table shows that significant transverse stiffness was obtained for walls 506 and 508, which had studs spaced at 1,220 mm on centre.

Finally, the stiffness of the end studs can have a significant effect on the transversal displacement of the entire wall. Other edge effects occur because of the edge support conditions of the wall. If a wall is supported at each end by walls in the perpendicular direction then the wall acts like a plate that is simply supported on all four edges. If a wall is supported only at the top and bottom then the end studs provide partial support because they are almost as stiff as the other composite studs in the wall but they only receive half of the load when the wall is loaded uniformly. The complete or partial end supports can reduce the maximum deflection in a wall to well below the deflection predicted based on a single bare or composite stud if the wall is not very long, like the walls that were tested. The edge effect was quantified for walls with the same configuration as wall 506 by analytically increasing the number of studs in a wall with a uniformly distributed load applied to it. The beam-spring analog model was used and incorporated the analytically predicted bending stiffness of the composite studs in wall 506 and the transverse bending stiffness matched to test results shown in Table 7.4. Free wall ends and simple supports at the top and bottom of the walls were assumed. The deflection at the mid-height of each stud under a uniformly distributed load was calculated.

Figure 7.26 shows the deflection of the central stud in a wall at the mid-height for several walls with an increasing number of studs. As can be seen, the deflection of the central stud can change

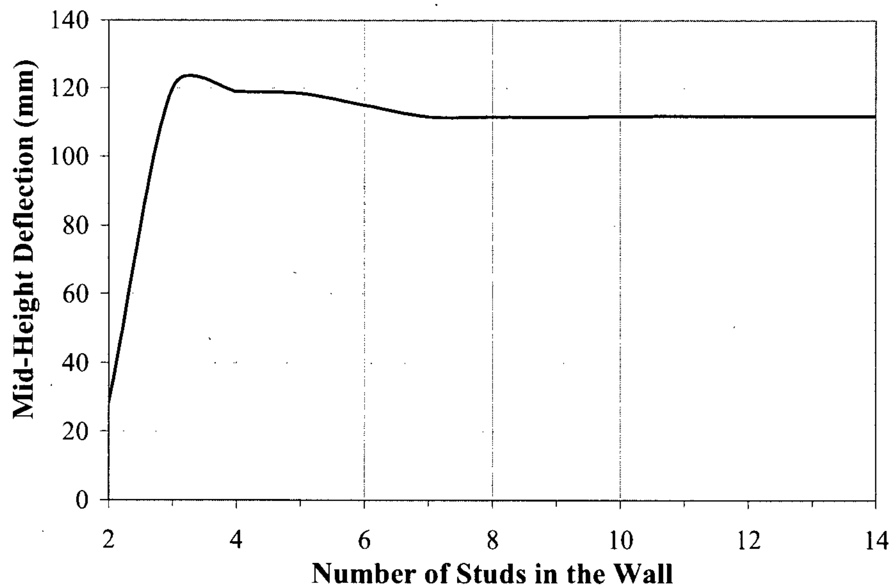

Figure 7.26. Analytically predicted mid-height deflection of the central stud of a wall with an increasing number of studs.

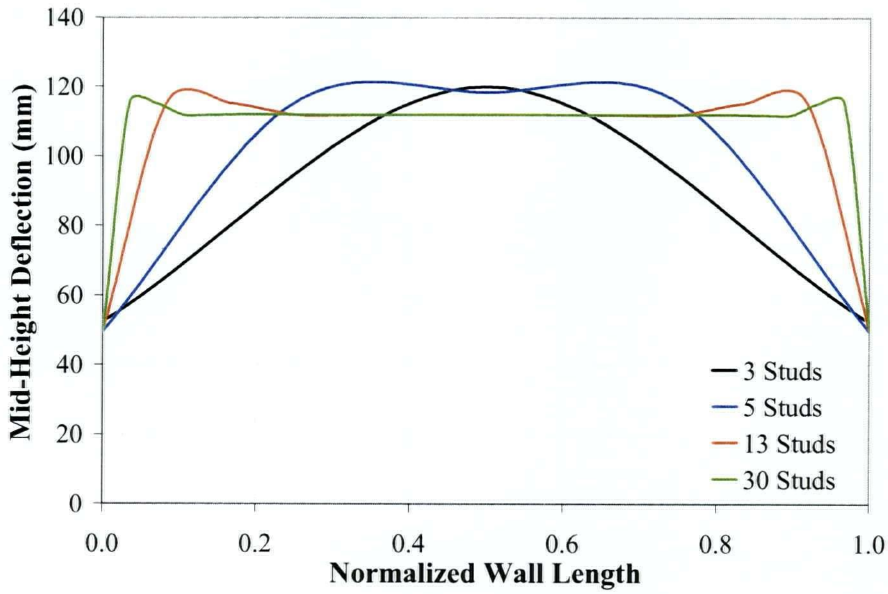

Figure 7.27. Analytically predicted mid-height deflection of each stud in a wall with an increasing number of studs.

significantly depending on the number of studs in the wall, especially for a wall with less than seven studs. The mid-height deflection of each stud in a wall is shown in Figure 7.27. The wall lengths have been normalized so that the total length of each wall is the same. The influence of plate action on the response of the wall is clearly evident.

In a wall with many studs, the majority of the studs displace the same amount because the studs or the support conditions at the edges of the wall do not affect them. For testing purposes, if narrow walls with few studs are tested under a uniformly distributed load, the maximum displacements of those walls will not be as large as the same wall configurations in an actual structure because the studs at the edges will add a disproportional amount of stiffness to the system. The effect of the edge studs on the displacement of the middle stud was not an issue for this study because uniform displacements were applied at the third points of the walls that were tested. Since the total applied load was measured, however, the experimental stiffness of each wall was therefore an average of the entire system.

7.3.5 Stud Connections and End Rotational Restraint

7.3.5.1 Axially Loaded Stud Connections

Wind can cause uplift suction on the leading edges of a roof resulting in an overall tension load on the supporting walls. For buildings with a light roof that spans long distances, such as in a large warehouse or industrial facility, these loads can be significant. Therefore, a continuous load path must be provided to transfer these uplift forces to the foundation of a building. For most regular wood-frame buildings constructed in Canada, a dedicated connector is not included at each stud in a wall to resist tensile forces and thus anchor the roof to the wall. The nailed connections of the sheathing to the end plates and the stud are deemed adequate to transfer the uplift load from the top plate to the stud and then from the stud to the bottom plate. Although the studs themselves are only end nailed to the plates, the sheathing connections provide a secondary load path that is usually sufficient. For tall wood-frame walls, however, the uplift forces can be quite high and connection details need to be designed to transfer these forces from the roof structure to the top plate of the walls. The studs need to be connected to the top and bottom plates of the wall by steel brackets with mechanical fasteners. This has been the practice in recently completed projects that incorporate tall wood-frame walls as primary supporting elements. It is generally assumed that the stud carries the tensile load alone without any contributions from the sheathing and that the sheathing does not transfer tension from the end plates to the studs. The bottom plate for both tall and regular walls is typically connected to the foundation with threaded anchors embedded in concrete. The need for a steel connector, and possibly an anchor bolt, at every stud in a tall wood-frame wall sets them apart from regular wood-frame walls. The need for such elaborate anchor details warrants investigation, however, since connectors and the labour required to install them can be relatively expensive in comparison to the cost of the stud itself. For buildings with many metres in length of walls, the cost of the connectors can be a significant portion of the overall cost of constructing the building.

To address this issue, four different types of connections were used in this study to connect the studs in the wall specimens to the end plates. A detailed description of each connection was provided in Section 7.2.1 and photos of the connections were shown in Figure 7.5. Seven walls were loaded under increasing tension loads without any transversal loads. The maximum tension load applied to each wall specimen is given in Table 7.5. Wall specimens 507, 508, and 512 were not loaded until failure because they were either used for further testing or exceeded the capacity of the test frame. All other wall specimens were loaded until failure occurred in tension. The design loads shown in Table 7.5 are the factored resistances of the connectors determined either from the values provided by the manufacturer or from calculations using the requirements set out in the Canadian Wood Design Code. They include resistance factors (ϕ) and the short term duration of loading factor (K_D). It should be noted that design values for wood screws are not currently available in the code. The fastenings for connection type D were therefore purposely designed to direct the mode of failure towards the nails. This avoided the need to determine an appropriate factored resistance of the screws. This also means, however, that the resistance of this connector could be enhanced by changing the fastener types.

The applied loads on the wall specimens tested exceeded all of the predicted design loads. The ratio of the maximum load applied to the predicted design load for each wall is shown in Table7.5. All of the test values exceeded predictions by a factor of approximately 2.0 or greater, except for wall 506, which had connection type D. The load-displacement response of each wall is shown in Figure 7.28 (a), (b), and (c). These loads were for the entire wall and not the individual connectors. The four modes of failure in tension that were observed are shown in

Table 7.5. Maximum axial load applied or point of axial failure.

Specimen Number	Connection Type	Specimen Type	Stud Spacing (mm)	Stud Material	Maximum Load, F_{max} (kN)	Design Load per Tension Connector (kN)	Total Design Load, F_{design} (kN)	Overstrength (F_{max} / F_{design})
504	B[a]	W2	610	LSL	99.21	7.06	21.18	4.68
506	D	W1	1220	LSL	40.92	7.25	21.75	1.88
507	B	W1	610	LSL	89.43[b]	7.06	35.30	2.53[b]
508	B	W4	1220	LSL	110.33[b]	7.06	21.18	5.21[b]
512	C	W1	610	LSL	67.15[b]	6.78	33.90	1.98[b]
513	C	W4	1220	LSL	110.32	6.78	20.34	5.42
514	A[a]	W1	610	SPF	51.03	4.97	14.91	3.42

Notes:
(a) Tension straps were used on every other stud, i.e. on three of the five studs in the wall.
(b) Wall specimen was not loaded until failure occurred.

Figure 7.29. The load-rotation response of the distribution beam, which was attached to the end plate at the roller-supported end of the walls, about the length of the beam for four of the wall specimens is shown in Figure 7.28 (d). Figure 7.28 (a) shows the load-displacement response of the two connector types used to connect the studs to the end plates for wall configuration W1 with LSL studs. Wall configuration W1 had studs spaced at 610 mm on centre with sheathing oriented perpendicular to the length of the studs. The figure shows that the stiffnesses of connector types B and type C were similar. Failure did not occur in the walls with these connector types.

The three walls that employed connection type B are shown in Figure 7.28 (b). Failure only occurred in wall 504, which had tension ties on only three of the five studs in the wall (Figure 7.29 (b)). The tension ties were attached to the studs well below the neutral axis of the walls. This induced an eccentric force at the bottom edge of the end plates. Because the roller-supported end of the wall was free to rotate, the force induced couple did not produce a large

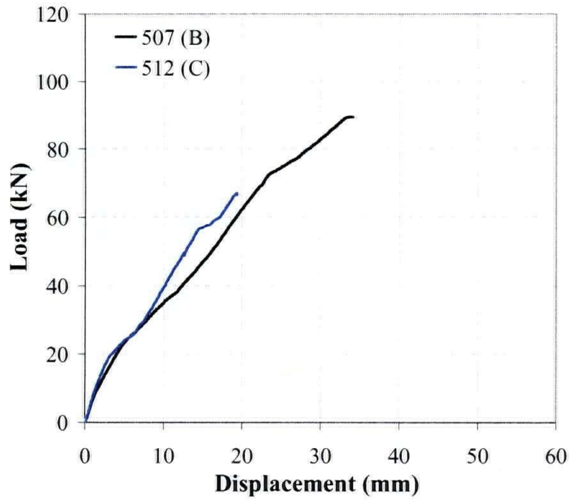

(a) Wall W1 with LSL studs.

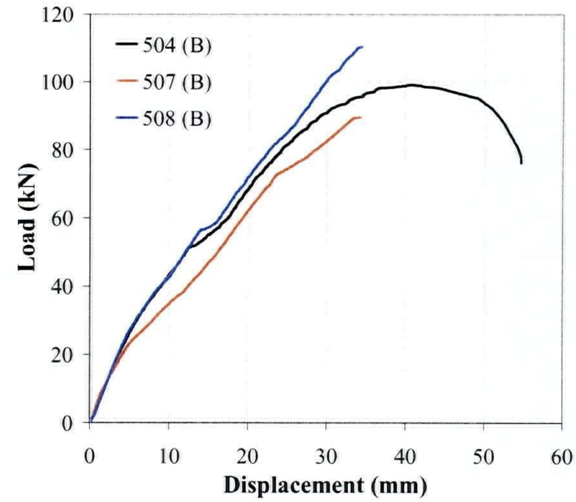

(b) Connection type B.

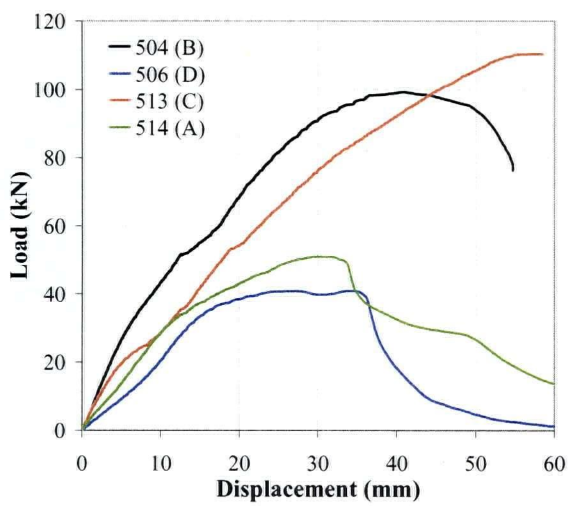

(c) Tension connectors on three studs.

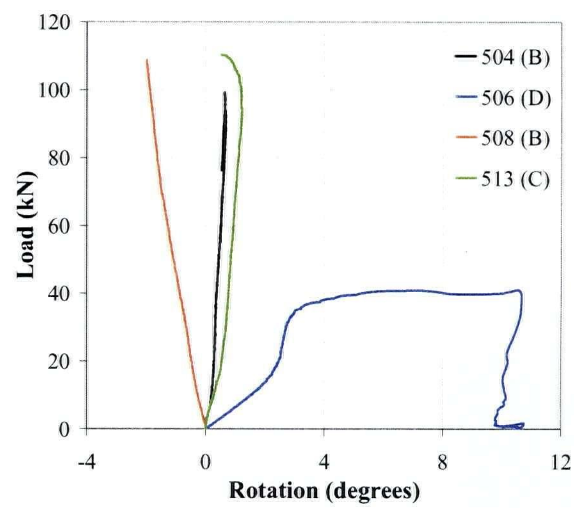

(d)

Figure 7.28. (a) to (c) Load-displacement and (d) load-rotation response of wall specimens under axial load only.

bending moment at the end of the wall. The wall was restricted from rotating at the foundation end. The connection of the sheathing to the end plates was weaker than the three tension ties in the wall, which resulted in the end of the stud rotating away from the end plate that was attached to the simulated foundation. The failure of the connectors and the withdrawal of the nails, which were attaching the joist hangers to the end plate, were uniform across the width of the wall. This mode of failure did not occur in wall 508, which also had only three tension ties, because the glued connection between the sheathing and the end plate was as strong as the tension ties. The eccentricity in wall 508 was quite significant as is evident from the rotation that occurred at the roller-supported end (Figure 7.28 (d)).

Figure 7.28 (c) compares four walls with the four different connection types with tension resisting elements, attached to three studs for walls with either five studs or three studs. The nails fastening the tension ties to the SPF studs in wall 514 withdrew, resulting in the failure of the wall (Figure 7.29 (a)). The failure in connection type C in wall 513 occurred when the flanges of the steel bracket on the end plates began to yield. Both of these modes of failure were ductile. Failure occurred in connection type D when the nails connecting the joist hangers to the studs withdrew (Figure 7.29 (d)). As the nails withdrew at the roller-supported end, large rotations of the end plate took place because tension forces were being transferred by the connection between the sheathing and the end plate (Figure 7.28 (d)). The screws connecting the joist hangers to the end plates remained intact.

Walls 504 and 514, which had tension ties on only three out of five studs, demonstrated that it was possible to surpass design load levels and achieve desirable modes of failure with this type of connection configuration. It should be kept in mind that the top plate of the tested specimens was attached to a relatively rigid steel beam, which ensured that all the tension ties experienced approximately the same displacements. In an actual wall, however, the double top plate and the sheathing would constitute a more flexible load path, which would make the tension force distribution more dependent on connector spacing and the distribution of wind loads on the roof. Further testing is required to validate the use of tension resisting elements on alternating studs in a tall wood-frame wall to better simulate the load distribution properties of the sheathing and the top plates.

(a)

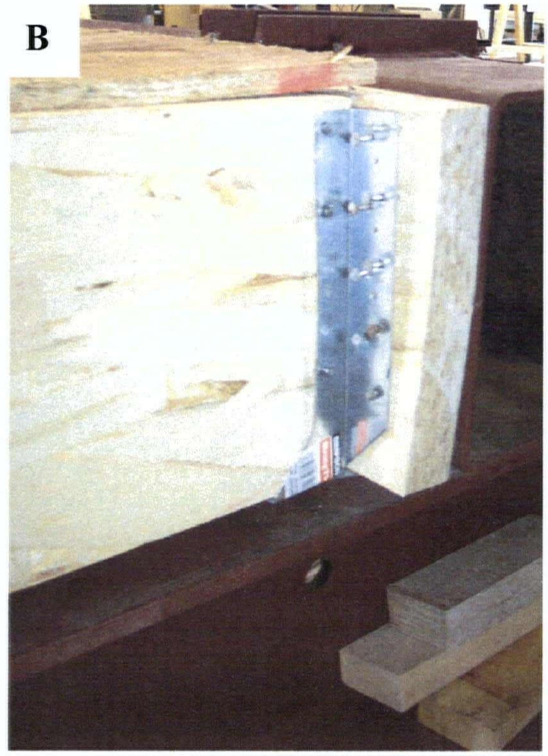

(b)

(c)

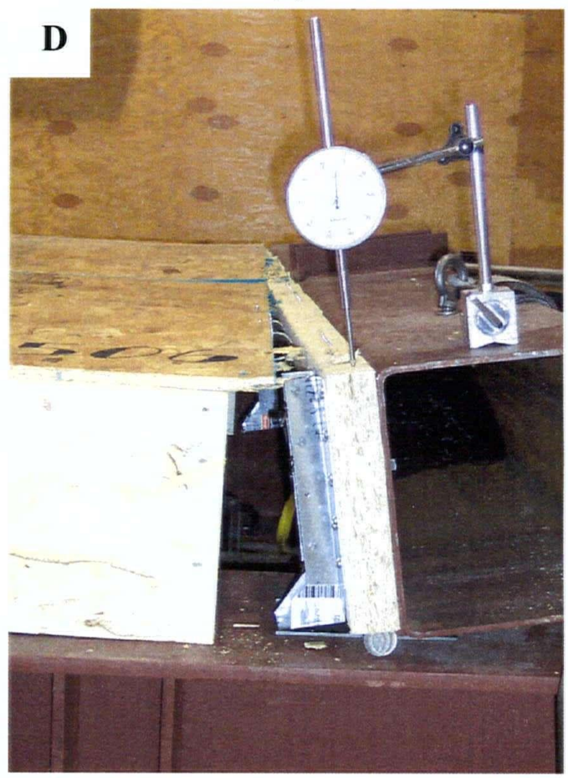

(d)

Figure 7.29. Failure modes of the full-scale wall stud connection types under axial load: (a) SPF joist hanger with tension strap; (b) LSL joist hanger with tension strap; (c) manufactured joist hanger; and (d) LSL joist hanger screwed to plate.

The results of the walls subjected to axial loads have lead to the following observations as they relate to the load-displacement responses of the walls:

(a) Off-the-shelf connector products generally performed well and are a viable alternative to specially fabricated connectors.

(b) The use of tension ties with deep studs produced an eccentric tension force transfer at the ends of the studs, which resulted in excessive rotations that seemed to precipitate early failures.

(c) Placing tension-resisting connectors on every other stud did not result in undesirable modes of failure due to the load distributional properties of the sheathing.

(d) The use of wood screws in conjunction with an off-the-shelf connector proved to be successful, as the mode of failure was not in the screws themselves. The use of screws removes the need for a tension tie at each stud connection.

(e) Further research should be conducted to determine if walls with larger intervals between tension capacity joist hangers would perform equally well.

As mentioned in Section 7.2.1, a connector similar to the one used in connection type C had been used in a building with tall wood-frame walls, constructed in Cranbrook, British Columbia. The connectors for that project were specifically designed and fabricated to resist the tensile and transversal forces in the studs. It was decided that the inclusion of these connectors would provide a useful reference point to recent construction practice. The connectors used in this testing program were made by a steel fabricator in Vancouver using the same specifications that were used for the building in Cranbrook. The building owner identified two negative aspects of those connectors after construction of the building was complete. Firstly, the cost of the connectors was unacceptably high relative to the cost of the studs. For this research project the purchase price of each type C connection was \$13.75, amounting to \$27.50 per stud. Including the cost of four lag screws, two bolts with nuts, and washers ($5), the total material cost for the connections at each stud was $32.50. Considering the material cost of each LSL stud ($48.80), 40% of the total material cost of each stud installed in the walls was attributable to the connections. Since studs are sold per linear foot and the walls in the Cranbrook building were approximately 50% taller than the wall specimens tested, the connections would represent 30% of the total material costs per stud for a similar wall configuration. This clearly emphasizes the importance of finding more cost-effective solutions to connect wall elements.

The second issue raised was the high amount of labour cost to properly install the stud connections. At each stud, at least six pre-drilled holes were required: two for the bolts through the studs and four into the double end plates for the lag screws. If the shank of the lag screws had an unthreaded portion, two pre-drilled holes were required for each lag screw, one for the threaded and one for the unthreaded portion of the shank. Each lag screw had to be installed by hand using a wrench in order to meet the requirements in the Canadian Wood Design Code. This clearly illustrates that, despite its apparent simplicity, this type of connection requires a significant amount of labour plus various pieces of equipment, such as a power drill, two or three drill bits, a wrench, and possibly an impact hammer for the bolt.

Connection types A and B, in contrast, consisted of off-the-shelf steel joist hangers and tension ties that were purchased from a local building supplier. The products were manufactured by Simpson Strong-Tie Co. and are commonly used in the construction of residential and commercial wood-frame structures. The same tension tie was used for both connection types. The cost for each tension tie was $3.50 and it was attached to the stud and plate with a total of 16 nails that cost approximately $0.20. Connection type A and B used joist hangers to resist the transversal loads applied to the studs. The purchase price for each joist hanger used for type A was approximately $1.00 and the purchase price for the hanger for type B was approximately

\$8.95. A cheaper joist hanger for type B could have been used but potential failure of the connections under high transversal loads was a concern, which favoured the use of this particular joist hanger. The hangers for connection types A and B were fastened to the end plates and each stud with 10 and 24 nails for a cost of \$0.15 and \$0.30, respectively. Therefore, the total material cost of the connectors per stud for connection type A was \$9.70 and \$25.90 for connection type B. LSL studs were used for connection type B and the percentage of the total material cost of the installed stud represented by the connector was 35%. SPF studs, which cost \$18.50 each, were used in conjunction with connection type A. The percentage of the total material cost of the installed stud represented by connection type A was 34%.

The same hanger employed in connection type B was used in connection type D. Fastening the joist hanger to the end plates with screws resisted the tension forces in the connection and eliminated the need for a tension tie. A total of 18 screws were used to fasten each hanger to the end plates and 6 nails were used to fasten the hanger to the studs for a cost of \$0.80. The total cost of the connectors per stud for connection type D was \$19.50, or 29% of the total material cost of the installed stud. Based on the performance of Wall 504, as discussed above, it was shown that it is possible to achieve a safe design by using tension ties on alternating studs. The use of tension ties on every other stud reduces the average total cost of the connections per stud from \$25.90 to \$24.05, or 33% of the average total material cost of each installed stud. The labour costs are also reduced due to a reduced number of nails that need to be fastened to each stud.

Of course, the cost of all the connector items listed above should be significantly lower when purchased in larger quantities, as would be the case in the construction of a large building. Since similar discounts could probably be expected for the stud materials, the above cost ratios can be expected to remain valid.

The most significant advantage of using off-the-shelf products over the specially fabricated connector is not so much the material cost savings outlined above, but the lower labour costs resulting from the ease of installation. All of the fasteners are nails or screws that do not require pre-drilled holes. In addition, the nails can be driven into place with a pneumatic nail gun. Although the nails used to fasten the hangers and tension ties in this study were driven by hand, nail guns with guides are available that can efficiently be used to attach joist hangers, tension ties, or any other type of connector that has pre-drilled nail holes.

7.3.5.2 End Rotational Restraint

The influence of the support conditions on the modes of failure of the walls tested under axial load is described in this section. The support conditions also affected the amount of transversal displacement that occurred in the walls under axial and transversal loads. All of the predictions compared to the transversal load-displacement responses of the walls tested that have been presented thus far have assumed that the walls were simply supported at the ends, or that each end of the wall was free to rotate. One end plate of each of the walls tested, however, was bolted to a rigid support beam that restrained the plate from rotating, as would occur in a real structure due to the attachment of the wall to a rigid foundation. This end rotational restraint increased the overall stiffness of the walls at the mid-height.

The effect of the end rotational restraint on the stiffness of a simply supported wall under transversal loads can be modeled by applying a rotational spring to one end of the wall. The reduction in deflection at the mid-height of the wall is then a function of the end rotational spring constant, K_r. An equation for the transversal displacement at the mid-height of a wall under third-point loading as a function of the end rotational spring constant is given as follows:

$$\Delta = \frac{PL^3}{648EI}\left[\frac{276+15B}{12+4B}\right], \text{ where} \tag{7.5}$$

$$B = \frac{K_r L}{EI}. \tag{7.6}$$

P denotes the load applied at each of the loading points and EI is the bending stiffness of the composite wall. Using the same principal, displacements at other points along the wall can be determined as a function of the end rotational spring constant. If the walls had been simply supported, the displacements along the length of the wall would have been symmetric about the middle of the walls. The transversal displacements of the walls tested were measured at equal distances from the middle of the walls near the ends of the walls (Plan 1 on Figure 7.10). By using these measured deflection values, an end rotational spring constant was calculated for the walls tested. The calculation of the spring constant for use in the deflection equation did not require the bending stiffness of the walls but did assume that the rotation at the end of the walls with the rotational restraint was equal to the transversal displacement a distance 0.03 times the length of the wall from the end of the wall divided by that distance. For small rotations, the error in the results due to this assumption can be considered negligible.

Figure 7.30 shows the total calculated end rotational restraint stiffness, K_r, with increasing transversal load for several wall specimens. As mentioned, the input data used to calculate those values were the deflections at each end of the walls. The deflections for transversal loads below approximately 10 kN were smaller than the margin of error for the data measurement devices; therefore, values in this load range were not used to calculate rotational end restraint stiffness. The end rotational restraint stiffness for walls with LSL studs with varying stud spacing and stud connector types are shown in Figure 7.30 (a). The solid lines represent walls with studs spaced at 610 mm on centre and the dashed lines represent walls with studs spaced at 1,220 mm on centre. Each different colour represents a different connection type: black for type B, blue for type C, and red for type D. What can be seen is that there is a wide spread between these values and no clear pattern. For the case of connection type B, the wall with studs spaced at 610 mm on centre had greater rotational stiffness than the wall with studs spaced at 1,220 mm on centre. The opposite is true, however, for the wall with connection type C. The results for the wall with connection type D fell in between the results for the walls with the other two connector types.

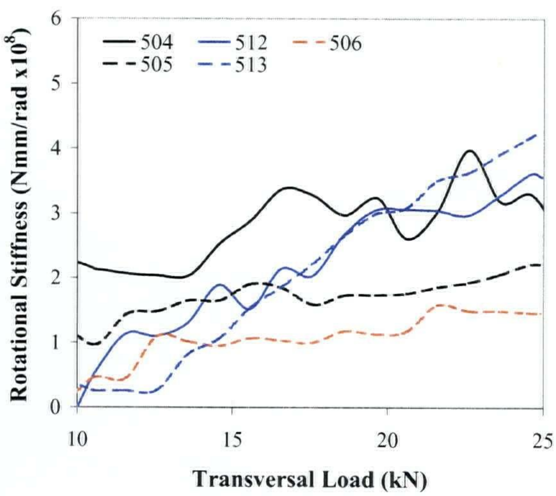

(a) Comparing the effect of stud spacing and connector type

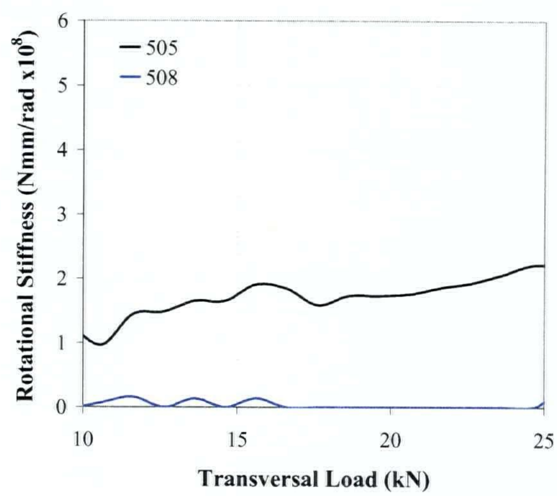

(b) Comparing the effect of sheathing connection stiffness

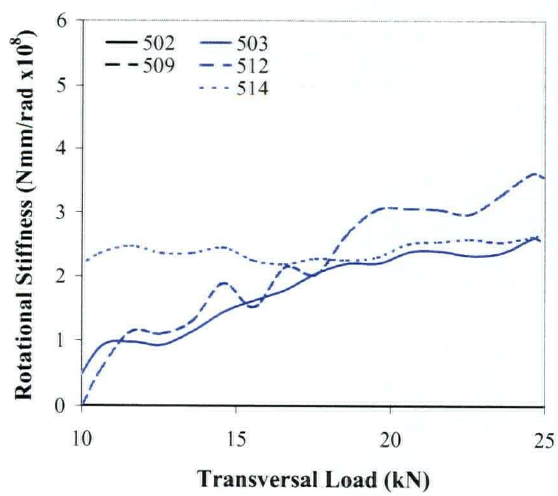

(c) Comparing the effect of stud material and sheathing type

Figure 7.30. Calculated end restraint rotational stiffness based on test results.

Two walls with LSL studs spaced at 1,220 mm on centre and continuous 15.5 mm thick OSB sheathing are presented in Figure 7.30 (b). The sheathing in wall 505 was connected to the frame with nails and the sheathing in wall 508 was connected with glue. The results shows that, in this case, end rotational restraint stiffness is independent of the sheathing connection stiffness, as the wall with a rigid connection had no measurable restraint compared with the wall with much lower connection stiffness provided by nails that had a nominal amount of restraint. Two sets of walls with similar framing configurations, sheathing types, and sheathing connection stiffnesses are presented in Figure 7.30 (c). Walls 502, 503, and 514 were constructed with SPF studs and the other two walls, 509 and 512, were constructed with LSL studs. Walls 502 and 509 were sheathed with 9.5 mm thick OSB and walls 503, 512, and 514 with 15.5 mm thick OSB. The walls with 15.5 mm thick sheathing had measurable end rotational restraint compared with the walls with 9.5 mm thick sheathing that had no measurable restraint.

The end rotational restraint stiffness for wall 504 with varying levels of axial load is presented in Figure 7.31. A negative axial load denotes compression. The variation in results is very high at lower transversal load levels. All of the curves converge to approximately the same level of end

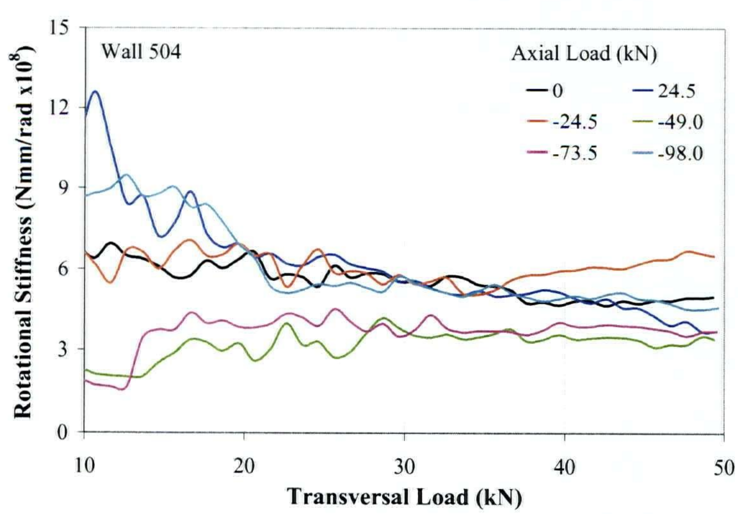

Figure 7.31. End restraint rotational stiffness of wall 504 with varied applied axial load.

rotational restraint stiffness at higher transversal loads. Two effects were believed to be interacting to produce the variable results. Each transversal load cycle reduced the amount of end rotational restraint by cycling the stud connections and thereby loosening the nailed connections. Each change in axial load level, however, would increase the amount of end rotational restraint. For an axial tension load, the nails in the stud connections fastening the hangers to the studs would be placed under shear loads along the length of the studs, temporarily increasing the rotational stiffness of the connection. For increasing levels of axial compression loads, the studs would bear against the end plates, temporarily increasing the end rotational stiffness until the end plate would crush perpendicular to grain. Although there was a large variation in results at low transversal load levels, end rotational restraint was independent of the level of axial load applied in this case.

Equation 7.5 showed how the displacement at the mid-height of a simply supported wall with a rotational spring at one end was a function of the rotational spring constant, the length of the wall, and the bending stiffness of the wall. Following the procedure outlined in Section 5.3.2, calculations for the composite stiffness of each wall specimen were used to determine the theoretical amount of reduction in the mid-height displacement of each wall due to the end rotational restraint stiffness values provided above. Figures 7.32 (a) through (c) show the amount of reduction for each of the walls presented in Figure 7.30. Because the constant B is inversely related to bending stiffness, with approximately the same level of end rotational restraint stiffness, a wall with a lower bending stiffness will receive a greater reduction in mid-height displacement. This can be seen for the walls that had larger stud spacing in Figure 7.32 (a), the wall that had lower connection stiffness in Figure 7.32 (b), and the walls that had SPF studs in Figure 7.32 (c).

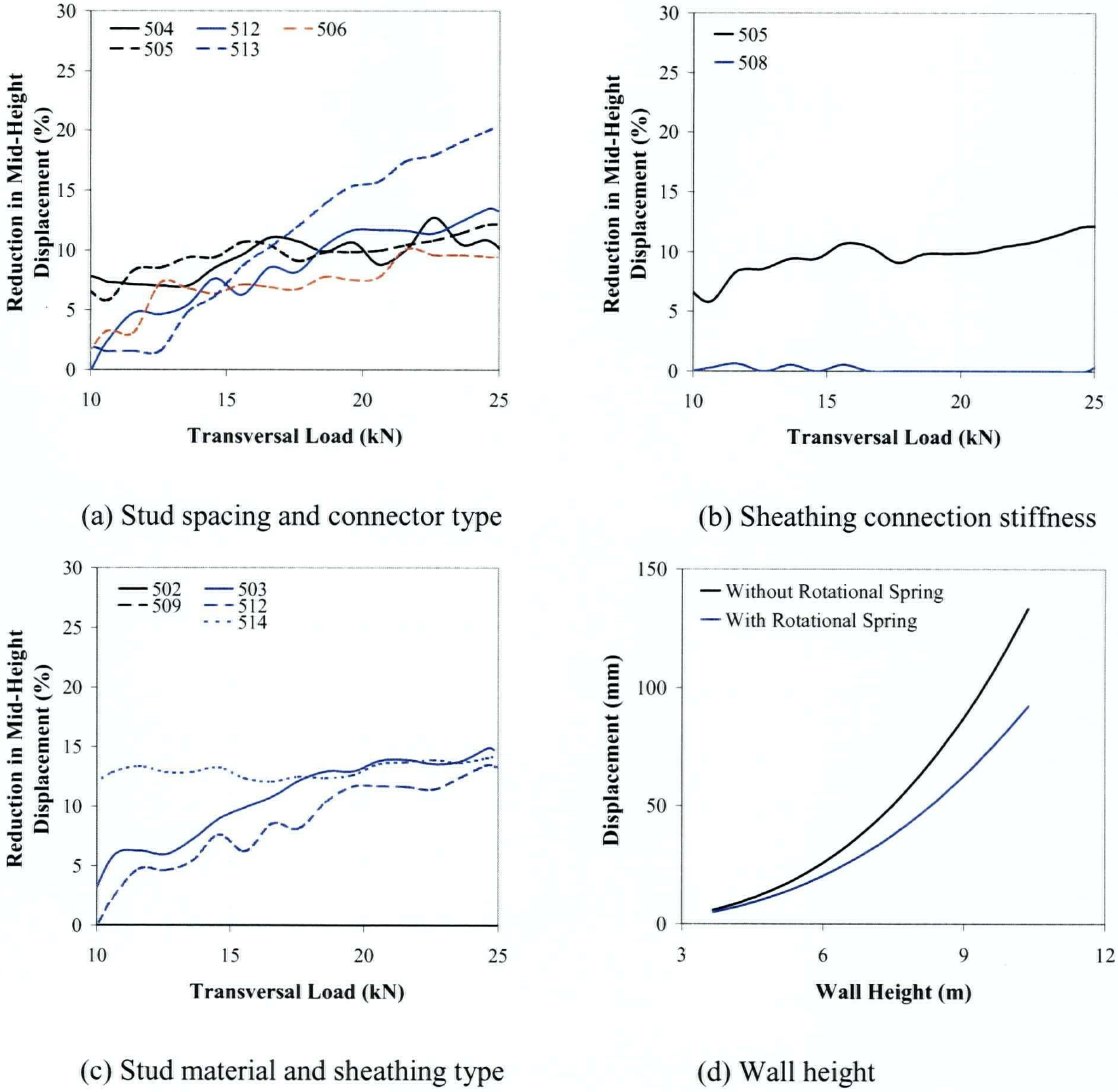

Figure 7.32. Calculated end restraint rotational stiffness based on the results of testing.

Figure 7.32 (d) shows the relationship between wall height and mid-height displacement for constant levels of end rotational restraint stiffness, wall bending stiffness, and transversal load. The properties calculated for wall 504 were used for this comparison. The constant B in Equation 7.6 is proportional to the height of the wall. Therefore, the percentage reduction in mid-height displacement increases with increasing wall height. Since the displacement of a wall is proportional to the height of the wall cubed, the effect of the end rotational restraint is not as significant for walls with increasing height.

In general, the tests showed that the end rotational restraint provided by the rigid foundation reduced the transversal displacements of the walls tested. The degree of end rotational restraint, however, varied significantly between wall specimens and no clear pattern could be discerned. As will be discussed next, some damage was observed in the stud connections of the walls that were loaded to very high transversal load levels. The damage appeared to reduce the amount of end rotational restraint at the high transversal load levels to the extent that the walls essentially behaved as if they were simply supported. Therefore, no benefit in end restraint was achieved at loads close to failure. For these reasons, it is recommended that the benefits of end rotational restraint not be included in the design of tall wood-frame walls.

7.3.6 Ultimate Strength and Modes of Failure in Bending

Several wall specimens were loaded in the transversal direction up to failure or at least well past the design load specified by the Canadian Wood Design Code. The transversal load that caused failure in a wall specimen or the maximum transversal load applied to each wall is given in Table 7.6. The axial load level was not the same for all of the walls tested to very high transversal load levels and is also presented in the table. The transversal load corresponding to the resistance in the Canadian Wood Design Code is given as well. This design load level was determined based on the current code provisions for wood-frame walls and include resistance factors (ϕ) and the short term duration of loading factor (K_D). Only the resistance of the stud members were taken into account and simple supports were assumed. The lateral stability factor in bending (K_L) was taken as 1.0 for all walls since sheathing and blocking supported the compression edges of all of the studs. The design load in bending was reduced due to the presence of the axial load using the linear interaction equation provided in Equation 7.1. Example calculations are provided in Appendix B. The overstrength factor in Table 7.6 is the ratio of the maximum applied transversal load (in some cases this was to failure) versus the design load.

Table 7.6. Maximum transversal load applied or point of failure in bending.

Specimen Number	Specimen Type	Stud Spacing (mm)	Stud Material	Connector Type	Axial Load (kN)	Maximum Load, F_{max} (kN)	Design Load[d], F_{design} (kN)	Overstrength (F_{max} / F_{design})
501	W1	610	SPF	A	-97.9	74.6[a]	12.4	6.02
502	W2	610	SPF	A	-97.9	53.2[a]	12.4	4.29
503	W1	610	SPF	A	-98.0	69.0[a]	12.4	5.56
505	W4	1220	LSL	B	-97.9	77.9	10.7	7.28
507	W1	610	LSL	B	-24.5	132.8[c]	31.2	4.26
508	W4	1220	LSL	B	-98.2	86.0[b,c]	10.7	8.04
509	W2	610	LSL	B	-98.0	90.0[c]	24.2	3.72
511	W5	610	LSL	B	-48.9	113.9[c]	28.7	3.97
512	W1	610	LSL	C	-97.9	90.2[c]	24.2	3.73

(a) Transversal load at first stud failure.
(b) Transversal load at first glue line failure.
(c) Wall specimen was not loaded until failure occurred.
(d) Factored transversal load determined using interaction equation with axial load and assuming wall is simply supported.

The load-displacement curves of all the walls loaded under high transversal loads are shown in Figure 7.33. All three of the walls with SPF studs loaded under high transversal loads failed in bending with one or more studs failing in tension (Figure 7.33 (a)). Similar to the results found from the T-beam tests presented in Chapter 5, the failure of each stud originated at defects on the tension face of the studs. Two examples of stud failures are shown in photos in Figure 7.34 (a) and (b). Wall 501 and 502 continued to resist increasing transversal load after the first stud failure\but wall 503 failed in a brittle manner after the first stud failure. Despite the stud failures, all three of the walls rebounded to their initial un-deflected position after the transversal loads were removed. In addition to the stud failures, large deformations were observed in the stud connections at high transversal loads (Figure 7.34 (c)). The overstrength values calculated for these walls at the point of first stud failure ranged from 4.29 to 6.02. Because of the large variability in the strength of SPF studs no conclusion can be drawn related to the increase in

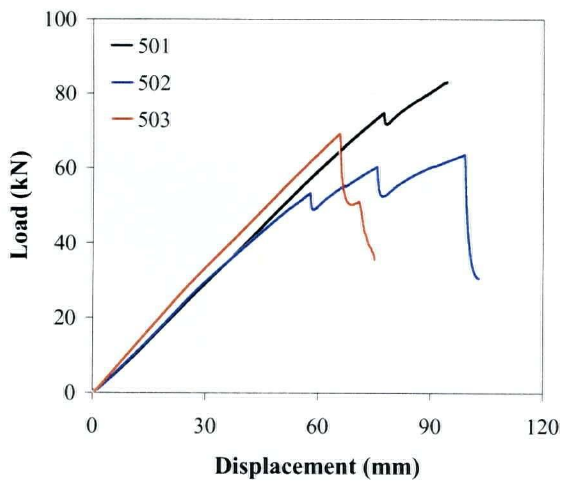

(a) Wall with SPF studs.

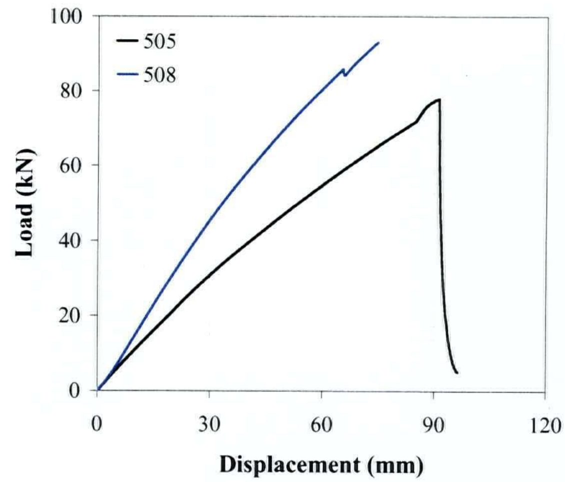

(b) Effect of connection stiffness.

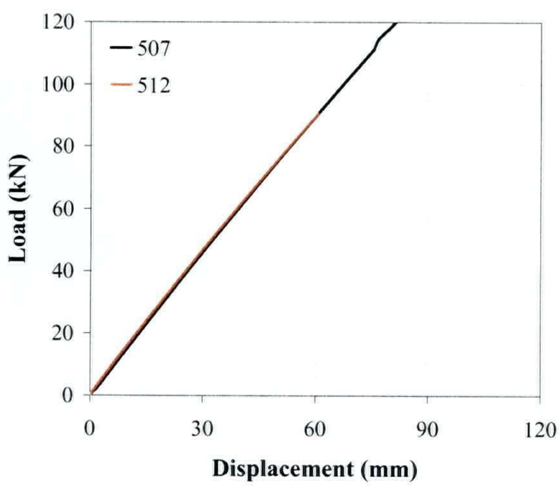

(c) Effect of connector type.

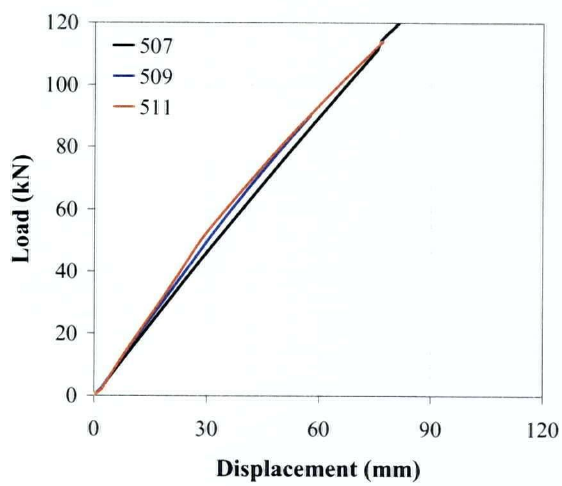

(d) Effect of sheathing type.

Figure 7.33. Various effects of load-displacement relationships of tall walls obtained from testing.

strength through composite action. A large number of walls would have to be tested in order to statistically determine the effect of composite action on maximum strength.

Two walls with LSL studs spaced at 1,220 mm on centre and continuous 15.5 mm thick OSB sheathing were loaded to high transversal load levels. The sheathing on wall 505 was connected using nails and the sheathing on wall 508 was connected using both glue and nails. Wall 505

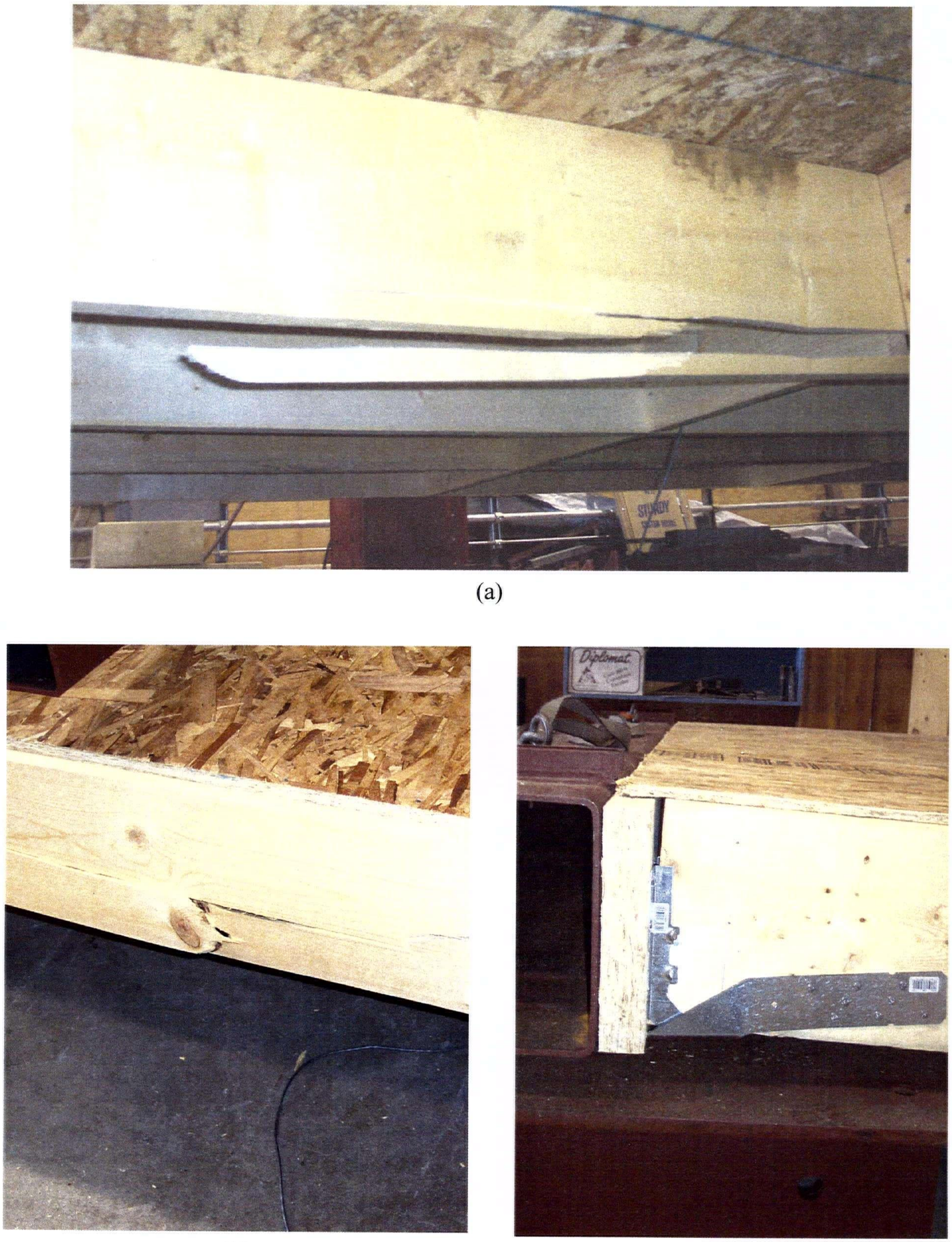

(a)

(b) (c)

Figure 7.34. Failure modes of the full-scale walls with SPF studs under transversal loads: (a) and (b) tension failure in wall studs; and (c) deformations in stud connection.

failed in a brittle manner when three adjacent studs failed in a combination of shear and bending at the loading point nearest to the roller-supported end of the wall (Figure 7.35 (c)). Additionally, the end plate of the wall at the roller-supported end split in half along the width of the wall (Figure 7.35 (a)). This occurred because the end plate was connected to the support beam with a single line of bolts along its centre, where the large load applied to the bottom of the end plate, by tension ties, caused significant transversal bending. Similar to the SPF walls loaded in the transversal direction to failure, large deformations were observed in the stud connections at the foundation end of the wall (Figure 7.35 (b)). The overstrength value calculated for wall 505 was 7.28. The maximum transversal load applied to wall 508 was not large enough to cause total failure of the wall but a failure in one of the glued connections between the sheathing and the studs was observed at a transversal load of 86.0 kN (Figure 7.33 (b)). No other damage was observed and the wall continued to resist increasing transversal loads with approximately the same stiffness as before glue line failure. The connection between the sheathing and the stud still resisted loads after the glue line failed, since the sheathing was also connected with nails, which then took over as primary connector elements. The overstrength value calculated for wall 508 was 8.04.

Walls 507 and 512 were constructed with 15.5 mm thick OSB sheathing connected with nails to LSL studs, which were spaced at 610 mm on centre. The stud connections for wall 507 were type B and the connections for wall 512 were type C. The load-displacement curves presented in Figure 7.33 (c) show no difference between these walls despite the fact that wall 512 had four times the applied axial load as wall 507. Wall 507 is also compared to walls with similar frames but with different sheathing configurations (Figure 7.33 (d)). As shown previously for lower load levels, no significant difference in stiffness was observed at high transversal load levels due

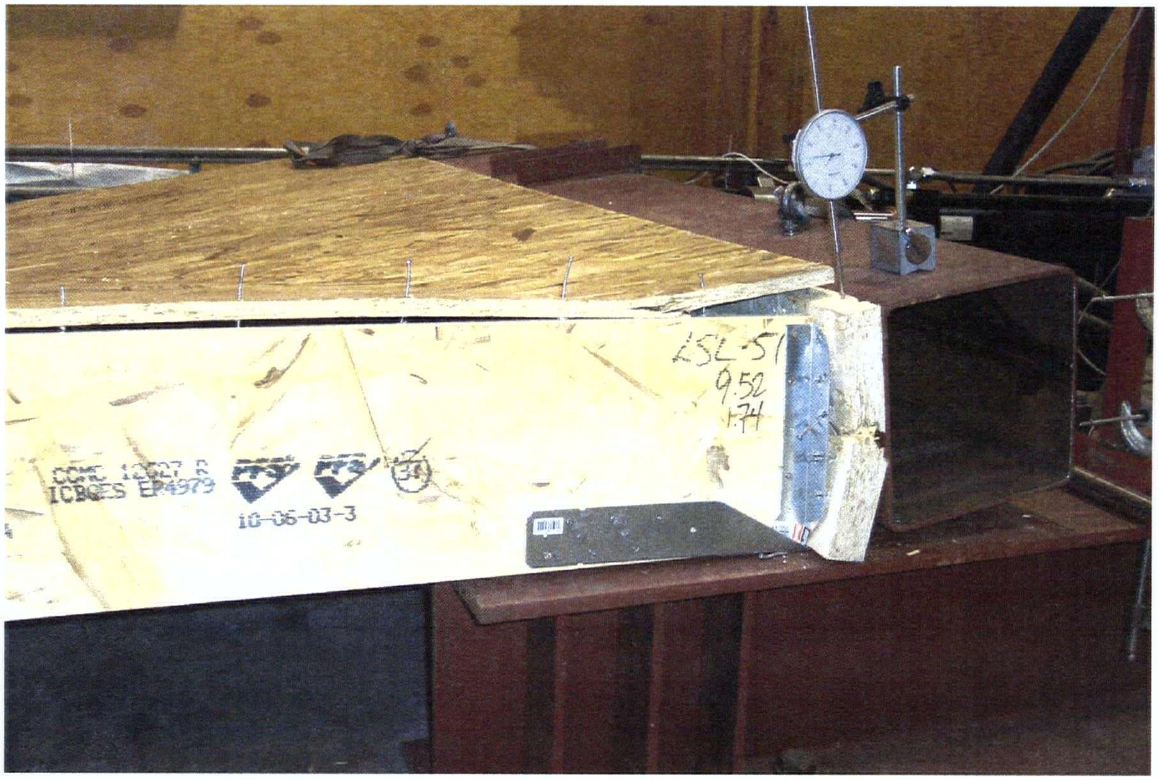

(a)

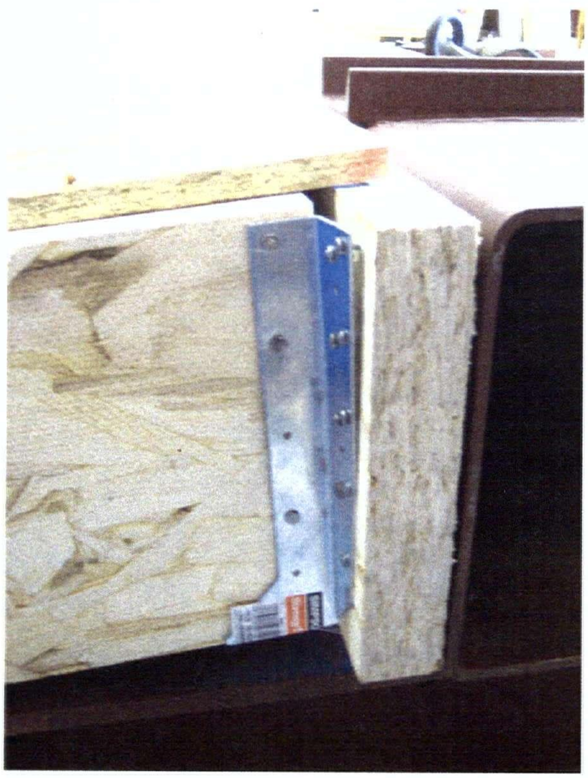

(b)

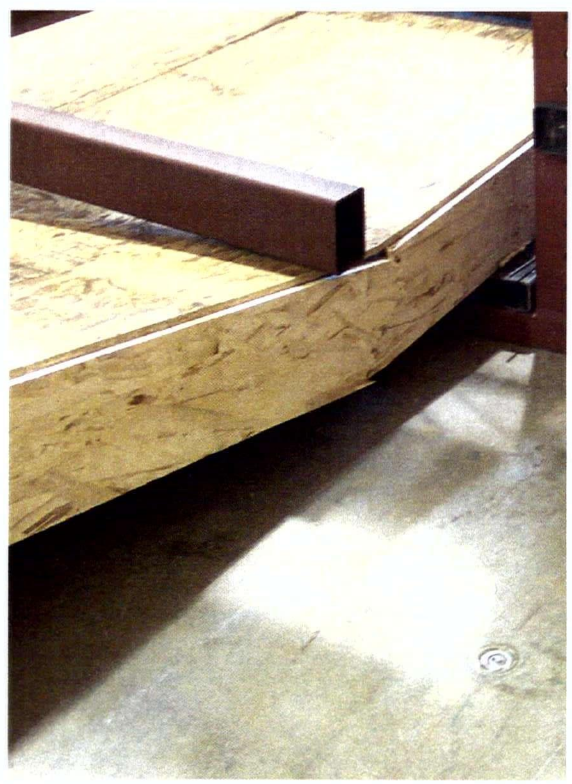

(c)

Figure 7.35. Failure modes of full-scale wall 505 under transversal loads: (a) splitting of the end plate at the roller-supported end; (b) deformations in stud connection; and (c) failure of an outside stud.

to the presence of gypsum wallboard on the tension face of wall 511 in comparison to wall 507, which did not have gypsum wallboard sheathing. The bending stiffness of wall 511 did, however, decrease more with increasing load than did wall 507. No significant difference in the response of wall 509, which had continuous 9.5 mm sheathing, was observed when compared to wall 507 either. The overstrength values for these four walls ranged from 3.72 to 4.26. No damage was observed in any of these walls.

The overstrength values that were determined based on the design specifications in the Canadian Wood Design Code show that the tall wood-frame wall specimens that were tested to high transversal loads, which sometimes resulted in failure, were well within the targets for safety specified for ultimate limit states. Even when the design values are adjusted for short term loading, it is felt that the specified design values for strength may be too conservative in some cases. It is difficult to draw conclusions on the appropriateness of the specified design strengths for the walls with SPF studs because of the large distribution in strength for the studs. Many composite walls would need to be tested using studs representative of the entire strength distribution for SPF framing members to obtain a sufficiently representative sample size for statistical analysis. A better definition for the ultimate limit state may also be required. For the walls tested, failure was defined as the load that caused the first stud to fail. Walls 501 and 502, however, continued to resist transversal loads up to 20% higher than the load at which the first stud failed.

The scatter of strength and stiffness for LSL studs is much less and some general conclusions can be made with regards to the walls tested with LSL studs. Wall 505 failed at a transversal load that was over seven times the design load. If it is assumed that there was no axial compression load applied to the wall, the overstrength factor reduces to 4.00 from 7.28 based on the resistance of the studs in bending alone. Wall 507, 509, 511, and 512 were all observed to be within their linear elastic ranges at predicted overstrength values of approximately 4.0. From these results, it is recommended that a reliability study be conducted using a computer model on the ultimate strength of tall wood-frame walls with both sawn lumber and engineered wood product stud members. The reliability analysis should incorporate the distribution of strength for each stud material determined from testing.

7.4 SUMMARY

Numerous aspects of the response of tall wood-frame walls under axial and transversal loads were determined after testing thirteen full-scale specimens. The wall specimens were constructed with the same types of materials that were used in the component tests described in previous chapters so that comparisons could be made with predicted results incorporating the previous test results.

The increase in stiffness of the composite walls over the bare studs determined from the load-displacement responses of the tests with axial and transversal loads were found to match well with the results obtained from the composite T-beam tests described in Chapter 5. Wall specimens with studs spaced at 1,220 mm on centre had greater increases in stiffness than were found in the T-beam tests due to the increased effective width of the sheathing.

The linear load interaction equation specified in the Canadian Wood Design Code was compared with the transversal stiffness results for six different levels of axial load. It was found to be conservative, especially at the higher axial compression load levels, even when using composite member properties to predict the response.

Theoretically, the bending stiffness of a composite member should be independent of the direction of loading. Three wall specimens showed similar bending stiffness values when loaded in both transversal directions.

The bending stiffness of a wall specimen with non-structural gypsum wallboard sheathing on the tension face did not show a significant increase compared with a wall specimen without gypsum wallboard over repeated transversal load cycles.

The current criterion for the transversal displacement of wood-frame walls is intended to limit damage to the structure and to non-structural attachments. Although the code prescribes that only the properties of the bare stud can be taken into account, the displacement criterion was set forth assuming that other factors such as composite action will reduce displacements. The maximum transversal displacements achieved in testing on walls without non-structural sheathing and the one wall with gypsum wallboard showed that the displacement criterion is conservative based on bare stud properties and the maximum allowable design displacements could be increased even if composite properties are included into design.

System factors prescribed in the code increase the bending strength of both sawn lumber and engineered wood product studs by accounting for the distribution of strength in a repetitive member system, the composite action of the sheathing, and the transverse distribution properties of the sheathing and blocking. Test results show that the significantly lower load-sharing factor ($K_H = 1.10$), that needs to be used when the bending capacity of a system with sawn lumber studs is calculated using composite member properties, may be too conservative. Furthermore, significant transverse stiffness was measured for wall specimens with engineered wood product studs spaced at 1,220 mm on centre and blocking, despite the fact that the code does not allow load-sharing factors to be applied to systems with framing members spaced at more than 600 mm on centre.

Several walls were loaded axially to determine the response of four different stud connection types. Off-the-shelf connector products performed well in testing and proved to be a viable alternative to specially fabricated connectors that have been used in the past. The use of one of these products, a tension tie, in combination with the deep studs used in the wall specimens produced an eccentric moment at the ends of the studs and resulted in excessive rotations that led to wall failures. Placing tension ties on every other stud did not result in additional undesirable modes of failure due to the load distributional properties of the sheathing. The need for tension ties can be removed by attaching joist hangers to the end plates with screws. A ductile mode of failure was observed by forcing the weakest point of the connection away from the screws.

The wall specimens were tested with realistic end conditions. A rigid foundation support provided end rotational restraint to the walls and reduced the transversal displacements of the walls. The amount of end rotational restraint provided by the rigid foundation varied greatly, however. Furthermore, excessive connection deformations lead to the deterioration of the end restraint prior to the failure of the walls under transversal loads. Therefore, it was recommended that the effect of end rotational restraints should not be accounted for in design.

Several wall specimens were loaded to very high transversal loads, which in some cases caused failure. The maximum loads achieved proved to be much larger than the specified loads prescribed by the code, especially for the walls with studs spaced at 1,220 mm on centre. This reinforced the need for future work on the inclusion of a system factor for studs spaced greater than 600 mm on centre and the conservative nature of the linear load interaction equation.

8. ANALYTICAL PREDICTION OF FULL-SCALE WALLS

The results from a series of tests on full-scale tall wood-frame walls under axial and transversal, or out-of-plane, loads were presented in the previous chapter. Several types of responses for the walls were quantified including the bending stiffness obtained from the load-displacement curves of the walls in two transversal load ranges and six levels of axial load, end rotational restraint stiffness at the foundation support, the ultimate strength in bending, and the ultimate strength under axial tension. The main objective of this chapter is to make analytical predictions of the load-displacement response of the walls tested. A detailed finite element computer program called PANEL, which incorporated the results of tests on tall wall components presented throughout this thesis, was used to predict the response of three walls loaded under axial and transversal loads. Several predictions have already been made in this thesis using an approximate formulation for determining the effective properties of composite members and a beam-spring analog. This method will also be compared to test results and to the results from finite element analyses. Satisfactory correlation between the predictions obtained from the finite element model and the test results would validate the use of the model for reliability analysis in order to obtain appropriate levels of safety for the factors used in design for this type of structural system. Correlation between the two analytical methods would further strengthen the appropriateness of using composite member properties in design.

8.1 ANALYTICAL MODELS

For predicting the load-displacement response of the full-scale tall wood-frame walls tested in the previous chapter, two types of analytical models were developed: a non-linear finite element model developed specifically for the analysis of wood-frame diaphragm structures and an analog linear model incorporating an approximate formulation for the effective properties of composite members. While the linear analog model can represent the load-displacement response of a wall accurately in specific load ranges using a single value for the connection stiffness between the sheathing and the studs in the wall, the non-linear finite element model can account for the non-linear properties of the connections and provide a better prediction over all load ranges. No data was obtained regarding the ultimate strength of the studs that were used in the walls tested. Therefore, analytical predictions were not made on the ultimate strength of the entire wall systems. Furthermore, since most of the walls tested to high axial loads failed in the stud connections, analytical predictions on ultimate strength were not attempted.

8.1.1 PANEL Finite Element Model

The finite element model was developed using the computer program PANEL (Foschi, 1999). It is one of several programs that were developed at the University of British Columbia to predict the response of wood-frame diaphragm structures. A structural idealization of a diaphragm with one layer of sheathing is shown in Figure 8.1. It consists of a finite strip formulation comprising an assemblage of T-beams. The deformations in the direction parallel to the frame members are represented by a Fourier series and in the direction perpendicular to the frame members by a one-dimensional finite element discretization. Lateral and torsional deformations of the framing members are included as degrees of freedom.

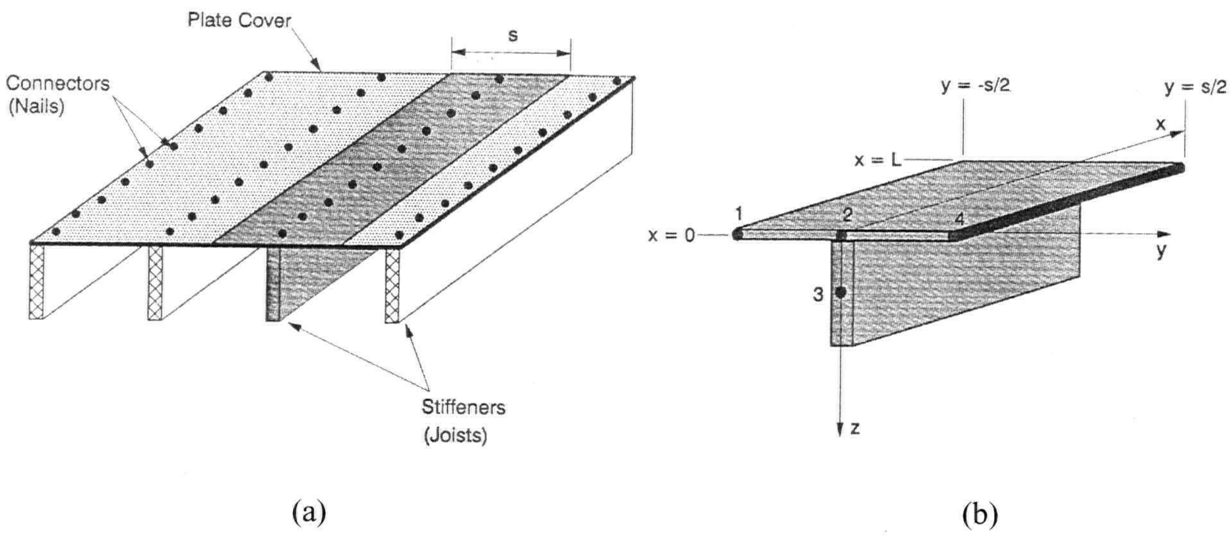

Figure 8.1. (a) Wood floor assembly and (b) T-beam element strip (Foschi, 1989).

The diaphragm structures consist of a frame connected to a top cover and a bottom cover if applicable. Wall structures can be modeled with openings for doors and windows. Loads can be applied in the transversal direction or in the plane of the diaphragm and can be applied simultaneously or incrementally until the ultimate capacity is reached. The program defines several criteria for ultimate failure, which include: excessive connection deformation, buckling of the covers, buckling of the frame, tearing of the edge of the covers implying local connection failure, and bending failure of the frame members. The solution may be obtained under either load or displacement control.

A model of wall specimen type W2 was developed to predict the load-displacement responses of full-scale wall test specimens 502, 504, and 509. A full description of the wall specimen type and the individual wall specimens was presented in Section 7.2.1. Wall 502 had spruce-pine-fir (SPF) sawn lumber studs and walls 504 and 509 had laminated strand lumber (LSL) studs. A schematic of the model is presented in Figure 8.2 and the input code is presented in Appendix C. The geometry of the model is defined by the position of the nodes at the four corners of the plate elements. The layout of the elements corresponds with the layout of the wall specimens that were tested and the position of the supports and loading points. A description of the full-scale wall test set-up was presented in Section 7.2.2. Nodes were placed in the model wall at the positions where transversal displacement measurement devices were located in the wall specimens and at the positions where the transversal loads were applied at the third points. Each end of the wall specimens that were tested was attached to a steel beam. One steel beam was held rigidly in place while the other was supported by rollers, which allowed it to rotate about its axis and to translate horizontally along the height of the wall. Since the roller was located under the steel beam, the total length of the wall specimens between supports was greater than the length of the specimens themselves. The total height of the modeled wall was made equal to the total supported length between supports. The length of the sheathing, however, was kept equal to the length of the sheets used for the wall specimens.

The transversal and axial loads in the full-scale wall test program were applied to the wall specimens using load control. The transversal loads were applied at the third points of the wall specimens themselves and not the third points of the total supported length of the test set-up. Although the difference between the two lengths was small, approximately 1%, this difference coupled with the partial end rotational restraint provided by the rigidly supported foundation end meant that the load applied at each of the two loaded points may not have been equal. The displacements applied to the wall at the third points, however, were approximately equal. Therefore, equal displacements were applied to the wall models at the stud locations corresponding to the loaded points on the wall specimens.

In actual wall structures loaded under uniformly distributed loads in the transversal direction, the variation in stud properties will certainly have an effect on the maximum displacements in the wall. Increasing the bending stiffness provided by the sheathing and the blocking in the direction

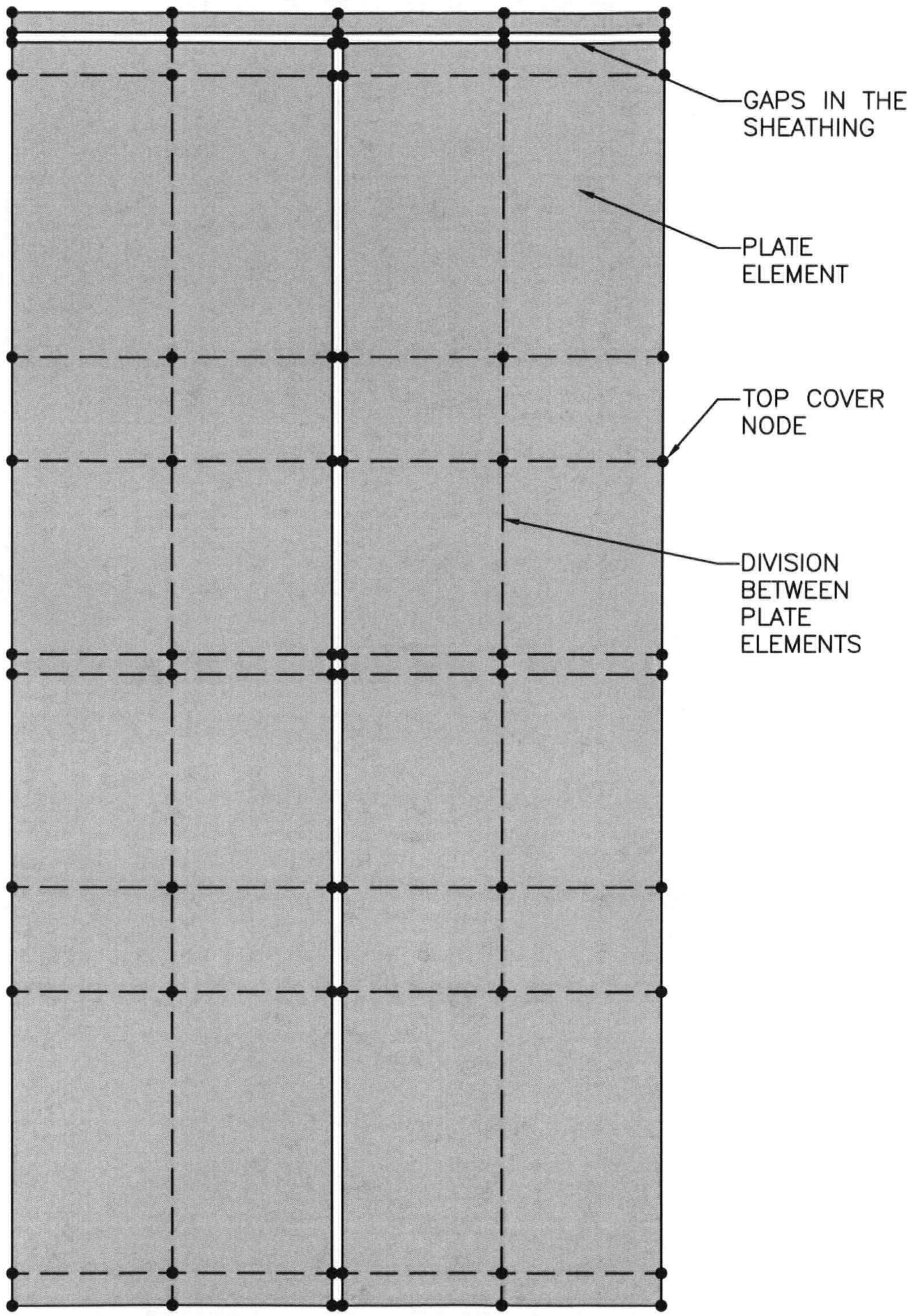

1 / 8.2 TOP COVER 1:25

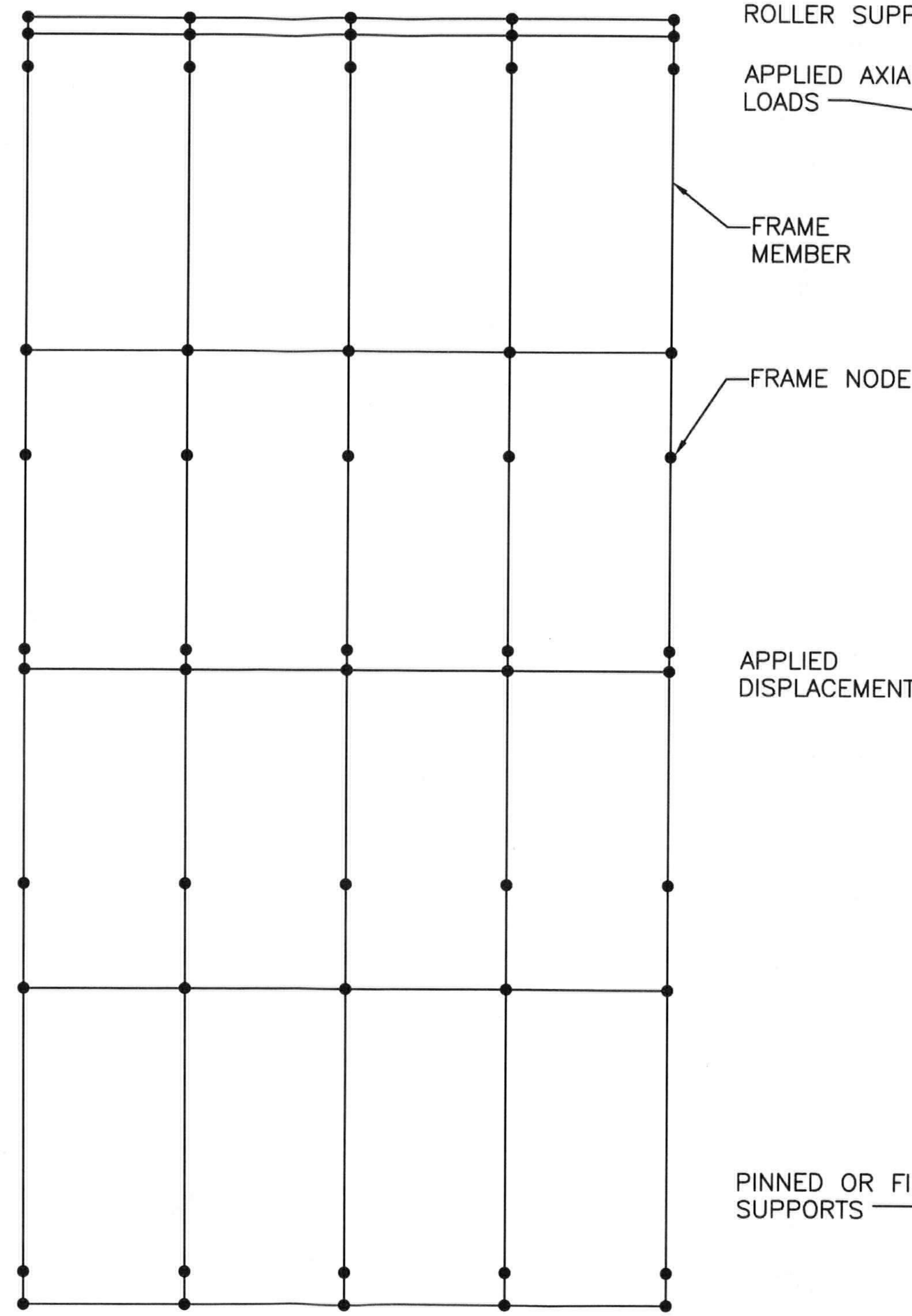

2 / 8.2 FRAME 1:25

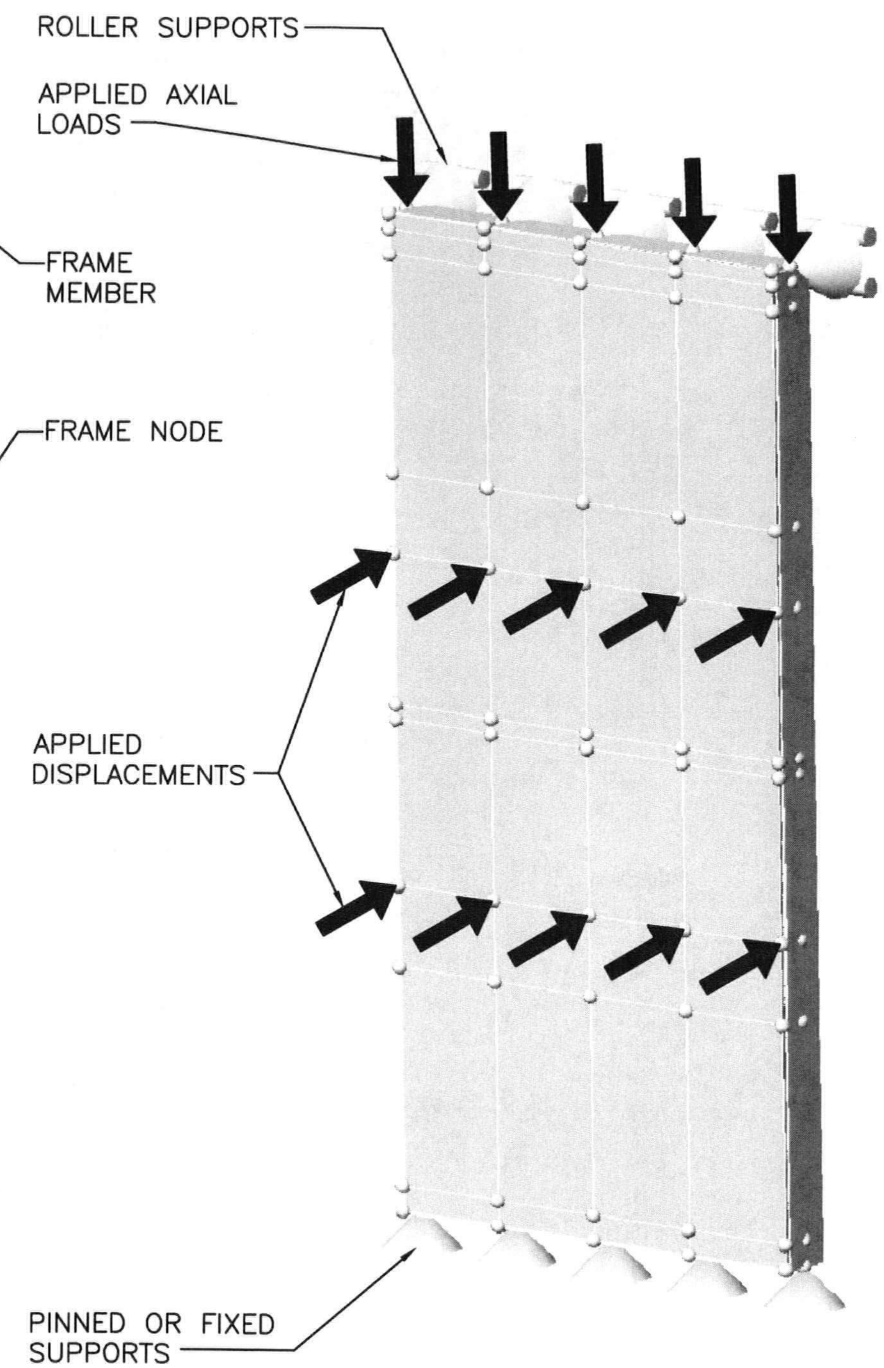

2 / 8.2 LAYOUT 1:25

Forintek Canada Corp.	TALL WALL STRUCTURAL PERFORMANCE	DRAWN DEL	DATE OCT-04
		SCALE AS SHOWN	APPROVED
	SCHEMATIC OF WALL TYPE W2 IN PANEL PROGRAM	DRAWING NUMBER FIG 8.2	REVISION PROJECT REF. 3910

perpendicular to the length of the studs can distribute the loads to the studs based on their relative stiffness and reduce the maximum displacement. When modeling this type of loading, applying the average properties of all of the studs to each of the studs in a wall, however, artificially increases the apparent stiffness of the sheathing and blocking and reduces the maximum displacements. Because equal displacements were applied to the model in Figure 8.2, the total load applied to the wall was equal, regardless of whether each stud had different stiffness properties or the average properties of all of the studs in the wall were used. No difference in the maximum displacements of wall models with these two configurations was found. The properties of the studs in wall specimen 502, which had the greatest variation of the three wall specimens modeled, were used to make this comparison. The average properties of the studs in a wall specimen, as obtained from testing and presented in Chapter 5 and Chapter 7, were used for each stud in the wall model for that particular specimen. The average properties of all of the studs tested for each stud material were used for the blocking members. The properties of the sheathing materials were also obtained from testing, as presented in Chapter 5.

The non-linear load-displacement responses of the connections in the four principal directions were applied along the edges of the plate elements in the model at the specified spacing. The four degrees of freedom were: displacement in the plane of the wall parallel and perpendicular to the length of the wall; withdrawal perpendicular to the face of the wall; and rotation between the studs and the sheathing. The program defines the same displacement function for each of these four degrees of freedom. The function is shown in Figure 8.3 and is given by (Foschi, 1974):

$$P = (P_o + K_1 u)\left(1 - e^{-\frac{K_o u}{P_o}}\right) \qquad \text{if } u < u_{max} \qquad (8.1)$$

$$P = P_o + K_1 u_{max} + K_E (u - u_{max}) \qquad \text{if } u > u_{max}. \qquad (8.2)$$

The parameters in the displacement function were determined in each direction for each wall specimen modeled from fastener testing that was conducted earlier in this study. A description of the load-slip test set-up for the properties of the connections parallel and perpendicular to the length of the studs was presented in Chapter 3. The nail withdrawal test set-up for the properties of the connections perpendicular to the face of the wall was described in Chapter 4. The test set-up to obtain the rotational response of nails was presented in Section 3.2.3.

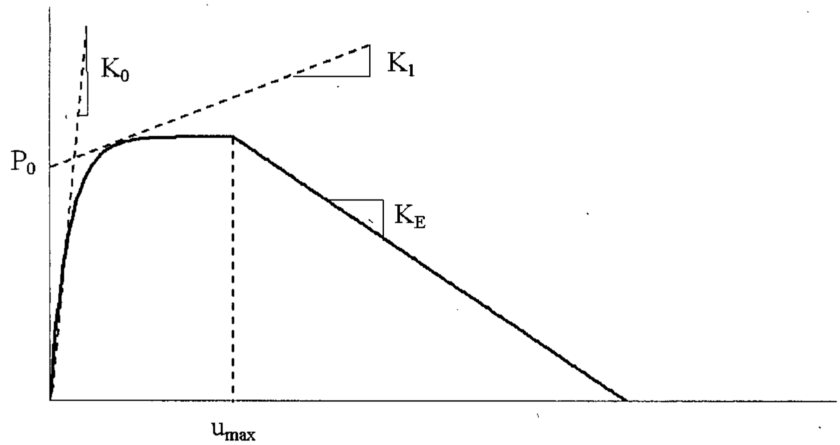

Figure 8.3. Definition of the connection parameters in the load-slip function by Foschi (1974).

8.1.2 Beam-Spring Analog Method

The linear model used to predict the load-displacement response of the full-scale wall specimens incorporated the formulation for composite member properties including the effective flange width as presented in Sections 5.3.2.1 and 5.3.2.2, and the beam-spring analog developed by McCutcheon that was presented in Section 2.5.6.2 (McCutcheon, 1984). This model also requires the material properties of the studs and the sheathing but only one value for the connectors: the load-slip response along the length of the studs. The individual connector stiffness for each wall was obtained, from the curve of the load-displacement response of the appropriate connection presented in Chapter 3, for the maximum slippage displacements measured in the wall specimens. The maximum slippage was approximately equal to what was measured for the T-beams constructed with the same materials presented in Chapter 5. Therefore, the same individual connector stiffness values presented in Table 5.6 were used for the linear models.

The progression of the beam-spring analog method used for the linear model is shown in Figure 8.4. A wall specimen is shown as it was constructed in the full-scale wall test set-up. The bending stiffness of the wall in the direction perpendicular to the length of the studs was determined. For a wall loaded uniformly in the transversal direction this bending stiffness would correspond to the sheathing and the blocking. A formula for determining the bending stiffness of the sheathing was presented in Section 2.5.6.2 and a discussion about the effect of blocking was presented in Section 7.3.4. The walls tested in this study were loaded at the third points by two steel beams. These beams were assumed to be rigid in comparison to the stiffness of the walls

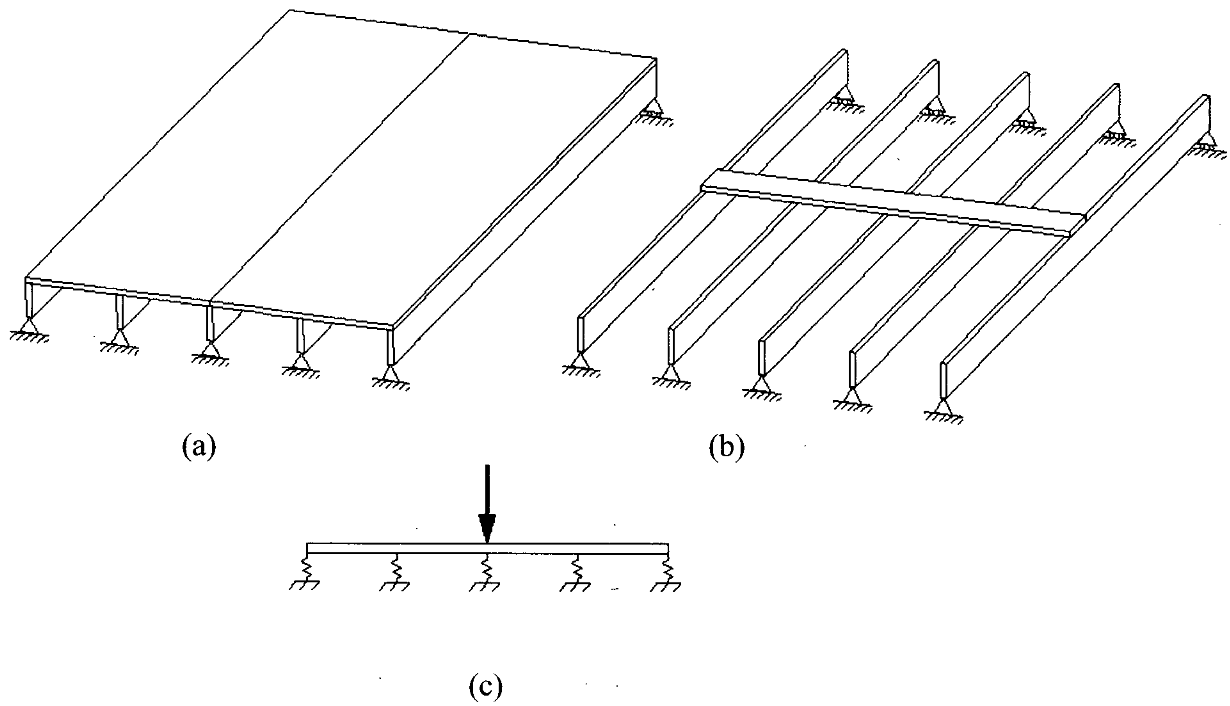

Figure 8.4. Progression of the beam-spring analog method. (a) composite wood-frame system, (b) transverse stiffness represented as an equivalent beam perpendicular to the load resisting elements, and (c) composite load resisting elements represented as springs supporting the equivalent transverse beam (McCutcheon, 1984).

themselves. An infinite bending stiffness perpendicular to the length of the studs was thus assumed (Figure 8.4 (b)). This assumption also corresponds to the equal applied displacements used in the PANEL model.

The bending stiffness of each composite member, comprising a stud connected to an effective width of sheathing with linear nail stiffness, under third point loading and with an axial load, was determined. This was done using beam theory and the stiffness reduction equation, due to the presence of the axial load, presented in Section 7.3.2. For wall specimens where an end rotational stiffness was measured, the bending stiffness was artificially increased using Equation 7.5 in Section 7.3.5.2. Each bending stiffness value determined was then used to represent a spring support for the transverse beam described previously (Figure 8.4 (c)). A stiffness matrix was then used to represent the entire system. An example of such a formulation is presented in Appendix C.

8.2 RESULTS AND DISCUSSION

The load-displacement responses at the mid-height of the central stud in walls 502, 504, and 509 are presented in Figures 8.5 to 8.8. The curves were obtained from the experimental tests, the PANEL finite element computer program, and from calculations using the beam-spring analog method. The wall geometries and loading configurations for each wall corresponded to the full-scale wall test set-up with third-point transversal loading and constant axial load. The axial load used for all of the curves was 48.9 kN compression. Load-displacement curves were determined for each wall that was modeled in PANEL with pinned supports at the foundation-supported end and with fixed supports. This was done to determine the sensitivity of end rotational restraint stiffness provided by the simulated foundation support. Where end rotational restraint stiffness was measured and a rotational stiffness was calculated for a wall specimen, a second linear load-displacement curve was determined using the beam-spring analog method to account for the increased bending stiffness. Comparisons of the bending stiffness obtained from two points on the load-displacement curves for the test results and using the beam-spring analog-method are presented for all six axial load levels that were applied to the wall specimens in Table 8.1.

Figure 8.5 shows the load-displacement response of wall 502 obtained from testing, the PANEL program, and determined using the beam-spring analog method. No end rotational restraint stiffness was measured during testing, so only one linear approximation was calculated. This was confirmed by the test results, which were located below the results obtained from PANEL with pinned supports at the foundation-supported end. The bending stiffness of the tested walls and the two predicted curves from the analytical methods assuming pinned supports, were very close, especially at transversal load levels beyond approximately 10 kN. The beam-spring analog method used only one value for connection stiffness so it did not account for the high degree of non-linearity in the initial loading range. The PANEL model, while more accurate, represented idealized support conditions that could not account for initial slack in the stud connections that may have reduced the initial stiffness of the wall.

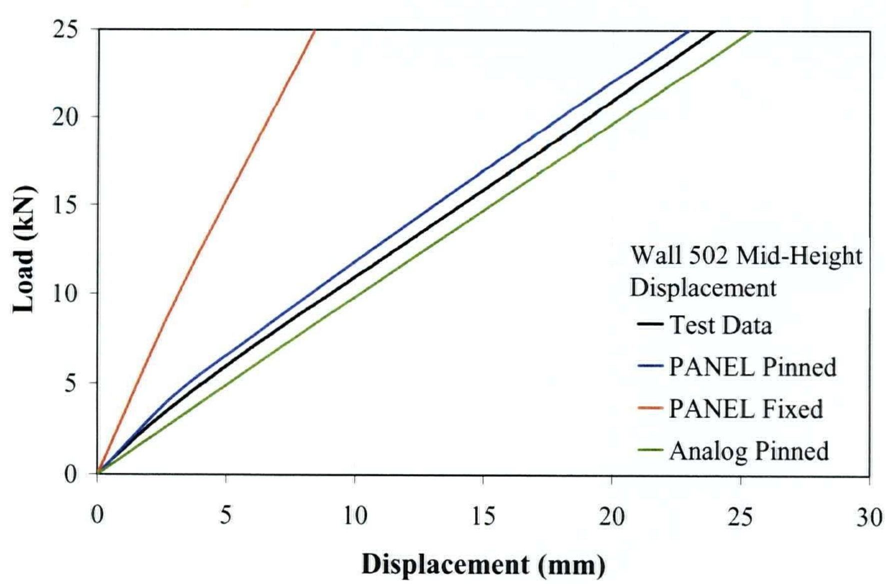

Figure 8.5. Load-displacement response comparison for wall 502.

It was mentioned previously that no difference was found between a wall modeled in PANEL with the average properties of the studs in the wall assigned to each stud and with each stud having its own properties. This was because the walls were modeled with applied displacements. This resulted in the relationship between the total load applied to the walls and the mid-height displacement at each stud being the same. The idealization of applied displacements used in the PANEL models was very accurate when the variation in the properties of the studs in the walls was low. For wall 502, however, the bending stiffnesses of the studs increased from one edge across the width of the wall. Although the load distribution beams did not bend during the tests, they were able to rotate and thus accommodate a linear variation of displacement across the wall. Figure 8.6 shows the effect of the variation in bending stiffness of the studs in wall 502. The mid-height displacement on one side of the wall was much less than on the other side. Because loads and not displacements were applied to the beam-spring analog model, the variation in displacement across the width of the walls could be determined. As can be seen, the predictions from this simplified linear model matched the test results closely across the width of the wall.

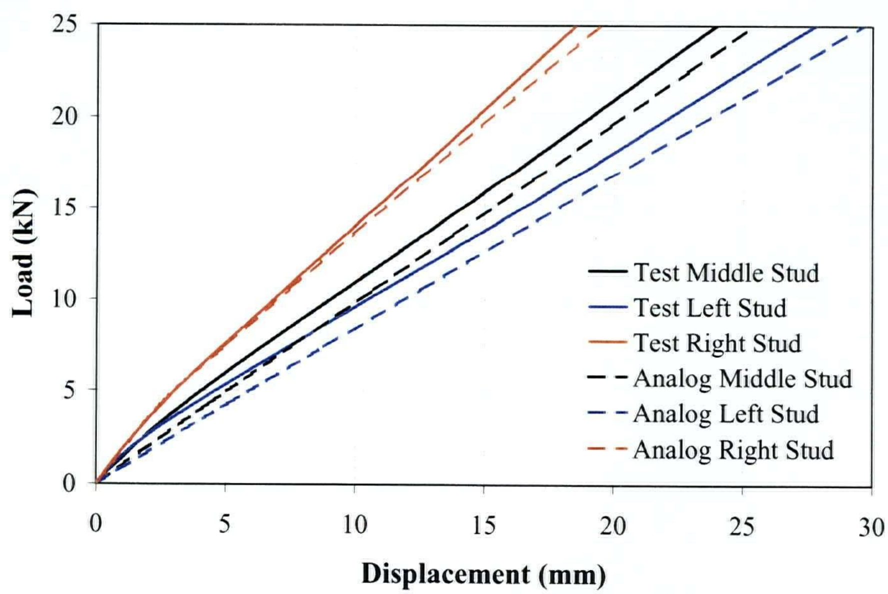

Figure 8.6. Load-displacement response comparison for three different studs in wall 502.

The results for wall specimen 504 are presented in Figure 8.7. Unlike the beam-spring model, the PANEL model accurately predicted the behaviour at the lower transversal load. Since end rotational restraint was measured for wall 504, a corresponding reduction in displacement of approximately 10% was calculated in Section 7.3.5.2. This corresponds well with the curves in the figure. The added bending stiffness due to the end rotational restraint was reduced with increasing transversal load as a result of deformations in the stud end connections. The prediction using the beam-spring method, and which included the effect of end rotational restraint, was not able to capture this degradation since it uses a linear connection stiffness. The largest effect of the rotational restraint occurred in the loading range where a non-linear response in the sheathing connectors occurred. The load-displacement response obtained from testing corresponded well with predictions assuming pinned supports after the initial non-linear loading range.

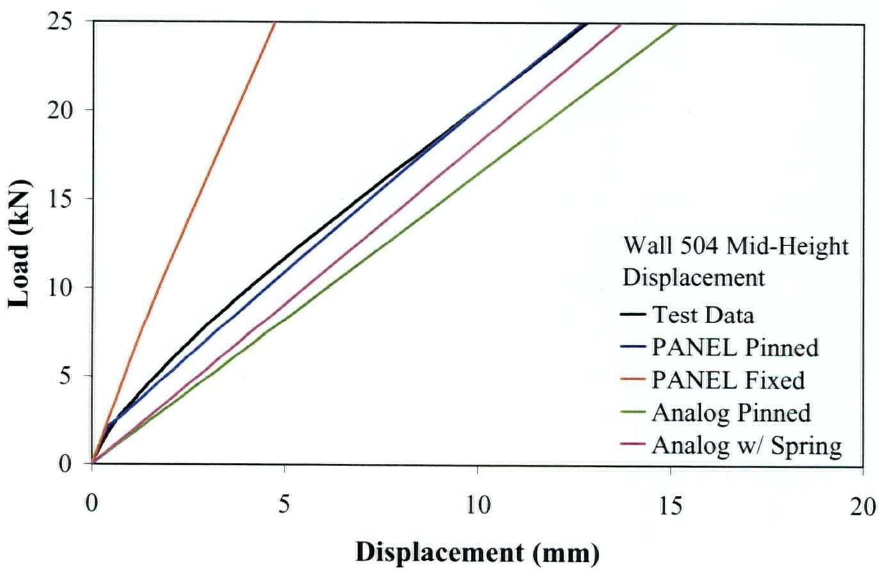

Figure 8.7. Load-displacement response comparison for wall 504.

The comparison between test results and predicted values for wall 509 were similar to those for wall 502. No significant end rotational restraint was observed for this wall specimen during testing and it is not surprising that the test results related quite closely to those obtained from the

PANEL model with pinned supports. Beyond the initial non-linear range, the bending stiffnesses for both predictions corresponded well with the test results. For all these walls, the fixity of the foundation-supported end had no significant effect on the load-displacement curve.

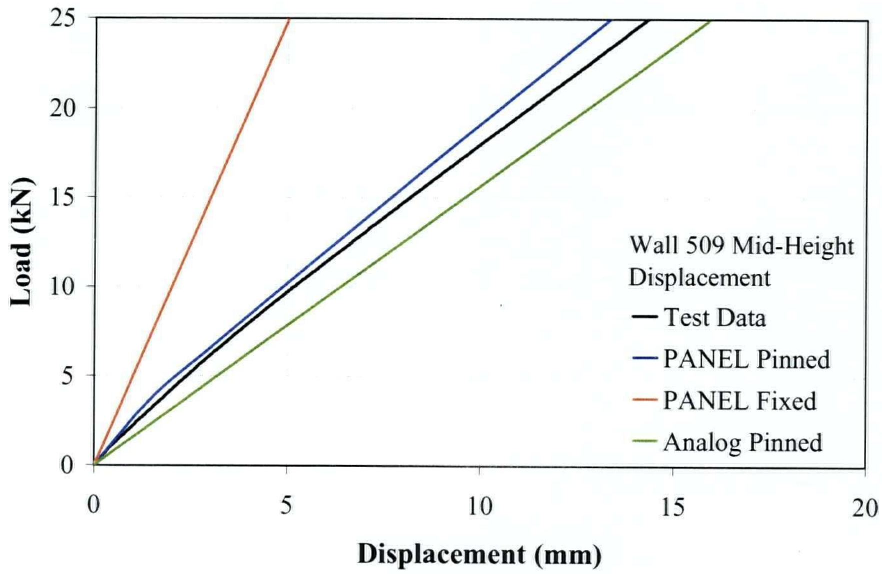

Figure 8.8. Load-displacement response comparison for wall 509.

A comparison between the bending stiffnesses determined from the slope of the transversal load-displacement curve for wall specimens tested at all six axial load levels, and the predicted values calculated using the beam-spring analog method, is presented in Table 8.1. Predictions for wall 511 were not included because the material properties of the non-structural gypsum wallboard sheathing, which was applied to the interior face of the wall specimen, were not obtained by testing. The transversal load range chosen for determining the bending stiffness was the same as that used for the full-scale wall tests, namely between 11.1 kN and 24.5 kN. The predicted values excluding and including the effects of the measured end rotational restraint stiffness are presented. The same rotational stiffness was used for all six axial load levels for a particular wall and was determined using the procedure described in Section 7.5.3.2. The predicted bending stiffnesses of each composite stud in the wall specimens are also presented. The effective

Table 8.1. Full-scale wall stiffness test values compared with linear beam-spring analog predictions.

Specimen Number/ Stud Numbers within Specimen	Predicted Effective Bending Stiffness of Composite Studs (Nmm^2)	Specimen Test Results			Prediction w/ Pin Ended Supports		Prediction w/ Rotational Spring Supports	
		Specimen Test Number	Axial Load (kN)	Bending Stiffness (11.1 - 24.5 kN) (N/mm)	Bending Stiffness (N/mm)	Percent Difference to Test Result	Bending Stiffness (N/mm)	Percent Difference to Test Result
501		01	0.0	1073	1056	-1.7	1083	0.9
SPF 01	5.203×10^{11}	02	24.5	1098	1084	-1.3	1112	1.3
SPF 12	3.185×10^{11}	03	-24.6	1037	1027	-1.0	1054	1.6
SPF 06	3.081×10^{11}	04	-49.0	1047	999	-4.6	1025	-2.1
SPF 14	5.650×10^{11}	05	-73.4	1034	971	-6.1	996	-3.7
SPF 08	5.295×10^{11}	06	-97.9	1006	942	-6.3	966	-3.9
502		01	0.0	964	1041	8.0	1041	8.0
SPF 02	4.058×10^{11}	02	24.5	1089	1069	-1.9	1069	-1.9
SPF 09	3.635×10^{11}	03	-24.5	1043	1012	-2.9	1012	-2.9
SPF 20	4.068×10^{11}	04	-48.9	1008	984	-2.4	984	-2.4
SPF 04	5.123×10^{11}	05	-73.4	996	956	-4.1	956	-4.1
SPF 05	5.216×10^{11}	06	-97.9	983	927	-5.7	927	-5.7
503		01	-0.1	1068	929	-13.0	1051	-1.6
SPF 25	3.312×10^{11}	02	24.4	1108	957	-13.7	1083	-2.3
SPF 26	4.056×10^{11}	03	-24.5	1049	900	-14.2	1019	-2.9
SPF 24	3.925×10^{11}	04	-49.0	1055	872	-17.3	987	-6.5
SPF 23	3.888×10^{11}	05	-73.4	1043	844	-19.1	955	-8.5
SPF 18	4.537×10^{11}	06	-98.0	1028	815	-20.7	922	-10.3
504		01	0.0	1755	1709	-2.6	1889	7.7
LSL 44	7.084×10^{11}	02	24.5	1831	1737	-5.1	1920	4.9
LSL 46	7.480×10^{11}	03	-24.5	1741	1680	-3.5	1858	6.7
LSL 45	7.525×10^{11}	04	-49.0	1700	1652	-2.8	1826	7.5
LSL 37	7.399×10^{11}	05	-73.5	1660	1624	-2.2	1795	8.1
LSL 41	6.793×10^{11}	06	-98.0	1622	1595	-1.7	1764	8.7
505		01	-0.1	1006	1003	-0.3	1115	10.9
LSL 51	7.138×10^{11}	02	24.5	1105	1031	-6.6	1147	3.8
LSL 48	7.110×10^{11}	03	-24.5	1057	975	-7.8	1084	2.6
LSL 47	7.048×10^{11}	04	-48.9	1018	946	-7.0	1052	3.4
		05	-73.4	984	918	-6.7	1021	3.7
		06	-97.9	955	890	-6.9	989	3.5
506		01	-0.1	874	887	1.5	961	9.9
LSL 17	6.371×10^{11}	02	24.5	850	916	7.8	991	16.7
LSL 16	6.431×10^{11}	03	-24.5	879	859	-2.3	930	5.8
LSL 18	6.040×10^{11}	04	-49.0	887	831	-6.4	899	1.3
		05	-73.4	878	802	-8.7	869	-1.1
		06	-97.9	868	774	-10.8	838	-3.4

Table 8.1 Continued. Full-scale wall stiffness test values compared with linear beam-spring analog predictions.

Specimen Number/ Stud Numbers within Specimen	Predicted Effective Bending Stiffness of Composite Studs (Nmm^2)	Specimen Test Results			Prediction w/ Pin Ended Supports		Prediction w/ Rotational Spring Supports	
		Specimen Test Number	Axial Load (kN)	Bending Stiffness (11.1 - 24.5 kN) (N/mm)	Bending Stiffness (N/mm)	Percent Difference to Test Result	Bending Stiffness (N/mm)	Percent Difference to Test Result
507		01	0.0	1548	1481	-4.3	1721	11.2
LSL 14	6.446E+11	02	22.3	1524	1507	-1.1	1751	14.9
LSL 13	6.222E+11	03	-97.7	1531	1368	-10.6	1590	3.9
LSL 04	6.364E+11	04	-73.4	1525	1396	-8.4	1622	6.4
LSL 06	5.974E+11	05	-49.0	1509	1425	-5.6	1655	9.7
LSL 05	6.449E+11	06	-24.5	1485	1453	-2.2	1688	13.7
508		01	0.0	1571	1611	2.5	1613	2.6
LSL 29	1.036E+12	02	24.5	1576	1639	4.0	1641	4.2
LSL 32	1.328E+12	03	-24.5	1584	1582	-0.1	1584	0.0
LSL 28	1.056E+12	04	-49.1	1580	1554	-1.7	1556	-1.5
		05	-73.5	1580	1525	-3.5	1527	-3.3
		06	-98.2	1544	1497	-3.1	1499	-3.0
509		01	0.1	1656	1627	-1.7	1627	-1.7
LSL 36	6.723E+11	02	24.5	1710	1656	-3.2	1656	-3.2
LSL 35	6.888E+11	03	-24.5	1653	1599	-3.3	1599	-3.3
LSL 33	7.406E+11	04	-48.9	1637	1570	-4.0	1570	-4.0
LSL 25	6.917E+11	05	-73.5	1628	1542	-5.3	1542	-5.3
LSL 27	6.615E+11	06	-98.0	1609	1514	-6.0	1514	-6.0
512		01	0.0	1488	1452	-2.4	1601	7.6
LSL 42	6.007E+11	02	24.6	1584	1480	-6.6	1632	3.0
LSL 43	6.460E+11	03	-24.5	1517	1424	-6.2	1569	3.4
LSL 52	5.937E+11	04	-49.0	1506	1395	-7.4	1538	2.1
LSL 50	6.163E+11	05	-73.4	1492	1367	-8.4	1507	1.0
LSL 49	6.264E+11	06	-97.9	1474	1339	-9.2	1476	0.1
513		01	0.0	962	1028	6.8	1171	21.7
LSL 42	7.165E+11	02	24.5	1101	1056	-4.1	1203	9.3
LSL 52	7.229E+11	03	-24.5	1042	999	-4.1	1139	9.3
LSL 49	7.425E+11	04	-49.0	1039	971	-6.5	1106	6.5
		05	-73.4	1033	942	-8.8	1074	4.0
		06	-97.9	1020	914	-10.4	1042	2.1
514		01	0.0	1137	1002	-11.9	1153	1.4
SPF 16	4.814E+11	02	24.5	1145	1030	-10.0	1186	3.6
SPF 17	4.264E+11	03	-24.5	1138	973	-14.5	1120	-1.6
SPF 22	4.796E+11	04	-49.1	1127	945	-16.2	1088	-3.5
SPF 19	3.324E+11	05	-73.6	1108	916	-17.3	1055	-4.8
SPF 15	4.070E+11	06	-98.0	1078	888	-17.6	1022	-5.1

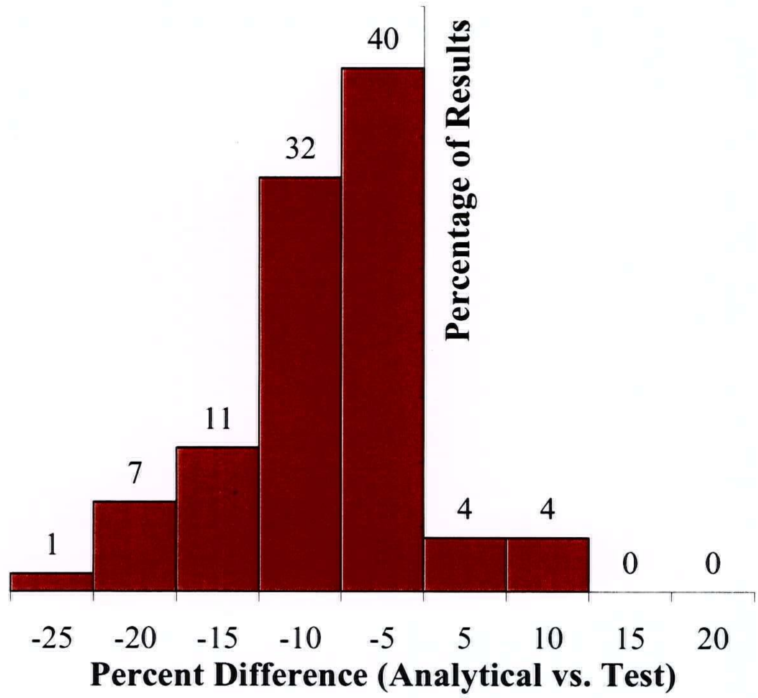

Figure 8.9. Histogram of analytical predictions versus test results for bending stiffness assuming pin ended supports.

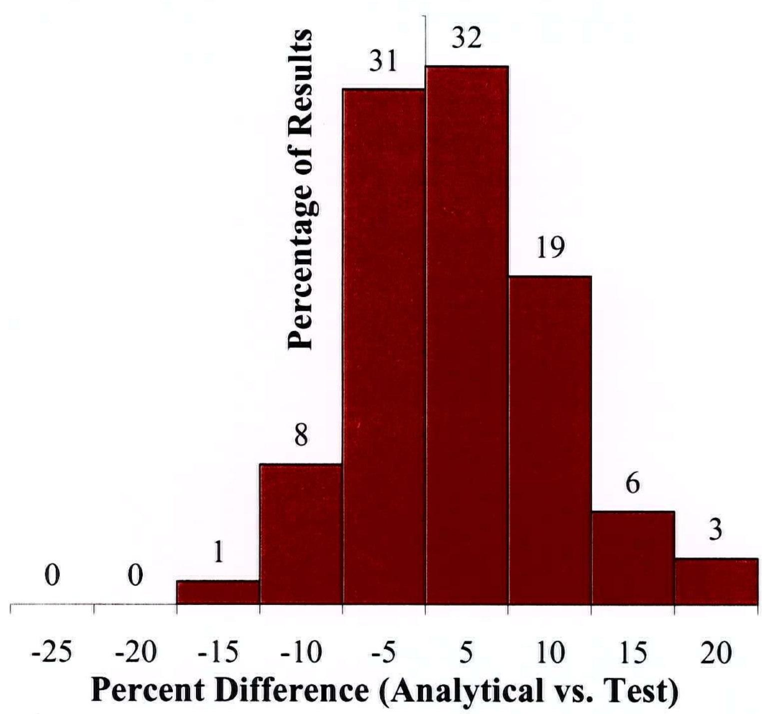

Figure 8.10. Histogram of analytical predictions versus test results for bending stiffness assuming one end of simply supported wall has a rotational spring.

stiffnesses for each composite stud in a wall are listed below the wall specimen number. Two histograms are shown in Figures 8.9 and 8.10 comparing the percent difference between bending stiffness values for the two prediction scenarios.

The histograms show that the predictions of bending stiffness were reasonably accurate for both assumed end support conditions. For the assumption of pinned supports at the foundation end (Figure 8.9) the predictions were conservative for the most part with 80% of the predictions falling within 10% of the results obtained from testing. The predictions that incorporated the end rotational restraint stiffness values (Figure 8.10) were unconservative for the most part but were more accurate with 90% of the predicted values falling within 10% of the test results.

8.3 SUMMARY

Analytical models to predict the load-displacement response of full-scale tall wood-frame walls under axial and transversal loads were presented in this chapter. Results were presented from a finite element computer program that accounted for the non-linear properties of the sheathing connectors and from a simpler beam-spring analog formulation that used a single linear connector stiffness value. Beyond the initial linear range both methods of prediction proved to be very accurate for the walls that were compared, while the finite element model also proved to be accurate in the initial non-linear range. The linear beam-spring analog method was compared to the results from most of the wall specimens that were tested in the full-scale wall testing program. The predicted values assuming that the foundation-supported end did not provide any rotational restraint were accurate and somewhat conservative. This method, which is simple enough to be used in engineering practice, is deemed to be sufficiently accurate for use in the design of tall wood-frame walls.

9. SUMMARY, CONCLUSIONS, AND RECOMMENDATIONS FOR FUTURE RESEARCH

9.1 SUMMARY

This thesis has addressed the structural performance of tall wood-frame walls under axial and transversal, or out-of-plane, loads. The background of this topic was discussed and the need for investigation of the behaviour of tall walls under axial and transversal loads was stressed. The topic was then addressed from several perspectives, using experimental and analytical studies. It can be stated that the objectives of this study were achieved and the study has yielded ample results, observations, comments, and design recommendations that can be very useful for engineering design practice and for code officials.

The main objectives in the first two experimental programs described were focused on characterising the lateral load-slip and withdrawal responses of connections between sheathing and studs in wood-frame walls using nails. The results obtained from these tests were necessary steps toward predicting the sectional properties of composite wood-frame structures under transversal loads that utilize engineered wood products and thick sheathing. Displacement controlled monotonic tests were conducted on several connections with four different stud materials, three different lengths of spiral nails, two different sheathing orientations, and five different thicknesses of two different types of sheathing. The four stud materials chosen were spruce-pine-fir No. 2 or better (SPF), laminated veneer lumber (LVL), laminated strand lumber (LSL), and SPF glued laminated lumber (glulam). The three nail lengths matched the particular sheathing thickness they were connecting to, so that an appropriate embedment length into the stud was maintained for each test. The sheathing material consisted of five thicknesses (9.5, 12.5, 15.5, 18.5, and 28.5 mm) of both Canadian softwood plywood (CSP) and oriented strandboard (OSB). The sheathing material was tested both parallel and perpendicular to the strong axis since sheathing in common construction practice can be installed with the strong axis being either vertical or horizontal. The tests revealed the load-displacement behaviour of connections with these different parameters.

In the third part of the experimental program, bending tests were performed on composite T-beams consisting of a 4,880 mm long stud and a 610 mm tributary width of sheathing. The components of the experimental test set-up were described and testing procedures were discussed. Two of the stud materials used in the connections test programs, SPF and LSL, were used in the T-beam test program. Three thicknesses of OSB sheathing (9.5, 15.5, and 28.5 mm) were used, oriented both parallel and perpendicular to the strong axis. Oversized OSB panels were employed to provide continuous sheathing over the entire length of some of the T-beam specimens. Glue was used to connect the sheathing to the studs in some of the T-beam specimens in addition to spiral nails of two different lengths. A total of twelve specimen group types were tested, eleven of which were tested monotonically. The other specimen group was tested under repeated increasing cycles of transversal load. Test data were used to determine the influence of the following parameters on the load-deformation characteristics of composite T-beams: stud material; sheathing thickness and orientation; sheathing-to-stud connection stiffness; the length between gaps in the sheathing; and monotonic and cyclic loading. In addition, test data were used for verification and calibration of analytical models to predict the composite properties and effective sheathing width of each T-beam. The analytical models incorporated the results of the lateral load-slip connection tests.

The fourth part of the experimental program consisted of lateral load tests on shearwalls with different OSB sheathing thicknesses and stud spacing. The purpose of the tests was to determine the buckling characteristics of the sheathing. To that end, displacement controlled monotonic pushover tests were conducted on three shearwalls with both thin and thick sheathing (9.5 mm and 18.5 mm), 610 mm and 1,220 mm stud spacing, and with varied sheathing connection stiffness. The framing members were all SPF studs and the sheathing material chosen for the testing was OSB. Each wall was initially tested with the sheathing panels connected to the wood frame with spiral nails and then a second test was conducted with the same sheathing panels connected to the frame with wood screws and washers. General trends on the occurrence of buckling and its effect on the lateral load carrying capacity of a shearwall were presented. A comparison with an analytical prediction for the buckling capacity of shearwalls was also made.

In the fifth, and final, experimental program, 4,880 mm tall by 2,440 mm wide full-scale wood-frame walls were tested under axial and transversal loads. Load controlled tests were conducted on thirteen walls with different: stud material and spacing; OSB sheathing thickness, orientation, and connection type; and stud connection type. One wall was tested with both exterior structural sheathing and interior gypsum wallboard sheathing. The stud materials used were SPF and LSL, spaced at either 610 mm or 1,220 mm on centre. The sheathing was connected to the studs with either spiral nails or with glue. Realistic end conditions were approximated and four different connection types were used to connect the studs and the end plates in two different connection configurations. The connections consisted of either off-the-shelf connector products or a specially fabricated connector similar to one used in a previously built tall wood-frame structure.

Test data were used to determine the influence of several aspects of tall wall construction on the load-deformation characteristics and ultimate load capacity of the full-scale specimens in both the axial and transversal directions. Constant axial load levels were applied to the wall specimens at the same time as several monotonic tests with linearly increasing transversal load. Several of the walls were inverted in the test frame and retested. Some of these walls were also loaded under axial tension only. The influence of the following on the transversal load-deflection response of the walls tested were investigated: stud material and spacing; OSB sheathing thickness, orientation, and connection type; axial load; direction of loading; non-structural sheathing; transverse, or in-plane, distributional effects; and end rotational restraint. The transversal load capacity and the influence of stud connection type on the axial tension capacity of the walls were discussed. In conjunction with all of the test programs described, additional tests were conducted to determine the material properties of stud and sheathing materials and spiral nails used.

In the final analytical part of the study, linear and non-linear analytical models to predict the load-displacement response of the tested full-scale walls were verified. Results were presented from a finite element computer program that accounted for the non-linear properties of the sheathing connectors and from a much simpler beam-spring analog formulation that used a single linear connector stiffness value. Comparisons between the non-linear finite element models were presented for three wall tests while a comparison for every full-scale wall test conducted was presented using the linear beam-spring analog model. The properties of the sheathing connectors were determined from the first two experimental programs described and from bending tests conducted on the individual spiral nails. The properties of each stud in the wall models and the sheathing material were determined from component tests conducted over the course of this study.

9.2 CONCLUSIONS AND DESIGN RECOMMENDATIONS

There have been several studies conducted over the past fifty years on the response of wood-frame floors under transversal loads, wood-frame walls under axial and transversal loads, and the composite components of both floors and walls. Those studies, however, have focused on diaphragms constructed in conventional ways with wall heights less than three metres, sawn lumber framing members spaced at a maximum of 610 mm on centre, and thin sheets of sheathing in standard sheet sizes. The results presented in this study are thus complementary to these previous studies and can in many ways be considered as an important research contribution to expand the application of composite wood-frame construction. The study has yielded extensive results and conclusions on parameters that influence the response of tall wood-frame walls under axial and transversal loads. These findings will be useful for design engineers and code officials by improving the understanding of the behaviour of these structures and in providing safe and economically competitive design alternatives to building owners. Some of the most important findings of the study are summarized as follows:

- The results of lateral load-slip nail connection tests have shown that having a connection with a high-density component, such as an engineered wood product stud, does not necessarily result in a stiffer or stronger connection. The mode of failure will usually find the weakest component of the system and therefore a further increase of the density of a stronger component in the connection does little to increase the overall strength of the connection. The strength of a connection was shown to increase significantly, however, when the failure mode was located in a dense stud or sheathing component or when the exchange of one component with a denser one moved the mode of failure to the other component. This was typically achieved by combining a dense stud with a dense sheathing material.

- Connections with LSL studs proved to be stronger on average than connections with the other stud materials as the LSL studs are much denser. The greatest average increase in connection strength that was achieved by changing one of its components, namely 86%, was by replacing an SPF stud with an LSL stud. Connections with the other three stud materials gave similar results, as the densities of these studs are similar, even though the manufacturing processes used to make them are not.

- The initial stiffness of the tested connections varied significantly between connection specimens, much more so than the ultimate strength. Connections consisting of LSL studs with OSB sheathing gave the highest values for initial stiffness.

- The results from nail withdrawal testing show that the response is related to the density of the stud material, the length of penetration, and the diameter of the nail, with the density of the stud being the most significant parameter. Once again, the highest withdrawal strength occurred in the connections with LSL studs since it was the densest stud material tested. The load-slip response of the sheathing and stud connections tested laterally were proportional to the withdrawal resistance of the nails in the studs, since withdrawal of the nail from the stud was the most common mode of failure.

- The variation of bending stiffness of the composite T-beams tested were found to be roughly equal to or lower than the coefficients of variation of the bending stiffness of the studs alone. The addition of the sheathing to the stud members did not increase the bending stiffness variability of the composite T-beam members, and in most cases reduced it significantly, compared to the bare studs.

- Testing has shown that the distance between the gaps in the sheathing had the greatest influence on the bending stiffness of the T-beam specimens tested under transversal loads. T-beam specimens that had continuous sheathing were significantly stiffer than those with at least one gap in the sheathing. The bending stiffness of tall wood-frame walls could therefore be increased significantly through the use of thick, oversized OSB sheathing products, which have become more widely available in recent years. Although the increase in stiffness of a composite stud member over the bare stud, due to changing the orientation of a standard 1,220 mm by 2,440 mm sheathing panel, was reported to be up to 30% in previous testing, it was not found to be significant for both the composite T-beams and tall wood-frame walls tested in this study. This is because the increase in stiffness is a function of the ratio of the distance between the gaps in the sheathing to the total height of the wall squared. For tall walls, the increase in this ratio due to changing the orientation of a standard sheathing panel is not as great as it is for a wall of regular height.

- The connection stiffness between the sheathing and the stud was also found to have a significant influence on the bending stiffness of the composite T-beam specimens tested, due to the incomplete composite interaction, or partial composite action, which exists between the sheathing and the framing members in wood-frame diaphragms. The incorporation of a method to account for the partial composite action into design standards would allow more cost-effective wall configurations to be selected. The majority of the analytical methods that are used to calculate composite action are based on the same assumptions and were found to give approximately the same results. Therefore, a simple approach was chosen to predict the results of the T-beams that were tested. This formulation included a method for predicting effective flange width based on structural mechanics. The predictions compared well with test results for specimens without gaps. A new length factor in the formulation of effective flange width, based on test results with glued connections, was determined to account for the effect of gaps in the sheathing. Using this new factor, the predicted stiffness values matched more closely with all T-beam test results.

- The sheathing in wood-frame diaphragms is connected to each framing member with a large number of nails, which results in significant load sharing among the fasteners. Therefore the average load-slip properties of the tested nailed connections, instead of a lower percentile value, were used in the analytical models to predict the response of the composite T-beams with nailed connections. The predictions using the average connection responses were found to be very conservative at low levels of transversal load, which can be attributed to the initial friction resistance between the sheathing and the stud. The model predictions were still conservative once the friction resistance was overcome. Only 20% of the predictions resulted in up to 10% larger bending stiffnesses than were obtained from tests.

- Despite the accurate comparisons between monotonically tested T-beams and analytical predictions, it is recognized that walls found in structures will undergo many loading cycles over the lifetime of a building. These cycles will most likely reduce the connection stiffness of mechanical fasteners and therefore the stiffness of the walls. Cyclic tests were thus conducted, which showed that the average bending stiffness of a composite T-beam can decrease by up to 25% after several cycles of increasing transversal load. The reduction in bending stiffness was found to vary linearly with the level of transversal load applied. In addition to loading cycles from external wind pressures, wood-frame walls may also undergo cyclic deformations due to changing moisture levels over time that can produce internal forces between the components of the composite structure. This can cause slippage between the sheathing and the studs and also lead to degradation in the overall bending stiffness of the system over time. A method to account for these reductions in connection stiffness must be developed before partial composite action can be incorporated into codified design.

- The creation of a T-beam by adding a flange to a stud will reduce the maximum bending stresses, but will also impart an additional tension stress over the depth of the stud as a result of the composite action. Therefore, each component of a composite beam must be designed as a member under combined axial and bending load using an interaction equation. Although the maximum stresses decrease, the stressed volume in tension of a composite T-beam was shown to increase as a result of composite action, thus negating the beneficial effect and potentially even increasing the probability of failure. It was found that the inclusion of partial composite action does not significantly affect the specified strength of composite T-beam members. The largest benefits are thus mainly limited to an increase in bending stiffness.

- The shearwalls that were tested under lateral in-plane loads with different sheathing thicknesses and stud spacing, but with the same sheathing-to-frame nailed connections and nail layout, were found to have approximately the same load-displacement responses. Thus, the response of shearwalls where the sheathing is connected to the frame with nails is directly related to the response of the nailed connections and is independent of the stud spacing. The responses of the shearwalls tested were found to become increasingly related to the properties of the sheathing as the stiffness of the connections between the sheathing and the frame increased.

- Buckling of the sheathing panels was measured in one of the shearwalls tested under lateral loads. The sheathing panels in that wall were connected to the frame with screws and washers, which provided very high connection stiffness to approximate near-rigid support conditions around the perimeter of each panel. The studs were spaced at 1,220 mm on centre. The lateral load-displacement response of the wall where the buckling of the sheathing was measured, was approximately equal to that of a wall with studs spaced at 610 mm on centre in which the sheathing did not buckle. Buckling of the sheathing panels of a shearwall under shear stresses did not constitute global failure of the shearwall. As a matter of fact, brittle failure of the frame was observed in two shearwalls where the sheathing was connected to the frame with screws and washers. In these cases the frame was not strong enough to resist the analytically predicted lateral load that would be required to induce buckling of the sheathing panels. The limit on the spacing of studs in a wood-frame shearwall specified in the Canadian Wood Design Manual, which is based on previous testing and analytical findings, and which is intended to prevent buckling of the sheathing as an ultimate mode of failure, was shown to not be applicable to the shearwalls that were tested in this study.

- The increase in stiffness of the composite walls over the bare studs, as determined from the load-displacement responses of the tests with axial and transversal loads, were found to match well with the results obtained from the composite T-beams tested. Wall specimens with studs spaced at 1220 mm on centre had greater increases in stiffness than were found in the T-beam tests due to the increased effective width of the sheathing.

- The linear load interaction equation specified in the Canadian Wood Design Code was found to be conservative when compared with the transversal stiffness test results of all of the full-scale walls for six different levels of axial load. The comparisons were found to be especially conservative at the higher axial compression load levels for stiffness predictions using both the code specified values of the studs only and with the composite stud members.

- The three wall specimens that were loaded in both transversal directions showed similar bending stiffness values in each direction, as theory would predict. The wall specimen tested with non-structural gypsum wallboard sheathing on the tension face did not have a significantly higher bending stiffness compared to a similar wall specimen without gypsum wallboard. The Canadian Wood Design Code prescribes that only the properties of the bare studs can be taken into account when determining transversal displacements of wood-frame walls with the implicit assumption that other factors such as composite action will reduce those displacements. The maximum transversal displacements achieved in testing on the composite full-scale tall walls tested, with and without non-structural sheathing, showed that the current transversal displacement criterion in the code of L/180 (the length of the wall divided by 180) is conservative and that the maximum allowable design displacements could be increased even if composite properties are included into design. The current criterion is intended to limit damage to the structure and to non-structural attachments. Transversal displacements of up to L/60 were measured in testing, however, without any observations of damage to the structural or non-structural components of the tall wood-frame walls.

- The system factor prescribed in the code, which takes account of the beneficial effect of load sharing in repetitive systems to reduce the likelihood of failure, has been examined in this study. For simple load sharing situations a modest 10% increase in characteristic bending strength is permitted for both sawn lumber and engineered wood product studs. In sheathed systems, such as walls and floors, a 40% benefit is gained, which also accounts for the composite action of the sheathing, and the transverse distribution properties of the sheathing and blocking. This implies, of course, that only the bare studs are accounted for when calculating the bending strength. Tests results show that the lower factor of 1.10, which is prescribed by the code if the composite properties of a system with sawn lumber studs are determined explicitly, may be overly conservative. Furthermore, the restriction of 610 mm maximum spacing of load sharing members may be too conservative, as considerable transverse load distribution occurred in the tested wall specimens with engineered wood product studs, blocked and spaced at 1,220 mm on centre. The transverse stiffness was measured for a number of walls and found to be significant enough to warrant some load sharing benefits in the design of such walls. For the wall specimens that were loaded to failure, the maximum loads achieved were considerably higher than the specified loads prescribed by the code, especially for the walls with studs spaced at 1,220 mm on centre. The inclusion of more comprehensive system factors for non-conventional systems such as these tall walls should be considered.

- Off-the-shelf connector products performed well in testing of full-scale walls under axial tension loads and proved to be a viable alternative to specially fabricated connectors that have been used in the past. Some caution is in order, however, since single tension ties, in combination with deep studs, were found to create significant eccentricity moments at the ends of the studs, which resulted in excessive rotations that led to wall failures. The frequency of tension ties was investigated and it was found that placing tension ties on every other stud did not result in undesirable secondary modes of failure, most probably due to the load distribution provided by the sheathing. The need for these tension ties, however, could also be eliminated by attaching joist hangers to the end plates with screws. A potentially brittle withdrawal mode of failure was avoided by forcing the weakest point of the connection away from the screws by assuring that the side nails would deform first.

- A realistic rigid foundation support was provided to the full-scale walls that were tested, which provided end rotational restraint that reduced transversal displacements in some of the walls. The amount of end rotational restraint varied greatly, as it was largely dependent on the extent of connection deformations, which in some cases ended up providing very little restraint, especially close to the failure point of the walls under transversal loads. Therefore, it is recommended here that the beneficial effect of end rotational restraint not be accounted for in design.

- Both of the analytical models that were used to predict the load-displacement response of full-scale tall wood-frame walls under combined axial and transversal loads proved to be very accurate, especially in the design load level range, where a linear elastic behaviour prevailed. The finite element model, which accounted for the non-linear properties of the sheathing connectors, gave a better overall response and proved to be accurate in the initial non-linear range as well. The predicted values, assuming no rotational restraint from the foundation-supported end, best represented test values, although they were slightly conservative. In the overall evaluation, considering effort and accuracy, the linear beam-spring analog method, which used a single linear connector stiffness value, is deemed to be sufficiently accurate and more user-friendly for use in the design of tall wood-frame walls.

9.3 RECOMMENDATIONS FOR FUTURE RESEARCH

During this study a large amount of valuable information was gathered on the behaviour of tall wood-frame walls. The results, however, have also shown the need for further research to investigate a number of outstanding topics pertaining to tall wood-frame walls. Some of the topics that research should be directed towards are as follows:

- This study has focused on the response of tall wood-frame walls under axial and transversal loads. The lateral and withdrawal loads applied to the connection specimens and the transversal loads applied to the composite T-beam and full-scale wall specimens represented the forces applied to a building by wind. Wind loading was considered as being quasi-static, as is commonly done in practice. Because of this assumption, most of the testing was conducted monotonically so that the loads were applied in one direction only and at rates slow enough so that the material strain rate effects would not influence the results. It could be argued that wind should be treated as a dynamic load condition and the effect of repeated loading needs closer investigation. In seismically active regions, the structure, and therefore the sheathing connections will be subjected to reversed cyclic loading due to earthquake motions. For these reasons, the cyclic response of laterally loaded sheathing-to-stud connections that utilize engineered wood products and thick sheathing is also needed.

- The use of oversized OSB sheathing panels has been shown to significantly increase the bending stiffness of tall wood-frame walls, to the extent that it becomes feasible to consider larger studs at wider spacing. The lateral load tests that were conducted on 2,440 mm tall walls with standard sheathing panel sizes showed that the limit on stud spacing in the Canadian Wood Design Code is not appropriate. Further research is needed, however, to understand the response of tall wood-frame walls with large stud spacing and oversized sheathing panels under in-plane lateral loads. The aspect ratio of the oversized sheathing panels may result in the response of tall shearwalls moving away from being shear dominated towards being dominated by bending of the panels.

- Increasing the stiffness of the connections between the sheathing and the studs has also been shown to be an effective means of increasing the bending stiffness of tall wood-frame walls. The greatest increase in bending stiffness in the composite T-beam and full-scale wall tests that were conducted was achieved by connecting the sheathing to the studs with glue in addition to spiral nails. The nails did not contribute to the connection stiffness until the glue bond had failed, which resulted in an abrupt decrease in stiffness. In addition, the stiffness of nailed connections alone was shown to increase when engineered wood products and longer nails were utilized. Brittle pull-through-the sheathing failure of the connections with dense engineered wood products and longer nails were far more likely than the more ductile mode of failure characterised by the sheathing and the nail pulling out of the stud, which is more commonly found with common lumber studs of lower density. When investigating the response of wood-frame walls under in-pane lateral loads due to earthquakes, connections that can maintain a high initial stiffness to limit drift under moderate loads, while achieving large yield displacements at high load levels, are ideal to provide ductility to absorb the seismic energy and prevent the structure from collapsing. For these reasons, further research is required to determine if the benefits gained from increased connection stiffness on the response of tall wood-frame walls under transversal loads are offset by reductions in ductility and energy absorption for the same walls when loaded laterally.

- It was shown that much more accurate analytical predictions were achieved with the incorporation of a new length factor into the formulations for effective flange width and partial composite action. The length factor was a function of the ratio between the length between the gaps in the sheathing and the total span length of a composite T-beam. A single relationship was proposed because approximately equal factors were determined at several ratios of gap-to-span length directly from tests conducted on composite T-beams with varied stud material and sheathing thickness. Further research is needed to determine if the length factor is applicable to all materials, composite member lengths, and composite cross-section types (I-beam and C-shape) and if the factor is a function of a greater number of parameters.

- The limited number of cyclic tests that were conducted on composite T-beams showed that many cycles of increasing transversal load decreased the bending stiffness of the beams. This was due to the degrading stiffness of the individual nailed connections between the sheathing and the studs along the length of the composite T-beam. In an actual structure, a wall will be loaded under numerous transversal wind loads that are smaller than the design event over the lifetime of the structure. In addition, wood-frame walls may also be exposed to changing moisture levels over time that can produce internal forces between the components of the composite structure. This could cause slippage between the sheathing and the studs and also lead to degradation in the overall bending stiffness of the system over time. To fully understand this phenomenon and to develop connection stiffness reduction factors for inclusion into design codes, several different connection specimens or composite members should be loaded with a protocol based on recorded wind speeds at numerous locations over the lifetime of a structure and exposed to varying moisture levels over an extended period of time.

- The transverse, or in-plane, load distribution effects of sheathing and blocking allow parallel members to provide mutual support in a structurally redundant system and thereby increase the capacity of the system beyond the predicted strength and stiffness of a single member alone. The lower system factor, $K_H = 1.10$, specified by the Canadian Wood Design Code when composite action is accounted for explicitly, may be too conservative and warrants further investigation. For the walls with engineered studs spaced at 1,220 mm on centre tested in this study, the average increase in stiffness over the predicted stiffness of the bare studs alone was approximately 30%. Significant stiffness in the transverse direction was measured for the one wall tested in this direction with studs spaced at 1,220 mm on centre. In addition, the two walls that had studs spaced at 1,220 mm on centre that were loaded to very high transversal loads had the highest overstrength ratios (7.28 and 8.04) of any of the walls tested. This contradicts the restriction in the code that states that diaphragms must have framing members spaced at a maximum of 610 mm on centre to include a system factor. Further research is therefore also required on the strength of walls with studs spaced greater than 610 mm on centre that have transverse load distribution elements, to determine if a system factor should be included in strength design calculations for these walls. It is recommended that a reliability study be conducted using a computer model on the ultimate strength of tall wood-frame walls in general with both sawn lumber and engineered wood product stud members.

- Because of the framing efficiencies gained through the use of engineered wood products, thick sheathing, and large stud spacing, the studs in tall wood-frame walls may be more susceptible to lateral-torsional buckling if they are not properly supported. A description of the discrepancies that currently exist in the published literature was presented. There is a need for further research into appropriate factors to account for lateral-torsional buckling in the design of tall wood-frame walls to address these discrepancies, which include: a universal definition of what constitutes structural sheathing to provide support to the compression edge of a stud; the use of buckling length coefficients in the design of tall walls; and if the lateral stability factors prescribed in the code for regular wood-frame walls are appropriate for tall walls..

- Off-the-shelf connectors were shown to resist the tension and shear loads in the studs of a tall wood-frame wall under axial and transversal loading. They proved to be cheaper and more easily installed than a specially fabricated connector that had been used in a previously built structure with tall wood-frame walls. In order to resist this combination of loads at each end of each stud, a joist hanger was paired with a stud tension tie or a joist hanger was connected to the end plates of a wall with screws. The current Canadian Wood Design Code does not provide design values for wood screws, however. Testing of full-scale tall walls has shown that using wood screws to fasten stud connectors to the end plates is a viable alternative to using tension ties and requires further research. The development of one stud connector that could resist both tension and shear loads and be easily installed with nails or wood screws would make tall wood-frame wall an even more economically competitive building alternative.

- Two of the full-scale walls that were tested under axial tension loading had tension ties on three out of the five studs in the wall. In this configuration the tension applied to the top plate of the wall was distributed to the studs that had tension ties by the end plates and by the sheathing. Undesirable modes of failure were not observed. This inexpensive method of resisting uplift forces may be an interesting alternative to hold downs, especially for long wood-frame walls where the overturning forces are relatively small.

In this case, tension ties designed to resist uplift forces due to wind suction may also be sufficient to resist the uplift forces due to overturning from seismic and wind loads. Further research is also needed on other suitable configurations for stud connectors to provide more economical construction solutions.

10. BIBLIOGRAPHY

AISI (2003). American Iron and Steel Institute website, http://www.steel.org.

Amana, E.J., and Booth, L.G. (1967). "Theoretical and experimental studies on nailed and glued plywood stressed-skin components: Part I. Theoretical study." *Journal of the Institute of Wood Science*, 4(1): 43-69.

Amana, E.J., and Booth, L.G. (1968). "Theoretical and experimental studies on nailed and glued plywood stressed-skin components: Part II. Experimental study." *Journal of the Institute of Wood Science*, 4(2): 19-34.

ASTM (1995). "Standard Test Method for Mechanical Fasteners in Wood – D 1761." *Annual Book of ASTM Standards,* American Society for Testing and Materials, 04(10).

Bessette, A. (1977). "An evaluation of elastomeric adhesive bonded design theory and the effect of panel gaps in T-beams." M.Sc. thesis, Washington State University, Pullman, WA.

Brooks, H. (1999). *The Tilt-Up Design and Construction Manual, Fifth Edition.* H.B.A. Publications, Newport Beach, CA.

Ceccotti, A. (2003). "Composite Structures." From: *Timber Engineering*, John Wiley & Sons Ltd., West Sussex, England, 409-427.

CEN (1995). *EN TC 124.117, European Committee for Standardization.* Timber structures test methods – cyclic testing of joints with mechanical fasteners, Comite' European de Normalisation, Brussels, Belgium.

Chui, Y.H., and Barclay, D.W. (1998). "Analysis of three-layer beams with non-identical layers and semi-rigid connections." *Canadian Journal of Civil Engineering*, NRC, 25: 271-276.

CMHC (1999). *Development of Generic Engineered Details for the Construction of Residential Tall Walls*, Canada Mortgage and Housing Corporation, Ottawa, ON.

CSA (2001). *Engineering Design in Wood (Limit States Design),* Canadian Standards Association CSA O86-01-2001, Etobicoke, ON.

CWC (1999). *Design and Costing Workbook*, Canadian Wood Council, Ottawa, ON.

CWC (2000). *Tall Walls Workbook*, Canadian Wood Council, Ottawa, ON.

CWC (2002). *Wood-Frame Housing – A North American Marvel*, Canadian Wood Council, Ottawa, ON.

FEMA (1997). *Windstorm Mitigation Manual for Light Frame Construction,* Federal Emergency Management Agency, Washington, DC.

Foschi, R.O. (1974). "Load-slip characteristics of nails." *Wood Science*, 7(1): 69-76.

Foschi, R.O. (1982). "Structural analysis of wood floor systems." *Journal of the Structural Division*, ASCE, 108(7): 1557-1574.

Foschi, R.O., Folz, B.R., and Yao, F.Z. (1989). "Reliability-based design of wood structures." Structural Research Series, Report No. 34, Department of Civil Engineering, University of British Columbia.

Foschi, R.O. (1989). "FAP: Floor analysis program." User's Manual Version 1.1, Department of Civil Engineering, University of British Columbia.

Foschi, R.O. (1993). "DAP: Diaphragm Analysis Program." Department of Civil Engineering, University of British Columbia.

Foschi, R.O. (1999). "PANEL: A general structural analysis for stressed-skin panels" and "SIP: A performance/reliability-based design for structural insulated panels." Foschi Engineering, Vancouver, BC.

Fragiacomo, M., and Ceccotti, A. (2004). "A simplified approach for long-term evaluation of timber-concrete composite beams." Proceedings of the World Conference on Timber Engineering, Lahti, Finland.

Gaston, C., Kozak, R., O'Conner, J. and Fell, D. (2001). *Potential for increased wood-use in North American non-residential markets.* Forintek Canada Corp., Vancouver, BC.

Girhammar, U.A., Bovim, N.I., and Kallsner, B. (2004). "Characteristics of sheahing-to-timber joints in wood shear walls." Proceedings of the World Conference on Timber Engineering, Lahti, Finland.

Girhammar, U.A., and Gopu, V.K.A. (1991). "Analysis of P-Δ effect in composite concrete/timber beam columns." *Structural Building Board*, Institute of Civil Engineers, 2(91): 39-54.

Girhammar, U.A., and Gopu, V.K.A. (1993). "Composite beam-columns with interlayer slip – exact analysis." *Journal of Structural Engineering*, ASCE, 119(4): 1265-1282.

Goodman, J.R., and Popov, E. (1968). "Layered beam systems with interlayer slip." *Journal of the Structural Division,* ASCE, 94(11): 2535-2547.

Goodman, J.R. (1969). "Layered wood systems with interlayer slip." *Wood Science*, 1(3): 148-158.

Granholm, H. (1949). "Om sammansatta balkar och pelare med sarskild hansyn till spikade trakonstruktioner (On composite beams and columns with particular regard to nailed timber structures)." *Chalmers Tekniska Hogskolas Handlingar,* No. 88.

Gromala, D.S. (1980). "Structural composite action in light-frame construction." Presentation at the International Union of Forest Research Organizations Conference, Oxford, England, Apr. 8-16.

Gromala, D.S. (1983). "Light-frame wall systems: performance and predictability." U.S. Department of Agriculture, Forest Service, Forest Products Laboratory Research Paper FPL 442, Madison, WI.

Gromala, D.S., and Polensek, A. (1984). "Light-frame wall research – axial and bending loads." *Housing Science*, 8(4): 383-393.

Hans, G.E., Galligan, W.L., Lehmann, W.F., Montrey, H.F., Moody, R.C., and Superfesky, M.J. (1977). "Five-year action plan for light-frame construction research." U.S. Department of Agriculture, Forest Service, Forest Products Laboratory Unnumbered Report, Madison, WI.

Hooley, R.F., and Madsen, B. (1964). "Lateral stability of glued laminated beams." *Journal of the Structural Division,* ASCE, 90(3): 201-218.

Hoyle, R.J. Jr. (1984). "Design of composite beams." *The Journal of Materials Education,* International Journal of Educational Modules for Material Science and Engineering, 6(6): 928-1026.

Itani, R.Y., and Brito, F.A. (1978). "Elastomeric bonded wood beams with transverse gaps." *Journal of the Structural Division,* ASCE, 104(10): 1595-1609.

Itani, R.Y. (1983). "Influence of sheathing gaps on wood floor systems." *Wood and Fiber Science*, 15(3): 190-202.

Jenkins, J.L., Polensek, A., and Bastendorff, K.M. (1979). "Stiffness of nailed wall joints under short and long term lateral loads." *Wood Science*, 11(3): 145-154.

Johns, K.C. (1991). "A continuous formula for timber columns." *Canadian Journal of Civil Engineering*, NRC, 18: 617-623.

Jurgen, E., Siebert, W., and Werner, H. (1990). "Nail and Nail Wire Bending Tests." Department of Timber Engineering, University Fridericiana Karlsruhe.

Kallsner, B. (1995). "Racking strength of wall diaphragms – discussion of the Eurocode 5 approach." CIB-W18/28-102-2, International Council for Building Research Studies and Documentation Working Commission W18 – Timber Structures, Copenhagen, Denmark.

Kasal, B., and Leichti, R.J. (1992). "Nonlinear finite-element model for light-frame stud walls." *Journal of Structural Engineering,* ASCE, 118(11): 3122-3134.

Kikuchi, S. (2000). "Effective width of stressed-skin panels." Proceedings of the World Conference on Timber Engineering, Whistler, BC.

Kreuzinger, H. (1995). "Mechanically jointed beams and columns." Lecture B-11, *Timber Engineering - STEP 1* Edited by H.J. Blass et. al., Structural Timber Education Programme, STEP/EUROFORTECH - funded under the EU Comett Programme, pp B11/1-8.

Kuenzi, E.W., and Wilkinson, T.L. (1971). "Composite beams – effect of adhesive or fastener rigidity." U.S. Department of Agriculture, Forest Service, Forest Products Laboratory Research Paper FPL 152, Madison, WI.

Liu, W-F., and Bulleit, W.M. (1995). "Overload behavior of sheathed lumber systems." *Journal of Structural Engineering*, ASCE, 121(7): 1110-1118.

McCutcheon, W.J. (1977). "Method for predicting the stiffness of wood-joist floor systems with partial composite action." U.S. Department of Agriculture, Forest Service, Forest Products Laboratory Research Paper FPL 289, Madison, WI.

McCutcheon, W.J. (1984). "Deflections of uniformly loaded floors: a beam-spring analog." U.S. Department of Agriculture, Forest Service, Forest Products Laboratory Research Paper FPL 449, Madison, WI.

McCutcheon, W.J. (1986). "Stiffness of framing members with partial composite action." *Journal of Structural Engineering*, ASCE, 112(7): 1623-1637.

McKeever, D. and Adair, C. (1998). "Wood products used in non-residential building construction." Wood Products Promotion Council (now called the Wood Products Council).

Newmark, N.M., Siess, C.P., and Viest, I.M. (1951). "Tests and Analysis of Composite Beams with Incomplete Interaction." Proceedings of the Society for Experimental Stress Analysis, 9(1): 75-92.

NBCC (1995). *National Building Code of Canada.* Canadian Commission on Building and Fire Codes, National Research Council of Canada.

NCMA (2003). National Concrete Association website, http://www.ncma.org.

Norris, C.B., Ericksen, W.S., and Kommers, W.J. (1952). "Flexural rigidity of a rectangular strip of sandwich construction – comparison between mathematical analysis and results of tests." U.S. Department of Agriculture, Forest Service, Forest Products Laboratory Research Paper FPL 1505A, Madison, WI.

Pellicane, P.J., and Robinson, G. (1997). "Effect of construction adhesive and joist variability on the deflection of light-frame floors." *Journal of Testing and Evaluation,* ASTM, 25(2): 163-173.

Pleshkov, P.F. (1952). *Teoriia rascheta dereviannyk sostavnnyhk sterzhnei (Theoretical studies of composite wood structures).* Moscow, 192 pp.

Polensek, A. (1975). "Finite element analysis for wood-stud walls under bending and compression loads." *Limited Distribution Report,* Forest Research Laboratory, Oregon State University, Corvallis, OR.

Polensek, A. (1976). "Rational design procedure for wood-stud walls under bending and compression loads." *Wood Science*, 9(1): 8-20.

Polensek, A. (1976b). "Finite element analysis of wood-stud walls." *Journal of the Structural Division*, ASCE, 102(7): 1317-1335.

Polensek, A. (1978). "Properties of components and joints for rational design procedure of wood-stud walls." *Wood Science*, 10(4): 167-175.

Polensek, A., and Atherton, G.H. (1976). "Compression-bending strength and stiffness of walls with utility grade studs." *Forest Products Journal*, 26(11): 17-25.

Polensek, A. (1982). "Effect of construction variables on performance of wood-stud walls." *Forest Products Journal*, 32(5): 37-41.

Polensek, A., and Gromala, D.S. (1979). "Wood-stud wall system: performance and probabilistic design for compression-bending loads." From: Behavior of Building Systems and Building Components, Vanderbilt University Department of Civil Engineering, Nashville, TN, 177-194.

Polensek, A., and Gromala, D.S. (1984). "Probability distributions for wood walls in bending." *Journal of Structural Engineering*, ASCE, 110(3): 619-636.

Polensek, A., and Kazic, M. (1991). "Reliability of nonlinear wood composites in bending." *Journal of Structural Engineering*, ASCE, 117(6): 1685-1702.

Polensek, A., and Schimel, B.D. (1986). "Rotational restraint of wood-stud wall supports." *Journal of Structural Engineering*, ASCE, 112(6): 1247-1262.

Raadschelders, J.G.M., and Blass, H.J. (1995). "Stressed skin panels." Lecture B-10, *Timber Engineering - STEP 1* Edited by H J Blass et al, Structural Timber Education Programme, STEP/EUROFORTECH - funded under the EU Comett Programme, pp B10/1-10.

Rosowsky, D., T.D. Reed, and K.G. Tyner (1998). "Establishing uplift design values for metal connectors in light-frame construction." *Journal of Testing and Evaluation,* ASTM, 26(4): 426-433.

Rosowsky, D., Schiff, S., Reinhold, T., Sparks, and P., Sill, B. (2000). "Experimental and analytical program: performance of light-frame wood structures under high wind loads." From: Wind Safety and Performance of Wood Buildings, Forest Products Society, Madison, WI, 67-83.

Ruhnke, J., and Schexnayder, F. (2002). "Description of tilt-up practice." *Practice Periodical on Structural Design and Construction.* 7(3): 103-110.

Sherwood, G., and Moody, R.C. (1989). "Light-frame wall and floor systems – analysis and performance." U.S. Department of Agriculture, Forest Service, Forest Products Laboratory General Technical Report FPL-GTR-59, 23-33.

Simpson Strong-Tie (2004). *Wood Construction Connectors: Canadian Limit States Design.* Simpson Strong-Tie Co., Dublin, CA.

Stefanescu, M., Foschi, R.O., Lam, F., Schiff, S.D., Rosowsky, D.V., Impson, D. and Twilley, R. (2000) "Testing of wood walls under combined vertical and out of plane (transverse) loading, and validation of the analysis program PANEL." Department of Civil Engineering and Department of Wood Science, University of British Columbia, Vancouver, B.C., and Department of Civil Engineering, Clemson University, Clemson, S.C.

Taylor, S.B. (2000). "Engineered wood building systems used in the construction of the Trus Joist Technology Center." Proceedings of the World Conference on Timber Engineering, Whistler, BC.

TCA (2003). Tilt-Up Concrete Association website, http://www.tilt-up.org.

Thompson, E.G., Goodman, J.R., and Vanderbilt, M.D. (1975). "Finite element analysis of layered wood systems." *Journal of the Structural Division,* ASCE, 101(12): 2659-2672.

Thompson, E.G., Vanderbilt, M.D., and Goodman, J.R. (1977). "FEAFLO: A program for the analysis of layered wood systems." *Computers and Structures,* Vol. 11: 237-248.

Tissell, J.R. (1990). "Structural panel shear walls." APA Research Report 154, Tacoma, WA.

Tremblay, G.A., Goodman, J.R., and Criswell, M.E. (1976). "Nonlinear analysis of layered T-beams with interlayer slip." *Wood Science*, 9(1): 21-30.

Trus Joist (2000). "TimberStrand LSL 1.5E Commercial Studs." Trus Joist, A Weyerhaeuser Business, Boise, ID.

Tucker, B.J. (1996). "Partial composite action and lateral distribution effects on wood-joist floor systems with various construction techniques." M.Sc. Thesis, Washington State University, Pullman, WA.

Kuhlmann, U., and Schanzlin, J. (2004). "Time dependent behaviour of timber-concrete-composite structures." Proceedings of the World Conference on Timber Engineering, Lahti, Finland.

USBC 2000. (2000). United States Bureau of the Census.

Wheat, D.L., Vanderbilt, M.D., and Goodman, J.R. (1983). "Wood floors with nonlinear nail stiffness." *Journal of Structural Engineering*, ASCE, 109(5): 1290-1302.

Wilson, E.L., and Habibulah, A. (2000). *SAP2000 Structural Analysis Users Manual*, Computers and Structures, Inc., Berkeley, CA.

WoodWorks (2003). WoodWorks website, http://www.wood-works.org.

Wolfe, R.W. (1990). "Performance of light-frame redundant assemblies," in: Proceedings of the 1990 International Timber Engineering Conference; Sugiyama, H. ed., Oct. 23-25, Tokyo, 1:124-131.

Yu, G. (2003). "Load sharing and system factors for light-frame wall systems." PhD Thesis, Oregon State University.

Zahn, J.J. (1984). "Bracing requirements for lateral stability." *Journal of Structural Engineering,* ASCE, 110(8): 1786-1802.

APPENDIX A: CONNECTION TEST RESULTS

The data presented in Chapters 3 and 4 are summaries of the complete connection load-displacement data collected during the course of this study. All of the load-displacement curves for the load-slip tests and for the nail withdrawal tests conducted will now be presented. The following abbreviations are used throughout:

CSP = Canadian Softwood Plywood,	LSL = Laminated Strand Lumber,
OSB = Orientated Strand Board,	Glulam = Glued Laminated Lumber,
SPF = Spruce-Pine-Fir,	PAR = Parallel,
LVL = Laminated Veneer Lumber,	PERP = Perpendicular,
AVG = Average,	STD = Standard Deviation.

Figure A.1 shows how the load-displacement results will be presented.

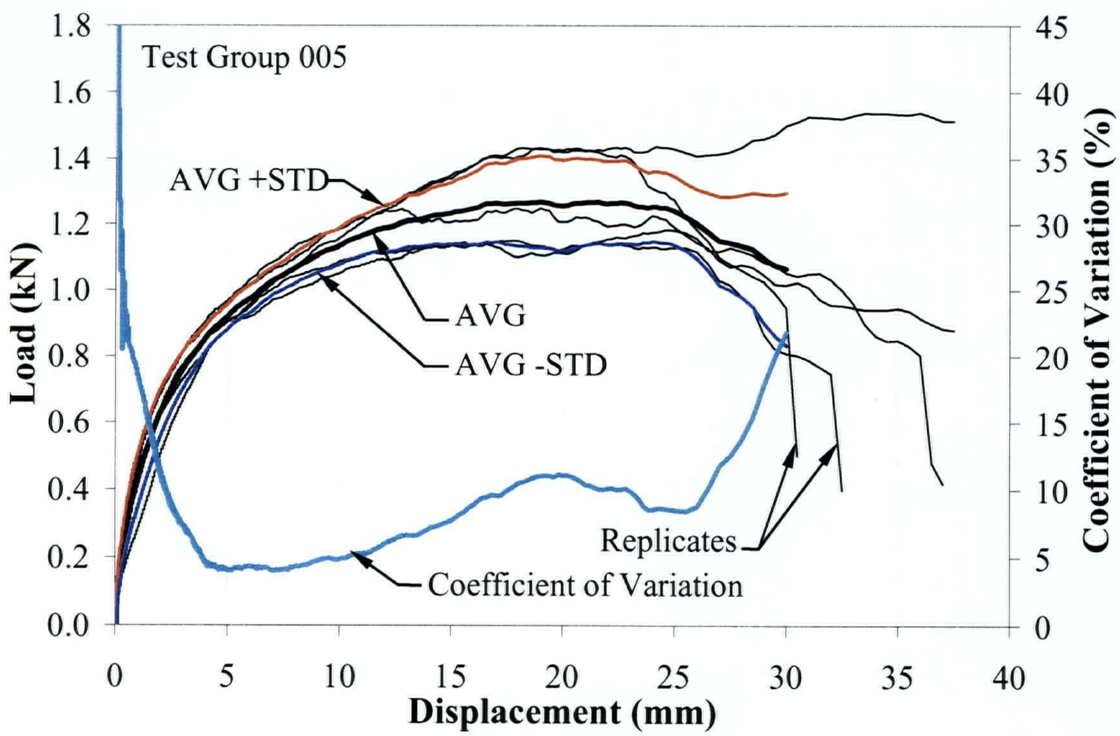

Figure A.1. Typical load-displacement results.

A.1 CONNECTION LOAD-SLIP TESTS

A summary of the connection load-slip test results is presented in Chapter 3. A schematic of the test set-up is shown in Figure 3.4. The relative density of each of the connection components is presented in Figure 3.5. The average properties of the spiral nails used are presented in Table 3.2 and Figure 3.8. Connection properties, as defined by the CEN protocol (CEN, 1995), are presented in tabular form. This protocol is described in detail in Section 2.7 of Chapter 2.

SPECIMEN GROUP 001

Description		Properties as defined by the CEN protocol	
Spiral nail length (mm)	65	Yield load F_y (kN)	0.781
Sheathing thickness (mm)	9.5	Yield displacement Δ_y (mm)	4.04
Sheathing material	CSP	Maximum load F_{max} (kN)	1.111
Sheathing orientation	PAR	Displacement at F_{max} (mm)	18.40
Stud material	SPF	Ultimate displacement Δ_u (mm)	24.20
Number of specimens	5	Initial stiffness (N/mm)	224
		Ductility (Δ_u/Δ_y)	5.99

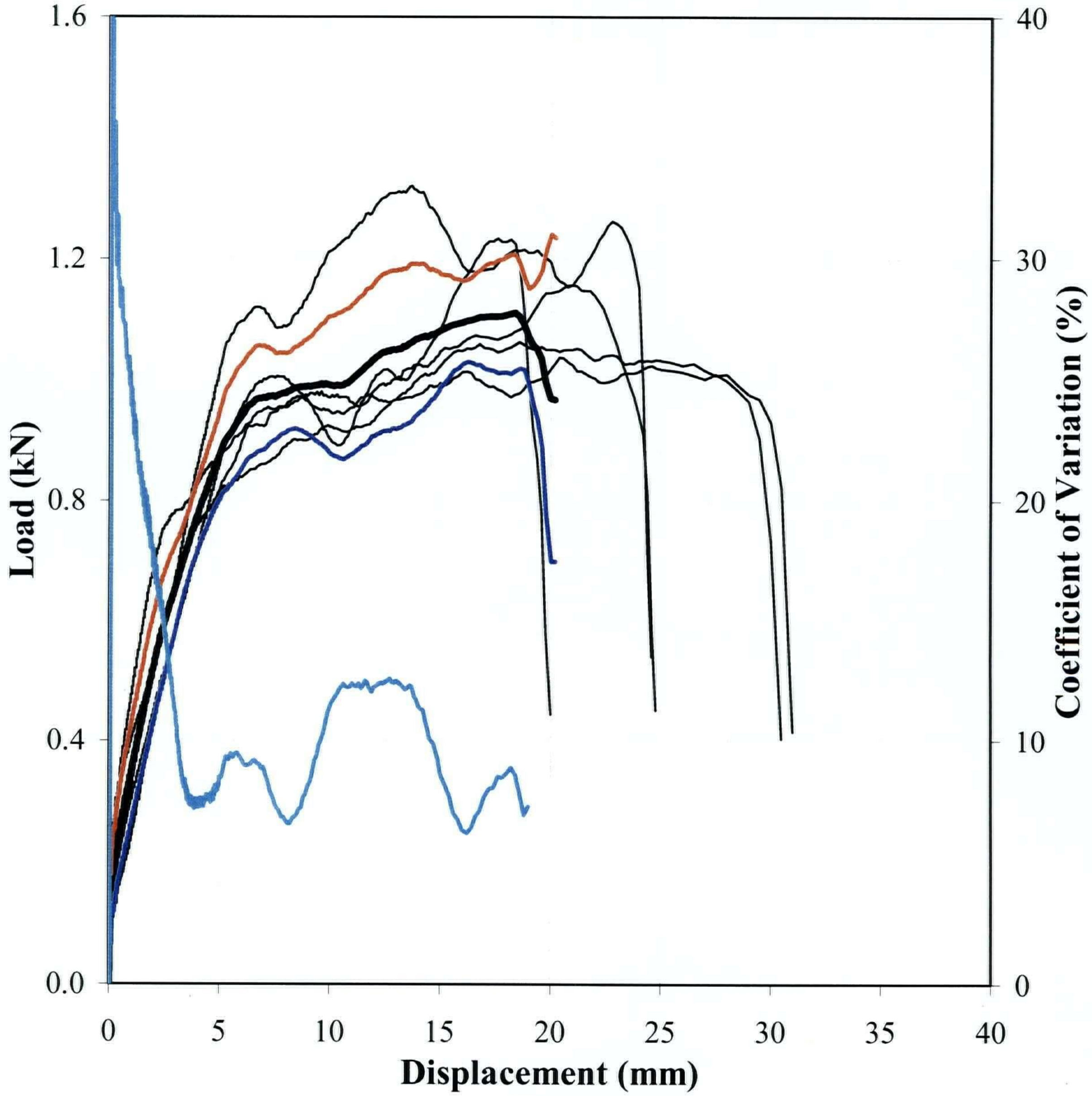

SPECIMEN GROUP 002

Description	
Spiral nail length (mm)	65
Sheathing thickness (mm)	15.5
Sheathing material	CSP
Sheathing orientation	PAR
Stud material	SPF
Number of specimens	5

Properties as defined by the CEN protocol	
Yield load F_y (kN)	0.714
Yield displacement Δ_y (mm)	3.48
Maximum load F_{max} (kN)	1.270
Displacement at F_{max} (mm)	27.00
Ultimate displacement Δ_u (mm)	30.50
Initial stiffness (N/mm)	225
Ductility (Δ_u/Δ_y)	8.76

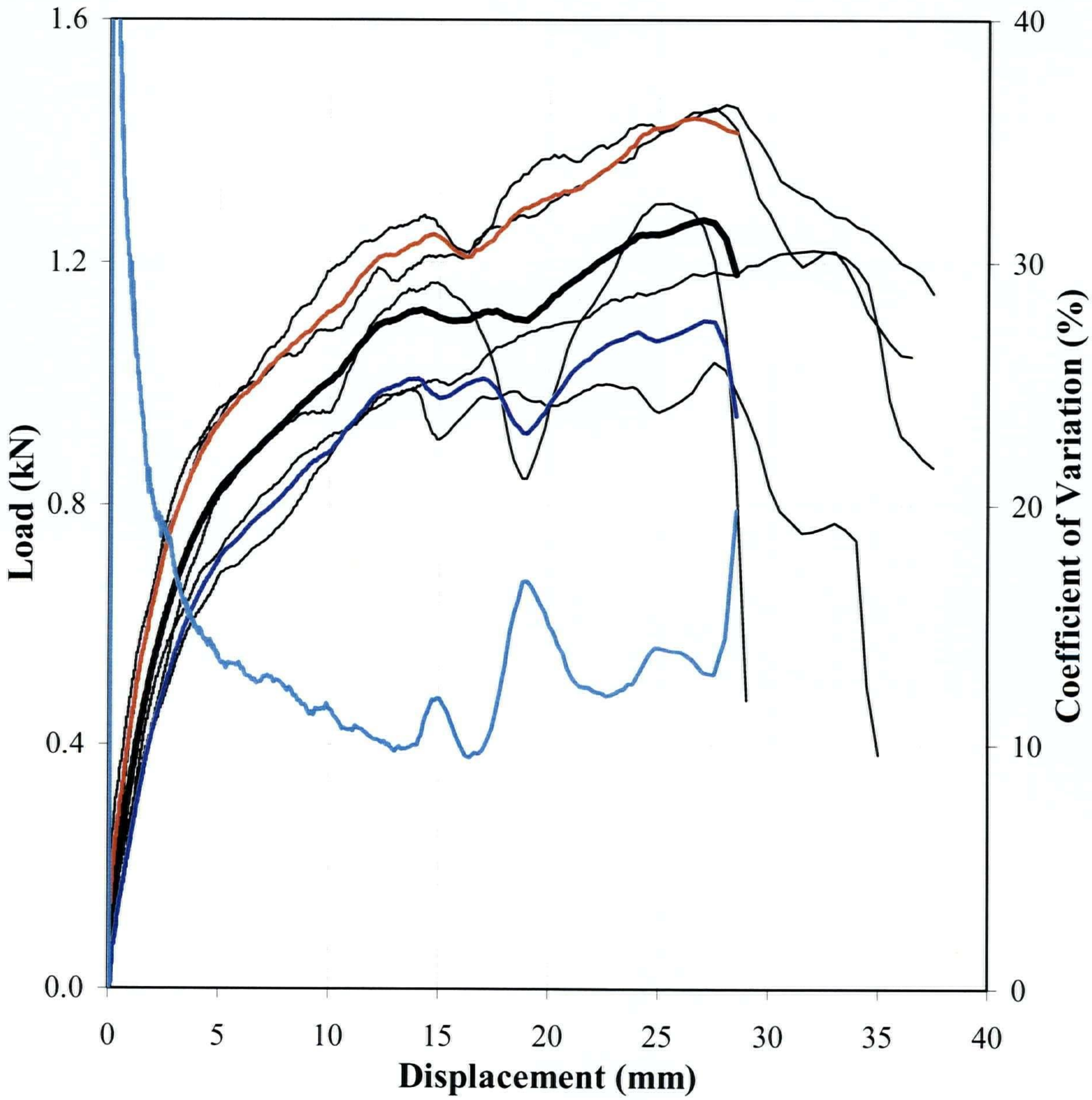

SPECIMEN GROUP 003

Description		Properties as defined by the CEN protocol	
Spiral nail length (mm)	65	Yield load F_y (kN)	0.619
Sheathing thickness (mm)	18.5	Yield displacement Δ_y (mm)	1.64
Sheathing material	CSP	Maximum load F_{max} (kN)	1.238
Sheathing orientation	PAR	Displacement at F_{max} (mm)	19.40
Stud material	SPF	Ultimate displacement Δ_u (mm)	28.00
Number of specimens	5	Initial stiffness (N/mm)	389
		Ductility (Δ_u/Δ_y)	17.07

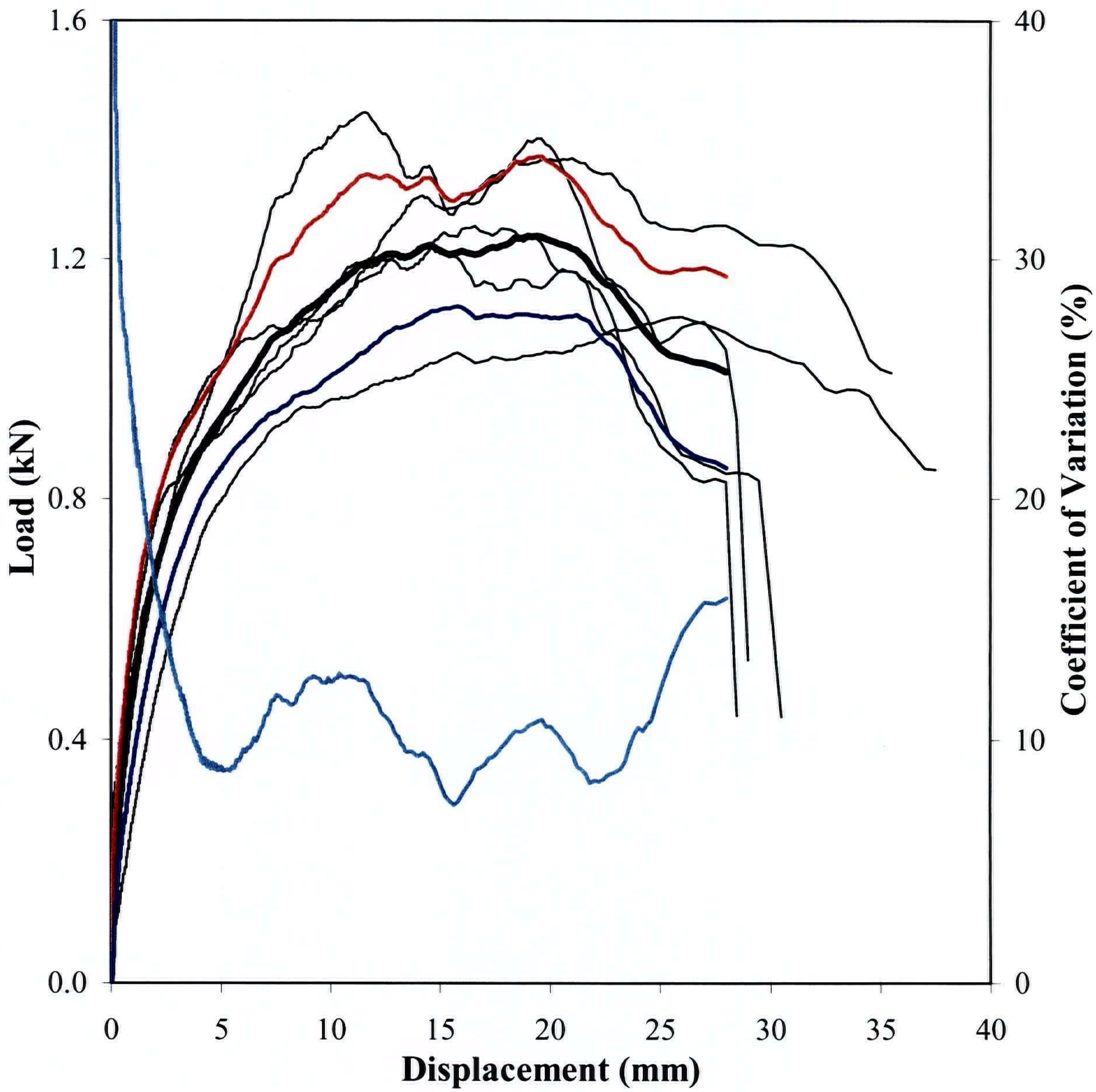

SPECIMEN GROUP 004

Description		Properties as defined by the CEN protocol	
Spiral nail length (mm)	65	Yield load F_y (kN)	0.745
Sheathing thickness (mm)	9.5	Yield displacement Δ_y (mm)	2.10
Sheathing material	OSB	Maximum load F_{max} (kN)	1.403
Sheathing orientation	PAR	Displacement at F_{max} (mm)	15.00
Stud material	SPF	Ultimate displacement Δ_u (mm)	24.40
Number of specimens	5	Initial stiffness (N/mm)	361
		Ductility (Δ_u/Δ_y)	11.62

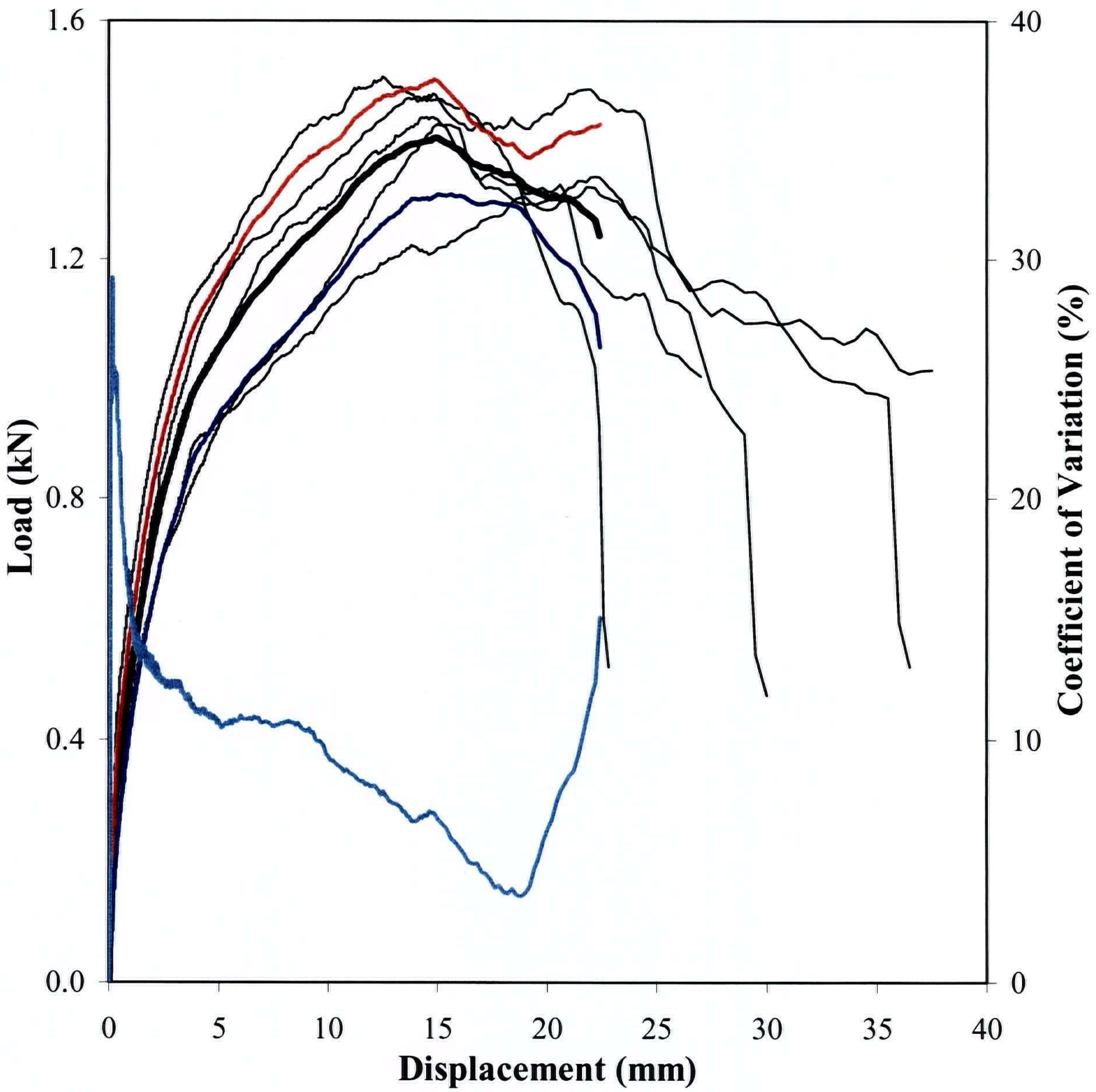

SPECIMEN GROUP 005

Description		Properties as defined by the CEN protocol	
Spiral nail length (mm)	65	Yield load F_y (kN)	0.672
Sheathing thickness (mm)	15.5	Yield displacement Δ_y (mm)	2.30
Sheathing material	OSB	Maximum load F_{max} (kN)	1.270
Sheathing orientation	PAR	Displacement at F_{max} (mm)	19.00
Stud material	SPF	Ultimate displacement Δ_u (mm)	30.50
Number of specimens	5	Initial stiffness (N/mm)	300
		Ductility (Δ_u/Δ_y)	13.62

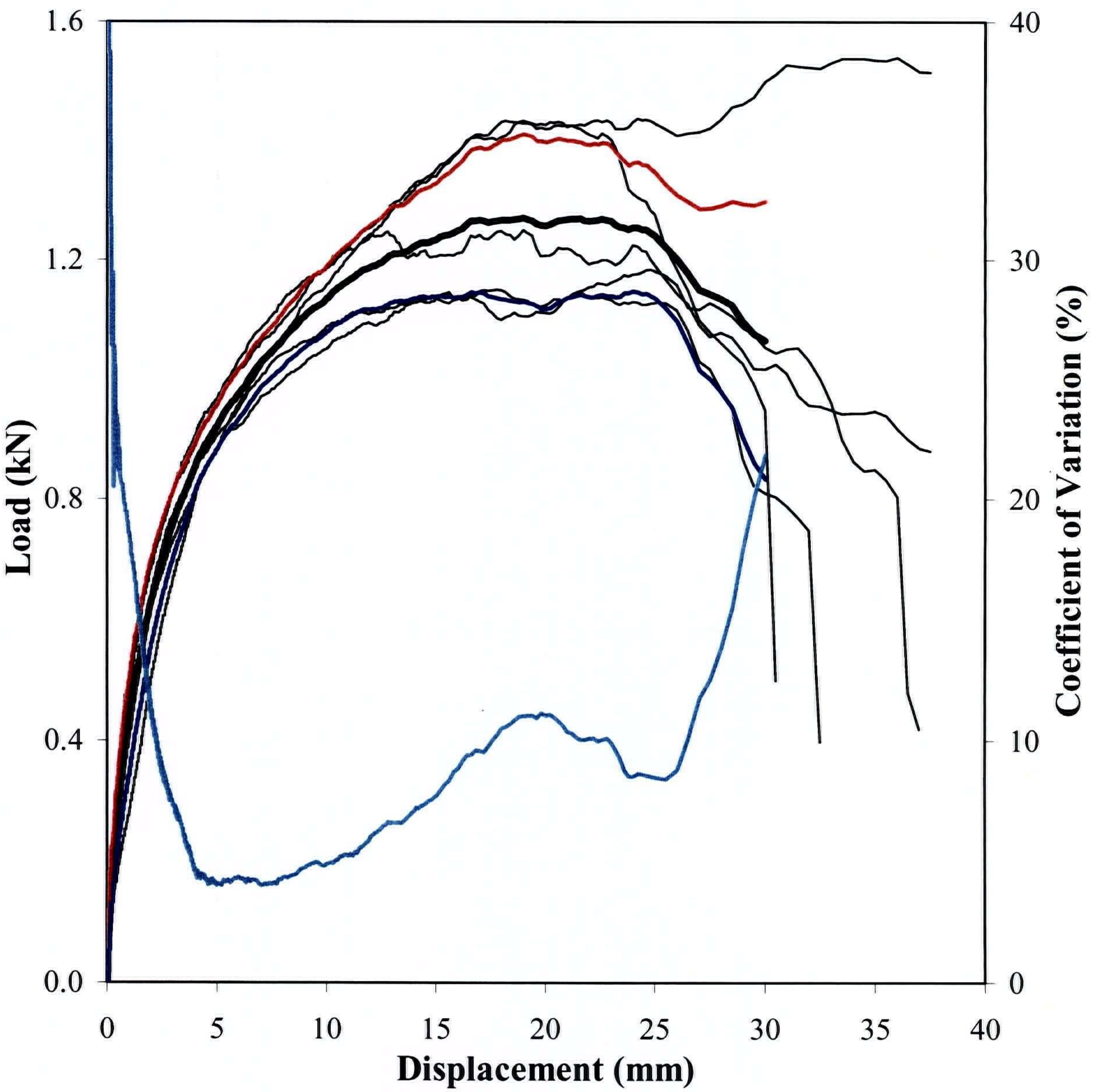

SPECIMEN GROUP 006

Description		Properties as defined by the CEN protocol	
Spiral nail length (mm)	65	Yield load F_y (kN)	0.601
Sheathing thickness (mm)	18.5	Yield displacement Δ_y (mm)	1.72
Sheathing material	OSB	Maximum load F_{max} (kN)	1.169
Sheathing orientation	PAR	Displacement at F_{max} (mm)	20.60
Stud material	SPF	Ultimate displacement Δ_u (mm)	31.00
Number of specimens	6	Initial stiffness (N/mm)	369
		Ductility (Δ_u/Δ_y)	18.02

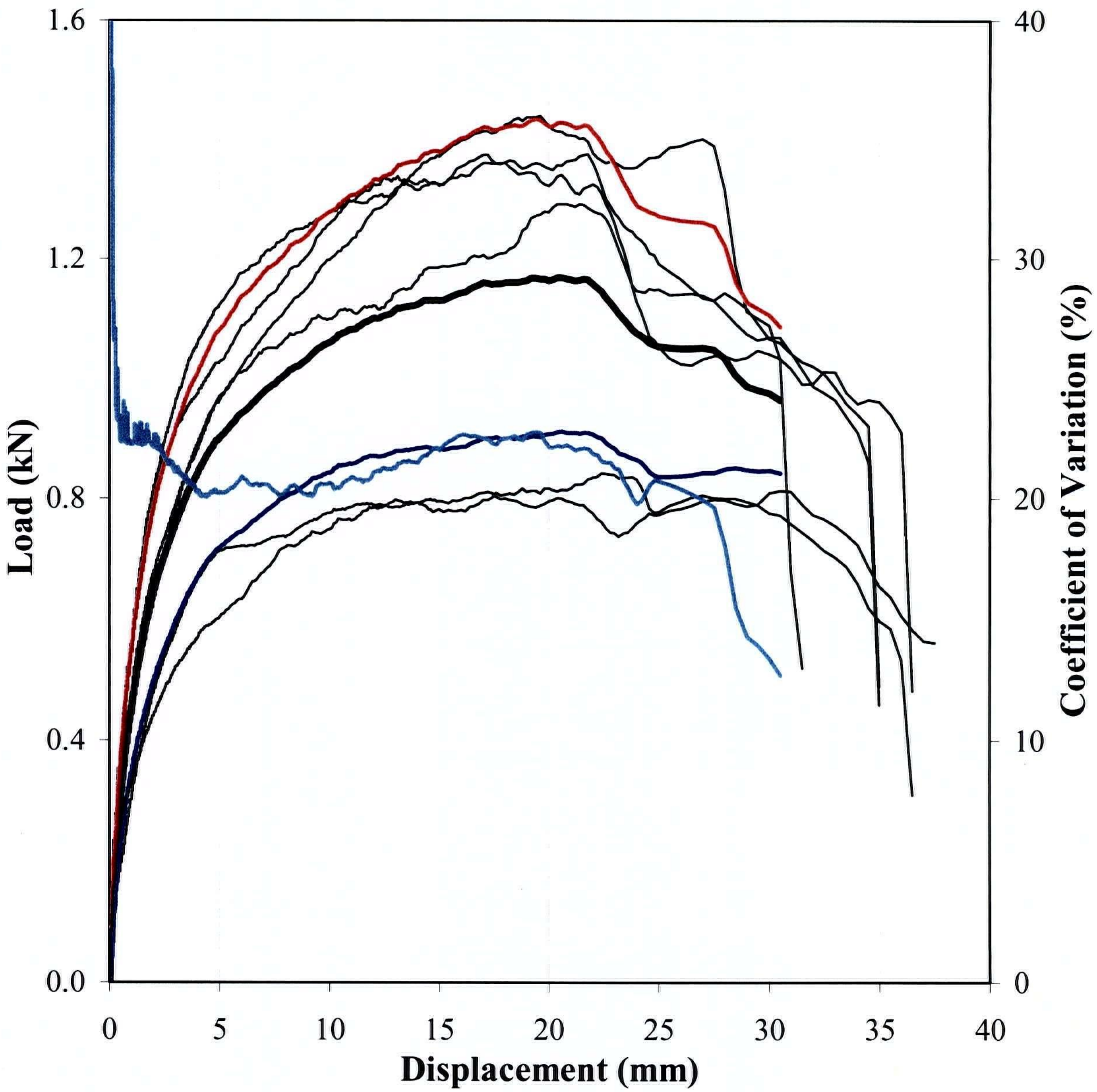

SPECIMEN GROUP 007

Description		Properties as defined by the CEN protocol	
Spiral nail length (mm)	65	Yield load F_y (kN)	0.643
Sheathing thickness (mm)	9.5	Yield displacement Δ_y (mm)	3.14
Sheathing material	CSP	Maximum load F_{max} (kN)	1.165
Sheathing orientation	PERP	Displacement at F_{max} (mm)	14.60
Stud material	SPF	Ultimate displacement Δ_u (mm)	18.40
Number of specimens	5	Initial stiffness (N/mm)	232
		Ductility (Δ_u/Δ_y)	5.86

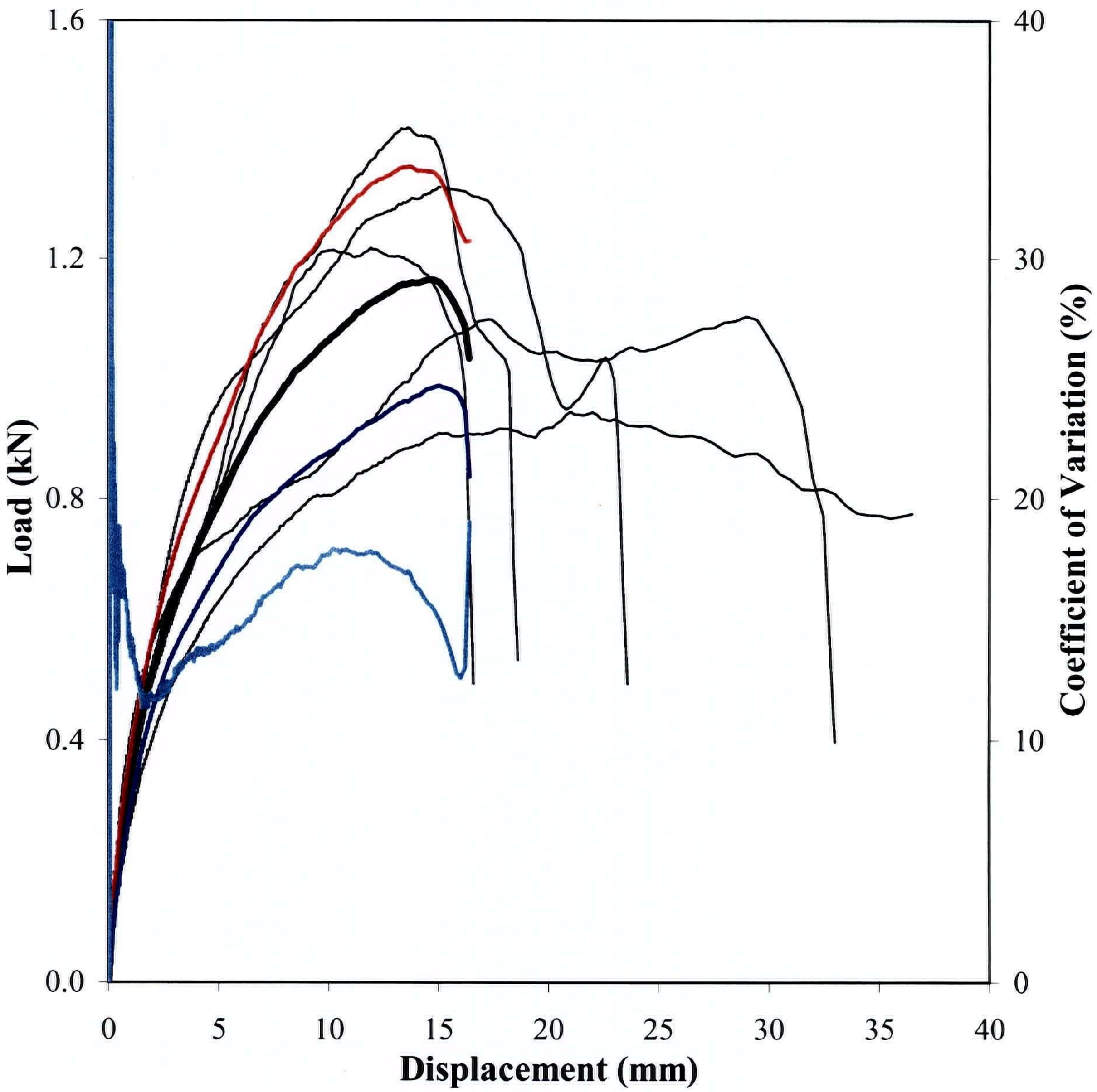

SPECIMEN GROUP 008

Description		Properties as defined by the CEN protocol	
Spiral nail length (mm)	65	Yield load F_y (kN)	0.545
Sheathing thickness (mm)	15.5	Yield displacement Δ_y (mm)	2.70
Sheathing material	CSP	Maximum load F_{max} (kN)	1.063
Sheathing orientation	PERP	Displacement at F_{max} (mm)	18.60
Stud material	SPF	Ultimate displacement Δ_u (mm)	33.00
Number of specimens	5	Initial stiffness (N/mm)	229
		Ductility (Δ_u/Δ_y)	12.22

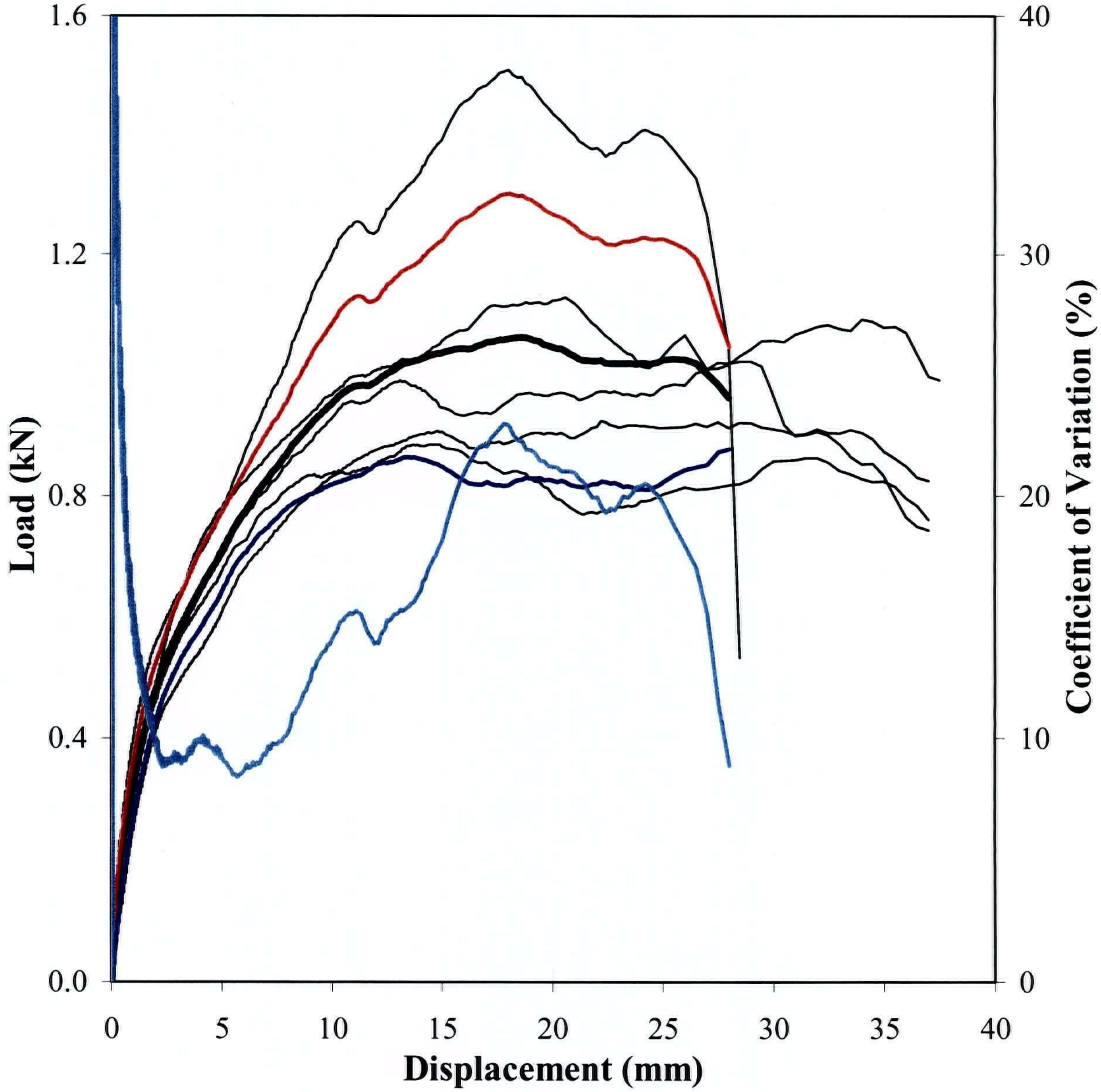

SPECIMEN GROUP 009

Description		**Properties as defined by the CEN protocol**	
Spiral nail length (mm)	65	Yield load F_y (kN)	0.578
Sheathing thickness (mm)	18.5	Yield displacement Δ_y (mm)	2.72
Sheathing material	CSP	Maximum load F_{max} (kN)	1.108
Sheathing orientation	PERP	Displacement at F_{max} (mm)	21.80
Stud material	SPF	Ultimate displacement Δ_u (mm)	35.00
Number of specimens	5	Initial stiffness (N/mm)	235
		Ductility (Δ_u/Δ_y)	12.87

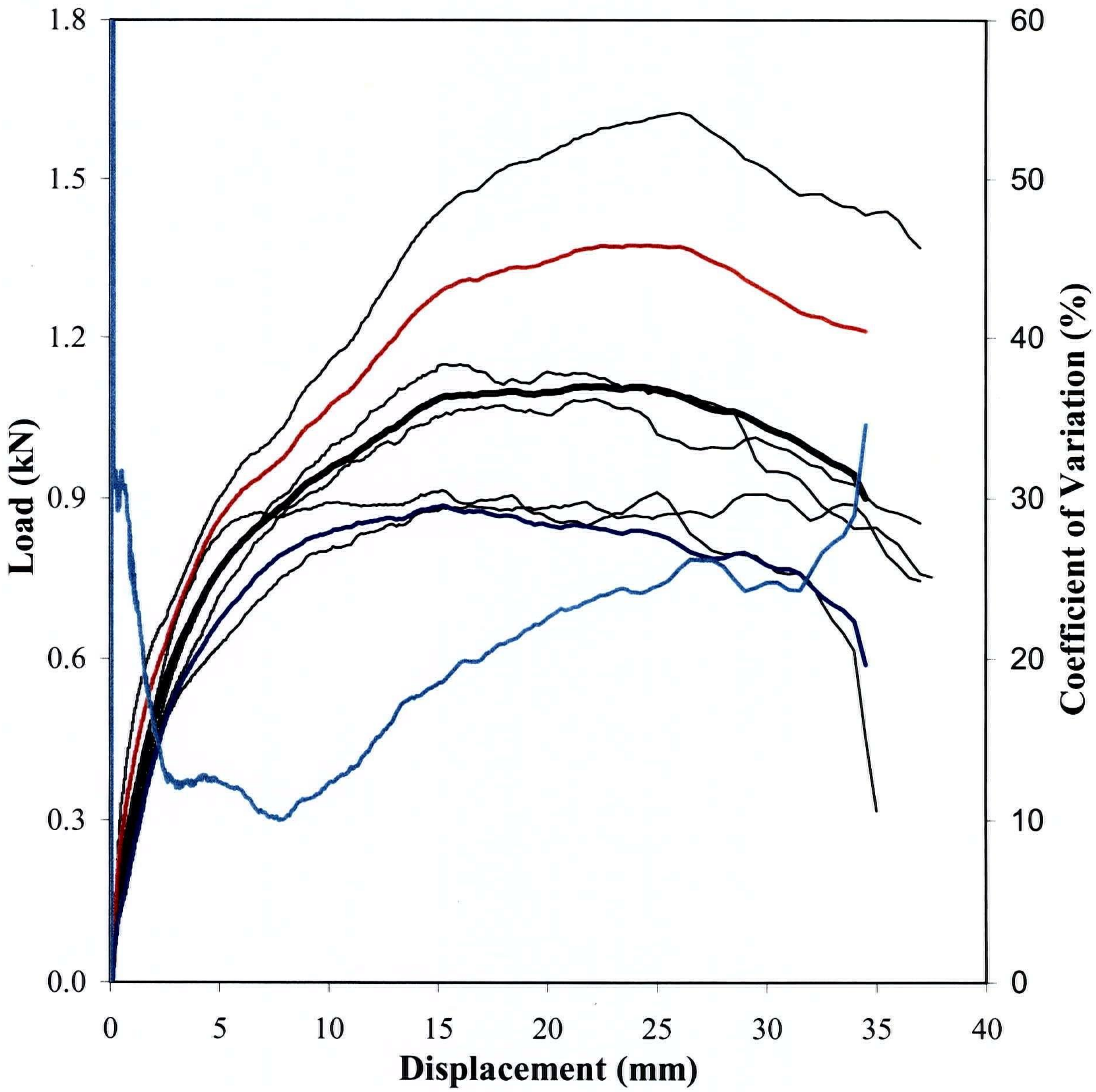

SPECIMEN GROUP 010

Description		Properties as defined by the CEN protocol	
Spiral nail length (mm)	65	Yield load F_y (kN)	0.686
Sheathing thickness (mm)	9.5	Yield displacement Δ_y (mm)	2.62
Sheathing material	OSB	Maximum load F_{max} (kN)	1.165
Sheathing orientation	PERP	Displacement at F_{max} (mm)	12.10
Stud material	SPF	Ultimate displacement Δ_u (mm)	23.60
Number of specimens	5	Initial stiffness (N/mm)	287
		Ductility (Δ_u/Δ_y)	9.01

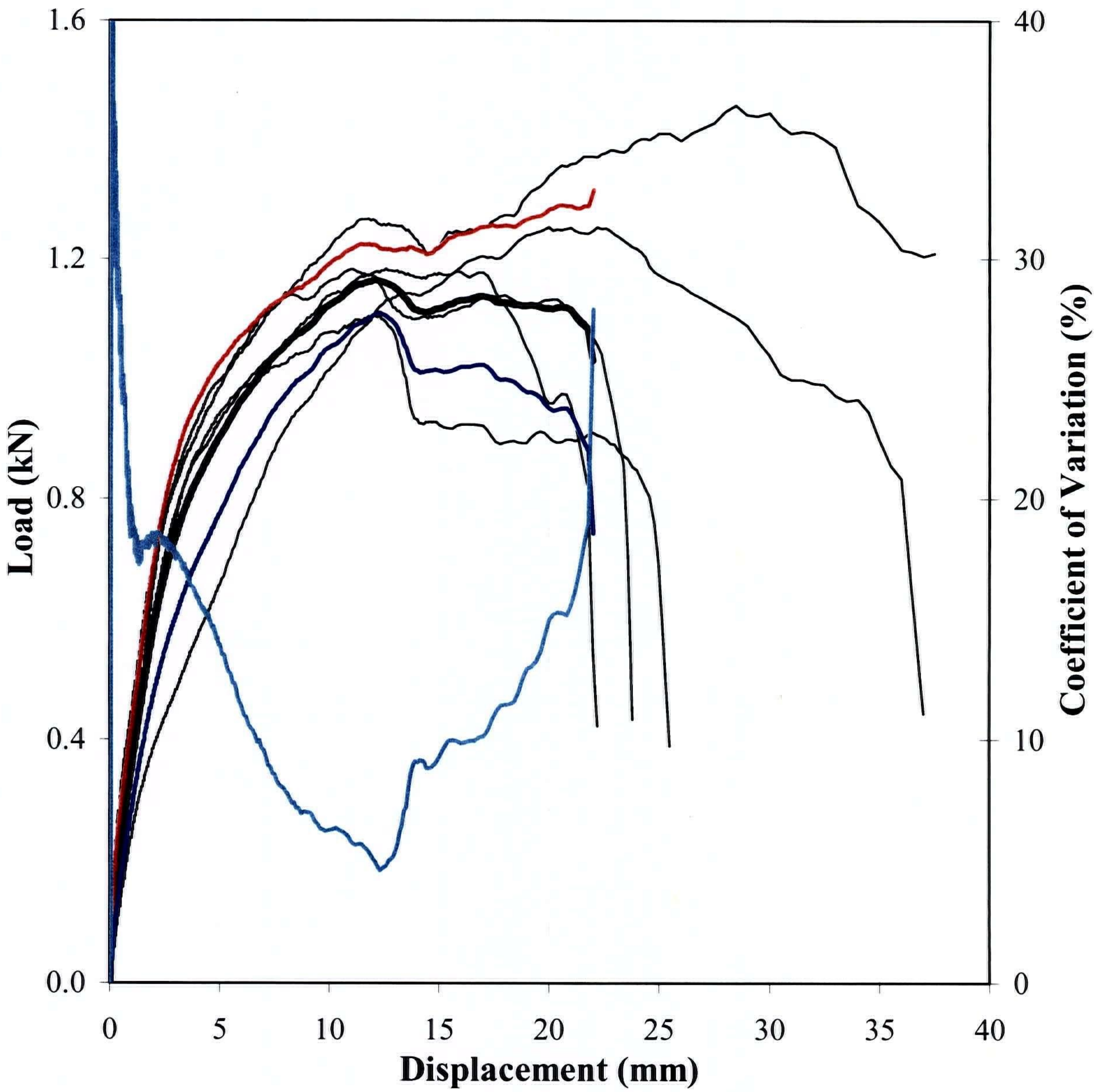

SPECIMEN GROUP 011

Description		**Properties as defined by the CEN protocol**	
Spiral nail length (mm)	65	Yield load F_y (kN)	0.623
Sheathing thickness (mm)	15.5	Yield displacement Δ_y (mm)	1.48
Sheathing material	OSB	Maximum load F_{max} (kN)	1.248
Sheathing orientation	PERP	Displacement at F_{max} (mm)	16.40
Stud material	SPF	Ultimate displacement Δ_u (mm)	26.00
Number of specimens	6	Initial stiffness (N/mm)	475
		Ductility (Δ_u/Δ_y)	17.57

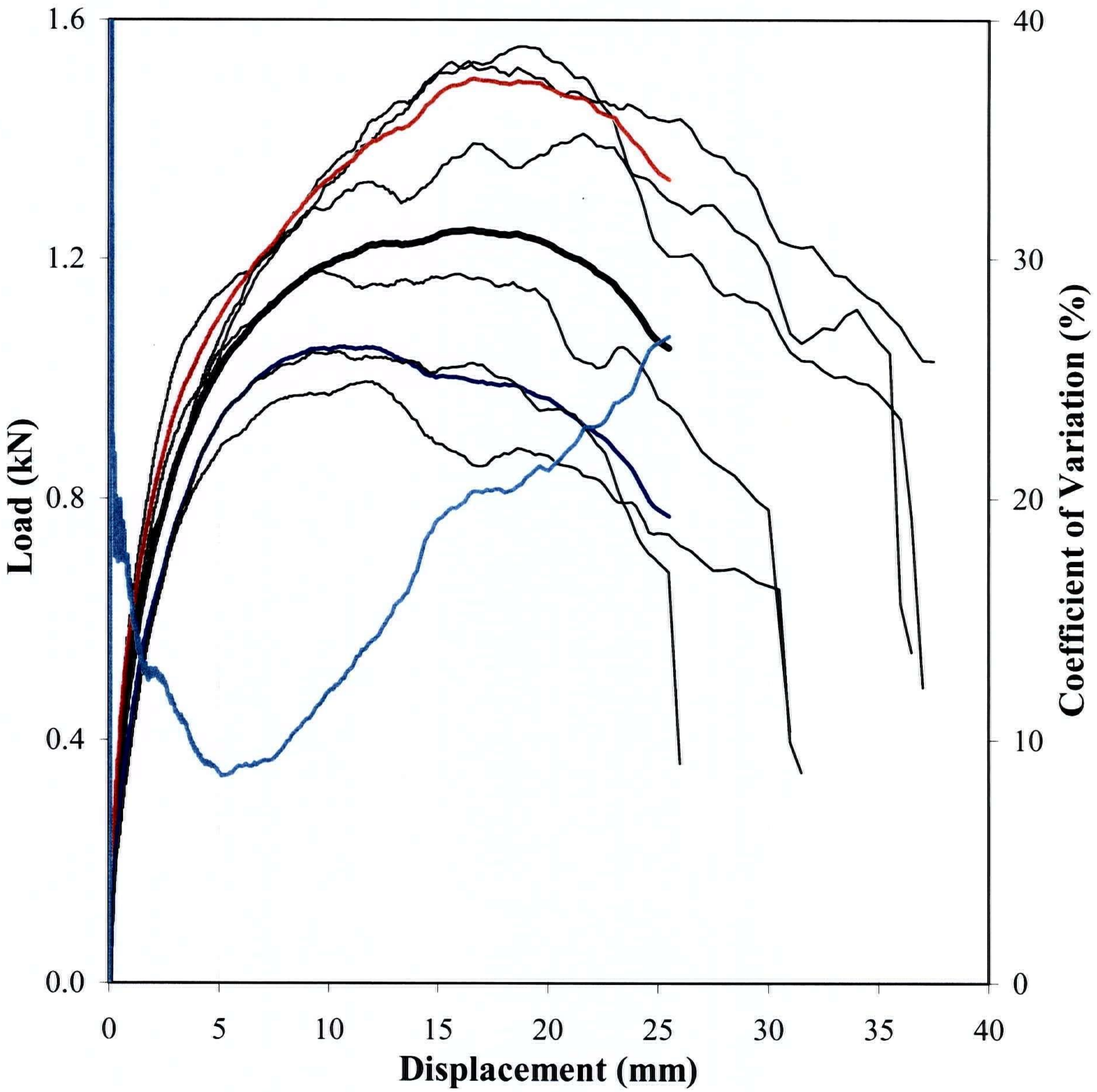

SPECIMEN GROUP 012

Description		Properties as defined by the CEN protocol	
Spiral nail length (mm)	65	Yield load F_y (kN)	0.526
Sheathing thickness (mm)	18.5	Yield displacement Δ_y (mm)	1.06
Sheathing material	OSB	Maximum load F_{max} (kN)	1.044
Sheathing orientation	PERP	Displacement at F_{max} (mm)	15.80
Stud material	SPF	Ultimate displacement Δ_u (mm)	26.00
Number of specimens	5	Initial stiffness (N/mm)	567
		Ductility (Δ_u/Δ_y)	24.53

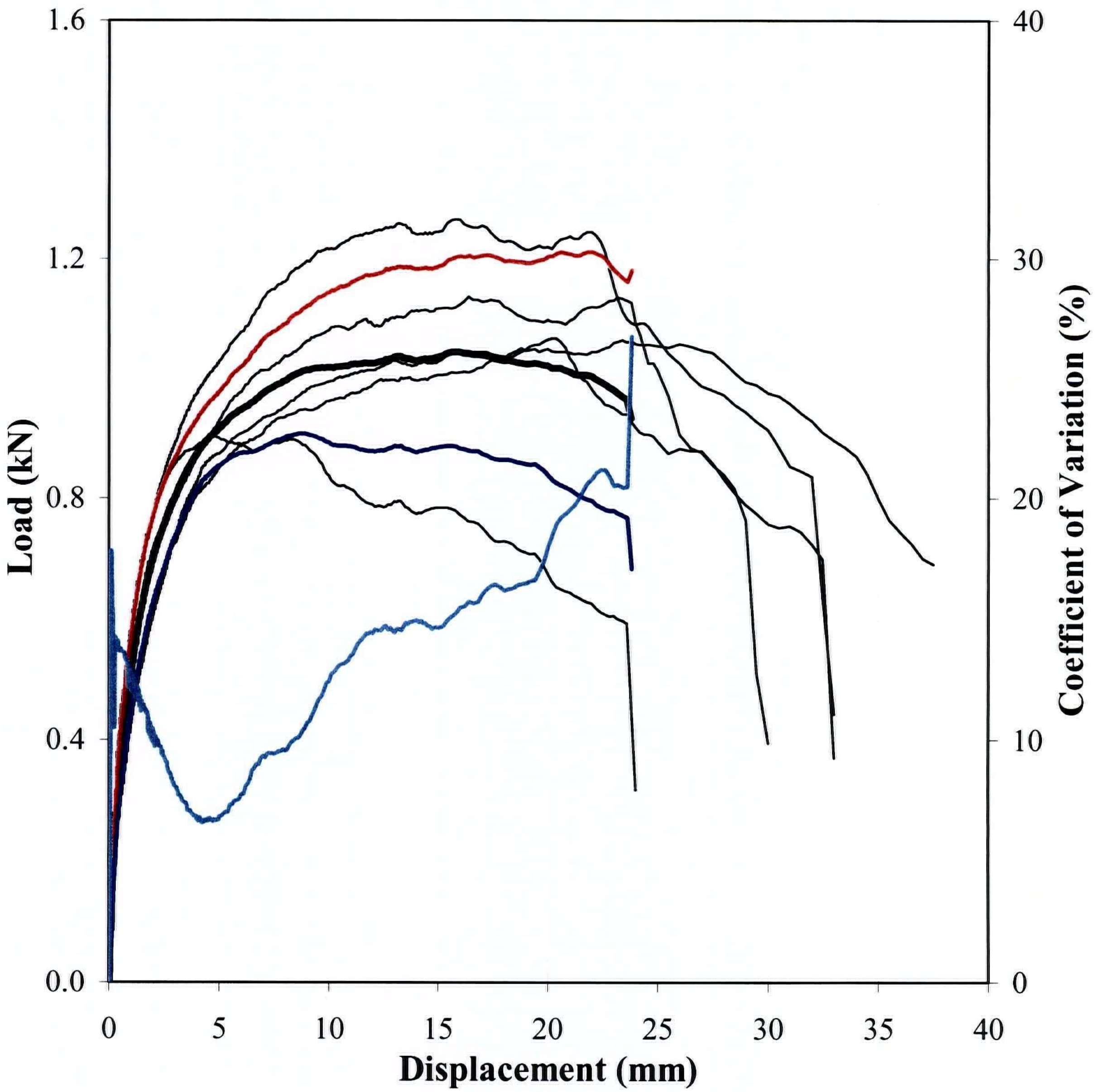

SPECIMEN GROUP 013

Description		Properties as defined by the CEN protocol	
Spiral nail length (mm)	65	Yield load F_y (kN)	0.732
Sheathing thickness (mm)	12.5	Yield displacement Δ_y (mm)	4.42
Sheathing material	CSP	Maximum load F_{max} (kN)	1.232
Sheathing orientation	PAR	Displacement at F_{max} (mm)	19.60
Stud material	LVL	Ultimate displacement Δ_u (mm)	25.00
Number of specimens	5	Initial stiffness (N/mm)	195
		Ductility (Δ_u/Δ_y)	5.66

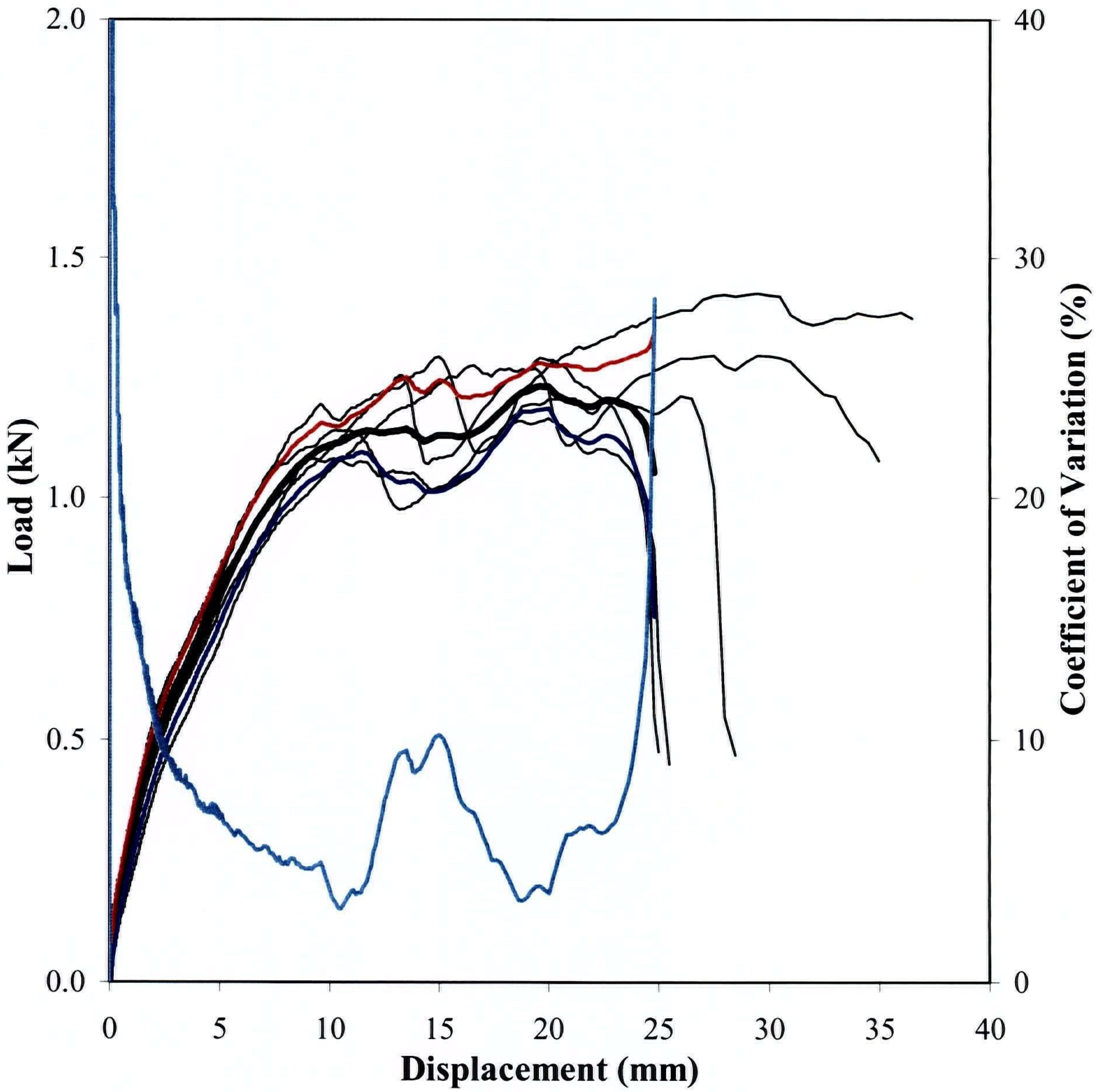

SPECIMEN GROUP 014

Description		Properties as defined by the CEN protocol	
Spiral nail length (mm)	65	Yield load F_y (kN)	0.841
Sheathing thickness (mm)	18.5	Yield displacement Δ_y (mm)	5.40
Sheathing material	CSP	Maximum load F_{max} (kN)	1.557
Sheathing orientation	PAR	Displacement at F_{max} (mm)	30.50
Stud material	LVL	Ultimate displacement Δ_u (mm)	35.50
Number of specimens	5	Initial stiffness (N/mm)	171
		Ductility (Δ_u/Δ_y)	6.57

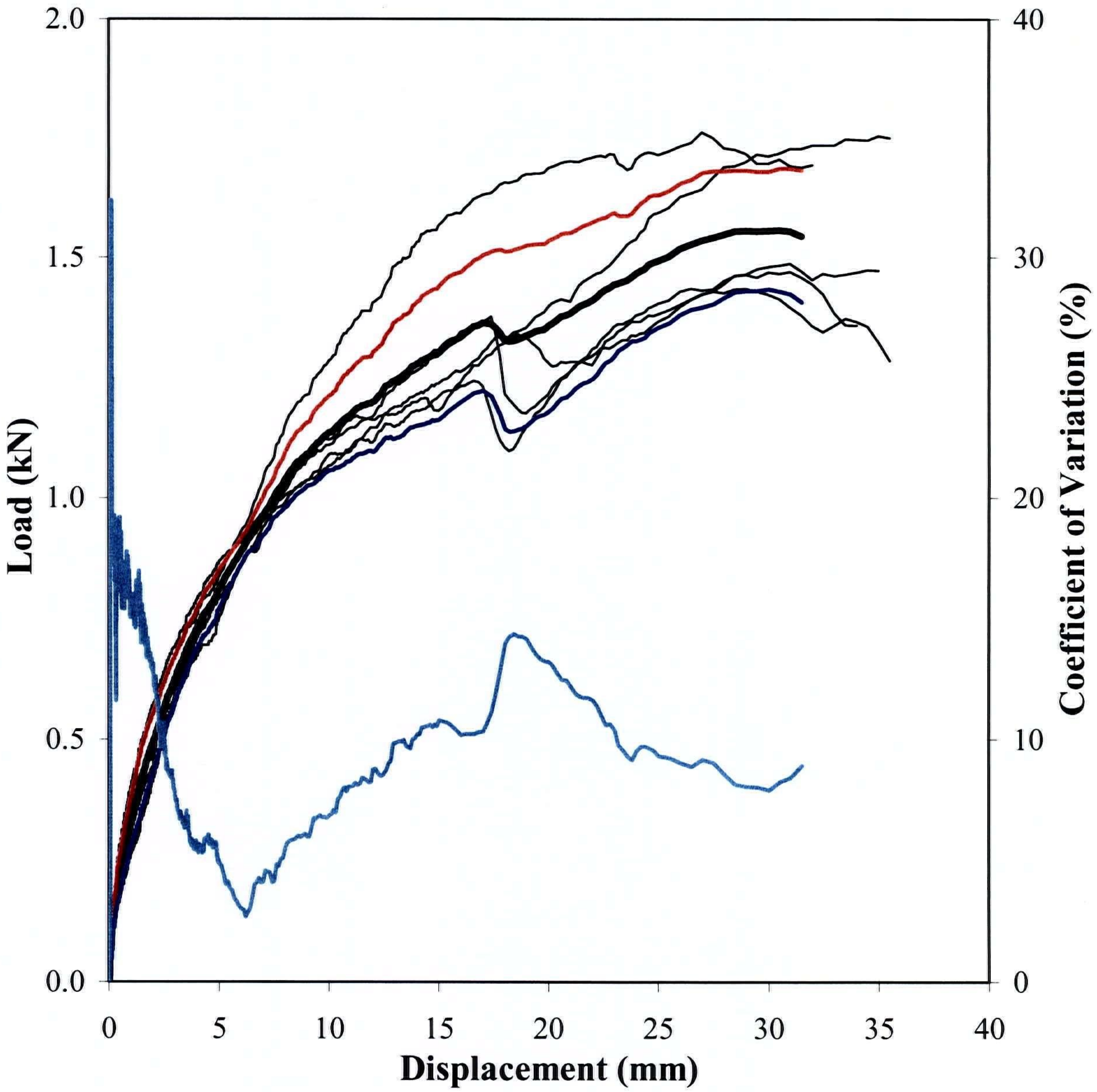

SPECIMEN GROUP 015

Description		Properties as defined by the CEN protocol	
Spiral nail length (mm)	76	Yield load F_y (kN)	1.023
Sheathing thickness (mm)	28.5	Yield displacement Δ_y (mm)	2.48
Sheathing material	CSP	Maximum load F_{max} (kN)	2.123
Sheathing orientation	PAR	Displacement at F_{max} (mm)	16.60
Stud material	LVL	Ultimate displacement Δ_u (mm)	37.50
Number of specimens	5	Initial stiffness (N/mm)	448
		Ductility (Δ_u/Δ_y)	15.12

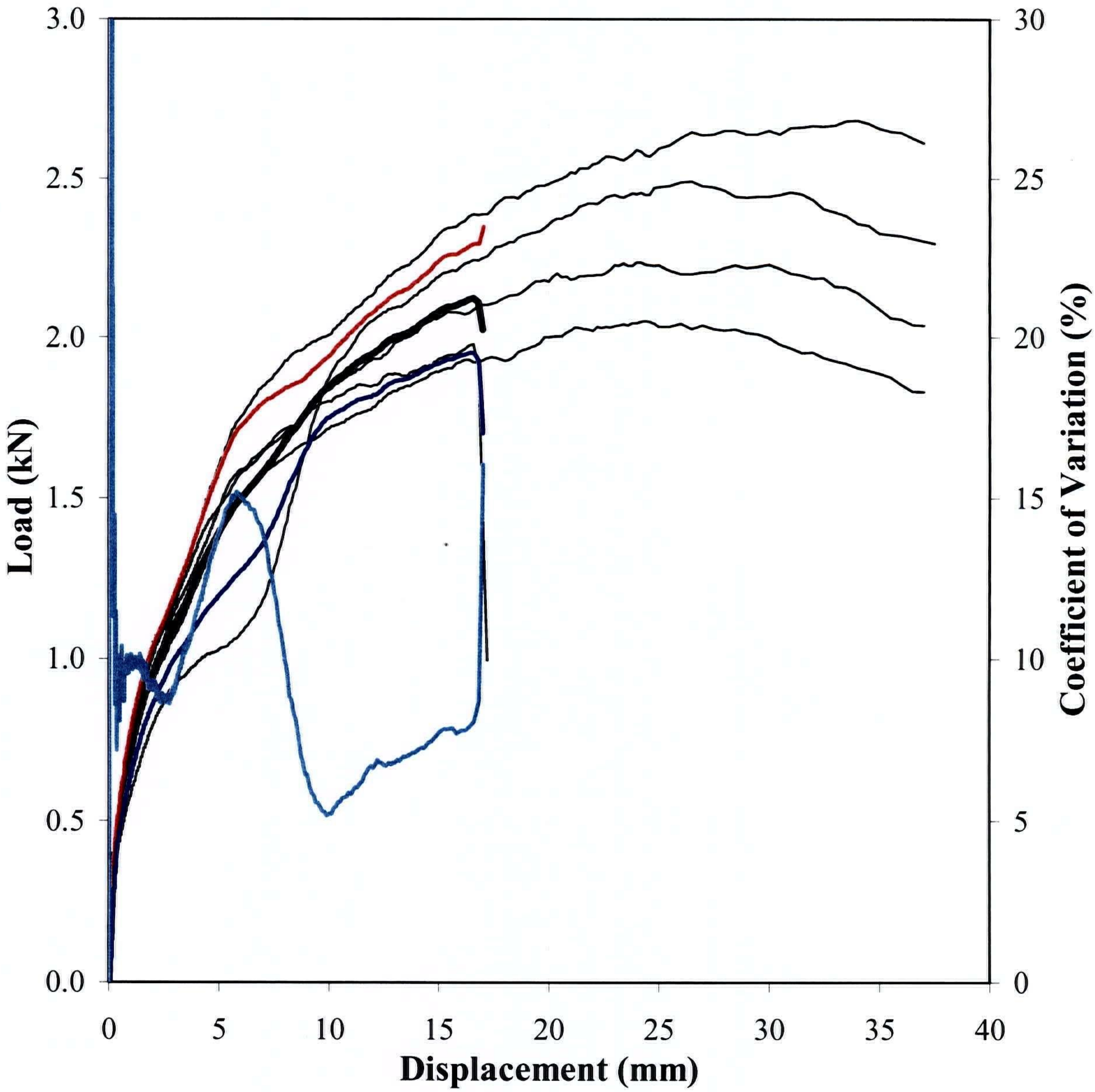

SPECIMEN GROUP 016

Description		Properties as defined by the CEN protocol	
Spiral nail length (mm)	65	Yield load F_y (kN)	0.673
Sheathing thickness (mm)	12.5	Yield displacement Δ_y (mm)	2.40
Sheathing material	OSB	Maximum load F_{max} (kN)	1.259
Sheathing orientation	PAR	Displacement at F_{max} (mm)	18.80
Stud material	LVL	Ultimate displacement Δ_u (mm)	36.50
Number of specimens	6	Initial stiffness (N/mm)	303
		Ductility (Δ_u/Δ_y)	15.21

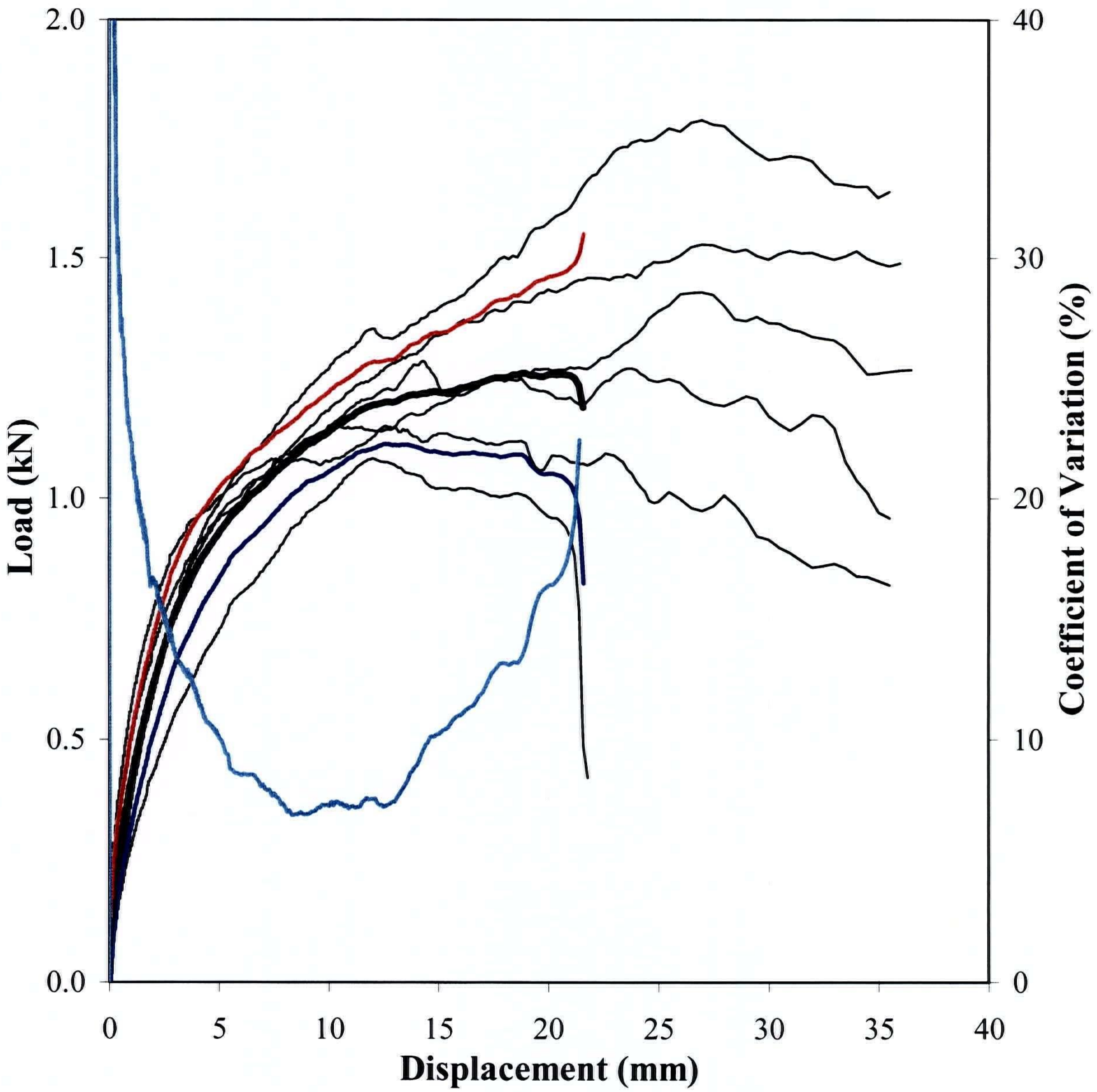

SPECIMEN GROUP 017

Description		Properties as defined by the CEN protocol	
Spiral nail length (mm)	65	Yield load F_y (kN)	0.672
Sheathing thickness (mm)	18.5	Yield displacement Δ_y (mm)	3.18
Sheathing material	OSB	Maximum load F_{max} (kN)	1.395
Sheathing orientation	PAR	Displacement at F_{max} (mm)	25.50
Stud material	LVL	Ultimate displacement Δ_u (mm)	37.00
Number of specimens	5	Initial stiffness (N/mm)	229
		Ductility (Δ_u/Δ_y)	11.64

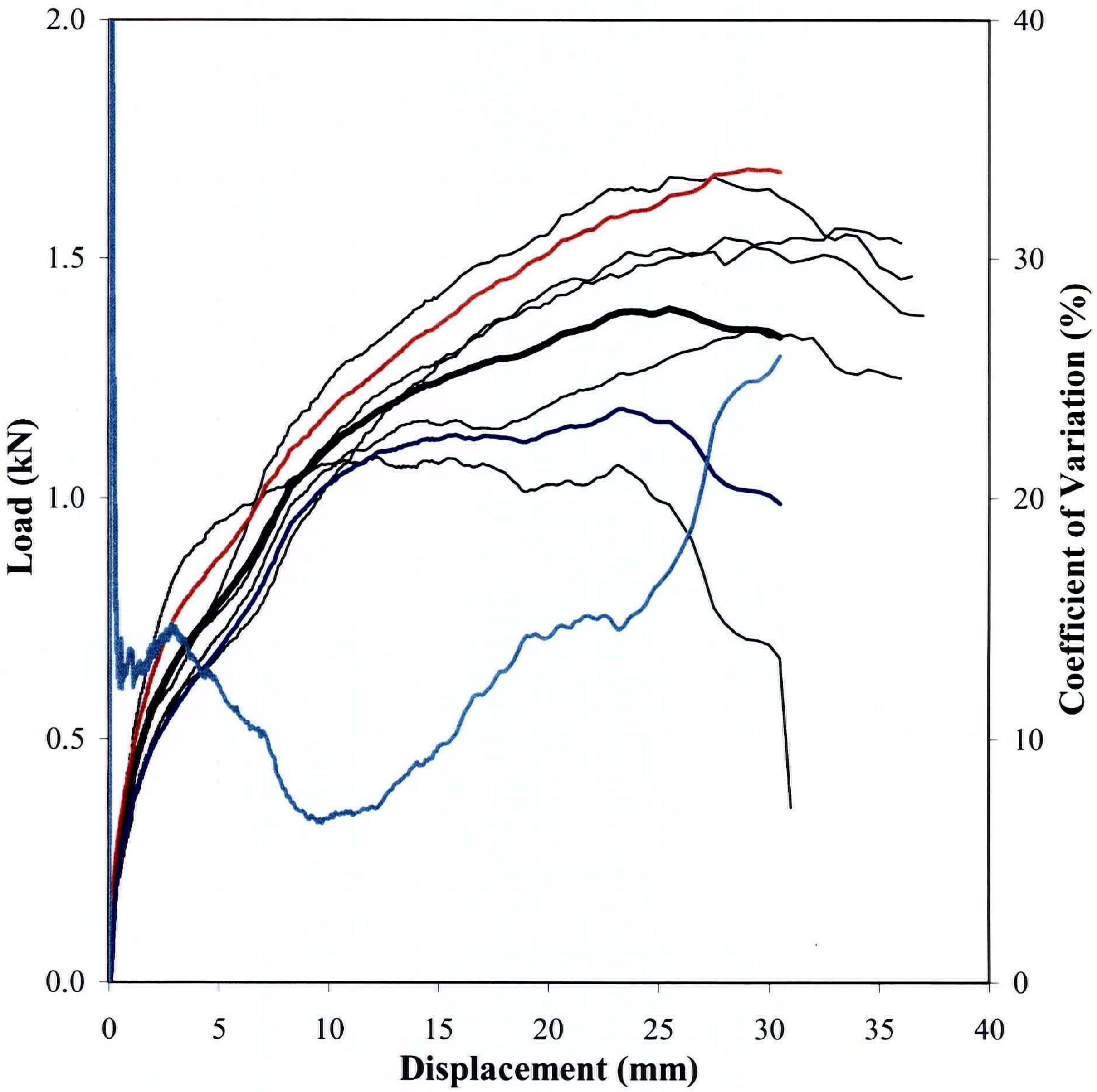

SPECIMEN GROUP 018

Description		Properties as defined by the CEN protocol	
Spiral nail length (mm)	76	Yield load F_y (kN)	0.836
Sheathing thickness (mm)	28.5	Yield displacement Δ_y (mm)	1.30
Sheathing material	OSB	Maximum load F_{max} (kN)	1.890
Sheathing orientation	PAR	Displacement at F_{max} (mm)	24.00
Stud material	LVL	Ultimate displacement Δ_u (mm)	37.50
Number of specimens	5	Initial stiffness (N/mm)	616
		Ductility (Δ_u/Δ_y)	28.85

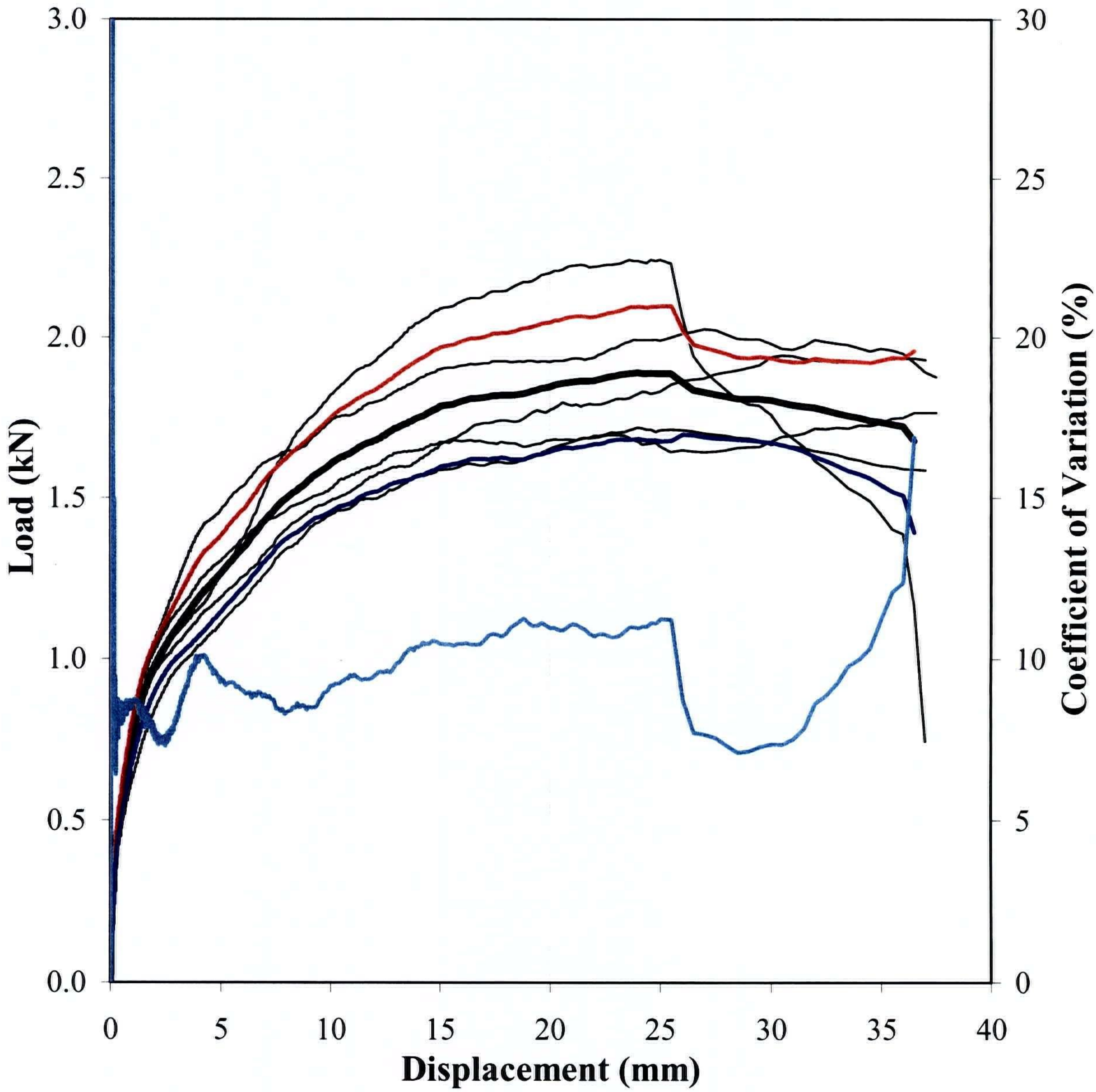

SPECIMEN GROUP 019

Description		Properties as defined by the CEN protocol	
Spiral nail length (mm)	65	Yield load F_y (kN)	0.808
Sheathing thickness (mm)	12.5	Yield displacement Δ_y (mm)	4.74
Sheathing material	CSP	Maximum load F_{max} (kN)	1.441
Sheathing orientation	PERP	Displacement at F_{max} (mm)	20.80
Stud material	LVL	Ultimate displacement Δ_u (mm)	35.00
Number of specimens	5	Initial stiffness (N/mm)	194
		Ductility (Δ_u/Δ_y)	7.38

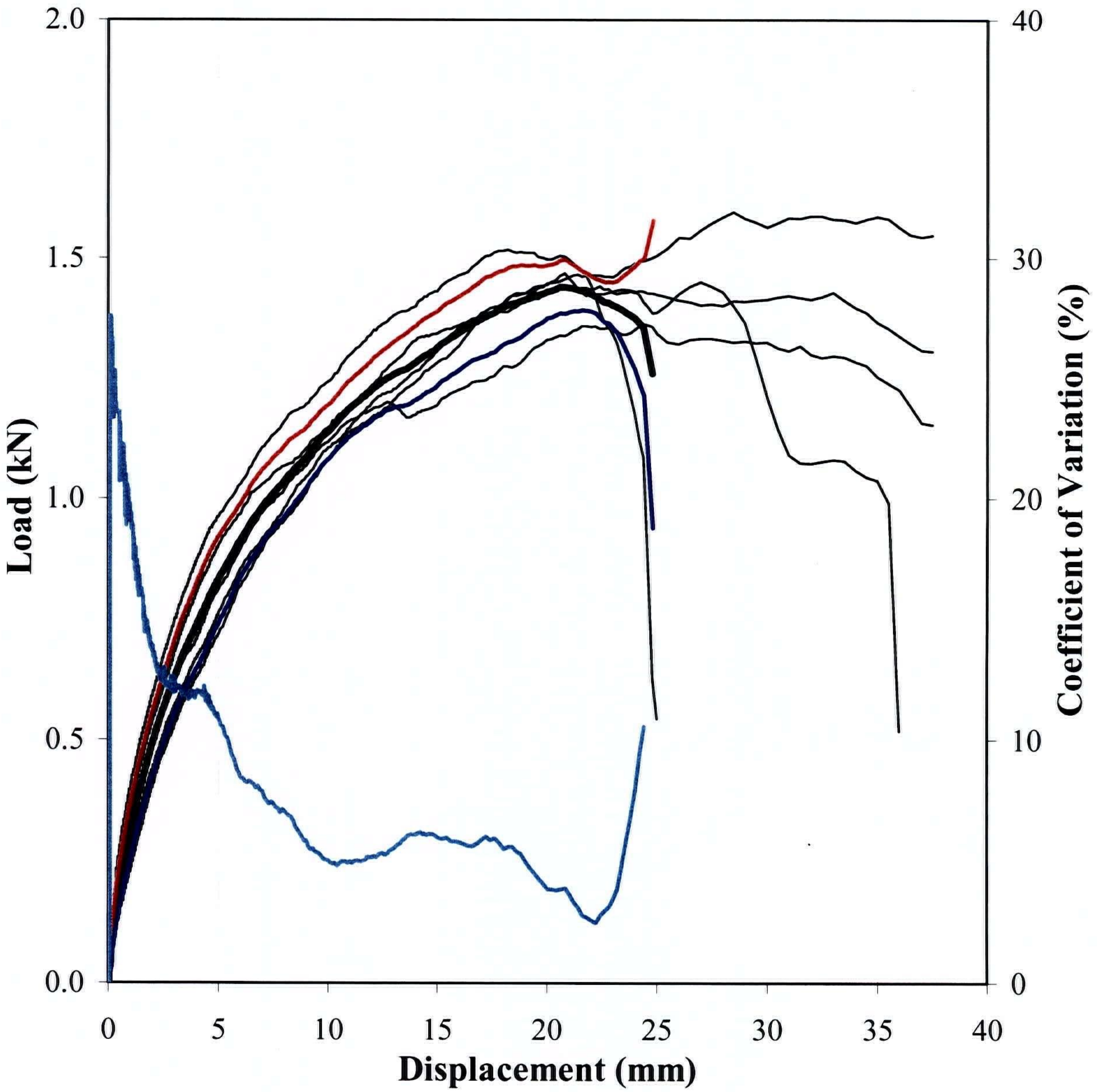

SPECIMEN GROUP 020

Description		Properties as defined by the CEN protocol	
Spiral nail length (mm)	65	Yield load F_y (kN)	0.837
Sheathing thickness (mm)	18.5	Yield displacement Δ_y (mm)	5.50
Sheathing material	CSP	Maximum load F_{max} (kN)	1.550
Sheathing orientation	PERP	Displacement at F_{max} (mm)	27.00
Stud material	LVL	Ultimate displacement Δ_u (mm)	37.50
Number of specimens	5	Initial stiffness (N/mm)	174
		Ductility (Δ_u/Δ_y)	6.82

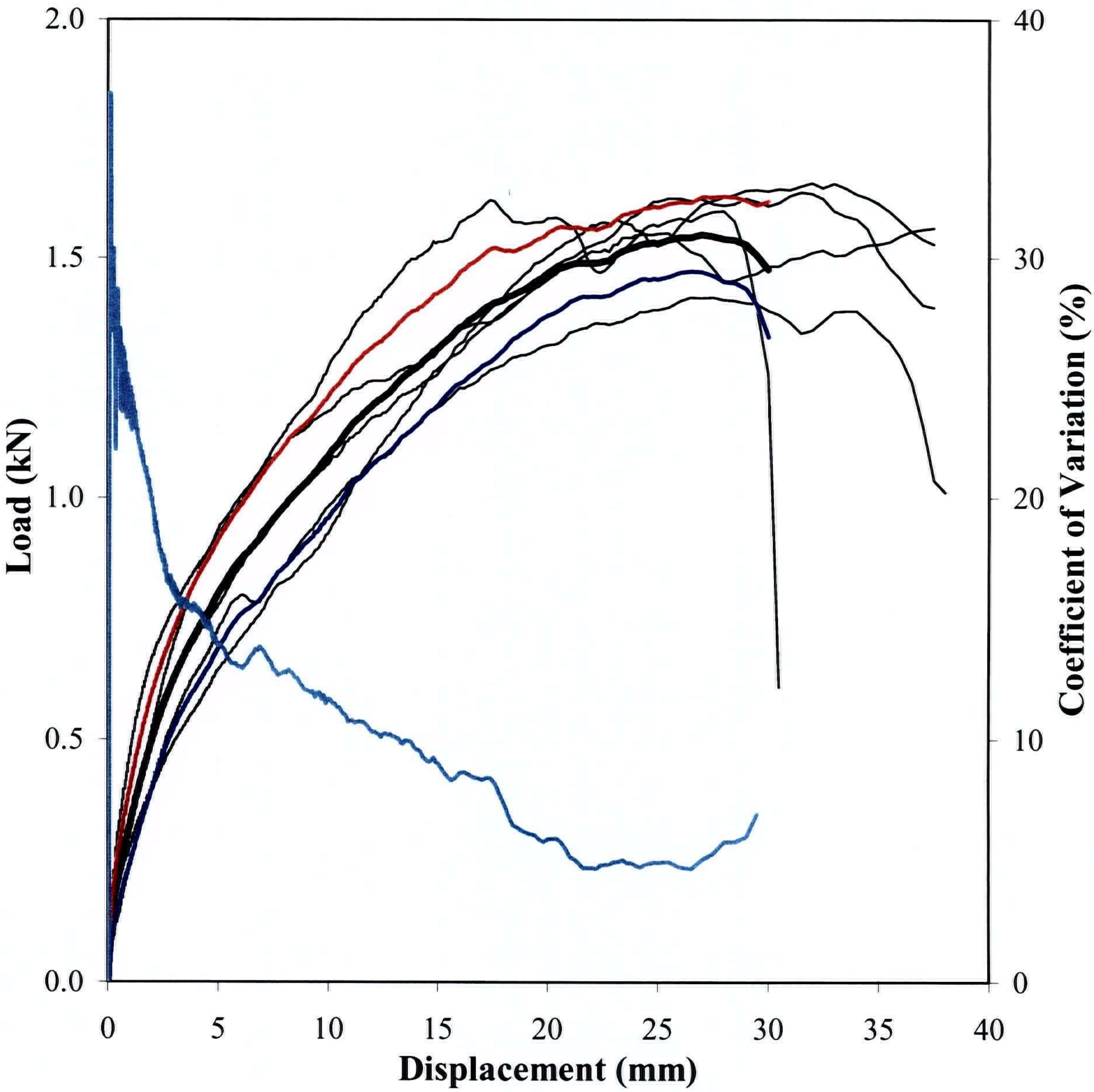

SPECIMEN GROUP 021

Description		**Properties as defined by the CEN protocol**	
Spiral nail length (mm)	76	Yield load F_y (kN)	1.167
Sheathing thickness (mm)	28.5	Yield displacement Δ_y (mm)	3.00
Sheathing material	CSP	Maximum load F_{max} (kN)	2.492
Sheathing orientation	PERP	Displacement at F_{max} (mm)	24.80
Stud material	LVL	Ultimate displacement Δ_u (mm)	38.00
Number of specimens	5	Initial stiffness (N/mm)	439
		Ductility (Δ_u/Δ_y)	12.67

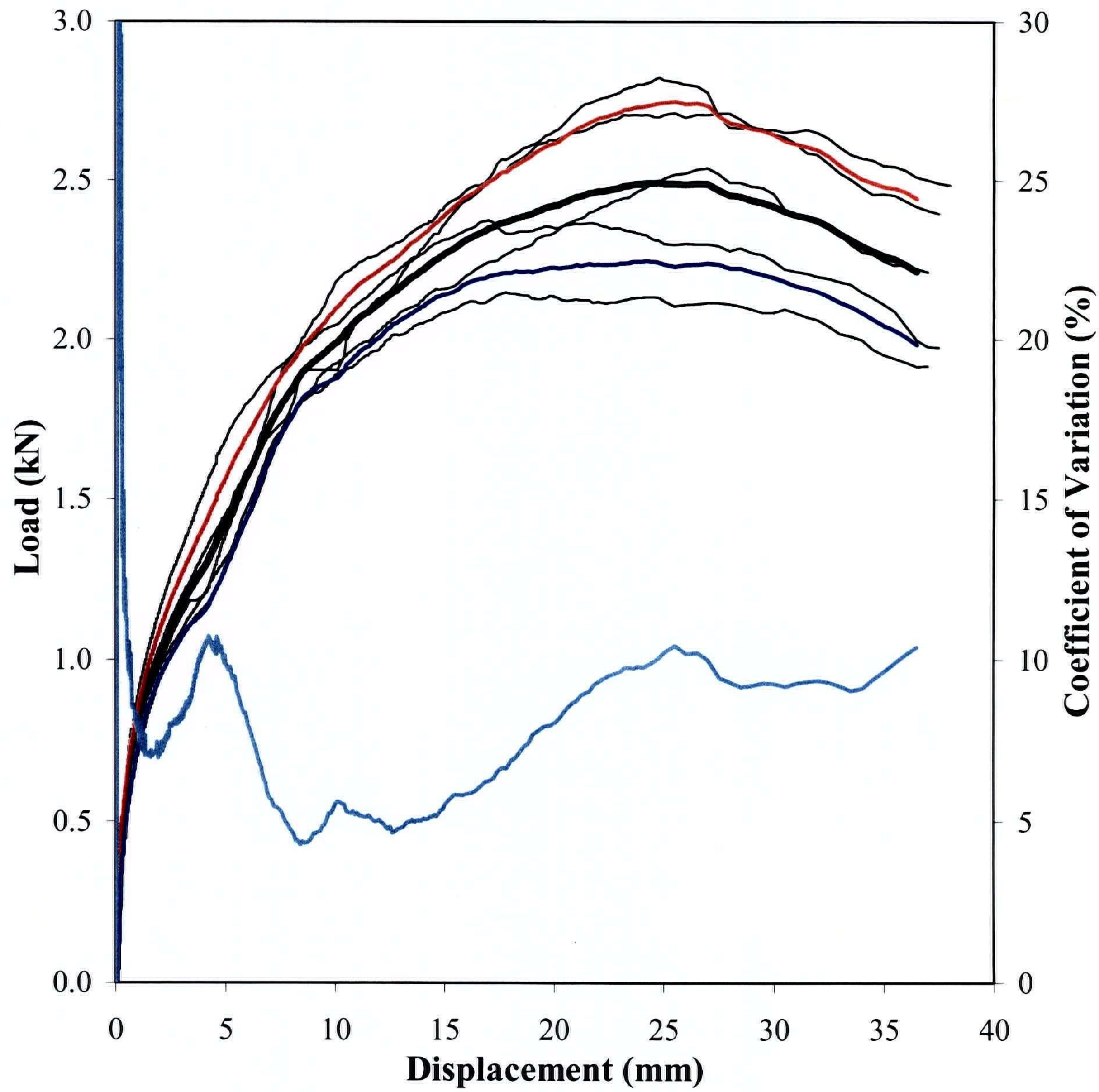

SPECIMEN GROUP 022

Description		**Properties as defined by the CEN protocol**	
Spiral nail length (mm)	65	Yield load F_y (kN)	0.718
Sheathing thickness (mm)	12.5	Yield displacement Δ_y (mm)	2.44
Sheathing material	OSB	Maximum load F_{max} (kN)	1.383
Sheathing orientation	PERP	Displacement at F_{max} (mm)	27.50
Stud material	LVL	Ultimate displacement Δ_u (mm)	38.00
Number of specimens	6	Initial stiffness (N/mm)	293
		Ductility (Δ_u/Δ_y)	15.57

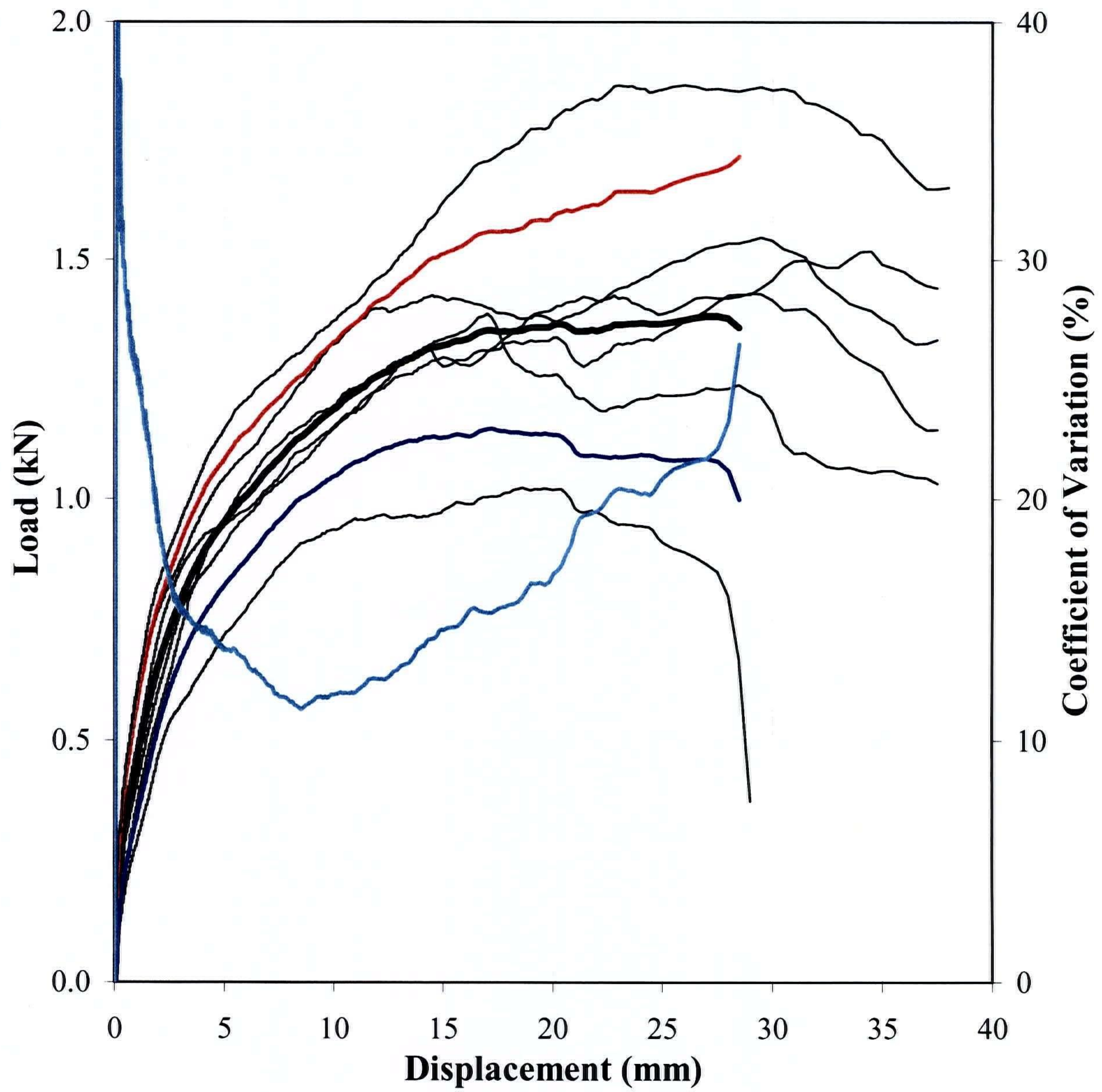

SPECIMEN GROUP 023

Description		**Properties as defined by the CEN protocol**	
Spiral nail length (mm)	65	Yield load F_y (kN)	0.651
Sheathing thickness (mm)	18.5	Yield displacement Δ_y (mm)	2.06
Sheathing material	OSB	Maximum load F_{max} (kN)	1.415
Sheathing orientation	PERP	Displacement at F_{max} (mm)	22.80
Stud material	LVL	Ultimate displacement Δ_u (mm)	34.50
Number of specimens	6	Initial stiffness (N/mm)	332
		Ductility (Δ_u/Δ_y)	16.75

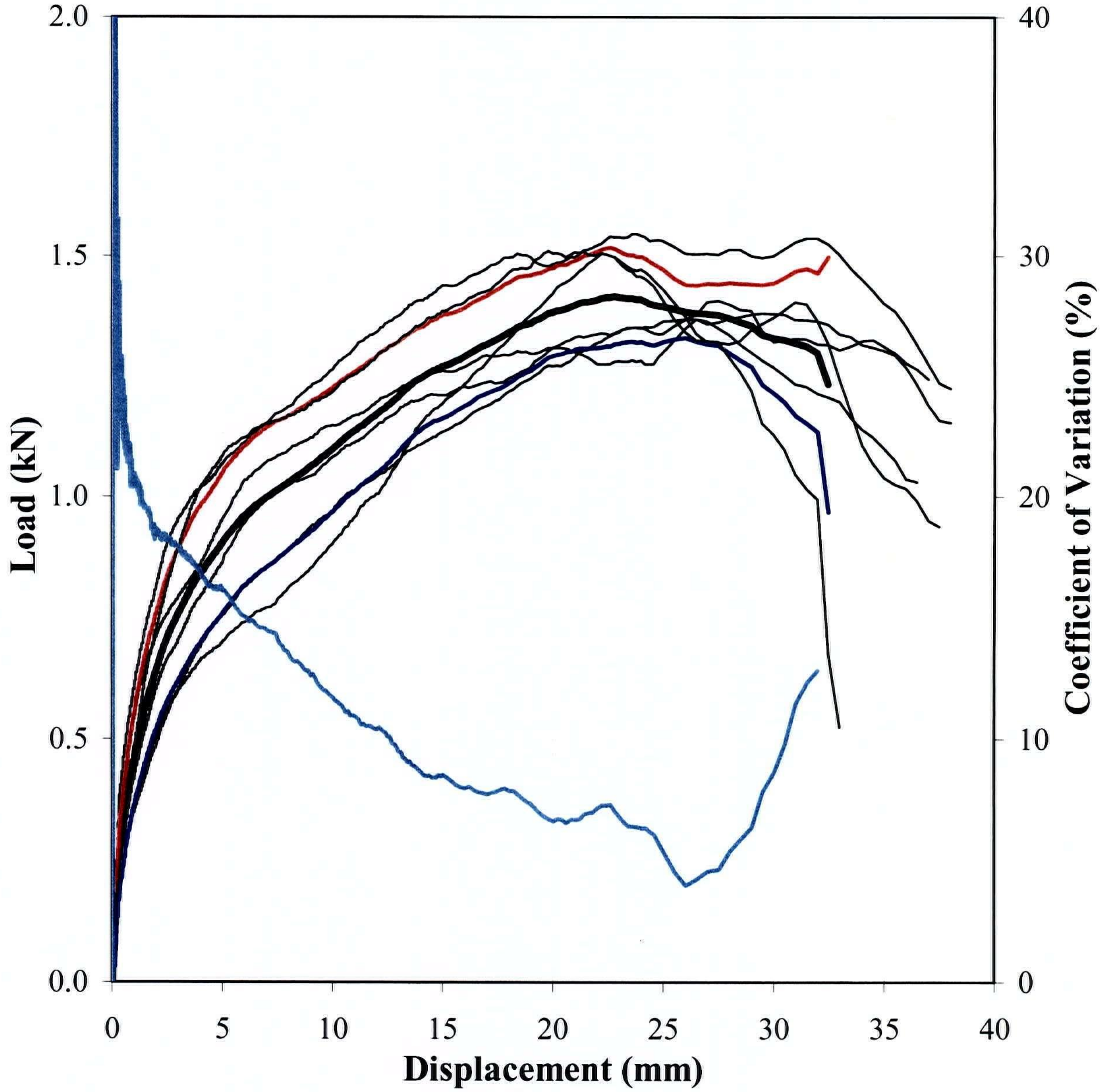

SPECIMEN GROUP 024

Description		Properties as defined by the CEN protocol	
Spiral nail length (mm)	76	Yield load F_y (kN)	0.937
Sheathing thickness (mm)	28.5	Yield displacement Δ_y (mm)	1.54
Sheathing material	OSB	Maximum load F_{max} (kN)	2.155
Sheathing orientation	PERP	Displacement at F_{max} (mm)	29.50
Stud material	LVL	Ultimate displacement Δ_u (mm)	41.50
Number of specimens	5	Initial stiffness (N/mm)	564
		Ductility (Δ_u/Δ_y)	26.95

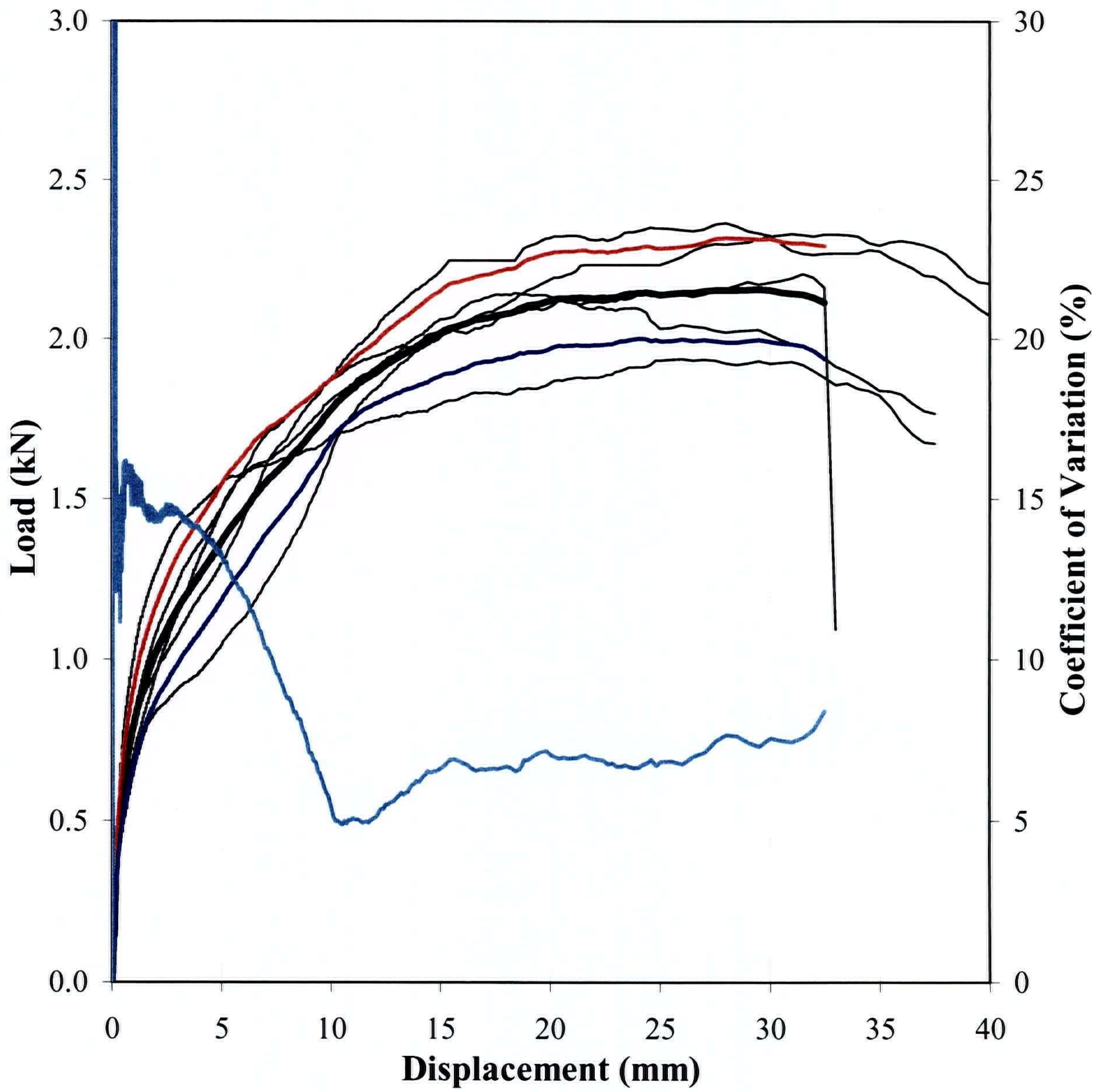

SPECIMEN GROUP 025

Description		Properties as defined by the CEN protocol	
Spiral nail length (mm)	65	Yield load F_y (kN)	0.651
Sheathing thickness (mm)	9.5	Yield displacement Δ_y (mm)	3.00
Sheathing material	CSP	Maximum load F_{max} (kN)	1.177
Sheathing orientation	PAR	Displacement at F_{max} (mm)	15.20
Stud material	LSL	Ultimate displacement Δ_u (mm)	17.40
Number of specimens	5	Initial stiffness (N/mm)	233
		Ductility (Δ_u/Δ_y)	5.80

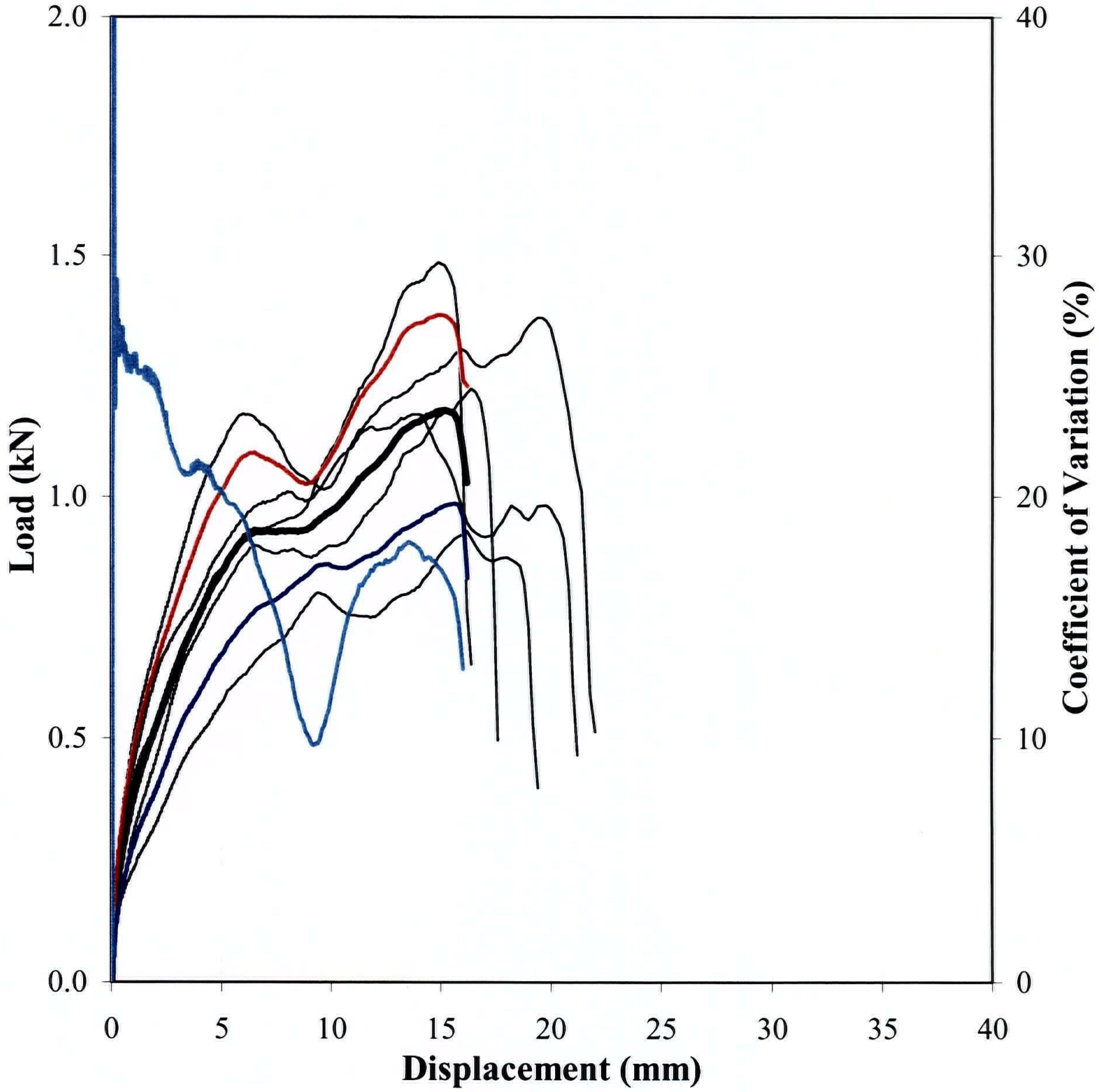

SPECIMEN GROUP 026

Description		Properties as defined by the CEN protocol	
Spiral nail length (mm)	65	Yield load F_y (kN)	0.759
Sheathing thickness (mm)	18.5	Yield displacement Δ_y (mm)	2.94
Sheathing material	CSP	Maximum load F_{max} (kN)	1.427
Sheathing orientation	PAR	Displacement at F_{max} (mm)	17.60
Stud material	LSL	Ultimate displacement Δ_u (mm)	22.00
Number of specimens	5	Initial stiffness (N/mm)	264
		Ductility (Δ_u/Δ_y)	7.48

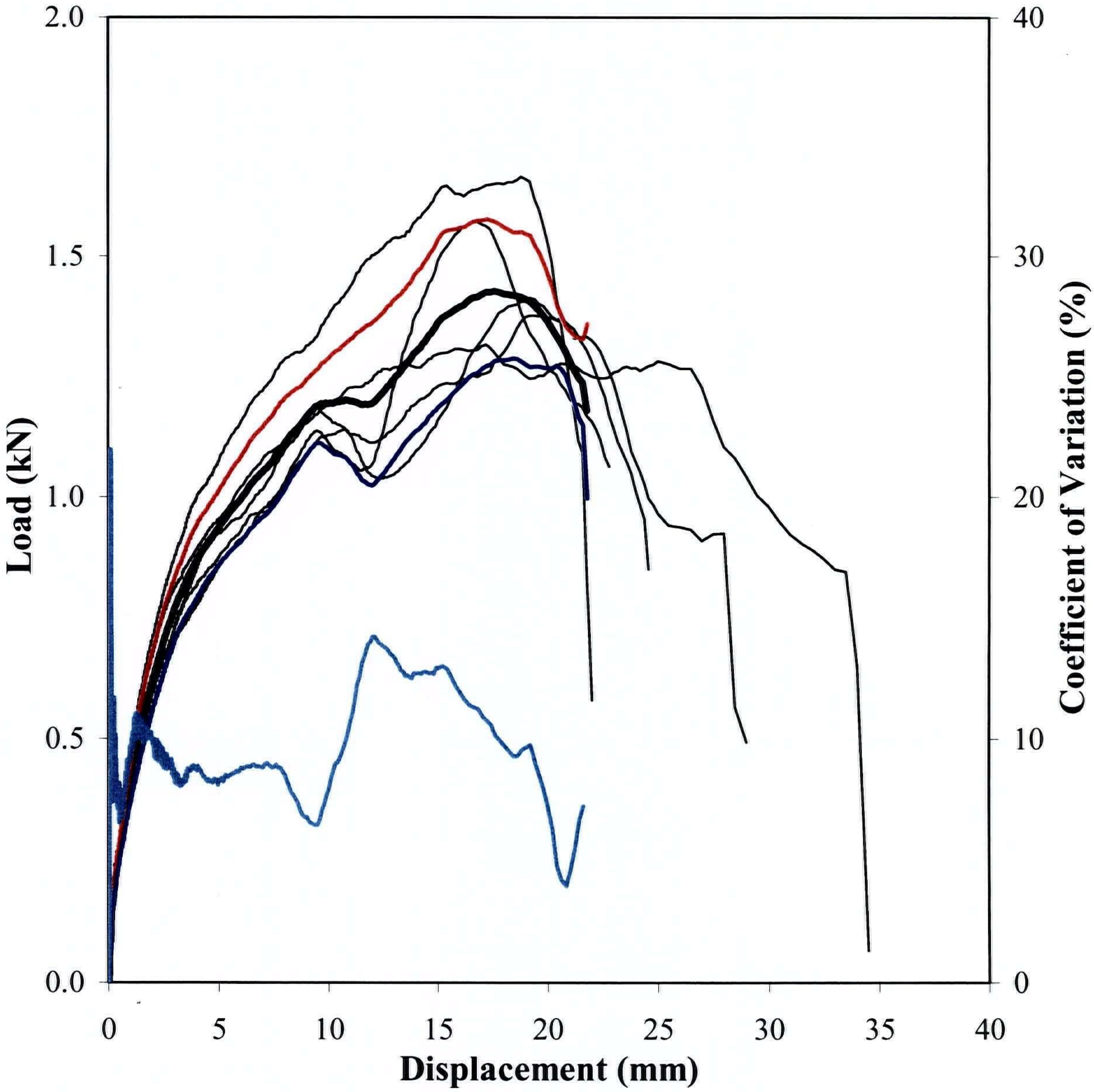

SPECIMEN GROUP 027

Description		Properties as defined by the CEN protocol	
Spiral nail length (mm)	76	Yield load F_y (kN)	1.557
Sheathing thickness (mm)	28.5	Yield displacement Δ_y (mm)	3.06
Sheathing material	CSP	Maximum load F_{max} (kN)	3.324
Sheathing orientation	PAR	Displacement at F_{max} (mm)	21.80
Stud material	LSL	Ultimate displacement Δ_u (mm)	30.00
Number of specimens	5	Initial stiffness (N/mm)	556
		Ductility (Δ_u/Δ_y)	9.80

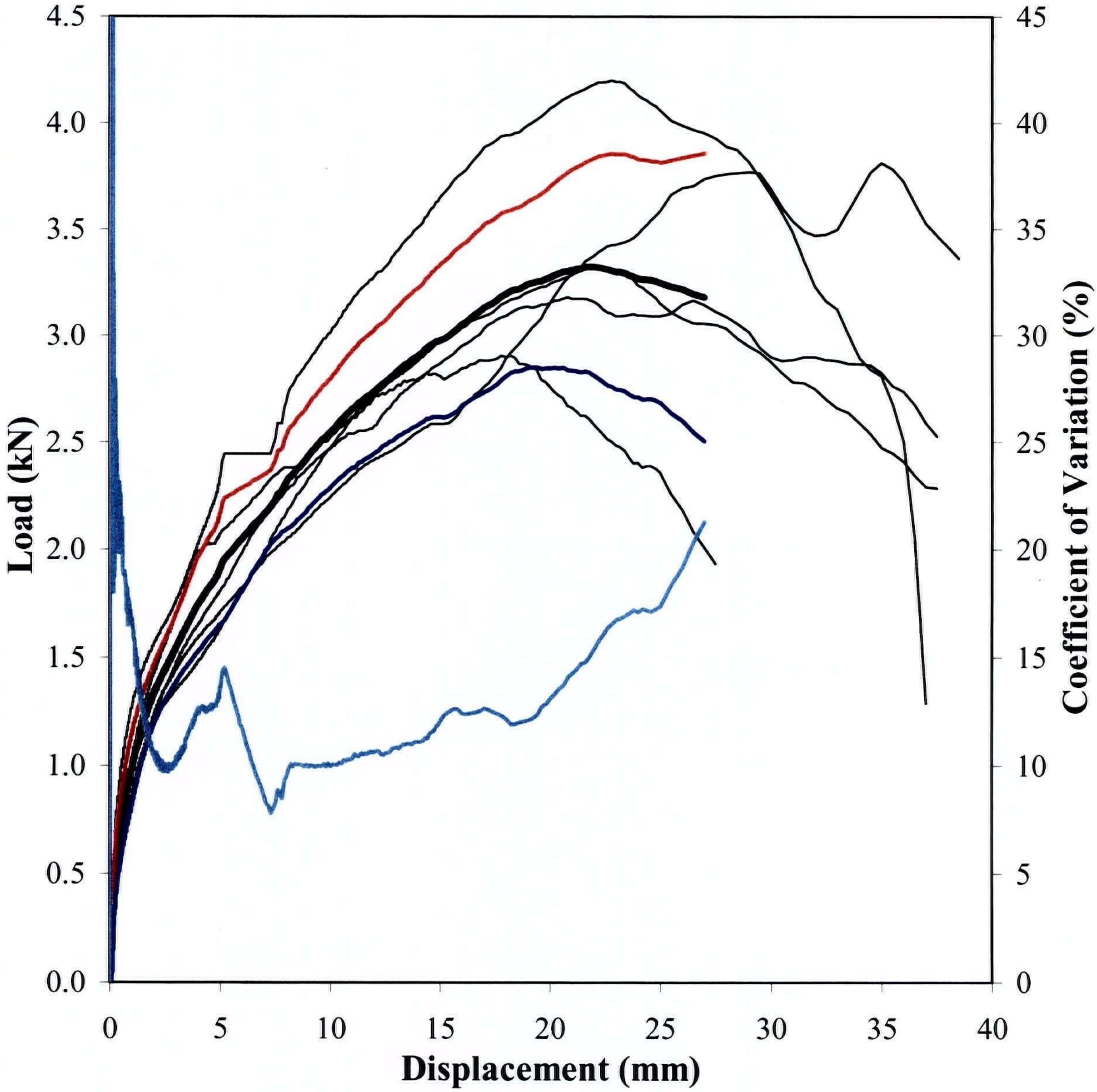

SPECIMEN GROUP 028

Description		Properties as defined by the CEN protocol	
Spiral nail length (mm)	65	Yield load F_y (kN)	0.863
Sheathing thickness (mm)	9.5	Yield displacement Δ_y (mm)	2.08
Sheathing material	OSB	Maximum load F_{max} (kN)	1.768
Sheathing orientation	PAR	Displacement at F_{max} (mm)	15.00
Stud material	LSL	Ultimate displacement Δ_u (mm)	17.80
Number of specimens	5	Initial stiffness (N/mm)	437
		Ductility (Δ_u/Δ_y)	8.56

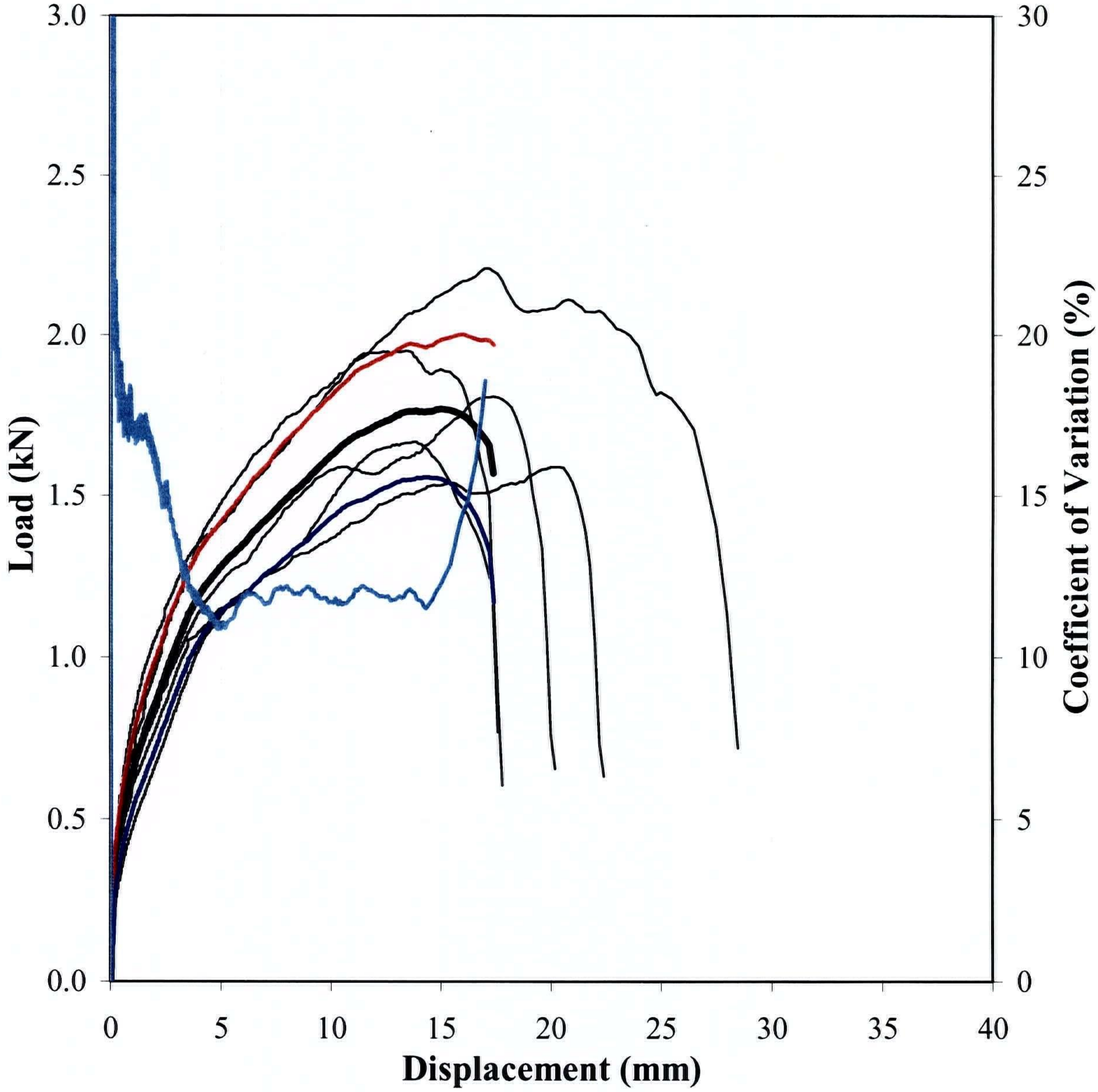

SPECIMEN GROUP 029

Description		Properties as defined by the CEN protocol	
Spiral nail length (mm)	65	Yield load F_y (kN)	0.766
Sheathing thickness (mm)	18.5	Yield displacement Δ_y (mm)	1.30
Sheathing material	OSB	Maximum load F_{max} (kN)	1.739
Sheathing orientation	PAR	Displacement at F_{max} (mm)	14.70
Stud material	LSL	Ultimate displacement Δ_u (mm)	21.60
Number of specimens	5	Initial stiffness (N/mm)	579
		Ductility (Δ_u/Δ_y)	16.62

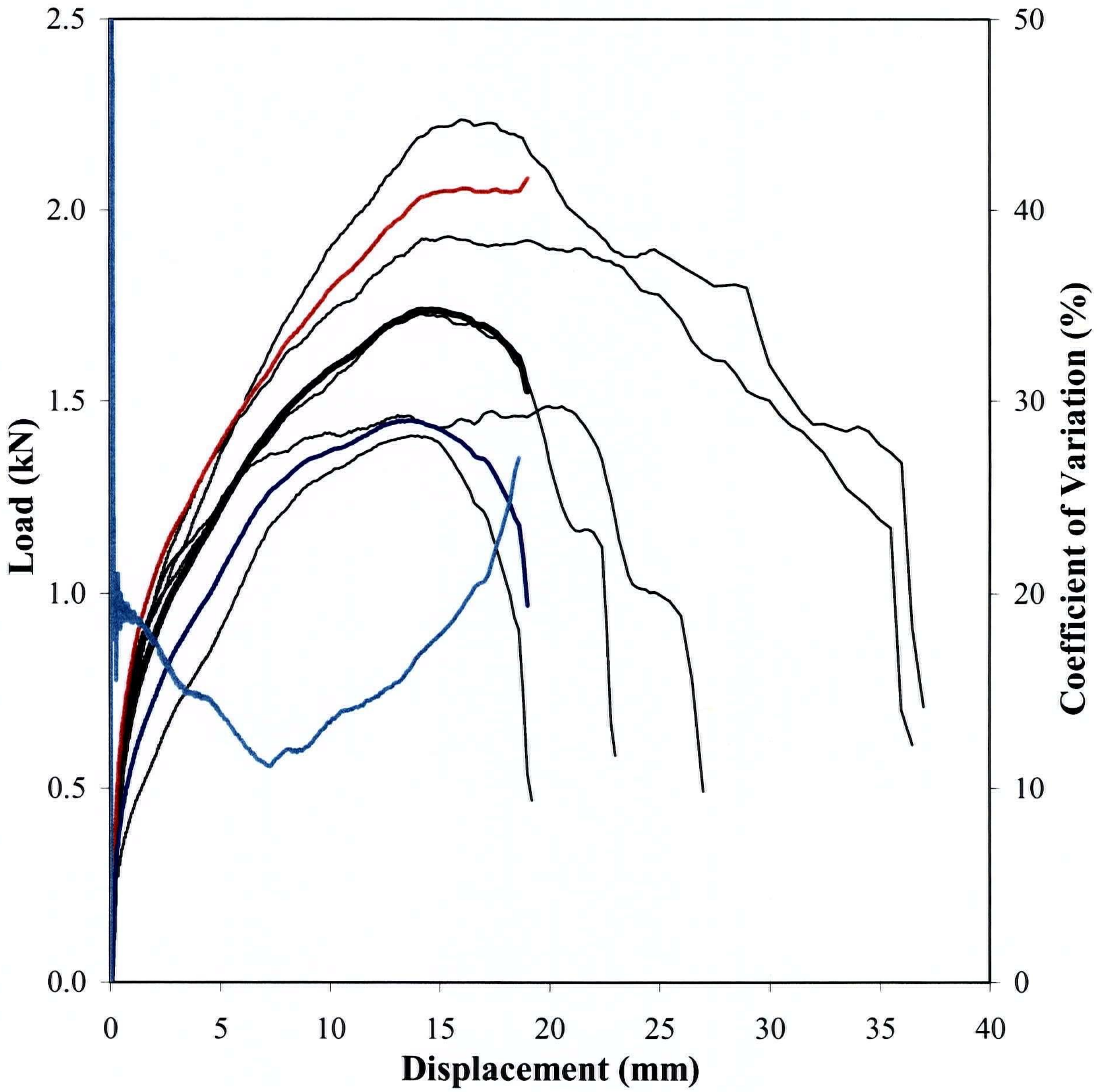

SPECIMEN GROUP 030

Description		**Properties as defined by the CEN protocol**	
Spiral nail length (mm)	76	Yield load F_y (kN)	1.379
Sheathing thickness (mm)	28.5	Yield displacement Δ_y (mm)	1.64
Sheathing material	OSB	Maximum load F_{max} (kN)	3.064
Sheathing orientation	PAR	Displacement at F_{max} (mm)	17.40
Stud material	LSL	Ultimate displacement Δ_u (mm)	25.50
Number of specimens	5	Initial stiffness (N/mm)	869
		Ductility (Δ_u/Δ_y)	15.55

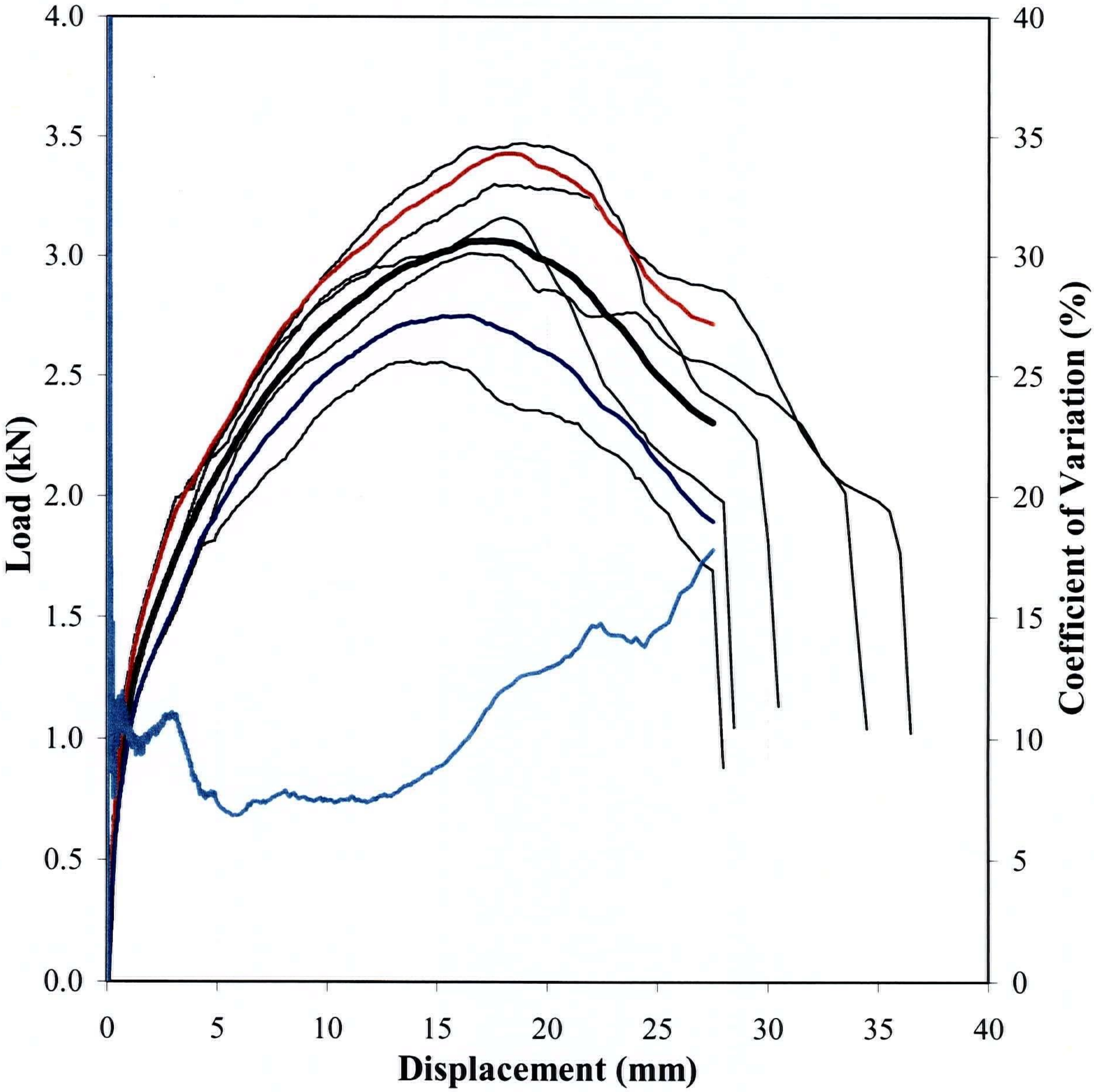

SPECIMEN GROUP 031

Description		Properties as defined by the CEN protocol	
Spiral nail length (mm)	65	Yield load F_y (kN)	0.698
Sheathing thickness (mm)	9.5	Yield displacement Δ_y (mm)	1.88
Sheathing material	CSP	Maximum load F_{max} (kN)	1.399
Sheathing orientation	PERP	Displacement at F_{max} (mm)	10.40
Stud material	LSL	Ultimate displacement Δ_u (mm)	13.20
Number of specimens	5	Initial stiffness (N/mm)	436
		Ductility (Δ_u/Δ_y)	7.02

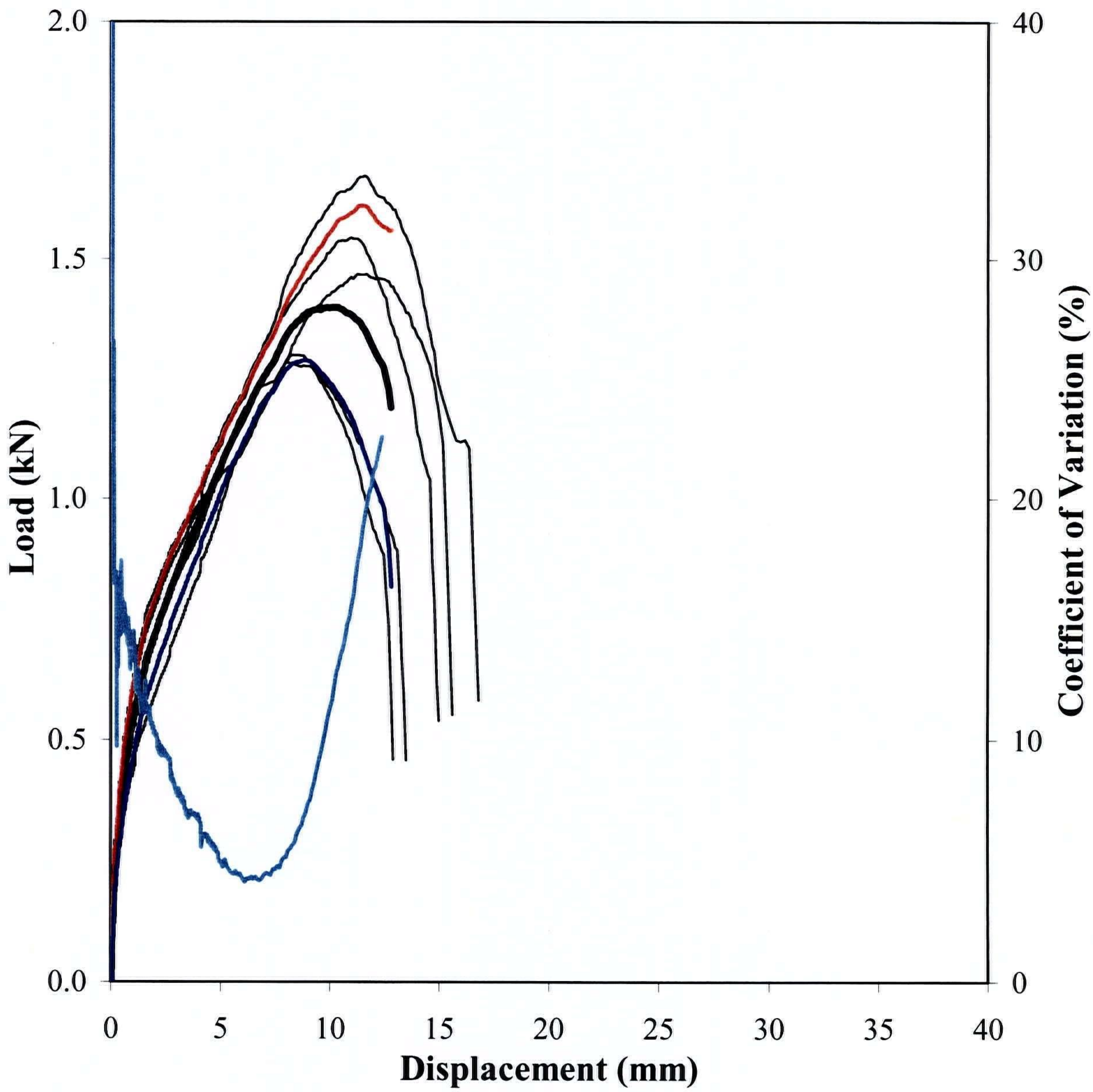

SPECIMEN GROUP 032

Description		Properties as defined by the CEN protocol	
Spiral nail length (mm)	65	Yield load F_y (kN)	0.977
Sheathing thickness (mm)	18.5	Yield displacement Δ_y (mm)	4.74
Sheathing material	CSP	Maximum load F_{max} (kN)	1.685
Sheathing orientation	PERP	Displacement at F_{max} (mm)	15.80
Stud material	LSL	Ultimate displacement Δ_u (mm)	23.80
Number of specimens	5	Initial stiffness (N/mm)	254
		Ductility (Δ_u/Δ_y)	5.02

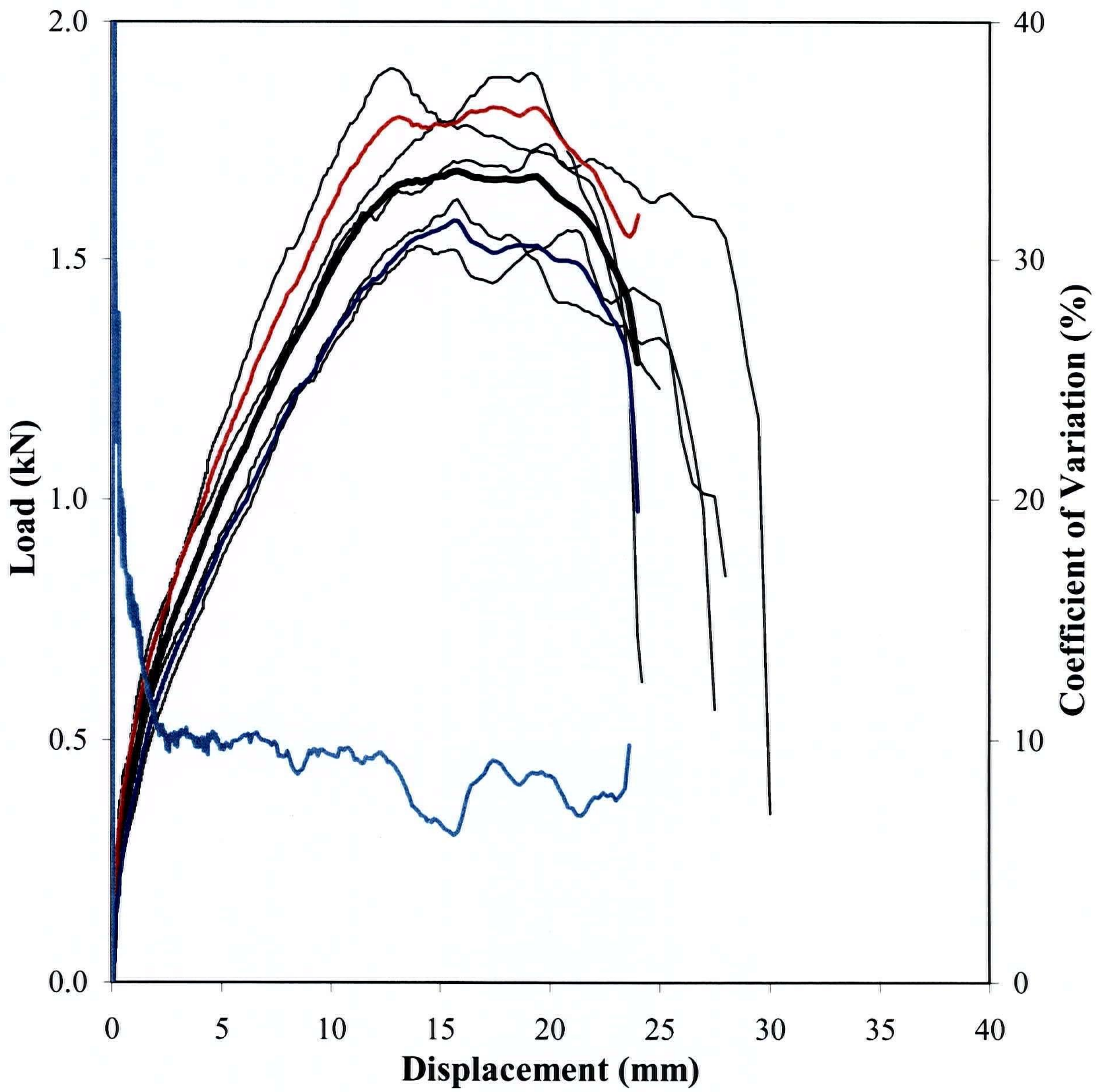

SPECIMEN GROUP 033

Description		**Properties as defined by the CEN protocol**	
Spiral nail length (mm)	76	Yield load F_y (kN)	1.508
Sheathing thickness (mm)	28.5	Yield displacement Δ_y (mm)	2.84
Sheathing material	CSP	Maximum load F_{max} (kN)	3.314
Sheathing orientation	PERP	Displacement at F_{max} (mm)	21.40
Stud material	LSL	Ultimate displacement Δ_u (mm)	29.50
Number of specimens	5	Initial stiffness (N/mm)	578
		Ductility (Δ_u/Δ_y)	10.39

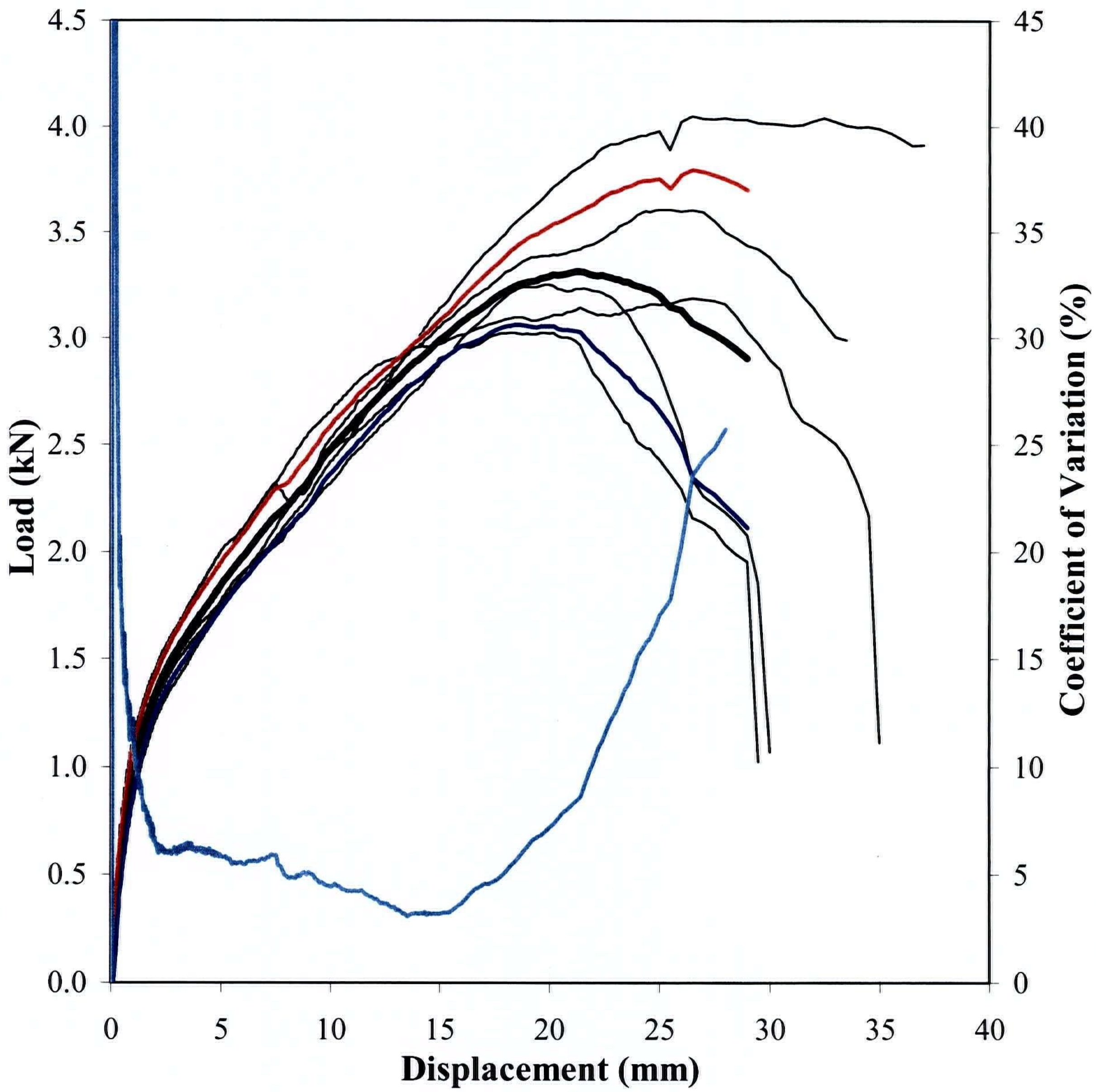

SPECIMEN GROUP 034

Description		Properties as defined by the CEN protocol	
Spiral nail length (mm)	65	Yield load F_y (kN)	0.855
Sheathing thickness (mm)	9.5	Yield displacement Δ_y (mm)	2.22
Sheathing material	OSB	Maximum load F_{max} (kN)	1.558
Sheathing orientation	PERP	Displacement at F_{max} (mm)	11.40
Stud material	LSL	Ultimate displacement Δ_u (mm)	15.60
Number of specimens	5	Initial stiffness (N/mm)	411
		Ductility (Δ_u/Δ_y)	7.03

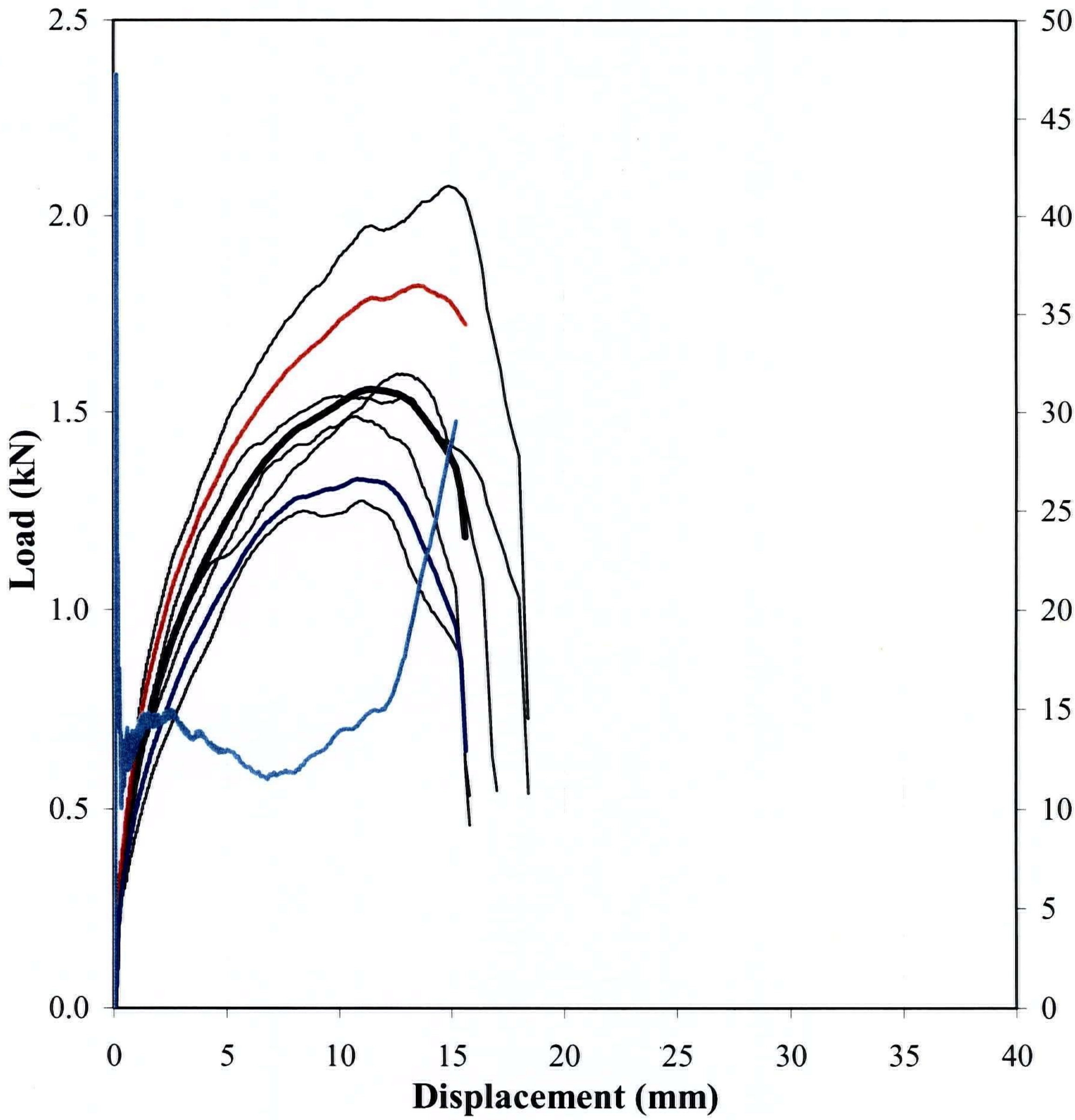

SPECIMEN GROUP 035

Description		Properties as defined by the CEN protocol	
Spiral nail length (mm)	65	Yield load F_y (kN)	0.855
Sheathing thickness (mm)	18.5	Yield displacement Δ_y (mm)	1.62
Sheathing material	OSB	Maximum load F_{max} (kN)	1.945
Sheathing orientation	PERP	Displacement at F_{max} (mm)	18.00
Stud material	LSL	Ultimate displacement Δ_u (mm)	22.40
Number of specimens	5	Initial stiffness (N/mm)	522
		Ductility (Δ_u/Δ_y)	13.83

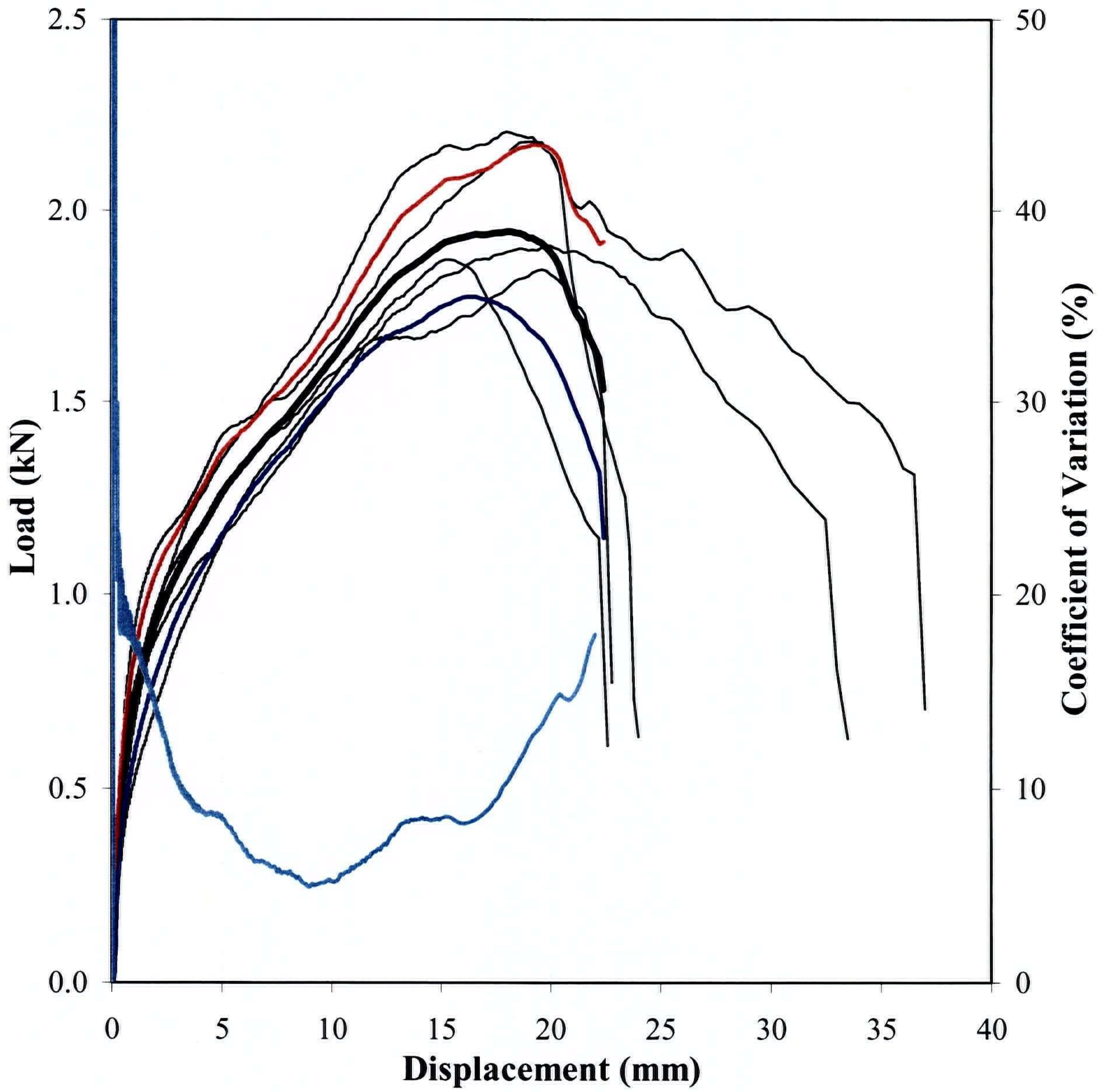

SPECIMEN GROUP 036

Description		Properties as defined by the CEN protocol	
Spiral nail length (mm)	76	Yield load F_y (kN)	1.404
Sheathing thickness (mm)	28.5	Yield displacement Δ_y (mm)	1.44
Sheathing material	OSB	Maximum load F_{max} (kN)	3.114
Sheathing orientation	PERP	Displacement at F_{max} (mm)	16.00
Stud material	LSL	Ultimate displacement Δ_u (mm)	24.40
Number of specimens	5	Initial stiffness (N/mm)	1036
		Ductility (Δ_u/Δ_y)	16.94

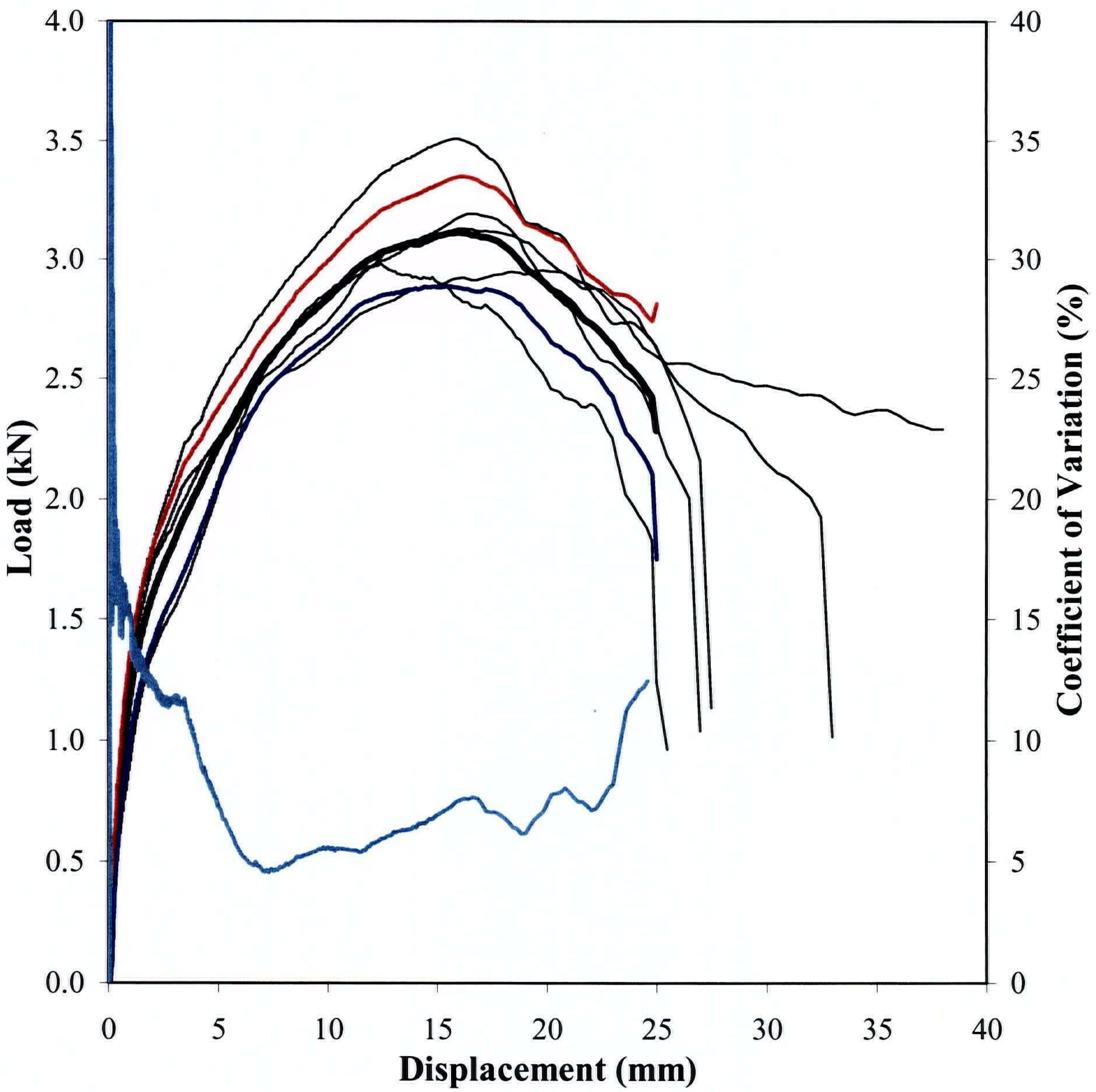

SPECIMEN GROUP 037

Description		Properties as defined by the CEN protocol	
Spiral nail length (mm)	65	Yield load F_y (kN)	0.626
Sheathing thickness (mm)	9.5	Yield displacement Δ_y (mm)	1.76
Sheathing material	CSP	Maximum load F_{max} (kN)	1.127
Sheathing orientation	PAR	Displacement at F_{max} (mm)	22.60
Stud material	Glulam	Ultimate displacement Δ_u (mm)	25.50
Number of specimens	5	Initial stiffness (N/mm)	358
		Ductility (Δ_u/Δ_y)	14.49

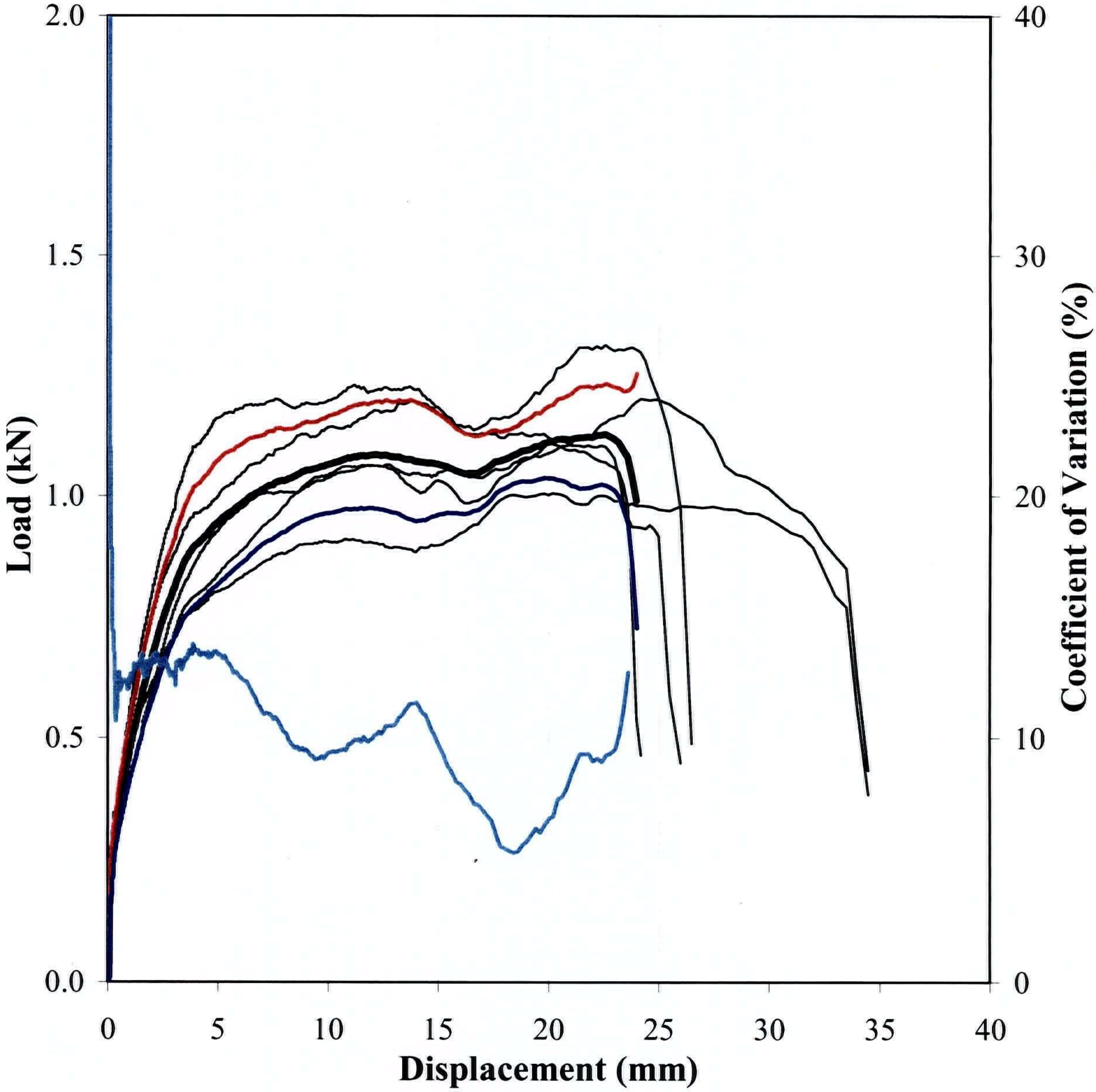

SPECIMEN GROUP 038

Description		Properties as defined by the CEN protocol	
Spiral nail length (mm)	65	Yield load F_y (kN)	0.704
Sheathing thickness (mm)	18.5	Yield displacement Δ_y (mm)	2.78
Sheathing material	CSP	Maximum load F_{max} (kN)	1.445
Sheathing orientation	PAR	Displacement at F_{max} (mm)	22.00
Stud material	Glulam	Ultimate displacement Δ_u (mm)	27.50
Number of specimens	5	Initial stiffness (N/mm)	268
		Ductility (Δ_u/Δ_y)	9.89

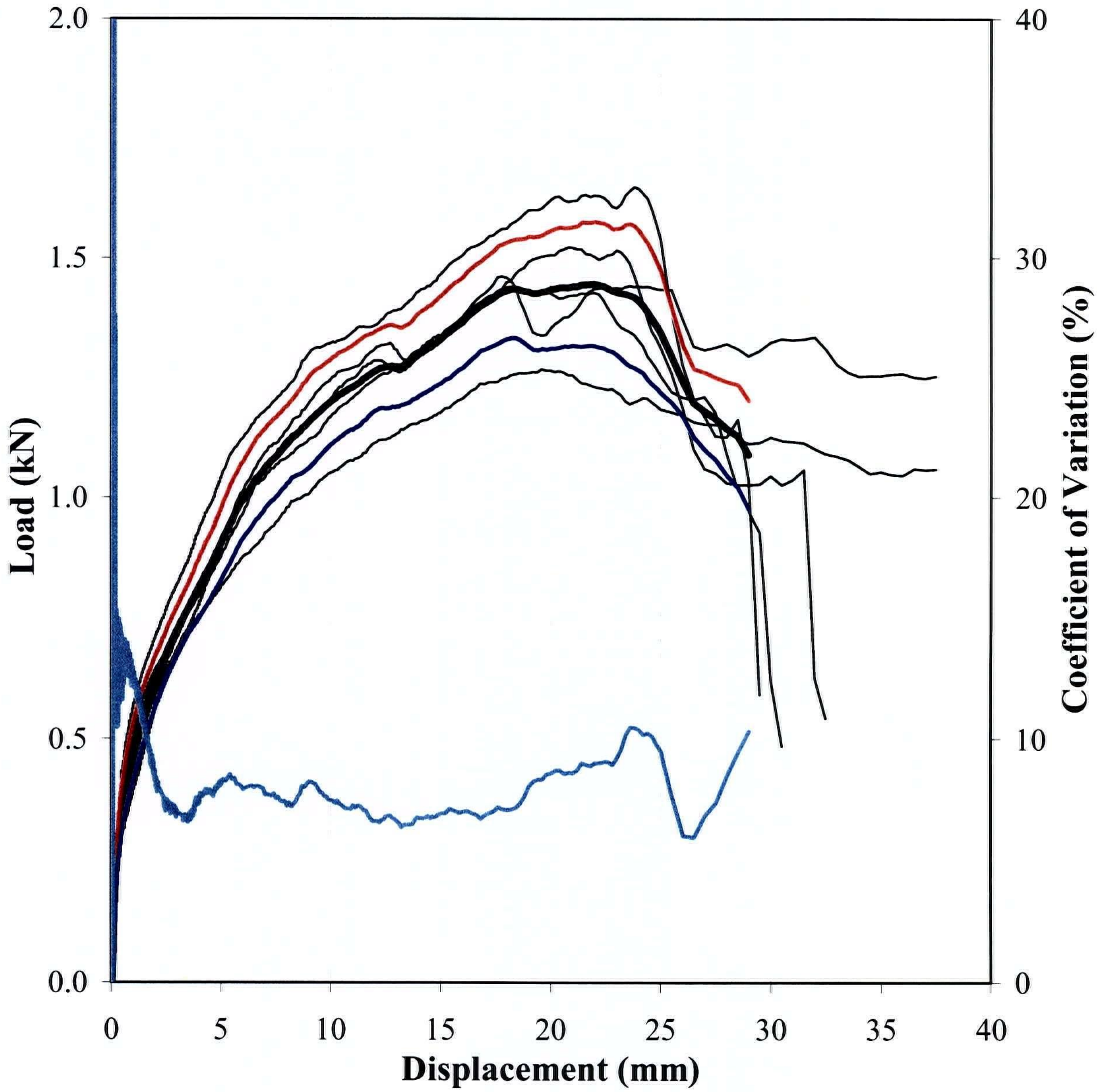

SPECIMEN GROUP 039

Description		Properties as defined by the CEN protocol	
Spiral nail length (mm)	76	Yield load F_y (kN)	0.956
Sheathing thickness (mm)	28.5	Yield displacement Δ_y (mm)	1.66
Sheathing material	CSP	Maximum load F_{max} (kN)	2.098
Sheathing orientation	PAR	Displacement at F_{max} (mm)	20.60
Stud material	Glulam	Ultimate displacement Δ_u (mm)	39.00
Number of specimens	5	Initial stiffness (N/mm)	591
		Ductility (Δ_u/Δ_y)	23.49

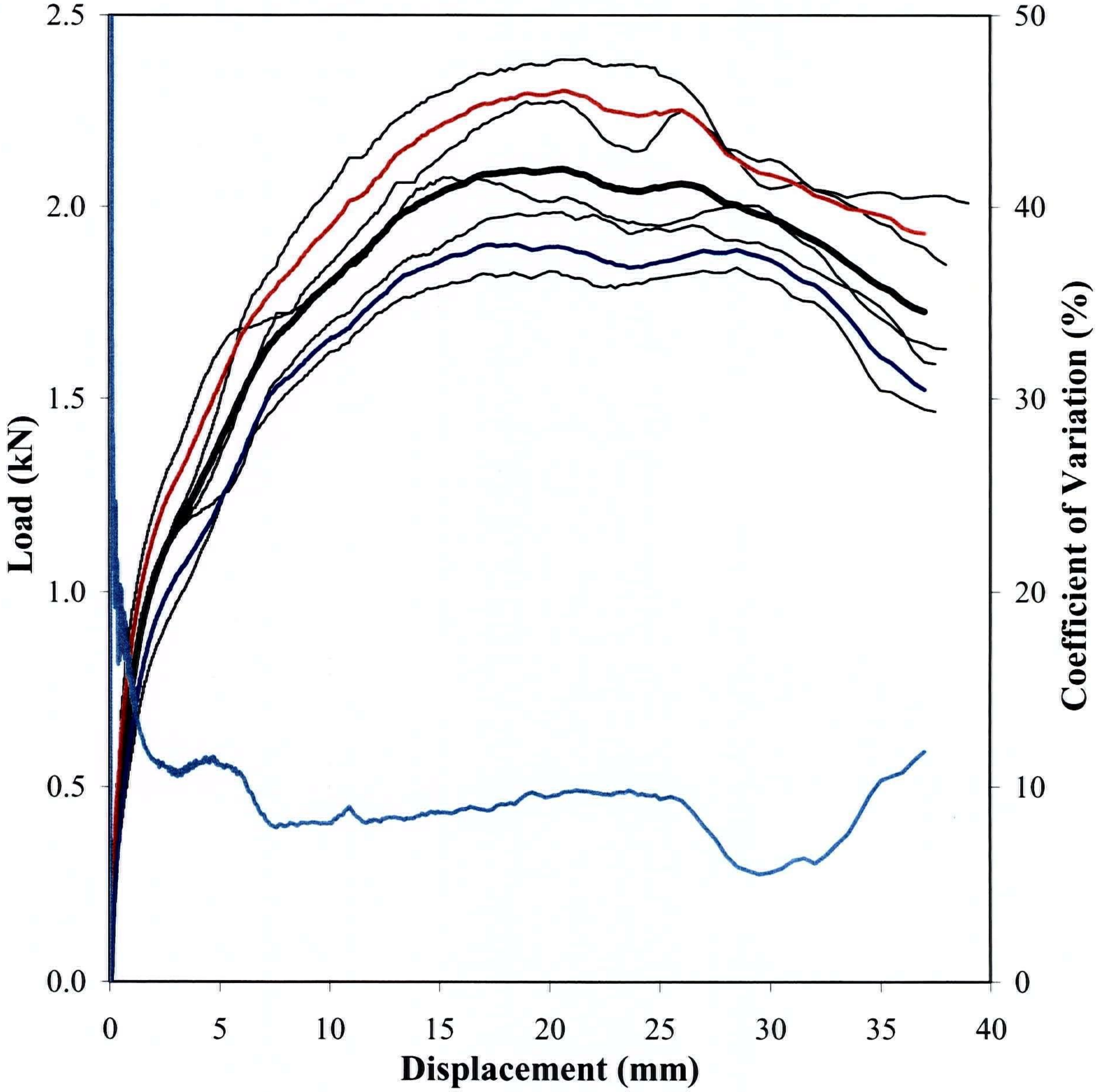

SPECIMEN GROUP 040

Description		Properties as defined by the CEN protocol	
Spiral nail length (mm)	65	Yield load F_y (kN)	0.615
Sheathing thickness (mm)	9.5	Yield displacement Δ_y (mm)	1.82
Sheathing material	OSB	Maximum load F_{max} (kN)	1.221
Sheathing orientation	PAR	Displacement at F_{max} (mm)	16.20
Stud material	Glulam	Ultimate displacement Δ_u (mm)	28.50
Number of specimens	5	Initial stiffness (N/mm)	367
		Ductility (Δ_u/Δ_y)	15.66

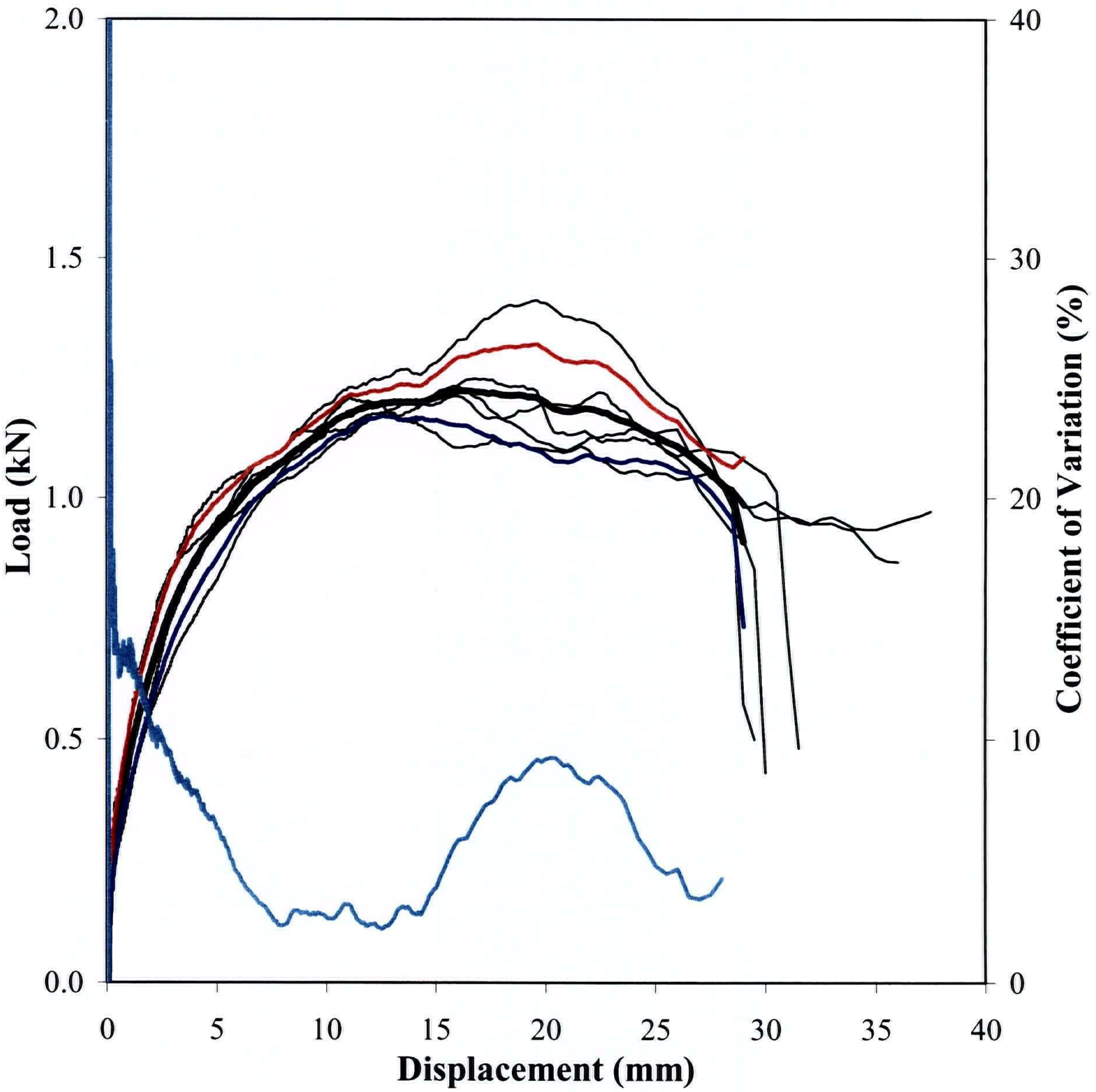

SPECIMEN GROUP 041

Description		Properties as defined by the CEN protocol	
Spiral nail length (mm)	65	Yield load F_y (kN)	0.604
Sheathing thickness (mm)	18.5	Yield displacement Δ_y (mm)	1.14
Sheathing material	OSB	Maximum load F_{max} (kN)	1.329
Sheathing orientation	PAR	Displacement at F_{max} (mm)	19.20
Stud material	Glulam	Ultimate displacement Δ_u (mm)	34.50
Number of specimens	5	Initial stiffness (N/mm)	491
		Ductility (Δ_u/Δ_y)	30.26

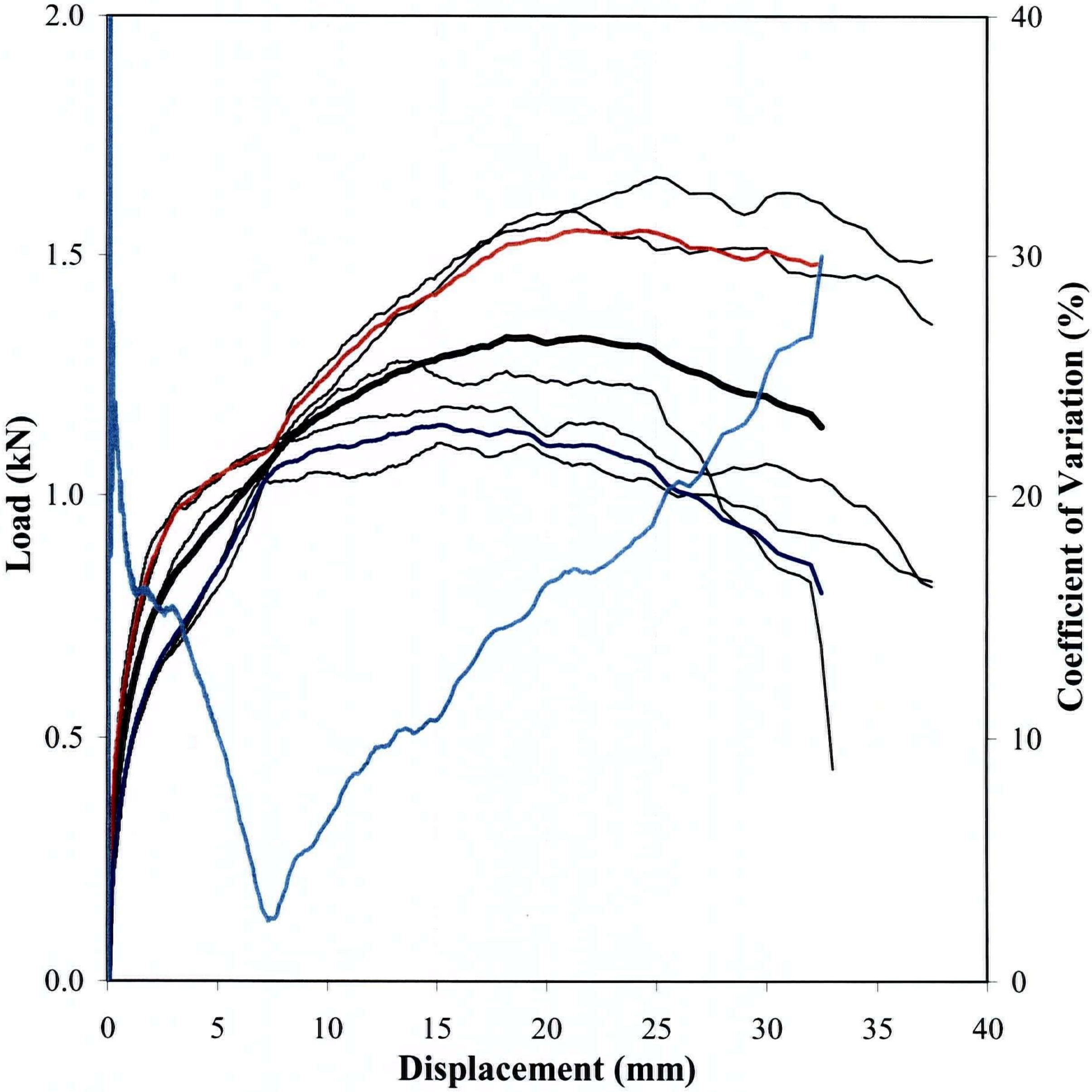

SPECIMEN GROUP 042

Description		Properties as defined by the CEN protocol	
Spiral nail length (mm)	76	Yield load F_y (kN)	0.860
Sheathing thickness (mm)	28.5	Yield displacement Δ_y (mm)	1.70
Sheathing material	OSB	Maximum load F_{max} (kN)	1.836
Sheathing orientation	PAR	Displacement at F_{max} (mm)	19.40
Stud material	Glulam	Ultimate displacement Δ_u (mm)	39.00
Number of specimens	5	Initial stiffness (N/mm)	531
		Ductility (Δ_u/Δ_y)	22.94

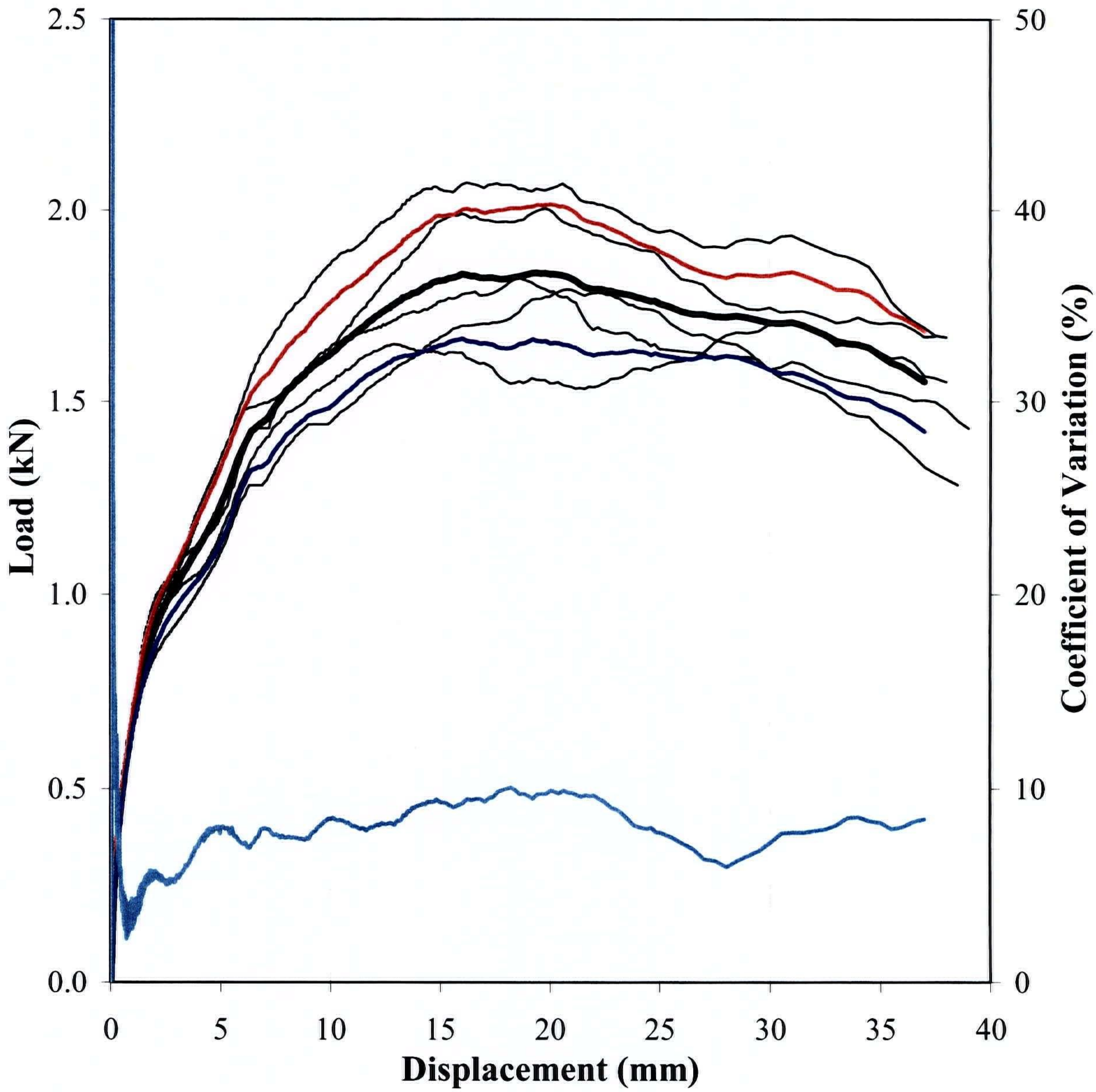

SPECIMEN GROUP 043

Description		Properties as defined by the CEN protocol	
Spiral nail length (mm)	65	Yield load F_y (kN)	0.713
Sheathing thickness (mm)	9.5	Yield displacement Δ_y (mm)	2.02
Sheathing material	CSP	Maximum load F_{max} (kN)	1.392
Sheathing orientation	PERP	Displacement at F_{max} (mm)	14.30
Stud material	Glulam	Ultimate displacement Δ_u (mm)	21.00
Number of specimens	5	Initial stiffness (N/mm)	377
		Ductility (Δ_u/Δ_y)	10.40

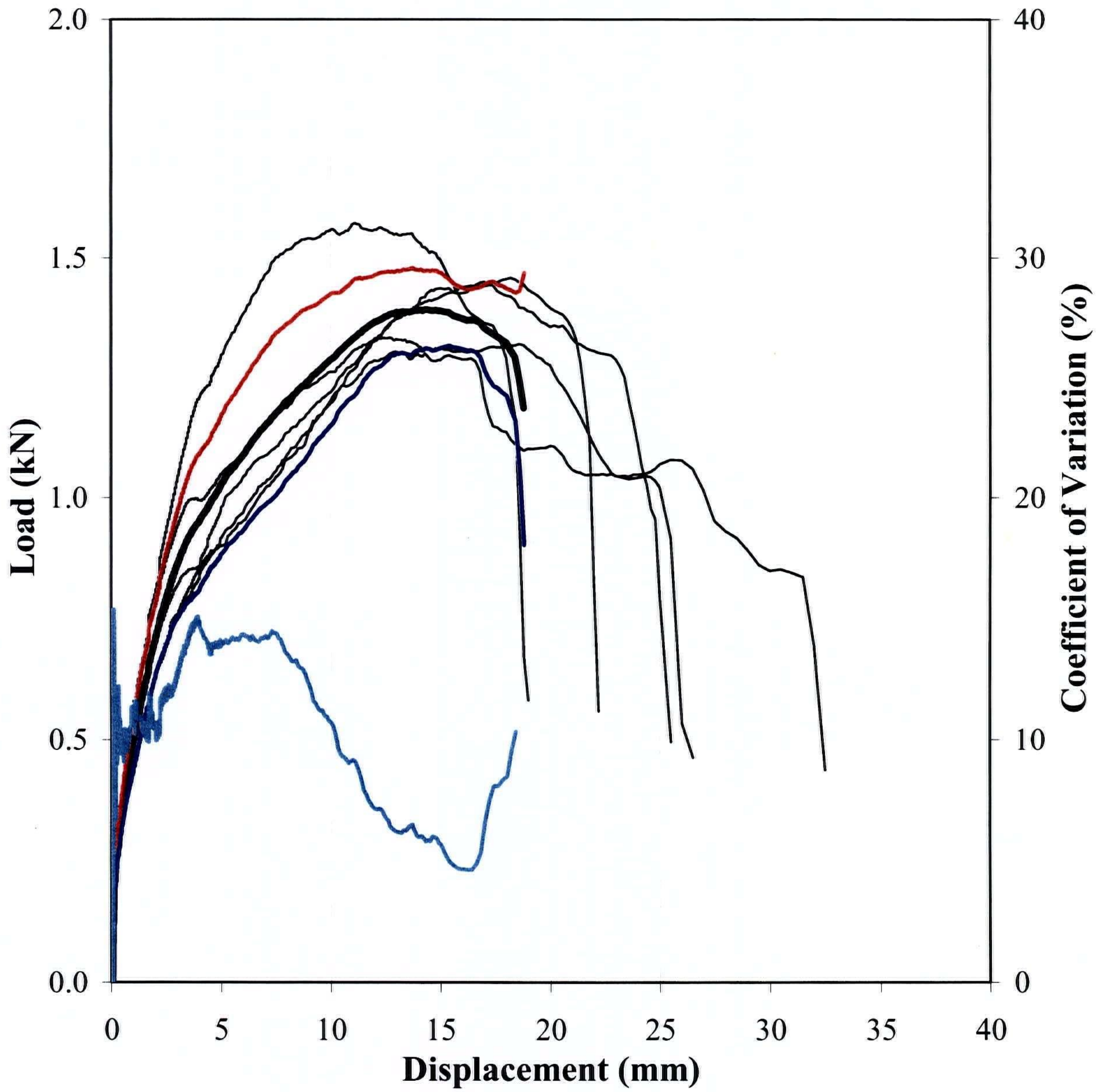

SPECIMEN GROUP 044

Description		Properties as defined by the CEN protocol	
Spiral nail length (mm)	65	Yield load F_y (kN)	0.624
Sheathing thickness (mm)	18.5	Yield displacement Δ_y (mm)	1.80
Sheathing material	CSP	Maximum load F_{max} (kN)	1.365
Sheathing orientation	PERP	Displacement at F_{max} (mm)	19.20
Stud material	Glulam	Ultimate displacement Δ_u (mm)	34.50
Number of specimens	5	Initial stiffness (N/mm)	359
		Ductility (Δ_u/Δ_y)	19.17

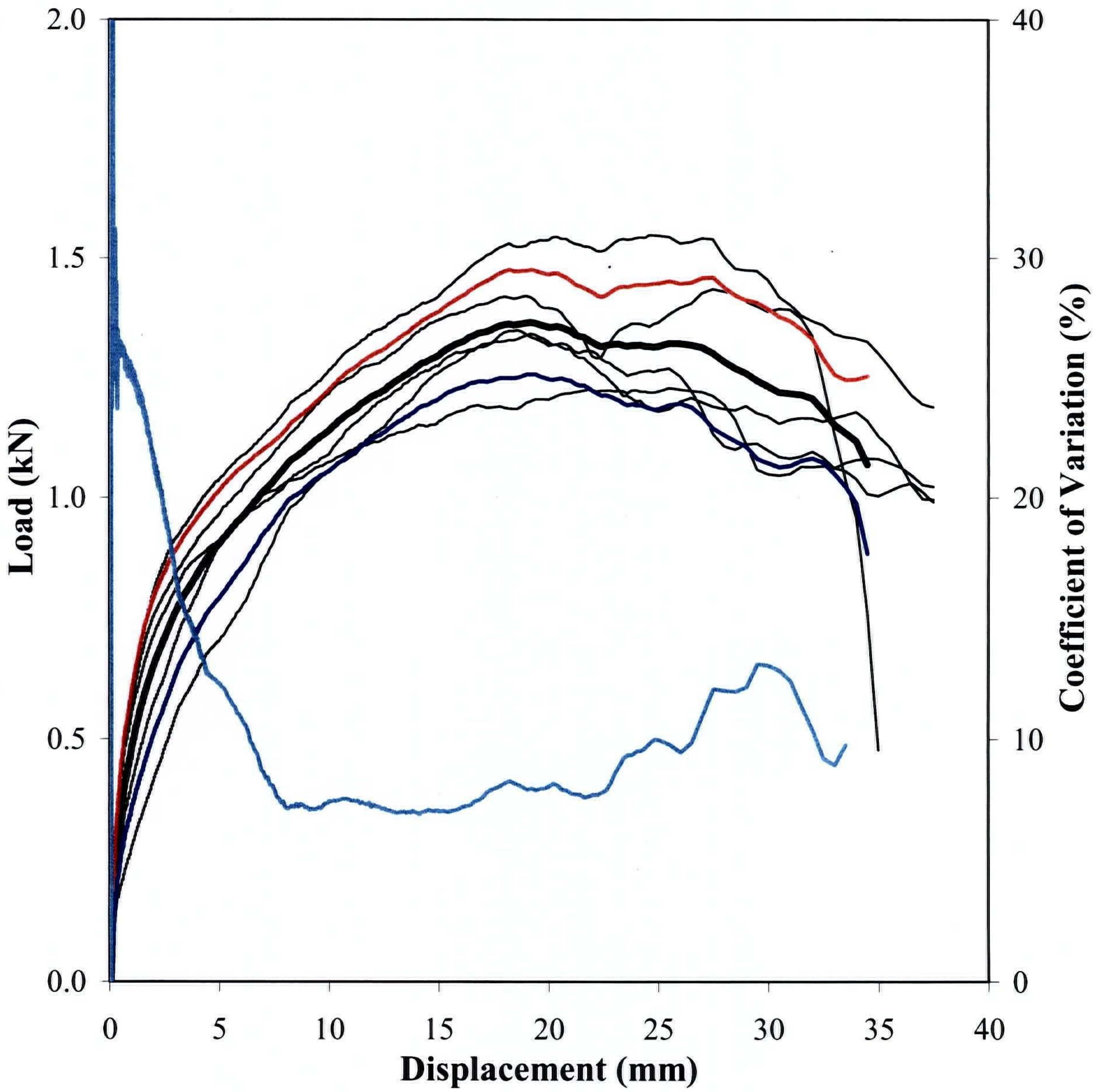

SPECIMEN GROUP 045

Description		Properties as defined by the CEN protocol	
Spiral nail length (mm)	76	Yield load F_y (kN)	0.901
Sheathing thickness (mm)	28.5	Yield displacement Δ_y (mm)	1.48
Sheathing material	CSP	Maximum load F_{max} (kN)	1.985
Sheathing orientation	PERP	Displacement at F_{max} (mm)	18.20
Stud material	Glulam	Ultimate displacement Δ_u (mm)	38.00
Number of specimens	5	Initial stiffness (N/mm)	625
		Ductility (Δ_u/Δ_y)	25.68

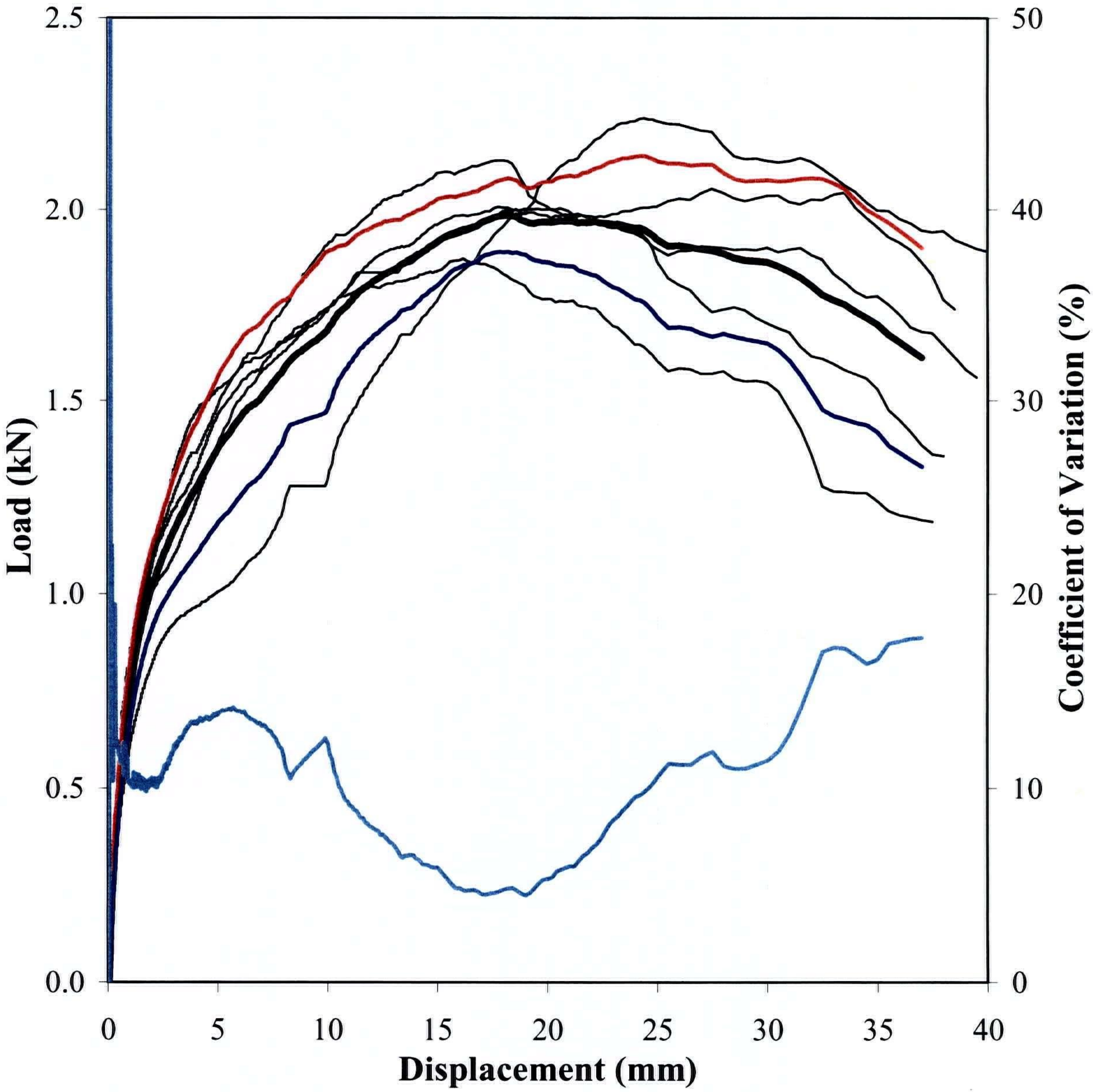

SPECIMEN GROUP 046

Description		Properties as defined by the CEN protocol	
Spiral nail length (mm)	65	Yield load F_y (kN)	0.773
Sheathing thickness (mm)	9.5	Yield displacement Δ_y (mm)	3.56
Sheathing material	OSB	Maximum load F_{max} (kN)	1.403
Sheathing orientation	PERP	Displacement at F_{max} (mm)	18.20
Stud material	Glulam	Ultimate displacement Δ_u (mm)	23.60
Number of specimens	5	Initial stiffness (N/mm)	228
		Ductility (Δ_u/Δ_y)	6.63

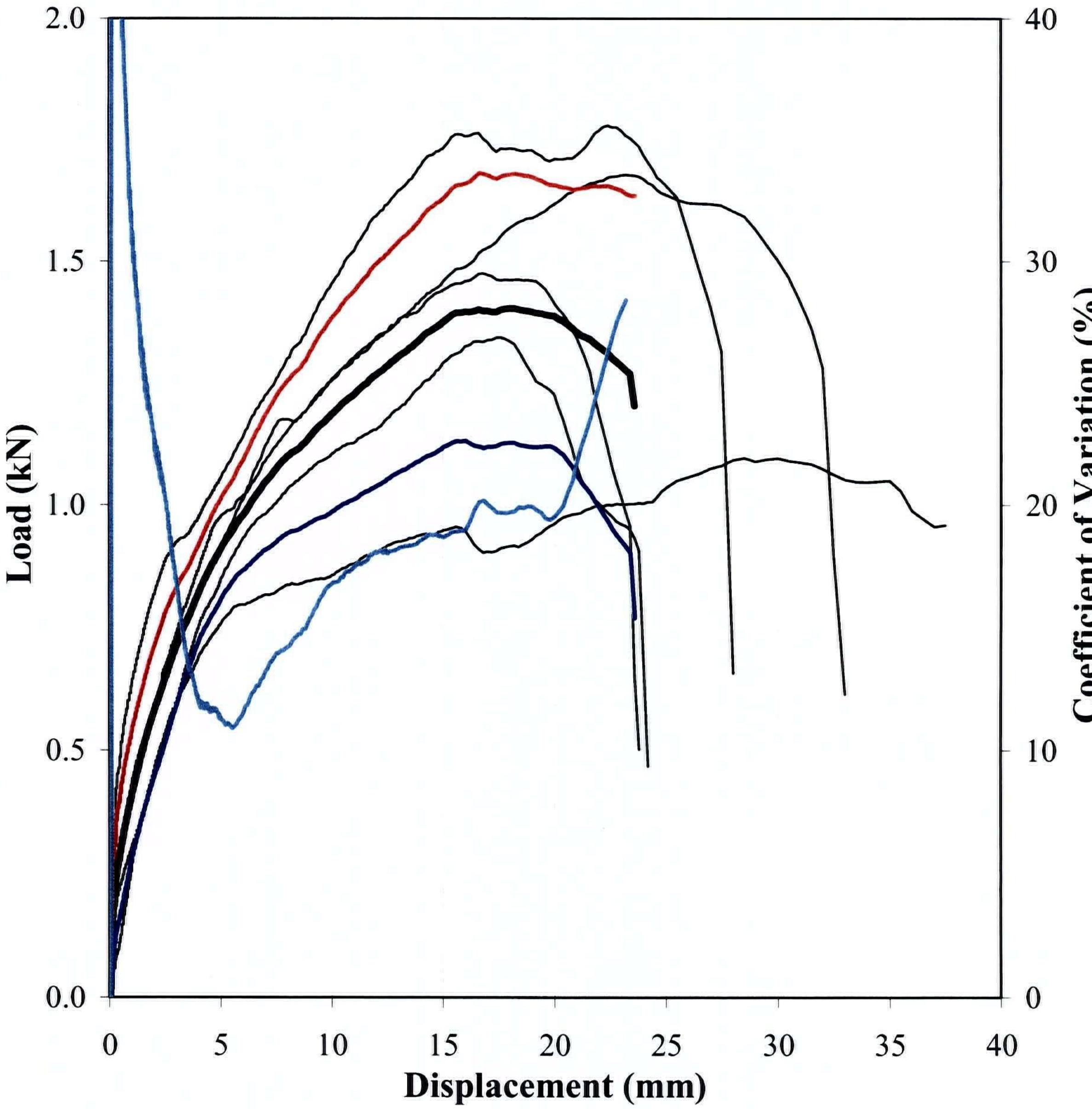

SPECIMEN GROUP 047

Description		Properties as defined by the CEN protocol	
Spiral nail length (mm)	65	Yield load F_y (kN)	0.588
Sheathing thickness (mm)	18.5	Yield displacement Δ_y (mm)	0.86
Sheathing material	OSB	Maximum load F_{max} (kN)	1.357
Sheathing orientation	PERP	Displacement at F_{max} (mm)	23.00
Stud material	Glulam	Ultimate displacement Δ_u (mm)	34.50
Number of specimens	5	Initial stiffness (N/mm)	690
		Ductility (Δ_u/Δ_y)	40.12

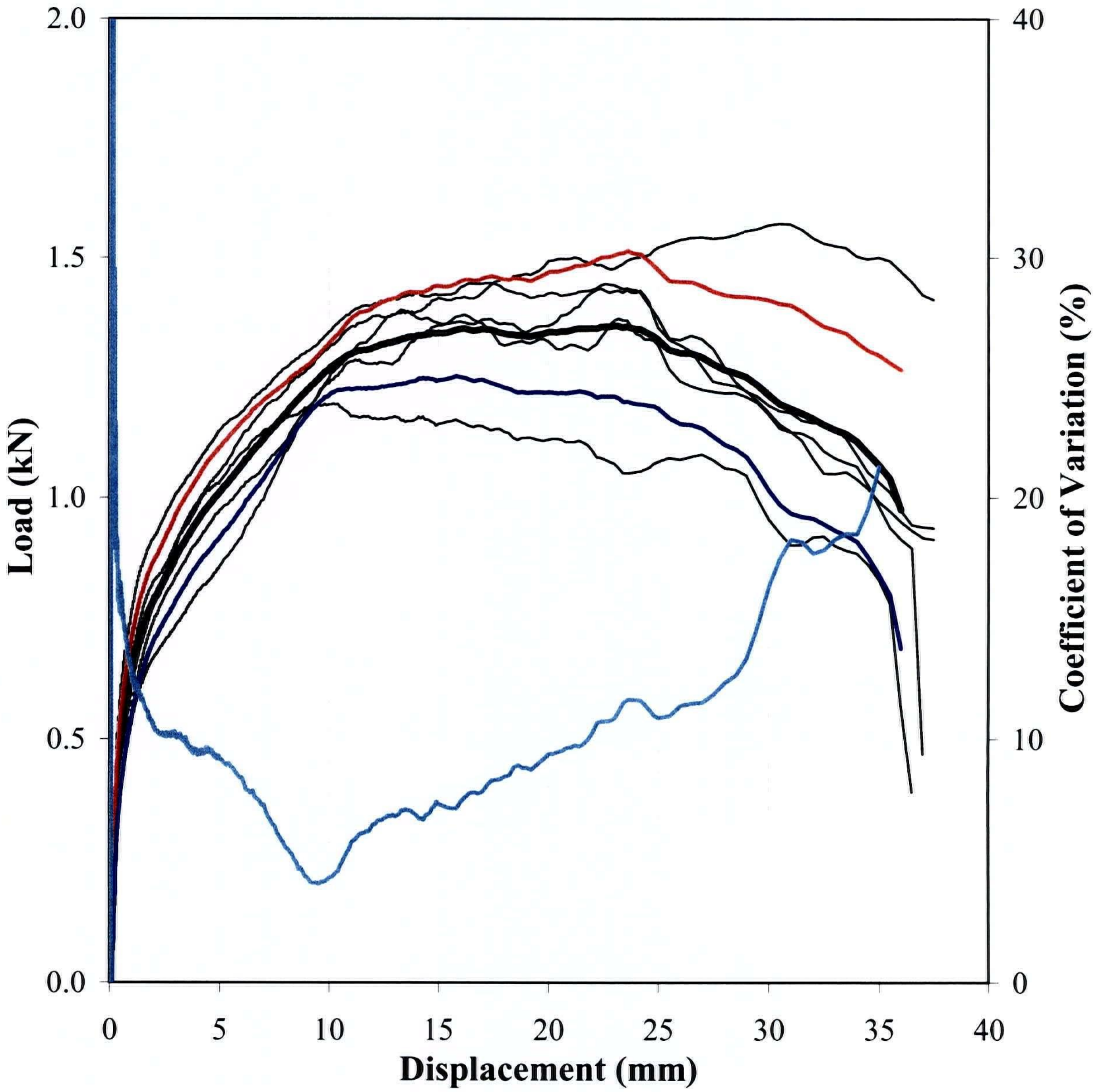

SPECIMEN GROUP 048

Description		Properties as defined by the CEN protocol	
Spiral nail length (mm)	76	Yield load F_y (kN)	0.903
Sheathing thickness (mm)	28.5	Yield displacement Δ_y (mm)	1.58
Sheathing material	OSB	Maximum load F_{max} (kN)	1.926
Sheathing orientation	PERP	Displacement at F_{max} (mm)	17.80
Stud material	Glulam	Ultimate displacement Δ_u (mm)	34.00
Number of specimens	5	Initial stiffness (N/mm)	618
		Ductility (Δ_u/Δ_y)	21.52

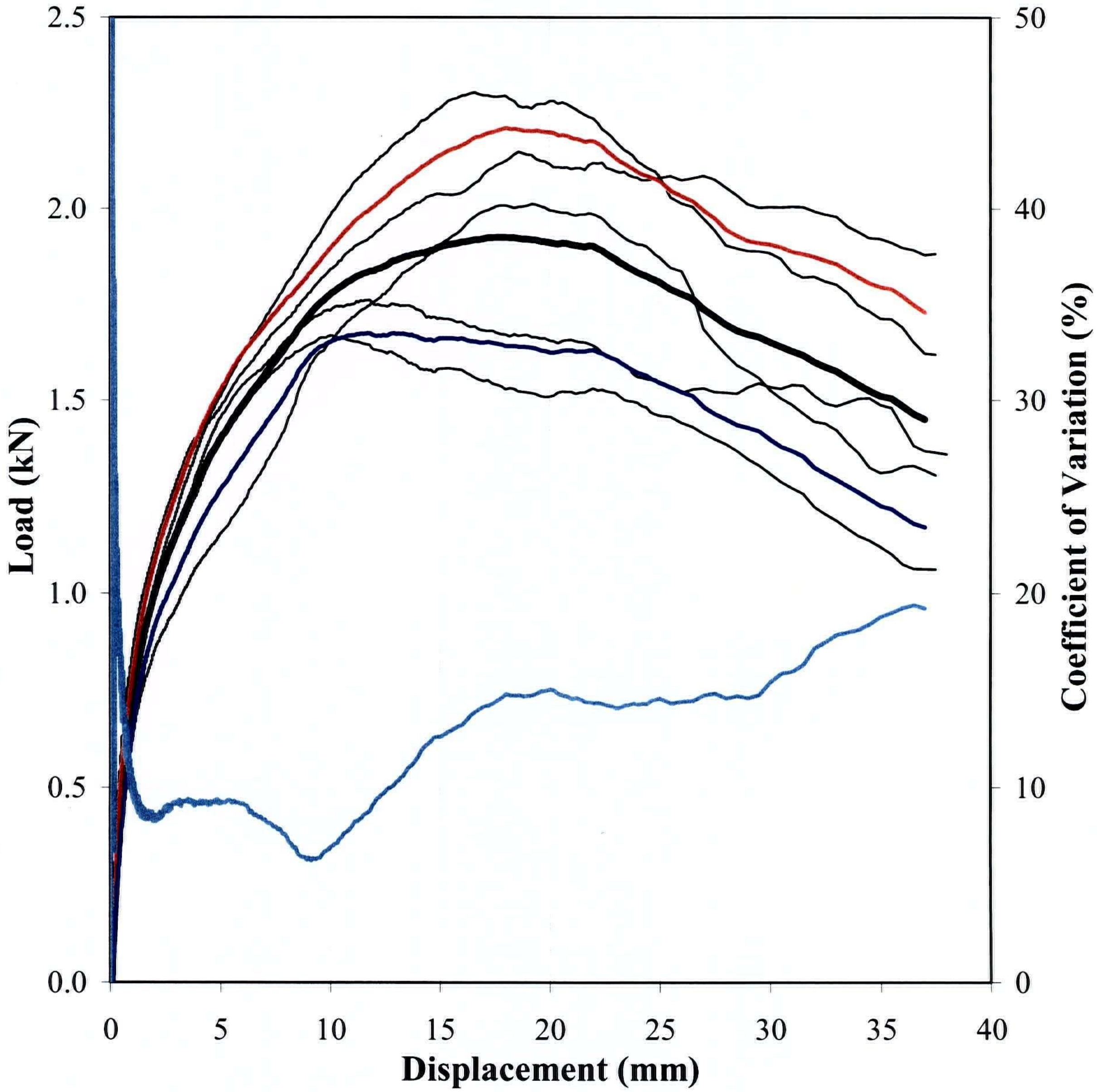

SPECIMEN GROUP 049

Description		Properties as defined by the CEN protocol	
Spiral nail length (mm)	102	Yield load F_y (kN)	1.307
Sheathing thickness (mm)	28.5	Yield displacement Δ_y (mm)	2.64
Sheathing material	CSP	Maximum load F_{max} (kN)	2.477
Sheathing orientation	PER	Displacement at F_{max} (mm)	22.20
Stud material	SPF	Ultimate displacement Δ_u (mm)	33.00
Number of specimens	5	Initial stiffness (N/mm)	526
		Ductility (Δ_u/Δ_y)	12.50

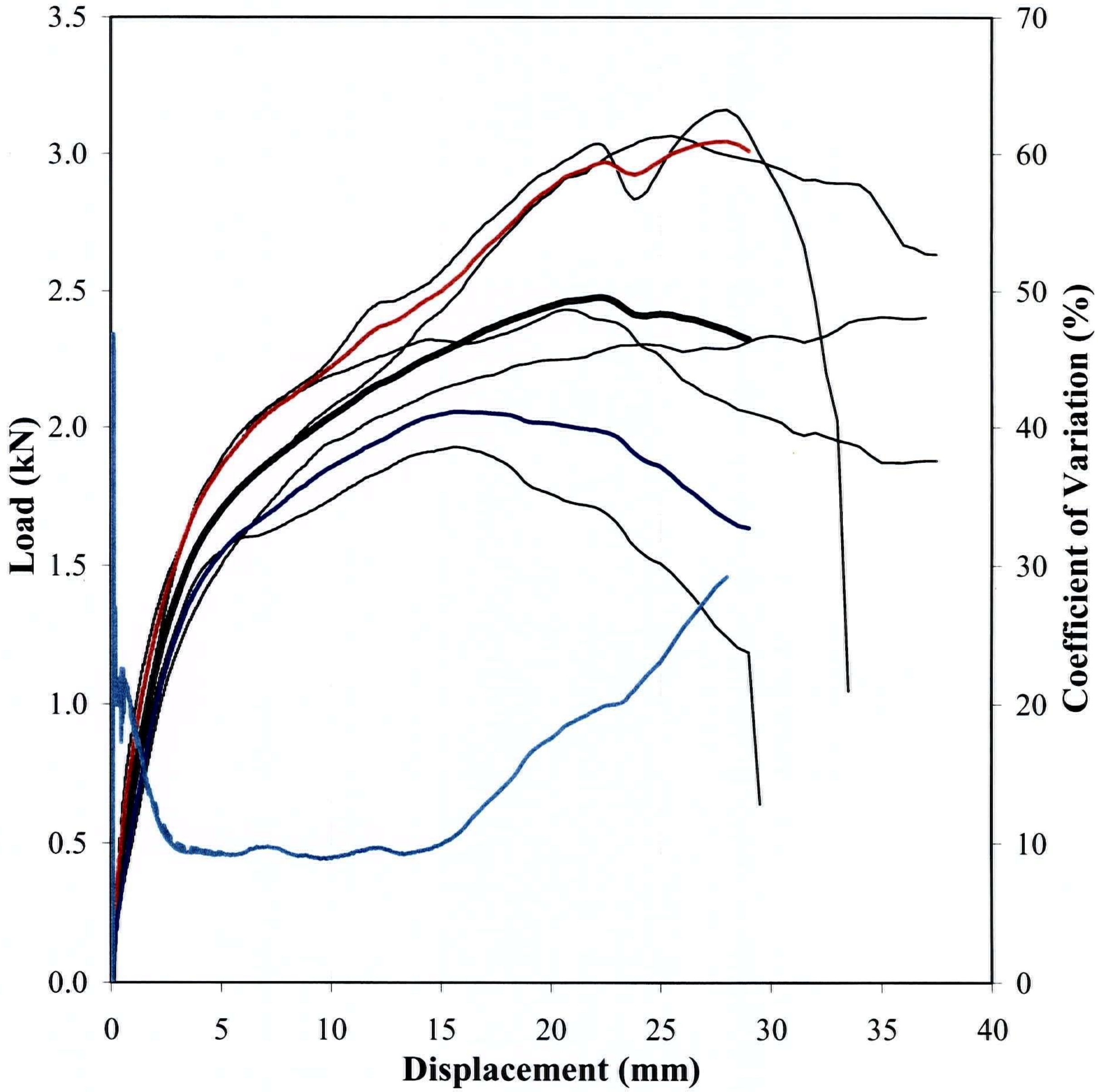

SPECIMEN GROUP 050

Description		Properties as defined by the CEN protocol	
Spiral nail length (mm)	102	Yield load F_y (kN)	1.166
Sheathing thickness (mm)	28.5	Yield displacement Δ_y (mm)	1.30
Sheathing material	OSB	Maximum load F_{max} (kN)	2.530
Sheathing orientation	PAR	Displacement at F_{max} (mm)	19.40
Stud material	SPF	Ultimate displacement Δ_u (mm)	31.50
Number of specimens	5	Initial stiffness (N/mm)	954
		Ductility (Δ_u/Δ_y)	24.23

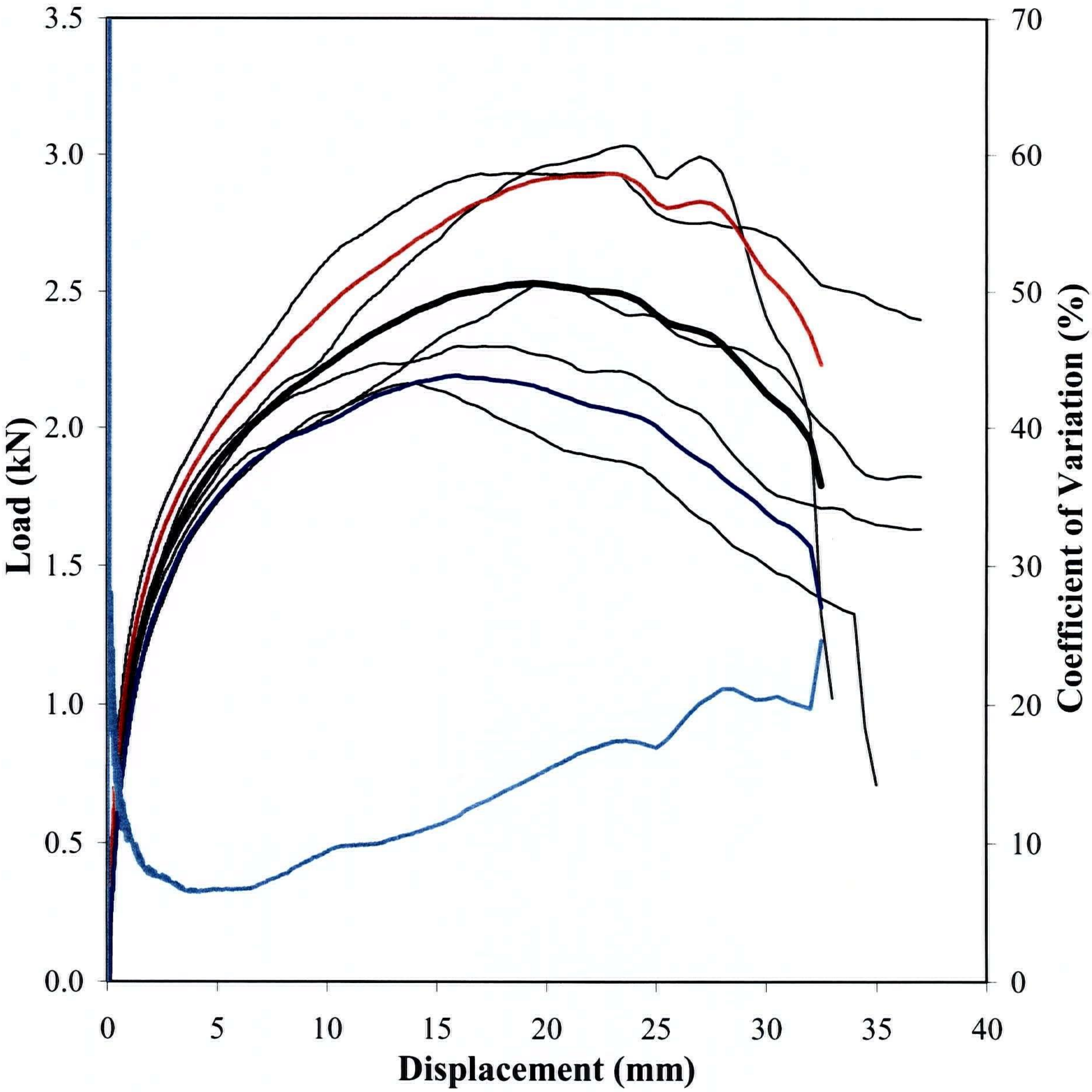

SPECIMEN GROUP 051

Description		**Properties as defined by the CEN protocol**	
Spiral nail length (mm)	102	Yield load F_y (kN)	1.670
Sheathing thickness (mm)	28.5	Yield displacement Δ_y (mm)	3.14
Sheathing material	CSP	Maximum load F_{max} (kN)	3.597
Sheathing orientation	PAR	Displacement at F_{max} (mm)	24.40
Stud material	LSL	Ultimate displacement Δ_u (mm)	34.50
Number of specimens	5	Initial stiffness (N/mm)	557
		Ductility (Δ_u/Δ_y)	10.99

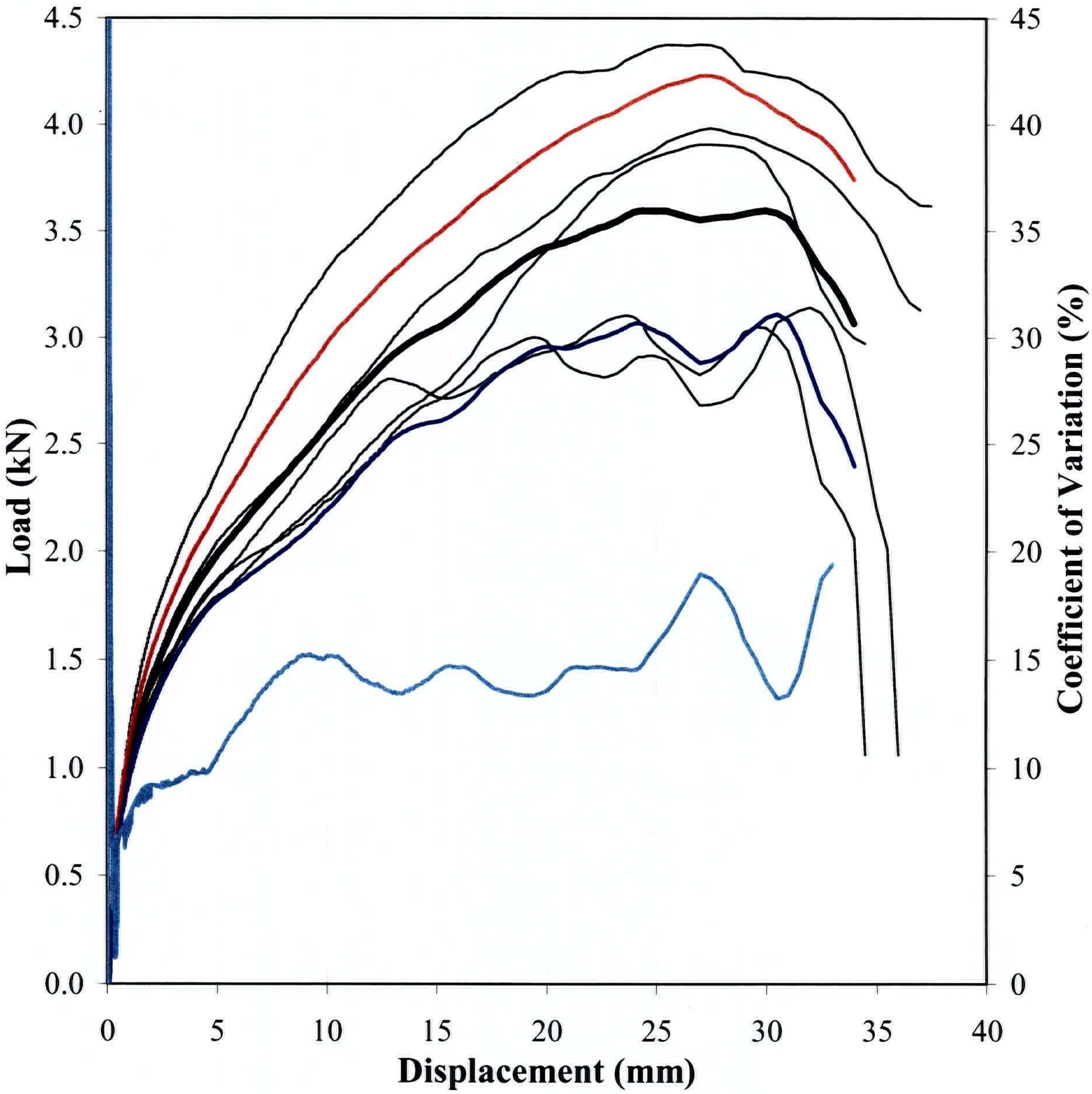

SPECIMEN GROUP 052

Description		Properties as defined by the CEN protocol	
Spiral nail length (mm)	102	Yield load F_y (kN)	1.294
Sheathing thickness (mm)	28.5	Yield displacement Δ_y (mm)	1.26
Sheathing material	OSB	Maximum load F_{max} (kN)	2.782
Sheathing orientation	PAR	Displacement at F_{max} (mm)	14.10
Stud material	LSL	Ultimate displacement Δ_u (mm)	21.40
Number of specimens	5	Initial stiffness (N/mm)	1076
		Ductility (Δ_u/Δ_y)	16.98

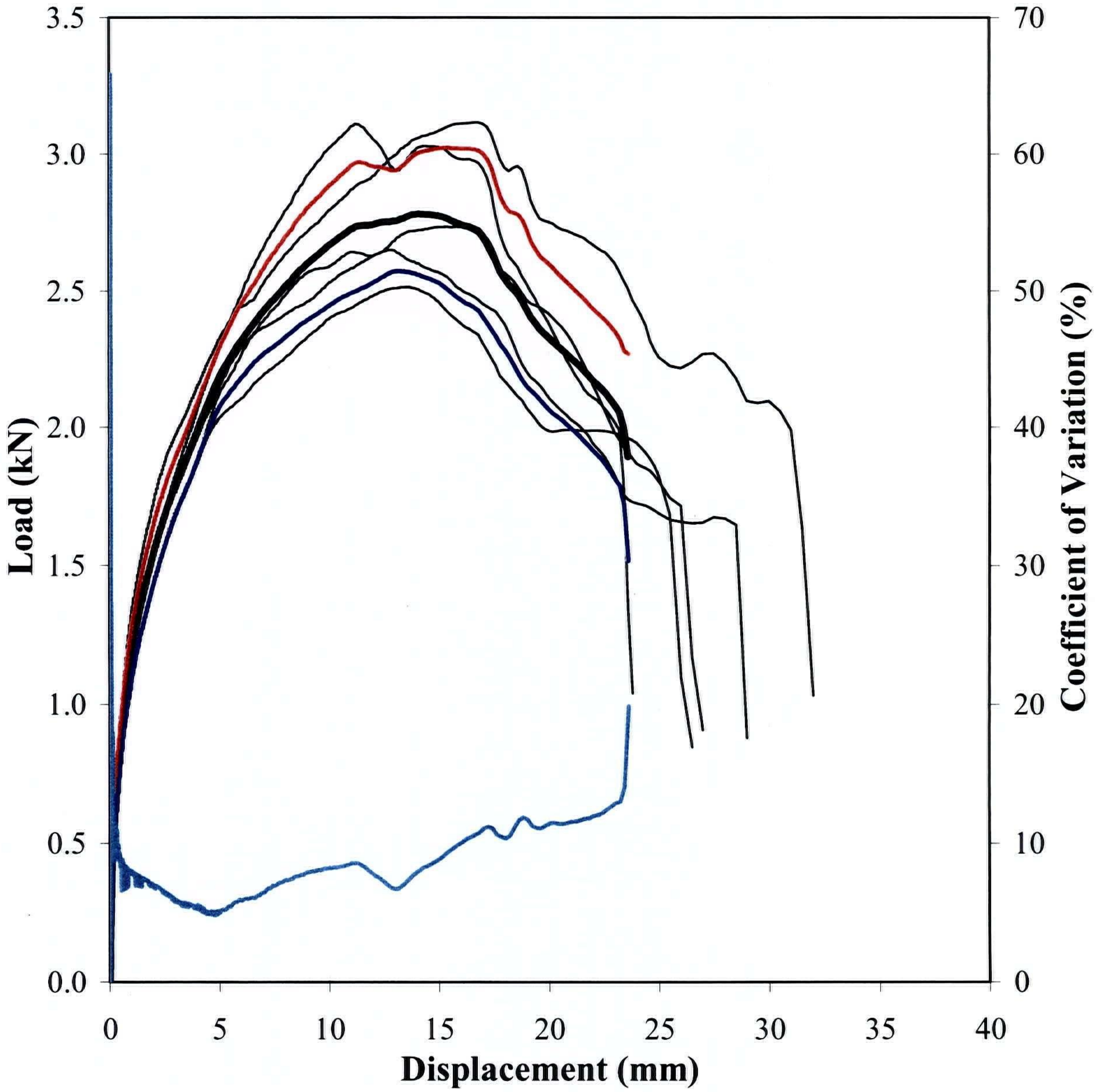

SPECIMEN GROUP 053

Description		Properties as defined by the CEN protocol	
Spiral nail length (mm)	65	Yield load F_y (kN)	0.890
Sheathing thickness (mm)	15.5	Yield displacement Δ_y (mm)	2.22
Sheathing material	OSB	Maximum load F_{max} (kN)	1.773
Sheathing orientation	PAR	Displacement at F_{max} (mm)	13.80
Stud material	LSL	Ultimate displacement Δ_u (mm)	22.80
Number of specimens	6	Initial stiffness (N/mm)	419
		Ductility (Δ_u/Δ_y)	10.27

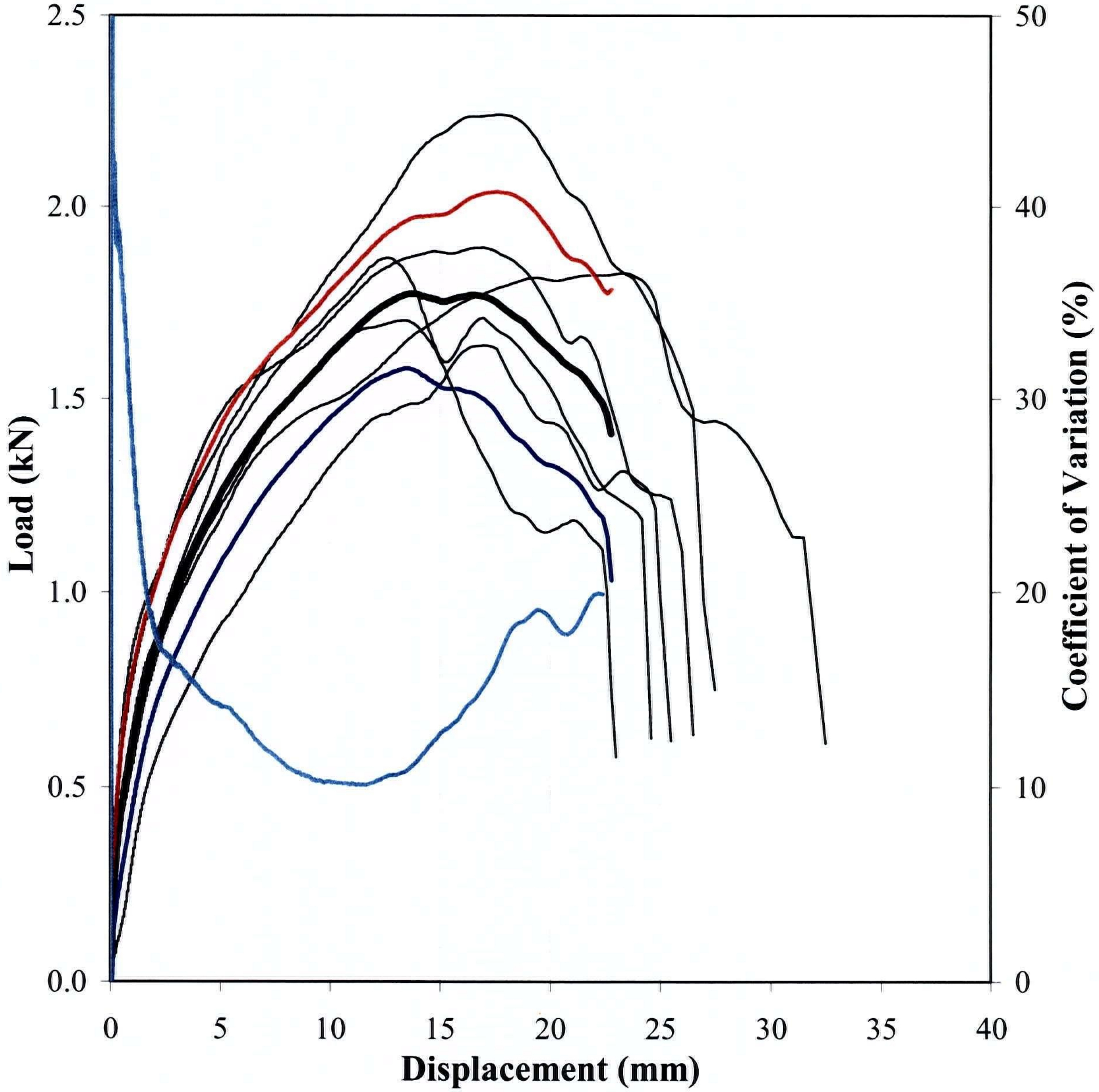

A.2 WITHDRAWAL TESTS

A summary of the withdrawal test results is presented in Chapter 4. A schematic of the test set-up is shown in Figure 4.3. The relative density of each of the connection components is presented in Figure 3.5 in Chapter 3. The average properties of the spiral nails used are presented in Table 3.2 and Figure 3.8 in Chapter 3. Connection properties, as defined by the CEN protocol (CEN, 1995), are presented in tabular form. This protocol is described in detail in Section 2.7 of Chapter 2.

SPECIMEN GROUP 101

Description		Properties as defined by the CEN protocol	
Spiral nail length (mm)	65	Yield load F_y (kN)	0.437
Stud material	SPF	Yield displacement Δ_y (mm)	0.36
Number of specimens	7	Maximum load F_{max} (kN)	0.694
		Displacement at F_{max} (mm)	3.22
		Ultimate displacement Δ_u (mm)	11.60
		Initial stiffness (N/mm)	1642
		Ductility (Δ_u/Δ_y)	32.22

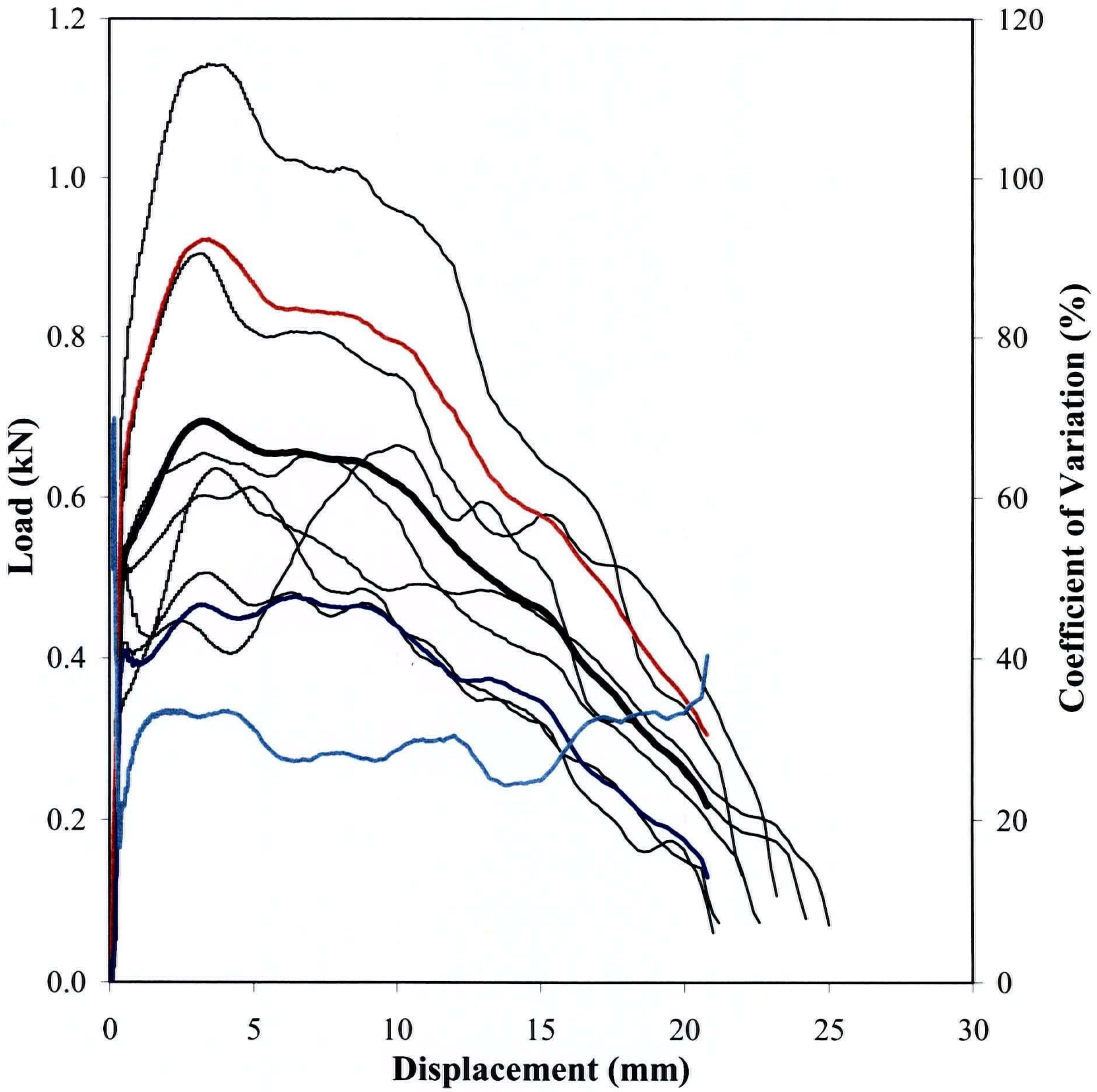

SPECIMEN GROUP 102

Description		Properties as defined by the CEN protocol	
Spiral nail length (mm)	65	Yield load F_y (kN)	0.527
Stud material	LVL	Yield displacement Δ_y (mm)	0.42
Number of specimens	7	Maximum load F_{max} (kN)	0.762
		Displacement at F_{max} (mm)	3.18
		Ultimate displacement Δ_u (mm)	13.20
		Initial stiffness (N/mm)	1806
		Ductility (Δ_u/Δ_y)	31.43

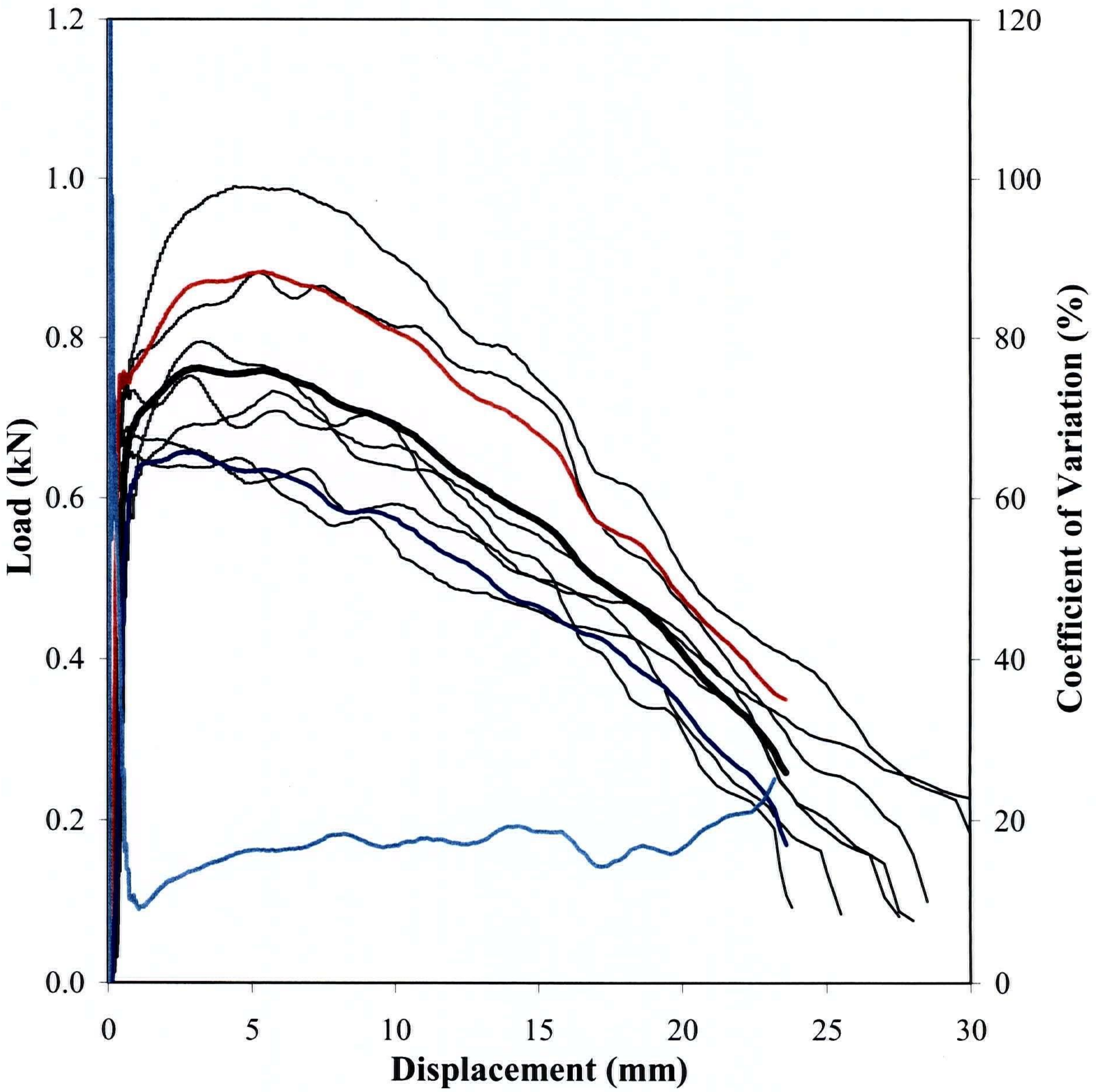

SPECIMEN GROUP 103

Description		**Properties as defined by the CEN protocol**	
Spiral nail length (mm)	76	Yield load F_y (kN)	1.307
Stud material	LVL	Yield displacement Δ_y (mm)	0.62
Number of specimens	7	Maximum load F_{max} (kN)	1.806
		Displacement at F_{max} (mm)	3.34
		Ultimate displacement Δ_u (mm)	11.00
		Initial stiffness (N/mm)	2681
		Ductility (Δ_u/Δ_y)	17.74

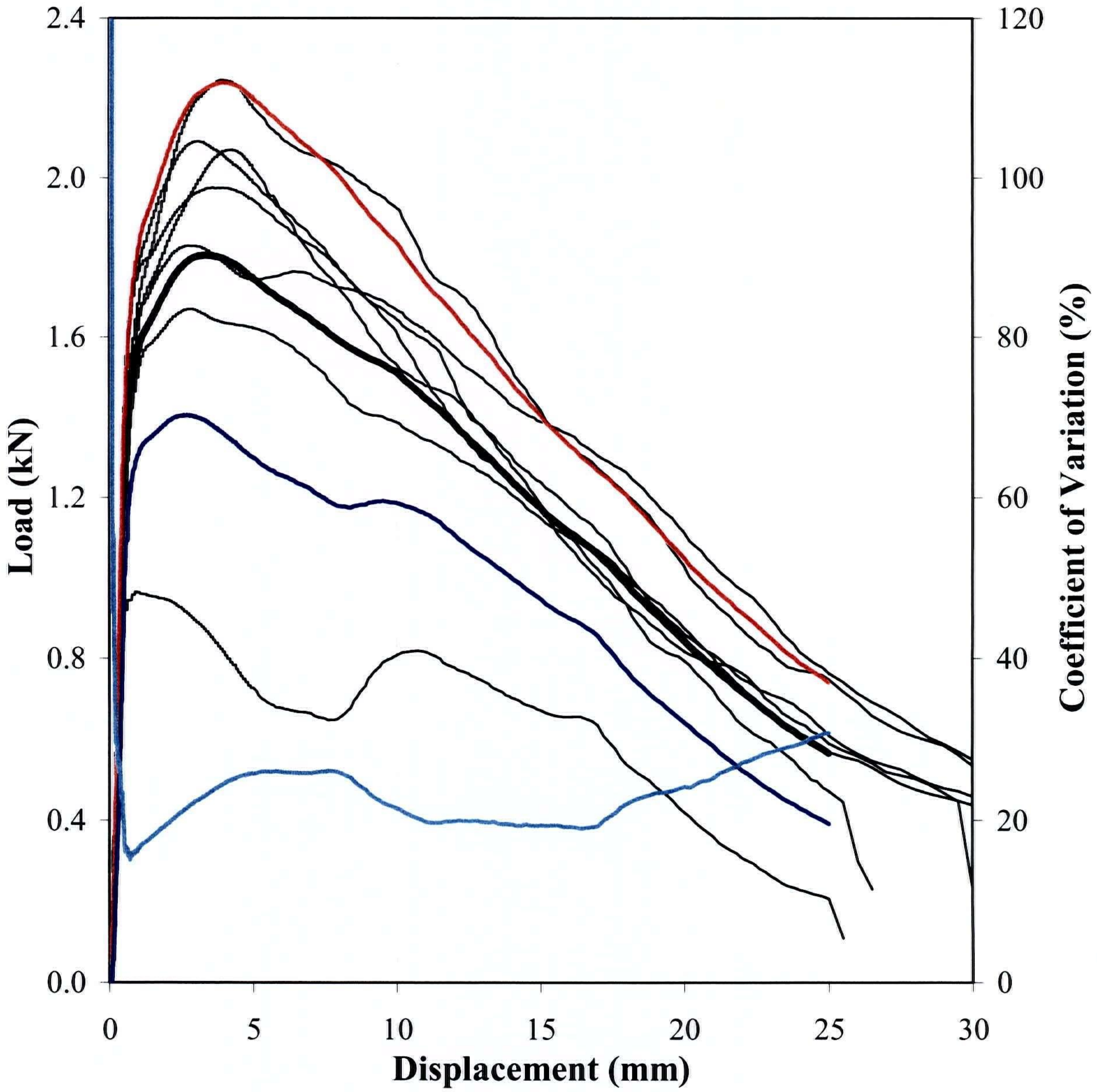

SPECIMEN GROUP 104

Description		Properties as defined by the CEN protocol	
Spiral nail length (mm)	65	Yield load F_y (kN)	0.879
Stud material	LSL	Yield displacement Δ_y (mm)	0.52
Number of specimens	9	Maximum load F_{max} (kN)	1.417
		Displacement at F_{max} (mm)	4.30
		Ultimate displacement Δ_u (mm)	8.10
		Initial stiffness (N/mm)	2184
		Ductility (Δ_u/Δ_y)	15.58

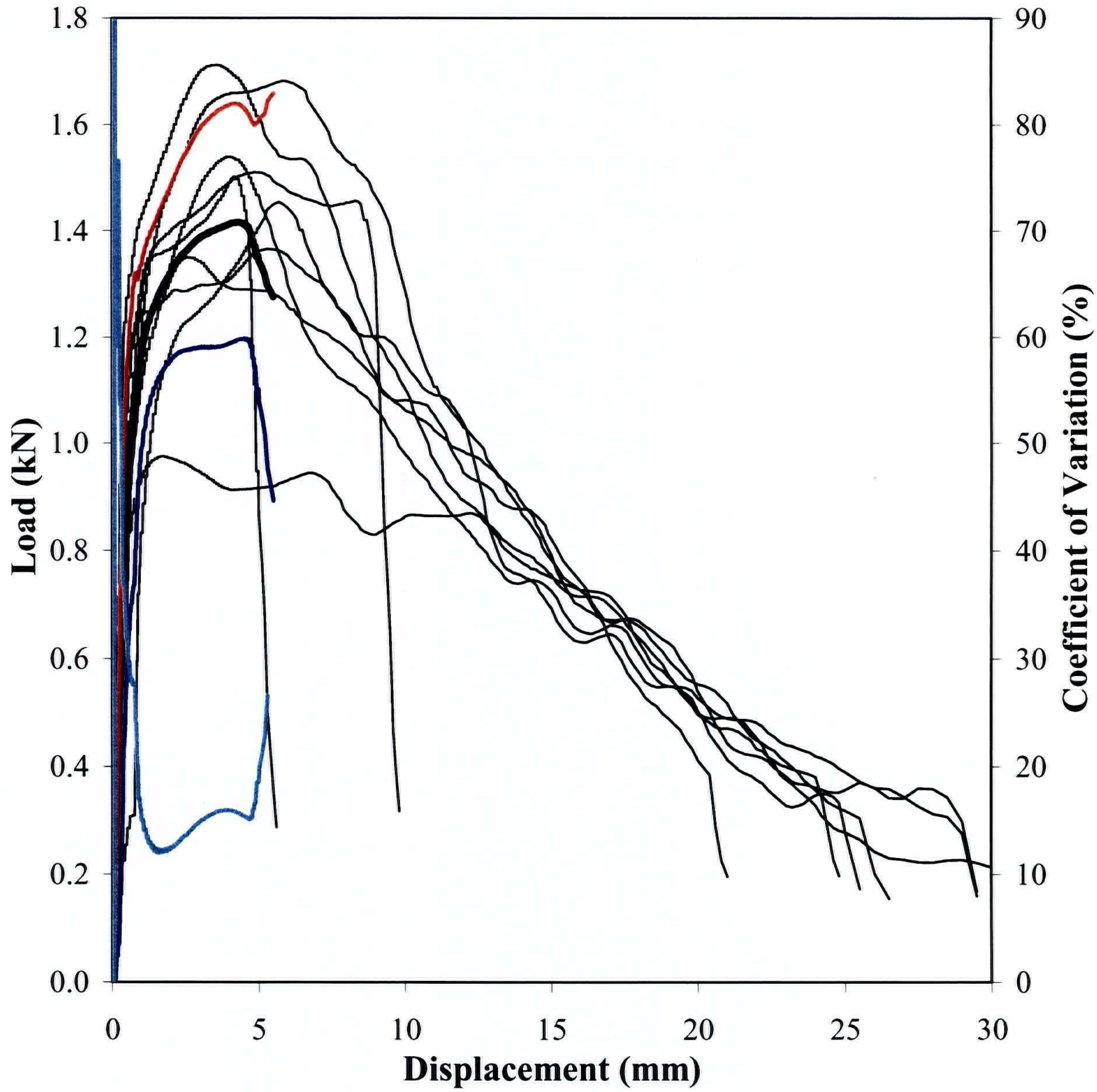

SPECIMEN GROUP 105

Description

Spiral nail length (mm)	76
Stud material	LSL
Number of specimens	10

Properties as defined by the CEN protocol

Yield load F_y (kN)	1.722
Yield displacement Δ_y (mm)	0.96
Maximum load F_{max} (kN)	2.170
Displacement at F_{max} (mm)	4.54
Ultimate displacement Δ_u (mm)	10.70
Initial stiffness (N/mm)	2054
Ductility (Δ_u/Δ_y)	11.15

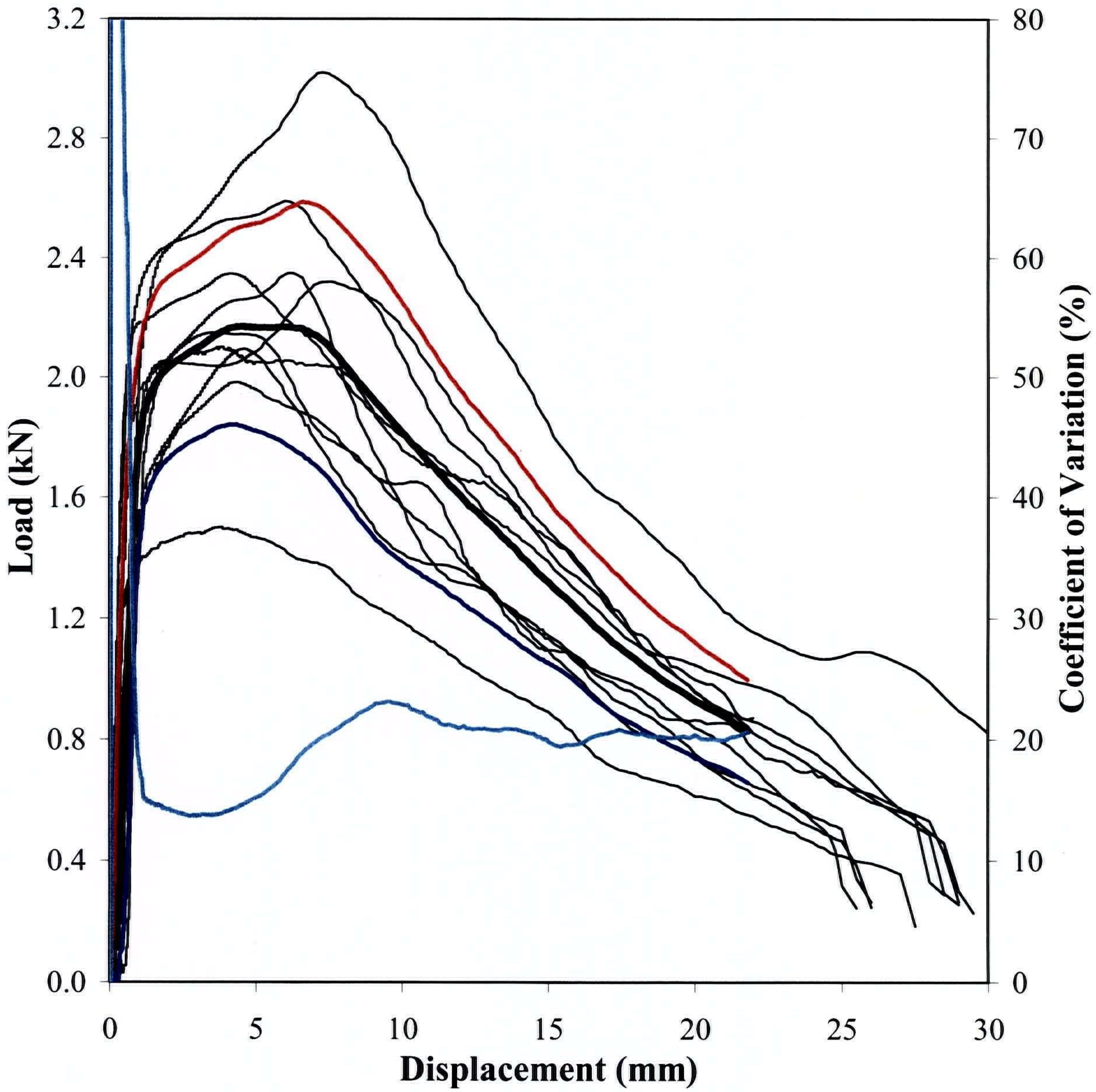

SPECIMEN GROUP 106

Description		Properties as defined by the CEN protocol	
Spiral nail length (mm)	65	Yield load F_y (kN)	0.409
Stud material	Glulam	Yield displacement Δ_y (mm)	0.50
Number of specimens	7	Maximum load F_{max} (kN)	0.694
		Displacement at F_{max} (mm)	5.40
		Ultimate displacement Δ_u (mm)	12.80
		Initial stiffness (N/mm)	1280
		Ductility (Δ_u/Δ_y)	25.60

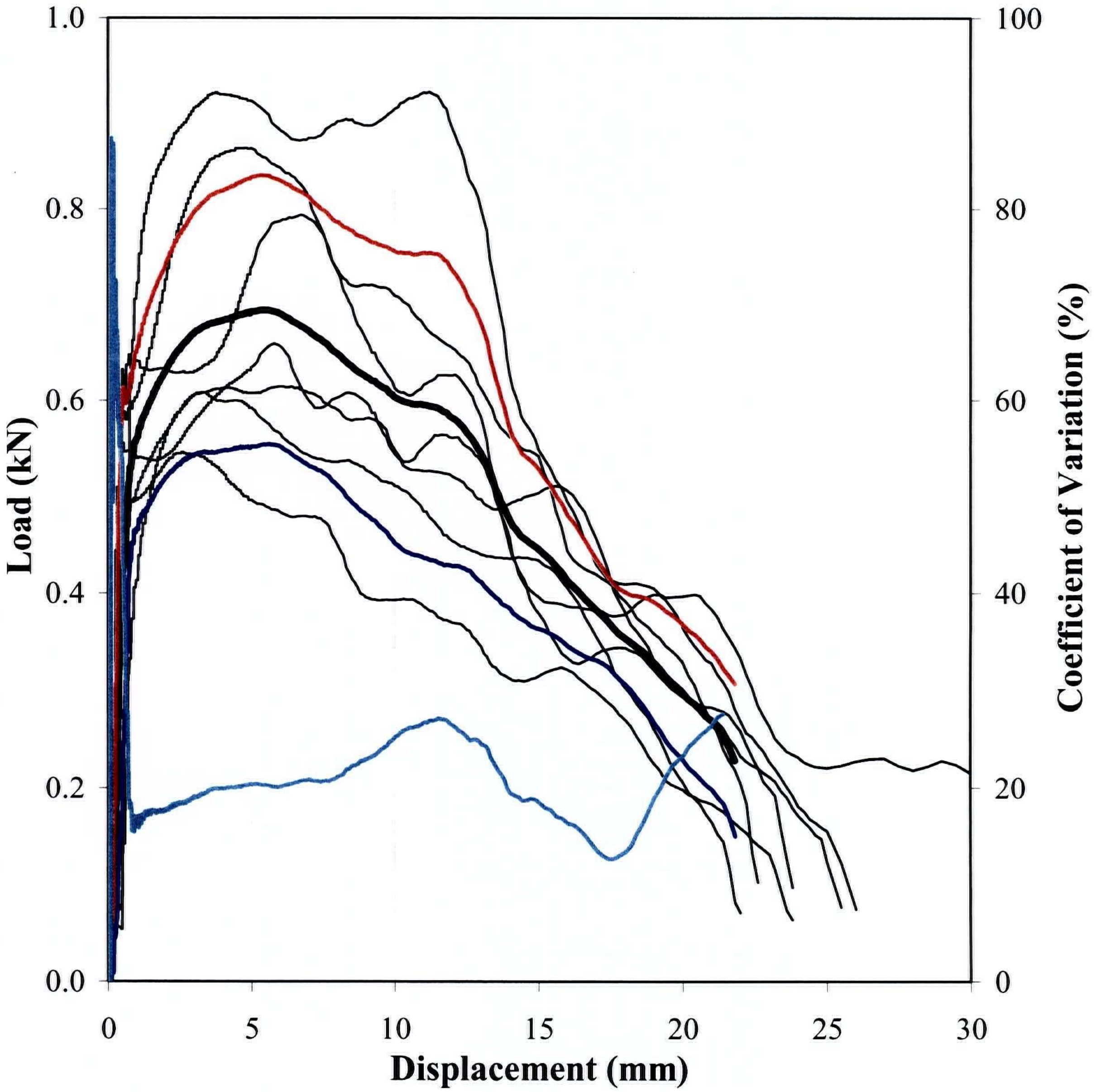

SPECIMEN GROUP 107

Description		Properties as defined by the CEN protocol	
Spiral nail length (mm)	76	Yield load F_y (kN)	0.979
Stud material	Glulam	Yield displacement Δ_y (mm)	0.60
Number of specimens	7	Maximum load F_{max} (kN)	1.417
		Displacement at F_{max} (mm)	4.10
		Ultimate displacement Δ_u (mm)	7.50
		Initial stiffness (N/mm)	1806
		Ductility (Δ_u/Δ_y)	12.50

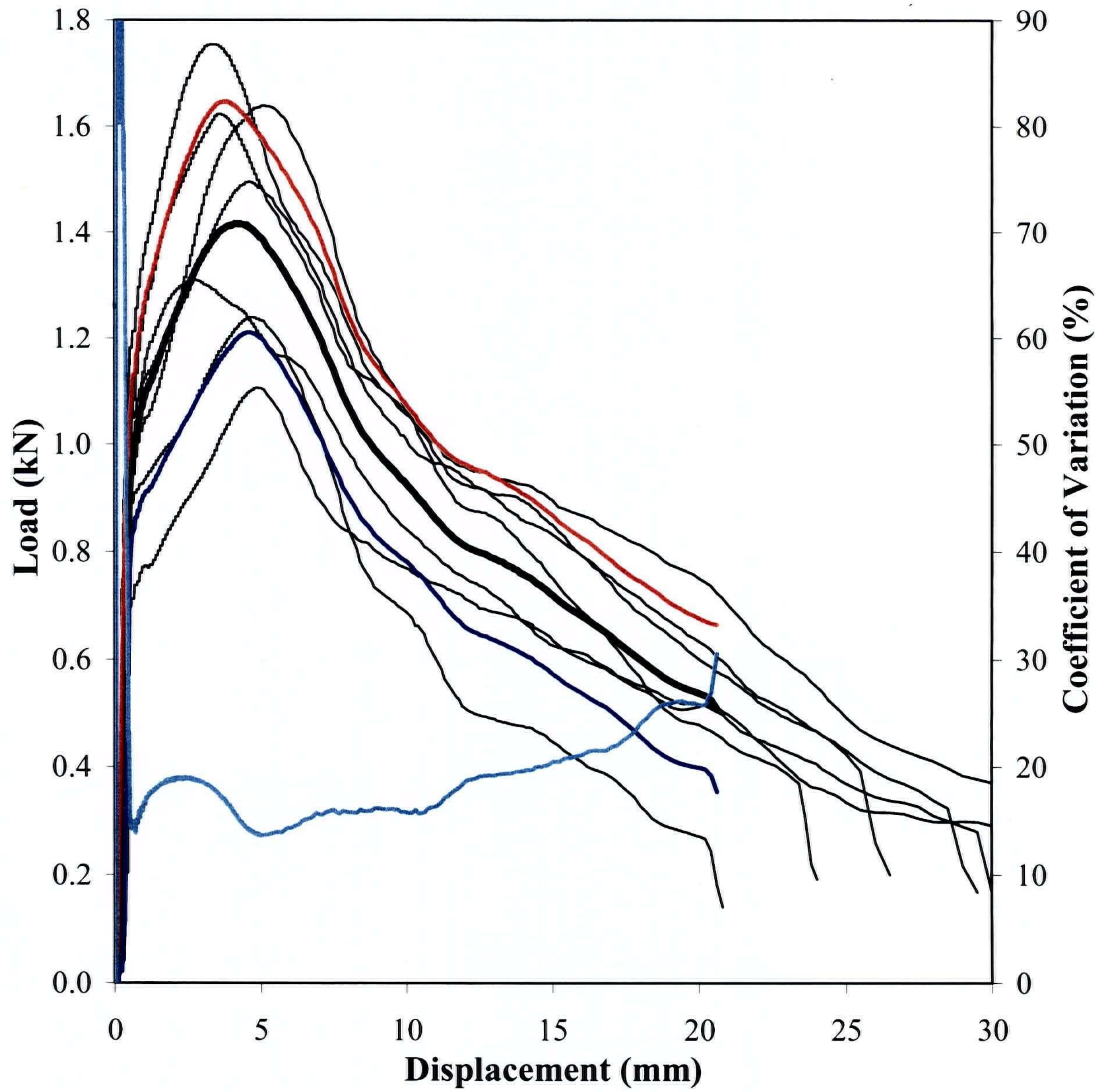

SPECIMEN GROUP 108

Description		**Properties as defined by the CEN protocol**	
Spiral nail length (mm)	102	Yield load F_y (kN)	1.273
Stud material	SPF	Yield displacement Δ_y (mm)	0.60
Number of specimens	7	Maximum load F_{max} (kN)	1.864
		Displacement at F_{max} (mm)	5.10
		Ultimate displacement Δ_u (mm)	14.20
		Initial stiffness (N/mm)	2802
		Ductility (Δ_u/Δ_y)	23.67

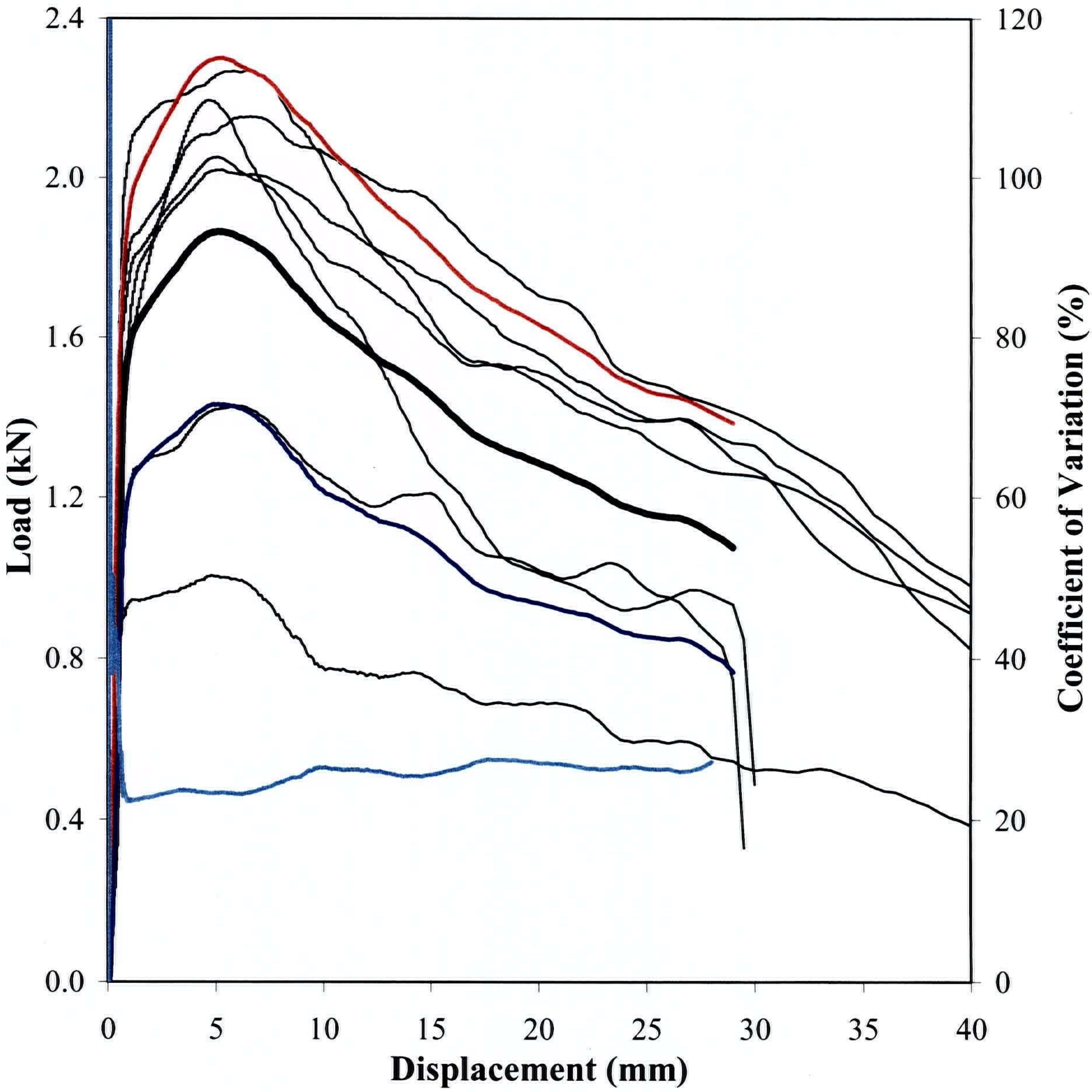

SPECIMEN GROUP 109

Description		Properties as defined by the CEN protocol	
Spiral nail length (mm)	102	Yield load F_y (kN)	1.705
Stud material	LSL	Yield displacement Δ_y (mm)	0.62
Number of specimens	9	Maximum load F_{max} (kN)	2.296
		Displacement at F_{max} (mm)	3.78
		Ultimate displacement Δ_u (mm)	14.00
		Initial stiffness (N/mm)	3885
		Ductility (Δ_u/Δ_y)	22.58

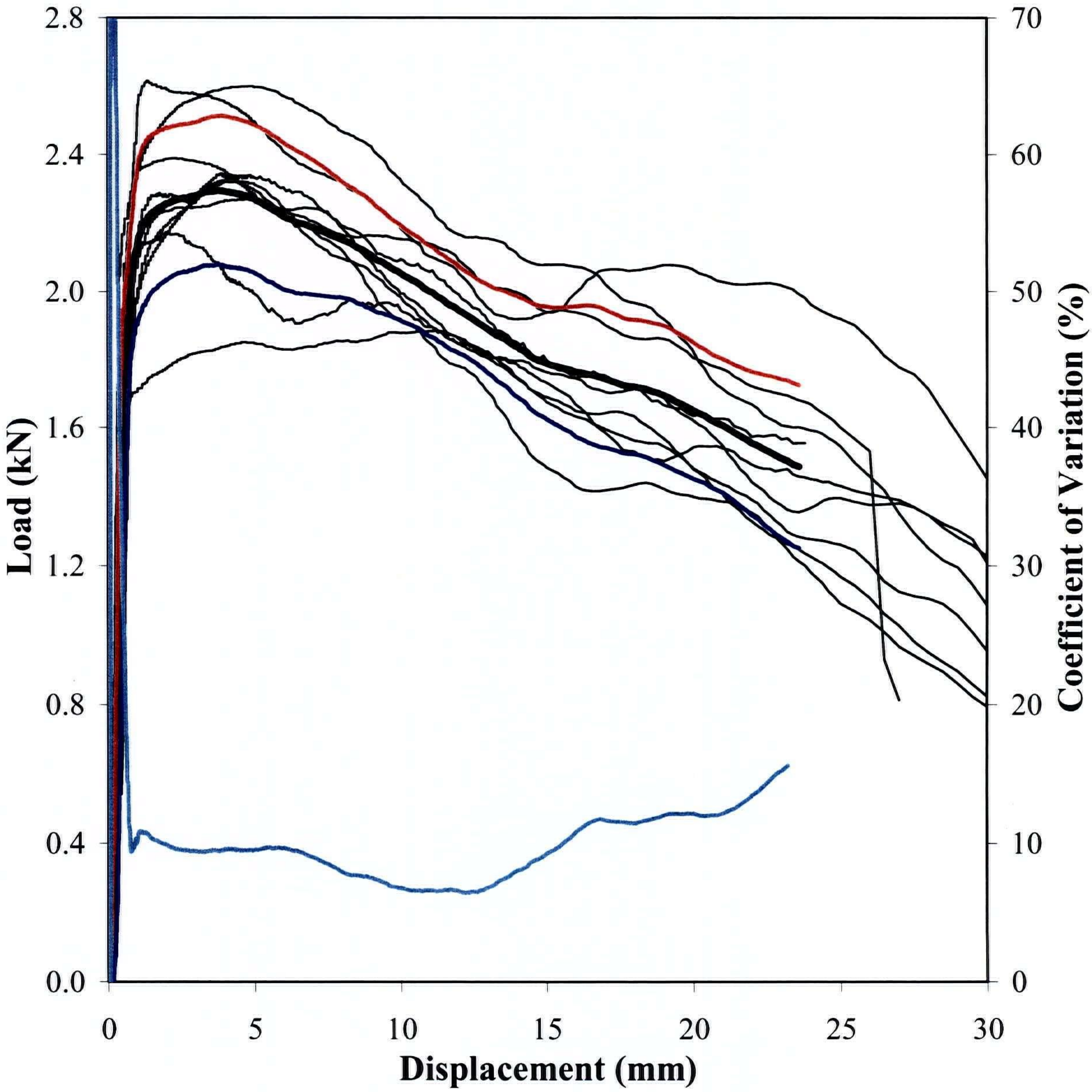

APPENDIX B: DESIGN EXAMPLE

B.1 TALL WALLS WORKBOOK DESIGN EXAMPLE

The following design example is taken from *Tall Walls Workbook: Single Storey Commercial Wood Structures*, a manual published by the Canadian Wood Council (CWC, 2000). It was intended to aid consulting structural engineers in the design of large wood-frame commercial structures. The example is based on the Cresbrook Value Added Centre built in 1999/2000. The design follows the assumptions outlined in the 1995 Edition of the National Building Code of Canada and the 1994 Edition of Engineering Design in Wood (Limit States Design), CSA O86.1-94. The example will be redone in Section B.2 incorporating the findings determined from this study.

3. Example

There are many aspects of wall construction that must be considered in a Tall Wall design. As a minimum, the following must be accounted for:

- Design of the studs
- Design of the stud connections
- Shearwall design including; overturning/hold-down design, shear panel design, shearwall chord design, base plate anchorage and drag strut design
- Design of the members around wall openings including; lintel design; jack post stud design, king post stud design and the design of the connections.
- Non-structural aspects of wall design including fire and thermal resistance.

This design example is based on the Crestbrook Value Added Centre built in 1999/2000. The example uses design assumptions outlined in the *National Building Code of Canada*, *CSA 086.1-94 Engineering Design in Wood (Limit States Design)* and Tembec's proprietary design information for Selectem™ 2.0E laminated veneer lumber.

Details in the design example are not necessarily the same as the final details used in the building construction. The details shown here have been adapted for more general building assumptions.

3.1 Overview of Building

Crestbrook Forest Industries is a lumber manufacturing facility in Cranbrook British Columbia. Additional space was required for their lumber remanufacturing and finger-joining operations. The facilities required large open areas without columns. As well, the North wall could not be load-bearing so that future plant expansion could be accommodated. Originally, a steel structure was specified but Tembec Forest Products, Crestbrook's parent company had recently adopted a policy which required wood to be considered for all their construction and used where cost effective. Analysis indicated a wood building could be constructed for the same cost as the pre-engineered steel building originally specified.

The building is a 2100 m^2 (22,300 ft^2) one storey wood frame with a concrete slab on grade floor and foundation. Figure 3.1 gives an overview of the building.

Figure 3.1
Isometric diagram of new building

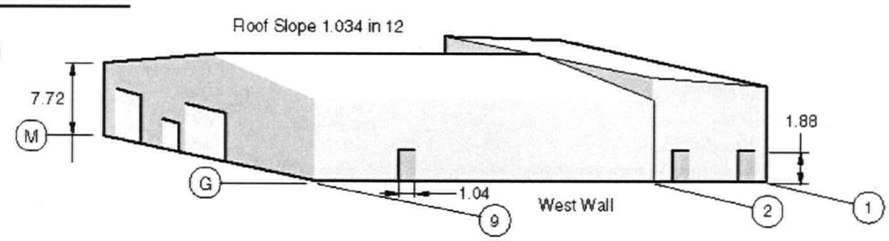

Figure 3.2
Roof framing plan

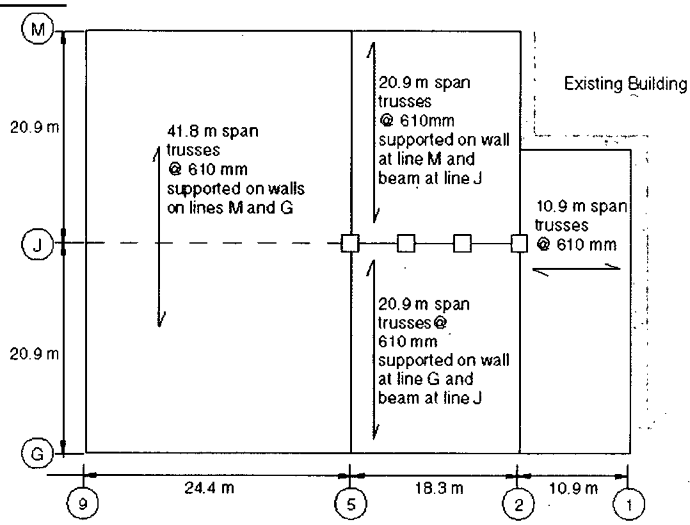

A roof framing plan is illustrated in Figure 3.2. The west wall, "Wall G" will be used for this example. The wall is 7.72 m (25 ft 4 in) tall and at the north end supports trusses spanning 41.8 m (137 ft).

Cranbrook has the following design data:

- Specified ground snow load, S_s, 2.7 kPa
- Associated rain load, S_r, 0.2 kPa
- 1/30 hourly wind pressure, $q_{1/30}$, 0.29 kPa
- 1/10 hourly wind pressure, $q_{1/10}$, 0.22 kPa
- Seismic design loads are minimal and did not affect the design of this structure.

3.2 Stud Design

Studs used in this project were 44 x 235 mm (1-3/4 x 9-1/4 in) SelecTem™ 2.0E studs manufactured by Tembec. Studs were spaced at 610 mm o/c and blocked at 1220 mm. Figure 3.3 shows a typical wall section. The stud length is the height of the wall minus the thickness of the top and bottom plates – 7.59 m. This stud design example will be for studs supporting the 41.8 m span trusses.

Load information

Stud axial loads

Roof dead load

Specified roof dead load	= 0.718 kPa
Roof load tributary width	= truss span/2 = 20.9 m
Specified roof dead load on wall	= 0.718 x 20.9 = 15.0 kN/m
Factored roof dead load on wall	= 1.25 x 15.0 = 18.8 kN/m

Figure 3.3
Typical wall section

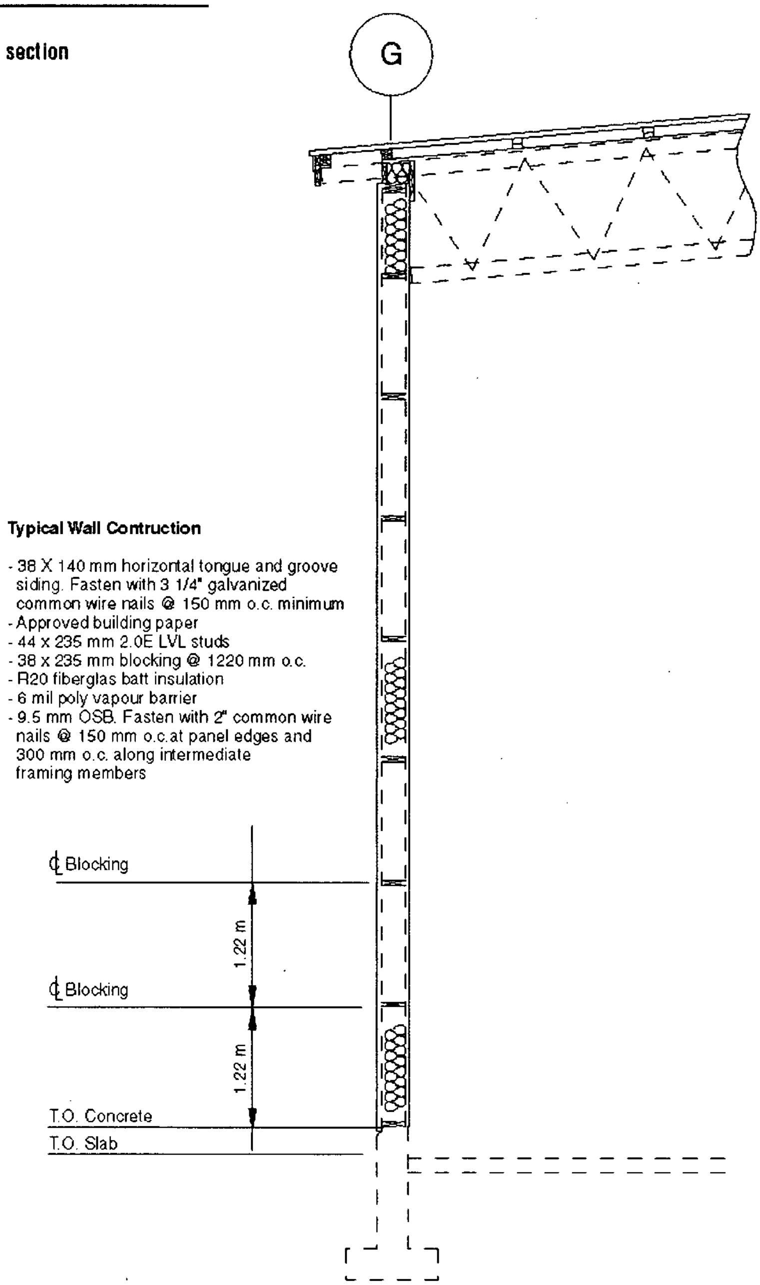

Wall dead load

Specified wall dead load = 0.40 kPa

The critical section for combined bending and axial loads on a stud is generally the mid-height of the stud. Therefore, consider half of the wall dead weight in the stud design.

Tributary height of wall dead load = 7.72/2 = 3.86 m

Specified wall dead load = 0.40 x 3.86
= 1.54 kN/m

Factored wall dead load = 1.25 x 1.54
= 1.93 kN/m

Roof snow load, S

$$S = S_s(C_b C_w C_s C_a) + S_r$$ NBCC 4.1.7.1 (1)

Ground snow load S_s = 2.7 kPa NBCC Appendix C

Associated rain load S_r = 0.2 kPa NBCC Appendix C

Basic roof snow factor C_b = 0.8 NBCC 4.1.7.1 (1)

All other factors C_w, C_s, C_a = 1.0

S = 2.7 x (0.8 x 1 x 1 x 1) + 0.2
= 2.36 kPa

Specified snow load on wall = 2.36 x 20.9
= 49.3 kN/m

Factored snow load on wall = 1.5 x 49.3
= 74.0 kN/m

Table 3.1
Summary of axial loads

	Specified Load	**Factored Load**
Wall + Roof Dead Load	16.5 kN/m	20.7 kN/m
Snow Load	49.3 kN/m	74.0 kN/m
Total Load	65.8 kN/m	94.7 kN/m
Stud Dead Load	10.1 kN	12.6 kN
Stud Snow Load	30.1 kN	45.1 kN
Total Stud Load	40.2 kN	57.7 kN

Stud wind loads

$$p = qC_eC_gC_p \pm qC_eC_{gi}C_{pi}$$ NBCC 4.1.8

Wind load for strength	$q_{1/30}$ = 0.29 kPa	NBCC Appendix C
Wind load for deflection	$q_{1/10}$ = 0.22 kPa	NBCC Appendix C
Exposure factor	C_e = 1.0	NBCC 4.1.8.1
External pressure coefficient and gust factor	C_pC_g = -2.0	NBCC Figure B8
Internal gust factor	C_{gi} = 1.0	NBCC Commentary B
Internal pressure coefficient	C_{pi} = ± 0.7	NBCC Commentary B

Table 3.2
Summary of wind loads

	Specified Load	Factored Load
Strength area load	0.783 kPa	1.17 kPa
Deflection area load	0.594 kPa	N/A
Strength stud load	0.478 kN/m	0.717 kN/m
Deflection stud load	0.362 kN/m	N/A

Stud resistance

Product design information for SelecTem™ 2.0E – Available from Tembec

Specified bending strength	f_b = 42.7 MPa
Specified shear strength	f_v = 3.65 MPa
Specified compression parallel to grain strength	f_c = 29.7 MPa
Specified compression perpendicular to grain strength	f_{cp} = 6.21 MPa
Specified tension strength	f_t = 29.0 MPa
Size factor for tension	K_{zt} = 1
Mean Modulus of Elasticity	E_{50} = 13800 MPa
5th percentile Modulus of Elasticity ($0.87E_{50}$)	E_{05} = 12000 MPa
Size factor in bending	K_{zb} = (305/d)0.15 = 1.04

Modification factors

Bending resistance factor	$\phi = 0.9$	CSA O86.1 Supplement, 13.4.5
Shear resistance factor	$\phi = 0.9$	CSA O86.1 Supplement, 13.4.5
Compression parallel to grain resistance factor	$\phi = 0.8$	CSA O86.1 Supplement, 13.4.5
Compression perpendicular to grain resistance factor	$\phi = 0.8$	CSA O86.1 Supplement, 13.4.5
Tension resistance factor	$\phi = 0.9$	CSA O86.1 Supplement, 13.4.5
Load duration factor:		
Load combinations with wind	$K_D = 1.15$	CSA O86.1 Supplement, 13.4.4
All other load combinations	$K_D = 1.00$	
System factor for bending	$K_H = 1.05$	CSA O86.1 Supplement, 13.4.4
Length of bearing factor	$K_B = 1.19$	CSA O86.1 5.5.7
Size factor for bearing	$K_{Zcp} = 1.15$	CSA O86.1 5.5.7

Resistance of 44 x 235 mm stud of length 7.62 m CSA O86.1 Supplement, 13.4.5

With wind loads:

$$\mathbf{M_r = \phi F_b S K_{Zb} K_L}$$
$$= 19.5 \text{ kN}\cdot\text{m}$$

$$\mathbf{V_r = \phi F_v \tfrac{2}{3} A}$$
$$= 26.0 \text{ kN}$$

$$\mathbf{P_r = \phi F_c A K_{Zc} K_c}$$
$$= 75.4 \text{ kN}$$

$$\mathbf{T_r = \phi F_t A_n K_{Zt}}$$
$$= 290 \text{ kN (for a member with a 1/2 in dia. bolt)}$$

Without wind loads:

$$\mathbf{M_r = \phi F_b S K_{Zb} K_L}$$
$$= 17.0 \text{ kN}\cdot\text{m}$$

$$\mathbf{P_r = \phi F_c A K_{Zc} K_c}$$
$$= 72.5 \text{ kN}$$

$$\mathbf{Q'_r = (\tfrac{2}{3}) \phi F_{cp} A'_b K_B K_{Zcp}}$$
$$= 59.8 \text{ kN}$$

Note: At the top plate, a 16000 mm^2 steel bearing plate is provided at the truss support.

$$A'_b = \frac{(16000 + 44 \times 235)}{2} \quad \text{but} \leq 1.5 \times 44 \times 235$$
$$= 13200 \text{ mm}^2$$

At the bottom plate, axial load from the stud is assumed to be distributed through the sill plate at a 45° angle as shown in Figure 3.4.

$$A_b' = b\left[\frac{L_{b1}+L_{b2}}{2}\right], \text{ but } \leq 1.5\,L_{b1}$$

$= 15500\ \text{mm}^2 > 13200$ Therefore, bearing of the top plate will govern

Figure 3.4
Bearing of stud on sill plate

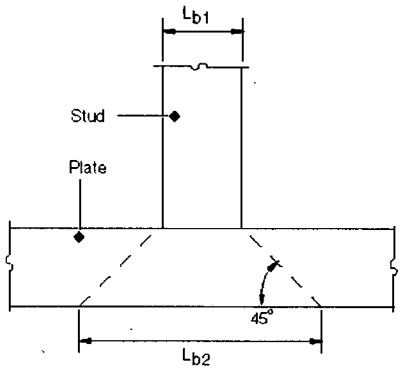

Load Case 1 – axial loads alone (1.25 D +1.5 L)

$P_f = 57.7$ kN per stud

Combined Loading:

Axial load may not be applied concentrically and is conservatively assumed to be applied at 1/6th the depth of the stud from the centre of the stud creating a moment as shown in Figure 3.5

The design should consider the more critical of:

- the unamplified moment at the top of the stud, and
- the amplified moment at the middle of the stud

(In the stud tables, the conservative case of amplified moment at the top of the stud was considered)

In this design example, the critical case is the amplified moment at the middle of the stud.

$$M'_f = \frac{1}{2}P_f \times \frac{d}{6}$$

$= 1.13$ kN•m per stud

The following formula is used for the amplified moment due to eccentric load

$$\frac{P_f}{P_r} + \frac{M_f}{M_r} \leq 1.0$$

$$M_f = M_f'\left[\frac{1}{1-\frac{P_f}{P_E}}\right]$$

Figure 3.5
Eccentric load, lateral load and moments on the stud

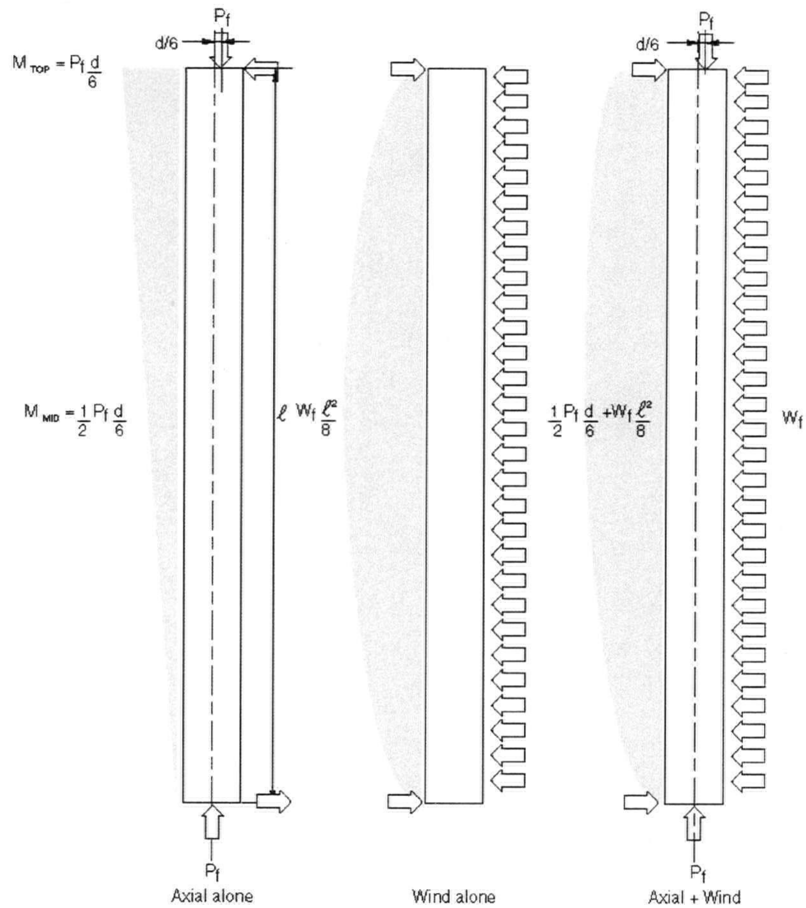

$$P_E = \frac{\pi^2 E_s I}{(K_e \ell)^2}$$

$= 112$ kN per stud

$E_s I = 657 \times 10^9$ N•mm²

$M_f = 2.33$ kN•m per stud

$$\frac{P_f}{P_r} + \frac{M_f}{M_r} \leq 1.0$$

$= 0.93 \leq 1.0$ (Acceptable)

Bearing on top and bottom plates

$Q_f = 57.7$ kN < 59.8 kN (Acceptable)

Load Case 2 - axial dead load plus wind load (1.25 D + 1.5 W)

Factored wind load (w_f) 0.717 kN/m per stud

Factored axial load (P_f) 12.6 kN per stud

Maximum moment (M'_f) at centre of stud

$$M'_f = \frac{w_f \ell^2}{8} + \frac{1}{2} P_f \times \frac{d}{6}$$

= 5.41 kN•m per stud

M_f = 6.10 kN•m per stud

Combined loading:

$$\frac{P_f}{P_r} + \frac{M_f}{M_r} \leq 1.0$$

= 0.48 ≤ 1.0 (Acceptable)

Shear:

$$V = w_f \times \frac{\ell}{2}$$

= 2.72 kN ≤ 26.0 kN (Acceptable)

Deflection:

Wall finishes, in this case OSB and lumber siding, are not brittle or subject to cracking. Acceptable total load deflection criteria is span/180 = 42 mm. Deflection is calculated at mid-span of the studs. In this Tall Wall example and the stud tables in Section 2, the deflections incorporate the deflections caused by the offset axial loads. The deflections from the wind loads and axial loads are amplified to account for the PΔ effect. These are conservative assumptions for determining stud deflection.

Specified wind load (w_s) = 0.362 kN/m per stud

Specified axial dead load (P_s) = 10.1 kN per stud

$$\Delta_T = \textbf{deflection from wind + deflection from eccentric load}$$

$$= \frac{5 w_s \ell^4}{384 EI} + \frac{P_s e \ell^2}{16 EI}$$

= 26.0 mm

$$\Delta_A = \textbf{amplified deflection to account for P}\Delta\textbf{ effect}$$

$$= \Delta_T \left[\frac{1}{1 - \frac{P_s}{P_E}} \right]$$

= 28.6 mm < 42 mm (Acceptable)

Load Case 3 - axial dead load + 0.7 axial live load + 0.7 wind load [1.25 D + 0.7 (1.5 L + 1.5 W)]

A load combination factor of 0.7 is used for combined wind load and snow load. NBCC 4.1.3.2

Factored wind load (w_f) 0.7 x 0.717 = 0.502 kN/m per stud

Factored axial load (P_f) 12.6 kN + 0.7 x 45.1 kN = 44.2 kN per stud

Maximum moment (M'_f) at centre of stud

$$M'_f = \frac{w_f \ell^2}{8} + \frac{1}{2} P_f \times \frac{d}{6}$$

= 4.48 kN•m per stud

M_f = 7.40 kN•m per stud

Combined loading:

$$\frac{P_f}{P_r} + \frac{M_f}{M_r} \leq 1.0$$

= 0.97 ≤ 1.0 (Acceptable)

Deflection:

Specified wind load (w_s) = 0.7 x 0.362 = 0.253 kN/m per stud

Specified axial dead load (P_s) = 10.1 + 0.7 x 30.1 = 31.2 kN per stud

Δ_T = **deflection from wind + deflection from eccentric load**

$$= \frac{5 w_s \ell^4}{384 EI} + \frac{P_s e \ell^2}{16 EI}$$

= 23.3 mm

Δ_A = **amplified deflection to account for PΔ effect**

$$= \Delta_T \left[\frac{1}{1 - \frac{P_s}{P_E}} \right]$$

= 32.4 mm < 42 mm (Acceptable)

Results:
Use 44 x 235 mm (1-3/4 x 9-1/4 in) SelecTem™ 2.0E spaced at 610 mm.

Other considerations:

1) Ensure that walls are laterally braced to prevent buckling about the narrow stud axis. The tongue and groove siding on the wall exterior, the OSB sheathing on the wall interior and the full depth blocking at 1.2 m will provide adequate bracing. For additional information on lateral bracing contact the stud manufacturer.
2) For wall segments used as shearwalls ensure all edges of sheathing are blocked. Blocking at 1.2 m intervals will provide edge support for all shearwall panels.

3.3 Stud Connection Design

Stud to wall plate connections must be designed to resist the uplift force on the stud and the wind loads resulting from the wind pressures/suctions on the face of the wall. For this project, special stud anchors were designed for the stud to plate connections. The top plate anchor is shown in Figure 3.6. SelecTem™ 2.0E studs have the same specific gravity as Hem-Fir and Tembec recommends using Hem-Fir connection design values for this product.

Figure 3.6
Stud to top plate connection

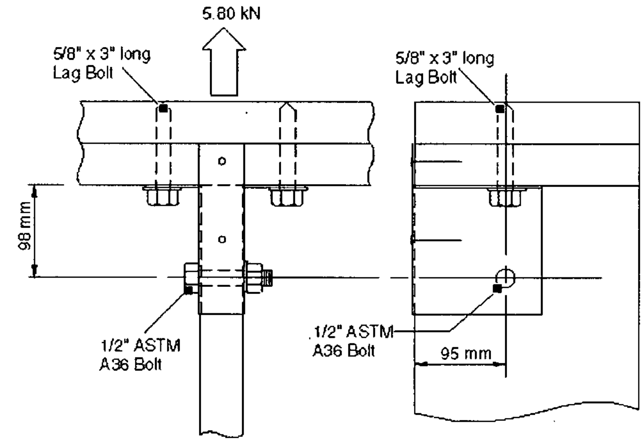

Load information

Factored uplift load at the eave (wind load – 0.85 roof dead load)

Critical wind uplift will be at the corner of the building — NBCC Figure B7

y = end zone width
= 6.18 m

End Zone

C_pC_g = -2.0 windward side of roof
= -1.0 leeward side of roof

C_{pi} = 0.7

C_e = 1.0

Wind uplift at eave

= 22.3 kN/m

Factored dead load at eave

= 15.0 kN/m x 0.85
= 12.8 kN/m

Net uplift at eave

= 9.5 kN/m

Uplift load/stud

= 9.5 x 0.61
= 5.80 kN

Wind pressures on stud

= stud shear load (pg 31)
= 2.72 kN

Uplift resistance

Top plate connected to stud anchor with lag screws

Two 5/8 in dia. x 3 in long lag screws

$\mathbf{P_{rw} = P'_{rw} L_t n_F K' J_E}$ pg 262

Length of threaded portion, L_t, in top plate pg 262

L_t = L/2 + 12.7 - tip
= 50.8 - 9.5
= 41.3 mm

n_F = 2

K_D = 1.15 = K'

P'_{rw} = 78 N/mm pg 262

P_{rw} = 7.41 kN > 5.80 kN (Acceptable)

Stud anchor connected to stud with single bolt loaded in double shear parallel to the grain

One 1/2 in dia. bolt

$\mathbf{P_r = P'_r n_s n_F K' J'}$ pg 250

Member end distance = 98 mm = 7.71 bolt diameters

J_L = 1.0 @ 10 dia. pg 239
= 0.75 @ 7 dia.
= 0.81 @ 7.71 dia.
= J'

K_D = 1.15 = K'

For 38 mm thick member, double shear, steel side plate

P'_r = 3.42 kN pg 252

P_r = 6.37 kN > 5.80 kN (Acceptable)

Resistance to wind pressures/suctions on the wall

Top plate connected to stud anchor with lag screws loaded perpendicular to the grain

Two 5/8 in dia. x 3 in long lag screws

Length of penetration, L_p, in top plate

L_p = length of lag screw - thickness of washer and steel in anchor - tip
= 76 - 9 - 9.5
= 57.5 mm

Standard length of penetration = 159 mm pg 262

Strength reduction for reduced penetration
= 57.5/159
= 0.36

n_{Fe} = 2

n_R = 1

K_D = 1.15 = K'

Q'_r = 5.61 kN pg 264

Q_r = $Q'_r n_{Fe} n_R K'$ x 0.36
= 4.65 kN > 2.72 kN (Acceptable)

Stud anchor connected to stud with single bolt loaded in double shear loaded perpendicular to the grain

One 1/2 in dia. bolt

Member edge distance = 95 mm = 7.5 dia. > 4 dia. (Acceptable)

$\mathbf{Q_r = Q'_r n_s n_F K' J_R}$ WDM pg 250

$n_s = 2$

$n_F = 1$

$K_D = 1.15 = K'$

For 38 mm thick member, double shear, steel side plate

$Q'_r = 1.49$ kN WDM pg 252

$Q_r = 3.43$ kN > 2.72 kN (Acceptable)

Results:
Stud anchor connections are adequate to resist the stud uplift and pressure/suction loads.

Other considerations:

1) Steel in stud anchor must be checked to ensure the anchor is capable of transferring the loads.
2) Stud to bottom plate anchor must also be checked. In this project, similar anchors were used at the top and bottom of the studs. The weight of the wall is beneficial to the connection at the bottom of the stud.
3) The connections between the roof framing and the top plate must be capable of resisting the uplift loads and the wind pressures/suctions. A load path must be detailed to ensure that the wind pressures/suctions, on the face of the wall, are resisted by the roof diaphragm acting in the plane of the roof sheathing.

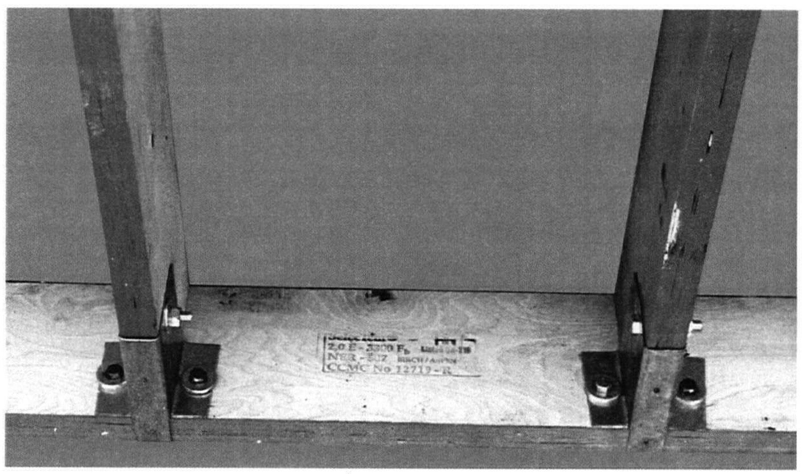

3.4 Shearwall Design

The Crestbrook Value Added Centre uses a system of diaphragms and shearwalls to resist the lateral loads. Wind pressures and suctions on the north and south end walls of the buildings are resisted by the end wall studs which transfer half of the wind load into the foundation and the other half to the roof diaphragm. The roof diaphragm acts as a deep beam and transfers the wind loads into east and west walls along Gridlines G and M. The walls on gridlines G and M must be designed as shearwalls to ensure that they are capable of transferring the shear loads at the eave level into the foundation at the base of the wall.

3.4.1 Lateral Load Path and Overturning

The diaphragm load on the roof is assumed to be uniformly distributed along the top of the wall plate. This load is transferred through the effective shear-wall segments to the foundation. All of Wall G is sheathed with OSB sheathing with only 3 door openings to reduce the shear capacity – see Figure 3.7. Therefore, most of the wall can be considered capable of transferring lateral loads.

A shearwall segment is defined as a section of a shearwall with uniform construction that forms a structural unit designed to resist lateral forces parallel to the plane of the wall. The wall segments around openings are not considered as part of the shearwall. As well, a wall section where the height of the wall is more than 3.5 times greater than the length of the segment is considered too narrow to carry load. This means there are three potential shearwall segments in Wall G as illustrated in Figure 3.7.

The wall sheathing nailed to the studs transfers the shear load from the top of the wall to the bottom of the wall. The overturning of each shearwall segment is resisted by dead loads on the wall segment and chords at the ends of the segments designed to transfer tension and compression forces into the foundation. Shearwall chords acting in tension require hold-down connections to the foundation. Where possible, wall geometry may be chosen to avoid using hold-down connections.

Load Information

Lateral loads

The factored roof diaphragm reaction at Wall G is 85 kN resulting from wind loads on the existing structure and the new Value Added Centre. The wall length is 53.9 m and the distributed diaphragm load along the top of the wall is 1.58 kN/m.

Dead loads

In wind load analysis, 85% of the specified dead load may be used to resist overturning. Since the roof dead load was considered to resist wind uplift, it will not be considered to resist overturning. Only the dead load of the wall will be considered in the overturning calculation.

Specified weight of wall = 0.4 kPa

Wall height = 7.72 m

Factored weight of the wall at the base of the wall

= 0.85 x 0.4 x 7.72

= 2.62 kN/m

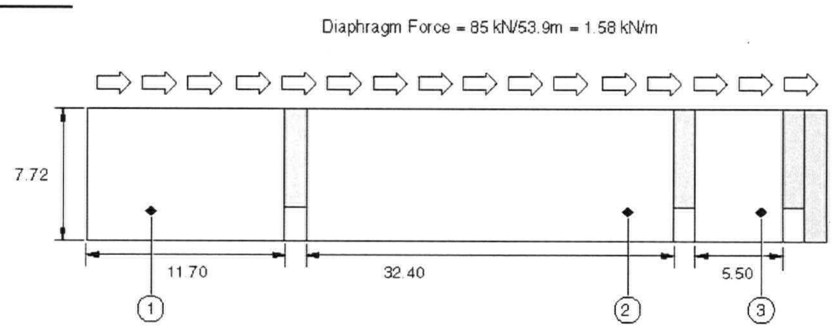

Figure 3.7
Wall G showing shearwall segments

Load paths

Each shearwall segment must be considered separately. In this analysis, all shearwall segments are constructed in the same manner. Due to the low aspect ratio, shear deformation is dominant and each shearwall segment is assumed to have the same stiffness per unit length and the load in each segment is assumed to be proportional to the length of the segment.

Figure 3.8 shows a free body diagram for a shearwall segment. The sheathed panels above the openings are conservatively ignored in the shearwall design.

Figure 3.8
Free body diagram of a shearwall segment

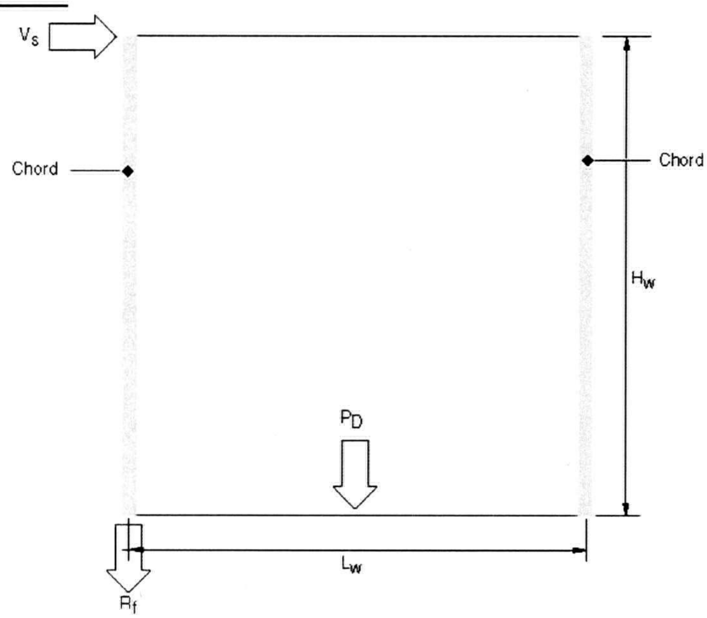

From static equilibrium

$$R_f = \frac{M_{overturning} - M_{resisting}}{L_w}$$

Where:

R_f = Hold-down force (positive is tension, negative is compression)

$M_{overturning}$ is the overturning moment
= $V_s \times H_w$

$M_{resisting}$ is the resisting moment
= $P_D \times L_w/2$

L_w = The length of the shearwall segment

H_w = The height of the shearwall
= 7.72 m

V_s = Load on the shearwall segment = $V_T \frac{L_w}{\Sigma L_w}$

V_T = Total shear load on the shearwall
= 85 kN

P_D = Total factored dead load on the shearwall segment
= 2.62 kN/m x L_w

Option 1 – 3 shearwall segments

ΣL_w = 11.7 + 32.4 + 5.5
= 49.6 m

	Length	**Overturning Moment**		**Resisting Moment**		
	L_w	V_s	V_sH_w	P_D	$P_DL_w/2$	R_f
Segment	m	kN	kN•m	kN	kN•m	kN
1	11.7	20.1	155	30.7	180	-2.14
2	32.4	55.4	428	84.9	1370	-29.1
3	5.5	9.42	72.6	14.4	39.6	6.00

Option 2 – Only consider segments 1 and 2 as resisting lateral load

ΣL_w = 11.7 + 32.35
= 44.1 m

	Length	**Overturning Moment**		**Resisting Moment**		
	L_w	V_s	V_sH_w	P_D	$P_DL_w/2$	R_f
Segment	m	kN	kN•m	kN	kN•m	kN
1	11.7	22.6	174	30.7	180	-0.51
2	32.4	62.4	481	84.9	1370	-27.4

In option 2, hold-downs would not be required. Base shearwall design on Option 2.

Results:
Only consider shearwall segments 1 and 2 in shearwall design.

Other considerations:

1) The top plate of the shearwall must be designed as a drag strut to transfer the diaphragm shear loads into the shearwall segments. See Section 3.4.5.

3.4.2 Shear Panel Design

Shear panels are 9.5 mm thick OSB nailed with 2 in common nails at 150 mm at panel edges and 300 mm at interior framing members. Alternatively, nailed plywood sheathing could be used for shear panels. OSB and plywood sheathing of the same thickness have equivalent shearwall shear capacity when nailed with the same size and number of nails. Panels are applied horizontally and blocking provides a nailing surface for all panel edges.

Shearwall capacity is given for 2 in nails used with 7.5 mm sheathing and 2-1/2 in nails used with 9.5 mm sheathing. The shearwall capacity is a function of the strength of the nail and the strength of the sheathing. Size of nail will govern shearwall capacity. Base shearwall capacity on 7.5 mm panel with 2 in common nails. Use capacity for Hem-Fir framing as recommended by Tembec.

Factored shear resistance of shearwall segments is 3.35 kN/m WDM pg 473

Factored shear load

$= V_T/\Sigma L_w$
$= 85/44.1$
$= 1.93$ kN/m $<$ 3.35 kN/m (Acceptable)

Results:
The interior sheathing consisting of 9.5 mm thick OSB nailed with 2 in common nails at 150 mm at the panel edges and 300 mm at interior framing members provides adequate shear resistance for lateral loads.

Other considerations:

1) Power nails cannot be substituted for common nails in shearwall construction. Power nails generally have smaller diameters and do not have the same capacity as common nails. See the power nail manufacturer for adjustments to shearwall capacity.

3.4.3 Chord Design

Typically, the chords of each shearwall segment will act in compression and tension alternately depending on the direction of the lateral load. Studs are usually doubled at the ends of the shearwall segments to act as the chords. The double member chord must be capable of resisting the chord force, roof gravity loads and wind loads on the face of the stud.

In the example given, there are no tie downs required, therefore there will not be tension in the chord, only compression.

Chord force

When calculating the compression force in the shearwall chord resulting from the shear force, the weight of the wall does not need to be considered. The weight of the wall is resisted by all of the studs in the shearwall segment. The design of the studs acting as chords must also consider the gravity loads and wind pressures/suctions on the stud.

Useful length of wall = L_w-300 mm to allow room for connections

$$R_{fc} = V_s \times H_w/(L_w-300)$$

Segment 1

$= 15.3$ kN

Segment 2

$= 15.0$ kN

Stud design

For studs used as a chord, check stud capacity considering extra axial load from chord. Check capacity of a double stud using resistance values from Section 3.2 Load Case 3 (pg 32).

Wind load on the face of the stud:

Since design is considering wind loads on multiple surfaces of the structure, use Figure B-7 of the Structural Commentaries to the NBCC – wind blowing on the end wall.

$C_pC_g = 0.9$ — NBCC Figure B7

Wind plus snow:

$w_f = 0.424 \times 0.7$
$= 0.297$ kN/m — per double stud

$P_f = 44.2$ kN $+ 0.7 \times 15.3$ kN
$= 54.9$ kN — per double stud

$P_r = 2 \times 75.4$
$= 151$ kN — per double stud

$M_r = 2 \times 19.5/1.05$
$= 37.1$ kN•m — per double stud

Combined loading:

$$\frac{P_f}{P_r} + \frac{M_f}{M_r} \leq 1.0$$

$= 0.48 \leq 1.0$ — (Acceptable)

Deflection:

$w_s = 0.150$ kN/m — per double stud

$P_s = 31.2 + 0.7 \times 15.3/1.5$
$= 38.3$ kN — per double stud

$\Delta_A = 10.9 \text{ mm} < 42 \text{ mm}$ — (Acceptable)

Results:
Two 44 x 235 mm (1-3/4 x 9-1/4 in) SelecTem™ 2.0E studs are acceptable as a shearwall chord.

Other considerations:

1) Studs around openings must be designed to resist the additional loads imposed at the openings – See Section 3.5.3 (pg 48).

3.4.4 Anchor Bolt Design

The anchor bolts which connect the base plate to the foundation, must be designed to resist the wind uplift force on the wall, the wind loads resulting from the wind pressures/suctions on the face of the wall and the wind shearwall shear forces acting parallel to the plane of the wall. For this project, 5/8 in dia. anchor bolts were used with a minimum embedment of 127 mm into the concrete. SelecTem™ 2.0E base plates have the same specific gravity as Hem-Fir and Tembec recommends using Hem-Fir connection design values for this product.

Load information

Factored uplift load at the eave (pg 33)

= (wind load – 0.85 roof dead load)
= 9.5 kN/m

Wind pressures (pg 33)

= 2.72/0.61
= 4.46 kN/m

Lateral shear loads along shearwall (pg 39)

= 1.93 kN/m

Uplift resistance

70 x 70 x 6 mm thick square washers resist wind uplift forces

Check bearing of washers on the wall plate.

Bearing area:

$$\mathbf{Q_r = \phi F_{cp} A_b K_B K_{Zcp}}$$

$$A_b = 70 \times 70 - \pi \times 18^2/4 = 4650 \text{ mm}^2$$

$$K_B = 1.13$$

$$K_{Zcp} = 1.15$$

$$Q_r = 34.5 \text{ kN}$$

Anchor bolt spacing for uplift:

= 34.5/9.5
= 3.63 m

Resistance to wind pressures/suctions on the wall

44 mm bottom plate; 5/8 in dia. anchor bolt; plate loaded perpendicular to grain

Design connection assuming wood and concrete have the same embedding strength and the concrete is twice as thick as the wood. CSA O86.1 10.4.2.3

$$\mathbf{Q_r = \phi Q_u n_s n_F J_R}$$

where:

$$\phi = 0.7$$

$$n_s = 1$$

$$n_F = 1$$

$$J_R = 1$$

$$Q_u = q_u(K_D K_{SF} K_T)$$

q_u is calculated in accordance with 10.4.4.2 using CSA O86.1 10.4.4.2

l_1 = 44 mm

l_2 = 88 mm

f_1 = 10.6 MPa

f_2 = 10.6 MPa

Q_r = 2.9 kN

Anchor bolt spacing for face loads:

= 2.9/4.46
= 0.65 m (Governs)

Resistance to lateral shear loads parallel to the wall

44 mm bottom plate; 5/8 in dia. anchor bolt; plate loaded parallel to grain

Design connection assuming wood and concrete have the same embedding strength and the concrete is twice as thick as the wood. CSA O86.1 10.4.2.3

$$P_r = \phi P_u n_s n_F J_F$$

where:

ϕ = 0.7

n_s = 1

n_F = 1

J_F = 1

$$P_u = p_u(K_D K_{SF} K_T)$$

p_u is calculated in accordance with 10.4.4.2 using CSA O86.1 10.4.4.2

l_1 = 44 mm

l_2 = 88 mm

f_1 = 24.4 MPa

f_2 = 24.4 MPa

P_r = 6.3 kN

Anchor bolt spacing for lateral loads:

= 6.3/1.93
= 3.26 m

Face loads will govern the spacing of the anchor bolts. Use 0.61 m anchor bolt spacing to match stud spacing.

Results:
Use 5/8 in dia. anchor bolts with 70 x 70 mm plate washers spaced at 0.61 m.

Other considerations:

1) The resistance of the concrete to the connection forces needs to be checked.

2) When anchor bolts are widely spaced, the bending capacity of the wall plate needs to be checked in both the strong and weak axis.

3.4.5 Drag Strut Design

A drag strut – also known as a collector, tie or diaphragm strut - is a diaphragm or shearwall boundary element parallel to the applied load that collects and transfers diaphragm shear forces to the shearwall segments. Typically the wall top plate acts as the drag strut and the connections in the top plate must be designed to resist the drag strut axial tension or axial compression forces.

The south 8.8 m segment of Wall G was not designed as a shearwall segment. Therefore, the diaphragm shear force at the south end of the wall has to be transferred to the shearwall segments at the north end of the wall. Figure 3.9 is a force diagram which illustrates the drag strut forces along wall G.

The maximum drag strut force is 13.9 kN. Since the shear force can occur from either the north or south direction, this can be either a tension force or a compression force. The maximum tension or compression stress in a single plate is 1.35 MPa. By observation, a single 44 x 235 mm member is capable of resisting this force. The plate members must be connected to provide continuity.

Figure 3.9
Drag strut forces along wall G

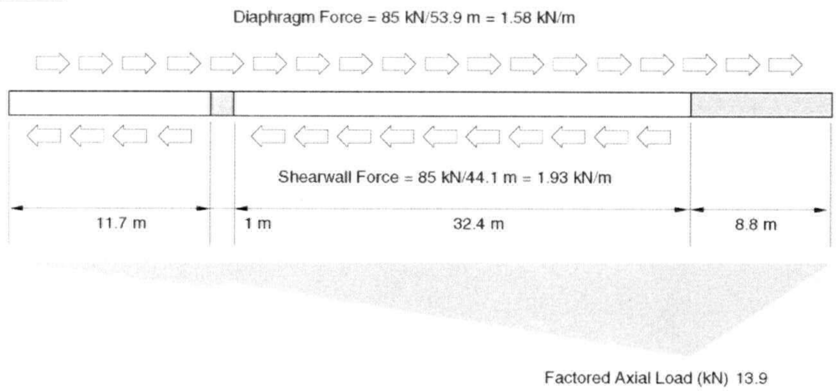

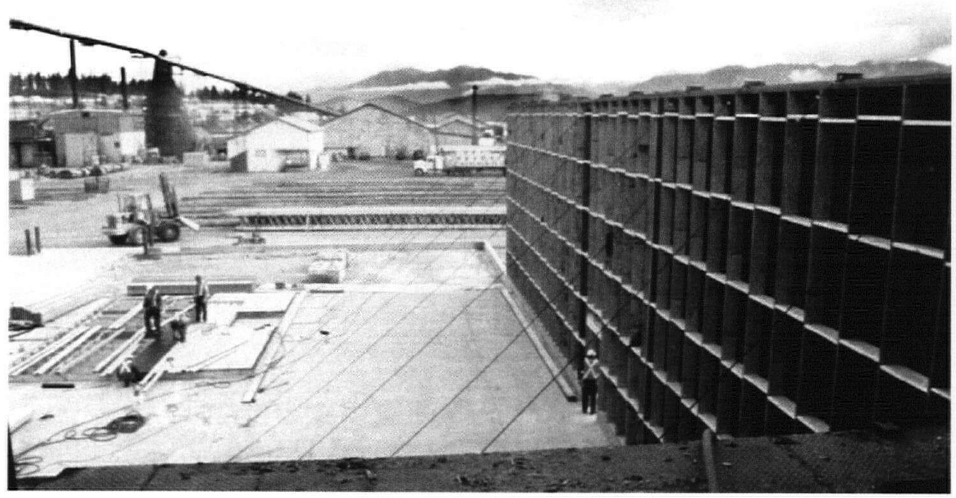

Drag strut connection

Stagger the butt joints in each of the top chord members and nail the top plates together.
Use 2 rows of 3-1/2 in common nails.

ϕn_u = 0.9 kN   pg 234

K_D = 1.15

Capacity per nail

= 1.0 kN

Number of nails/row

= 13.9/(2 x1)
= 7

Space nails at 300 mm.

Stagger end joints in the top plate 2.1 m.

Figure 3.10
Top plate designed as drag strut

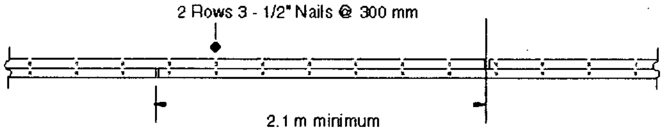

Results:
Design the wall top plate to act as a drag strut. Stagger end joints in the wall plate members a minimum of 2.1 m. Nail plates with 2 rows of 3-1/2" nails spaced at 300 mm.

Other considerations:

1) The wall top plate is often used as the diaphragm chord. The splice connections in the top plate should be designed for the most critical of the diaphragm chord force or the drag strut force.

B.2 REVISED EXAMPLE INCORPORATING RESEARCH FINDINGS

The design example in the previous section has been redone incorporating applicable findings obtained over the course of this study. The same geometry, materials, support conditions, and applied loads were used wherever possible. This section does not attempt to optimize the tall wall in the previous design example. The advantages that can be gained through incorporating design changes such as increasing stud spacing and sheathing connector stiffness have been described in Chapters 5, 6, and 7. The objective of this section is to clearly demonstrate how the method that was used throughout this study to determine the composite properties of a tall wood-frame wall can be applied to this design example. Recommendations for the use of an alternate stud connection consisting of off-the-shelf connectors are also made.

B.2.1 Wall Design

Studs are not designed independently when composite action is taken into account. The stud spacing, sheathing thickness, and sheathing connector type and spacing all effect the strength and stiffness of the composite wall. The studs used in this design example are 44 mm by 235 mm SelecTem™ LVL 2.0E studs manufactured by Tembec. Studs were spaced at 610 mm on centre and blocked at 1,220 mm. The sheathing used is 12.5 mm thick OSB and is connected to studs with 65 mm long spiral nails spaced at 152 mm on centre. Connection load-slip response data is available for this combination of stud, sheathing, and nail type from the tests that were described in Chapter 3. The sheathing is oriented so that the axis of greatest strength is parallel to the height of the studs. The composite wall length used for design is the height of the wall minus the thickness of the top and bottom plates – 7.59 m. It was shown in Section 7.3.5.2 that the amount of end rotational restraint provided by the foundation is minimal and variable. In addition, Section 8.2 showed that analytical predictions assuming pin-supported wall ends matched test results closely. Therefore, the assumption that the wall is pin supported at the top and bottom is valid. The design example is for a composite wall supporting trusses spanning 41.8 m spaced at 610 mm on centre. It is assumed that the spacing of the trusses is independent from the spacing of the studs in the wall. The top wall plate must be able to support the end reaction from a truss in between two adjacent studs.

B.2.1.1 Load Information

The same applied loads presented in Section B.1 were used in this design example. The dead weight of the wall is assumed to be the same as the previous design example. Summaries of the axial and wind loads on the wall and composite studs are presented in Tables B.1 and B.2.

Table B.1. Summary of axial loads.

	Specified Load	Factored Load
Wall + Roof Deal Load	16.5 kN/m	20.7 kN/m
Snow Load	49.3 kN/m	74.0 kN/m
Total Load	65.8 kN/m	94.7 kN/m
Composite Stud Dead Load	10.1 kN	12.6 kN
Composite Stud Snow Load	30.1 kN	45.1 kN
Total Composite Stud Load	40.2 kN	57.7 kN

Table B.2. Summary of wind loads.

	Specified Load	Factored Load
Strength area load	0.783 kPa	1.17 kPa
Deflection area load	0.594 kPa	N/A
Strength composite stud load	0.478 kN/m	0.717 kN/m
Deflection composite stud load	0.362 kN/m	N/A

B.2.1.2 Composite Stud Resistance

The following worksheet demonstrates the methodology used to design a tall wood-frame wall under axial and transversal loads incorporating the effects of composite action. The adequacy of the composite stud will only be checked against the applied forces for Load Case 3 from the previous example. Design information for SelecTem™ LVL 2.0E studs and 12.5 mm OSB sheathing with an A rating grade, taken from Table 7.3C in CSA O86-01, are presented. Firstly, the effective width of the sheathing will be determined. The length factor presented in Chapter 5 will be included in this calculation to account for gaps in the sheathing. The effective bending stiffness, which is a function of the modulus of elasticity of the stud, will then be determined. The effective bending stiffness will be used to calculate both the maximum deflections under specified loads and the forces in each component of the composite stud under factored loads. The code dictates that the mean modulus of elasticity of the stud shall be used for serviceability limit states, such as displacements, and that the 5th percentile modulus of elasticity of the stud shall be used for ultimate limit states, such as bending and axial strength.

For design purposes, the stud alone is assumed to resist the axial load. The specified axial strength of a member and the predicted axial load that will cause the member to buckle (Euler buckling load) are, however, functions of the bending stiffness of the member. Therefore, accounting for the composite properties of the stud increases the predicted axial capacity of the wall. The effects of composite action are not included in the system factor for walls constructed with engineered wood products, as the code only requires that transverse load distribution elements be present to use this factor. The design wall has blocking and structural sheathing on one face so the system factor can be applied.

INPUT PARAMETERS:

Stud Properties:

$b := 44$	mm	Width
$d := 235$	mm	Depth
$f_b := 42.7$	MPa	Specified bending strength
$f_v := 3.65$	MPa	Specified shear strength
$f_c := 29.7$	MPa	Specified compression parallel to grain strength
$f_t := 29.0$	MPa	Specified tension strength
$E_{50} := 13800$	MPa	Mean modulus of elasticity
$E_{05} := 12000$	MPa	5th percentile modulus of elasticity ($E_{05} = 0.87E$ for engineered lumber)

Sheathing Properties:

$t := 12.5$	mm	Thickness
$m_{p0} := 500$	Nmm/mm	Bending strength per unit width parallel to studs
$m_{p90} := 160$	Nmm/mm	Bending strength per unit width perpendicular to studs
$t_{p0} := 100$	N/mm	Axial tension strength per unit width parallel to studs
$t_{p90} := 50$	N/mm	Axial tension strength per unit width perpendicular to studs
$p_{p0} := 100$	N/mm	Axial compression strength per unit width parallel to studs
$p_{p90} := 50$	N/mm	Axial compression strength per unit width perpendicular to studs
$v_p := 40$	N/mm	Shear strength per unit width
$B_{b0} := 1300000$	Nmm^2/mm	Bending stiffness per unit width parallel to studs
$B_{b90} := 390000$	Nmm^2/mm	Bending stiffness per unit width perpendicular to studs
$B_{a0} := 60000$	N/mm	Axial stiffness per unit width parallel to studs
$B_{a90} := 25000$	N/mm	Axial stiffness per unit width perpendicular to studs
$B_v := 12000$	N/mm	Shear rigidity per unit width
$\mu_{xy} := 0.2$		Poisson's ratio

Wall Geometry Properties:

$L := 7590$	mm	Height of the wall (assuming ends are pinned)
$L_{gap} := 2440$	mm	Length between gaps in the exterior sheathing parallel to studs
$s_s := 610$	mm	Stud spacing

Connection Properties:

$s_K := 152$	mm	Sheathing connection spacing
$K := 440$	N/mm	Individual connector stiffness

DETERMINATION OF EQUIVALENT FLANGE WIDTH:

$b_f := s_s - b$ mm Web spacing

$$L_L := L \cdot \left[3.6 \left(\frac{L_{gap}}{L} \right)^4 - 4.1 \cdot \left(\frac{L_{gap}}{L} \right)^3 + 0.94 \left(\frac{L_{gap}}{L} \right)^2 + 0.49 \left(\frac{L_{gap}}{L} \right) \right]$$

$L_L = 1191$ mm Length factor to account for the effect of gaps in the sheathing on the prediction of effective flange width

$E_{a0} := \frac{B_{a0}}{t}$ MPa Sheathing axial modulus of elasticity parallel to studs

$E_{a90} := \frac{B_{a90}}{t}$ MPa Sheathing axial modulus of elasticity perpendicular to studs

$G := \frac{B_v}{t}$ MPa Sheathing shear modulus of elasticity

$$c := \frac{E_{a0}}{E_{a90}} \qquad a := \frac{E_{a0}}{2 \cdot G} - \mu_{xy}$$

$$\lambda_1 := \sqrt{a + \sqrt{a^2 - c}} \qquad \lambda_2 := \sqrt{a - \sqrt{a^2 - c}}$$

$$\alpha_1 := \frac{\lambda_1 \cdot \pi \cdot b_f}{2 \cdot L_L} \qquad \alpha_2 := \frac{\lambda_2 \cdot \pi \cdot b_f}{2 \cdot L_L}$$

$$b_{ef} := \frac{\left(\lambda_1 \cdot \tanh(\alpha_1) - \lambda_2 \cdot \tanh(\alpha_2)\right)}{\pi \cdot \left(\lambda_1^2 - \lambda_2^2\right)} \cdot 2 \cdot L_L$$

$b_{ef} = 313$ mm Effective flange width

DETERMINATION OF EQUIVALENT BENDING AND AXIAL STIFFNESS:

Wall Stud:

$A := b \cdot d$	mm^2	Wall stud area
$S := \frac{b \cdot d^2}{6}$	mm^3	Wall stud section modulus
$I := \frac{b \cdot d^3}{12}$	mm^4	Wall stud moment of inertia

Sheathing:

$EA_0 := B_{a0} \cdot b_{ef}$	N	Sheathing axial stiffness parallel to studs
$EI_0 := B_{b0} \cdot b_{ef}$	Nmm^2	Sheathing bending stiffness parallel to studs
$k := \frac{K}{s_K}$	N/mm/mm	Sheathing connection slip modulus

Equivalent Bending Stiffness:

$$\gamma := \frac{1}{1 + \frac{\pi^2 \cdot EA_0}{k \cdot \left(L_{gap}\right)^2}} \qquad \gamma = 0.085$$

Connection coefficient factors:
1.0 = fully composite section
0.0 = no composite action

$h_s := \frac{t + d}{2}$ — mm — Distance between stud and sheathing centroids

$a(E) := \frac{\gamma \cdot EA_0 \cdot h_s}{\gamma \cdot EA_0 + E \cdot A}$ — mm — Distance from centroid of stud to centre of axial rigidity

$a_s(E) := h_s - a(E)$ — mm — Distance from centre of axial rigidity to centroid of sheathing

$$EI_{eff}(E) := E \cdot I + E \cdot A \cdot a(E)^2 + EI_0 + \gamma \cdot EA_0 \cdot a_s(E)^2$$

$EI_{eff}(E_{50}) = 6.813 \times 10^{11}$ Nmm^2 — Effective bending stiffness of the composite stud member

$EA_{eff}(E) := E \cdot A + \gamma \cdot EA_0$ N — Effective axial stiffness of composite stud member

DETERMINATION OF COMPOSITE MEMBER COMPONENT RESISTANCES:

Stud Bending Strength:

$\phi_b := 0.90$		Bending resistance factor
$K_D := 1.15$		Load duration factor for wind
$K_H := 1.04$		System factor
$K_S := 1.00$		Exposure Factor
$K_T := 1.00$		Treatment factor
$K_L := 1.00$		Length factor (meets the requirements of Clause 5.5.4.2)
$K_{zb} := \left(\frac{305}{d}\right)^{0.15}$	$K_{zb} = 1.04$	Size factor in bending
$F_b := f_b \cdot (K_D \cdot K_H \cdot K_S \cdot K_T)$	MPa	Factored bending strength

$$M_r := \frac{\phi_b \cdot F_b \cdot S \cdot K_{zb} \cdot K_L}{10^6}$$

$M_r = 19.4$	kNm	Bending moment resistance of the bare stud member

Stud Axial Strength:

$\phi_c := 0.80$		Compression parallel to grain resistance factor
$K_{zc} := 1.0$		Size factor
$F_c := f_c \cdot (K_D \cdot K_S \cdot K_T)$	MPa	Factored compression strength
$r(E) := \sqrt{\frac{EI_{eff}(E)}{EA_{eff}(E)}}$	mm	Partially composite stud member radius of gyration
$\lambda(E) := \frac{L}{\sqrt{12} \cdot r(E)}$		Partially composite stud member effective slenderness
$K_{ceff}(E) := \left(1.0 + \frac{F_c \cdot K_{zc} \cdot \lambda(E)^3}{35 \cdot E \cdot K_S \cdot K_T}\right)^{-1}$		Partially composite stud member effective slenderness factor

$$P_r(E) := \frac{\phi_c \cdot F_c \cdot A \cdot K_{zc} \cdot K_{ceff}(E)}{10^3}$$

$P_r(E_{05}) = 78.0$	kN	Stud member effective axial resistance increased due to the increased stability provided by composite action

Stud Shear Strength:

$\phi_v := 0.90$ Shear resistance factor

$K_{zv} := 1.0$ Size factor

$F_v := f_v \cdot (K_D \cdot K_S \cdot K_T)$ MPa Factored shear strength

$$V_r := \phi_v \cdot F_v \cdot \frac{2 \cdot A}{3 \cdot 10^3} \cdot K_{zv}$$

$V_r = 26.0$ kN Stud member shear resistance

Stud Tension Strength:

$\phi_t := 0.90$ Tension resistance factor

$K_{zt} := 1.0$ Size factor

$F_t := f_t \cdot (K_D \cdot K_S \cdot K_T)$ MPa Factored tension strength

$$T_r := \phi_t \cdot F_t \cdot \frac{A}{10^3} \cdot K_{zt}$$

$T_r = 310.4$ kN Stud member tension resistance (net area is equal to gross cross sectional area because a bolted connection will not be used for this example)

Sheathing Bending Strength:

$\phi_{mp} := 0.95$ Bending resistance factor

$M_p := m_{p0} \cdot (K_D \cdot K_S \cdot K_T)$ MPa Factored bending strength

$$M_{pr} := \phi_{mp} \cdot M_p \cdot \frac{b_{ef}}{10^6}$$

$M_{pr} = 0.17$ kNm Sheathing bending resistance

Sheathing Compression Strength:

$\phi_{pp} := 0.95$ Compression parallel to panel edge resistance factor

$P_p := p_{p0} \cdot (K_D \cdot K_S \cdot K_T)$ MPa Factored compression strength

$$P_{pr} := \phi_{mp} \cdot P_p \cdot \frac{b_{ef}}{10^3}$$

$P_{pr} = 34.2$ kNm Sheathing compression resistance

LOAD CASE 3:

$w_f := 0.7 \cdot 0.717$

$w_f = 0.502$ kN/m Factored wind load

$P_f := 12.6 + 0.7 \cdot 45.1$

$P_f = 44.2$ kN Factored axial load

$$M := \frac{w_f \cdot \left(\frac{L}{10^3}\right)^2}{8} + \frac{1}{2} \cdot P_f \cdot \frac{d}{6 \cdot 10^3}$$

$M = 4.48$ kNm Unamplified bending moment at the middle of the wall

$$P_E(E) := \frac{\pi^2 \cdot EI_{eff}(E)}{L^2} \cdot \frac{1}{10^3}$$

$P_E(E_{50}) = 117$ kN Euler buckling load

$$M_f := M \cdot \left(\frac{1}{1 - \frac{P_f}{P_E(E_{50})}}\right)$$

$M_f = 7.21$ kNm Amplified bending moment at the middle of the wall. Because the wall has gaps, the worst case is for a gap to occur in the middle of the wall and therefore the maximum bending moment will equal this value. For a wall without a gap in the middle of the wall, the maximum moment in the stud is as follows.

$$M_s := \frac{E_{50} \cdot I \cdot M_f}{EI_{eff}(E_{50})}$$

$M_s = 6.95$ kNm

$$V_f := \frac{w_f \cdot L}{2 \cdot 10^3}$$

$V_f = 1.905$ kN Maximum shear force at the ends of the wall

$$T_s := \frac{\gamma \cdot a(E_{50}) \cdot E_{50} \cdot A \cdot M_f \cdot 10^3}{EI_{eff}(E_{50})}$$

$T_s = 0.18$ kN Tension force in the stud due to composite action for a member without a gap in the middle of the wall

$M_{sh} := \frac{EI_0 \cdot M_f}{EI_{eff}(E_{50})}$ $M_{sh} = 0.004$ kNm Bending moment in the sheathing due to composite action for a member without gaps in the sheathing at the middle of the wall

$P_{sh} := \frac{\gamma \cdot a_s(E_{50}) \cdot EA_0 \cdot M_f \cdot 10^3}{EI_{eff}(E_{50})}$

$P_{sh} = 2.07$ kN Compression force in the sheathing due to composite action for a member without gaps in the sheathing at the middle of the wall

Design Check of the Stud of a Composite Member with a Gap at the Middle of the Wall:

$\frac{P_f}{P_r(E_{05})} + \frac{M_f}{M_r} = 0.94$ ≤ 1.0 (Acceptable)

$\frac{V_f}{V_r} = 0.073$ ≤ 1.0 (Acceptable)

Design Check of the Stud of a Composite Member without a Gap at the Middle of the Wall:

$\frac{P_f - T_s}{P_r(E_{05})} + \frac{M_s}{M_r} = 0.92$ ≤ 1.0 (Acceptable)

Design Check of the Stud of a Composite Member without a Gap at the Middle of the Wall and with an Applied Axial Tension Force due to Wind Uplift:

$T_f := 5.80$ kN Net uplift at the eave

$$M_f := \frac{w_f \cdot \left(\frac{L}{10^3}\right)^2}{8} + \frac{1}{2} \cdot T_f \cdot \frac{d}{6 \cdot 10^3}$$

$M_f = 3.73$ kNm Bending moment at the middle of the wall

$M_s := \frac{E_{50} \cdot I \cdot M_f}{EI_{eff}(E_{50})}$ $M_s = 3.59$ kNm Bending moment in the stud at the middle of the wall for a wall without a gap in the middle

$T_s := \frac{\gamma \cdot a(E_{50}) \cdot E_{50} \cdot A \cdot M_f \cdot 10^3}{EI_{eff}(E_{50})}$

$T_s = 0.09$ kN Tension force in the stud due to composite action for a member without a gap in the middle of the wall

$\frac{T_f + T_s}{T_r} + \frac{M_s}{M_r} = 0.20$ ≤ 1.0 (Acceptable)

- Design Check of the Sheathing of a Composite Member without a Gap at the Middle of the Wall:

$$\frac{P_{sh}}{P_{pr}} + \frac{M_{sh}}{M_{pr}} = 0.09 \qquad . \le 1.0$$ (Acceptable)

- Design Check of the Maximum Allowable Displacement at the Middle of the Wall:

$w_s := 0.7 \cdot 0.362$

$w_s = 0.253$ kN/m Specified wind load

$P_s := 10.1 + 0.7 \cdot 30.1$

$P_s = 31.2$ kN Specified axial load

$$\Delta := \frac{5 \cdot w_s \cdot L^4}{384\, EI_{eff}(E_{50})} + \frac{P_s \cdot 10^3 \cdot \frac{d}{6} \cdot L^2}{16 \cdot EI_{eff}(E_{50})} \qquad \Delta = 22.5$$ mm Unamplified displacement at the middle of the wall

$$\Delta_A := \Delta \cdot \left(\frac{1}{1 - \frac{P_s}{P_E(E_{50})}} \right) \qquad \Delta_A = 30.7$$ mm Amplified displacement at the middle of the wall

$$. \le . \frac{L}{180} = 42.2$$ (Acceptable)

B.2.1.3 Stud Connection Design

Tests on full-scale wall specimens have shown that utilizing off-the-shelf connectors is a feasible alternative to using specially fabricated stud connectors. The design loads to be applied to the connectors for this design example are 5.80 kN in tension and 2.72 kN in shear. Wood connector manufacturers provide factored resistance values for their products. For this example, an H6 hurricane tie connector and an HU9 face mounted joist hanger, both produced by Simpson Strong-Tie Company, were chosen to resist the applied tension and shear forces, respectively. These two connectors were used in the full-scale wall tests with connection type B, which is described in Chapter 7 and shown in Figure 7.5 (b). Tembec recommends using the same specific gravity as hemlock-fir (Hem-Fir) sawn lumber when designing connections for their SelecTem™ LVL product. Simpson Strong-Tie only provides design values for Douglas fir-larch (D.Fir-L) and spruce-pine-fir (SPF) sawn lumber products. Both of these connectors resist the tension and shear forces applied to them through the lateral resistances of the nails. The Canadian Wood Design Code provides unit lateral resistances for nails for all three species groups. It was deemed appropriate to interpolate the design resistances provided by Simpson Strong-Tie for these two connectors with the ratios of unit lateral resistances provided by the code. The factored resistances for the connectors were calculated to be 5.92 kN in tension and 6.22 kN in shear, respectively. Both of these values are larger than the applied forces and are deemed to be adequate for use in construction.

The factored shear resistance value is for the face mounted joist hanger in the weak (uplift) direction. These hangers are designed for wood-frame floor or roof construction. The uplift suction forces on the connectors due to wind are not as large as the downward forces due to the weight of the diaphragm and the downward applied loads in these applications. Because of the geometry of the connection, the shear resistance in one direction is not as great as the shear resistance in the other direction, which is consistent with the applied forces. The suction force on a wall due to wind can be approximately the same as the compression force, however, so the minimum resistance value for the connector was chosen for design.

APPENDIX C: ANALYTICAL MODELS

C.1 PANEL FINITE ELEMENT MODEL

The following is a sample input data file for the computer program PANEL described in Section 8.1.1. This example is for wall specimen 502, which is described in detail in Section 7.2.1. A schematic of this wall model was presented in Figure 8.2. The input data is in inch and pound units of measurement. Text that is italicized describes the input data.

5	*Number of files plotting individual results*
40 7 70 0 0 55	*Number of: elements, element size types, nodes in the top cover, 0 equals no bottom cover, nodes in the bottom cover, and nodes in the frame*
4 10	*Number of: element columns and the elements in each column*
1 0.000000E+00 0.000000E+00	*Element node number and its position in the X and Y coordinates*
2 0.000000E+00 0.487500E+01	
3 0.000000E+00 0.473750E+02	
4 0.000000E+00 0.631250E+02	
5 0.000000E+00 0.953750E+02	
6 0.000000E+00 0.983750E+02	
7 0.000000E+00 0.127625E+03	
8 0.000000E+00 0.143375E+03	
9 0.000000E+00 0.185875E+03	
10 0.000000E+00 0.190750E+03	
11 0.000000E+00 0.190750E+03	
12 0.000000E+00 0.193250E+03	
13 0.240000E+02 0.000000E+00	
14 0.240000E+02 0.487500E+01	
15 0.240000E+02 0.473750E+02	
16 0.240000E+02 0.631250E+02	
17 0.240000E+02 0.953750E+02	
18 0.240000E+02 0.983750E+02	
19 0.240000E+02 0.127625E+03	
20 0.240000E+02 0.143375E+03	
21 0.240000E+02 0.185875E+03	
22 0.240000E+02 0.190750E+03	
23 0.240000E+02 0.190750E+03	
24 0.240000E+02 0.193250E+03	
25 0.480000E+02 0.000000E+00	

26	0.480000E+02	0.487500E+01
27	0.480000E+02	0.473750E+02
28	0.480000E+02	0.631250E+02
29	0.480000E+02	0.953750E+02
30	0.480000E+02	0.983750E+02
31	0.480000E+02	0.127625E+03
32	0.480000E+02	0.143375E+03
33	0.480000E+02	0.185875E+03
34	0.480000E+02	0.190750E+03
35	0.480000E+02	0.190750E+03
36	0.480000E+02	0.193250E+03
37	0.480000E+02	0.000000E+00
38	0.480000E+02	0.487500E+01
39	0.480000E+02	0.473750E+02
40	0.480000E+02	0.631250E+02
41	0.480000E+02	0.953750E+02
42	0.480000E+02	0.983750E+02
43	0.480000E+02	0.127625E+03
44	0.480000E+02	0.143375E+03
45	0.480000E+02	0.185875E+03
46	0.480000E+02	0.190750E+03
47	0.720000E+02	0.000000E+00
48	0.720000E+02	0.487500E+01
49	0.720000E+02	0.473750E+02
50	0.720000E+02	0.631250E+02
51	0.720000E+02	0.953750E+02
52	0.720000E+02	0.983750E+02
53	0.720000E+02	0.127625E+03
54	0.720000E+02	0.143375E+03
55	0.720000E+02	0.185875E+03
56	0.720000E+02	0.190750E+03
57	0.720000E+02	0.190750E+03
58	0.720000E+02	0.193250E+03
59	0.960000E+02	0.000000E+00
60	0.960000E+02	0.487500E+01
61	0.960000E+02	0.473750E+02
62	0.960000E+02	0.631250E+02
63	0.960000E+02	0.953750E+02
64	0.960000E+02	0.983750E+02
65	0.960000E+02	0.127625E+03
66	0.960000E+02	0.143375E+03
67	0.960000E+02	0.185875E+03
68	0.960000E+02	0.190750E+03
69	0.960000E+02	0.190750E+03
70	0.960000E+02	0.193250E+03
1	0.240000E+02	0.487500E+01
2	0.240000E+02	0.425000E+02
3	0.240000E+02	0.157500E+02
4	0.240000E+02	0.322500E+02

5 0.240000E+02 0.300000E+01	
6 0.240000E+02 0.292500E+02	
7 0.240000E+02 0.250000E+01	
1 1	*Number of frame types and connection types*
1 0.100000E+01	*Frame type number and configuration code (1 equals dimensional lumber)*
1 0.12769E+07 0.75112E+05 0.14961E+01 0.92126E+01	
	Frame type number and properties: E, G, b, d
1 1	*Connection type number and frame type number*
0.202000E+03 0.205000E+03 0.428300E+04 0.570000E+00 -0.126000E+03	
0.191000E+03 0.160000E+03 0.268400E+04 0.490000E+00 -0.860000E+02	
0.112000E+03 0.400000E+03 0.142750E+05 0.110000E+00 -0.571000E+02	
0.212000E+03 0.100000E+02 0.152000E+04 0.890000E+00 -0.127000E+03	
	Connection displacement function parameters P_0, K_1, K_0, u_{max}, *and* K_E *parallel to the frame member, perpendicular to the frame member, in withdrawal, and in rotation*
1 1 1	*Element number, element type number, 1 equals that an element is present*
1 13 14 2	*Node numbers of the element counter clockwise*
71 82 83 72	*Node number of the frame counter clockwise*
2 2 1	
2 14 15 3	
72 83 84 73	
3 3 1	
3 15 16 4	
73 84 85 74	
4 4 1	
4 16 17 5	
74 85 86 75	
5 5 1	
5 17 18 6	
75 86 87 76	
6 6 1	
6 18 19 7	
76 87 88 77	
7 3 1	
7 19 20 8	
77 88 89 78	
8 2 1	
8 20 21 9	
78 89 90 79	
9 1 1	
9 21 22 10	
79 90 91 80	
10 7 0	
11 23 24 12	
80 91 92 81	
11 1 1	

13 25 26 14
82 93 94 83
12 2 1
14 26 27 15
83 94 95 84
13 3 1
15 27 28 16
84 95 96 85
14 4 1
16 28 29 17
85 96 97 86
15 5 1
17 29 30 18
86 97 98 87
16 6 1
18 30 31 19
87 98 99 88
17 3 1
19 31 32 20
88 99 100 89
18 2 1
20 32 33 21
89 100 101 90
19 1 1
21 33 34 22
90 101 102 91
20 7 0
23 35 36 24
91 102 103 92
21 1 1
37 47 48 38
93 104 105 94
22 2 1
38 48 49 39
94 105 106 95
23 3 1
39 49 50 40
95 106 107 96
24 4 1
40 50 51 41
96 107 108 97
25 5 1
41 51 52 42
97 108 109 98
26 6 1
42 52 53 43
98 109 110 99
27 3 1
43 53 54 44

99 110 111 100
28 2 1
44 54 55 45
100 111 112 101
29 1 1
45 55 56 46
101 112 113 102
30 7 0
35 57 58 36
102 113 114 103
31 1 1
47 59 60 48
104 115 116 105
32 2 1
48 60 61 49
105 116 117 106
33 3 1
49 61 62 50
106 117 118 107
34 4 1
50 62 63 51
107 118 119 108
35 5 1
51 63 64 52
108 119 120 109
36 6 1
52 64 65 53
109 120 121 110
37 3 1
53 65 66 54
110 121 122 111
38 2 1
54 66 67 55
111 122 123 112
39 1 1
55 67 68 56
112 123 124 113
40 7 0
57 69 70 58
113 124 125 114
0.381100E+00 *Top cover thickness*
0.1090974E+07 0.415678E+06 0.174045E+06 0.200000E+00 0.760000E-01
Top cover properties E_{PAR}, E_{PERP}, G, ν_{LARGE}, and ν_{SMALL}
0.200000E+01 *2 equals top cover strong direction in Y*
1 1 1 0 1 *Element number and frame type number counter clockwise around the element*
2 0 1 1 1
3 0 1 0 1
4 0 1 1 1

```
 5 0 1 0 1
 6 0 1 0 1
 7 0 1 1 1
 8 0 1 0 1
 9 0 1 1 1
10 0 1 1 1
11 1 1 0 0
12 0 1 1 0
13 0 1 0 0
14 0 1 1 0
15 0 1 0 0
16 0 1 0 0
17 0 1 1 0
18 0 1 0 0
19 0 1 1 0
20 0 1 1 0
21 1 1 0 0
22 0 1 1 0
23 0 1 0 0
24 0 1 1 0
25 0 1 0 0
26 0 1 0 0
27 0 1 1 0
28 0 1 0 0
29 0 1 1 0
30 0 1 1 0
31 1 1 0 0
32 0 1 1 0
33 0 1 0 0
34 0 1 1 0
35 0 1 0 0
36 0 1 0 0
37 0 1 1 0
38 0 1 0 0
39 0 1 1 0
40 0 1 1 0
 1 1 1 0 1 0.600000E+01 0.600000E+01 0.000000E+00 0.600000E+01
```

Element number, connection type number counter clockwise around the element, and connector spacing

```
 2 0 1 1 1 0.000000E+00 0.600000E+01 0.600000E+01 0.600000E+01
 3 0 1 0 1 0.000000E+00 0.600000E+01 0.000000E+00 0.600000E+01
 4 0 1 1 1 0.000000E+00 0.600000E+01 0.600000E+01 0.600000E+01
 5 0 1 0 1 0.000000E+00 0.600000E+01 0.000000E+00 0.600000E+01
 6 0 1 0 1 0.000000E+00 0.600000E+01 0.000000E+00 0.600000E+01
 7 0 1 1 1 0.000000E+00 0.600000E+01 0.600000E+01 0.600000E+01
 8 0 1 0 1 0.000000E+00 0.600000E+01 0.000000E+00 0.600000E+01
 9 0 1 1 1 0.000000E+00 0.600000E+01 0.600000E+01 0.600000E+01
10 1 1 1 1 0.600000E+01 0.600000E+01 0.600000E+01 0.600000E+01
```

11	1	1	0	0	0.600000E+01	0.600000E+01	0.000000E+00	0.000000E+00
12	0	1	1	0	0.000000E+00	0.600000E+01	0.600000E+01	0.000000E+00
13	0	1	0	0	0.000000E+00	0.600000E+01	0.000000E+00	0.000000E+00
14	0	1	1	0	0.000000E+00	0.600000E+01	0.600000E+01	0.000000E+00
15	0	1	0	0	0.000000E+00	0.600000E+01	0.000000E+00	0.000000E+00
16	0	1	0	0	0.000000E+00	0.600000E+01	0.000000E+00	0.000000E+00
17	0	1	1	0	0.000000E+00	0.600000E+01	0.600000E+01	0.000000E+00
18	0	1	0	0	0.000000E+00	0.600000E+01	0.000000E+00	0.000000E+00
19	0	1	1	0	0.000000E+00	0.600000E+01	0.600000E+01	0.000000E+00
20	1	1	1	0	0.600000E+01	0.600000E+01	0.600000E+01	0.000000E+00
21	1	1	0	1	0.600000E+01	0.600000E+01	0.000000E+00	0.600000E+01
22	0	1	1	1	0.000000E+00	0.600000E+01	0.600000E+01	0.600000E+01
23	0	1	0	1	0.000000E+00	0.600000E+01	0.000000E+00	0.600000E+01
24	0	1	1	1	0.000000E+00	0.600000E+01	0.600000E+01	0.600000E+01
25	0	1	0	1	0.000000E+00	0.600000E+01	0.000000E+00	0.600000E+01
26	0	1	0	1	0.000000E+00	0.600000E+01	0.000000E+00	0.600000E+01
27	0	1	1	1	0.000000E+00	0.600000E+01	0.600000E+01	0.600000E+01
28	0	1	0	1	0.000000E+00	0.600000E+01	0.000000E+00	0.600000E+01
29	0	1	1	1	0.000000E+00	0.600000E+01	0.600000E+01	0.600000E+01
30	1	1	1	0	0.600000E+01	0.600000E+01	0.600000E+01	0.000000E+00
31	1	1	0	0	0.600000E+01	0.600000E+01	0.000000E+00	0.000000E+00
32	0	1	1	0	0.000000E+00	0.600000E+01	0.600000E+01	0.000000E+00
33	0	1	0	0	0.000000E+00	0.600000E+01	0.000000E+00	0.000000E+00
34	0	1	1	0	0.000000E+00	0.600000E+01	0.600000E+01	0.000000E+00
35	0	1	0	0	0.000000E+00	0.600000E+01	0.000000E+00	0.000000E+00
36	0	1	0	0	0.000000E+00	0.600000E+01	0.000000E+00	0.000000E+00
37	0	1	1	0	0.000000E+00	0.600000E+01	0.600000E+01	0.000000E+00
38	0	1	0	0	0.000000E+00	0.600000E+01	0.000000E+00	0.000000E+00
39	0	1	1	0	0.000000E+00	0.600000E+01	0.600000E+01	0.000000E+00
40	1	1	1	0	0.600000E+01	0.600000E+01	0.600000E+01	0.000000E+00

10 *Number of nodes with support conditions*
71 3 1 2 4 0 *Node number, number of degrees of freedom*
81 2 1 4 0 *supported, support codes, and 0 equals no freedom*
82 3 1 2 4 0 *allowed for any of the support codes. 3 support*
92 2 1 4 0 *conditions corresponds to a pinned condition and 2*
93 3 1 2 4 0 *corresponds to a roller support. A fixed support*
103 2 1 4 0 *4 support conditions: 1 disp. in X, 2 disp. in Y, 4*
104 3 1 2 4 0 *disp. in Z, and 6 rotation about XY.*
114 2 1 4 0
115 3 1 2 4 0
125 2 1 4 0
2 *2 equals displacement control*
10 *Number of displacement increments*
5 *Number of nodes with concentrated loads*
81 0.000000E+00 -0.068800E+04 0.000000E+00 0 0 0
Node number, concentrated loads in X, Y, and Z, load increments in X, Y, and Z
0 *0 for no eccentricity applied to vertical loads*
92 0.000000E+00 -0.137500E+04 0.000000E+00 0 0 0

0	
103 0.000000E+00 -0.137500E+04 0.000000E+00 0 0 0	
0	
114 0.000000E+00 -0.137500E+04 0.000000E+00 0 0 0	
0	
125 0.000000E+00 -0.068800E+04 0.000000E+00 0 0 0	
0	
0	*Number of elements with distributed loads*
10	*Number of nodes with applied displacements*
74 4 -0.100000E+00	*Node number, direction of applied displacement,*
77 4 -0.100000E+00	*and magnitude of applied displacement*
85 4 -0.100000E+00	
88 4 -0.100000E+00	
96 4 -0.100000E+00	
99 4 -0.100000E+00	
107 4 -0.100000E+00	
110 4 -0.100000E+00	
118 4 -0.100000E+00	
121 4 -0.100000E+00	
76 4	*Node number to be plotted and coordinate response*
94 4	*to be plotted*
98 4	
101 4	
120 4	
0	*0 equals cover tearing forces ignored*
0	*0 equals maximum bending stress of framing members ignored*

C.2 BEAM-SPRING ANALOG

The following is a sample calculation for determining the bending stiffness of a composite full-scale wall specimen using the beam-spring analog method, described in Section 8.1.2. This example is also for wall specimen 502, which is described in detail in Section 7.2.1. Highlighted text indicates an input parameter.

INPUT PARAMETERS:

Stud Properties:

$b := 38$	mm	Width
$d := 234$	mm	Depth
$j := 0..4$		5 studs in the wall
$E := \begin{pmatrix} 8224 \\ 6711 \\ 7746 \\ 10293 \\ 11046 \end{pmatrix}$	MPa	Calculated modulus of elasticity for each stud in the wall obtained from testing

Sheathing Properties:

$t := 9.68$	mm	Thickness
$B_{b0} := 567800$	Nmm^2/mm	Bending stiffness per unit width parallel to studs
$B_{b90} := 216400$	Nmm^2/mm	Bending stiffness per unit width perpendicular to studs
$B_{a0} := 42600$	N/mm	Axial stiffness per unit width parallel to studs
$B_{a90} := 23300$	N/mm	Axial stiffness per unit width perpendicular to studs
$B_v := 11600$	N/mm	Shear rigidity per unit width
$\mu_{xy} := 0.2$		Poisson's ratio

Wall Geometry Properties:

$L := 4928$	mm	Height of the wall (assuming ends are pinned)
$L_{gap0} := 4880$	mm	Length between gaps in the exterior sheathing parallel to studs
$L_{gap90} := 1220$	mm	Length between gaps in the exterior sheathing parallel to studs
$s_s := 610$	mm	Stud spacing

Connection Properties:

$s_K := 152$	mm	Sheathing connection spacing
$K := 440$	N/mm	Individual connector stiffness

Load Properties:

$i := 0..10$		Number of transverse load steps
$P_t := 2447$	N	Transverse load increment
$P_a := 48.9$	kN	Total axial load applied

DETERMINATION OF EQUIVALENT FLANGE WIDTH:

$$b_f := \begin{pmatrix} \frac{s_s}{2} - b \\ s_s - b \\ s_s - b \\ s_s - b \\ \frac{s_s}{2} - b \end{pmatrix}$$ mm Web spacing

$$L_L := L \cdot \left[3.6 \left(\frac{L_{gap0}}{L} \right)^4 - 4.1 \cdot \left(\frac{L_{gap0}}{L} \right)^3 + 0.94 \left(\frac{L_{gap0}}{L} \right)^2 + 0.49 \left(\frac{L_{gap0}}{L} \right) \right]$$

$L_L = 4373$ mm Length factor to account for the effect of gaps in the sheathing on the prediction of effective flange width

$E_{a0} := \frac{B_{a0}}{t}$ MPa Sheathing axial modulus of elasticity parallel to studs

$E_{a90} := \frac{B_{a90}}{t}$ MPa Sheathing axial modulus of elasticity perpendicular to studs

$G := \frac{B_v}{t}$ MPa Sheathing shear modulus of elasticity

$c := \frac{E_{a0}}{E_{a90}}$ $a := \frac{E_{a0}}{2 \cdot G} - \mu_{xy}$

$\lambda_1 := \sqrt{a + \sqrt{a^2 - c}}$ $\lambda_2 := \sqrt{a - \sqrt{a^2 - c}}$ $\alpha_{1_j} := \frac{\lambda_1 \cdot \pi \cdot b_{f_j}}{2 \cdot L_L}$ $\alpha_{2_j} := \frac{\lambda_2 \cdot \pi \cdot b_{f_j}}{2 \cdot L_L}$

$$b_{ef_j} := \frac{\left(\lambda_1 \cdot \tanh\left(\alpha_{1_j}\right) - \lambda_2 \cdot \tanh\left(\alpha_{2_j}\right)\right)}{\pi \cdot \left(\lambda_1^2 - \lambda_2^2\right)} \cdot 2 \cdot L_L$$

$$b_{ef} = \begin{pmatrix} 264 \\ 547 \\ 547 \\ 547 \\ 264 \end{pmatrix}$$ mm Effective flange width

$$\eta_j := \frac{EI_{eff_j}}{E_j \cdot I} \cdot 100 - 100 \qquad \eta = \begin{pmatrix} 18 \\ 27 \\ 24 \\ 18 \\ 14 \end{pmatrix}$$

Percent increase of partially composite member bending stiffness over bare stud bending stiffness

$$EA_{eff_j} := E_j \cdot A + \gamma_j \cdot EA_{0_j} \qquad \text{N}$$

Effective axial stiffness of composite stud member

$$k_j := \frac{1296\, EI_{eff_j}}{23 \cdot L^3} \qquad k = \begin{pmatrix} 185.632 \\ 162.806 \\ 182.963 \\ 232.255 \\ 239.953 \end{pmatrix} \quad \text{N/mm}$$

Bending stiffness of each composite member

$$K_r := 0 \qquad \text{Nmm/rad}$$

Calculated rotational end restraint stiffness from testing for the entire wall

$$EI_{SUM} := EI_{eff_0} + EI_{eff_1} + EI_{eff_2} + EI_{eff_3} + EI_{eff_4}$$

$$B := \frac{K_r \cdot L}{EI_{SUM}} \qquad B = 0$$

$$\zeta := \frac{23}{\frac{(276+15 \cdot B)}{(12+4 \cdot B)}} \qquad \zeta = 1$$

Increase in stiffness factor due to the presence of rotational restraint

$$P_E := \frac{\pi^2 \cdot EI_{SUM}}{L^2} \qquad P_E = 866278 \quad \text{N}$$

Euler buckling load of partially composite member

$$\psi := 1 - \frac{P_a \cdot 1000}{P_E} \qquad \psi = 0.944$$

Reduction in stiffness factor due to axial load

$$k_j := k_j \cdot \zeta \cdot \psi$$

Factored bending stiffness of each composite member

$$EI_b := 10^{23}$$

Bending stiffness in the transverse direction (set to a very large number to account for steel load distribution beams)

Beam-Spring Analog Stiffness Matrix

$$K := \begin{pmatrix}
12\cdot\frac{EI_b}{s_s^3}+k_0 & 6\cdot\frac{EI_b}{s_s^2} & -12\cdot\frac{EI_b}{s_s^3} & 6\cdot\frac{EI_b}{s_s^2} & 0 & 0 & 0 & 0 & 0 & 0 \\
6\cdot\frac{EI_b}{s_s^2} & 4\cdot\frac{EI_b}{s_s} & -6\cdot\frac{EI_b}{s_s^2} & 2\cdot\frac{EI_b}{s_s} & 0 & 0 & 0 & 0 & 0 & 0 \\
-12\cdot\frac{EI_b}{s_s^3} & -6\cdot\frac{EI_b}{s_s^2} & 24\cdot\frac{EI_b}{s_s^3}+k_1 & 0 & -12\cdot\frac{EI_b}{s_s^3} & 6\cdot\frac{EI_b}{s_s^2} & 0 & 0 & 0 & 0 \\
6\cdot\frac{EI_b}{s_s^2} & 2\cdot\frac{EI_b}{s_s} & 0 & 8\cdot\frac{EI_b}{s_s} & -6\cdot\frac{EI_b}{s_s^2} & 2\cdot\frac{EI_b}{s_s} & 0 & 0 & 0 & 0 \\
0 & 0 & -12\cdot\frac{EI_b}{s_s^3} & -6\cdot\frac{EI_b}{s_s^2} & 24\cdot\frac{EI_b}{s_s^3}+k_2 & 0 & -12\cdot\frac{EI_b}{s_s^3} & 6\cdot\frac{EI_b}{s_s^2} & 0 & 0 \\
0 & 0 & 6\cdot\frac{EI_b}{s_s^2} & 2\cdot\frac{EI_b}{s_s} & 0 & 8\cdot\frac{EI_b}{s_s} & -6\cdot\frac{EI_b}{s_s^2} & 2\cdot\frac{EI_b}{s_s} & 0 & 0 \\
0 & 0 & 0 & 0 & -12\cdot\frac{EI_b}{s_s^3} & -6\cdot\frac{EI_b}{s_s^2} & 24\cdot\frac{EI_b}{s_s^3}+k_3 & 0 & -12\cdot\frac{EI_b}{s_s^3} & 6\cdot\frac{EI_b}{s_s^2} \\
0 & 0 & 0 & 0 & 6\cdot\frac{EI_b}{s_s^2} & 2\cdot\frac{EI_b}{s_s} & 0 & 8\cdot\frac{EI_b}{s_s} & -6\cdot\frac{EI_b}{s_s^2} & 2\cdot\frac{EI_b}{s_s} \\
0 & 0 & 0 & 0 & 0 & 0 & -12\cdot\frac{EI_b}{s_s^3} & -6\cdot\frac{EI_b}{s_s^2} & 12\cdot\frac{EI_b}{s_s^3}+k_4 & -6\cdot\frac{EI_b}{s_s^2} \\
0 & 0 & 0 & 0 & 0 & 0 & 6\cdot\frac{EI_b}{s_s^2} & 2\cdot\frac{EI_b}{s_s} & -6\cdot\frac{EI_b}{s_s^2} & 4\cdot\frac{EI_b}{s_s}
\end{pmatrix}$$

$$R(i) := \begin{pmatrix} 0 \\ 0 \\ 0 \\ 0 \\ P_t \cdot i \\ 0 \\ 0 \\ 0 \\ 0 \\ 0 \end{pmatrix} \qquad S(i) := (K)^{-1} \cdot R(i) \qquad D(i) := \begin{pmatrix} S(i)_0 \\ S(i)_2 \\ S(i)_4 \\ S(i)_6 \\ S(i)_8 \end{pmatrix}$$

Equivalent Wall Stiffness at Each Stud: $\dfrac{P_t}{D(1)_j} = \begin{pmatrix} 798 \\ 860 \\ 933 \\ 1019 \\ 1122 \end{pmatrix}$

$S(i)_0 =$	$S(i)_4 =$	$S(i)_8 =$
0.00	0.00	0.00
3.07	2.62	2.18
6.13	5.25	4.36
9.20	7.87	6.54
12.27	10.50	8.72
15.33	13.12	10.91
18.40	15.74	13.09
21.47	18.37	15.27
24.53	20.99	17.45
27.60	23.61	19.63
30.67	26.24	21.81

Mid-Height Wall Deflection vs Transverse